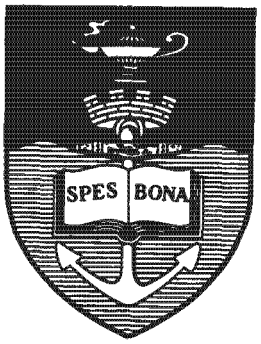
The copyright of this thesis vests in the author. No quotation from it or information derived from it is to be published without full acknowledgement of the source. The thesis is to be used for private study or non-commercial research purposes only.

Published by the University of Cape Town (UCT) in terms of the non-exclusive license granted to UCT by the author.

University of Cape Town



Sedimentary facies from the Head of the Cape Canyon: Insights into the Cenozoic evolution of the western margin of South Africa

University of Cape Town

Rochelle Anne Wigley
Bsc Hons (Rhodes), MSc (UCT)

Submitted in fulfilment of the requirements of the degree of
DOCTOR OF PHILOSOPHY
in the
Department of Geological Sciences
Faculty of Science
University of Cape Town
November 2004

DECLARATION

I, **Rochelle Anne Wigley**, submit this thesis in fulfilment of the requirements for the degree of Doctor of Philosophy in Geology. I hereby declare that the work presented in this thesis is my own, except where otherwise stated. Chapter 5 is a copy of a paper published in *Marine Geology*, of which I am second author. This thesis reports the results of original work that I have undertaken from March 2000 to February 2005 in the Department of Geological Sciences at the University of Cape Town.

Signed by candidate

Rochelle Anne Wigley

20 February 2005

ACKNOWLEDGMENTS

For my father and grandfather

I would like to express my sincere appreciation to the following people and institutions:

- Assoc. Prof. John Compton for all his guidance, encouragement and many invaluable scientific discussions
- Dr John Rogers for all his support, his knowledge of the western margin of southern Africa and his meticulous attention to detail
- Dr Ian McMillan (formerly of De Beers Marine) for his invaluable assistance in the identification of the foraminiferal assemblages and their depositional environments, which added a valuable component to this thesis
- Werner Marine Research (Pty) Ltd for supplying the cores used in this study
- Sue de Villiers, of the University of Cape Town, for the palynological analyses of Cretaceous samples
- Mariam Bamford, of the Bernard Price Institute for Palaeontological Research at the University of the Witwatersrand, for the work she did on the Cretaceous wood samples
- Andreas Spath, University of Cape Town, for all his assistance with the microprobe and laser-ablation ICP-MS analyses
- Assoc. Prof. Dave Reid, University of Cape Town, for his assistance with all computer-related issues
- The technical support staff from the Department of Geological Sciences
- De Beers Marine (Pty) Ltd and the National Research Foundation for their financial support
- And lastly to all those people, you know who you are (including Mum, Helen & the Geological Department of Sainsbury's), without whose encouragement and continual support this may never have happened

THANK YOU

University of Cape Town

ABSTRACT

Cenozoic sedimentary successions have a restricted distribution and are largely incomplete due to erosion and non-deposition on the western margin of southern Africa. For this reason, much controversy and uncertainty remains on the geological evolution of the western margin. The wide western margin is largely devoid of bathymetric features, except for the deeply incised Cape Canyon that crosscuts the continental slope and shelf ~150 km to the northwest of Cape Town. The Head of the Cape Canyon forms a well-developed trough landwards of the Western Ridge, which separates the middle and outer shelf. More than 50 cores, up to 6 m in length, at water depths between 190 and 450 m were recovered from the Head of the Cape Canyon region. Siliciclastic, authigenic and biogenic sediments, varying in age from Cretaceous to Holocene provide the basis of a detailed sedimentary analysis. The diversity of lithostratigraphic units recovered from the condensed sedimentary record provide a unique opportunity to define in detail, for the first time, a late Cenozoic stratigraphic record for the western outer continental shelf. The depositional history is documented by an integration of bio-, Sr-isotopic and lithostratigraphy in order to ascertain the relative importance of such factors as sea-level fluctuations, tectonism, palaeoclimate and palaeoceanographic conditions on the Cenozoic evolution of the western margin.

The late Cenozoic sediments of the study area unconformably overlie unconsolidated middle Cretaceous interbedded woody quartzose sands and kaolinitic muds. The middle Albian to lower Cenomanian sediments are recovered only in the deepest parts of the canyon and adjacent to upfaulted blocks of Cretaceous strata and record deposition in brackish swamps or mud flats crosscut by sand banks and channel infill quartz sand under humid, temperate conditions. A large regional hiatus separates the Cretaceous from the upper Oligocene to lower/middle Miocene (Langhian) carbonate sediments on the outer shelf. Upper Oligocene (25.8-27.3 Ma) quartzose foraminiferal sediment was deposited in a low-energy, inner shelf, subtropical warm water environment during a relative sea-level lowstand. The presence of abundant authigenic phosphorite and phospho-glauconite and evidence for bottom current activity in the overlying upper Oligocene sediments is interpreted to reflect the onset of warm-water upwelling on the continental shelf. The main peak in phosphogenesis and hardground formation at the Oligocene/Miocene transition is linked to increased wind-driven coastal upwelling related to large climatic shifts at this time (~23.5 Ma). The stratigraphic sequences recognised in these carbonate sediments are ascribed to three to four relative sea-level fluctuations, reflecting a combination of eustasy and margin subsidence during a long-term late Oligocene to early Miocene marine transgression.

University of Cape Town

Early Miocene calcareous deposition was brought abruptly to an end at around 18 Ma by uplift, estimated to be in the order of 200 m, of the western margin.

The upper Oligocene/lower Miocene carbonate succession dips gently to the west signifying the influence of sediment loading and downwarping associated with the seawards tilt of the western margin as a result of the mid Miocene and later uplift events of the coastal platform. The middle to late Miocene sedimentary record is recovered only in a single core and the depositional environment is largely interpreted from reworked sediments having a Pliocene final depositional age. The abundance of quartz in the middle Miocene sediment suggests increased terrigenous input after uplift of the interior. Rapid ice sheet expansion, intensification of Southern Ocean circulation and the establishment of ocean stratification with rapid cooling of bottom waters during the later middle Miocene influenced sedimentation on the margin. The onset of cold-water upwelling and associated local oceanographic changes resulted in the establishment of hydrographic conditions similar to the modern Benguela system with a coast-parallel mudbelt present on the middle shelf. Glauconite-rich sediments on the middle to outer shelf indicate overall low accumulation rates and multiple reworking events of organic-rich clayey sediments during the middle to late Miocene/early Pliocene. Deposition of a prograding wedge of inner shelf delta front quartzose very fine sands indicates increased fluvial output in the middle Miocene (15.8-9.1 Ma) in hydrographic conditions similar to the modern shelf. Sea-level fluctuations of the middle Pliocene reworked this quartzose muddy sand out across the outer shelf, where the Pliocene foraminifera indicate dysoxic bottom water conditions.

The Pliocene sediments are unconformably overlain by a number of distinct Pleistocene facies that reflect the influence of the canyon bathymetry on the depositional environment. It is argued that a late Pliocene/early Pleistocene uplift of the western margin resulted in the fault-controlled incision of the Head of the Cape Canyon along the seaward flank of the buoyant Agulhas-Columbine basement block. The outer shelf and Western Ridge sediments were reworked during the Pleistocene, whereas quartz-rich sediments from increased fluvial input associated with uplift were trapped within the Cape Canyon Head region. The late Pleistocene and Holocene are associated with active erosion and incision of the canyon.

The late Cenozoic evolution of the western margin, recorded in the complex condensed sediment record of Concession 20D, is characterised by low sediment accumulation rates and multiple reworking events. The integrated stratigraphic interpretation emphasises the close link between sequence boundaries in the sediment record of the passive western margin and sea-level fluctuations as well as the important influence of local tectonic activity, fluvial sediment input, palaeoceanographic and climatic changes.

University of Cape Town

GLOSSARY OF TERMS AND ABBREVIATIONS

(See Figure 3.11)



Faecal-rich muddy sand

Medium sand

Fine to very fine sand

Shelly sand

Foraminifera-rich sand

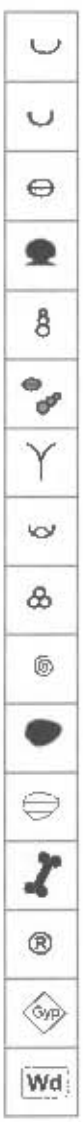
Shell lag/interval

Ooze (>60% biogenic)



Contact gradational

Bioturbation



Bivalves and other shell fragments
(Ⓞ: Oyster)

Phosphatised shell fragments

Articulated bivalves

Pecten sp.

Gastropod

Phosphatised mollusc casts

Bryozoa

Brachiopod

Foraminifera

Larger benthic foraminifera

Pebbles (>2mm)
Ph Phosphorite
Qz Quartz

Limestone

Bone (fragments)

Reduced patches

Gypsum crystallization

Wood fragments

ABBREVIATIONS:

Minerals:

Qz: Quartz
Glc: Glauconite
Ph: Phosphorite (Compton *et al., in press*)
PCG: Phosphate-cemented grains
PCL: Phosphate replaced limestone
SPG: Skeletal phosphorite grain (Sk: bone, otolith, T: Teeth)
PP: Pelletal Phosphorite
Cc: Calcite
Calc: Calcareous
ShF: Shell fragments
Bv: Bivalve (Pc - Pecten)
G: Gastropod
Bry: Bryozoa
Br: Brachiopod (art - articulated)
Ech: Echinoid (S - spine; P - plate)
Dent. Dentalium
SkF: Skeletal Fragments
F: Foraminifera (pF - planktonic; bF - benthic)
FP: Faecal pellets
Ost: Ostracods
SSp: Sponge Spicules
HS: Holothurian sclerites

Colours
Amb: Amber
Brn: Brown
Blk: Black
Grn: Green

Modified Wentworth Grade Scale after Dunbar and Rodgers (1957).

PEBBLES:

veP Very coarse (32 mm - 64 mm)
cP Coarse (16 mm to 32 mm)
mP Medium (8 mm to 16 mm)
fP Fine (4 mm to 8 mm)
vfP Very fine (2 m to 4mm) also referred to as granules (gran.)

SAND:

veS. Very coarse (1 mm - 2 mm)
cS Coarse (500 µm to 1 mm)
mS Medium (250 µm to 500 µm)
fS Fine (125 µm to 250 µm)
vfS Very fine (63 µm to 125 µm)

Powers (1953) roundness scale

ang: angular
rnd: rounded
subang/rnd: subangular/rounded
v-ang/rnd: very angular/rounded

Sorting Φ values for grain size analysis after Folk (1965).

.00-.32Φ: Very well sorted
.33-.37Φ: Very well to well sorted
.38-.47Φ: Well sorted
.48-.52Φ: Well to moderately well sorted
.53-.68Φ: Moderately well sorted
.69-.73Φ: Moderately well to moderately sorted

Glauconite grey scale summary.



University of Cape Town

TABLE OF CONTENTS

1 THESIS OBJECTIVES AND OVERVIEW 1-1
1.1 INTRODUCTION 1-1
1.2 OBJECTIVES 1-2
1.3 MAJOR THEMES AND STRUCTURE OF THE THESIS 1-3

2 LITERATURE REVIEW 2-1
2.1 RIFTING OF THE WESTERN MARGIN OF SOUTHERN AFRICA 2-3
2.1.1 Tertiary Uplift and Erosion Cycles 2-7
2.1.2 Modern and Palaeo-Drainage Systems 2-9
2.2 SEA LEVEL VARIATIONS 2-11
2.3 PALAEO-CLIMATE 2-13
2.4 ATLANTIC OCEAN / BENGUELA SYSTEM 2-15
2.5 GEOLOGICAL EVOLUTION OF THE WESTERN MARGIN 2-16
2.5.1 Pre-Cretaceous Basement Geology 2-16
2.5.2 Onshore Tertiary Deposits 2-18
2.5.3 The Offshore Geological Record 2-18
2.5.3.1 Cretaceous 2-22
2.5.3.2 Cenozoic 2-23
2.5.3.3 Lower Tertiary / Palaeogene 2-25
2.5.3.4 Upper Tertiary / Neogene 2-27
2.5.3.5 Pleistocene and Holocene 2-29

3 INTRODUCTION TO THE STUDY AREA, METHODOLOGY AND TERMINOLOGY 3-1
3.1 WESTERN MARGIN 3-1
3.2 SAMPLE COLLECTION AND GEOPHYSICAL DATA 3-4
3.2.1 Bathymetry of Concession 20d 3-7
3.2.2 Seismic Profiles 3-11
3.3 PROCESSING AND ANALYSIS 3-14
3.4 GENERAL TERMINOLOGY 3-16
3.4.1 Introduction 3-16
3.4.2 Sequence Stratigraphy 3-17
3.4.3 Sea Level 3-20
3.5 GENERAL STRATIGRAPHY AND LEGEND 3-23

4 CRETACEOUS WOODY QUARTZOSE SAND 4-1
4.1 INTRODUCTION 4-1
4.2 GEOLOGICAL SETTING 4-2
4.3 CRETACEOUS STRATIGRAPHY OF THE STUDY AREA 4-5
4.4 LITHOLOGY OF THE WOODY QUARTZOSE SAND 4-8
4.5 AGE OF THE WOODY QUARTZOSE SAND 4-12
4.6 PALAEOENVIRONMENTAL RECONSTRUCTION OF THE STUDY AREA 4-15
4.7 CONCLUSIONS 4-19

5 LATE CENOZOIC PHOSPHOGENESIS ON THE WESTERN SHELF OF SOUTH AFRICA IN THE VICINITY OF THE CAPE CANYON 5-1
ABSTRACT 5-2
1 INTRODUCTION 5-2
2 GEOLOGICAL SETTING 5-3
3 METHODS 5-6
4 RESULTS 5-11
4.1 Stratigraphy 5-11
4.2 Phosphorite Grains 5-16
5 DISCUSSION 5-16
5.1 Depositional Age Model Based on Biostratigraphy and Sr Isotope Ratios 5-16
5.1.2 Miocene Successions 5-17
5.1.3 Pliocene Successions 5-18
5.1.4 Pleistocene Successions 5-18
5.2 Phosphogenic Episodes 5-19
5.3 Phosphogenesis and Climate 5-20

University of Cape Town

6 OLIGOCENE-MIOCENE SUCCESSION 6-1
6.1 QUARTZOSE FORAMINIFERAL MUDDY SAND 6-1
6.1.1 Lithostratigraphy of the Quartzose Foraminiferal Muddy Sand 6-1
6.1.2 Age of the Quartzose Foraminiferal Muddy Sand 6-6
6.1.3 Depositional Environment of the Quartzose Foraminiferal Muddy Sand 6-7
6.2 QUARTZOSE GLAUCONITIC CALCAREOUS SAND 6-8
6.2.1 Lithostratigraphy of the Quartzose Glauconitic Calcareous Sand 6-9
6.2.2 Age of the Quartzose Glauconitic Calcareous Sand 6-15
6.2.3 Depositional Environment of the Quartzose Glauconitic Calcareous Sand 6-16
6.3 GLAUCONITIC CALCAREOUS SAND 6-17
6.3.1 Lithostratigraphy of the Glauconitic Calcareous Sand 6-18
6.3.2 Age of the Glauconitic Calcareous Sand 6-21
6.3.3 Depositional Environment of the Glauconitic Calcareous Sand 6-21
6.4 FORAMINIFERAL OOZE 6-22
6.5 MIOCENE SEDIMENTS OF THE SOUTHERN AFRICAN MARGIN 6-24
6.6 GRAVELLY CALCAREOUS QUARTZOSE MUDDY SAND (CORE 319) 6-27
6.6.1 Depositional Environment of the Gravelly Calcareous Quartzose Muddy Sand 6-30
6.7 OLIGOCENE-MIOCENE GEOLOGICAL EVOLUTION OF THE MARGIN 6-31

7 PLIOCENE SUCCESSION 7-1
7.1 GLAUCONITIC SAND UNIT 7-1
7.1.1 Lithostratigraphy of the Glauconitic Sand Sub-unit 7-7
7.1.1.1 Phosphorite Gravel Facies of the Outer Shelf 7-7
7.1.1.2 Glauconitic Sand Facies of the Outer Shelf 7-15
7.1.2 Lithostratigraphy of the Glauconitic Muddy Sand Sub-unit 7-17
7.2 QUARTZOSE MUDDY SAND UNIT 7-24
7.2.1 Lithostratigraphy of the Quartzose Muddy Sand Unit 7-24
7.3 DEPOSITIONAL HISTORY OF PLIOCENE SUCCESSION 7-32
7.3.1 Age of the Pliocene Succession 7-32
7.3.2 Depositional History of the Pliocene Succession 7-39
7.3.3 Reworked Miocene in the Pliocene Succession 7-45
7.3.3.1 Quartzose Delta Front Deposits 7-45
7.3.3.2 Glauconitization 7-53

8 QUATERNARY SUCCESSION 8-1
8.1 CALCAREOUS GLAUCONITIC SAND OF THE OUTER SHELF SUCCESSION 8-1
8.1.1 Age of the Calcareous Glauconitic Sand 8-4
8.1.2 Upper Slope Cores 8-6
8.1.3 Depositional Environment of the Calcareous Glauconitic Sand 8-6
8.2 CALCAREOUS QUARTZOSE VERY FINE SAND 8-9
8.2.1 Age of the Calcareous Quartzose Very Fine Sand 8-15
8.2.2 Depositional Environment of the Calcareous Quartzose Very Fine Sand 8-15
8.3 THE GLAUCONITIC QUARTZOSE SAND 8-16
8.3.1 Age of the Glauconitic Quartzose Sand 8-27
8.3.2 Depositional Environment of the Glauconitic Quartzose Sand 8-28
8.4 HOLOCENE FAECAL–RICH MUDDY SAND 8-29
8.5 QUATERNARY EVOLUTION OF CONCESSION 20D 8-33

9 TEXTURE AND GEOCHEMISTRY OF GLAUCONITE GRAINS 9-1
9.1 GLAUCONITE MORPHOLOGY 9-2
9.2 MAJOR ELEMENT GEOCHEMISTRY 9-8
9.3 RARE-EARTH ELEMENT GEOCHEMISTRY 9-16

10 SYNOPSIS 10-1
10.1 STRATIGRAPHY 10-1
10.2 GEOLOGICAL EVOLUTION OF THE WESTERN MARGIN (FIGURE 10.1) 10-3

REFERENCES R-1

APPENDIX 1 – CORE LOGS A1-1
APPENDIX 2 – PALYNOLOGICAL ASSEMBLAGE A2-1
APPENDIX 2 – REE DATA A3-1

University of Cape Town

LIST OF TABLES

Table 2.1	A summary of the Pickford and Senut (1999) Cenozoic sea level variations, based largely on littoral mammalian fossil studies and fluvial assemblages deposited during sea-level transgressions (Pether, 1994a).	2-13
Table 2.2	A summary of the onshore Late Cenozoic geology of the southwestern Cape coast after Tankard, 1974, 1975, 1976; Dingle *et al.*, 1983; Rogers, 1980, 1982; Coetzee and Rogers, 1982; Hendey, 1982; Theron *et al.*, 1992; Rogers *et al.*, 1990; Senut *et al.*, 1996; Dale and McMillan, 1999b; Pether *et al.*, 2000 and Franceschini, 2003.	2-20
Table 2.3	A summary of the Late Cenozoic marine packages of the Namaqua and the south-western Cape coast (after Rogers *et al.*, 1990; Pether, 1994; Dale and McMillan, 1999b; Pether *et al.*, 2000 and Franceschini, 2003).	2-21
Table 2.4	A summary of the relationship between seismic records and sediment data for the Orange Shelf. The core sediment data refers to the records from the Ocean Drilling Program (ODP) Sites 1085, 1086 and 1087 of Leg 175 (Shipboard Scientific Party, 1998a, b, c).	2-24
Table 3.1	Summary of the Sr-ages of selected sand-sized bulk foraminiferal assemblages recalculated using the McArthur *et al.* (2001) look-up tables with an estimated $^{87}Sr/^{86}Sr$ error value of 20 X 10^{-6}.	3-7
Table 4.1	A summary of the Cretaceous record for the western margin of southern Africa after 1: Brown *et al.* (1995); 2: Dale and McMillan, 1997; 3: McMillan (*in prep.*); 4: McMillan (1990); 5: Petroleum Agency SA (2002) and 6: Stevenson and McMillan (*in press*).	4-3
Table 4.2	Summary of results of the wood biostratigraphy (M. Bamford, *pers. comm.* 2002).	4-13
Table 5.1	Sr isotope analysis	5-7
Table 5.2	Foraminiferal assemblages of selected samples.	5-9
Table 6.1	The relative abundance (% of grains) of the components present in the sand fraction of the Quartzose Foraminiferal Muddy Sand.	6-3
Table 6.2	The foraminiferal assemblage of Sample 324-8 (I. McMillan, *pers. comm.*, 2002).	6-6
Table 6.3	The relative percent grain types of the sand fraction of the Quartzose Glauconitic Calcareous Sand determined by point-counting a minimum of 300 grains. Foraminifera include only those species not replaced or infilled by phospho-glauconite.	6-11
Table 6.4	The foraminiferal assemblage of the Quartzose Glauconitic Calcareous Sand	6-15
Table 6.5	The relative percent grain types of the sand fraction of the Glauconitic Calcareous Sand as determined by point-counting a minimum of 300 grains.	6-18
Table 6.6	The stratigraphy of lower Miocene sediments found on the outer shelf and upper slope (seawards of 120 m) of the western margin of southern Africa (after Dale and McMillan, 2003b; McMillan, 1989, 1990; Corbett, 1996).	6-26
Table 6.7	The composition of the basal gravel (568-572 cm) and overlying sands (520-524 cm) of the Gravelly Calcareous Quartzose Muddy Sand determined by point-counting a minimum of 300 grains.	6-27
Table 7.1	A summary of the scattered pebbles and small cobbles found within the glauconite-rich sediments of the outer shelf.	7-5
Table 7.2	The composition of the Pliocene Glauconitic Sand Sub-unit and, for comparison, the Quaternary glauconite-rich sediments (in italics) of the outer shelf as determined by point-counting a minimum of 300 grains	7-15
Table 7.3	The composition (reported as the percent grain types by number) of the Glauconitic Muddy Sand and Glauconite Sand facies as determined by point-counting a minimum of 300 grains. .	7-21
Table 7.4	The available Sr-age data of the Quartzose Muddy Sand (Compton *et al.*, 2004)	7-33
Table 7.5	A summary of the interpretation of the foraminiferal assemblage (I. McMillan *pers. comm.*, 2003).	7-38
Table 8.1	The composition of the Glauconitic Sand Unit was determined by point-counting a minimum of 300 grains.	8-4
Table 8.2	A summary of the foraminiferal assemblage of Samples 128-3 & 128-5 from the Calcareous Glauconitic Sand (I. McMillan *pers. comm.*, 2003).	8-4
Table 8.3	The composition of the Holocene Faecal-rich Muddy Sand of the outer shelf unit as determined by point-counting a minimum of 300 grains.	8-31
Table 9.1	The age and location of Eocene and Cretaceous glauconitic sediments analysed in this study from the southern Namibian margin.	9-15
Table 9.2	The PAAS REE abundance (in ppm) used in all normalization calculations (Taylor and McLennan, 1985).	9-18

University of Cape Town

LIST OF FIGURES

CHAPTER 2

Figure 2.1 A summary of the western margin of southern Africa, including the bathymetry, main orographic features, onshore morphology and a summary of palaeo-drainage systems. 2-2

Figure 2.2 A simplified map of the western margin of southern Africa with the localities mentioned in the text shown. 2-4

Figure 2.3 An idealized cross-section across the central Orange Basin of southern Africa, illustrating sediment distribution, prominent seismic reflectors and faults of the Orange Basin. 2-5

Figure 2.4 The Cenozoic sea-level curve for the west coast of southern Africa. 2-12

Figure 2.5 Geology of the southwest African continent. 2-17

Figure 2.6 The distribution of onshore Cenozoic sediments in the southwest Cape. 2-19

Figure 2.7 A simplified cross-section of the western continental margin of the northern Orange Basin. 2-22

Figure 2.8 Distribution of the composition and texture of the unconsolidated surficial Holocene sediments. 2-25

Figure 2.9 A: Distribution of Late Tertiary sediments (T1-T4) . 2-26
B: A summary of the seismic section and geology of the Cape Canyon.

CHAPTER 3

Figure 3.1 The bathymetry of the western margin showing the major bathymetric features. 3-2

Figure 3.2 The location of the study area, Offshore Diamond Concession 20D, in relation to the Cape Canyon on the western margin off Cape Columbine. 3-3

Figure 3.3 The location of the WMR cores and dredges in Concession 20D in relation to the track charts of the seismic lines undertaken by Benguela Conncessions (Pty) Ltd. 3-6

Figure 3.4. Definition of the bathymetric features of Concession 20D. 3-9

Figure 3.5. The core locations within Concession 20D and the Canyon Head region, with the selected transects and core numbers included in the close-up. All WMR cores shown with a small +. 3-10

Figure 3.6 Interpreted east-west mini-airgun profile of the Central Transect across the Cape Canyon Head to Outer Shelf. 3-12

Figure 3.7 Interpreted Chirp profile across the Eastern Flank just to the south of the Central Transect (Figure 3.4). 3-13

Figure 3.8 Interpreted Chirp profile of the Northern Transect across the Cape Canyon Head region and Western Ridge, with <20 m of Tertiary sediments (T) above the high reflectivity Cretaceous sediments with bathymetric profile inset. 3-13

Figure 3.9 Interpreted Chirp profile of the Southern Transect across the Cape Canyon Head region showing only an occasional thin veneer of Tertiary sediments above the high reflectivity Cretaceous sediments with bathymetric profile inset. 3-14

Figure 3.10 A: The Haq *et al.* (1987, 1988) eustatic curve with long-term and third-order cycles shown. 3-22
B: The global deep-sea oxygen isotope record of Zachos *et al.* (2001).

Figure 3.11 A generalised stratigraphic column for Concession 20D, summarising the sedimentary units described in the subsequent chapters. 3-24

CHAPTER 4

Figure 4.1 The location of Concession 20D (grey polygon) relative to the West Coast of southern Africa. 4-2

Figure 4.2 A schematic cross section across the central Orange Basin. 4-5

Figure 4.3 The distribution of the Woody Quartz Sand. 4-6

Figure 4.4 A cross section of the Southern Transect (Figure 4.3) with the core logs for the three cores that intersect the Woody Quartzose Sand. 4-7

Figure 4.5 Photographs of the Woody Quartzose Sand from split cores, showing the bioturbated contact between the Cretaceous Woody Quartzose Sand and a typical Pleistocene phosphorite- and quartz-dominated gravel lag. 4-7

Figure 4.6 A summary of the recovered thickness of the Woody Quartzose Sand. 4-9

Figure 4.7 A summary of the Cretaceous Woody Quartzose Sand grain size textures. 4-9

Figure 4.8 Frequency curves showing the particle-size distribution of the sand fraction of the Woody Quartzose Sand. 4-9

Figure 4.9 Photomicrographs of the sand fraction of the Woody Quartzose Sand. 4-10

Figure 4.10 Examples of the megaspores (A (Henrisporites) and B) and megaspore cast (C) from the Woody Quartzose Sand of Samples 178A-5 and 179-2. 4-10

University of Cape Town

Figure 4.11 SEM images of surface textures of quartz grains from Samples 177-3 (A,C & D) and 177-5 (B) of the Woody Quartzose Sand. 4-11
Figure 4.12 Pyritised wood fragments (A & B) and framboidal pyrite (C) from the Woody Quartzose Sand (Sample 178A-5). 4-12
Figure 4.13 A summary of the XRD records for the mud fraction (<63 μm) of the Woody Quartzose Sand. 4-12
Figure 4.14 The palaeogeographic map of the continents during the mid Cretaceous (96 Ma) using the Scotese Paleomap Program, showing the approximate location of Concession 20D and the two DSDP Sites 360 and 361. 4-16
Figure 4.15 A schematic stratigraphic column for the Quartzose Woody Sand, based on Core 178A. 4-19

CHAPTER 5

Figure 5.1 Bathymetry of the western continental margin of southern Africa (Dingle *et al.*, 1987). 5-4
Figure 5.2 Detailed bathymetry (20 m contours) of study area showing the location of vibracores. 5-5
Figure 5.3 Stratigraphy of vibracores of the deep water, western area of the outer shelf. Ages are derived from Sr isotope ratios (Table 1). 5-12
Figure 5.4 Stratigraphy of vibracores of the northern end of the Head of the Cape Canyon area on the outer shelf. Ages are derived from Sr isotope ratios (Table 1). 5-13
Figure 5.5 Stratigraphy of vibracores of the southern end of the Head of the Cape Canyon area on the outer shelf. Ages are derived from Sr isotope ratios (Table 1). 5-14
Figure 5.6 Comparison of proposed sea-level fluctuations (Haq *et al.*, 1987), simplified stratigraphy of the outer shelf successions, the age distribution of reworked biogenic grains (dashed boxes) and phosphorite grains from this study, the marine oxygen and carbon isotope records (Zachos *et al.*, 2001) and climate events. 5-15

CHAPTER 6

Figure 6.1 The stratigraphy of the Lower Miocene Calcareous Unit. 6-2
Figure 6.2 The distribution of the Quartzose Foraminiferal Muddy Sand facies on the Southern Rocky Plateau of the Western Ridge in Concession 20D. 6-3
Figure 6.3 Photographs of the sand fraction of the Quartzose Foraminiferal Muddy Sand from Sample 324-8. 6-4
Figure 6.4 A summary of Quartzose Foraminiferal Muddy Sand grain size textures. 6-4
Figure 6.5 Typical coarse quartz grains with orange surface coatings from Sample 324-8 (152-156 cm). 6-5
Figure 6.6 An *Operculina* sp. test (A) from Sample 324-8 and a close-up (B) of the white square in the centre showing the extensive surface recrystallisation. 6-5
Figure 6.7 XRD records for the mud fraction (<63 μm) of the Quartzose Foraminiferal Muddy Sand. 6-6
Figure 6.8 The distribution of the Quartzose Glauconitic Calcareous Sand facies in Concession 20D. 6-9
Figure 6.9 Photographs of the sand and gravel fraction of the Quartzose Glauconitic Calcareous Sand of Sample 324-5 (77-82 cm). 6-10
Figure 6.10 A summary of Quartzose Glauconitic Calcareous Sand grain size textures. 6-11
Figure 6.11 The weight percent non-magnetic and paramagnetic fractions for the Quartzose Glauconitic Calcareous Sand. 6-11
Figure 6.12 A photograph of the sand fraction of Sample 159-5. 6-12
Figure 6.13 SEM images of typical well-rounded coarse quartz grains from Sample 324-5. 6-12
Figure 6.14 The magnetic fraction of Sample 159-5 is dominated by earthy, green-brown, phospho-glauconite grains. 6-14
Figure 6.15 A dark green glauconite grain *in situ* in a zooecium of a bryozoan fragment in Sample 324-6. 6-15
Figure 6.16 *Victoriella conoidea* (A-C) and *Rupertina stabilis* (D) from Sample 159-5. 6-16
Figure 6.17 The distribution of the Glauconitic Calcareous Sand facies in Concession 20D. 6-18
Figure 6.18 A summary of the Glauconitic Calcareous Sand grain size textures. 6-19
Figure 6.19 Photographs of the sand and gravel fraction of the Glauconitic Calcareous Sand. 6-20
Figure 6.20 The weight percent non-magnetic (quartz and calcareous grains) and paramagnetic (glauconite) fractions for the Glauconitic Calcareous Sand facies. 6-21
Figure 6.21 The distribution of the Foraminiferal Ooze facies in Concession 20D. 6-23
Figure 6.22 A summary of Foraminiferal Ooze grain size textures. 6-23
Figure 6.23 Distribution of the Gravelly Calcareous Quartzose Muddy Sand. 6-28
Figure 6.24 A summary of the Gravelly Calcareous Quartzose Muddy Sand stratigraphy in Core 319. 6-29
Figure 6.25 A summary of the Sr-derived ages of the upper Oligocene to Miocene sedimentary facies and relevant global climatic and tectonic events. 6-32

University of Cape Town

CHAPTER 7

Figure 7. 1	Pliocene stratigraphy of the study area.	7-2
Figure 7.2	The sediment isopachs for the glauconite-rich sediments from Concession 20D.	7-3
Figure 7.3.	Stratigraphy of the glauconite-rich sediments of the Outer Shelf in Core 128 (Figure 7.2).	7-4
Figure 7.4	The wt % non-magnetic *vs* paramagnetic components of the sand fractions from the Central Transect.	7-6
Figure 7.5	A SEM image showing coccoliths in a suture of a typical lobate glauconite grain.	7-6
Figure 7.6	A summary of the grain size textures for the Phosphorite Gravel.	7-8
Figure 7.7	The recovery of vibrocores from the Southern Rocky Plateau (shaded area) was poor and a number of vibrocore attempts failed.	7-8
Figure 7.8	Photographs of layered phosphorite pebbles from the shoe of Core 228A and a small cobble recovered from the Glauconitic Sand facies at the base of Core 116 (Figure 7.2).	7-10
Figure 7.9	A photomicrograph of a thin-section from the layered phosphorite of Core 228A.	7-11
Figure 7.10	A close-up photomicrograph of the area shown as a black box in Figure 7.9.	7-12
Figure 7.11	A photomicrograph of the upper erosional surface (2) above the Coarse Quartz Shelly Sand interval of the layered phosphorite from Core 116.	7-13
Figure 7.12	Green glauconite grains (paramagnetic fraction) of the Glauconitic Sand facies.	7-16
Figure 7.13	A summary of the grain size textures for the Glauconitic Sand facies.	7-17
Figure 7.14	The Glauconitic Sand facies commonly has *in situ* cemented aggregates of sand, which are common near the base of Core 119.	7-18
Figure 7.15	SEM images of cemented aggregates from the Glauconitic Sand facies of Cores 119 (A-D) and 120 (E-H).	7-19
Figure 7.16	The stratigraphy of the Pliocene Glauconitic Muddy Sand Unit in Core 30.	7-20
Figure 7.17	A summary of the XRD records for the mud fraction (<63 μm) of the Glauconitic Muddy Sand facies of Core 30.	7-22
Figure 7.18	The percent sand and stratigraphy of the two upper slope Cores 146 and 147.	7-23
Figure 7.19	The distribution of the Quartzose Muddy Sand Unit in the Cape Canyon Head Area.	7-25
Figure 7.20	Core photographs of the Quartzose Muddy Sand Unit (core width ±8.25 cm).	7-25
Figure 7.21	A summary of the Quartzose Muddy Sand grain size textures.	7-26
Figure 7.22	A summary of the paramagnetic (glauconite) and non-magnetic (quartz, phosphorite and foraminifera) weight percent present in the sand fraction of the Quartzose Muddy Sand.	7-27
Figure 7.23	The sand fraction of the Quartzose Muddy Sand.	7-27
Figure 7.24	Frequency curves showing the particle-size distribution of the sand fractions of the Quartzose Muddy Sand facies from the Northern, Central and Southern Transects.	7-28
Figure 7.25	Weight % $CaCO_3$ determined by acid leaching, using dilute (10%) HCl, of the sand fraction (63 μm - 2mm) of the Quartzose Muddy Sand.	7-29
Figure 7.26	XRD records for the mud fraction (<63 μm) of the Quartzose Muddy Sand facies composed of calcite, quartz, feldspar with a non-expandable 10 Å sheet-silicate and kaolinite present.	7-30
Figure 7.27	The slumped stratigraphy of the Pliocene Quartzose Muddy Sand and Pleistocene Glauconitic Quartzose Sand in Core 16.	7-32
Figure 7.28	The foraminiferal assemblage of the Pliocene Quartz Muddy Sand facies, which includes the distinct Pliocene assemblage (A), together with Miocene to Pliocene species (B) and a reworked Miocene assemblage (C).	7-34
Figure 7.29	The Pliocene Succession and the middle Miocene Gravelly Calcareous Quartzose Muddy Sand together with the Sr-ages of reworked foraminifera, skeletal phosphorite grains and phosphorite gravels recovered from the Pliocene Succession.	7-37
Figure 7.30	A sketch of the proposed mid Miocene to Plio/Pleistocene geological history of the western margin in the vicinity of the Northern Transect in Concession 20D.	7-41
Figure 7.31	The distribution of Cenozoic sediments in the western Cape.	7-48
Figure 7.32	The section of the core log for G30878, the holostratotype core of the Elandsfontyn Formation after Rogers (1980) with samples locations for this study superimposed.	7-50
Figure 7.33	SEM images of the blue-tarnished iron sulphides from G30878-7.	7-51
Figure 7.34	XRD records for the mud fraction (<63 μm) of the Elandsfontyn Formation from A) G30878 and B) the Saldanha Steel boreholes.	7-52

CHAPTER 8

Figure 8.1	The stratigraphy of the glauconite-rich sediments of Core 128 (see Figure 7.3).	8-2
Figure 8.2	A summary of the grain size textures for the Calcareous Glauconitic Sand.	8-3
Figure 8.3	The percent sand and stratigraphy for the two upper slope Cores 146 and 147.	8-5

UNIVERSITY of the WESTERN CAPE

Figure 8.4	The distribution of the Calcareous Quartzose Very Fine Sand facies in the Canyon Head region of Concession 20D.	8-10
Figure 8.5	The stratigraphy of the Calcareous Quartzose Very Fine Sand facies of Core 348.	8-11
Figure 8.6	A summary of the textural nomenclature of the Calcareous Quartzose Very Fine Sand.	8-12
Figure 8.7	Frequency curves showing the particle-size distribution of the sand fractions of the Calcareous Quartzose Very Fine Sand.	8-12
Figure 8.8	Weight percent $CaCO_3$ of the sand fraction of the Calcareous Quartzose Very Fine Sand.	8-13
Figure 8.9	The weight percent non-magnetic (quartz) and paramagnetic (glauconite) components of the acid leached sand fraction of the Calcareous Quartzose Very Fine Sand.	8-13
Figure 8.10	The predominantly cold water (upwelling) late Pleistocene assemblage of the Calcareous Quartzose Very Fine Sand facies.	8-14
Figure 8.11	The XRD records for the mud fraction (<63 μm) of the Calcareous Quartzose Very Fine Sand facies is dominated by calcite, quartz and feldspar, with only minor clay peaks present.	8-15
Figure 8.12	The sediment isopachs for the Glauconite Quartzose Sand Unit.	8-17
Figure 8.13	Stratigraphic sections of cores that include the Glauconitic Quartzose Sand Unit from the Northern, Central and Southern Transects.	8-18
Figure 8.14	Frequency curves showing the particle-size distribution of the sand fractions of the Glauconitic Quartzose Sand.	8-19
Figure 8.15	A summary of the non-magnetic (quartz) and paramagnetic (glauconite) weight percent present in the acid-leached (carbonate-free) sand fraction of the Glauconitic Quartzose Sand.	8-20
Figure 8.16	A summary of the Glauconitic Quartzose Sand grain size textures.	8-21
Figure 8.17	Weight percent $CaCO_3$ of the sand fraction of the Glauconitic Quartzose Sand Unit.	8-22
Figure 8.18	The XRD records show that the mud fraction (<63 μm) of the Glauconitic Quartzose Sand Unit from the Northern Transect.	8-24
Figure 8.19	The sand fraction of the Glauconitic Quartzose Sand of Samples 107-2 (A) and 110-4 (B) recovered along the Central Transect.	8-25
Figure 8.20	SEM images (A) and the EDS determined composition (B) of the glauconitic surface coating of green-stained quartz.	8-26
Figure 8.21	A summary of the grain size textures of the Holocene Faecal-rich Muddy Sand.	8-30
Figure 8.22	The XRD records show that the mud fraction (<63 μm) of the Holocene sediments from the Northern Transect.	8-32
Figure 8.23	The interpreted mini-gun seismic record along the Central Transect of Concession 20D, showing location of cores.	8-33
Figure 8.24	A wireframe projection of the Canyon Head area showing the distribution of the Pleistocene Glauconitic Quartzose Sand in relation to the underlying siliciclastics sediments of the area.	8-35
Figure 8.25	The location of Concession 20D in relation to the modern rivers, where the shaded area shows the extent of the basement high of Brown *et al.* (1995).	8-36

CHAPTER 9

Figure 9.1	SEM images of infilled benthic (A) and planktic (B-D) foraminifera from the Pliocene Phosphorite Gravel facies (Samples 128-7 and 129-4).	9-3
Figure 9.2	Representative SEM images of broken Pliocene, Pleistocene and Holocene glauconite pellets from Concession 20D.	9-4
Figure 9.3	Sutures in glauconite pellets (A) and foraminiferal infills (B-D), where rosette (A and B) and box-work (D) textures typical of evolved glauconite (>6.5% K2O) are common (Odin and Matter, 1981).	9-5
Figure 9.4	Representative SEM backscatter and normal secondary collector images of glauconite pellets from the Pliocene Sample 128-7 (A), Pleistocene Samples 110-4 (B) and 112-4 (C) and Holocene Sample 112-1 (D).	9-5
Figure 9.5	High-resolution SEM images of glauconite pellets from Concession 20D shows the complex relationship between lamellar textured glauconite and CFA.	9-6
Figure 9.6	Thin section photomicrographs of glauconite pellets from the four outer shelf glauconite-rich facies.	9-9
Figure 9.7	The glauconite compositions from Core 128 as determined by microprobe analysis.	9-10
Figure 9.8	The glauconite compositions from Sample 128-1 showing the within-grain range in compositions determined by microprobe analysis.	9-11
Figure 9.9	Holocene glauconite (Sample 128-1) compositions determined by microprobe analysis.	9-12
Figure 9.10	Pleistocene glauconite (Sample 128-3) compositions determined by microprobe analysis.	9-13
Figure 9.11	Pliocene glauconite (Sample 128-7) compositions determined by microprobe analysis.	9-14
Figure 9.12	Photomicrographs of southern Namibian Eocene glauconite grains from samples DN 1418 (A), DN 1407 (B) and No. 3949 (C) and thin-section of glauconite pellets from DN 1418.	9-16

University of Cape Town

Figure 9.13 SEM images of southern Namibian Eocene glauconite pellets. 9-17
Figure 9.14 The absolute trace and REE compositions for CFA-glauconite mixed-mineral pellets from the Pliocene glauconite-rich sediment units. 9-18
Figure 9.15 PAAS-normalized REE diagrams for CFA-glauconite mixed-mineral pellets from the Holocene (Sample 128-1), Pleistocene (128-3) and Pliocene (sample numbers in legend) glauconite-rich facies. 9-19
Figure 9.15 continued PAAS-normalized REE diagrams for CFA-glauconite mixed-mineral pellets from the Pliocene basal lag (Sample 128-10) and Lower Miocene (sample numbers in legend) glauconite-rich facies and from Eocene and Cretaceous samples. 9-20
Figure 9.16 A summary of the range in PAAS-normalised REE abundances from Figure 9.14 for CFA-glauconite mixed-mineral pellets from the major lithostratigraphic units of Concession 20D. 9-21
Figure 9.17 The relationship between the Ce- and Eu-anomalies for various CFA-glauconite mixed-mineral pellets. 9-21

CHAPTER 10

Figure 10.1 The late Cenozoic stratigraphy of Concession 20D related to relative sea-level fluctuations, tectonic activity and palaeoceanography. 10-4

University of Cape Town

1 THESIS OBJECTIVES AND OVERVIEW

1.1 INTRODUCTION

The west coast of southern Africa is a passive margin formed by the Early Cretaceous breakup of Gondwana, with the offshore sediment succession recording the changing palaeo-environments from the early rifting phase, through the drift phase to the modern environment (Gerrard and Smith, 1982). The western margin of the southern Cape Basin was built up largely during the Cretaceous and the rapid development of this passive margin slowed down considerably in the Tertiary (Dingle *et al.*, 1983). The Tertiary sediment record of the west coast continental shelf is largely characterised by non-deposition, erosion and large-scale slumping events (Dingle, 1971a). However, a thin veneer of Tertiary sediments is present on the shelf, with a thicker succession preserved on the upper continental slope (Dingle *et al.*, 1983). Exposures are largely limited, particularly of the lower Tertiary, with outcrops confined to a narrow inner continental shelf zone and relatively little is known about the lithofacies and stratigraphy of the succession (Dingle *et al.*, 1983).

Very little research into the evolution of the southern Africa margin has taken place subsequent to a number of initial studies undertaken in the late 1970s to early 1980s (Rogers and Bremner, 1991 and references within). This published literature on the sediments and evolution of the west coast relied largely on surface grab and dredge samples, deep petroleum exploration boreholes and the initial geophysical surveys undertaken in the early 1970s (Siesser *et al.*, 1974; Emery *et al.*, 1975). The 1500 km stretch of the southern African coast from St. Helena Bay in the south to Conception Bay in Namibia is commonly referred to as the "diamond coast" and has been mined for marine and alluvial diamonds since the first diamond was discovered in Lüderitz in 1908 (*e.g.* De Decker and Woodborne, 1996). The economic value of the diamond deposits of the western margin of southern Africa is largely responsible for the relative dearth of published research on the continental shelf and adjacent coastal region, with the accessibility to the results of any research undertaken largely limited by the confidentiality clauses of the respective mining houses.

The Neogene slope sediments of the Orange Slope region have been the focus of a number of recent studies, following the drilling undertaken on ODP Leg 175 in 1997 (Wefer *et al.*, 1998). The ODP Sites 1085, 1086 and 1087, located on the slopes of the Orange Basin, provide the first detailed record of the evolution of the upper Tertiary slope sediments. In addition, the passive-margin deep-sea fans of the Atlantic margins have been the focus of renewed interest, because of the recent discovery of giant hydrocarbon fields (Eschard, 2001), resulting in considerable interest in the post-rifting evolution of the western margin of Africa.

The cores used in this study were all collected during the reconnaissance exploration programme undertaken in the Deep-Water Offshore Diamond Concession 20D, a ~3000 km^2 area offshore Cape Columbine in 200-500 m water depths. The head of the Cape Canyon forms a significant bathymetric

University of Cape Town

feature in the eastern portion of Concession 20D (Simpson and Forder, 1968). The Cape Canyon is the only substantial cross-margin bathymetric feature on the western margin and forms a deeply incised submarine canyon with a maximum of ±800 m vertical relief on the slope and can be traced for ±200 km to a water depth of at least 3600 m (Dingle, 1970a).

1.2 OBJECTIVES

The following section provides an overview of the major objectives addressed in this thesis. This study provides an integrated understanding of the evolution of the western margin considering aspects of the tectonic regime, palaeoceanography and climate change together with continental and margin geomorphology.

DEPOSITIONAL HISTORY OF THE WESTERN MARGIN

The stratigraphic succession of a passive continental margin provides a detailed record of its geological history and the definition of the lithostratigraphy is an essential tool in the interpretation of the depositional evolution of the continental margin (Miller *et al.*, 1997, 1998; Lavier *et al.*, 2001). A diversity of lithostratigraphic types have been recovered from the very condensed sedimentary record of Concession 20D. An understanding of the upper Cenozoic lithostratigraphy of the sediments of Concession 20D provides the framework to evaluate the major factors that have modified the passive continental margin off Cape Columbine, and by extrapolation, the western margin of southern Africa in general. An integration of litho-, bio- and Sr-isotope stratigraphy is used to provide the first detailed late Cenozoic age-model for deposition on this margin. This study will clarify the relative influence of eustasy, ocean-circulation and climatic changes , active tectonism and the evolution of drainage patterns affecting the relative sea level and accommodation space of the western continental margin.

UPWELLING HISTORY OF THE WESTERN MARGIN

The Benguela Current is one of the four major eastern boundary currents of the world's oceans with the coastal region dominated by the Benguela upwelling system (Shannon and Nelson, 1996). The authigenic minerals, glauconite and phosphorite, present in the sedimentary record of Concession 20D, will be used to address some of the questions regarding the early evolution of the Benguela upwelling system, which is still poorly understood. Information from coastal-upwelling zones of the Atlantic is sparse and the Miocene evolution of the Benguela System is traditionally based on extrapolations of cores collected during DSDP Leg 40 and ODP Leg 175 (Siesser, 1980; Diester-Haass *et al.*, 2002).

LINKING ONSHORE AND OFFSHORE RECORDS

Cenozoic deposits along the west coast of southern Africa have long been a focus of interest, because of the economic quantities of diamonds contained within basal gravel units. However, the stratigraphic succession, age, depositional environment and correlation between outcrops remain poorly understood (Pether, 1994a; Pether *et al.*, 2000). Recent studies have largely concentrated on the major fluvial and palaeo-fluvial systems (De Wit *et al.*, 2000), and studies by Pickford (1998; 2000) and Pickford and

University of Cape Town

Senut (1999) have used vertebrate fossil assemblages to date the fluvial and littoral terraces of the Namaqualand and Namibian coastal strip. But, to date, the correlation between the onshore and offshore sedimentary records has not been studied intensively.

Terrigenous sedimentation on the continental margin is dominated by fluvial input, although an aeolian component may be present (Rogers, 1977). Diverse opinions exist in the literature regarding the evolution of the southern African river systems (Chapter 2). The terrigenous component of the Concession 20D sediment record is evaluated in terms of a possible fluvial origin, including an analysis of fluvial sediments of the onshore Elandsfontyn Formation to allow comparison. Aspects such as provenance, denudation and deposition as well as the palaeo-topographical controls on the major drainage axes, sea-level changes (eustatic and tectonic) and the timing of events were also considered. This comparison was undertaken in order to assess whether any inferences regarding the onshore fluvial systems can be made using the sediment record of Concession 20D.

CANYON FORMATION

Although the Cape Canyon is one of the most significant bathymetric features of the western margin of southern Africa, it has received little attention in the literature (Simpson and Forder, 1968; Dingle, 1970b). An understanding of both the timing and processes involved in the formation of the Cape Canyon are significant in terms of an understanding of the general continental margin evolution. In addition, the age of canyon formation will have important implications for the provenance of terrestrial (and authigenic) signatures observed in southern Cape Basin sediments. The Cape Canyon has a large influence on Quaternary sedimentation of the western margin and the stratigraphy of deposits in and adjacent to the Cape Canyon are used to provide evidence for canyon formation.

University of Cape Town

1.3 MAJOR THEMES AND STRUCTURE OF THE THESIS

A detailed review, summarizing the literature available for the western margin of southern Africa and focusing on those issues most relevant to this thesis, is presented in Chapter 2. The regional geological evolution is discussed, starting with the rifting and rift morphology, as well as timing of uplift events and the associated escarpment retreat of the western margin. The post-rift Tertiary evolution is discussed in relation to differential uplift rates, palaeo-drainage patterns, palaeo-climatic conditions, sea-level fluctuations and palaeoceanography. The geological record of the adjacent coastal region is examined as a possible source for the sediments of the western margin. Finally, the currently available information for the onshore and offshore Tertiary sediments is presented. The extensive literature review presents much of the early work undertaken on the margin and includes details from many of the local and in-house publications not readily available internationally. No attempt is made to untangle the often contentious issues in the review, rather these are followed up on in the appropriate thesis discussion sections.

Chapter 3 introduces the geological setting of the continental shelf off Cape Columbine in the Offshore Diamond Mining Concession 20D, the exploration work undertaken by Werner Marine Research (Pty) Ltd, the sampling and methodology used in this study and the stratigraphy of Concession 20D. In addition, a section on the eustatic sea-level curve and the role of relative sea level on sequence stratigraphic models is in included as these elements are utilized in all the subsequent discussions.

The sediments of Concession 20D are subdivided into four lithostratigraphic successions on the basis of age, composition and depositional history. The primary subdivision is based on age with both Cretaceous and upper Cenozoic sediments recovered in Concession 20D. The unconsolidated Cretaceous basement sediments are discussed in Chapter 4. The sediment composition, micro- and macro-scale textures, age and depositional palaeo-environment of the Woody Quartzose Sand unit are discussed in context of the available information in the literature for Cretaceous sediments of the western margin. A co-authored paper, published in *Marine Geology Volume 206* (2004), is included as Chapter 5. This paper summarises the chronostratigraphy used throughout the subsequent Cenozoic Chapters 6-8.

The Cenozoic sediments recovered in Concession 20D are composed of variable proportions of calcareous, authigenic and siliciclastic grains. The calcareous components include foraminifera, mollusc shell fragments and bryozoa, in addition to minor amounts of echinoid plates and spines, ostracods and encrusting algae. Glauconite and phosphorite (carbonate-fluorapatite) are the predominant authigenic minerals present, with pyrite included within some glauconite and phosphorite grains. Quartz is the predominant siliciclastic mineral, but feldspar, mica and lithic siliciclastic fragments are also present.

The upper Cenozoic lithostratigraphic units are discussed in Chapters 6-8. Chapter 6 focuses on the upper Oligocene to lower Miocene stratigraphy of Concession 20D with four lithostratigraphic facies defined and their sedimentology, age and interpreted depositional environments discussed in detail. The lithostratigraphy of the Upper Oligocene/Lower Miocene Calcareous Unit is compared to the carbonate successions of the southern and western margin of southern Africa. The only known example of an *in situ* middle to upper Miocene succession from the southern African margin was recovered in Core 319. The description and discussion of the calcareous quartzose sediment of Core 319 is included within Chapter 6 because this unit clearly defines the end of the carbonate-rich deposition on the western margin. The changes in depositional environment, recorded within the Upper Oligocene/Lower Miocene Calcareous Unit, are interpreted in terms of eustatic sea-level fluctuations, tectonics, sedimentation rates, changing global oceanographic and climatic systems. The geological evolution of the upper Oligocene/lower Miocene sediment succession is interpreted to be representative of the southern African margin in general.

The complex condensed glauconite- and very fine sand-size quartz-rich sedimentary succession, which records a Pliocene depositional age, is described in Chapter 7. The Pliocene succession includes two units with significantly different glauconite and quartz abundances. The Glauconitic Sand Unit is

University of Cape Town

further subdivided on the basis of texture and quartz abundance and the distribution, lithostratigraphy and age of the two sub-units are described. The lithostratigraphy of the Quartzose Muddy Sand Unit, which contains both Pliocene and reworked middle to upper Miocene foraminifera, is described. The presence of reworked upper Miocene foraminifera within these Pliocene-aged sediments is used to speculate on the inferred upper Miocene depositional environment and the possible onshore fluvial sources for the quartz sand, including the Elandsfontyn Formation, are examined. The variations in sediment compositions, within and between the different Pliocene units, are used to interpret the changing depositional environments.

Chapter 8 addresses the Quaternary sediments of Concession 20D, where the Pleistocene sediments, in particular, show a strong correlation between their composition and distribution on the margin. The sediment facies of the upper slope and outer shelf, Western Ridge and Cape Canyon Head region are described. The various depositional environments and the implications for the geological evolution of the western margin are discussed.

The texture and composition of the authigenic mineral, glauconite, ranging in age from Cretaceous to Holocene, is the focus of Chapter 9. The morphology and geochemistry of glauconite pellets from various glauconite-rich units are compared to ascertain whether the observed morphological and textural variations correspond to geochemical or mineralogical differences. The term glauconite is used for all green pellets and is used without any mineralogical implications. The term phospho-glauconite or CFA-glauconite mixed-mineral is used in this thesis to denote grains that consist of a mixture of carbonate fluorapatite (CFA) and glauconite, a common grain type in the study area. Differences in normalised REE patterns are used to make inferences on the changing depositional environment.

Finally, Chapter 10 presents a summary of the lithostratigraphic units and interpreted depositional environments. Chapter 10 synthesizes the discussions presented in the individual chapters in order to address questions regarding the evolution of the western continental margin of southern Africa during the late Cenozoic.

University of Cape Town

2 LITERATURE REVIEW

The main objective of this chapter is to present a review of the current literature available for the regional geological history of the western continental margin of southern Africa from continental break-up to the modern depositional environment, concentrating on those issues most relevant to this study, as well as poorly constrained and unresolved issues. The extremely condensed sediment record of Concession 20D, with mid-Cretaceous sediments overlain by a late Oligocene to Holocene succession, requires a fairly extensive literature review to provide the background for the interpretation of the depositional environments.

The western margin of southern Africa is bounded by the Walvis Ridge to the north and by the Agulhas Ridge to the south, with numerous seamounts of volcanic origin present (Figure 2.1; Shannon and Nelson, 1996). Rogers and Bremner (1991) subdivided the continental margin into the Agulhas Bank, the Olifants Shelf (Cape Point Valley to Childs Bank) and the Orange Shelf (Childs Bank to Orange Banks). The margin is divided into four distinct morphological zones; the nearshore rocky platform (inner shelf), the continental shelf, the continental slope and the continental rise. The continental rise and slope extend far (approximately 600 km) offshore, into the Cape Basin, with most of the outer-margin morphology shaped by post-Pliocene slumping events (Dingle and Robson, 1992). The continental shelf is generally wide and relatively deep (approximately 200 km wide between the Olifants and Orange Rivers) and has a poorly defined shelf break (Birch, 1975; Du Plessis *et al.*, 1972). However, two distinct shelf breaks, a middle (200-380 m) and outer (500 m) shelf break occur such that the shelf is divided into an inner, middle and outer shelf (Birch *et al.*, 1991; Shannon and Nelson, 1996). The inner shelf is a rocky pre-Cretaceous basement platform, which varies in width from 1-6 km, widening to ~35 km off St. Helena Bay and to the west of Cape Town (Birch *et al.*, 1991). The inner shelf has an irregular sediment cover with deposits typically confined to bedrock depressions (Birch *et al.*, 1991). A steep edge marks the seaward extent of this inner-shelf platform at a water depth of 90 m off the Orange to 150 m west of Cape Point (120-140 m in the Cape Columbine area). The middle shelf extends from the base of the rocky inner shelf platform to the middle shelf break. The middle shelf, from south of the Orange River mouth to St Helena Bay, is partially covered by an extensive Holocene mudbelt that extends to ~130 m water depth (Birch, 1975; Rogers, 1977).

The outer shelf is generally very uniform although local bathymetric highs (Figure 2.1), such as Childs Bank (200 m) and Orange Banks (200 m) do occur (Shannon and Nelson, 1996). Dingle *et al.* (1983) referred to a Palaeogene shelf-edge ridge extending from offshore the Orange River to the Cape Columbine area. The outer shelf between Cape Town and Hondeklip Bay is characterised by a rocky erosional surface with patchy residual cover (Birch, 1975). Rare relict submarine canyons cross the shelf and slope such as the Cape Point Valley, which lies south of the Cape Peninsula and the Cape Canyon, offshore off the Cape Columbine area. The Cape Canyon represents the largest of the cross-margin canyons and this study focuses on the upper reaches of the canyon.

University of Cape Town

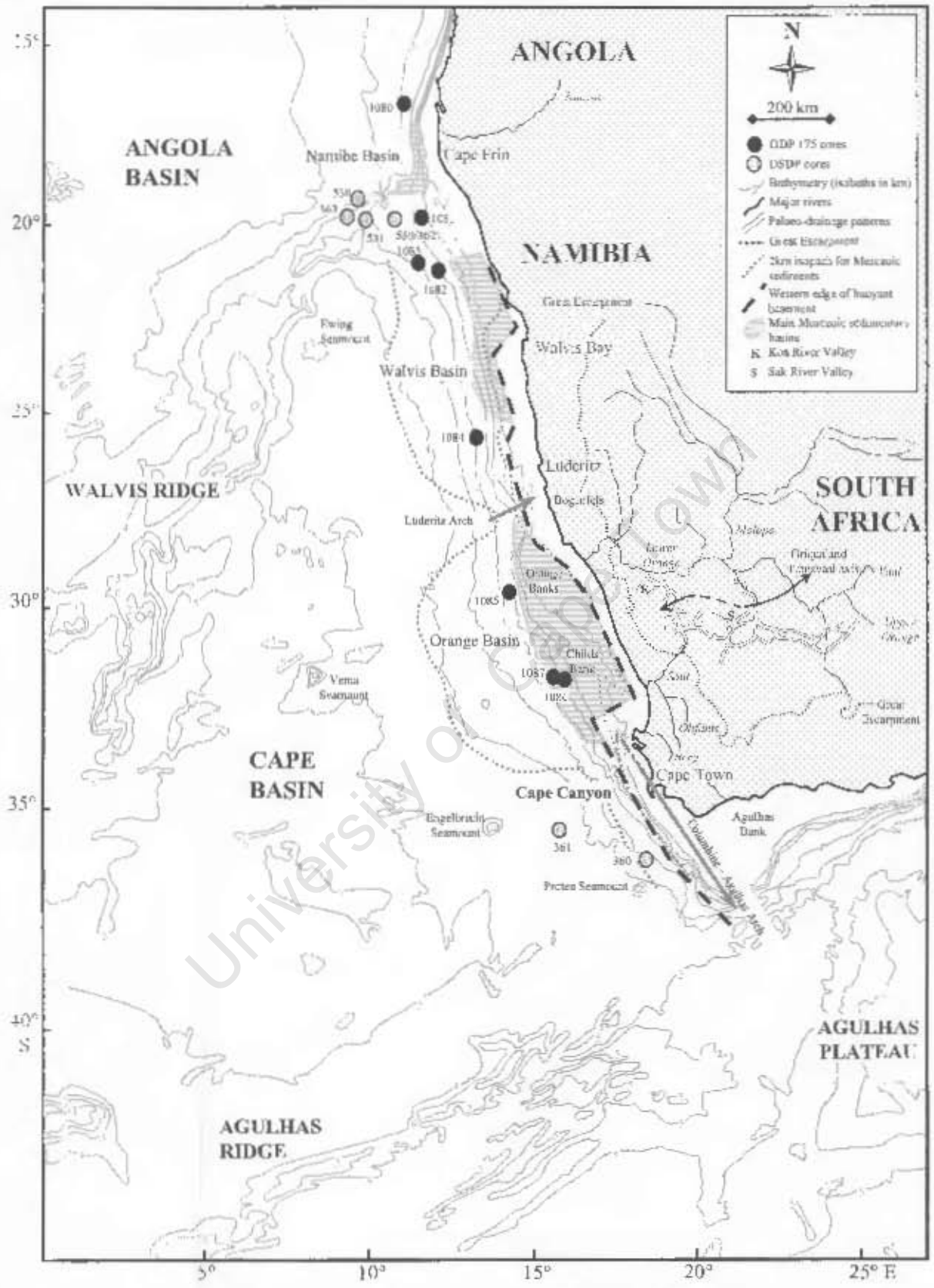


Figure 2.1. A summary of the western margin of southern Africa, including the bathymetry, main orographic features, onshore morphology and a summary of palaeo-drainage systems. (After Dingle *et al.* (1983); Dingle and Robson (1992); SOEKOR (1994, 1996); Shannon and Nelson (1996); Partridge and Maud (1987); Gilchrist and Summerfield (1990); Shannon (1985); Maslanyi *et al.* (1992), Malan (1974) cited in Dingle and Hendey (1984) and Wefer *et al.* (1998).

University of Cape Town

From Cape Point to the Kunene River (±17°S) the margin lacks embayments, apart from a few exceptions, such as Lüderitz and Walvis Bay (Figure 2.1). However, south of ±32°S, several prominent headlands occur with granite outcrops at Cape Columbine and Cape Town forming boundaries to exposed bays to the north and protected bays to the south of each headland. A large number of raised (and drowned) terraces occur on the western margin (Martin, 1973), with the sedimentary packages of upper Tertiary and Quaternary raised terraces referred to as the 90 m, 50 m, 30 m, 8-12 m, 4-6 m and 2-3 m Packages (Pether *et al.*, 2000). The gently sloping coastal platform of the western margin is separated from the adjacent western interior plateau by a rim of high terrain, or marginal upwarp, referred to as the Great Escarpment reaching heights of 2300 m (Figure 2.1 and 2.2), located between 50 to ≥500 km from the present coastline (Martin, 1973; Partridge and Maud, 2000).

2.1 RIFTING OF THE WESTERN MARGIN OF SOUTHERN AFRICA

The passive margin formed from clean-break separation and only minor shearing of western Gondwana during the early Cretaceous (Dingle *et al.*, 1983; Fouché *et al.*, 1992). Onset of continental drift is believed to have started between 126 and 121 Ma (Fouché *et al.*, 1992) along a zone of weakness between the buoyant pre-Cretaceous basement to the east and the main N-S horst and graben lineament adjacent to it (Dingle *et al.*, 1983), although the determination of the exact timing of break-up is still unresolved (Fouché *et al.*, 1992). The onset of continental break-up is recorded in the linear array of four major basins developed parallel to the coast, within the zone of maximum subsidence (Maslanyj *et al.*, 1992). The four basins are the Orange, Lüderitz, Walvis and Namibe, with the Orange and Walvis basins being the largest (Figure 2.1). The extent of the Orange Basin is largely controlled by the presence of two relatively buoyant pre-Cretaceous basement blocks, namely the Lüderitz or Kudu (Brown *et al.*, 1995) Arch to the North and the Columbine-Agulhas Arch to the south (Scrutton and Dingle, 1976). The Lüderitz or Kudu Arch, offshore from the Bogenfels area, separates the Orange and Walvis Basins. The Columbine-Agulhas Arch, a buoyant basement block composed predominantly of Cambrian granites, with a drape of Ordovician to Devonian (Cape Supergroup) sediments (Dingle *et al.*, 1983), defines the southern end of the Orange Basin (Dingle, 1980a). The Columbine-Agulhas Arch is terminated to the south by the Agulhas Fracture Zone, so that this buoyant basement block lies between the rifted western and sheared southeast margins. The basins of the western margin were initially clearly defined by north-south striking basement structural controls (horst and grabens), but lost much of their surface identity through the cumulative effects of accelerated oceanward progradation of the coastal margin, downwarping and the oceanward shift of sediment depocentres (Dingle *et al.*, 1983). These rift basins were the main sediment depocentres during the Mesozoic with the continental shelf largely built up by terrigenous sediments, although volcanic rocks are also present (Brown *et al.*, 1995). Examination of the Mesozoic sediment isopachs suggests that the rift basins overlie both continental and newly formed oceanic crust (Austin and Uchupi, 1982; Dingle *et al.*, 1983). Similarly, nine Mesozoic-Tertiary extensional basins are present along 2000 km of the east coast of southern America and include from south to north, the North Malvina, San Jorge, Rawson–Valdes, Colorado and Salado Basins (*e.g.* Hinz *et al.*, 1999). Aizawa *et al.* (2000) suggested that interpretation of the Namibian offshore seismic

University of Cape Town

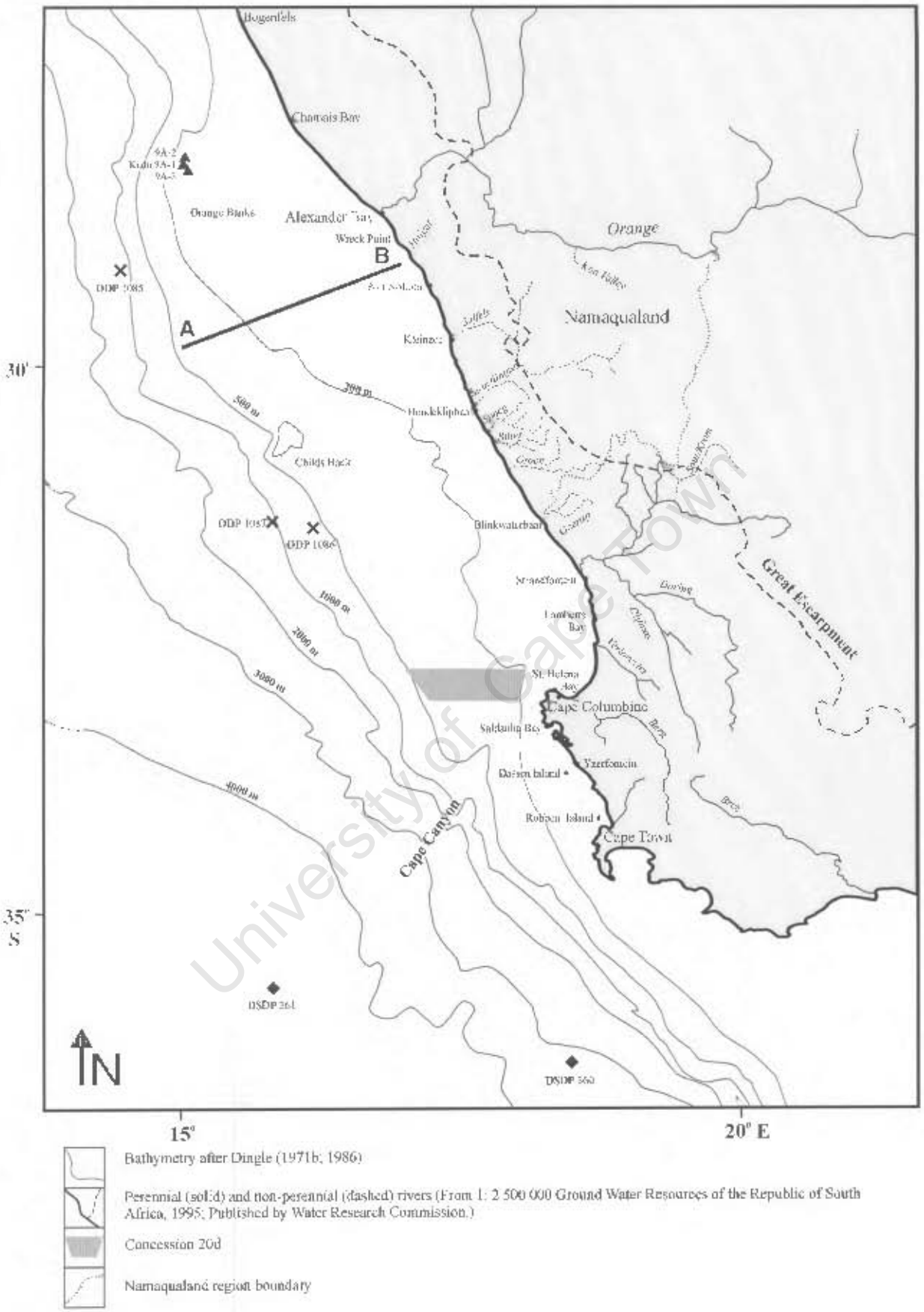


Figure 2.2. A simplified map of the western margin of southern Africa with the localities mentioned in the text shown. Borehole locations after Bolli *et al.* (1978); McMillan (1990) and Wefer *et al.* (1998). A schematic cross-section A-B is included as Figure 2.7.

University of Cape Town

records shows that the dominant structural element controlling the western margin evolution for the last ~130 Ma is a coast parallel "hinge zone" in the continental lithosphere, which forms a boundary between areas of subsidence and areas of uplift. The Namibian/Atlantic Hinge Line is offset by structural-zone boundaries along the Namibian and Angolan margin (Clemson *et al.*, 1997; Cramez and Jackson, 2000).

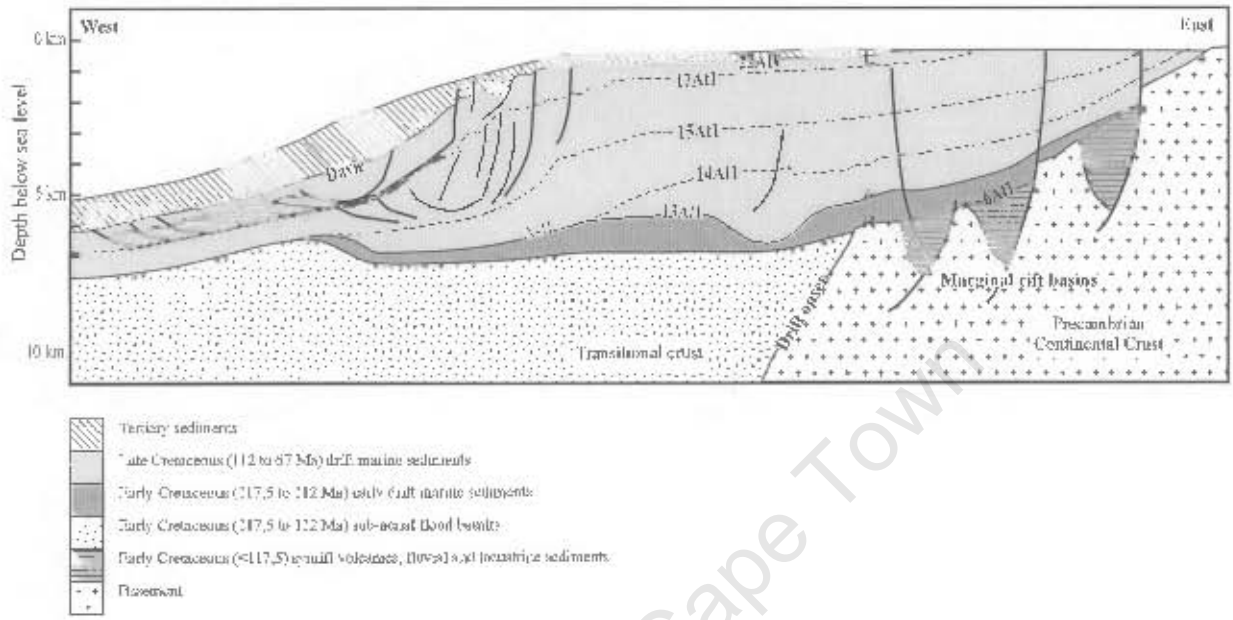


Figure 2.3. An idealized cross-section across the central Orange Basin of southern Africa, illustrating sediment distribution, prominent seismic reflectors and faults (heavy lines) of the Orange Basin (after the poster display by the Petroleum Agency SA for the AAPG 2002 conference, Houston, Texas and modified from Gerrard and Smith, 1982; Dingle *et al.*, 1983 and SOEKOR, 1994, 1996). The nomenclature of the major reflectors varies considerably in the literature, with the most commonly used shown.

Following the initial rifting phase, the tectonic-sedimentary history is subdivided into the initial narrow-ocean early-drift phase followed by the open-ocean drift phase (Gerrard and Smith, 1982). A number of prominent reflectors demarcating the rift to drift transition are recognised from seismic records for the ocean basin and outer margin off most of the west (and south) coast of southern Africa (Figure 2.3). Studies undertaken by SOEKOR (1994, 1996) suggested that an early drift interval (seismic reflectors 6At1 to 13At1) represents the transition from rifting to full drift or the transition from terrigenous sediments to onset of marine deposition (Dingle *et al.*, 1983). Therefore, the mid-Cretaceous 13At1 unconformity (equivalent to Atlantis II or A-II) marks the onset of full drift and open-ocean conditions (Figure 2.3). The 13At1 boundary probably also reflects the fundamental change in crustal subsidence and basin formation from the horst and graben style sedimentary basins, with well-developed boundary faults, to a more regional downwarping (epeirogenic subsidence) and the development of elongate marginal basins (Dingle *et al.*, 1983). The exact timing of this mid-Cretaceous unconformity is debated, with ages varying from Albian (Dingle *et al.*, 1983), mid-Aptian (Brown *et al.*, 1995; SOEKOR, 1996) to late Aptian (Bolli *et al.*, 1978). The Cretaceous drift sediment sequence reaches a thickness of more than 8000 m in the Orange Basin, with pre-13At1 sediments reaching maximum known thicknesses of 2200 m (Brown *et al.*, 1995). The regionally extensive marine planation surface, which marks the end of the Cretaceous sedimentation is referred to as the Davie unconformity (Figure 2.3) and can be traced

University of Cape Town

records shows that the dominant structural element controlling the western margin evolution for the last ~130 Ma is a coast parallel "hinge zone" in the continental lithosphere, which forms a boundary between areas of subsidence and areas of uplift. The Namibian/Atlantic Hinge Line is offset by structural-zone boundaries along the Namibian and Angolan margin (Clemson *et al.*, 1997; Cramez and Jackson, 2000).

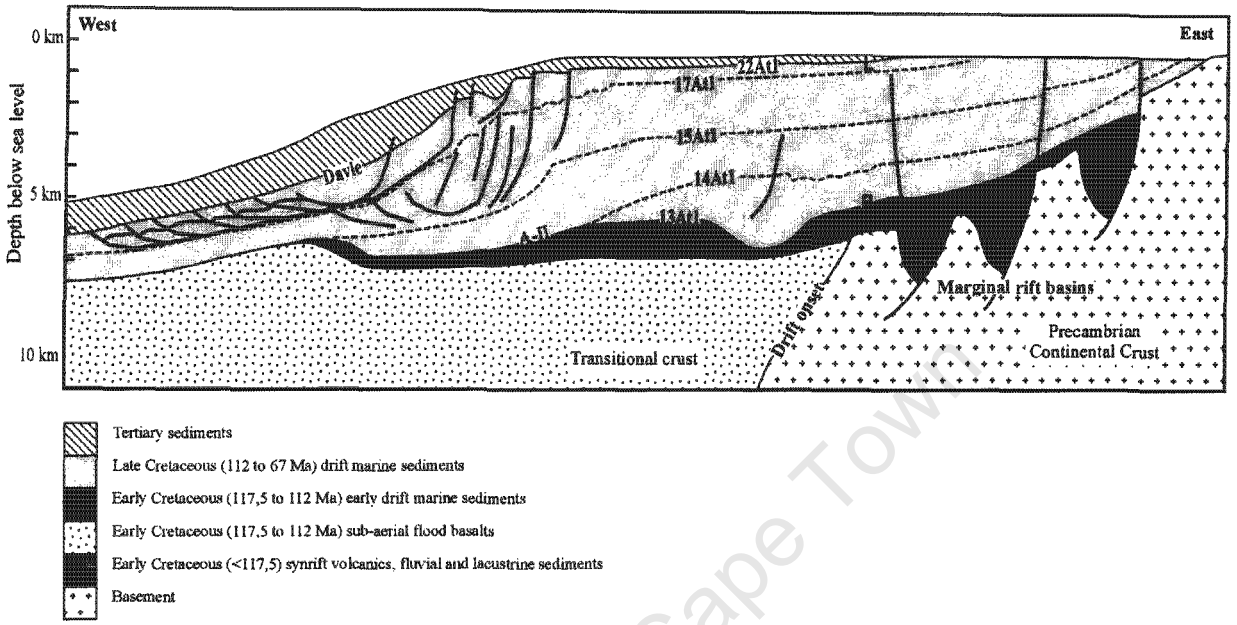


Figure 2.3. An idealized cross-section across the central Orange Basin of southern Africa, illustrating sediment distribution, prominent seismic reflectors and faults (heavy lines) of the Orange Basin (after the poster display by the Petroleum Agency SA for the AAPG 2002 conference, Houston, Texas and modified from Gerrard and Smith, 1982; Dingle *et al.*, 1983 and SOEKOR, 1994, 1996). The nomenclature of the major reflectors varies considerably in the literature, with the most commonly used shown.

Following the initial rifting phase, the tectonic-sedimentary history is subdivided into the initial narrow-ocean early-drift phase followed by the open-ocean drift phase (Gerrard and Smith, 1982). A number of prominent reflectors demarcating the rift to drift transition are recognised from seismic records for the ocean basin and outer margin off most of the west (and south) coast of southern Africa (Figure 2.3). Studies undertaken by SOEKOR (1994, 1996) suggested that an early drift interval (seismic reflectors 6At1 to 13At1) represents the transition from rifting to full drift or the transition from terrigenous sediments to onset of marine deposition (Dingle *et al.*, 1983). Therefore, the mid-Cretaceous 13At1 unconformity (equivalent to Atlantis II or A-II) marks the onset of full drift and open-ocean conditions (Figure 2.3). The 13At1 boundary probably also reflects the fundamental change in crustal subsidence and basin formation from the horst and graben style sedimentary basins, with well-developed boundary faults, to a more regional downwarping (epeirogenic subsidence) and the development of elongate marginal basins (Dingle *et al.*, 1983). The exact timing of this mid-Cretaceous unconformity is debated, with ages varying from Albian (Dingle *et al.*, 1983), mid-Aptian (Brown *et al.*, 1995; SOEKOR, 1996) to late Aptian (Bolli *et al.*, 1978). The Cretaceous drift sediment sequence reaches a thickness of more than 8000 m in the Orange Basin, with pre-13At1 sediments reaching maximum known thicknesses of 2200 m (Brown *et al.*, 1995). The regionally extensive marine planation surface, which marks the end of the Cretaceous sedimentation is referred to as the Davie unconformity (Figure 2.3) and can be traced

University of Cape Town

from the inner shelf to the lower continental rise. It is assigned a late Maastrichtian/early Palaeocene age on the shelf (Dingle *et al.*, 1983) to a latest Palaeocene/earliest Eocene age in DSDP Site 362 on the Walvis Ridge (Figure 2.1).

The morphology of the continental margin is commonly described as a high-elevation rifted margin (*e.g.* Partridge and Maud, 1987; Gilchrist and Summerfield, 1990; Burke, 1996; Partridge and Maud, 2000). Major seaward-facing escarpments are prominent macrogeomorphological features of many high-elevation passive continental margins, including southern Africa, western India and southeastern Australia (Gallagher and Brown, 1999). However, the timing of the events leading to the elevation of southern African are in dispute, where many authors infer a high elevation of the continental areas prior to rifting with estimated elevations of ±1500 m of the western interior (Gilchrist and Summerfield, 1990; Ollier and Pain, 1997; Partridge and Maud, 2000). Gallagher and Brown (1999) showed, using fission-track data from Namibia, that two dominant phases of denudation can be identified, namely an early Cretaceous rift-related event and a latest Cretaceous (~80-60 Ma) event associated with tectonic reactivation of regional structures. Brown *et al.* (1990; 2000) noted that the accelerated phase of cooling identified in the latest Cretaceous (~80–60 Ma) correlates with sedimentation patterns derived from borehole data for the adjacent offshore Orange and Walvis basins, where the major volume of sediments were deposited in late Cretaceous-early Tertiary (Rust and Summerfield, 1990). In contrast, Aizawa *et al.* (2000) described a latest Maastrichtian to earliest Paleocene (Cretaceous/Tertiary) uplift of ~1 km close to the present coast line (decreasing to little to no evidence for uplift at 50 km offshore), of the northern Orange Basin and argue that the Great Escarpment was consequently initiated by erosion (shallow-marine bevelling) of this uplifted basement. Apatite fission-track supports a late Cretaceous (~70 Ma) uplift of northern Namibia with a net vertical displacement of ~2 km estimated using the palaeo-temperature range (120-80° C) across the Damara Omaruru Lineament (Raab *et al.*, 2002). In contradiction to all of the above arguments, Burke (1996) argued that, during the early Tertiary, the African continent was low-lying and that many of Africa's deeply weathered rocks, including laterite and bauxite developed during this 65 to 30 Ma interval. Burke (1996) argued that the elevation of the African Plate (in response to the African Superswell) occurred approximately at 30 Ma due to isostatic uplift when the lateral movement of the African Plate slowed above an underlying mantle plume. He argued that uplift was initiated at a time of peak volcanic activity on the African Plate and that the Great Escarpment is consequently a young (<30 Ma) erosional feature of a similar age to the well-defined marine unconformity described for southern Africa.

The presence of an escarpment, up to 100 Ma after rifting, has important implications in the offshore depositional history because the escarpment functions as a barrier, deflecting rivers away from the rifted margin and preventing the transport of sediments from the large internal continental drainage basins to the newly formed rifted basins (Gilchrist and Summerfield, 1990). The Great Escarpment is traditionally interpreted to have been retreating inland since its initial formation, although it still forms a significant topographic feature (Partridge and Maud, 2000). Recent fission-track and cosmogenic isotope studies in Namibia indicated that retreat of the escarpment since the Eocene has been minimal

University of Cape Town

(~5 m/Ma for the coastal plains and ~10 m/Ma for the inland area) and that, in Namibia at least, the escarpment is pinned at a drainage divide (Cockburn *et al.*, 2000).

2.1.1 TERTIARY UPLIFT AND EROSION CYCLES

A number of studies have emphasised the importance of Tertiary tectonism and the associated uplift of the southern African landmass as a mechanism to describe the beach terraces of the West Coast and the series of palaeo-surfaces, reflecting cycles of erosion, located on both sides of the Great Escarpment (Partridge and Maud, 1987, 2000; Partridge, 1998; De Wit *et al.*, 2000). The following section is a review of the terminology, evidence and arguments for and against cycles of erosion and uplift following rifting to explain the presence of the erosional surfaces (Partridge and Maud, 1987, 2000; Burke, 1996; De Wit, 1993, 1999; Spönemann and Hagedorn, 2000; De Wit *et al.*, 2000). The Gondwana pre-rift surface (King and King, 1959) is preserved only as a widespread Jurassic unconformity beneath the earliest marine sediments (Partridge and Maud, 1987).

The African Surface, cut at two levels above and below the Great Escarpment, results from erosion following the rifting of Gondwana with thicknesses of up to 1650 m to 1800 m removed during this post-rifting denudation cycle (Partridge and Maud, 1987; Partridge, 1998; Gilchrist and Summerfield, 1990), where Brown *et al.*, (1990) argued that fission-track analyses indicate as much as 3 km of material has been removed. The African Surface occurs as a vast undulating plain across the subcontinent, with only minor erosional residuals and high-lying areas preserved (*e.g.* Cape Fold Belt mountains, Lesotho highlands, Langeberg and Kuruman ranges of northern Cape). The African Surface has deeply kaolinised weathering profiles with massive laterite and silcrete duricrusts (Partridge and Maud, 1987). The polycyclic nature of the Cretaceous erosional events resulted in widespread epeirogenic sedimentation, in several pulses, off the continental shelf, with a general slowing of shelf sedimentation culminating in the Oligocene hiatus (the terminal stages of planation, where little sediment was contributed to the shelf via drainage systems). A middle to late Oligocene erosional hiatus is well known off the western Atlantic Ocean margin (Siesser and Dingle, 1981; Cramez and Jackson, 2000; Lavier *et al.*, 2001). A reconstruction of the tectonic history of the West African margin was done using sequential backstripping of two seismic profiles across the Congo and Angola margin (Lavier *et al.*, 2001). They noted that the Eocene-Oligocene transition is interpreted as an erosional event resulting from mass wasting and erosion, with the removal of as much as 1000 m of sediment, associated with changes in ocean currents and the initiation of upwelling off the African coast north of the Walvis Ridge (Lavier *et al.*, 2001). The African cycle of erosion stripped most of the pre-Mesozoic Karoo cover from the western interior and margin so that post-Cretaceous drainage is largely governed by pre-Karoo topography (Partridge and Maud, 2000).

Disturbance of the African surface occurred in response to uplift of the subcontinent, during the latest Oligocene (Burke, 1996) or the early Miocene (Partridge and Maud, 1987, 2000, Partridge, 1998; Spönemann and Hagedorn, 2000). Partridge (1998) suggested that uplift occurred at 16-19 Ma during

University of Cape Town

the lower to middle Miocene (Burdigalian to Langhian) as evidenced by minor increases in terrestrial input in the Orange Basin (Dingle *et al.*, 1983). Movement is believed to have occurred along a number of discrete axes, with the greatest amount of uplift of ~100-200 m along a line roughly coinciding with the Great Escarpment (Partridge, 1998). Most of the movement in the Miocene resulted in the elevation of marine and coastal deposits, with the Columbine-Agulhas Axis reactivated during this time with downwarping to the southwest (Partridge and Maud, 1987). The overall asymmetry of the Miocene uplift resulted in a slight westward tilt to the subcontinent (Partridge and Maud, 1987). This uplift and erosion was associated with the return to widespread shelf sedimentation following the Oligocene hiatus, although sediment output was considerably lower than during the Cretaceous (Partridge and Maud, 1987). Partridge and Maud (1987) suggested that several major offshore slumps, described by Dingle (1980b) and Dingle *et al.* (1983), were triggered by uplift and increased sedimentation rates at this time. This cycle of uplift and erosion produced the Post-African I Surface. A second major erosional event is recorded in the sediments of the West African margin in the early Miocene, resulting from the increased rate of tectonic uplift (Lavier *et al.*, 2001). Lavier *et al.* (2001) estimated uplift in the Miocene for this area of at least 500 m (Angola) to 330 m (Congo) on the assumption that the shelf break in the Miocene was at a similar depth to the present-day shelf break at 130 m.

Further uplift of the southern African continent occurred during the Pliocene along virtually the same axes of the Miocene uplift. Pliocene movement was typically of a greater amplitude, with an even more marked asymmetry in the movement, causing accentuated westward tilting of the subcontinent (Partridge and Maud, 1987, 2000; Partridge, 1998; Pickford, 1998, 2000; Brown *et al.*, 2000; Pether *et al.*, 2000). Differential uplift rates are used to explain the differences in heights above sea level of marine terraces along the West Coast of Southern Africa. Apatite fission-track ages, between Cape Town and Lüderitz show a general decrease in age northwards, supporting an asymmetric tilting of the subcontinent with increased uplift to the north (Gallagher and Brown, 1999). Partridge (1998) noted that uplift along the eastern part of the subcontinent was of the order of 700-900 m, and suggests uplift of only ±90-100 m along the western extremes of the Griqualand-Transvaal Axis (Figure 2.1). This uplift resulted in a marked rejuvenation along major inland-drainage systems. Again, massive offshore Pliocene slumps may have been triggered by this uplift event (Dingle, 1980b; Partridge and Maud, 1987). This cycle of uplift and erosion produced the Post-African II Surface. Recent work using cosmogenic ^{21}Ne dating of pediment surfaces by Van der Wateren and Dunai (2001) indicated that accelerated denudation began around 2.81±0.11 Ma in the central Namib Desert, but they interpreted this to signify increasingly wet conditions in this region, in response to changes in the Plio/Pleistocene global climate, rather than requiring an increased rate of uplift. The late Neogene tectonic history of the southwestern African margin is similarly controversial. Roberts and Brink (2002) suggested that some 40-50 m subsidence, rather than uplift, of the Namaqualand coast occurred sometime between the early to late Pliocene, based on the age and elevation of sea-level highstand deposits of the western margin. In contrast, Dale and McMillan (2003b) correlated the offshore Pliocene units with the onshore 90 m Package (Pether *et al.*, 2000) and argued that the distribution of these sediments indicates 90 m of uplift of the shelf between Bogenfels and Blinkwaterbaai (Figure 2.2).

University of Cape Town

Partridge and Maud (1987) noted that no significant faulting accompanies the uplift in any of the above-mentioned erosional cycles. They suggested a tentative link between onshore denudation and deposition on the continental margin and isostatic uplift of the interior, although Partridge (1998) proposed that this continued uplift through the Cenozoic results rather from buoyancy forces arising from the thermal anomalies associated with the continued southward development of the African Superswell (Burke, 1996). However, there is growing evidence for late Tertiary to Quaternary tectonic activity in the southwestern Cape with the dominant Pleistocene stress field characterised by extension towards N25° (NNE-SSW) and a prominent ESE-WNW strike of faulting (Andreoli *et al.*, 1996). Ransome *et al.* (1993; cited in Andreoli *et al.*, 1996) proposed that a broad neotectonic seismic zone exists, striking NW-SE, along the axis of Miocene uplift of the Columbine-Agulhas Arch. The neotectonic activity was initiated in the Miocene and largely induced by three major stress fields orientated E, NNE and NW (Andreoli *et al.*, 1996).

In contrast to the arguments favouring uplift, Hendey (1982) and Dingle and Hendey (1984) argued that the marine benches and land surfaces could be explained simply by eustatic fluctuations in sea level, with new base levels initiating new cycles of erosion. They developed their model further and suggest that river capture and changes in palaeo-drainage systems of southern Africa could also be related to changes in sea level. Pickford (1998) similarly argued that the Cenozoic onshore marine deposits of southern Africa can be ascribed largely, if not solely, to eustatic sea-level fluctuations because his reconstruction of the sea level curve for Namaqualand and Namibia, based on mammalian biochronology, closely resembled the Australian sea level curve of Quilty (1977). However, the present altitude of the deposits may be, partly, the result of differential uplift (Pickford, 1998).

University of Cape Town

2.1.2 MODERN AND PALAEO-DRAINAGE SYSTEMS

The major perennial rivers of the West Coast of southern Africa today, the Berg, Olifants, Orange and Kunene rivers (Du Toit, 1954) are shown in Figures 2.1 and 2.2, where the majority of the coastal rivers are non-perennial, typically short in length and have a limited catchment area. The Great Escarpment of the western margin is only breached twice, at 28° and 31° south (Figure 2.2), by the Orange River in the north and by the Sout/Krom, an ephemeral tributary of the Olifants River in the south (Dingle and Hendey, 1984). The Orange and Olifants rivers and secondary rivers, such as the Buffels, are believed to have supplied the majority of diamonds to western continental margin (Corbett, 1996).

The major westward-flowing drainage systems are interpreted by Cox (1989) to have been initiated sometime during the early Jurassic (±190 Ma) as a classic example of drainage away from topographic doming associated with the Karoo plume and the newly formed Indian Ocean. The Mesozoic Kalahari River cuts a considerable gorge through the Cape-Angola (Paraná) high, suggesting that this drainage system was well established prior to the onset of rifting along the western margin. Gilchrist and Summerfield (1990) argued that continental rifting creates a significantly lower base level along the newly formed high-elevation margins, with the consequent development of two distinct drainage

systems. The coastal drainage systems, which tend to be small, are associated with aggressive denudation because of the high local relief and hence produce most of the sediments deposited in the offshore basins. The inland drainage systems with the low local relief inland of the escarpment produces lower denudation rates. The early Cretaceous break-up of Gondwana associated with the formation of the Atlantic Ocean initiated a new cycle of erosion, which consequently altered the major drainage-systems. Two major westward-flowing river systems subsequently evolved, namely the Karoo (also referred to as the Palaeo-Orange) and Kalahari rivers. The courses of these palaeo-rivers appear to mimic pre-Karoo topography, due to the resistant nature of the underlying regionally metamorphosed basement (Malherbe *et al.*, 1986). A number of studies, however, following conclusions made by Du Toit (1910), have noted that the drainage systems of southern Africa have changed considerably since the rifting of Gondwana (Dingle *et al.*, 1983; Dingle and Hendey, 1984; Malherbe *et al.*, 1986; Partridge and Maud, 1987; De Wit *et al.*, 2000 and Moore and Moore, 2004). The palaeo-drainage channels of the central interior, interpreted from satellite images by Malan (1974, cited in Dingle and Hendey, 1984) are included in Figure 2.1 as a general indication of the possible Mesozoic/Cenozoic drainage patterns. Although there is little agreement in the literature on the details and timing of these changes, there is general agreement that the drainage systems were most active during the late Cretaceous, middle Miocene, (late Miocene (Pickford, 2000)) and Plio/Pleistocene, reflecting more humid onshore climates (De Wit, 1993, 1999; De Wit *et al.*, 2000; Moore and Moore, 2004).

Dingle and Hendey (1984) argued that the Karoo River changed the location of its river mouth twice since the mid-Cretaceous, switching from a northern exit (in the vicinity of the present-day position of Orange River mouth) in the Cretaceous to a southern exit (in the vicinity of the present day Olifants River in Figure 2.2) from latest Cretaceous to end Oligocene, switching back to a northern exit from the early Miocene. A number of studies of sediment thicknesses in the Orange Basin supported the existence of two major drainage systems (Gerrard and Smith, 1982; Dingle *et al.*, 1983; Rust and Summerfield, 1990), where Dingle and Hendey (1984) utilised sediment isopach evidence to support alternating discharge points. Dingle and Hendey (1984) supported their hypothesis of a southern exit of the Karoo River from the Cretaceous to end-Oligocene by emphasizing 1) that the excavated valleys associated with the southern breach in the escarpment require a much larger river than the existing Krom River (Figure 2.2); 2) upcore changes in the DSDP Site 361 (Figure 2.1) Paleocene to Oligocene clay chemistry with increased montmorillonite (at the expense of illite) during the Palaeogene reflecting the input of altered Karoo volcanic rocks (Stormberg lavas) from the Upper Orange catchment area; 3) that switches in the position of the river mouths were associated with sea-level regressions and consequent rejuvenation and down-cutting would have promoted river capture.

Recent literature, using geomorphological, sedimentological and zoological evidence from a number of Namaqualand fluvial deposits exploited by the alluvial diamond mining industry, has argued for only a single switch in the position of the Karoo River mouth (Partridge and Maud, 1987, 2000; Partridge, 1998; De Wit, 1993, 1999). During the Cretaceous, the Karoo River drained the area to the south of the Cargonian Highlands (along the Griqualand-Transvaal Axis in the northwestern Cape) and the upper

University of Cape Town

Orange/Vaal system linked to the Olifants River via the Sout/Krom River and discharged in the vicinity of the present day Olifants River mouth (Figure 2.2). In contrast, the Kalahari River drained southern Namibia and Botswana, where the lower Orange River linked up with the proto-Molopo River and formed the northern drainage system (De Wit, 1993, 1999). Similarly, Brown *et al.* (1995) argued that the palaeo-Olifants River was the dominant sediment supply to the Orange Basin in the early Cretaceous between 117.5 to 103 Ma (Hauterivian to mid-Albian), after which the Orange River switched to the northern exit, where the Orange River delta system has been the dominant sediment source onto the western margin since the mid-Albian.

De Wit (1993, 1999) argued that the extreme denudation during the humid and tropical Cretaceous, in response to uplift of the Griqualand-Transvaal Axis (Figure 2.1) would have resulted in the exhumation of resistant pre-Mesozoic topographic highs. Two of these areas in the Northern Cape, the Doringberg Hills and the Cargonian Highlands are believed to have played an important role, as major geomorphic barriers, in the development of the palaeo-drainage systems. De Wit (1993, 1999) therefore inferred that a combination of regional asymmetrical tilting, associated with uplift and denudation, resulted in the Kalahari River capturing the Karoo River sometime early in the Tertiary, soon after the end-Cretaceous climatic deterioration. De Wit (1993) proposed, on geomorphological evidence, that the drainage patterns of the southern African continental area have not changed much since the early Tertiary, although, during the Miocene, the lower Karoo catchment area was drained by the Koa River, a left-bank tributary to the Orange River (Figure 2.2). In summary, De Wit (1993) argued that the evolution of the Cenozoic drainage patterns is dynamically related to the uplift events and climatic changes that affected the subcontinent. Pickford (2000) correlated the Neogene fluvial terraces of the Karoo River with the marine/littoral Packages of Namaqualand (Figure 2.2), so that the 90 m Package is equivalent to the composite Proto-Orange Terrace I (early Miocene Auchus to basal middle Miocene Arrisdrift); the 50 m Package is associated with the Meso-Orange Terrace II and the 30 m Package is associated with the Meso-Orange Terrace I, although the last two correlations are inferred only, because no fossil dates are available (Section 2.5.2). Pickford (2000) consequently argued that the accumulation of the fluvial deposits of the Karoo River can be explained as deposition in response to changing sea levels.

2.2 SEA LEVEL VARIATIONS

The Tertiary sea level curve for southern Africa (Dingle and Scrutton, 1974; revised by Siesser and Dingle, 1981), extensively referred to in the southern African literature (Figure 2.4A), is a generalised curve showing the *gross direction* of sea-level movement around southern Africa during the Tertiary and includes a tectonic component. It is based on the reported ages of onshore deposits, seismic evidence and a small number of analyses of marine samples. However, Siesser and Dingle (1981) noted that it is difficult to assess Tertiary eustatic changes in sea level, because of the differential uplift of the southern African subcontinent, which is further complicated by the asymmetry of the uplift. In addition, there is a scarcity of onshore deposits with material suitable for dating and considerable controversy exists in the literature on the ages of the existing deposits. However, over the past decade, the Namibia

University of Cape Town

Palaeontology Expedition (Pickford, 2000) has been actively involved in establishing a Tertiary geochronological framework for Namibia and the Namaqualand, largely based on the geochronology of vertebrate and bivalve fossils after Pether (1994a) (Figure 2.4B and Table 2.1). Although the two sea level curves for southern Africa (Figure 2.4A & B) are quite different, both are characterized by a marked regressive event in the late Oligocene. The widespread Oligocene–early Miocene erosional unconformity is used as evidence for a drop in sea level of the order of 500 m during the Oligocene regression (Siesser and Dingle, 1981). Pickford and Senut (1999) only described the Oligocene regression as being associated with a considerable drop in sea level, and noted that the incision of valleys into the Namibian Unconformity Surface on the coastal plains of the Namib occurred during this lowstand. These valleys can be followed out onto the shelf for some of the major rivers (*e.g.* the Orange and Kaukausib), where the Kaukausib River course can be traced seaward to –130 m south of Lüderitz, off Elizabeth Bay (Murray *et al.*, 1970; Day *et al.*, 1992). Cramez and Jackson (2000) also mentioned a drop in sea level of ~300 m during the Oligocene (~30 Ma) for the Angolan margin.

University of Cape Town

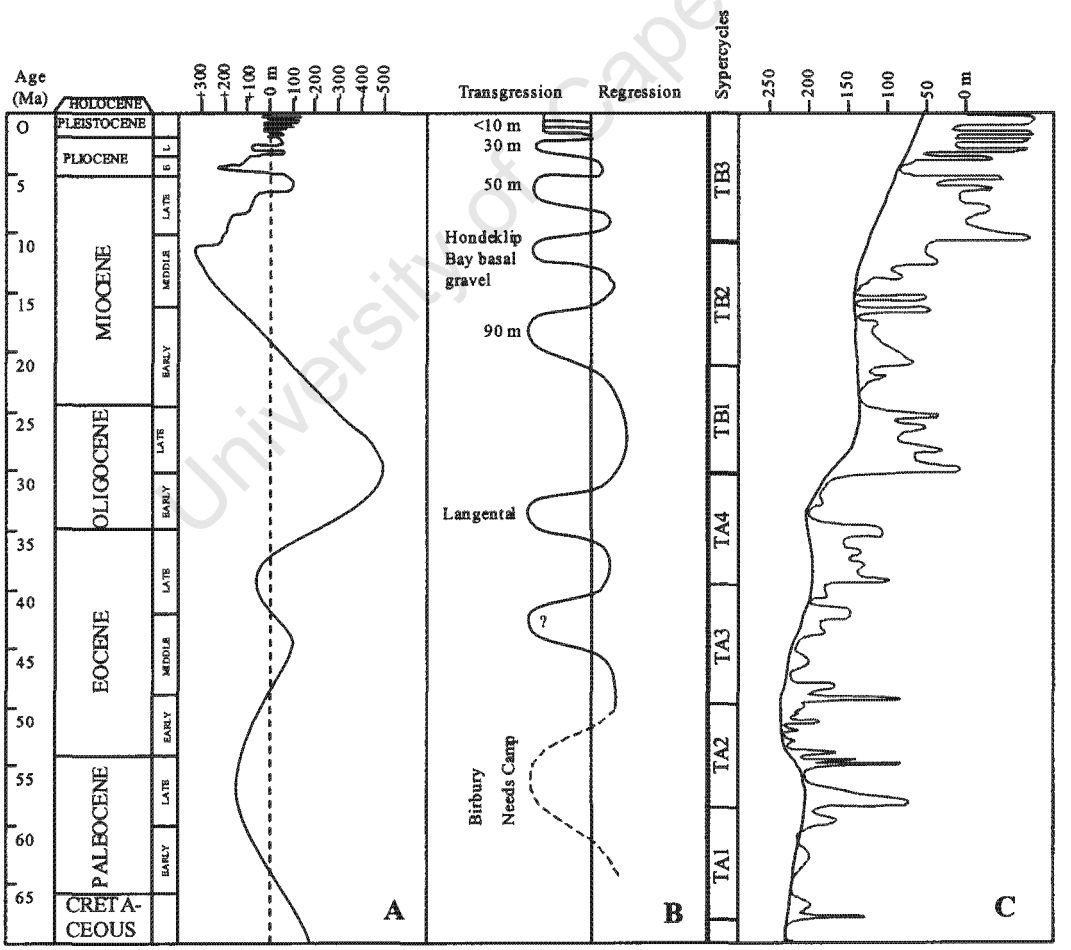


Figure 2.4. The Cenozoic sea-level curve for the west coast of southern Africa after A) Siesser and Dingle (1981) modified after Hendey (1982), Dingle *et al.* (1983) and Dale and McMillan (1999a) and B) Pickford (1998). C) The global eustatic sea-level curve of Haq *et al.* (1987; 1988) modified by Berggren *et al.* (1995).

The Cenozoic sediment history of the western margin of southern Africa is still poorly understood (Pether *et al.*, 2000) and the uplift history of southern Africa is poorly constrained, with little consensus regarding the scale and the timing of the uplift events. Consequently, the sea level curves of Siesser and Dingle (1981) and Pickford (2000) are discussed in relation to the modified global sea level curve of Haq *et al* (1987; 1988) recalibrated to Berggren *et al.* (1995) after Miller *et al.* (1997; 1998), as an independent reference, when discussing Cenozoic sea-level changes along the western margin. The relevance of a global sea level curve is discussed in more detail in Section 3.4.

Table 2.1. A summary of the Pickford and Senut (1999) Cenozoic sea level variations, based largely on littoral mammalian fossil studies and fluvial assemblages deposited during sea-level transgressions (Pether, 1994a).

	Age (Ma)	Sea level relative to present	Sediments (Section 2.7.3)	Package names proposed by Pickford (2000)
Late Pleistocene to Holocene transgressions		< 10 m	Three <10 m Packages	*Donax serra*
			30 m Package	*Donax rogersi*
Plio-Pleistocene boundary transgression	~2.6-2.3	30 m higher		
Pliocene regression			50 m Package	*Donax haughtoni*
Late late Miocene transgression	~7-5	50 m higher		
			Gravels below 50 m Package	*Agnotherium tetralophodon*
Late middle Miocene transgression	~12-10			
Middle Miocene regression			90 m Package	*Kenyasus nguruwe*
Late early Miocene transgression	~20-17.5	Between 50 and 90 m higher		
Oligocene regression		Considerably lower		

University of Cape Town

2.3 PALAEO-CLIMATE

Relatively little is known about the early Cenozoic environment, largely due to a paucity of onshore deposits. Ward and Corbett (1990) suggested that the aridity of the western margin began in the Eocene, based on the aeolianites from the Buntfeldschuh and Bogenfels deposits of southern Namibia, although Tankard and Rogers (1978) noted that a dry temperate climate and summer rain is indicated by the upper Eocene/Oligocene Banke lacustrine deposits of Namaqualand. Kaolinisation, as evidence of a humid climate, occurred prior to the middle Eocene in southern Namibia (previously referred to in the literature as the Cretaceous kaolin weathering), but appears to have persisted into the Oligocene in the south, as evidenced by kaolinisation below the lower Miocene deposits of the Namaqualand coast (Pether, 1994a; Pickford and Senut, 1999) and in the Noordhoek area (Rogers, 1982; Partridge and Maud, 1987; Pickford and Senut, 1999). The Oligocene, in general, is a period of very low offshore sedimentation rates (Partridge and Maud, 1987; Pickford and Senut, 1999), which probably implies low erosion rates reflecting the advanced stage of planation (Partridge and Maud, 1987).

The Palaeogene proto-Namib desert phase of Ward and Corbett (1990) is followed by a Pluvial phase in the early Miocene. Evidence from a number of onshore diamond-bearing placer deposits supports widespread fluvial activity during the early to middle Miocene (Bosluispan/Geelvloer fluvial phase of De Wit, 1993, 1999). Faunal evidence from a number of sites supports humid conditions sufficient to support a woodland environment around 19-16 Ma (Partridge, 1998). The mammal, crocodile and tortoise fossil record preserved in the fluvial grits and gravels at Bosluispan within the Koa/Geelvloer palaeo-river valley (Figure 2.2) of the Northern Cape are interpreted to represent a riparian woodland environment and a more tropical climate, with the main depositional event at 15-16 Ma (Senut *et al.*, 1996). A similar environment and age (± 17-19 Ma) are suggested for the Arrisdrift sediments of southern Namibia (De Wit *et al.*, 2000). Similarly, Smith and Mason (2002) described the middle Miocene (±16-10 Ma) Karpfenkliff Conglomerate Formation in the central Namib Desert, which are alluvial-fan deposits, related to an increased rainfall during the mid Miocene. Additional evidence for a middle Miocene warm-humid climate is supplied by the Al-rich illite chemistry from ODP Site 1088 and 1092 (Leg 177) on the Agulhas and Meteor Rise (Diekmann *et al.*, 2003).

The climate along the western margin of southern Africa changed dramatically around ~15 Ma (middle Miocene) from a tropical to sub-tropical to a cooler, more arid temperate climate, denoting the onset of desert conditions in the Namib (De Wit *et al.*, 2000; Pickford and Senut, 1999). Pollen studies showed that arid to hyper-arid conditions have existed along the western margin of Namibia since the Miocene (Van Zinderen Bakker, 1984). Detailed mammal fossil and ostrich eggshell biochronology has dated the onset of aeolianite deposition in the Namib at ~17-16 Ma (Pickford, 2000), although Pether *et al.* (2000) suggested that it may be older with a Palaeogene proto-Namib Desert phase followed by the main aeolian deposition (Tsondab Sandstone) in the early to middle Miocene. An onshore source of sediment was considerably reduced with increasing aridity of the western margin (De Wit *et al.*, 2000).

Ward and Corbett (1990) described a pedogenic phase following the early–mid Miocene Pluvial phase. The pedogenic phase of the earliest to mid late Miocene is followed by the Namib Desert phase (Ward and Corbett, 1990) and silicification of surface deposits during the late Miocene is commonly observed (Pickford and Senut, 1999). Increased aridification during the late Miocene/Pliocene resulted in a decrease in river flow and deposition in the fluvial channels, followed by the formation of extensive calcrete deposits during the late Pliocene (Malherbe *et al.*, 1986). Pickford and Senut (1999) argued that active erosion continued until the early Pliocene as the *Hipparion namaquense* fossils in the underlying granitic sands at Bosluispan, based on a comparison with other African specimens, imply an early Pliocene age (~4-6 Ma). They suggested that the widespread calcretes of northern Namaqualand are most likely younger than early Pliocene and are not late Miocene in age (Ward and Corbett, 1990). Hendey (1982) noted the macrofauna of the Mio/Pliocene Varswater Formation from Langebaanweg, inland from Saldanha Bay, recorded a change from a more tropical to a more temperate climate.

Slight warming during the late Pliocene with an associated slightly wetter climate is inferred from the terrestrial grazer fossils of the Namaqualand area, where grasslands overtook the arid interior (De Wit,

University of Cape Town

1993, 1999). Similarly, Van der Wateren and Dunai (2001), and references therein, argued that ^{21}Ne cosmogenic ages indicate a late Pliocene wetter climate, based on the inferred timing of canyon incisions at the base of the Great Escarpment.

2.4 ATLANTIC OCEAN / BENGUELA SYSTEM

The Benguela Current, flowing equatorwards along the western margin of southern Africa, is one of four global eastern boundary currents, where trade wind-driven coastal upwelling occurs (Shannon and Nelson, 1996). Seven principal upwelling cells occur off the western margin of southern Africa, namely the Cape Peninsula, Columbine, Namaqua, Lüderitz, Central Namibia, Northern Namibia and Kunene cells from south to north (Lutjeharms and Meeuwis, 1987; Shannon and Nelson, 1996). The perennial Lüderitz cell, with upwelling filaments extending up to 150-200 km offshore, forms an oceanographic divide between the Northern and Southern Benguela regions (Giraudeau, 1993; Dingle 1995; Shannon and Nelson, 1996). Upwelling in the southernmost Cape Peninsula and Columbine cells is the most seasonal, being strongest in mid-summer under the influence of strong southeasterly winds (Lutjeharms and Meeuwis, 1987). The Agulhas Retroflection forms the southern boundary to the Benguela system and the Angola-Benguela front, the northern boundary.

The development of the Benguela system through the Neogene has been an important component in the evolution of the west margin of southern Africa (Diester-Haass *et al.*, 2002). Upwelling is associated with increased productivity and accumulation of organic-rich sediments in the shelf/inshore region. In addition, the widespread occurrence of authigenic mineralization on the continental shelf and extensive phosphatisation of lower Miocene calcareous sediments and limestones exposed at the sea-bed has been linked to increased upwelling (Pether, 1994b). The onset of increased onshore aridity and the formation of the Namib have been coupled to the establishment of cold-water Benguela upwelling (Ward and Corbett, 1990). A late Miocene to late Pliocene age for the intensification of upwelling is proposed (Siesser, 1978b; Siesser, 1980; Diester-Haass *et al.*, 1992; Wefer *et al.*, 1998; Diester-Haass *et al.*, 2002). Siesser (1978b, 1980) argued that sedimentological, palaeontological and geochemical evidence from DSDP Site 362 on the Walvis Ridge indicated an onset of upwelling in the early late Miocene (~10 Ma) in the Northern Benguela region. The establishment of extensive eastern Antarctic ice sheets in the middle Miocene at ~14 Ma (Lawver and Gahagan, 2003) would have resulted in intensified trade winds due to an increased thermal gradient, resulting in increased Benguela upwelling (Berger and Wefer, 1996a; Uenzelmann-Neben *et al.*, 2002). Diester-Haass *et al.* (1992) suggested that the Benguela Current has shifted northwards since the middle Miocene, so that upwelling was initiated on the Walvis Ridge at 10.5 Ma, where upwelling was more intense during interglacial periods until 5.4 Ma. Recent work based on sediments from three ODP sites (1085-1087) in the Southern Benguela region, show that palaeoproductivity increased dramatically in the late Miocene at 6.7-6.5 Ma (Diester-Haass *et al.*, 2002). They argued that this high export productivity is simply not a local signal indicating the onset of upwelling, but rather reflects a response to changes in the global palaeoceanographic conditions (Berger and Wefer, 1996b).

University of Cape Town

2.5 GEOLOGICAL EVOLUTION OF THE WESTERN MARGIN

2.5.1 PRE-CRETACEOUS BASEMENT GEOLOGY

The Pre-Cretaceous basement geology of the western margin of southern Africa (Figure 2.5) is dominated by the late Proterozoic to early Paleozoic Pan-African volcano-sedimentary Gariep and Saldania mobile belts, overlying the metamorphic rocks of the 1500-900 Ma Namaqua Province (Thomas *et al.*, 1996; Frimmel and Frank, 1998). A network of Pan-African mobile belts formed during collision/subduction events associated with the assembly of Gondwana following the reversal of rifting at ±780-740 Ma of Rodinia (Rozendaal *et al.*, 1999; Frimmel and Frank, 1998).

The Malmesbury Group, which represents the main exposure of the southern Saldania Belt, crops out to the north of Cape Town (Rozendaal *et al.*, 1999). Three distinct terranes are defined within the Malmesbury Group by northwest-trending fault zones, namely the Tygerberg, Swartland and Boland terranes (from southwest to northeast), with an increasing complexity in the volcanosedimentary record to the north (Rozendaal *et al.*, 1999). The Malmesbury volcanic and sedimentary succession represents a variety of environments, from a rifted-margin succession in the northwest (Boland to Swartland terranes) to deeper-marine flysch-like deposits in the Tygerberg terrane (Rozendaal *et al.*, 1999). Closure of the rifted basins (proto-Atlantic) and collision/subduction between 600 and 545 Ma is associated with intrusion of the granitoids of the Cape Granite Suite. A minimum age for the Malmesbury Group is constrained by the 547±5 Ma age obtained for the Cape Granite Suite using SHRIMP zircon ages (Da Silva, 1997 cited in Rozendaal *et al.*, 1999). The granitoids of the Cape Granite Suite are all subduction-related and include S-, I- and A-types, resulting from three intrusive phases (Scheepers, 1995). Precursor mafic and intermediate volcanics are associated with Phase I and III of the Cape Granite Suite (Scheepers, 1995). The Colenso Fault, which separates the Tygerberg terrane to the southwest from the Swartland terrane to the northeast, extends from just northwest of Stellenbosch to the coast at Paternoster. This fault also separates the older S-type granites in the southwest from the younger I-type granites in the north, suggesting a deep crustal scale for this fault (Rozendaal *et al.*, 1999). In the Olifants River area, the southern remnant of the Gariep mobile belt is preserved together with the predominantly siliciclastic sediments (Nama and Vanrhynsdorp Group) of the syn-to post-orogenic Nama Foreland Basin (Frimmel and Frank, 1998).

The Ordovician (~500 Ma) to Carboniferous Cape Supergroup (~330 Ma) unconformably overlies the Malmesbury Group and the Cape Granites (SACS, 1980). The siliciclastic sediments of the Cape Supergroup can be subdivided into the Table Mountain, Bokkeveld and Witteberg groups, where the Bokkeveld Group is distinguished by its more argillaceous character (SACS, 1980; Broquet, 1992). The Cape Supergroup records a ~170 Ma poorly understood sedimentary history of widespread fluvial systems delivering sediments to a mid- to high latitude epicontinental sea. The Cape Supergroup is overlain by the Karoo Supergroup deposited in a retroarc foreland basin, which initially covered most of southwestern Gondwana (Cole, 1992). Deposition commenced with the Dwyka Group tillites in the late Carboniferous, which are overlain by a succession of offshore, deltaic and terrestrial sediments of the

University of Cape Town

Ecca, Beaufort and Stormberg Groups until late Triassic-early Jurassic. Sedimentation ceased with the extrusion of the early Jurassic Stormberg basaltic lavas (Cole, 1992; SACS, 1980).

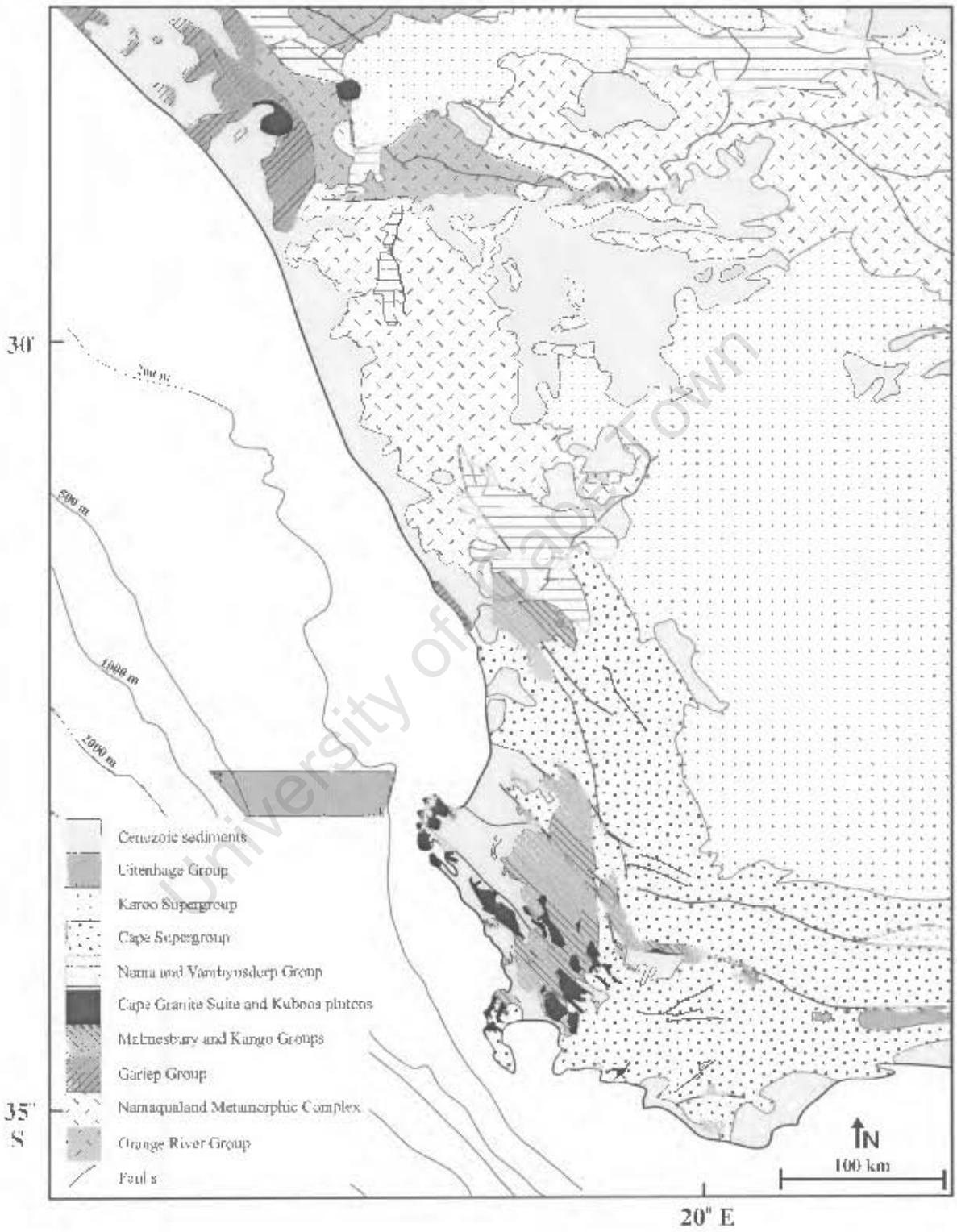


Figure 2.5. Geology of the southwest African continent after Hammerbeck and Allcock (1985) and modified after Scheepers (1995) and Rozendaal *et al.* (1999). The study area, Concession 20D, is shown as a grey polygon on the continental shelf.

University of Cape Town

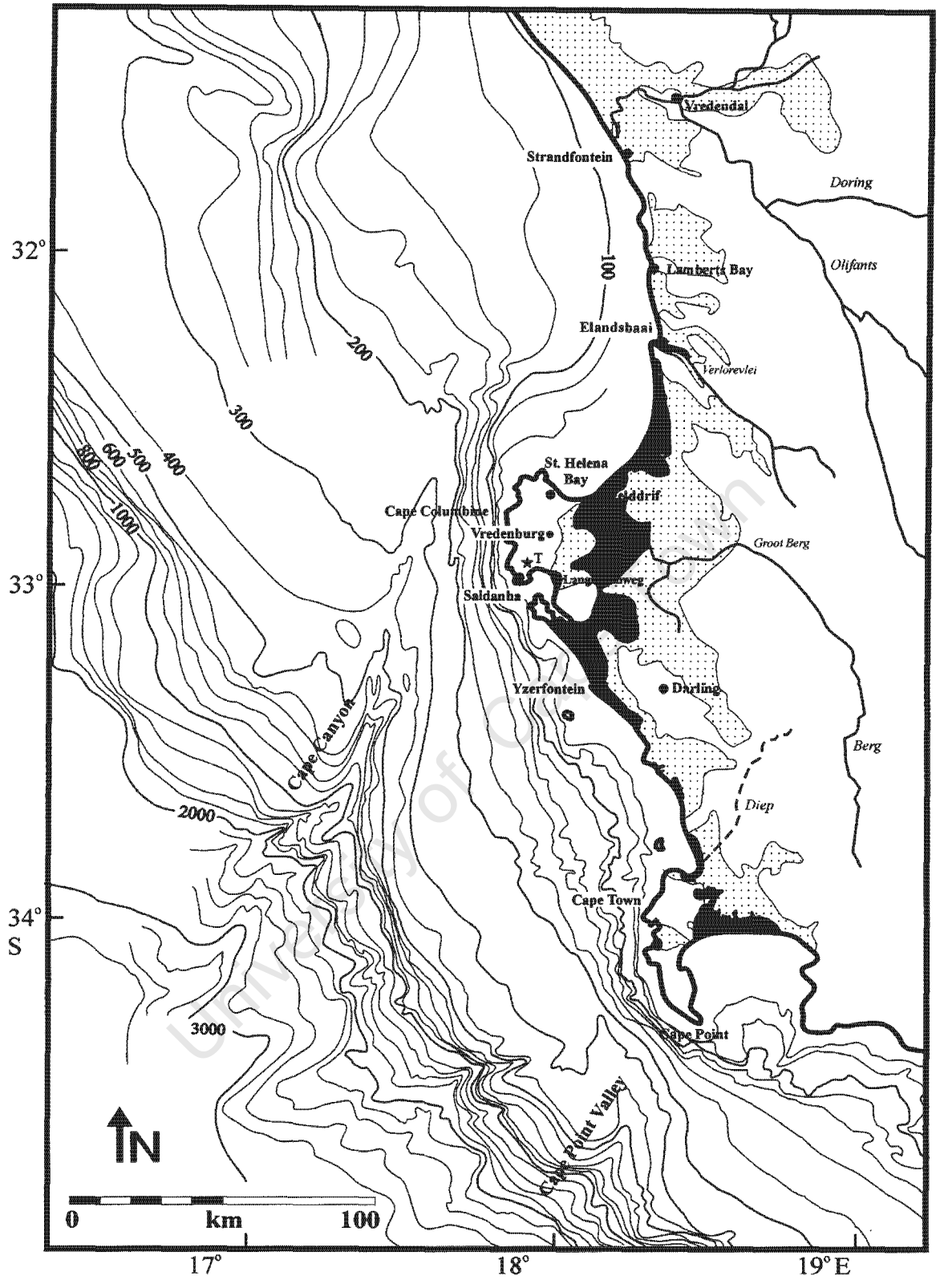
2.5.2 ONSHORE TERTIARY DEPOSITS

Three subgroups occur within the Cenozoic deposits of the West Coast of southern Africa, namely those of the Namibian, the Namaqua (Olifants to Orange Rivers) and the southwest Cape coasts (Pether *et al.*, 2000). Early Tertiary (Palaeogene) sediments are absent from the southwest Cape and Namaqua coasts, although the age of the kaolinised fluvial palaeo-channel deposits is poorly constrained (Pether *et al.*, 2000). Dale and McMillan (1999b) described the Eocene coastline as a low-energy environment with mainly fine-grained beaches. Only scattered Palaeogene deposits are found on the Namibian coast between the Orange River and Lüderitz (Dingle *et al.*, 1983). The Palaeogene deposits include the ~64 Ma Chalcedon-Tafelberg Formation and other silcrete cappings, the ~ 55 Ma Blaubock Gravels and the Eocene (42 Ma) marine and terrestrial units of the Buntfeldschuh Formation and Langental (marine) Beds (Pether *et al.*, 2000). The scattered outcrops of Neogene cover of the southwest Cape are best developed in the Saldanha region (Figure 2.6), where up to 120 m of sediment overlie the granitic basement (Rogers, 1980, 1982; Dingle *et al.*, 1983). The literature for the onshore record is often incomplete and inconsistent, with little consensus reached regarding the depositional age of the sediments and correlation among outcrops (Table 2.2). In contrast, the Namaqua coast has a more consistent series of elevated marine packages (Table 2.3), which have been extensively studied because of the significant diamond content in their basal gravels, with each package named after the elevation of its trangressive maximum (Pether *et al.*, 2000). The older three packages have warm-water molluscan assemblages, whereas the younger units have cold-water assemblages (Pether *et al.*, 2000).

2.5.3 THE OFFSHORE GEOLOGICAL RECORD

The bulk of the western continental margin is constructed of terrigenous Mesozoic sediments (Figure 2.7) with a veneer of middle to upper Tertiary sediments (Rogers and Bremner, 1991). The upper Tertiary sediments occur largely as a coast-parallel lens on the outer shelf and continental slope, but a thinner cover extends seawards far into the Cape Basin (Dingle, 1973a, Dingle *et al.*, 1983). Dingle (1973b; 1973c) noted that maximum Cenozoic sedimentation appears to occur in areas of maximum Mesozoic sedimentation, with deposition occurring as outbuilding lenses on the high-gradient regions of the Cretaceous continental slope. Dingle (1973a) suggested that the present width of the continental margin can be related to the thickness of the Cretaceous sediments, as discharge from the palaeo-drainage built a thick sediment wedge out over the margin, thereby acting as a further sediment trap for later sediment discharge. However, Tankard (1976) proposed that the late Eocene/early Oligocene volcanic activity of the Klinghardt extrusives of the Bogenfels area (Namibia) and the Agulhas Arch intrusives are evidence for crustal instability during the early Tertiary and defined a "tilt-axis" by this volcanic activity (that runs roughly parallel to the present coastline). He argued that tilting and warping has occurred since the early Tertiary as an explanation for the abnormally deep (±400 m) shelf break of the western margin (Figure 2.2).

University of Cape Town



LEGEND:

- Cenozoic sediments (Cole and Roberts, 1996)
- Bedrock topography <-20 to 0 m for areas south of Elandsbaai (Rogers, 1980)
- ★ Quarries (T: Tabakbaai; V: Varswater)
- Bathymetry (60 - 300 m in 20 m intervals; 1,000 - 3,600 m in 200 m intervals) after Dingle (1971b) and Dingle *et al.* (1987)
- Perennial (solid) and non-perennial (dashed) rivers (From 1: 2 500 000 Ground Water Resources of the Republic of South Africa, 1995; Published by Water Research Commission.)

Figure 2.6. The distribution of onshore Cenozoic sediments in the southwest Cape.

Table 2.2. A summary of the onshore Late Cenozoic geology of the southwestern Cape coast after Tankard, 1974, 1975, 1976; Dingle *et al.*, 1983; Rogers, 1980, 1982; Coetzee and Rogers, 1982; Hendey, 1982; Theron *et al.*, 1992; Rogers *et al.*, 1990; Senut *et al.*, 1996; Dale and McMillan, 1999b; Pether *et al.*, 2000 and Franceschini, 2003.

AGE		FORMATION		LITHOLOGY
Holocene	SANDVELD GROUP	Witsand$_2$		Aeolian calcareous quartzose coastal dunes, partly vegetated or unvegetated (Rogers, 1980).
Pleistocene		Langebaan$_1$		Aeolian calcrete-capped calcareous sandstone with *Trigonephrus globulus* and other terrestrial snails reaches a maximum thickness of 88 m (Rogers, 1980, 1982; Tankard, 1976). Interdune areas frequently associated with ferricrete horizons. The aeolinites hosts numerous fossils and the deposits range in age from mid- to late-Pleistocene (Pether *et al.*, 2000).
		Velddrif$_1$	Includes Milnerton Member of Rogers (1982).	Littoral calcrete-capped coquina deposited during Last Interglacial (~120 ka) when sea-level at +5 m (Tankard, 1976). The Milnerton Member is a local deposit related to the Diep River. It includes fluvial gravel, marine clay and littoral sand (ex-Rietvlei Formation (Diep River and Killarney members) of Rogers, 1980, 1982).
		Springfontyn$_2$	*Tentative inclusion of interbedded sand and mud of the Papkuils Member*	Aeolian well sorted, fine to medium, quartzose sand with a maximum thickness of ~68m, includes intermittent peaty layers (Pether *et al.*, 2000). All surficial quartz sands (Theron *et al.*, 1992) of the greater Cape Town area included into this formation.
		Post-Pliocene deposits were all included into Bredasdorp Formation of Rogers (1980, 1982.)		
Pliocene / Miocene (~5 Ma) [a] a: vertebrate fossils stratigraphy (Hendey, 1982) (Dale & McMillan (1999b) assign a Late Pliocene / Early Pleistocene biostratigraphic age) *Late Miocene hiatus* +30 m late Miocene regression Late Pliocene / Early Pleistocene age based on echinoid spines abundances (Dale & McMillan, 1999b)		Varswater$_1$ Saldanha Formation$_1$ *Conglomeritic Phosphorites from the Bomgat stratotype area are subsumed into the Gravel Member (Pether et al., 2000)*	*Informal subdivision: Varswater Quarry:* • Calcareous Sand Member (Anyskop) • Pelletal Phosphorite Member or Muishondfontyn Member$_a$ • Quartzose Sand Member Gravel Member or Koningsvlei Member[a] *(Includes the Strandfontein Member, the Duynefontyn and Silwerstroom Members, the Bookram Member)* a: Roberts (*pers. comm.*, 2002)	The Varswater Formation attains maximum thickness of 60 m (Pether *et al.*, 2000) • The fine bio-calcarenites, with sparse marine benthic foraminifera and sparse phosphatised grains assigned to Anyskop Member of Langebaan Formation (Pether *et al.*, 2000). • A moderately sorted medium to fine phosphatic-quartzose sand, with lenses and concretions of phosphatic sandstone with a maximum thickness of 25-28 m (Tankard, 1976). Shallow marine depositional environment (Tankard, 1976). • A moderately sorted fine to coarse quartzose sands, generally lacking phosphate with subordinate clay and lignitic clay; maximum thickness of ~15 m (Tankard, 1976; Pether *et al.*, 2000). Fluvial channels include abundant fossils (Hendey, 1982). Floodplain-estuarine-shallow marine depositional environment (Tankard, 1974; Rogers *et al.*, 1990). • 2m thick phosphatic gravel, including clasts of reworked phosphorite, and locally, coquina above a bedded microsphorite (Hendey, 1982; Tankard, 1975) (Tankard, 1975 notes that the coarse well rounded to fine sub-rounded quartz grains in a microsphorite matrix show characteristics (conchoidal breakage patterns and random V-shaped notches) of a high-energy littoral environment).
Middle Miocene [a] **OR** Late Middle Miocene [b] **OR** Mio/Pliocene [c] Latest Pliocene/Early Pleistocene [c] a: Pether *et al.* (2000) b: Roberts and Brink (2002) c: Franceschini (2003) d: Dale & McMillan (1999b)		Prospect Hill$_2$	• *Described from two excavations as:* *Upper quarry* *Lower quarry (or Diazville Member) 7* • *Lies unconformably above 40 m boulder beach, which is equated with 90 m Package of Namaqualand* [7]	Pether *et al.* (2000) describe the Prospect Hill Formation as a bioclastic carbonate (5-15% well rounded quartz) aeolianite banked up (maximum thickness of 70 m) against the basement granitic ridge, extending for 25 km form Saldanha to Paternoster (Roberts and Brink, 2002). Typically red (Fe) stained and included highly indurated pedogenic calcretes. The fossil egg shell of *Diamontornis wardi* found in this unit assigned an age of 12-10 Ma by Senut *et al.* (1996). Dale and McMillan (1999b) assign ages using foraminiferal stratigraphy. A latest Miocene / Pliocene age determined by Sr-isotope stratigraphy (Franceschini, 2003)
Early-mid to late Miocene Trangression Supercycle TB2 of Haq *et al.* (1987) (Roberts and Brink, 2002)		Elandsfontyn$_3$		Angular quartz gravelly sands and peaty clays (carbonate and phosphorite free) deposited in a tropical meandering fluvial system (Rogers, 1980, 1982; Coetzee and Rogers, 1982). (Partridge and Maud. 1987) link the sedimentation of the Elandsfontyn Formation with the Post-African I cycle of erosion)

1: Formation nomenclature approved by the SACS, 2: Formation nomenclature not yet recognised by the SACS; 3: Formation nomenclature not recognised by the SACS
SACS: Lithostratigraphic units recommended for use in publications and reports of the Council for Geoscience from http://www.geoscience.org.za/sacs/newlith.htm (Last revised on 17-Jul-2002).

University of Cape Town

Table 2.3. A summary of the Late Cenozoic marine packages of the Namaqua and the south-western Cape coast after Rogers *et al.*, 1990; Pether, 1994; Dale and McMillan, 1999b; Pether *et al.*, 2000 and Franceschini, 2003.

AGE	Formations of southwest Coast	Package	Namaqualand Coast [1,2,3]	Southwest Coast [4]
Early/Mid Holocene		2 m		Depositional environment grading from estuarine salt-marsh and mud flats through beach sands to aeolianites in a ±1.5 m succession adjacent to the Berg River Mouth deposited since sea-level attained its present day position in the mid-Holocene
Eemian/Weichselian		4 m		?Marine calcarenites and aeolianites limited to sites very close to present day coast and is the most widely distributed succession
Late Pleistocene (latest Cromerian. Earliest Elsterian) [4]		8-10 m (8-12 m) [1,3]	<12m packages assigned latest Pleistocene ages by Rogers *et al.* (1990)	Aeolianites, shelly calcarenites to green sandy clays deposited in lagoonal and estuarine environments
Late Pliocene (~3.3 Ma) [1, 2, 6] **OR** Early Pleistocene [3, 4]	Calcareous Sand Member and Pelletal Phosphorite Member of Varswater *(now Anyskop Member of Langebaan Formation)* [4] Prospect Hill "lower quarry" [7]	30 m (Includes "29-34 m beach" & "17-21 m complex") [2]	Lower shoreface prograding through upper shoreface to reworked/obscured foreshore sands, where the upper shoreface facies extensively preserved. Decalcification and pedogenic reddening common (Pether *et al.*, 2000). Meso-Orange terrace I[8]	Calcarenite outcrops in Tabakbaai Quarry [5] (or lower part of the Prospect Hill Formation deposit) and in the Langebaanweg-Varswater area.
Pliocene / Miocene (~5 Ma) [1] **OR** Latest Pliocene / Early Pleistocene [4]	Varswater [1] **OR** Prospect Hill "upper quarry" [4]	50 m (old 45-50 m Complex) [2]	Shoreline progradation deposit composed of a boulder beach basal gravel overlain by predominantly lower shoreface fine green sands (Rogers *et al.*, 1990) Meso-Orange terrace II[8]	Calcarenite outcrops in Tabakbaai Quarry [5] (or upper part of the Prospect Hill Formation deposit) and on western flank of Prospect Hill
Early-mid to late Miocene [1] **OR** Early to basal Mid Miocene [6] **OR** Early Pliocene [3]		90 m	Basal gravel with abundant silcrete overlain by reddened coarse to medium grained sands with heavy mineral laminae, with a Sr-age of 16 Ma (M. Lavelle, *pers. comm.* - cited in Pether *et al.*, 2000) Proto-Orange terrace II[8]	Absent

1: Pether *et al.* (2000); 2: Pether (1994); 3: Rogers *et al.* (1990); 4: Dale and McMillan (1999b); 5: Terminology after Franceschini (2003) as quarry also referred to as Prospect Hill and Diazville in the literature; 6: Pickford and Senut (1999); 7: Roberts and Brink (2002); 8: Pickford (2000).

University of Cape Town

Apart from a number of major slumps, referred to as the Cape Town, Childs Bank and Chamais slumps, the entire outer margin, at least between Childs Bank and Cape Town, is characterised by low-angle rotated slump masses, where the age of these rotational slumps is post-lower Pliocene as evidenced by the sediment succession in borehole DSDP Site 360 (Bolli *et al.*, 1978; Dingle, 1980b). The most likely trigger mechanism for slumping is interpreted as tectonic activity with additional contributions by along-slope undercutting by Antarctic Bottom Water (Dingle, 1980b; Dingle and Robson, 1992). Dingle (1980b) noted that most areas of slumping typically record multiple slump-events.

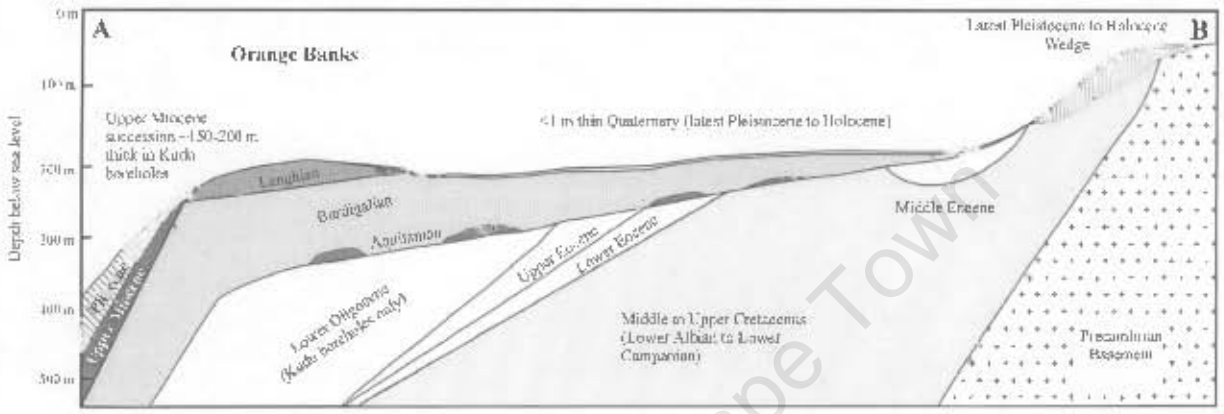


Figure 2.7. A simplified cross-section of the western continental margin of the northern Orange Basin after Corbett (1996) and modified by I. McMillan (*pers. comm.*, 2003) (refer to Figure 2.2 for location). McMillan (2003b) notes that the Lower Oligocene is observed only in the Kudu boreholes and appears to be absent from the rest of the Orange Basin further to the south.

2.5.3.1 CRETACEOUS

The Cretaceous sedimentary succession has been subdivided into three groups on the basis of well-defined horizons in the seismic record, with the rift succession overlain by an early drift and drift succession (*e.g.* Gerrard and Smith, 1982 and Section 2.1). The Cretaceous units of the continental shelf are overstepped by Palaeogene sediments and only very occasional inliers are exposed on the continental margin (Figure 2.7), although Upper Cretaceous sediments crop out ~60 m above present sea level in the Bogenfels area (Klinger, 1977). The Cretaceous rift-drift succession is therefore largely interpreted from borehole data (Chapter 4). Although the Cretaceous was a period of strong upward and outward building of the South African continental margin, local small buoyant blocks, such as the Columbine-Agulhas Arch, occur, which are largely devoid of sedimentation (Dingle, 1970b). Partridge (1998) argues that the massive volume of post-rifting Cretaceous erosion onshore and deposition in the offshore basins is evidence of the pre-rifting elevation of the continent, where an increase in sediment supply along the western margin during the late Cenomanian to Maastrichtian resulted in rapid up-building of the shelf (Rust and Summerfield, 1990; Dingle and Robson, 1992). The prograding outer edge of this sediment body is characterised by a large number of slumps and other post-depositional features (Dingle and Robson, 1992). These Late Cretaceous drift sediments beneath the Davie reflector form a lens, with maximum thicknesses in the vicinity of the present-day shelf break (Dingle *et al.*, 1983). Early

University of Cape Town

Cretaceous slumping events are recognised, where rapid sediment rates probably triggered the slumping (Dingle *et al.*, 1983).

The end of Cretaceous sedimentation is recorded by the Davie seismic horizon and signifies a distinct sedimentary hiatus in the marine record, reflecting a sea-level regression with a large proportion of the shelf deposits exposed to shallow-marine or subaerial erosion, so that Tertiary sediments lie unconformably above Mesozoic sediments (Bolli *et al.*, 1978; Dingle, 1973a). North of ~32° S the Cretaceous-Tertiary contact deepens from 300 to 800 m below the sea floor (Du Plessis *et al.*, 1972; Figure 2.2). The Cretaceous-Tertiary unconformity is intersected between 559-600 m below the sea-floor in the Kudu 9A boreholes (McMillan, 1990; Figure 2.2). The Davie unconformity is interpreted to result from uplift of the Orange Basin margin, with 1 km of uplift suggested by Aizawa *et al.* (2000).

2.5.3.2 CENOZOIC

The Cenozoic sedimentary history of southern Africa is characterised largely by low sea levels and marine erosion (Dingle, 1973c; Siesser and Dingle, 1981) and large-scale downslope mass movement of these sediments is commonly observed (Dingle and Robson, 1992). Cenozoic sediments form a coast-parallel lens on the continental margin, with the thickest and most extensive deposits found on the outer shelf and slope (Dingle *et al.*, 1983). Cenozoic sediment thicknesses on the slope are typically in the order of 1 to 1.5 km, although thicker successions are preserved off the local Orange River depocentre (Dingle *et al.*, 1983). Sediment rates decreased during the Cenozoic, particularly in the late Tertiary, with the establishment of the Benguela eastern boundary current upwelling system resulting in increased aridity along the West Coast (Dingle, 1980b; Dingle and Robson, 1992). Sites 1085, 1086 and 1087 (Figure 2.1), drilled during ODP Leg 175 (Wefer *et al.*, 1998) provided eleven high-resolution seismic-reflection profiles that allow for direct correlation (Table 2.4) between the detailed sediment record and the seismic profiles down to 600 m below sea-floor (Table 2.4; Wefer *et al.*, 1998; Uenzelmann-Neben *et al.*, 2002).

The bathymetry and surficial cover of the continental margin is described in detail in a trilogy of PhD theses (Birch, 1975; Rogers, 1977 and Bremner, 1981) with the marine sedimentology summarised in Figure 2.8 reflecting the classification of the surficial sediments from these studies. Biogenic and authigenic sediments dominate the Cenozoic sediment succession, which reflects the Benguela system input (Rogers and Bremner, 1991). West of Saldanha Bay and Cape Town, muddy quartzose sands mantle the inner and middle shelf, glauconitic sediment predominates on the outer shelf and foraminiferal ooze covers the continental shelf/slope (Rogers and Bremner, 1991). This broad sediment pattern is, however, complicated by the exposure of lower Tertiary and Cretaceous material within, and near to, the Cape Canyon (Dingle *et al.*, 1983). The Tertiary sediment history of the western margin can be divided into a lower Palaeogene and upper Neogene Tertiary succession, where a late Oligocene to early Miocene hiatus is commonly observed as an unconformity on seismic records (Dingle *et al.*, 1983). A similar erosional plane is observed on seismic records from the Agulhas Bank (Dingle, 1971a).

University of Cape Town

McMillan (1989) suggested an early Oligocene (Rupelian) to early Miocene (Aquitanian) age for this unconformity, which is present off the entire South African coastline. Dingle (1971a, 1973c), therefore, subdivided the Tertiary succession of the western continental margin into four time-equivalent, seismostratigraphic units on the basis of correlation of unconformities in the seismic records, with the major division between lower Tertiary (T_1) and upper Tertiary sediments. The upper Tertiary sediments are further subdivided into three subgroups, namely: T_2, T_3 and T_4. Figures 2.9A and B summarise the distribution of these sediment subgroups off the south-western margin of southern Africa.

Table 2.4. A summary of the relationship between seismic records and sediment data for the Orange Shelf. The core sediment data refers to the records from the Ocean Drilling Program (ODP) Sites 1085, 1086 and 1087 of Leg 175 (Shipboard Scientific Party, 1998a, b, and c).

Seismic stratigraphic units	ODP Leg 175 lithological units (Wefer *et al.*, 1998)	Seismic character and interpretation
CB-1		50-58 m thick. Incisions interrupt sea-floor indicating slide scarps or channels. Strong signal amplitudes and continuous style imply high impedance contrasts – supported by fluctuating grain sizes in 1086 and 1087 - Hemipelagic ooze with a glacial-interglacial cycle signature (or short-period sea-level changes).
	IA Nannofossil ooze	Reflector CB-A: ~1.5 to 1.6 Ma
CB-2		240-550 m thick (240m in 1086; 375 m in 1087, and 550 m thick at 1085 probably due to increased productivity associated with increased upwelling or may be a result of erosion in the south with larger scale glide scarps.) Weak reflectors, with continuous well-stratified layering, indicating a homogenous lithology due to hemipelagic deposition of clay and ooze. (Foramineral-nannofossil ooze in 1085-1087) Unit thins out towards shelf break and merges (toplap termination) with CB-1, indicating non-deposition/erosion on shelf (perhaps due to due to stronger currents).
	IA-B Nannofossil ooze	Reflector CB-B: 9.2-11.7 Ma (14.4 Ma at 1085 - older in the north). Undulated and disrupted by slide scarps and faults
CB-3	II Microfaulted clay-rich nannofossil ooze	235m in 1086; 330 m in 1087, and 155 m thick at 1085. Closely spaced reflectors of moderate amplitude due to hemipelagic sedimentation – with higher amplitudes reflecting carbonate content variations (lithification) caused by fluctuations in the CCD and dissolution. Similarly show toplap onto CB-1 due to erosion. Upper parts of the unit significantly disturbed by slide scarps. Reflector CB-C: ~14-28 Ma (age estimated using sedimentation rates)
CB-4		240m in 1086; 125 m in 1087, and 170 m thick at 1085. High amplitude due to hemipelagic sedimentation – with higher amplitudes reflecting carbonate content variations (lithification) caused by fluctuations in the CCD and dissolution. Reflector CB-D or Davie (base of Neogene?)

University of Cape Town

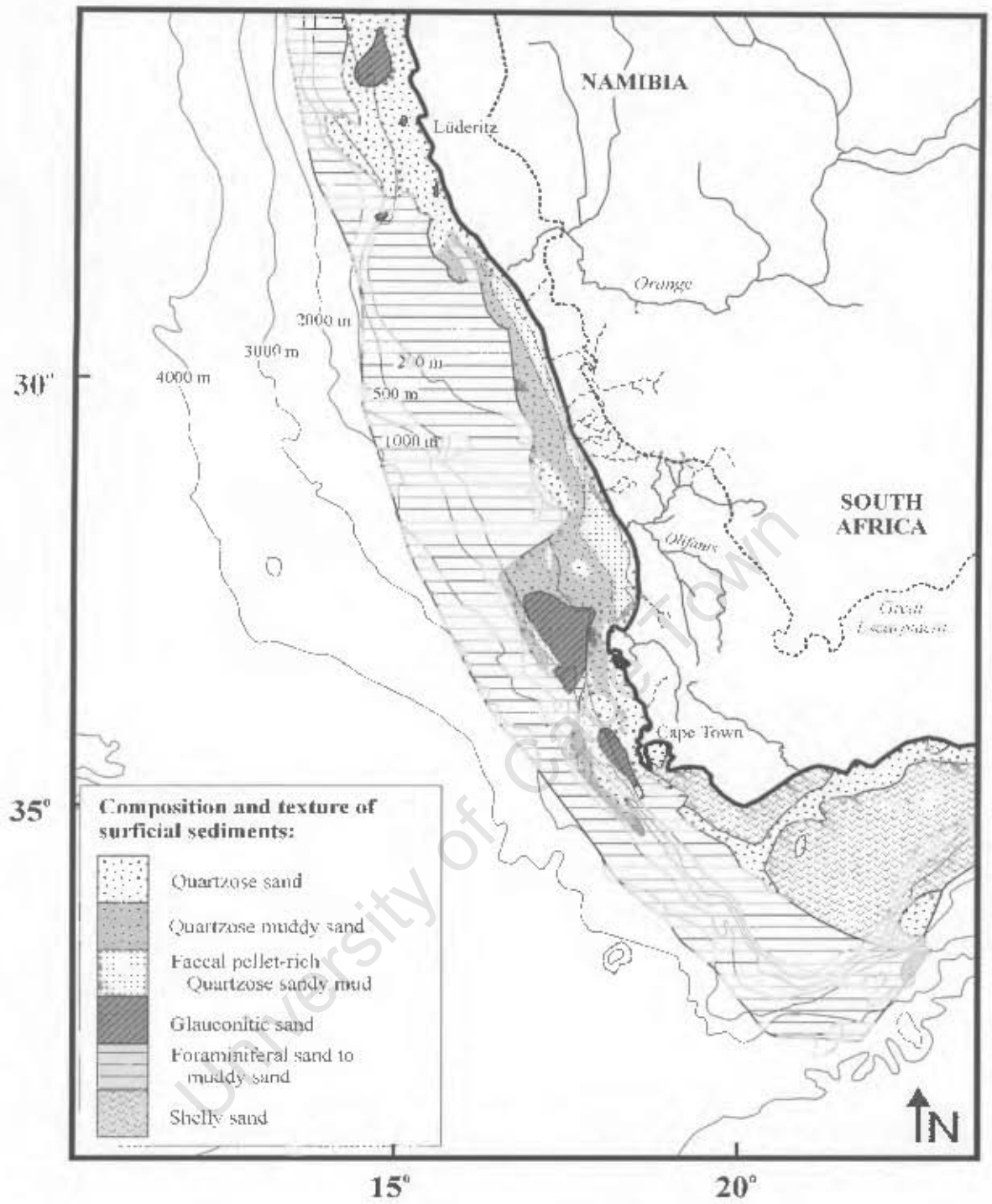


Figure 2.8. Distribution of the composition and texture of the unconsolidated surficial Holocene sediments after Rogers and Bremner (1991), Birch (1975) and Rogers (1977).

University of Cape Town

2.5.3.3 LOWER TERTIARY / PALAEOGENE

Palaeogene sediments underlie most of the western continental margin (Figure 2.7), although exposure is limited to a narrow, coast-parallel strip (Dingle *et al.*, 1983). The Palaeogene is dominated by strong upbuilding of the shelf (Dingle, 1971a) and Palaeogene sediments form a seaward-thickening wedge, which has a maximum thickness of 900 m southwest of the Orange River (Dingle *et al.*, 1983). The Lower Tertiary (T_1) unit is assigned a minimum ?Palaeocene/Eocene age by Dingle (1971a). A similar age is assigned to the sediments above the Davie unconformity in DSDP Site 361 (Bolli *et al.*, 1978).

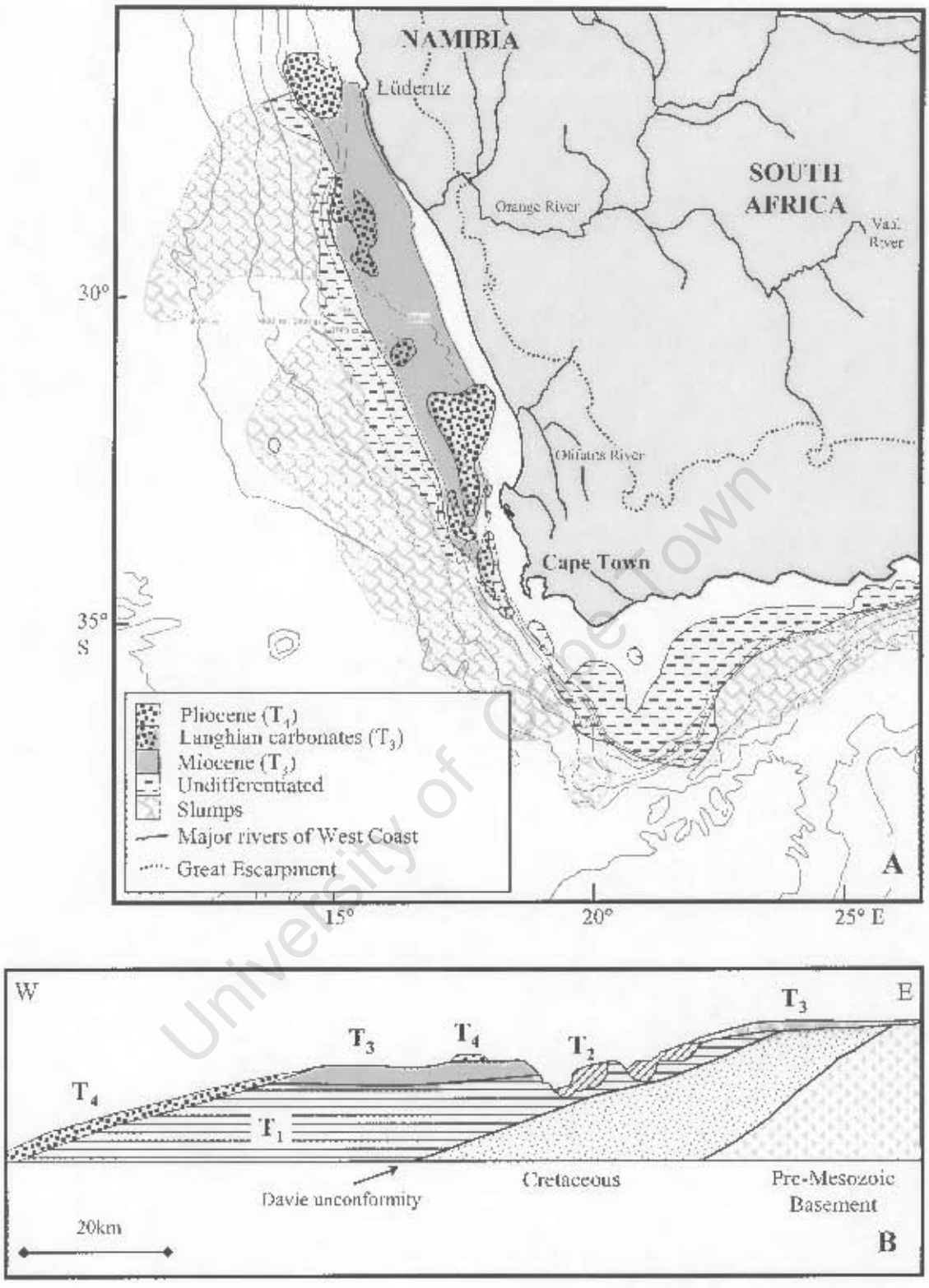


Figure 2.9. A: Distribution of Late Tertiary sediments (T_1-T_4) modified after Dingle (1971a); Dingle *et al.* (1983) after I. McMillan, *pers. comm.* (2002). Refer to text for explanation of Tertiary units. The Orange Banks is now considered Langhian (I. McMillan *pers. comm.*, 2002) and not Pliocene as originally proposed by Dingle (1971a; 1973c).
B: A summary of the seismic section and geology of the Cape Canyon (Line 20 off Yzerfontein) after Dingle (1971a; 1973c).

University of Cape Town

Relatively little is known about the lithofacies and internal stratigraphy of the lower Tertiary succession (Dingle *et al.*, 1983) and the lower Cenozoic sediments are described largely from borehole data (Dingle *et al.*, 1983). The Kudu 9A-1 borehole, located offshore of the Orange River, within this thick Palaeogene succession, has a thin outer shelf/upper slope upper Palaeocene to lower Eocene foraminifera-rich clay unconformably overlain by upper Eocene and lower Oligocene middle to outer shelf shelly clays and silts with abundant foraminifera (McLachlan and McMillan, 1979; McMillan, 1990; Dingle *et al.*, 1983). The dominance of biogenic material in the Palaeogene units suggest low terrestrial input (McLachlan and McMillan, 1979), where the large benthic foraminifera from various Eocene (*Discocyclina* spp.) and lower Oligocene (*Nummulites* and *Operculina* sp.) deposits suggest warm water (McLachlan and McMillan, 1979). Dale and McMillan (1999b) noted that middle Eocene (42-40 Ma) green clays were deposited in poorly oxygenated waters. Rogers (1977) described quartzose limestone and lime mudstones cropping out on the middle shelf region (50-200 m) between 25° and 30° south. Comparison with south-coast deposits (Siesser, 1972) suggests a Palaeocene-Eocene age. Some of these limestones have been extensively cemented by a carbonate-fluorapatite cement (Rogers, 1977), although few phosphatised samples were dredged to the north of 30° S.

Erosional unconformities define both the upper and lower contacts of the lower Cenozoic succession (McLachlan and McMillan, 1979). The upper contact is a well-defined and extensive reflector observed on seismic records, which has been interpreted as an erosional surface resulting from a late Oligocene lowstand (Dingle *et al.*, 1983). McMillan (1990) noted that the lower Miocene (upper Aquitanian to Langhian) is found unconformably above the lower Oligocene in the Kudu 9A-1 to –3 boreholes and states that the absence of an upper Oligocene unit is typical of South African continental shelf deposits. Dingle and Robson (1992) noted that faulting was a continual feature of the lower Tertiary to the west and south of Cape Town, which has resulted in a thick sediment succession at the base of the end-Cretaceous continental slope.

University of Cape Town

2.5.3.4 UPPER TERTIARY / NEOGENE

The Lower Tertiary (T_1) sedimentary period was brought to a close by a major regression (Dingle, 1971a, 1973c). The lower to upper Tertiary (T_1 to T_2) unconformity is associated with large-scale erosional event on the South African margin and it has been proposed that the erosion of the Cape Canyon by the palaeo-Olifants River during a sea-level regression was initiated at this time (Dingle, 1971a, 1973c; Dingle *et al.*, 1983). The upper Tertiary succession of the western margin is more complex than the underlying sediments and Dingle (1971a) subdivided the succession into three lithological units (T_2, T_3 and T_4), which are confined to the outer shelf and in the vicinity of the Cape Canyon.

The T_2 beds are interpreted to represent Oligocene cut-and-fill structures, which have eroded into the Eocene clays and possibly into the Upper Cretaceous in the Cape Canyon during the Oligocene regression (Dingle, 1971a). The T_2 sediments are interpreted as having a fluviatile to shallow-marine

origin, formed under conditions of rapidly changing sea level. The series of infilled channels in the Cape Canyon record a complex history of fluvial activity, where the T_2 deposits represent the initiation of the Cape Canyon sedimentary history. Dingle (1971a) suggested that these sediments were deposited during a major hiatus between the lower and upper Tertiary sediment successions. The fluvial/shallow marine conditions are brought to a close by another major transgression and the deposition of the T_3 sediments.

Lower Miocene sediments (T_{3a}/T_{3b})

Lower Miocene (T_3) sediments cover most of the shelf and upper slope and form a seaward-thickening wedge (Figure 2.8), where the Miocene unit tends to be flat-lying or dip seawards at a very shallow angle (Dingle *et al.*, 1983). Dingle (1973c) proposed that the lower Miocene sedimentation was strongly influenced by the Lower Tertiary ridge, a narrow magnetic high lying between 29° and 32°S on the mid to outer shelf, with a marked thinning of deposits above this ridge. The outer-shelf unconsolidated Miocene sediments are capped by a 10-20 cm thick carbonate-cemented crust/hardground, where extensive erosion from the upper Miocene to the Pleistocene has planed off the upper surface of the lower Miocene unit (McMillan, 1989). The limestones are all phosphatised to some degree, with phosphorite conglomerates (>18% P_2O_5) recognised. Phosphatisation of the Miocene carbonate sediment succession is common along the west and south coast continental margin of southern Africa (Parker, 1971; Parker and Siesser, 1972; Siesser, 1978a), where the average P_2O_5 concentration of these rocks is 15 %. Francolite has replaced the micrite matrix of the *in situ* Miocene limestones under submarine conditions (Parker and Siesser, 1972). Below the surface hardground, cementing is generally poor, and the sediments are either stiff clays or compacted biogenic sands (I. McMillan *pers. comm.*, 2003). Three distinct sedimentary units have been recognised in the lower to middle Miocene or T_3 succession, with the Aquitanian, Burdigalian and Langhian units separated by erosional surfaces (McMillan, 1989, 1990; Dingle *et al.*, 2001).

Lower Miocene sediments are interpreted to extend from just below the sea-floor to a depth of approximately 300 m in the Kudu 9A boreholes (McMillan, 1990), and the maximum recorded thickness of the Miocene carbonate unit is ~180-200 m on the outer shelf (Corbet, 1996; I. McMillan, *pers. comm.*, 2003). The dominance of biogenic material suggests low terrestrial input and well-oxygenated water; lithic fragments, glauconite and phosphorite are generally rare (McMillan, 1990). The large benthic foraminiferal assemblage (*Heterostegina* and *Miogypsina* in particular) suggests warmer water temperatures (Christison, 1985; McMillan, 1986) and the ostracod assemblage supports a sub-tropical/ tropical climate until at least the Langhian (Dingle *et al.*, 2001). The ostracod assemblage of the western continental shelf indicates that sub-tropical conditions prevailed, with water temperatures >20°C, during the early to middle Miocene (Aquitanian to Langhian), where the ostracod assemblage of slope sediments (ODP Site 1087) show a significant faunal change in the middle Miocene (16-13 Ma) (Dingle *et al.*, 2001).

University of Cape Town

A local erosional unconformity is recognised in the Miocene succession to the west of the Cape Canyon, where the T_{3b} unit lies unconformably above the T_{3a} unit. The T_{3b} unit has been interpreted to represent a second cycle of erosion in shallow marine/fluviatile conditions (Dingle, 1971a). The return to shallow marine/fluvial activity at the end of the T_{3b} phase resulted in further cut-and-fill type deposits in the Cape Canyon (Dingle, 1971a). A veneer, usually no thicker than about 50 cm, of Quaternary sediments is deposited above these Miocene calcareous sediments (Compton *et al.*, 2002; McMillan, 1989; I. McMillan, *pers.comm.*, 2003; Rogers, 1977.

Pliocene sediments (T_4)

The horizontal Pliocene T_4 beds were largely removed by post-Pliocene erosion with only perched outliers remaining on the middle and outer shelf (Dingle, 1971a, 1973c; Dingle *et al.*, 1983) although up to 160–180 m of Pliocene material is locally preserved in the Cape Canyon/Saldanha region (Dingle *et al.*, 1983; Dale and McMillan, 2003a). A thick (<1200 m) Pliocene sediment succession is preserved on the upper continental slope at water depths greater than 500 m from Cape Town to Lüderitz (Dale and McMillan, 2003a; Figure 2.7). Pliocene sediments, at least between Childs Bank and Cape Town, are extensively affected by post-Pliocene slumping where the entire outer margin is affected by low-angle rotated slump masses (Dingle, 1980b; Dingle *et al.*, 1983).

Birch (1975) proposed that the terrigenous sediments were reworked out onto the outer shelf during the major late Tertiary transgressive/regressive cycle (T_4) of Dingle (1970b; 1971a). However, the composition of the lower Pliocene sediments is reported to be calcareous clays with a high proportion of authigenic minerals and little terrigenous material (Dingle *et al.*, 1983; Dale and McMillan, 2003a). Dingle *et al.* (1983) proposed a shallow-marine, locally high-energy, environment of deposition, with low terrigenous input and a strong Benguela upwelling signature. The Pliocene is characterised by low oxygen concentrations at the sea-floor, resulting in foraminiferal assemblages dominated by only a few benthic foraminifera species, such as *Epistomella pulchella*, *Nuttallides* sp. and ribbed and spinose *Uvigerina* spp. The uppermost lower Pliocene (upper Zanclean) succession contains the cold-water planktic species (*Globigerina pachyderma*), which marks a decrease in water temperature from the warmer than present temperatures of the early and middle Miocene (McMillan, 1986).

2.5.3.5 PLEISTOCENE AND HOLOCENE

The majority of the Quaternary deposits of the continental shelf are located at the base of the pre-Cretaceous inner-shelf platform as a wedge deposited on the inner shelf slope in water depths of 30-120 m (Williamson and Stevenson, 1999). Quaternary sediments range in thickness between 5 to 60 m (Birch *et al.*, 1991), where the 2–8 m thick Holocene mud-belt lies above the Pleistocene sand wedge in the middle shelf region (Birch *et al.*, 1991). Pleistocene and Holocene sediments are typically present as a thin veneer (≤1 m), reflecting continued erosion and reworking during repeated late Pleistocene lower sea levels together with, in general, a low input of terrestrial material onto the continental shelf throughout the Quaternary (McMillan, 1993; Corbett, 1996). The vast majority of the offshore

University of Cape Town

Quaternary deposits are confined to the deltas of the Orange, Olifants and Berg rivers (Figure 2.2). The sand fraction of littoral sediments tends to move northwards along the inner shelf by longshore drift (Rogers, 1977). However, the suspended fine fraction is deposited on the middle shelf between 70 and 120 m water depth, by a poleward-flowing bottom current (De Decker undercurrent) as far south as Cape Town (Rogers, 1977; Birch *et al.*, 1991; Rogers and Bremner, 1991; Shannon and Nelson, 1996; Figure 2.8). The mudbelt, which is about 40 km wide has an average vertical thickness of 15 m, but it can be as thick as 35 m in the Orange River prodelta. Seaward of the mudbelt, the continental shelf is covered by a coarse, relict sand, diluted with Holocene mud (Rogers and Li, 2002).

Erosion and reworking, during the regressive-transgressive cycles of the late Quaternary, left few complete sediment records for this time and the best Pleistocene records are therefore preserved on the continental slope (McMillan, 1993). In addition, Birch *et al.* (1991) suggested that the paucity of Quaternary sediments could be the result of winnowing by strong current and water action during sea-level regressions, and that much of the sediment could have been lost over the shelf break into the adjacent Cape Basin. The Cape Canyon would also have acted as a conduit for sediment transport (Dingle, 1973a). The Quaternary sediment succession from the Orange River Prodelta is typically a fining-upward transgressive sequence with a very condensed (LGM) basal gravel overlain by a ~2 m thick mud (Compton *et al.*, 2002). Occasionally, a similar fining-upward unit is recognised below the LGM transgressive system tract (Williamson and Stevenson, 1999).

University of Cape Town

3 INTRODUCTION TO THE STUDY AREA, METHODOLOGY AND TERMINOLOGY

3.1 WESTERN MARGIN

The terminology used in this study follows the conventions established by previous studies on the western margin of southern Africa (Dingle, 1973c; Birch, 1975; Rogers, 1977; Dingle *et al.*, 1983). The morphology the western margin (Figure 3.1) is described in detail in Chapter 2. The continental shelf of the western margin is generally wide, reaching a maximum width of ~200 km off the Olifants River. The continental shelf is largely devoid of any distinct bathymetric features except for Childs Bank, a flat-topped plateau at 200 m water depth at the edge of the shelf, west of Hondeklip Bay. However, the shelf break maintains an approximate NNW-SSE strike resulting in it considerably narrowing of the shelf to the south of St. Helena Bay (Figure 3.1). The shelf is at its narrowest at ~60 km west of Cape Columbine and the Cape Peninsula (Figure 3.1; Birch, 1975). The narrow shelf off Cape Columbine shows a pronounced inner-shelf slope, where the narrowness and steepness of the shelf obscures the relationship between the middle to inner shelf, although Birch (1975) notes that the rocky platform is between 5.5 and 9 km wide west of Cape Columbine and with the inner (rocky platform) to middle shelf transition is reported to occur at ~140 m water depth west of Cape Columbine (Birch *et al.*, 1991). The narrow and rugged continental shelf and steep continental slope south of St. Helena Bay reflects the buoyant continental margin above the Columbine-Agulhas Arch, which has remained buoyant since the Palaeozoic (Dingle, 1979; Dingle *et al.*, 1983).

The Cape Canyon (Figure 3.2) was first mapped by Simpson and Forder (1968). A project to investigate the structure, sedimentology and oceanography of the Cape Canyon was initiated by SANCOR (South African National Committee for Oceanographic Research) in 1984 using bathymetric and seismic data collected by the *Thomas B Davie* in 1979 and the *Africana II* in 1984 (Dingle, 1986). The Cape Canyon has a longitudinal extent of at least 200 km and can be traced to a water depth of at least 3600 m (Dingle, 1970a), where the topography of the distal end is rugged and complex (Dingle, 1986). The head of the Cape Canyon is located ±25 km west of Cape Columbine, where it forms a well-developed trench on the continental shelf, 100 m deep and 4 km wide in water depths of ~200 m (Dingle, 1986). The canyon no longer represents a distinct bathymetric feature 8 km to the northeast (Dingle, 1986). The Cape Canyon becomes progressively broader and deeper south of Cape Columbine, and adjacent to Cape Town at a water depth of 1500 m, the canyon has a local relief in the order of 500-800 m (Simpson and Forder, 1968; Dingle, 1986). Dingle (1986) subdivided the Cape Canyon into three sectors on the basis of wall morphology and thalweg (line joining deepest points in the channel) gradient. The proximal sector, in water depths of ≤450-500 m, is up to 3 km wide, has relatively smooth walls, a mean up-canyon orientation of 015° and a remarkably constant gradient (1:400). The middle sector, in water depths of 500 to 1000 m, shows complex wall morphologies most likely due to slumping (Dingle, 1986), with canyon-parallel and oblique depressions and gullies, which give rise to two thalwegs. The mean orientation of the canyon is similar to the proximal sector, but the thalwegs change to an

University of Cape Town

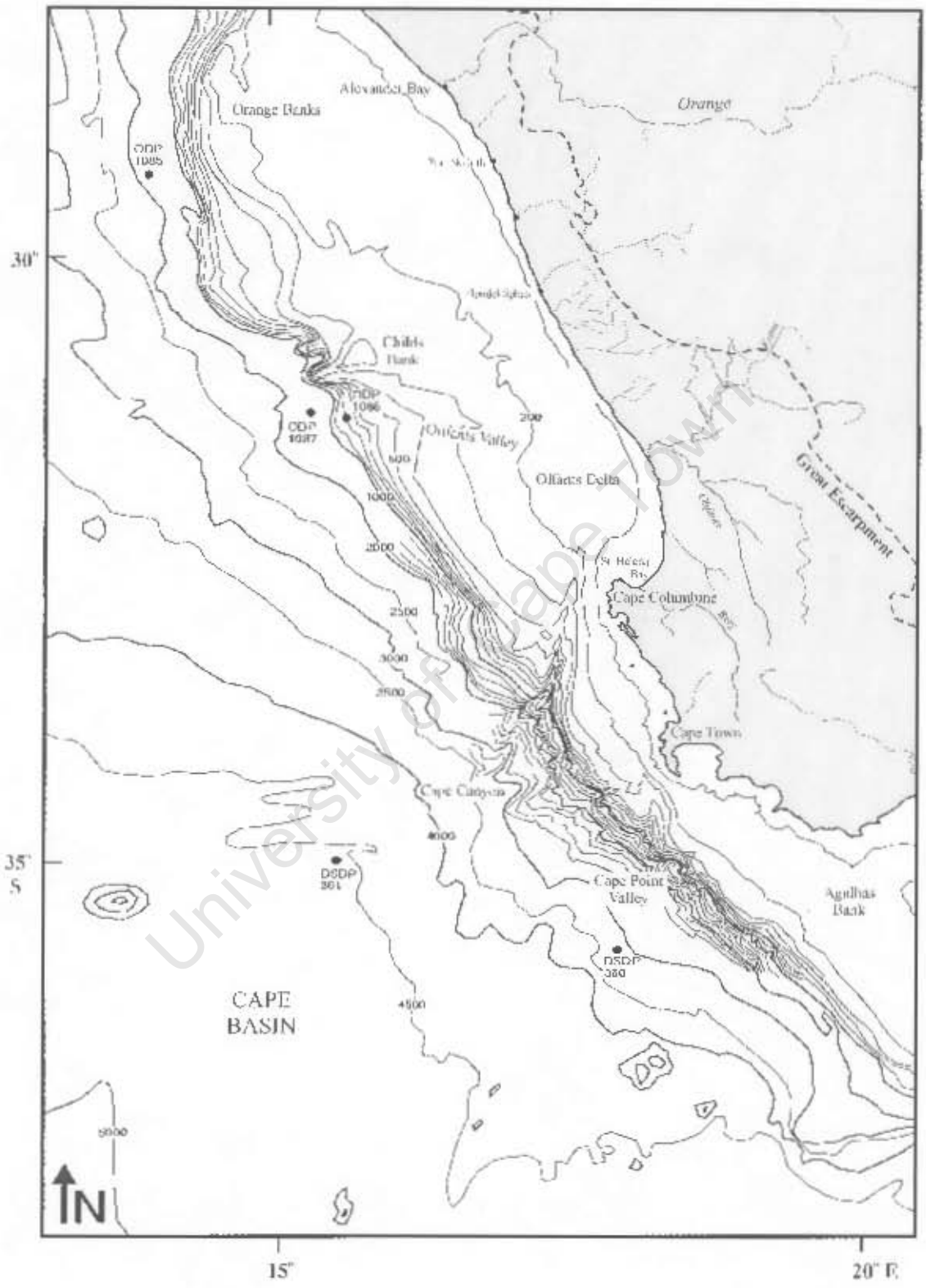
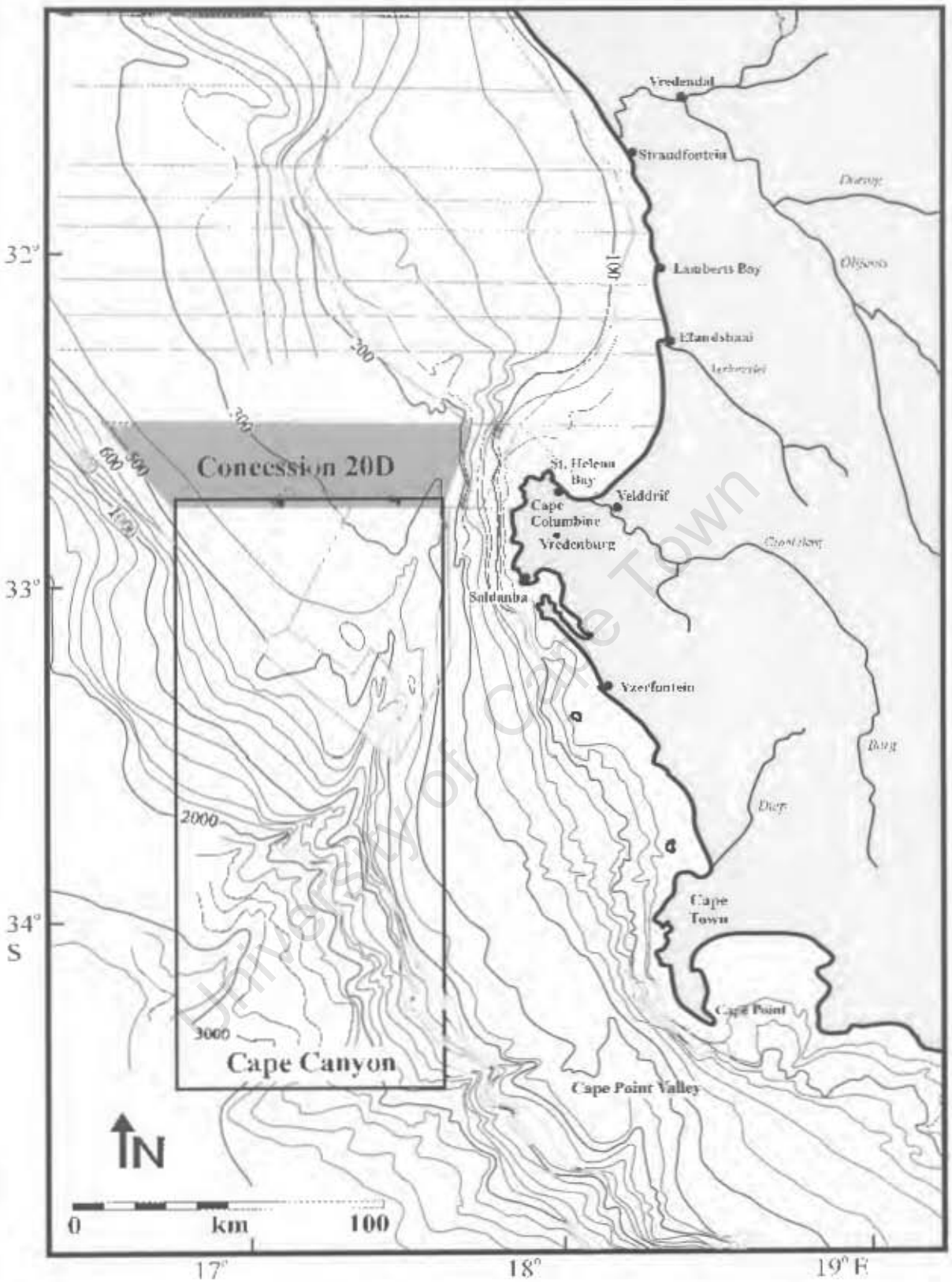


Figure 3.1. The bathymetry of the western margin showing the major bathymetric features (after Birch (1975), Dingle *et al.* (1987).

University of Cape Town



University of Cape Town

LEGEND:

Bathymetry (60 - 300 m in 20 m intervals; 1,000 - 3,600 m in 200m intervals) after Dingle *et al.* (1987).

Primary (dark) and secondary (light) drainage patterns

Offshore Diamond Concessions

Figure 3.2. The location of the study area, Offshore Diamond Concession 20D, in relation to the Cape Canyon on the western margin off Cape Columbine.

orientation of 061° when the canyon emerges onto the upper slope. The distal canyon, at water depths >1000 m is narrow, deeply incised and slightly sinuous. Mass transfer of sediments down the axis of the canyon in the proximal to middle sectors, would explain the steepening of the more distal canyon where the change in orientation could reflect the need to bypass the partial blocking of the canyon by slumped sediments. Simpson and Forder (1968) noted that there is no ready explanation for the NNE/SSW trend of the Cape Canyon, which cuts obliquely across the continental margin (Figure 3.1).

A number of arguments have been proposed regarding the formation of the Cape Canyon. Simpson and Forder (1968) suggested that turbidity currents are responsible for the excavation of the Cape Canyon, which is still actively in progress, since none of their profiles indicate sediment accumulation at the foot of the canyon. Tankard (1976) suggests that the presence of the Cape Canyon probable affected the sedimentation history along the western margin in the St. Helena Bay area, by acting as a sediment conduit. Dingle (1971a) suggested that the Cape Canyon was initiated as a series of channels that were eroded and infilled during the Oligocene regression. Because the head of the Cape Canyon crosses the shelf only 70 km from the modern Olifants River mouth, it has been proposed that the Cape Canyon was cut by the proto-Olifants River during the Oligocene lowstand (Dingle, 1971a; Dingle and Hendey, 1984; Dingle, 1992/1993). Dingle proposed that the Karoo River (palaeo-Orange) used the southern breach in the Great Escarpment at ~31°S from the Cretaceous to end-Oligocene. A thick wedge of muddy sediments, which has prograded seawards from the Olifants River area, cause a strong seaward bulge in the isobaths north of Cape Columbine and it is most likely that the head of the Cape Canyon lies buried beneath this sediment wedge (Dingle, 1971a, 1971b; Stevenson, 1992).

Dingle and Robson (1992) describe a large sedimentary cone (submarine fan) developed at the distal end of the canyon, extending across the continental rise, with the extent of the original fan obscured by Neogene slumping events and erosion by Antarctic Bottom Water (Dingle and Robson, 1992). Dingle (1980b) notes that the main *en echelon* glide-plane associated with the Cape Town Slump on the continental slope appears to swing along the trend of the Cape Canyon so that the Cape Town Slump is deflected to the west around the Canyon shoulder. Dingle (1980b) therefore suggests that the distal parts of the Canyon (below ±1000 m) may not be a simple canyon profile, but a complex of north-trending tensional depressions associated with the Cape Town Slump, which, in turn, suggests that the margin-oblique orientation of the canyon may be in some way controlled by slump glide-planes.

3.2 SAMPLE COLLECTION AND GEOPHYSICAL DATA

The study area for this thesis is the deep-water Offshore Diamond Concession 20D (Figure 3.1). Concession 20D extends from the 190-200 m isobath in the east to ~500 m water depth, adjacent to Cape Columbine on the western margin and encompasses an area of 2,918 km^2. The head of the Cape Canyon, which is the focus of this study, lies in the eastern sector of Concession 20D. The four corner coordinates for Concession 20D, from the top right (NE) in a clockwise order are, 32°33'30"S/17°42'58"E; 32°49'39"S/17°37'42"E; 32°49'39"S/16°44'26"E and 32°33'30"S/16°30'44"E.

University of Cape Town

The exploration programme of Concession 20D, which provided the material for this study was undertaken by Werner Marine Research (Pty) Ltd, subsequently referred to as WMR, while the writer was an employee. I was involved in most aspects of the exploration programme, and spent a month at sea, during which time 300 of the cores from Concession 20D were collected and logged. Two reconnaissance sampling survey cruises, *i.e.* Leg I (28 /03 to 03/04 and 23 to24/04/96) and Leg II (27/04 to 23/05/96), were carried out in Concession 20D, on behalf of WMR by RACAL Survey Limited on board the *M/V Kommandor Therese*. Bathymetric lines were collected along the ship's track and additional bathymetric data were acquired during weather downtime during both cruises. WMR concluded its exploration programme of Concession 20D and the company ceased operations in 1998.

Bathymetric data were obtained using an Atlas Deso 25 Echo Sounder; TSS 320 Heave Compensator; Hull mounted 33/210 kHz Transducers and a Valeport 600 CTP Probe. A total of 1,467 line kilometres of bathymetric data were collected from Concession 20D. All charted bathymetric soundings were processed onboard and reduced to Lowest Astronomical Tide (LAT), based on predicted tide tables for Saldanha, where LAT is 0.91m below Mean Sea Level (MSL) at Saldanha. The data were filtered for spiking and a 1 m resolution was retained. The contoured bathymetric data used during this study are summarized in Figure 3.3. The bathymetric data, as well as all other spatial data, are presented as UTM coordinates using the WGS 84 spheroid and the 15° Central Meridian with a false Easting of 500,000 m and a false Northing of 10,000,000 m.

Sediments were collected using the Alluvial Mining 6 m Vibrocorer, comprising a 7.8 m long frame, a 6 m demountable tripod base, a vibrating piston head and a detachable core barrel. In use, the core barrel is primed with a 6.45 m long PVC core liner with an internal diameter of 84.14 mm. The base is sealed with a rosette-type brass core catcher and core cutter. A total of 359 acceptable cores (>1 m) were collected from Concession 20D during the sampling operation (Figure 3.3), with the vast majority of the samples collected from the Cape Canyon Head region. The <6 m cores were cut into 1 m sections and each section cut in half, length-ways, using a band-saw onboard. Half of each core was plastic-wrapped and archived. The geologists onboard drew a preliminary descriptive core log, based largely on the macroscopic characteristics of the sediments, although occasional subsamples were collected and examined under the microscope when time allowed. Samples rich in gravel were jigged (using a 2 mm wire mesh jig-sieve) and the gravel fraction bagged. Preliminary studies, undertaken by the WMR geologists, resulted in a large number of facies types being loosely defined on the basis of composition, grain size, colour and micro-/macrofaunal content.

WMR geologists selected a number of samples for detailed biostratigraphic and chemostratigraphic analyses in order to refine the stratigraphic relationship between sediment types. Eight representative samples selected for chemostratigraphic analysis were submitted to J. Harmer at the Council for Geoscience in Pretoria for Sr-isotope dating (Table 3.1). The samples were washed and sieved at the Werner Marine Research (Pty) Ltd laboratory. Mixed foraminifera-carbonate fragments were picked, except for a sample from Core 72, where glauconite was picked due to a low faunal content.

University of Cape Town

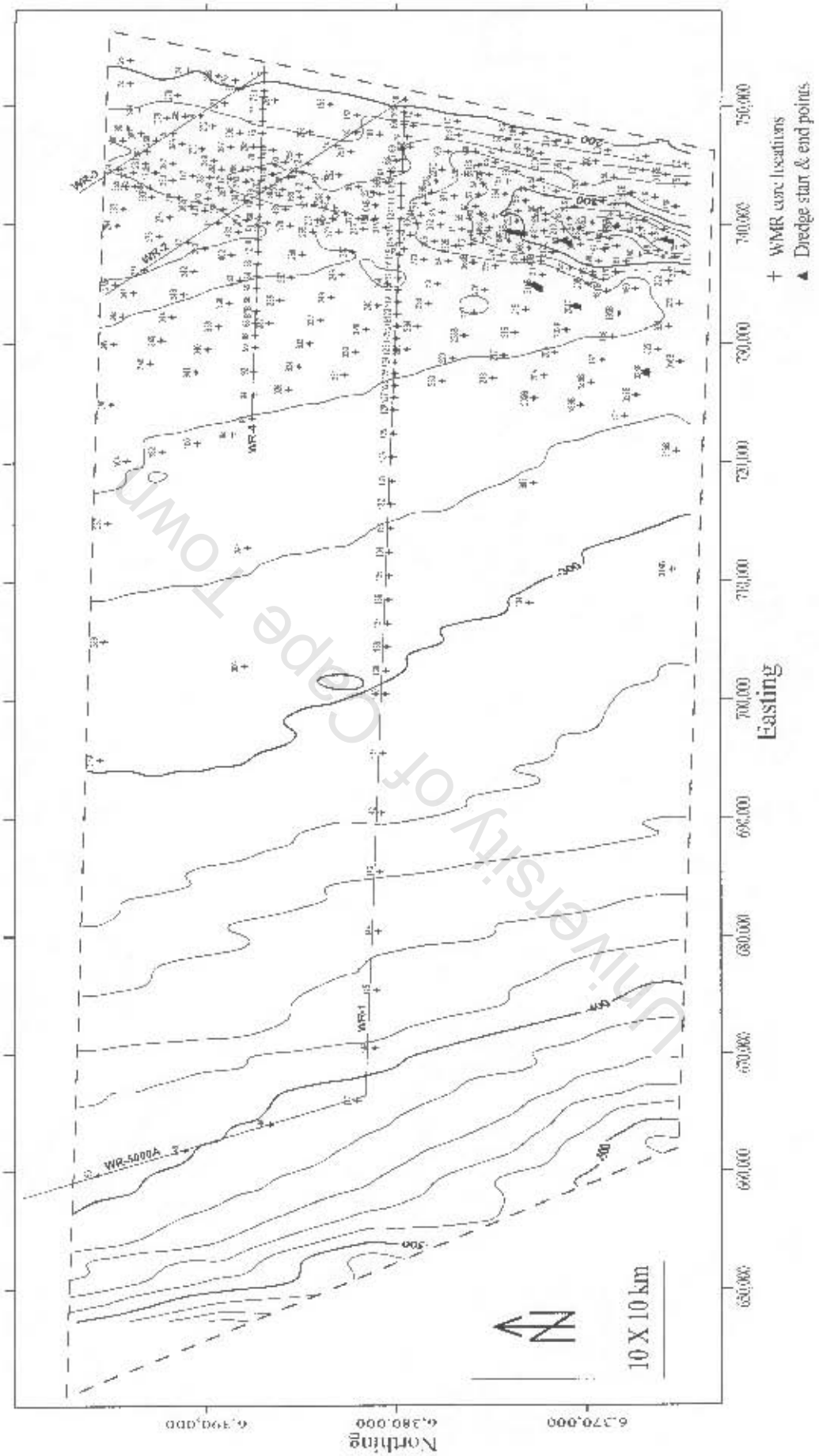


Figure 3.3. The location of the WMR cores and dredges in Concession 20D in relation to the track charts of the seismic lines undertaken by Benguela Concessions (Pty) Ltd.

University of Cape Town

In addition, two wood samples from Core 151 (=2.65 m) and Core 179 (90-95 cm) were selected and sent for dating to M. Bamford at the Bernard Price Institute for Palaeontological Research at the University of the Witwatersrand, Johannesburg. The research undertaken by the geologists at WMR produced a preliminary stratigraphic section for the sediments of Concession 20D. One of the most important results of this preliminary research, was the recognition of the three end-member calcareous, authigenic and siliciclastic sediment types in Concession 20D. Although WMR developed an initial framework for the more detailed study undertaken here, the WMR stratigraphy is not included, because it has been considerably modified during this study.

Table 3.1: Summary of the Sr-ages of selected sand-sized bulk foraminiferal assemblages recalculated using the McArthur *et al.* (2001) look-up tables with an estimated $^{87}Sr/^{86}Sr$ error value of 20 X 10^{-6}.

Sample No.	Depth	$^{87}Sr/^{86}Sr$	Age (Ma)	WMR Facies
WP-361	1.40 m	"modern sea water"	<0.5	Quartz sand
WP-381	2.10 m	0.709078	1.5	Quartz-glauconite sand
WP-72	1.00 m	0.709029	1.8-4.7	Shell rich quartz muddy sand
WP-186	1.34 m		No results	Glauconite sand with forams
WP-90	2.25 m	0.708404	19.8-20.7	Pelagic ooze
WP-230	4.00 m	0.708430	19.4-20.3	Mixed carbonate
WP-159	0.90 m	0.708219 0.708227	23.5-24.4 23.3-24.3	Bryozoa-rich pelagic ooze
WP-324	1.48 m	0.708082	25.8-27.2	Red-stained carbonate

A crude plough, attached to a 44 gallon drum, was designed and constructed on board the *M/V Kommandor Therese*. Four sites on the Southern Rocky Plateau and three sites within the Main Channel and Western Flank were dredged (Figure 3.3). The dredge samples were jigged through a 2 mm wire mesh jig-sieve and described by onboard geologists. A subsample of the jigged material was retained from the dredges.

Five seismic lines covering a total of 135 km were run over Concession 20D by Benguela Concessions (Pty) Ltd from 14-28 March 1996. Two of the survey lines lie in an E-W direction (WR-1 and WR-4) and the remaining lines trend NW-SE (WR-2, -3 and WL5000A). The geophysical data were acquired by the deployment of a mini-airgun and hydrophone array. In addition, thirty-one lines, covering a distance of 630 km, were run in Concession 20D by Underwater Surveys (Pty) Ltd from 15-21 November 1996. The cruise included twenty-four WNW-ESE lines (±1.5 km spacing between lines); 3 NNE-SSW lines (± 3.5 km spacing between lines) and a further four E-W lines (± 10 km spacing between lines). The seismic lines run during this survey followed as closely as possible, the core locations sampled during the RACAL survey. The X-STAR towfish was used to obtain shallow-penetration sub-bottom profiles utilising Chirp technology.

3.2.1 BATHYMETRY OF CONCESSION 20D

In contrast to the general uniformity of the outer shelf of the western margin, a number of clearly defined bathymetric features can be identified in Concession 20D (Figure 3.4). The Upper Slope to

University of Cape Town

Outer Shelf transition is marked by a slight decrease in the gradient in water depths shallower than ~450 m. The Outer Shelf of Concession 20D is relatively wide and flat and devoid of any substantial relief, with a gradient of ±0.005 between Cores 129 and 147 (Figure 3.3). The Northern Depression of Figure 3.4 is separated from the Outer Shelf by the Western Ridge, but the Western Ridge flattens out to the south into the Southern Rocky Plateau. The Western Ridge deepens from <210 m in the north to approximately 240-250 m in the south. The Southern Rocky Plateau is defined as the largely flat-lying area on the western flank of the canyon south of the Central Transect (Figure 3.4). The area lies approximately between the 280 m bathymetric contours in an east-west direction and includes a narrow ~10 m deep trough (Figure 3.4). Core recovery was poor from this area, where approximately a third of the cores collected had a recovery of less than 100 cm, with multiple attempts having no recovery at all at seven locations. The Cape Canyon is a well-defined, deeply incised feature in the south of the Cape Canyon Head region, where the canyon is divided into two regions by a central seaward bulge in the eastern flank. The Northern Depression is a broad (<10 km) relatively shallow basin (<50 m), where the irregular surface reflects the presence of a number of poorly defined channels. The Main Channel becomes increasingly narrow and more deeply incised to the south, with a maximum relief of ~160 m in the very south of the concession area. The canyon flanks are relatively steep, although the Eastern Flank flattens out slightly to the south. The bathymetry of the Western Flank is considerably more variable than that of the smooth Eastern Flank, where depressions with steep sides resembling glide-plane scars are present. Such features could indicate slumps that would have supplied sediment into the Main Channel.

Three transects across the north, central and south areas of the concession (Figure 3.5) were selected for sampling to include the representative bathymetric features, available seismic-survey line data and the majority of sediment types recovered in WMR cores. The Northern and Southern Transects run roughly perpendicular to the main channel axis along the original coring operations track. The Central Transect is slightly oblique to the canyon axis and follows one of the E-W mini-airgun seismic-survey track by Benguela Concessions (Pty) Ltd. Additional cores were sampled where required (discussed in relevant sections) and sediment data were available from Compton *et al.* (2004).

University of Cape Town

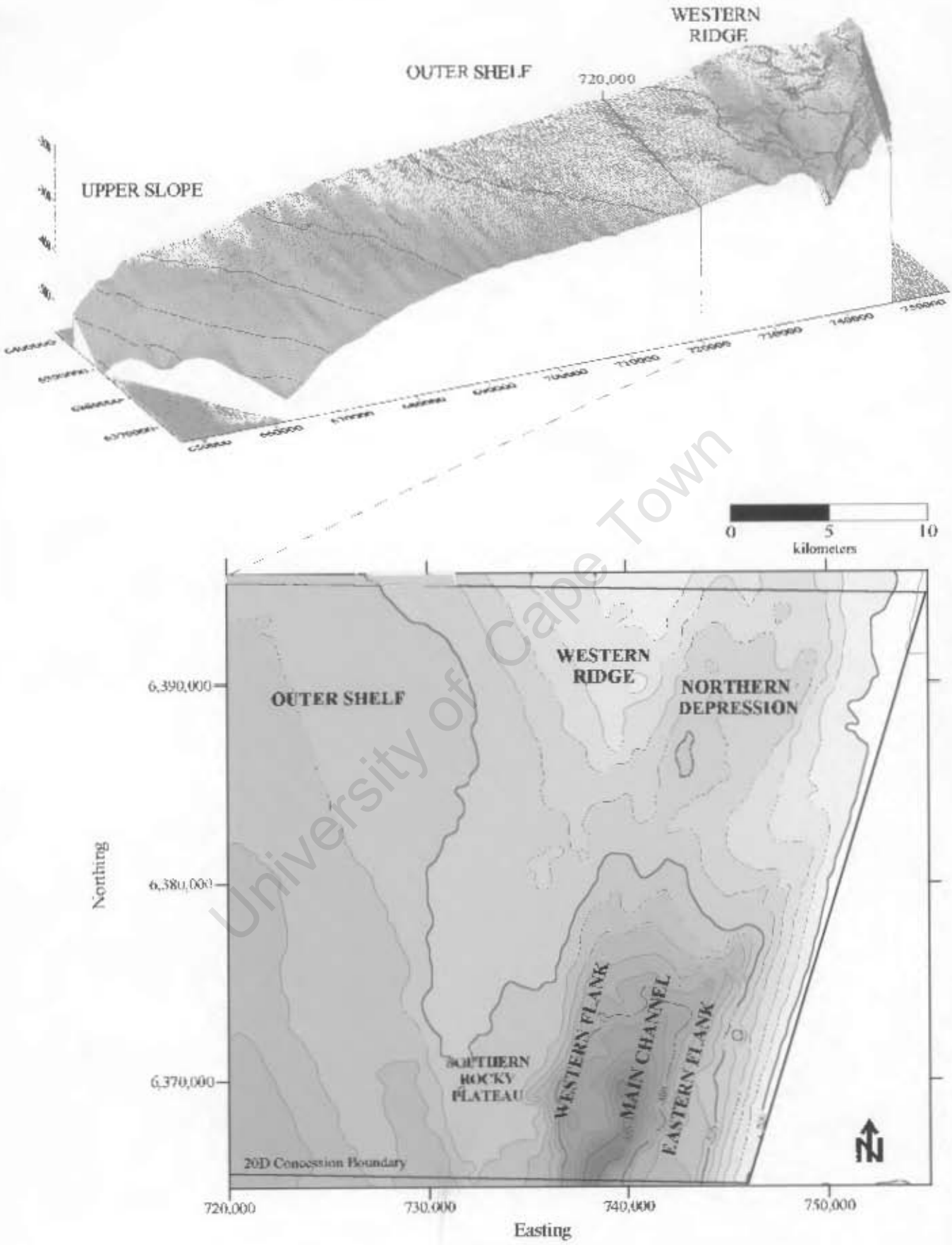


Figure 3.4. Definition of the bathymetric features of Concession 20D. (Bathymetry in 50 m intervals below 200 m in the wire-frame projection.)

University of Cape Town

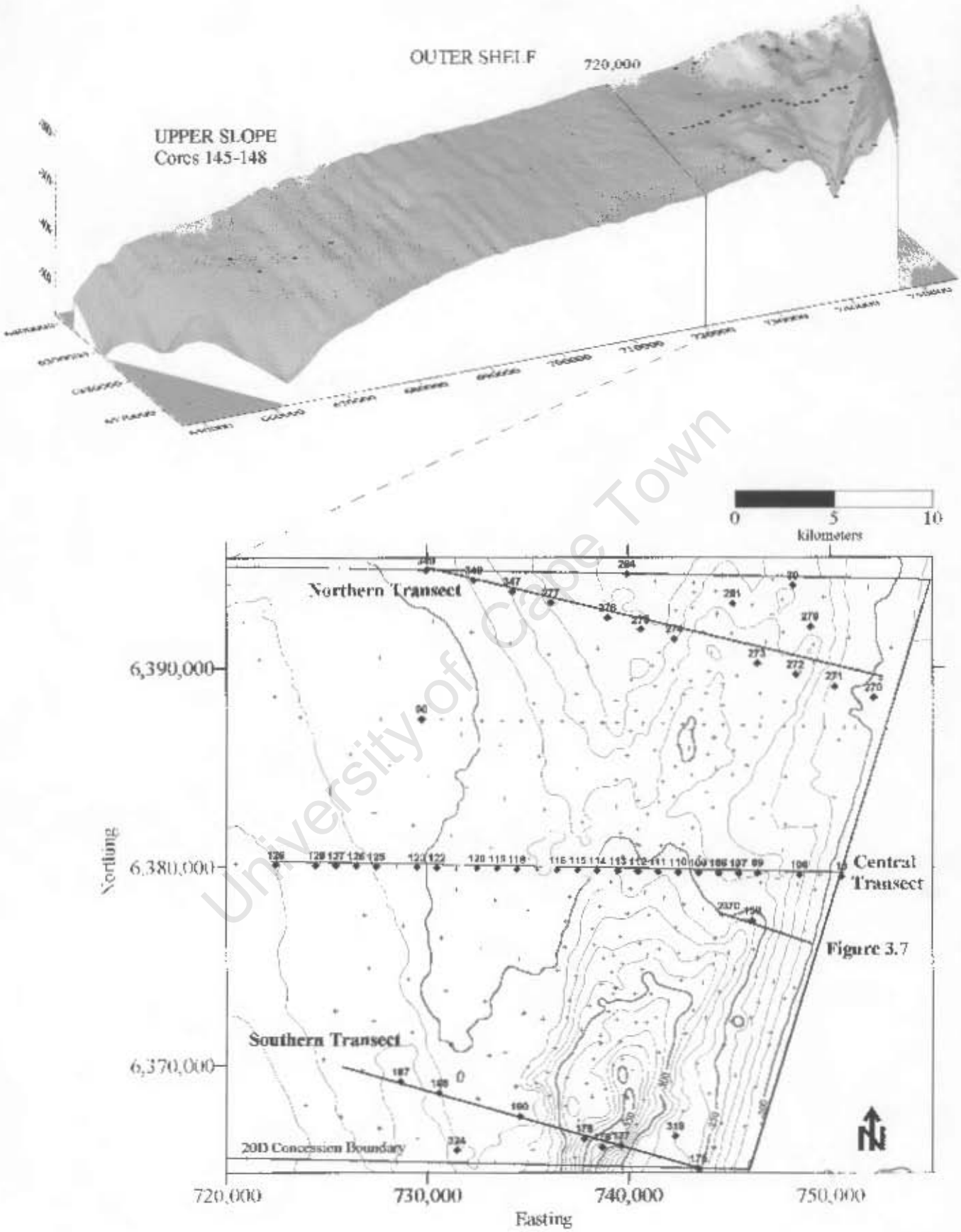


Figure 3.7

Figure 3.5. The core locations within Concession 20D and the Canyon Head region, with the selected transects and core numbers included in the close-up. All WMR cores shown with a small +.

University of Cape Town

3.2.2 SEISMIC PROFILES

Only paper copies of both the mini-airgun and Chirp seismic profiles were available and no data corrections could be made, although the bathymetry recorded in the seismic profiles are generally similar enough to true bathymetric for the purpose of this interpretation. The available records for the selected transects were examined, even though, in general, the quality of the data was poor. A photocopy of the original paper record was cut and pasted in order to correct for vertical shifts and artificial breaks in the seismic data. A scanned copy of the original seismic record and the interpreted profiles, with core locations, are included in Figures 3.6 to 3.9.

The quality of the mini-airgun record along the Central Transect is greatly reduced by the presence of multiples (Figure 3.6). However, a prominent undulating palaeosurface/angular unconformity is present below the Cape Canyon Head region. The palaeosurface defines three broad depressions, with a maximum depth of ~ 50 m, where the sea-floor surface mimics these depressions. A number of deep seaward-dipping low-angle reflectors are present below the palaeosurface in the high reflectivity Cretaceous sediments. Inferred normal and antithetic reverse faults are common below the palaeosurface in the Cape Canyon Head region, suggesting a structural control for the formation of the Cape Canyon.

The palaeosurface, identified in the Chirp profile, was intersected just to the south of the Central Transect (Figures 3.5 and 3.7) in Core 237C where Pleistocene sediments overlie Cretaceous sediments, indicating that the palaeosurface represents the Cretaceous-Tertiary (KT) boundary in the study area. Lower Miocene calcareous sediments were recovered from Core 159 (Figure 3.7) suggesting that similar sediments are present at depth in the disturbed sediments below Core 69 in Figure 3.6. The high-reflectivity Cretaceous sediments are clearly visible in the Chirp profiles from the northern and southern transects, where no obvious Tertiary reflectors are recognised (Figure 3.8 and 3.9). A Cretaceous high underlies the Western Ridge in the north, whereas almost no Tertiary sediments are preserved along the Southern Transect.

University of Cape Town

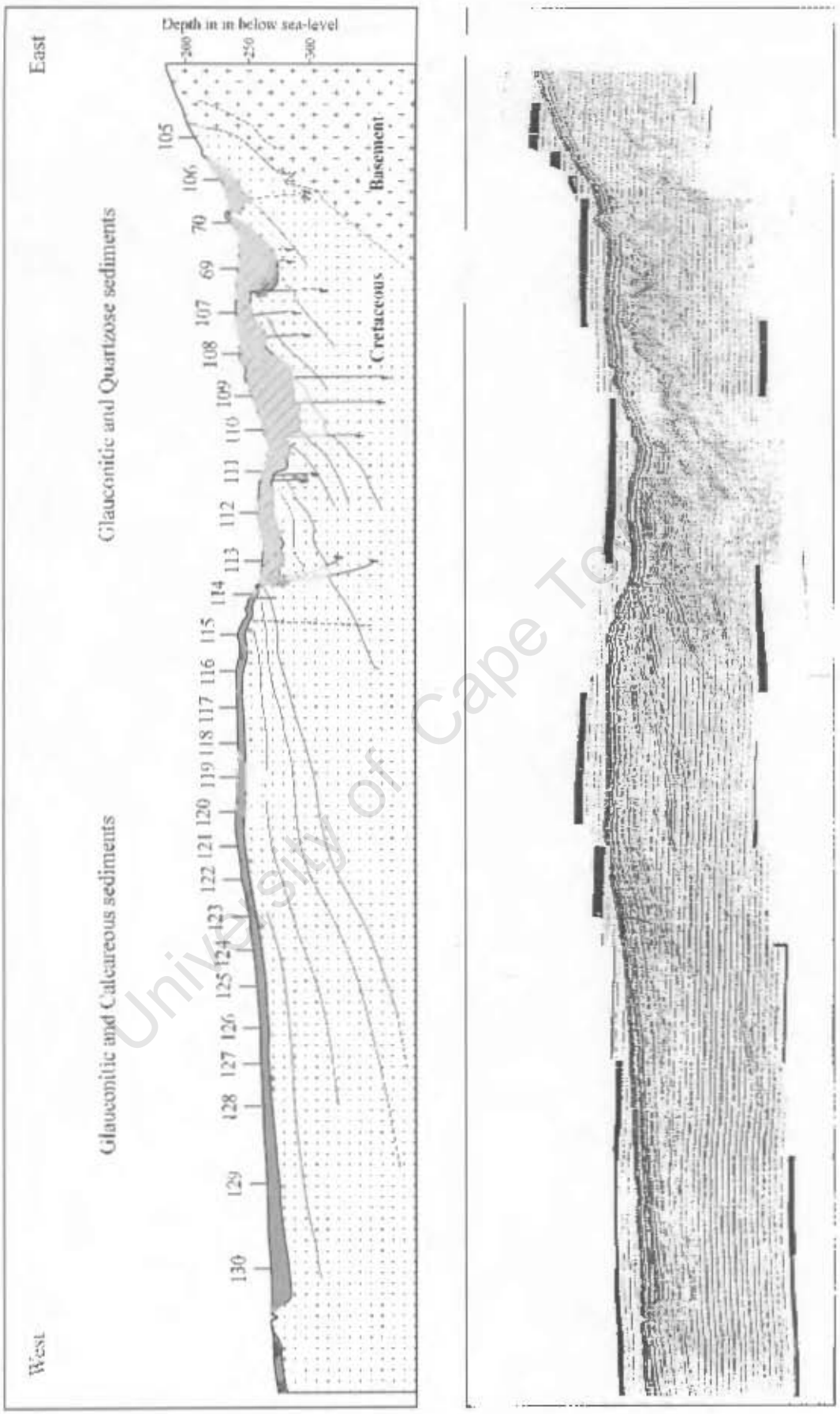


Figure 3.6. Interpreted east-west mini-airgun profile of the Central Transect across the Cape Canyon Head to Outer Shelf. Cenozoic sediments coloured grey with dominant sediment components shown. (f=fault)

University of Cape Town

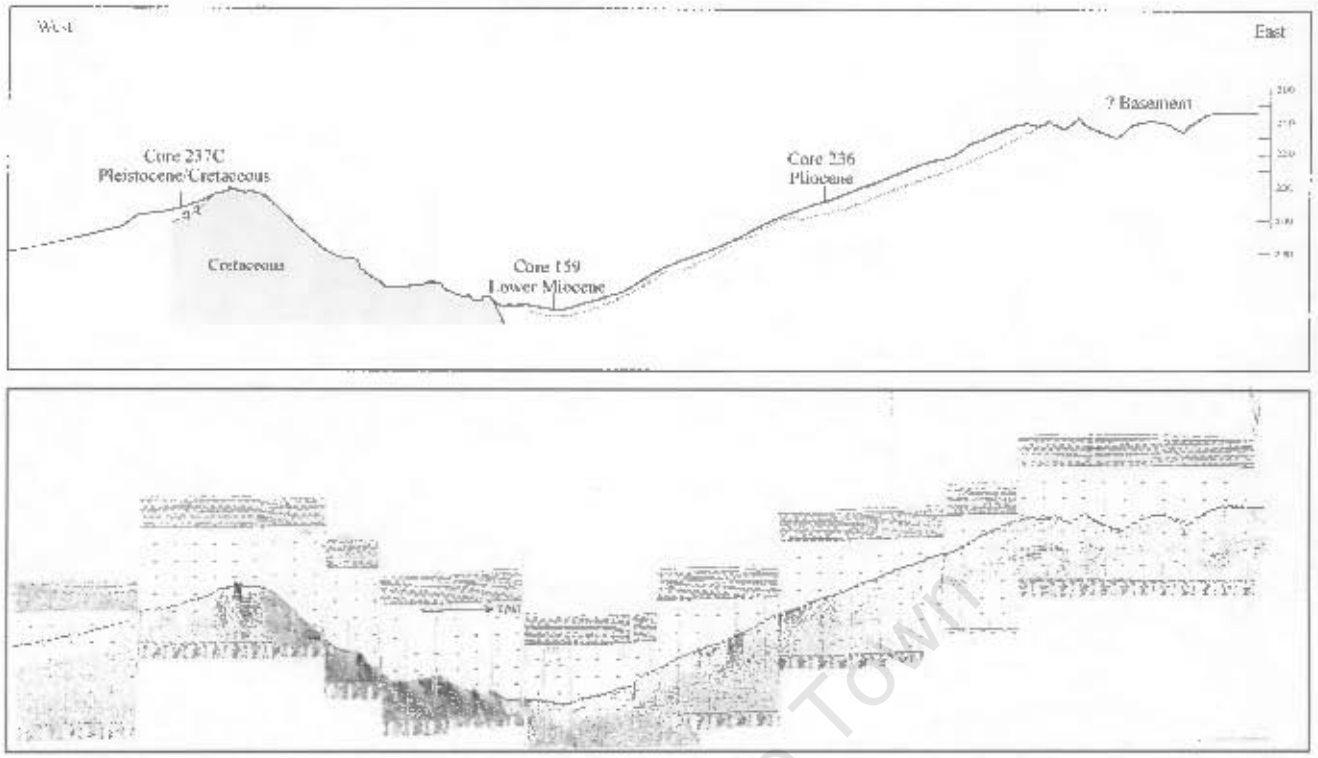


Figure 3.7. Interpreted Chirp profile across the Eastern Flank just to the south of the Central Transect (Figure 3.5).

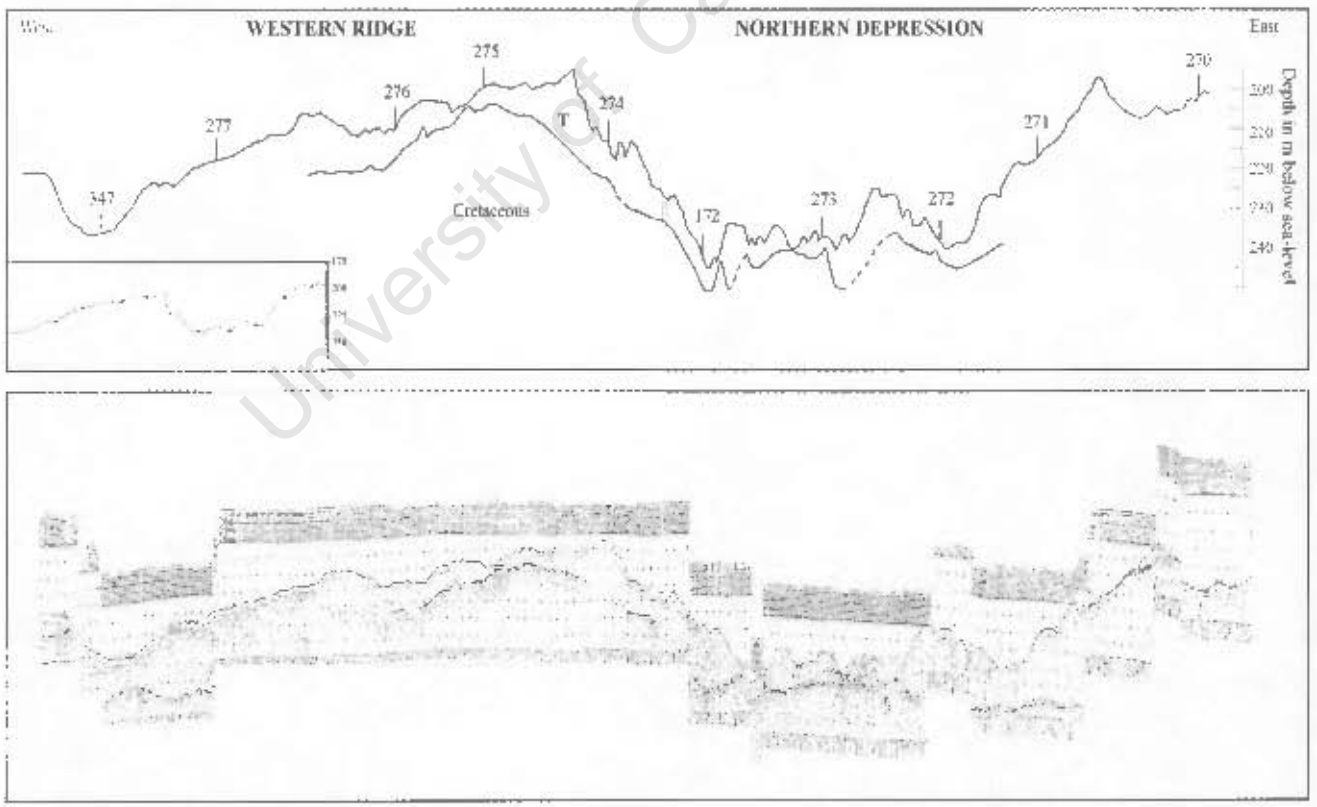


Figure 3.8. Interpreted Chirp profile of the Northern Transect across the Cape Canyon Head region and Western Ridge, with <20 m of Tertiary sediments (T) above the high reflectivity Cretaceous sediments with bathymetric profile inset.

University of Cape Town

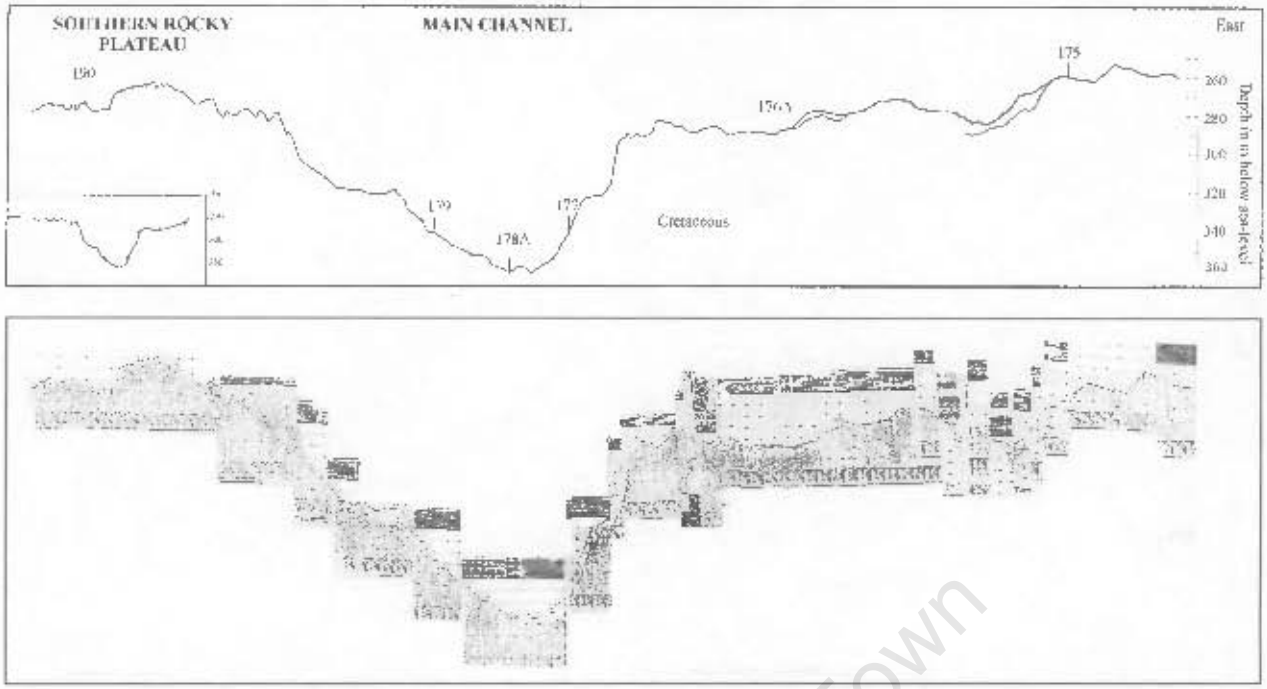


Figure 3.9. Interpreted Chirp profile of the Southern Transect across the Cape Canyon Head region showing only an occasional thin veneer of Tertiary sediments above the high reflectivity Cretaceous sediments with bathymetric profile inset.

University of Cape Town

3.3 PROCESSING AND ANALYSIS

- Selected cores were opened, described and core logs were drawn. Samples were collected from near the top and bottom of observable units. Additional samples were taken, if required, from within thicker units and where any other obvious variations were observed.
- A ~75 g subsample split was taken and remaining material retained as a reference sample.
- The bulk mass of each subsample was measured.
- The subsample was soaked in tap water overnight and was disaggregated by agitation in an ultrasonic bath for ±10-20 seconds on addition of water to the bulk sample and again prior to sieving.
- Samples were wet-sieved through a 63 µm (4 phi) stainless steel sieve using ±1 litre water.
- The mud fraction was allowed to settle for a minimum of 48 hours before the water was siphoned off. Smear slides were made for XRD analysis, using wherever possible, the upper clay-rich layer.
- The mud fraction was oven dried at ±90°C, weighed and bagged.
- The >63 µm fraction was oven dried at ±90°C. The dried sediment was sieved using 2mm (-1 phi) sieve to separate the gravel (>2mm) from sand fraction (≥63µm ≤2mm).
- The gravel fraction was weighed, described, and bagged. Pebble and cobble grades were defined using the Dunbar and Rodgers (1957) modified Wentworth Grade Scale.
- The sand fraction was weighed, described and bagged. Sediments were assigned a textural nomenclature using the graphical methods outlined in Folk (1965).

1. The sand fractions were described using a binocular microscope. The compositions, grain size, shape and sorting of the grains were described and compared to standard comparative schemes

summarized in the legend of Figure 3.11. Any surface-textures and cementing was noted. Selected sand samples were photographed using the Electron Microscope Unit (EMU) Ziess Axiocam camera (and software) on a light microscope.

2. Point counting was carried out, using a modified ribbon method, after Galehouse (1971). A complete split subsample was sprinkled onto a picking tray and all grains within a square were picked along diagonal transects until a minimum of 300 grains were picked.
3. The complete foraminiferal assemblage was picked from selected samples and submitted to Dr. I.K. McMillan at the De Beers Marine Geolaboratory Mineral Resources Unit for identification and interpreted depositional environment. Selected species were mounted for SEM imaging.
4. 10g subsamples were taken using a sediment sample splitter and acid-leached using a 10% HCl solution to determine acid-soluble (carbonate) content. The samples were left in acid for at least 8 hours before rinsing at least three times with tap water. The leached samples were oven-dried at ±100°C and weighed. If the wt % $CaCO_3$ was less than ~2%, the sand fraction was examined under the microscope, while adding drops of 10% HCl to check whether the sample had trace amounts of carbonate material present.
5. Approximately 2g subsamples were taken using a sample splitter and grain-size analyses were undertaken using the settling column in the Sediment Laboratory at UCT. The principles of the settling were described by Flemming (1976) and Flemming and Thum (1978)
6. 10g subsamples were taken using the sediment sample splitter and run through the Franz Isodynamic Magnetic Separator. The separator was run using the technique and settings outlined in Birch (1971), with a pitch of 20°, a roll of 6° and a current of 0.7 Amps. Samples were run at low vibrations and the separates then run independently to improve separation at variable vibration levels (4-9).
7. Selected samples were analysed using the Philips PW1390 Powder X-Ray Diffractometer in the Department of Geological Sciences at UCT. Smear slides were run using standard departmental operating procedures. Samples were scanned from 4 to 45° 2-Theta, using a step size of 0.05 and counting times of 1.5 sec/step.
8. Selected samples, sputter coated with gold-palladium (for imaging only), or evaporation coated with carbon (for EDS), were photographed using the Leica S440 fully analytical Scanning Electron Microscope (SEM) of the EMU at UCT. The S440 is equipped for energy dispersive x-ray (EDS) analysis with a Fisons Kevex detector utilizing Sigma software, with representative samples analysed. EDS parameters: Acquire time: 100 seconds, Beam Current >150 picoAmps, Working Distance 25 mm. All of the subsequent EDS scans plot counts (Y-axis) *vs* keV (X-axis).
9. The mineral composition of selected glauconite pellets was determined on 30 μm polished thin-sections using the Cameca Camebax 4 channel electron microprobe in the Department of Geological Sciences at UCT and standard departmental operating procedures.
10. Selected samples were analysed, with the assistance of A. Spath, by laser ablation inductively coupled plasma mass spectrometry (ICP-MS) at UCT using a Perkin Elmer/Sciex Elan 6000 and a CETAC LSX-200 laser ablation module (frequency-quadrupled Nd-Yag laser operating at 266 nm). Calibration was achieved using the NIST-620 and NIS-612 synthetic glass standards.

University of Cape Town

Instrument drift was corrected for by standardization against Si. Laser operating parameters: beam diameter - 100 μm; pulse energy - 5 mJ.pulse^{-1}; pulse repetition rate - 5 Hz.

3.4 GENERAL TERMINOLOGY

3.4.1 INTRODUCTION

Vail *et al.* (1977) constructed a composite global sea level model of the relative changes in sea level from the study by EXXON petroleum geologists of seismic stratigraphic sequences, integrating magneto-, chrono- and biostratigraphic data, from a number of different continental margins. Vail *et al.* (1977) documented three orders of magnitude within this eustatic curve. First-order cycles, of 200-300 million years duration, are modified by long-term (second-order) cycles of 10–80 million years duration. The long-term trend is further modified by short-term or third-order cycles (<1-10 million years in duration), which Vail *et al.* (1977) argued were likely to result from glacial-interglacial cycles. This global sea-level model has been the subject of considerable debate since first published by the EXXON group, largely as no direct method exists for determining the apparent magnitude of sea-level change (Kendall and Lerche, 1988). It has been argued that a global curve, based largely on work undertaken in the northern hemisphere is not a robust interpretive tool (Miall, 1992; Carter, 1998; Miall and Miall, 2001). In addition, Carter (1998) and Miall (1995) noted that the age-resolution of the sediment record is, in general, too poor to allow for a robust comparison between regions, further weakening arguments for a global signature. Haq *et al.* (1988) also acknowledged that the estimation of the relative rise in sea level using coastal-onlap models (landwards sediment encroachment above an unconformity surface) requires an assumption of the changing area of continents onlapped by sea. The determination of this area requires an often-unavailable detailed knowledge of palaeogeography of the shoreline and adjacent interior.

The major factors influencing relative sea-level change include eustatic sea level, subsidence rate (thermal subsidence due to lithospheric cooling, active tectonics, flexural response to sediment and water loading), sediment supply, sediment compaction, local active tectonism and climate (Haq *et al.*, 1988; Posamentier *et al.*, 1988; Helland-Hansen and Gjelberg, 1994; Miller *et al.*, 1998; John *et al.*, 2004). Many of these factors are interrelated, further complicating the extraction of a global signature. These factors, together with eustasy, all play a major role in governing the amount of accommodation space on the continental margin for the deposition and preservation of stratigraphic sequences. Extracting a eustatic sea-level signature requires, firstly, an estimate of the actual changes in volume of ocean water (due to factors as such as changes in water temperature or ice volume) or changes in the volume of the ocean basins (due to changes in basin shape by, for example, changes in the spreading rates at mid ocean ridges *etc.*). This "global" signature is then modified by a number of local factors, which all need to be recognised and assessed before the eustatic signal can be determined.

However, the eustatic sea-level model has gained general acceptance in the literature as a useful tool for developing an integrated approach to the interpretation of sedimentary successions of passive

University of Cape Town

continental margins. Glacio-eustatic sea-level fluctuations are recorded, in part by the $\delta^{18}O$ marine isotopic record, and have large amplitudes during icehouse conditions, which have existed since the Eocene (Coe and Church, 2003a). The term *relative sea level* is used in this thesis to reflect the sum of all factors that influence sea level in the study area, such as changes in the eustatic sea level, tectonic movement and sedimentation rates as defined by Vail *et al.* (1977), Kendall and Lerche (1988), Posamentier *et al.* (1988), Schlager (1993), Church and Coe (2003), Coe and Church (2003b) and many others.

3.4.2 SEQUENCE STRATIGRAPHY

Sequence stratigraphy is a method commonly used to study repetitive, genetically-related strata bound by sequence boundaries, within a chronostratigraphic time-frame (Vail *et al.*, 1977; Van Wagoner *et al.*, 1988; Hellan-Hansen and Gjelberg, 1994; Coe and Church, 2003b). The method requires the integration of seismic, lithologic and biostratigraphic data. The following commonly used definitions in sequence stratigraphy are based on Van Wagoner *et al.* (1988) unless stated otherwise. The fundamental unit of sequence stratigraphy is the *depositional sequence*, bounded at top and bottom by *sequence boundaries*. Sequence boundaries are unconformities (and their correlative conformities) that result from subaerial exposure, and in some cases, marine erosion, where a significant hiatus is indicated. Sequence boundaries are interpreted in terms of relative changes in sea level, where eustatic sea level is modified by local tectonism. Whether or not sequence boundaries represent a chronostratigraphic boundary is largely still debated. Sequences are divided into *systems tracts*, defined by their position within the sequence and by the stacking patterns of *parasequence sets* (a parasequence being a conformable succession of genetically related beds) bounded by marine-flooding surfaces across which there is evidence of an abrupt increase in water depth, often associated with minor marine erosion and non-deposition. One of the fundamental principles of sequence stratigraphy is in recognising the sequence and systems tract boundaries (Van Wagoner *et al.*, 1988, Catuneanu *et al.*, 1998; Carter, 1998; Coe and Church, 2003b).

University of Cape Town

The importance of eustasy was inferred by observation of similar predictable stratal patterns in a variety of plate tectonic settings, where systems tracts are associated with specific segments of the sea-level curve (e.g. Vail *et al.*, 1977; Posamentier, 1988; Posamentier and Vail, 1988). Sequence stratigraphic models predict that eustatic cycles will produce a sequence composed of a predictable succession of systems tracts assuming that there is space in the basin to accumulate sediment (accommodation space) (Posamentier *et al.*, 1988; Helland-Hansen and Gjelberg, 1994). A relative rise in sea level increases accommodation space where passive margins generally show increased rates of subsidence basinwards (Posamentier *et al.*, 1988). In general, a seaward shift in deposition (*progradation*) occurs when the rate of deposition is greater than the rate of accommodation; building up (*aggradation*) occurs when the rate of deposition equals rate of accommodation and landwards encroachment (*retrogradation*) reflects a rate of deposition, which is less than the rate of accommodation (Van Wagoner *et al.*, 1988).

The impact of relative sea level on stratal patterns has been recognised with two major sequence boundaries (Type 1 & 2) defined, depending on local tectonics (Posamentier *et al.*, 1988; Posamentier and Vail, 1988). A *Type 1 boundary* occurs when the rate of eustatic fall is greater than the rate of basin subsidence, producing a relative drop in sea level, whereas a *Type 2 boundary* occurs when the rate of eustatic fall is less than the rate of basin subsidence resulting in either no change or a rise in relative sea level. The sequences that occur between these two boundary types differ significantly and highlights the importance of integrating eustasy with local tectonics (subsidence rate) in sequence stratigraphic models (Posamentier, 1988; Posamentier and Vail, 1988).

The commonly recognised systems tracts, within a complete relative sea-level cycle, are summarised below (e.g. Vail *et al.*, 1977; Loutit *et al.*, 1988; Posamentier, 1988; Posamentier and Vail, 1988; Van Wagoner *et al.*, 1988; Helland-Hansen and Gjelberg, 1994; Coe and Church, 2003b):

- *A Lowstand Systems Tract* (LST) occurs during a relative fall in sea level (rate of eustatic fall greater than the rate of subsidence) and is associated with, for example, fan deposits, turbidites and debris-flow deposition, canyon formation and incised valley erosion. The base of the LST is defined by a subaerial exposure surface and correlates with the depositional surface of lowest relative sea level.
- A *Lowstand Wedge* (LW), initially included with the LST, is a regressive unit characterised by progradational parasequence stacking patterns, initiated in latter part of rapid eustatic fall and subsequent lowstand, where rate of subsidence is greater than the rate of eustatic fall, implying slow rise in relative sea level (Helland-Hansen and Gjelberg, 1994). The upper boundary of LW is defined by the transgressive surface, the first significant marine-flooding surface within the sequence.
- The *Transgressive Systems Tract* (TST) is characterised by one or more retrogradational parasequence sets (rate of deposition is less than the rate of accommodation) above the basal flooding surface. The top of the TST is a downlap surface, which marks the change from a retrogradational to an aggradational parasequence. Condensed sections are typical of the TST, which are interpreted to be deposited during rapid eustatic rise where accommodation space is rapidly increasing (Posamentier *et al.*, 1988). Condensed sections are intervals of greatly reduced sediment accumulation rates of deeper water pelagic to hemipelagic sediments, often associated with authigenic minerals, produced during a rapid relative sea level rise. They are associated with apparent hiatuses and often occur as thin, slightly burrowed, lithified beds or hardgrounds (Loutit *et al.*, 1988). Surfaces of non-deposition are often referred to as downlap surfaces in sequence-stratigraphic models. Condensed sections are easily recognized and hence are a useful stratigraphic tool (Loutit *et al.*, 1988).
- The *Highstand Systems Tract* (HST) is commonly widespread on the shelf and is characterised by one or more aggradational parasequence sets succeeded by one or more progradational parasequence sets. HSTs are interpreted to indicate deposition at or near eustatic highstands during the late stages of a relative rise in sea level. The upper surface of the HST marks the sequence boundary.

A number of models have been proposed of the idealised stratigraphy of sediments deposited during a single sea-level cycle (*e.g.* Vail *et al.*, 1977; Loutit *et al.*, 1988; Posamentier, 1988; Posamentier and

University of Cape Town

Vail, 1988; Carter, 1998). These models rely on the reproducibility of systems tracts during successive cycles of relative sea level rise and fall, with the variable stacking patterns of systems tracts (parasequences) reflecting local changes in sediment supply and accommodation space. In contrast, many authors (*e.g.* Helland-Hansen and Gjelberg, 1994; Carter, 1998, Miall and Miall, 2001 and references cited therein) argued that the sequence stratigraphic models described above are over-simplified, are based on unreproducible assumptions and do not account for the individual character of different depositional environments. They argued that the preservation of different stacking patterns is more dependent on local factors such as accommodation space, tectonics and sediment supply than on timing within cycles of relative sea level rise and fall. In addition, Helland-Hansen and Gjelberg (1994) have argued that an understanding of the variability of basin-fill depositional processes are fundamental, otherwise models based largely on relative sea level can be misleading.

Sequence stratigraphic models are largely based on interpretation of siliciclastic shoreline deposits, but it has been argued that carbonate sequence stratigraphy follows a similar set of rules defined for siliciclastic systems (*e.g.* Sarg, 1988; Caron *et al.*, 2004). Sarg (1988) argued that two types of sequences can be recognised within carbonate deposits, with systems tracts similarly reflecting differences in relative sea level. However, the controlling factors of carbonate deposition require that in addition to relative sea level, depositional setting (basin topography/platform type) and climate be taken into account. The type of carbonate or mixed carbonate/siliciclastic sediment deposited depends, in part, on climate (Brachert *et al.*, 2003; Caron *et al.*, 2004). In addition, care needs to be taken when interpreting cool-water, transitional and temperate carbonate sediments, because the depositional setting, particularly shelf morphology, is important. The width and gradient of the carbonate platform govern such factors as production, concentration and dilution by siliciclastic sediments (Brachert *et al.*, 2003; Coffey and Read, 2004.) Caron *et al.* (2004) noted that more integrated studies, including environmental factors fundamental to carbonate production, provide a useful process-driven stratigraphic framework for assessing complex carbonate-facies distribution. They noted that recognition of sequence boundaries is important and argued that transgressive surfaces of erosion associated with reworking and winnowing, developed during relative sea level rise, are best used as boundary surfaces for cool-water carbonates.

Relative changes in sea level will clearly have a large impact on sedimentation and the sediment succession preserved on continental margins. The problem is sorting out the contribution from eustasy, tectonism and sediment supply, since these factors are rarely known independently. Many authors have argued against oversimplification and rigid adherence to sequence stratigraphic models. However, there is a general consensus in the literature that the integration of sequence stratigraphy (physical framework), biostratigraphy and local tectonic/depositional setting provides a powerful tool for dating and correlating continental margin sequences (Loutit *et al.*, 1988; Schlager, 1993; Carter, 1998, Abreu and Anderson, 1998; Miller *et al.*, 1998; Zachos *et al., 2001;* McHugh *et al.*, 2002; Brachert *et al.*, 2003; Caron *et al.*, 2004; Holbourn *et al.*, 2004; Li *et al*, 2004). Although the records available for this study on the west coast of southern Africa preclude detailed sequence stratigraphic and biostratigraphic

University of Cape Town

studies, this thesis attempts to provide as integrated an approach as possible to understanding the evolution of the condensed Tertiary sediment record of the western margin of southern Africa.

3.4.3 SEA LEVEL

Sequence stratigraphic models have used the coastal onlap patterns of stratigraphic sequences to quantify a globally averaged sea-level history, based on stratigraphic correlations interpreted to reflect a relative (and eustatic) sea level. Stratigraphic correlations are based on the recognition of simultaneous depositional sequences in the seismic record from different continental margins (Vail *et al.*, 1977). However, it has been argued by many that this "global" sea level model reflects an assembly of local relative sea level events, which are controlled as much by local tectonics as they are by eustasy (Kendall and Lerche, 1988; Carter, 1998; Miall and Miall, 2001; and references cited therein).

Although changes in relative sea level are generally accepted, it has been argued that their global synchroneity, amplitude and rate are still largely unquantified (Carter, 1998; Miall and Miall, 2001; Spezzaferri *et al.*, 2002; John *et al.*, 2004.). Kendall and Lerche (1988) and Miller *et al.* (1998) argued that, although a chart defining the exact magnitude of eustatic sea level cannot be determined, the relative size of the excursions in eustatic sea level can be estimated as a useful stratigraphic tool. Many have therefore argued that global sea level models can be powerful predictive tools, particularly as changes observed in the sediment record of passive margins with low subsidence rates and low terrigenous sediment input are likely to be most strongly influenced by fluctuations in sea level (Sugarman and Miller, 1997; Carter, 1998; Miller *et al.*, 1998; Harris and Whiting, 2000; Monteverde *et al.*, 2000).

The New Jersey passive margin has been studied extensively in order to evaluate the relationship between sequence boundaries in the sediment record and sea level fluctuations, as well as the influence of other factors, such as subsidence rates, sediment supply and climate (Sugarman and Miller, 1997; Miller *et al.*, 1998; Monteverde *et al.*, 2000). Miller *et al.* (1996; 1998) summarise the vast amount of research undertaken on this margin and conclude that variations in the size of ice sheets (glacioeustatic sea level) has been the primary control on the formation of sequence boundaries since 42 Ma (middle Eocene). They argued that the New Jersey coastal plain sequences show a close link between continental slope and coastal plain sequence boundaries and variations in sea level, where the ages of sequence boundaries correlate well with both marine oxygen isotope studies and the modified EXXON sea level curve of Haq *et al.* (1987, 1988).

A number of studies undertaken elsewhere show a similar association between global fluctuations in sea level and the sediment record. Sequence boundaries in the sediment records from other Atlantic passive margins including the Bragantina and Pará Platforms of northeastern Brazil are interpreted to reflect global sea-level changes during the late Cenozoic, where these boundaries are correlated with discontinuity surfaces that occur in the São Luís and Grajaú Basins at least 1000 km to the east (Rossetti, 2001). The upper Oligocene to lower Miocene sediment succession of northern Brazil lies

University of Cape Town

between two major unconformities, with the sediments occurring above Cretaceous basement and below an unconformity at the early to middle Miocene transition (Rossetti, 2001). Similarly, a number of studies on the eight basins (namely Bremer, Eucla, St. Vincent, Murray, Otway, Torquay, Port Phillip and Gippsland basins from west to east) along the southern Australian passive margin attest to the importance of sea-level fluctuations and sequence boundaries (Gallagher and Holdgate, 2000; Gallagher *et al.*, 2001). Gallagher *et al.* (2001) noted that early Miocene transportation of inner to middle shelf foraminifera species to the outer shelf in the Gippsland Basin of southeast Australia can be correlated with the third-order sea level cycles of Haq *et al.* (1987, 1988). The Miocene coal seams of the Gippsland Basin have also been attributed to third-order eustatic cycles, where changes in sea level are shown to be important in the development and properties of these coal seams (Holdgate *et al.*, 1995).

Oxygen isotope stratigraphy, developed from deep-sea pelagic sections, is a widely recognized proxy for glacial-interglacial cycles and therefore provides an independent tool to assess relative changes in sea level (Abreu and Anderson, 1998; Williams, 1988; Zachos *et al.*, 2001; Spezzaferri *et al.*, 2002; Coe and Church, 2003a), although inaccuracies in the oxygen isotope curves may reflect incorrect assumptions on temperature and salinity, both of which affect the $\delta^{18}O$ value. Coe and Church (2003a) noted that changes in the ice volume resulting in a 1‰ change in the $\delta^{18}O$ value is equivalent to approximately 100 m change in global sea level. It has been acknowledged that the similarities between the eustatic and oxygen isotope curves do not stand up to a rigorous statistical comparison, but it has been argued that the glacial-interglacial control on sequence stratigraphic stratal stacking is clearly indicated (Abreau and Anderson, 1998; Zachos *et al.*, 2001, Coe and Church, 2003a). A considerable amount of recent literature based largely on continuous cores drilled in ocean basins by the collaborative Ocean Drilling Program (ODP), combines sequence stratigraphy, biostratigraphy and oxygen isotope curves of benthic foraminifera to support the link between sequence boundaries and glacial-interglacial cycles, particularly for the Neogene and Quaternary (Coe and Church, 2003a). For example, research by Holbourn *et al.* (2004) and Li *et al.* (2004) on cool-water carbonates from the Great Australian Bight show a remarkable coincidence between identified regional hiatuses in the sediment record based on biostratigraphic, $\delta^{18}O$ and $\delta^{13}C$ analyses and the third-order boundaries in the eustatic curve of Hardenbol *et al.* (1998), suggesting a significant eustatic control. They do not discount, however, the possibility that these hiatuses are influenced by tectonoeustatic controls, and describe longer-term mega-hiatuses that they argued are likely to be correlated with three major regional tectonic events.

As emphasised in Chapter 2, the Cenozoic evolution of the western margin of southern Africa is poorly constrained, with little consensus regarding tectonic history, palaeoclimate or sediment history. In the absence of well-constrained local datums, the global sea-level model and oxygen isotope curve, with all their inherent controversy, are used as predictive tools to assess some of the possible processes recorded in the sediment record of Concession 20D. Figure 3.10 shows the proposed Haq *et al.* (1987, 1988) eustatic curve, replotted to the Berggren *et al.* (1995) time scale after Miller *et al.* (1997; 1998) together with the $\delta^{18}O$ curve (Zachos *et al,* 2001). These proposed records are used as a starting point of comparison for the sediment record throughout this thesis. The proposed eustatic sea level model is

University of Cape Town

primarily used to assess relative changes (rising, highstand, falling and lowstand) in sea level. The absolute magnitude of relative sea level changes cannot be resolved as the magnitude of the local tectonic overprint is unknown.

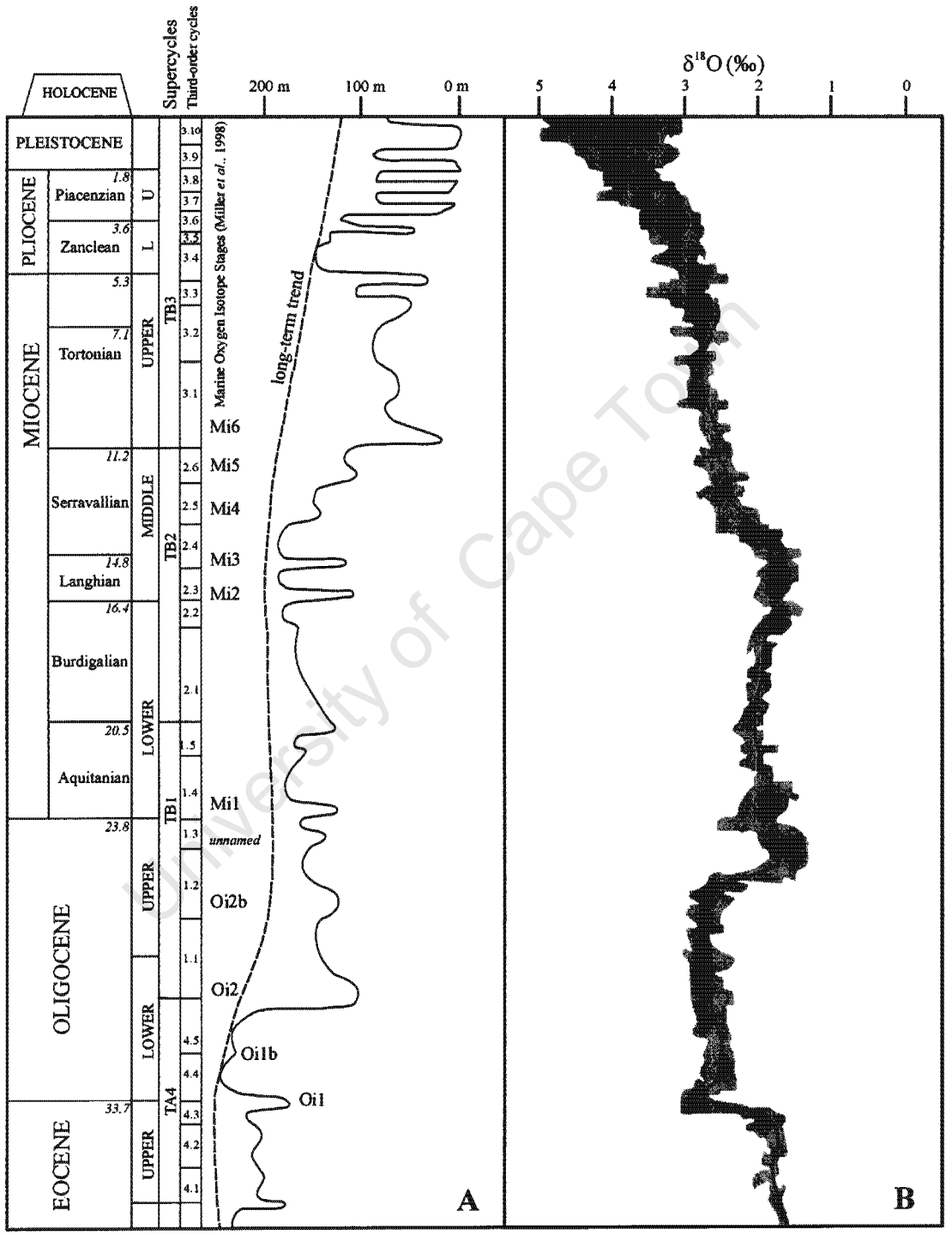


Figure 3.10. A: The Haq *et al.* (1987, 1988) eustatic curve with long-term (dashed line) and third-order cycles (solid line) shown. The supercycle sequences and third-order glacial-interglacial cycles are re-calibrated to the Berggren *et al.* (1995) time scale after Miller *et al.* (1997; 1998). B: The global deep-sea oxygen isotope record of Zachos *et al.* (2001).

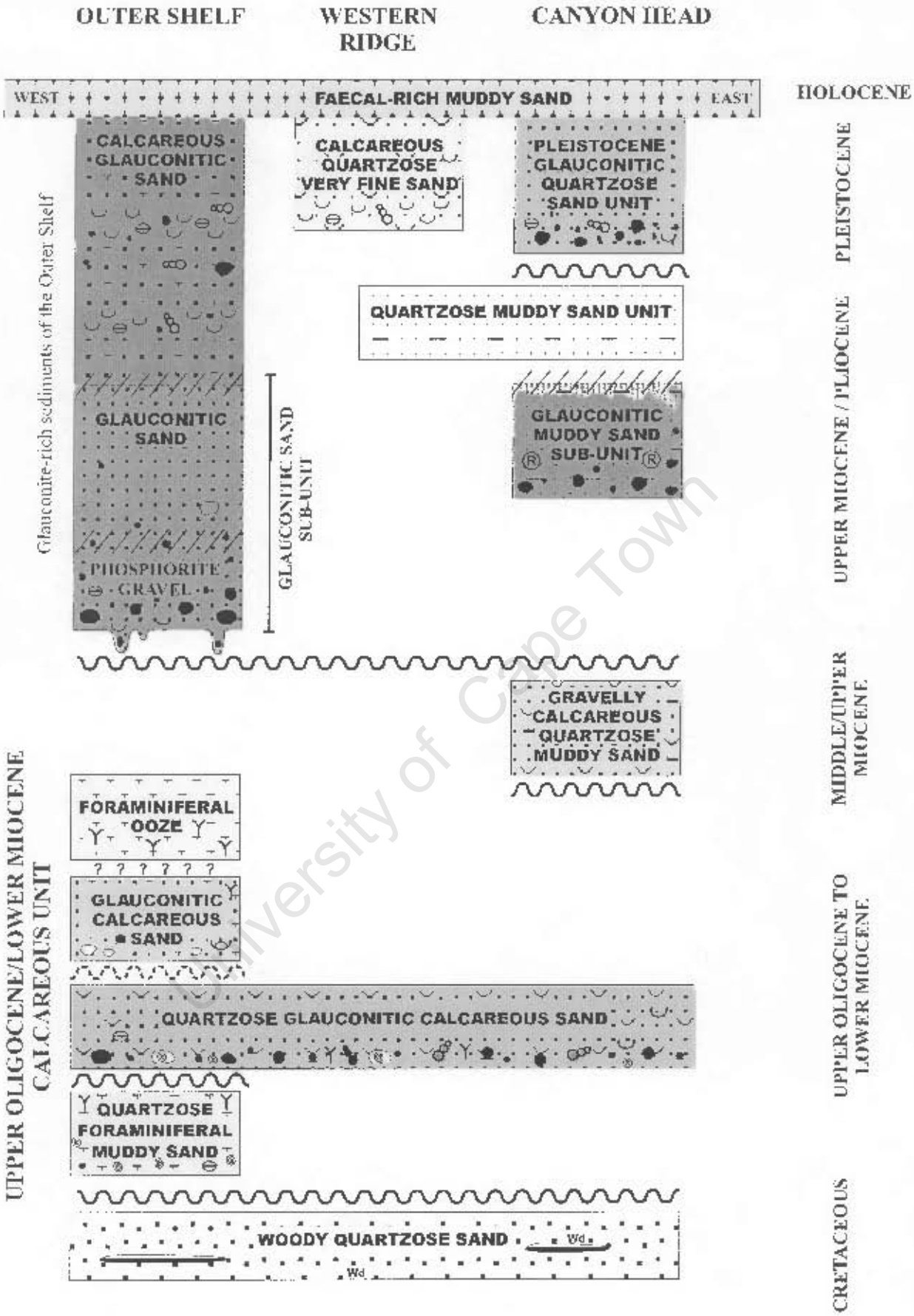
University of Cape Town

3.5 GENERAL STRATIGRAPHY AND LEGEND

Four distinct stratigraphic successions were defined on the basis of age and sediment composition in Concession 20D. Insufficient spatial data are available to make use of, in general, sequence stratigraphic terminology. The simplified stratigraphy of the study area, indicating the unit, sub-unit and facies names utilised throughout the thesis is provided here for reference (Figure 3.11).

The unconsolidated Cretaceous Woody Quartzose Sand is overlain by a Tertiary sedimentary succession. The Tertiary sediments can be subdivided into three lithostratigraphic units. The Lower Miocene Calcareous Sand Unit dips gently to the west, where the sediments young seawards of the Western Ridge. The lower Miocene sediments are overlain by a complex condensed section of reworked glauconitic and quartzose sediments, which were deposited in the Pliocene. In contrast to the underlying sedimentary units, the Pleistocene successions show a well-defined relationship between sediment composition and distribution within Concession 20D. The unconsolidated sedimentary units and facies were named according to the dominant compositional components, using the guidelines outlined in the ODP Explanatory Notes of Leg 175 that recovered sediments from the western African margin (Wefer *et al.*, 1998). The term "ooze" was used when the calcareous component comprised >60% of the sediment, otherwise the sediments were classified according to grain texture, modified by major compositional components listed in order of increasing abundance. Minor to subordinate, but significant, modifiers were indicated by the "–rich" suffix. The definitions of the facies within the stratigraphic succession of Concession 20D were solely based on the sediments recovered from the cores analysed during this study, and no use was made of the initial WMR classification scheme. The sediments of the WMR cores were then assigned to Units and facies based on the original onboard sediment description in the core logs.

University of Cape Town



University of Cape Town

Figure 3.11. A generalised stratigraphic column for Concession 20D, summarising the sedimentary units described in the subsequent chapters. The legend, on the following page, shows lithology fill patterns, symbols, contact types, terminology and abbreviations used.

LEGEND



Faecal-rich muddy sand

Medium sand

Fine to very fine sand

Shelly sand

Foraminifera-rich sand

Shell lag/interval

Ooze (>60% biogenic)

Contact gradational

Bioturbation

Bivalves and other shell fragments
(Ⓞ: Oyster)

Phosphatised shell fragments

Articulated bivalves

Pecten sp.

Gastropod

Phosphatised mollusc casts

Bryozoa

Brachiopod

Foraminifera

Larger benthic foraminifera

Pebbles (>2mm)
Ph: Phosphorite
Qz: Quartz

Limestone

Bone (fragments)

Reduced patches

Gypsum crystallization

Wood fragments

ABBREVIATIONS:

Minerals:
Qz: Quartz
Glc: Glauconite
Ph: Phosphorite (Compton *et al.*, 2004)
CFA: Carbonate-fluorapatite
PCG: Phosphate-cemented grains
PCL: Phosphate replaced limestone
SPG: Skeletal phosphorite grain (Sk: bone, otolith, T: Teeth)
PP: Pelletal Phosphorite
Cc: Calcite
Calc: Calcareous
ShF: Shell fragments
Bv: Bivalve (Pe - Pecten)
G: Gastropod
Bry: Bryozoa
Br: Brachiopod (art - articulated)
Ech: Echinoid (S - spine; P - plate)
Dent. Dentalium
SkF: Skeletal Fragments
F: Foraminifera (pF - planktonic, bF - benthic)
FP: Faecal pellets
Ost: Ostracods
SSp: Sponge Spicules
HS: Holothurian sclerites

Colours
Amb: Amber
Brn: Brown
Blk: Black
Gn: Green

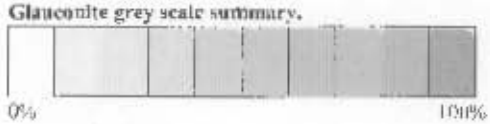
Modified Wentworth Grade Scale after Dunbar and Rodgers (1957).
PEBBLES:
vcP Very coarse (32 mm - 64 mm)
cP Coarse (16 mm to 32 mm)
mP Medium (8 mm to 16 mm)
fP Fine (4 mm to 8 mm)
vfP Very fine (2 m to 4mm) also referred to as granules (gran.)
SAND:
vcS Very coarse (1 mm - 2 mm)
cS Coarse (500 µm to 1 mm)
mS Medium (250 µm to 500 µm)
fS Fine (125 µm to 250 µm)
vfS Very fine (63 µm to 125 µm)

Powers (1953) roundness scale
ang: angular
rnd: rounded
subang/rnd: subangular/rounded
v-ang/rnd: very angular/rounded

Sorting Φ values for grain size analysis after Folk (1965).
.00-.32Φ: Very well sorted
.33-.37Φ: Very well to well sorted
.38-.47Φ: Well sorted
.48-.52Φ: Well to moderately well sorted
.53-.68Φ: Moderately well sorted
.69-.73Φ: Moderately well to moderately sorted
.74-1.0Φ: Moderately sorted

Semi-quantitative proportion estimates after Ingram (1965).
dominant: 50-100%
subordinate: 5-50%
minor: trace to 5%
trace: isolated grains

Glauconite grey scale summary.



University of Cape Town

Figure 3.11 continued.

4 CRETACEOUS WOODY QUARTZOSE SAND

4.1 INTRODUCTION

The passive western margin of southern Africa (Figure 4.1) developed since the break up of Gondwana, where rifting of the western margin of southern Africa started between 126 and 121 Ma (Fouché *et al.*, 1992; Section 2.2). The rift to drift evolution is recorded in the ≥8 km thick sediment succession of the Orange Basin (Gerrard and Smith, 1982; Dingle *et al.*, 1983; Brown *et al.*, 1995). The Cretaceous succession is covered by a veneer of Tertiary sediments, where the thickness of the Tertiary cover is <1 m in the proximal Orange Basin, thickening to 300 to 800 m on the outer shelf to upper slope (Du Plessis *et al.*, 1972; Compton *et al.*, 2002). The Cretaceous/Tertiary boundary was intersected at ~600 m below the sea floor in the Kudu oil-exploration boreholes on the Orange Banks off the Orange River mouth (McMillan, 1990) (Figure 4.1). Upper Cretaceous sediments outcrop or subcrop on the mid to inner shelf, where these possibly low-grade diamondiferous (upper Cretaceous to) lower Tertiary sediments have been reworked during the sediment-starved late Tertiary to produce a diamondiferous gravel lag, which is typically less than a few metres thick, at the base of the Pleistocene succession (McMillan, 1993; Kuhns, 1995). Details of the offshore Cretaceous records have largely been limited by the confidentiality clauses of the mining houses exploiting the economic diamond and oil deposits.

In contrast to the thickness of the offshore Cretaceous sediment record, onshore Cretaceous deposits are very rare in southern Africa along the West Coast, although numerous kimberlite crater-lake deposits occur in Namaqualand (Scholtz, 1985). The only known onshore Cretaceous marine deposit is an about 20 cm thick, mollusc-rich silty limestone of the Wanderfeld IV Beds, which crops out just inland of Bogenfels in the Sperrgebiet of southern Namibia (Figure 4.1) and is dated as mid to late Cretaceous, *i.e.* Cenomanian (Klinger, 1977) or lower Santonian (McMillan, 1992). Non-marine Cretaceous outcrops are also scarce, although river-channel deposits are reported, such as at Kangnas (±140 km due east of the Orange River mouth) and the lower Cretaceous (Hauterivian) carbonaceous fluvial sediments on the farm Karreedoornvlei, ±20 km north of Kleinzee (Figure 4.1; Dingle *et al.*, 1983; Rogers *et al.*, 1990). The offshore Cretaceous record has been studied from a seismic-stratigraphic viewpoint in some detail, because of potential economic oil deposits (Gerrard and Smith, 1982; Brown *et al.*, 1995). However, the mid to late Cretaceous palaeoenvironments and sedimentary history on the western margin, in particular, are poorly constrained (Bamford and Stevenson, 2002). The presence of Cretaceous sediments at the base of the sediment succession in the main channel of the Cape Canyon in Concession 20D provided a unique opportunity for a detailed study of this sediment. The main objectives of this chapter are to determine the sedimentology and age of the Cretaceous unit to provide constraints on the palaeoenvironmental conditions prevailing in the Cape Columbine area during the Cretaceous.

University of Cape Town

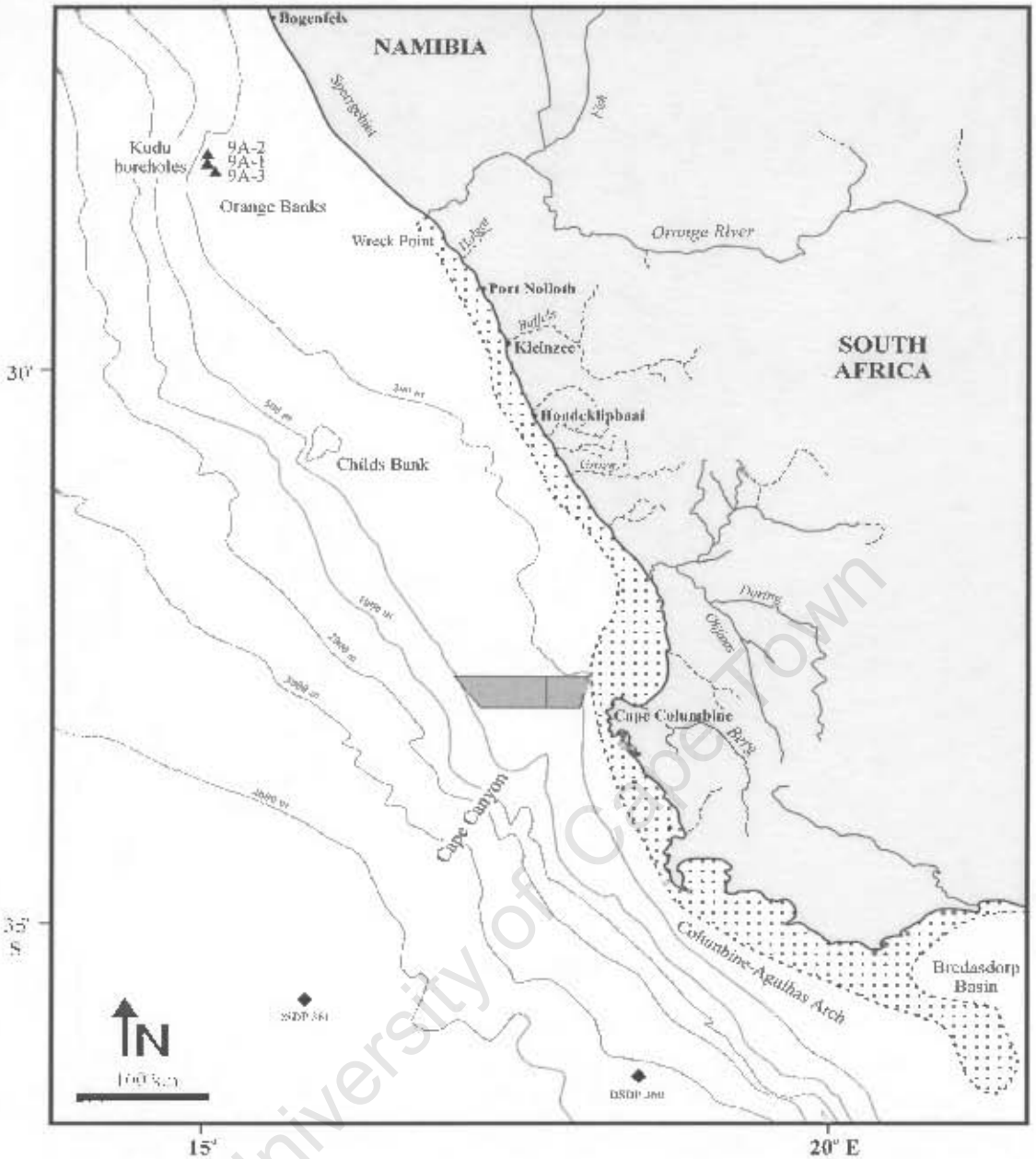


Figure 4.1. The location of Concession 20D (grey polygon) relative to the West Coast of southern Africa, with relevant SOEKOR (▲) and DSDP (◆) boreholes shown. The stippled area shows the extent of the pre-Cretaceous basement high of Brown *et al.* (1995).

University of Cape Town

4.2 GEOLOGICAL SETTING

The Cretaceous sedimentary succession on the western margin of southern Africa is subdivided into three distinct seismo-stratigraphic groups on the basis of well-defined seismic reflectors, with the rift succession overlain by an early drift and drift succession, respectively (Table 4.1; Gerrard and Smith, 1982). The rift succession is dominated by synrift volcanics and fluvial, aeolian and lacustrine mainly siliciclastic sediments (Gerrard and Smith, 1982). The early drift succession is characterised by significant variations in lithology and includes red beds, aeolian continental sediments, with evaporite horizons towards the base of the succession (~117.5-112 Ma), interbedded with grey marine sediments and with minor basaltic lavas (Gerrard and Smith, 1982; Dingle *et al.*, 1983; Wickens and McLachlan,

1990; Dingle, 1992/1993; Brown *et al.*, 1995). An Aptian fall in sea level during the early drift succession (112-103 Ma) resulted in erosion of the 13At1 unconformity surface, representing the closing stages of the early drift phase (Brown *et al.*, 1995). The drift succession is dominated by open-marine siliciclastic sandstones, shales and siltstones, where the foraminiferal assemblages indicated oxygenated bottom waters (Dingle and Robson, 1992). Maximum accumulations in the late Cretaceous occurred in the Walvis and Orange Basins with sediment thicknesses of ~5.1 km in the drift succession (between the 13At1/Alf and 22At1/Davie unconformities) preserved in the Orange Basin (Dingle and Robson, 1992). The post-rift Cretaceous succession (particularly super sequences (Sseqs) 13 and 14; Table 4.1) is condensed on the flanks of the Columbine-Agulhas Arch with only 3.5 km of post-rift sediments preserved, most likely reflecting repeated uplift and intensive erosion events (Brown *et al.*, 1995).

Table 4.1. A summary of the Cretaceous record for the western margin of southern Africa after 1: Brown *et al.* (1995); 2: Dale and McMillan, 1997; 3: McMillan (*in prep.*); 4: McMillan (1990); 5: Petroleum Agency SA (2002) and 6: Stevenson and McMillan (*in press*).

Age (Ma) and standard chronostratigraphy for southern Africa[1]			Major U/C[5]	Super-sequence[2]			Palaeo-drainage[1]	DSDP361		Red Beds[3]	Tectonic Events
LATE	66	Maastrichtian	Davie	15-20	DRIFT	~93—80 Ma: Episodic gravity faulting of aggradational clastic shelf and slope system[1]	105 Ma: Northern exit (palaeo-Orange) with Orange River delta established as major depo-centre	6	Middle Albian to latest Santonian, proximal Orange Basin sediments[3]		Major uplift at 80 Ma[4].
	74	Campanian	17At1								Thick Santonian fluvial to marginal marine succession (1800 m) in Kudu boreholes[4,6]
	84	Santonian	80 Ma	15-16							Upper Coniacian*: includes thin red beds in succession[5]
	88	Coniacian									Lower Turonian*: includes thin red beds in succession[5]
	91	Turonian	15At1								~92 Ma: free connection between N & S Atlantic[5]
	92	Cenomanian	93 Ma			net aggradation					
EARLY	96	Albian	14At1	14		major marine flooding and subsequent progradation	103 Ma: Southern exit (palaeo-Olifants)	No palynomorph record			Middle Albian (14At1) to Lower Cenomian: 3000 m thick proximal fluvial deposits with red beds[3,6]
	105	Aptian	109 Ma	13				7			*Major drainage shifts from Olifants to Orange River*[1]
	113	Barremian	13At1/Alf								* cyclical fluvial to innermost shelf[6]
	116.5	Hauterivian	112 Ma	6-12	EARLY DRIFT	aggradation	117.5-103 Ma: Northern exit (palaeo-Olifants)				~112 Ma: Open Ocean[5]; uplift and tilting[1]
	121	Valanginian	6At1								~117.5 Ma: Drift onset[1]
	126	Berriasian	117.5 Ma 1At1		RIFT						~121 Ma: Onset of transform motion in Bredasdorp Basin[5]
	142										~121-126 Ma: Onset of rifting of western margin of southern Africa (Fouché *et al.*, 1992)

University of Cape Town

Large rivers are believed to have drained onto the western margin during the Aptian to Campanian drift phase from 112-80 Ma years ago with terrigenous sediments discharging from the palaeo-drainage systems as large deltas prograded across the Continent-Ocean Boundary (COB) and fed submarine fans in the newly formed ocean (Dale and McMillan, 1998b). The middle Albian to upper Santonian drift succession is dominated by alluvial facies (Corbett, 1996) although a number of thin (<5 m thick) marine incursions are recorded especially in the Turonian/Coniacian (Dale and McMillan, 1997). The alluvial sediment succession consists of a variety of white, red and pale grey kaolinitic clays and clean gritty sand with red beds (Table 4.1) and ferruginised horizons (hardgrounds) deposited in a coastal-plain environment. The alluvial sediments include variable amounts of lignite and wood, amber, plant material, spores and seeds (Dale and McMillan, 1997; 1998b). Framboidal pyrite, lignite and megaspores are observed throughout this succession until the Santonian in the deep oil exploration Kudu 9A boreholes off the West Coast (Figure 4.1; McMillan, 1990). Cementation by iron and manganese oxides of the more permeable upper Cretaceous/lower Tertiary units is common along the Namaqualand and Namibian middle shelf, where these cemented horizons are more resistant to erosion and form seaward-dipping outcrops (Kuhns, 1995; Corbett, 1996). In addition, Rogers (1977) described the petrography of a suite of scarp-forming, ferruginous sandstones, which were dredged from a belt of irregular topography on the middle shelf in water depths of 130 to 160 m off Hondeklip Bay and Port Nolloth (Figure 4.1). He assigned a late Cretaceous-Palaeocene age by comparison with the Pomona Silcrete Beds. Bamford and Stevenson (2002) suggested that the ferricrete horizons formed during the late Cretaceous (Turonian to Coniacian), where waterlogged, highly reducing conditions persisted in the deeply incised valleys of the coastal plain. The thick sedimentary Cretaceous succession, dominated by siliciclastic sediments, indicates that large-scale fluvial systems supplied the sediment that accumulated on the continental margin off Namaqualand during the late Cretaceous drift phase (Kuhns, 1995; Corbett, 1996; Dale and McMillan, 1998b; Corbett and Burrell, 2001; Bamford and Stevenson, 2002).

The sedimentology and age of the distal Orange Basin Cretaceous succession is largely based on the work undertaken on the deep oil-exploration boreholes (McMillan, *in prep.*), with the foraminiferal assemblages of the Cretaceous succession recorded in the deeper off-delta Kudu boreholes described by McMillan (1990). The proximal (continental shelf) succession is largely dated by up-dip projection on seismic sections, with a middle Albian to upper Santonian succession cropping out at the sea floor in the proximal Orange Basin (Figure 4.2; Dale and McMillan, 1997). In addition, upper Cretaceous sediments, which occur below a thin veneer of Quaternary sediments on the inner shelf, are commonly recovered during diamond exploration coring operations and have been dated using the predominantly agglutinated foraminiferal assemblage present in the marine transgressive sequences (Dale and McMillan, 1997; Compton *et al.*, 2002). The shallow seaward dip of the Cretaceous sequence (Figure 4.2; Brown *et al.*, 1995) results in the oldest sediments cropping out adjacent to the coast, the strata progressively younging seawards, with lower Campanian and upper Maastrichtian packages occurring beneath the Tertiary sedimentary wedge only under the outer shelf/slope region (Dale and McMillan, 1997; Bamford and Stevenson, 2002).

University of Cape Town

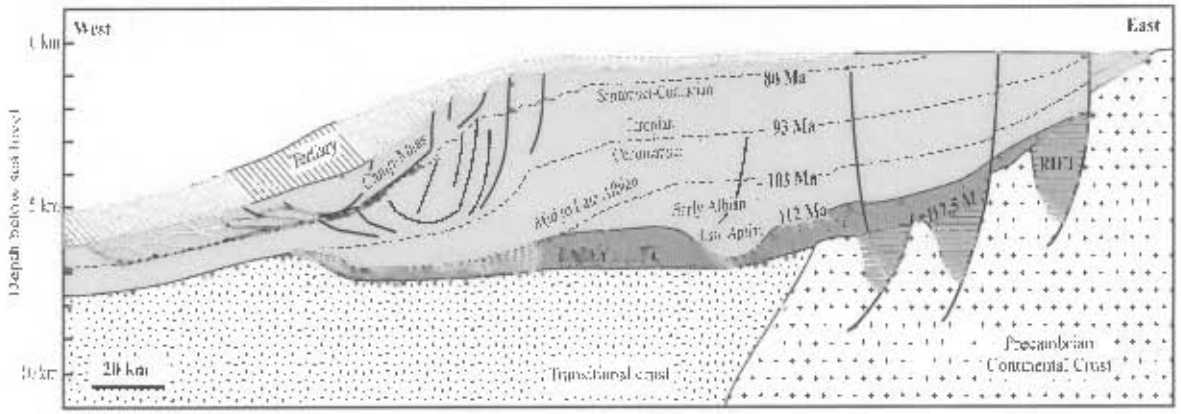


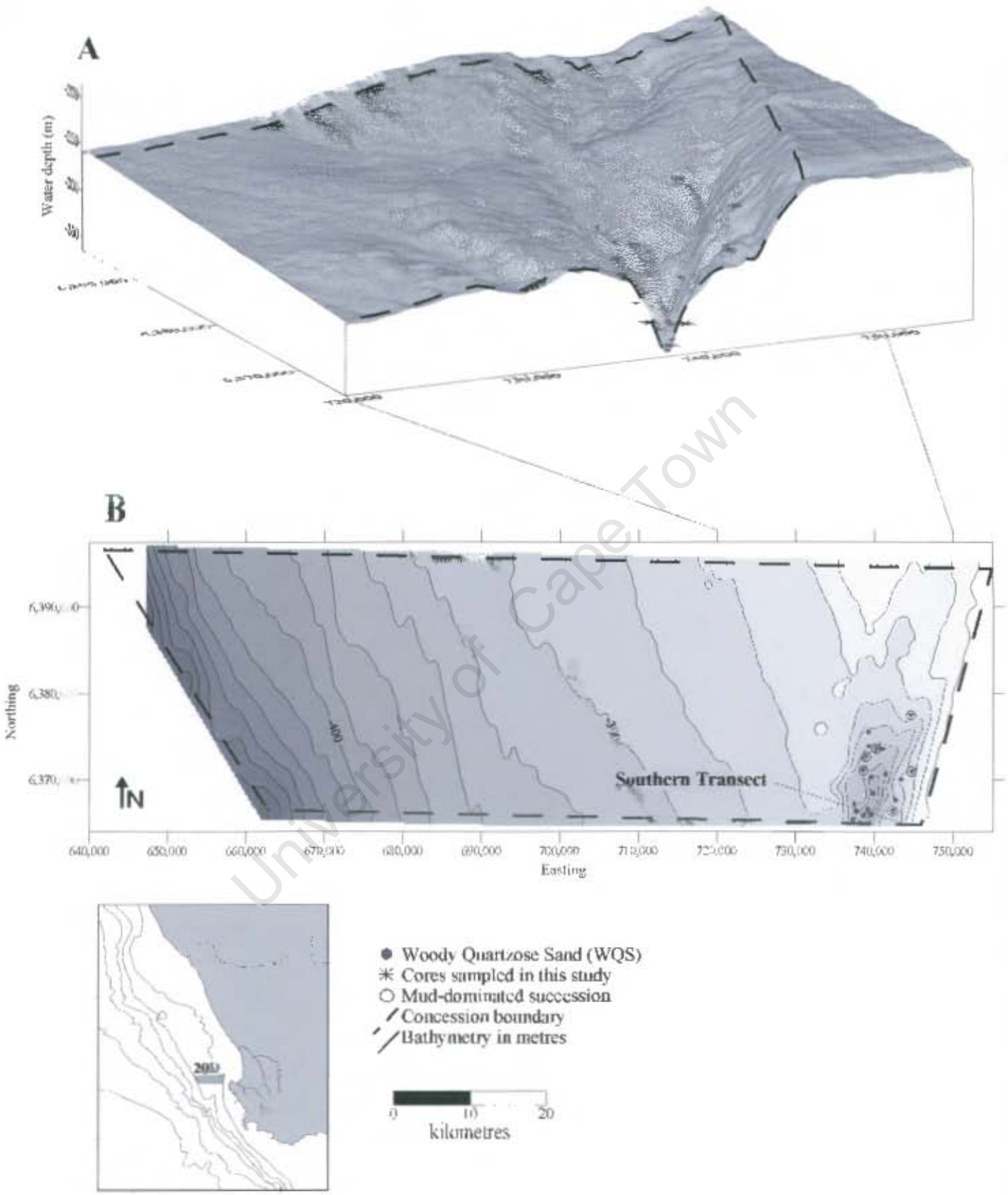
Figure 4.2. A schematic cross section across the central Orange Basin after the poster display by the Petroleum Agency SA for the AAPG 2002 conference, Houston, Texas (see Figure 2.3).

4.3 CRETACEOUS STRATIGRAPHY OF THE STUDY AREA

The oldest sedimentary unit recovered in the study area is defined as the Woody Quartzose Sand unit. The Woody Quartzose Sand was recovered in a number of cores collected in the deepest central part of the main channel in the south of the Cape Canyon Head area at water depths greater than 290 m (Figure 4.3). However, the Woody Quartz Sand unit was recovered from cores in shallower water depths (≤ 248 m) on the steep eastern flank of the canyon, and in a single outlier, Core 237, to the north. The northern erosional outlier is located above the up-faulted block of unconsolidated Cretaceous clayey sediments observed in the mini-gun and chirp seismic profiles and described in more detail in Chapter 3. The Woody Quartzose Sand unit was recovered in three of the cores of the southern transect (Figure 4.3) from within the main channel of the Cape Canyon (Figure 4.4). Eight representative sediment samples were analysed from the three cores (see Appendix 1).

The Woody Quartzose Sand succession is unconformably overlain by the basal gravel lag of the Pleistocene quartzose glauconitic sediments of the Cape Canyon Head succession, which is discussed in detail in Chapter 8. The exception to this stratigraphic relationship is observed in Core 319 (Compton *et al.*, 2004), where the Cretaceous mud-rich interval is overlain by a thin limonitic lower Miocene gravel interval and a middle to upper Miocene (16.9-17.5 Ma) calcareous muddy sand (Chapter 6). Core 359 has a sharply defined erosional contact and is the only core studied in which no basal lag occurs between the brown mud of the Woody Quartzose Sand and the overlying Pleistocene sand. The upper ±30 cm of the Woody Quartzose Sand, below the basal lag, is commonly bioturbated. Large burrows up to 5 cm in diameter are filled with sand and gravel of the overlying sediments (Figure 4.5). The gravel lag is dominated by pebble- to cobble-size dark brown phosphorite, phosphatised shell fragments, quartz and shell fragments. Minor amounts of wood, sharks teeth, agate pebbles and limestone gravel occur in some of the lag layers. Reworked Cretaceous material was observed in the gravel-lag deposits of the overlying Pleistocene sand in some of the cores from the main channel of the Cape Canyon (*e.g.* Core 178). Ferricrete cobbles are a common component of these gravel lag deposits and ferricrete nodules and carbonate clasts are observed at the erosional contact in Core 319 (Compton *et al.*, 2004).

University of Cape Town



University of Cape Town

Figure 4.3. The distribution of the Woody Quartz Sand in A) A wire-frame projection of the Cape Canyon Head region only and in B) the whole of Concession 205. The cross-section of the Southern Transect is illustrated in Figure 4.4.

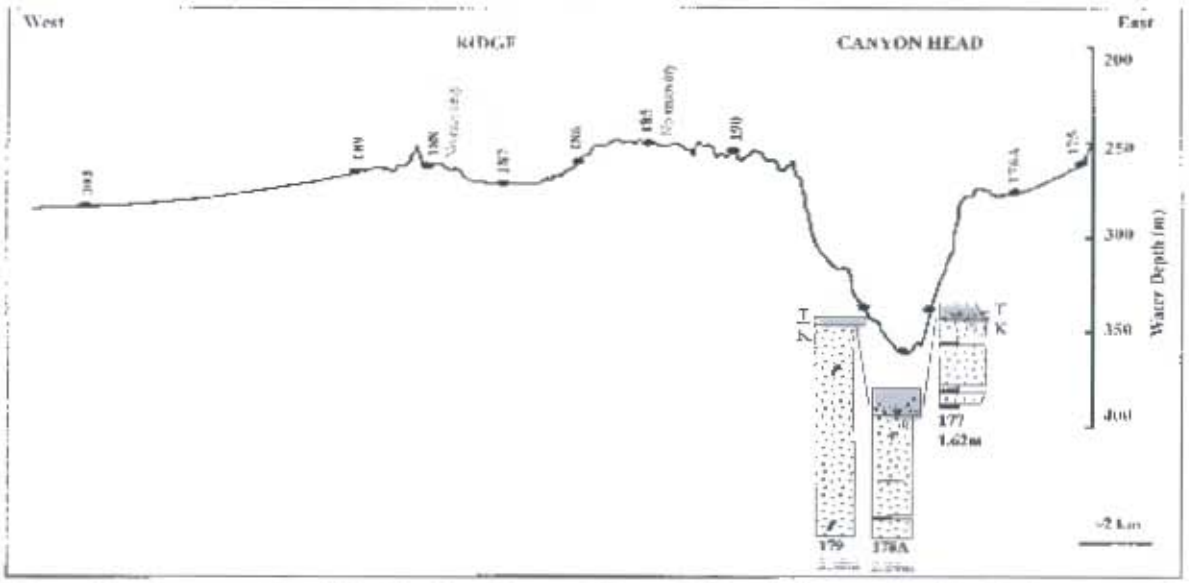


Figure 4.4. A cross section of the Southern Transect (Figure 4.3) with the core logs for the three cores that intersect the the Woody Quartzose Sand unit.

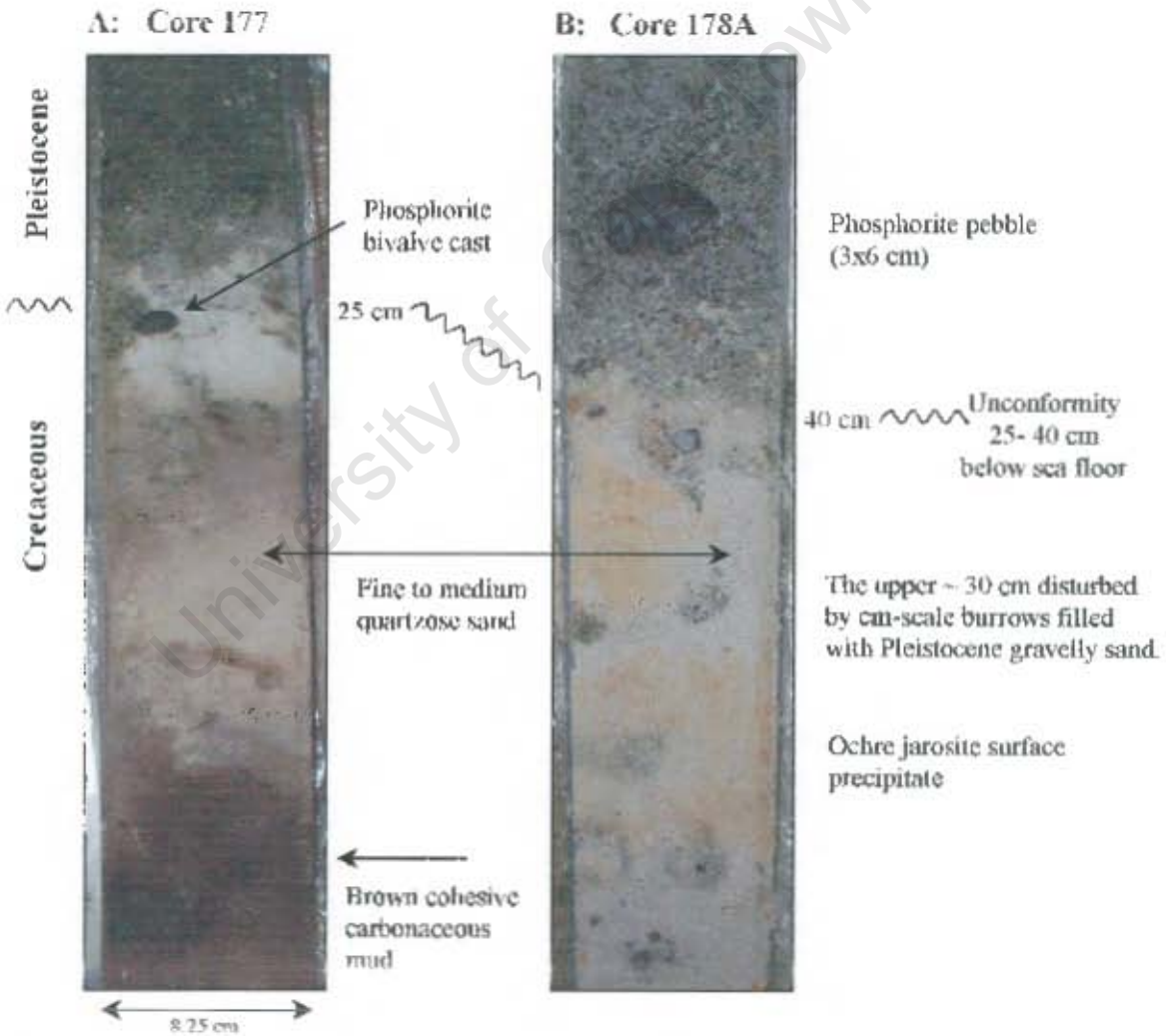


Figure 4.5. Photographs of the Woody Quartzose Sand from split cores, showing the bioturbated contact between the Cretaceous Woody Quartzose Sand and a typical Pleistocene phosphorite- and quartz-dominated gravel lag. The variation between pink sand and brown mud-rich layers is shown in Core 177 (**A**). The post-coring alteration of sulphides results in the formation of ochre-coloured jarosite visible on the cut core surface of Core 178A (**B**).

University of Canterbury

Late Cenozoic reworking or slumping of the Woody Quartzose Sand sediments is preserved in Core 153A, collected within the main channel, where a 10 cm thick interval of the Woody Quartzose Sand unit is interbedded within younger quartz glauconite-rich Cenozoic sediments.

4.4 LITHOLOGY OF THE WOODY QUARTZOSE SAND

The Woody Quartzose Sand unit is composed of unconsolidated interbedded pink-grey coloured quartzose sand and brown kaolinitic mud (Figure 4.4 and 4.6) with scattered wood fragments in both sandy and muddy layers. The Woody Quartzose Sand facies varies between a 4 m thick sand (*e.g.* Core 192A) and a > 3 m thick cohesive mud (*e.g.* Core 237B). The location of mud-dominated cores is indicated in Figure 4.3. The mud-dominated sediments are found along the flanks of the canyon and in the northern erosional outlier above the upfaulted block of Cretaceous sediments (Figure 4.3; Chapter 3). Interbedded sand and mud layers are common, varying from thin (≤5 mm) carbonaceous muddy laminations to <45 cm thick mud layers in a predominantly sandy sediment (*e.g.* Cores 177 and 178A in Figure 4.4). The Woody Quartzose Sand varies between a sand and a sandy mud according to the Folk (1965) classification (Figure 4.7). The slightly gravelly sand and the gravelly muddy sand reflect the presence of wood fragments (<10 cm) in the sediment. The Woody Quartzose Sand includes both fining-upward and coarsening-upward units, where a decrease in mud up-core is associated with an increasing mean grain size in Core 177, whereas Core 179 has an up-core increase in mud content.

The sand fraction varies from a fine (2-3 phi) to a medium (1-2 phi) sand and is well to moderately well sorted (Figure 4.8). The sand fraction is dominated (>95%) by subangular to subrounded quartz grains, with minor to trace amounts of well-rounded quartz grains present (Figure 4.9). Medium sand-size wood fragments produce a bimodal grain size distribution in some samples (Samples 197-2 and 178-4) in Figure 4.8. The wood fragments are carbonised (M.Bamford *pers. comm.*, 2002) and often associated with abundant pyrite. The quartz grains have a frosted appearance and a slight pink colour. Minor quantities of ochre-stained quartz grains are present in all samples and trace to minor amounts of muscovite are present. Minor gypsum crystallization on the surface of quartz grains in the sandy samples is observed in some samples. Traces of megaspores, pyrite framboids, pyrite-cemented quartz grains, partially pyritised (plant) woody material and yellow amber grains (>250µm <2mm) are present in the sand fractions of the mud-rich samples (Figure 4.9; Figure 4.10). One of the megaspore species is identified as *Henrisporites* Potonié, 1956, a well-known form in Cretaceous sediments (de Villiers and Wigley, *in prep.*). No foraminifera were observed in any of the samples studied. The surfaces of the quartz grains have a weathered and deeply etched appearance with linked etch pits (Figure 4.11). The precipitates observed on the surfaces of the ochre-stained quartz grains are shown in Figure 4.11 to be a diagenetic Fe (and Ti) oxide.

The Woody Quartzose Sand samples were all tested individually for the presence of carbonate material by adding a 10% HCl acid solution onto the sample under a binocular microscope. The samples were $CaCO_3$-free, although a single sample, 177-5, collected from the base of the core, including trace amounts of very fine to fine sand-size, very worn, indeterminate carbonate fragments. Wood fragments,

University of Cape Town

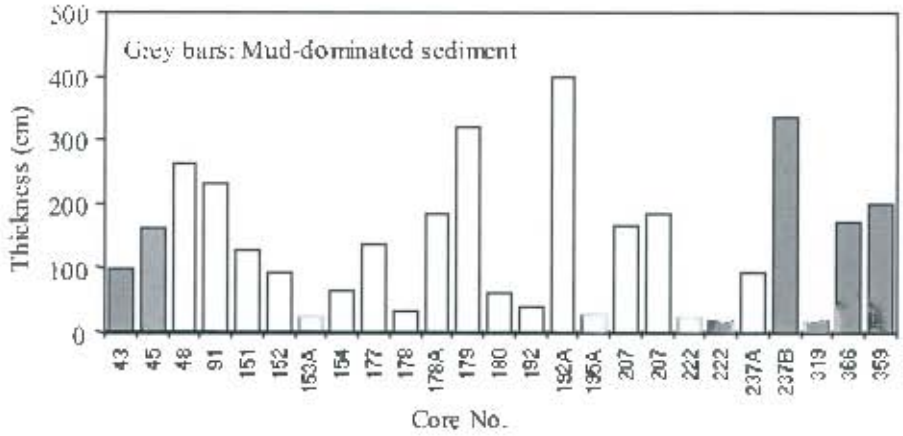


Figure 4.6. A summary of the recovered thickness of the Woody Quartzose Sand.

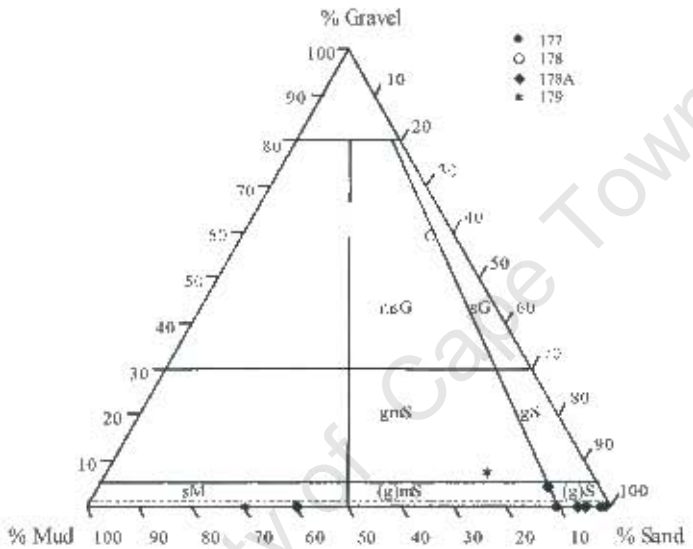


Figure 4.7. A summary of the Cretaceous Woody Quartzose Sand grain size textures

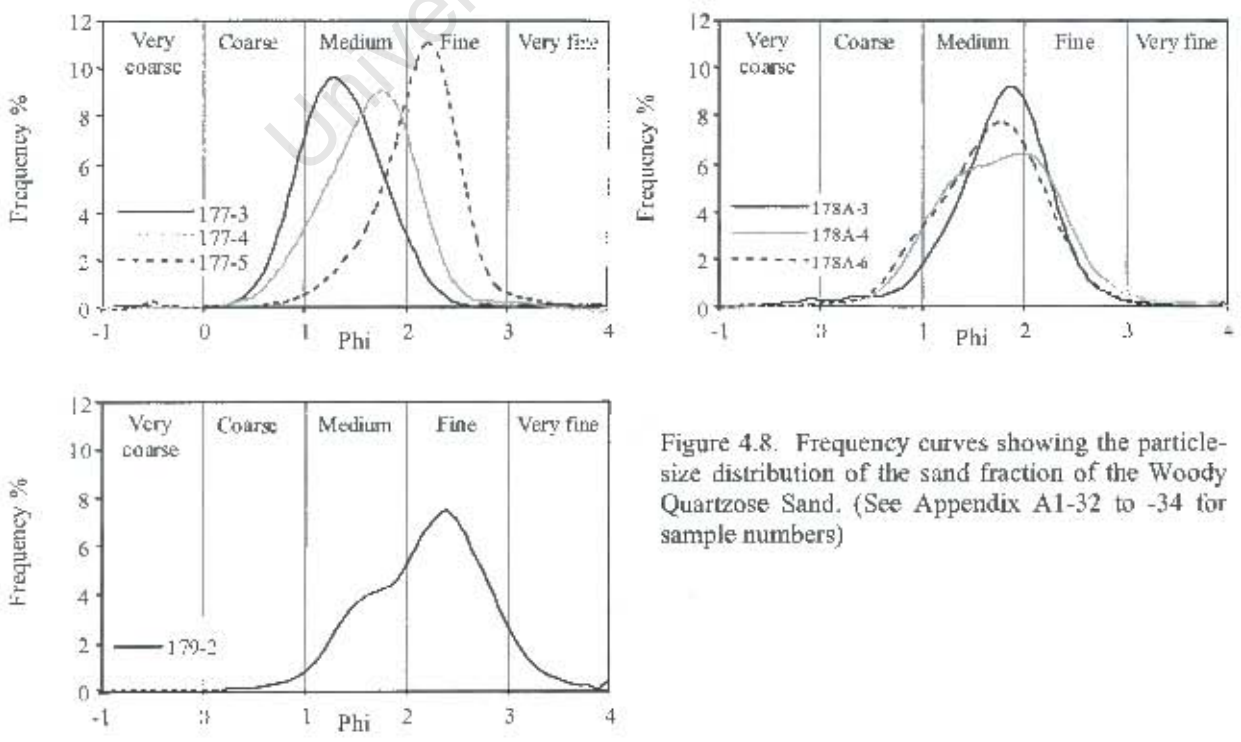


Figure 4.8. Frequency curves showing the particle-size distribution of the sand fraction of the Woody Quartzose Sand. (See Appendix A1-32 to -34 for sample numbers)

University of Cape Town

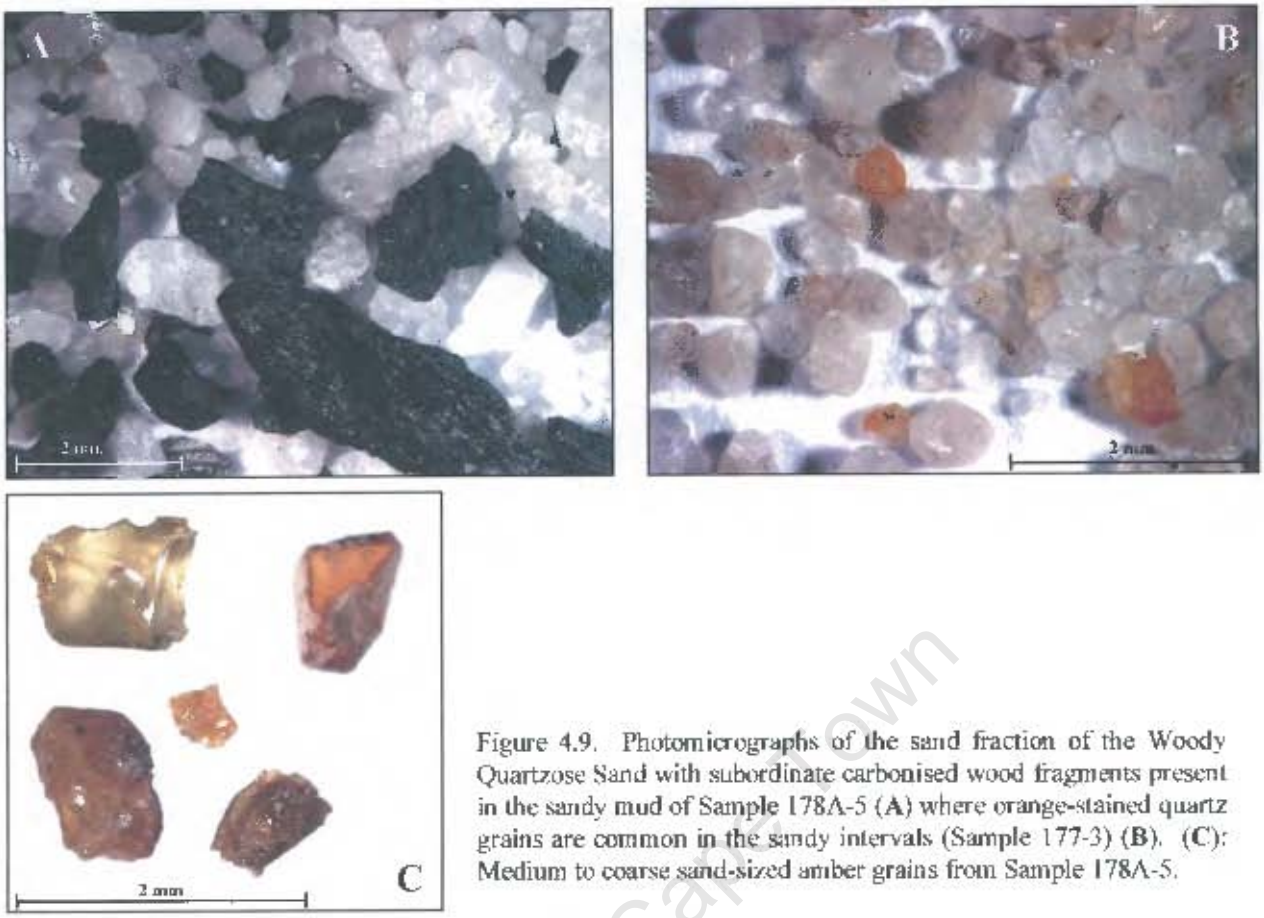


Figure 4.9. Photomicrographs of the sand fraction of the Woody Quartzose Sand with subordinate carbonised wood fragments present in the sandy mud of Sample 178A-5 (A) where orange-stained quartz grains are common in the sandy intervals (Sample 177-3) (B). (C): Medium to coarse sand-sized amber grains from Sample 178A-5.



Figure 4.10. Examples of the megaspores (A *(Henrisporites)* and B) and megaspore cast (C) from the Woody Quartzose Sand of Samples 178A-5 and 179-2.

up to 10 cm in size, are found scattered within both the sand and mud-dominated intervals. The gravel fraction of the Woody Quartzose Sand, where present, is composed entirely of wood fragments. The wood is typically pyritised, either partially (Figure 4.12) or completely pseudomorphed by pyrite. Framboidal pyrite aggregates and pyrite-cemented quartz aggregates are a minor component of the gravel and sand fraction. The mud fraction (<63 μm) is dominated by kaolinite with minor amounts of quartz and a 10 Å sheet silicate (Figure 4.13). Jarosite is identified in Sample 178-6. Natrojarosite and jarosite have similar XRD patterns, where many of the differences in peak position are obscured beneath the muscovite and kaolinite peaks in this record. However, the peaks present at ±14.8 and 15.4 °2-Theta suggests that jarosite rather than natrojarosite (a peak at 16 °2-Theta) is present. Although the cores were collected in 1996 and only sampled in 2002, the preservation of the core material was good. However, ochre-coloured jarosite crystallization is common along the cut surface of the cores (Figure

4.5B) and the presence of gypsum crystallization does suggest that post-coring oxidation of at least some of the pyrite has occurred (Kraus, 1998; Postma, 1983). Although Siesser and Rogers (1976) argued for an authigenic origin for the gypsum present in the organic-rich sediments off Namibia, recent sulphur isotopic analyses of this marine gypsum by Eckardt and Spiro (1999) showed that the gypsum is characterized by light sulphur isotopes ($\delta^{34}S$ of -34.8 to -4.5‰) and cannot therefore be precipitated directly from seawater ($\delta^{34}S$ of +20 to +22‰), but formed from the oxidation of pyrite.

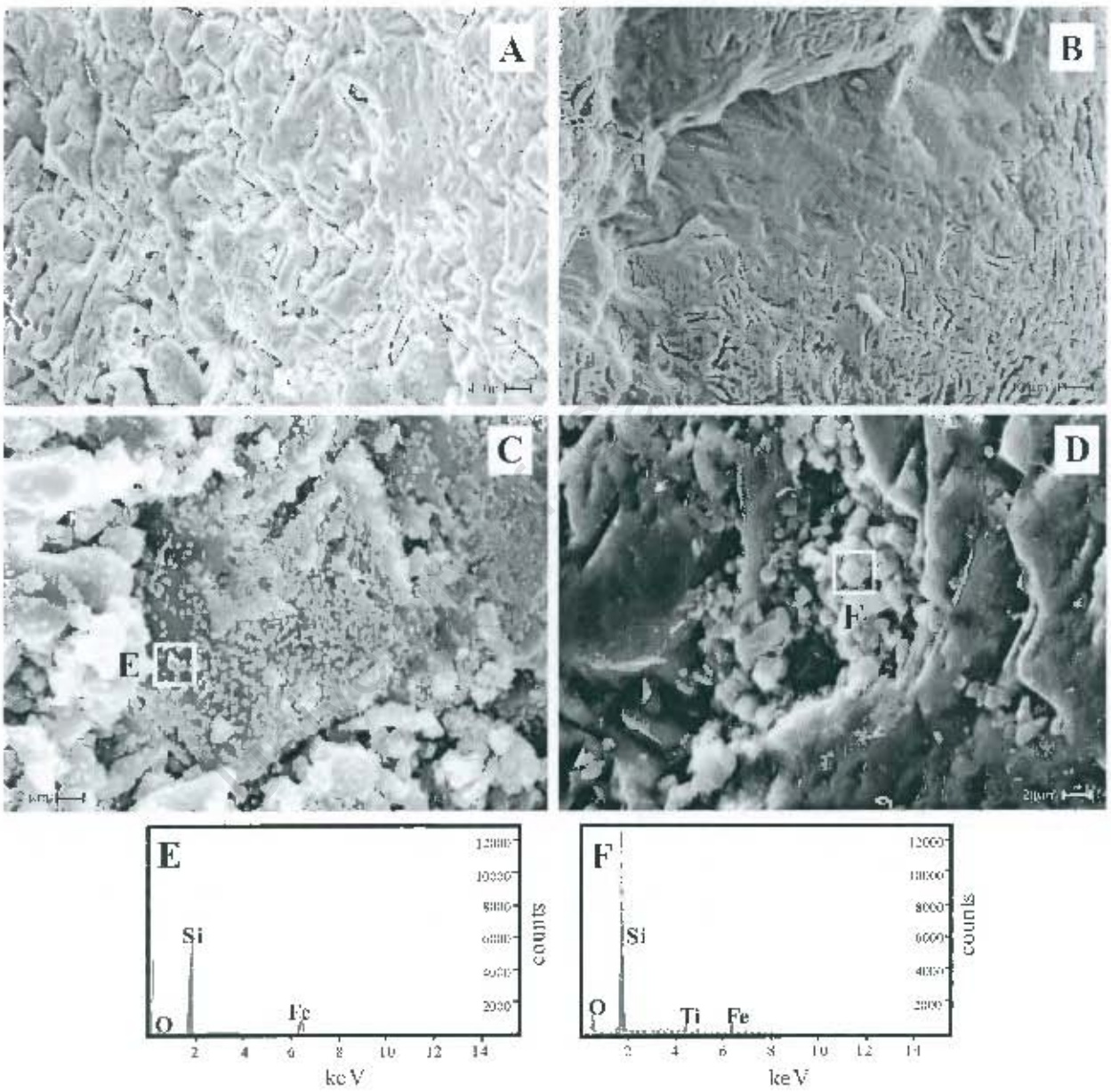


Figure 4.11. SEM images of surface textures of quartz grains from Samples 177-3 (A,C & D) and 177-5 (B) of the Woody Quartzose Sand. Photographs A and B show the etched surfaces of a typical frosted subangular quartz grain. The quartz grain (A) has an orange-coloured surface coating visible at low magnification. Photographs C and D and the EDS scans (marked with a white squares labeled E and F), taken from two different areas clearly illustrate that the tiny surface precipitates on this quartz grain are a Fe (-Ti) oxide. A number of other spot analyses from this and other quartz grains all showed Fe-dominated scans similar to that shown in C.

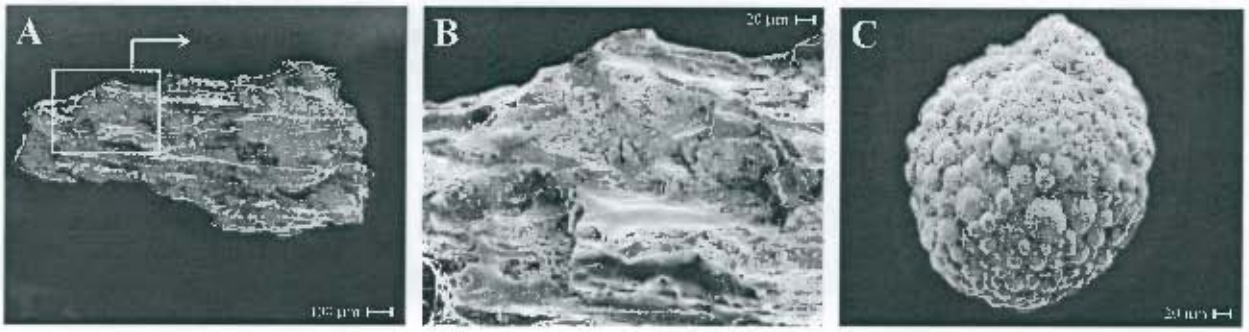


Figure 4.12. Pyritised wood fragments (A & B) and framboidal pyrite (C) from the Woody Quartzose Sand (Sample 178A-5).

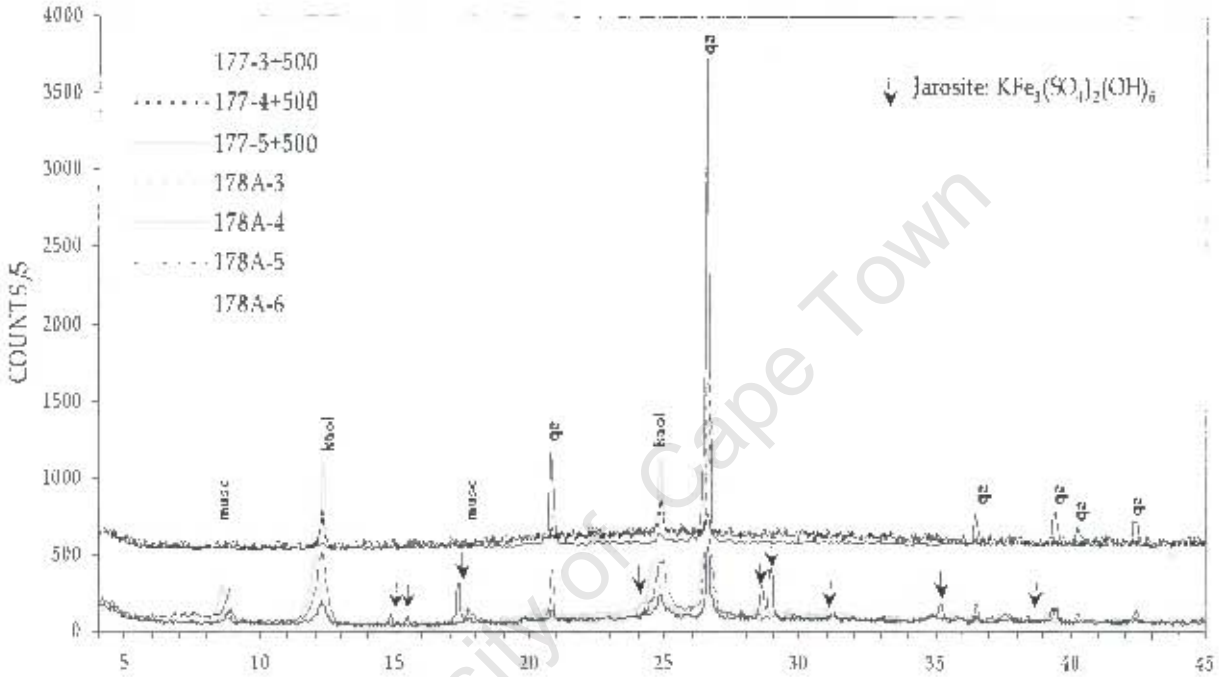


Figure 4.13. A summary of the XRD records for the mud fraction (<63 μm) of the Woody Quartzose Sand.

University of Cape Town

4.5 AGE OF THE WOODY QUARTZOSE SAND

The age of the Woody Quartzose Sand was determined from pollen and wood fragments. Cretaceous sediments offshore southern Africa have been dated using foraminifera (Bolli *et al.*, 1978; McLachlan and McMillan, 1979; McMillan, 1990; Compton *et al.*, 2002), but foraminifera were absent from the samples processed in this study. Stratigraphically, the Woody Quartzose Sand is typically found below a Quaternary gravel lag (Figure 4.5). However, the oldest reworked grains on the Cretaceous/Tertiary contact in Core 319 are skeletal phosphorite grains with an early Miocene Sr-derived age of 21.7-23.1 Ma (Compton *et al.*, 2004).

A number of carbonized wood samples were selected and sent for dating to M. Bamford at the Bernard Price Institute for Palaeontological Research at the University of the Witwatersrand, Johannesburg (Table 4.2). The wood was difficult to section as the material shrank badly and did not make good thin sections (M. Bamford, *pers. comm.* 2002). The wood assemblage supports a Cretaceous age for the deposition for the Woody Quartzose Sand unit. The younger age implied by angiosperm wood of Core

179 may suggest a later reworking of the sediments and further work is required to confirm these initial results and to resolve these discrepancies in ages. However, because the Woody Quartzose Sand is found stratigraphically below the lower Miocene gravel lag in Core 319, the younger Miocene angiosperm age seems unlikely. M. Bamford (*pers. comm.*, 2002) notes that the wood samples collected from the Cape Canyon Head area of Concession 20D are quite different from the predominantly late Cretaceous (Coniacian) Podocarpaceae wood found offshore of Namaqualand (Bamford and Stevenson, 2002; Bamford and Corbett, 1994, 1995)

Table 4.2. Summary of results of the wood biostratigraphy (M. Bamford, *pers. comm.* 2002).

Sample Number	Depth	Comments	Age
Core 151 (BP/16/611 from WMR)	±265 cm	Poorly preserved gymnosperm	Permian to Cretaceous
Core 151	340-345 cm	Gymnosperm	Permian to Cretaceous
Core 179 (BP/16/612 from WMR)	90-95 cm	Angiosperm wood similar to that found in the Miocene Auchas and Arrisdrift deposits.	Latest Cretaceous to Miocene?
Core 179	Two small pieces at 70 cm	Gymnosperm (*Araucarian*)	Permian to Cretaceous
Core 180	Broken pieces collected between 90-100 cm	Gymnosperm	Permian to Cretaceous
Core 356	261 cm	Fragments would not stick onto a slide - no result.	

In order to refine the general Cretaceous age obtained from the wood samples, two samples (178A-5 and 179-2), both from mud-rich intervals, were selected for palynological analyses by S. de Villiers (EGS Palynology Laboratory, UCT) using standard maceration techniques (Doher, 1980). The palynomorph assemblages identified for the two samples are summarized in Appendix 2.

The palynomorph assemblage is dominated by ferns and other lower plants, primitive angiosperms and conifers (S. de Villiers, *pers. comm.*, 2003). The palynomorphs recovered from Samples 178A–5 and 179–2 were compared to the assemblage recorded by McLachlan and Pieterse (1978) from DSDP 361 (Figure 4.1), because this is the only complete Cretaceous palynological record available for southern Africa. The Cretaceous sedimentary record for DSDP 361 is subdivided into two units, namely the lower to upper Aptian Unit 7 and the upper Aptian to Maastrichtian Unit 6 (Melguen, 1978; Siesser, 1978), where the palynomorph assemblage of the two units is quite distinct (McLachlan & Pieterse, 1978). No palynomorph record is available from the lower two cores (25 and 26) of Unit 6 and so the upper Cretaceous palynomorph record, therefore, extends back only to the Cenomanian (McLachlan & Pieterse, 1978). Many palynomorphs found in the Woody Quartzose Sand samples are common to the lower parts of Unit 6 of DSDP Site 361, such as *Clavatipollenites*, *Equisetosporites* and *Nyssapollenites* as well as Taxodiaceae pollen. However, an important difference was noted in that no *Classopollis* pollen (Cheirolepidaceae Family: group of extinct conifers of coastal environments) was found in Samples 178A-5 and 179-2 (de Villiers and Wigley, *in. press*). Taxodiaceae pollen have never been found in Africa before (de Villiers and Wigley, *in prep.*). However, their presence is not unexpected,

University of Cape Town

because other gymnosperm groups are well represented in the palynofloral assemblage, such as the podocarps and cheirolepidaleans. The Family Taxodiaceae pollen identified in the Woody Quartzose Sand unit was misidentified by McLachlan and Pieterse (1978) as *Schizosporis cooksonii* (Pocock, 1962) and is found towards the base of Unit 6 (Cenomanian to Maastrichtian) in DSDP Site 361 (De Villiers and Wigley, *in prep.*), suggesting an earliest late or mid Cretaceous age for the Woody Quartzose Sand unit.

The presence of amber, mica, wood fragments, megaspores and plant material represent additional evidence in support of an Albian to Santonian age for these sediments (Dale and McMillan, 1997, 1998b; I. McMillan, *pers. comm.*, 2002). Gomez *et al.* (2002) reported the first published record of Cretaceous amber in Africa from the lower Cretaceous (middle to upper Valanginian) Kirkwood Formation, although the presence of amber and megaspores are typical of upper Cretaceous sediments along the West Coast of southern Africa (Dale and McMillan, 1997, 1998b). Gomez *et al.* (2002) noted that the amber in the upper Aptian-lower Albian Brazilian Crato Formation (Santana Group, Araripe Basin) is the only other reported evidence of Cretaceous amber in the southern hemisphere.

The Fe-oxide precipitates on the surface of the ochre-stained quartz grains are interpreted as a diagenetic precipitation of authigenic haematite, characteristic of continental red beds (Turner, 1980). Stevenson and McMillan (*in press.*) described three distinct units containing red-beds within the upper Cretaceous sediment succession of the Orange Basin (Table 4.1). The continental red-bed association of the Woody Quartzose Sand is most likely to be correlated with the middle Albian to lower Cenomanian proximal fluvial succession (Table 4.1). The correlation with the middle Albian to lower Cenomanian unit reflects the nearshore location of the cores, at the eastern edge of Concession 20D adjacent to the pre-Cretaceous basement high (Figure 4.1), where the oldest of the seaward-dipping Cretaceous strata is recovered. The presence of a ferricrete gravel component in the basal lag lying unconformably above the Woody Quartzose Sand unit represents additional circumstantial evidence supporting a mid Cretaceous age for the unit, as a Turonian to Coniacian age is assigned to the ferricrete horizons off Namaqualand (Bamford and Stevenson, 2002).

To summarise, the palynological data suggest an early late Cretaceous age (De Villiers and Wigley, *in prep.*), narrowing down the general Cretaceous age provided by the wood analyses (M. Bamford, *pers. comm.*, 2002). The location of the samples on the inner shelf adjacent to the pre-Cretaceous basement high implies a middle Albian to Cenomanian age (Petroleum Agency SA, 2002; McMillan, *in prep.*), which is supported by the presence of amber and the evidence for red-bed diagenesis in the Woody Quartzose Sand unit. The Woody Quartzose Sand is, therefore, interpreted to be Albian to Cenomanian in age (mid Cretaceous).

University of Cape Town

4.6 PALAEOENVIRONMENTAL RECONSTRUCTION OF THE STUDY AREA

A number of different factors, including sediment composition, as well as micro- and macro-scale textures displayed by the sediments of the Woody Quartzose Sand unit are considered in order to infer the palaeoenvironmental conditions prevailing during deposition in the mid Cretaceous. The first important question addressed is whether these sediments were deposited in a subaerial or submarine environment. Agglutinated benthic foraminifera are common in Upper Cretaceous (Turonian and Coniacian) marine and estuarine environments (Dale and McMillan, 1997) and the absence of any foraminiferal assemblage suggests an upper delta plain/fluvial depositional environment for the Woody Quartzose Sand.

The abundance of organic material in the Woody Quartzose Sand supports a diagenetic origin for the pyrite. The formation of pyrite resulting from the degradation of organic matter in anoxic marine sediments is well documented (Berner, 1984; Raiswell and Berner, 1985). However, pyrite is also found associated with poorly drained wetland ecosystems, which have waterlogged anoxic conditions and abundant organic matter (Postma, 1983; Giblin and Wieder, 1992; Kraus, 1998), where the H_2S released during early diagenesis may be fixed as pyrite (Berner, 1984; Giblin and Wieder, 1992). In contrast to the pervasiveness of pyrite in marine environments and brackish water swamps, freshwater wetlands are dominated by organic sulphur with much lower concentrations of pyrite (Giblin and Wieder, 1992). The abundance of pyrite in the samples therefore may imply a marine to brackish water swamp environment. The location of the study area on the margin of the ancient landmass of Figure 4.14 indicates that a coastal environment is most likely. Typical marine siliciclastic sediments have a relatively narrow range in the C/S ratio (Berner, 1984; Raiswell and Berner, 1985; Morse and Berner, 1995), and the C/S ratio is a useful tool to determine palaeodepositional environment. Future work, utilizing this technique, would help confirm the palaeodepositional environment.

A number of microtextural features observed for the quartz sand grains imply a subaerial depositional environment. Severe etching of the quartz grains is typical of humid tropical continental weathering environments (Eswaran and Stoops, 1979; Malengreau and Sposito, 1997; Schulz and White, 1999), where conditions of high rainfall, low pH and high concentrations of organic acids favour quartz dissolution (Pye and Mazzullo, 1994). Howard *et al.* (1995) described the weathering and etching of quartz as a micromorphological progression from smaller to larger triangular/rhombohedral to irregular shaped etched pits to an interconnected or anastomosing network of miniature grooves and crevasses, finally resulting in bulk decomposition of the grains. They noted that a preferential or selective dissolution pattern, commonly observed, suggests a crystallographic control to dissolution. The linked etch pits on the quartz-grain surfaces, observed in the Woody Quartzose Sand unit, therefore reflect considerable dissolution of the quartz grains (Krinsley and Doornkamp, 1973; Howard *et al.*, 1995) and suggest that a humid tropical environment existed during deposition of these sediments. In addition, the diagenetic precipitation of haematite on quartz-grain surfaces is a common process in tropical or humid continental environments (Pye, 1983), with alternating wet and dry periods favouring rapid weathering

University of Cape Town

(Padmanabhan and Mermut, 1996). In addition, the diagenetic processes involved in the formation of continental red beds are also evidenced by dissolution features on quartz grains and the paucity of unstable silicate grains (Turner, 1980). Pye and Mazzullo (1994) note that chemical weathering favours an increased angularity of quartz grains.

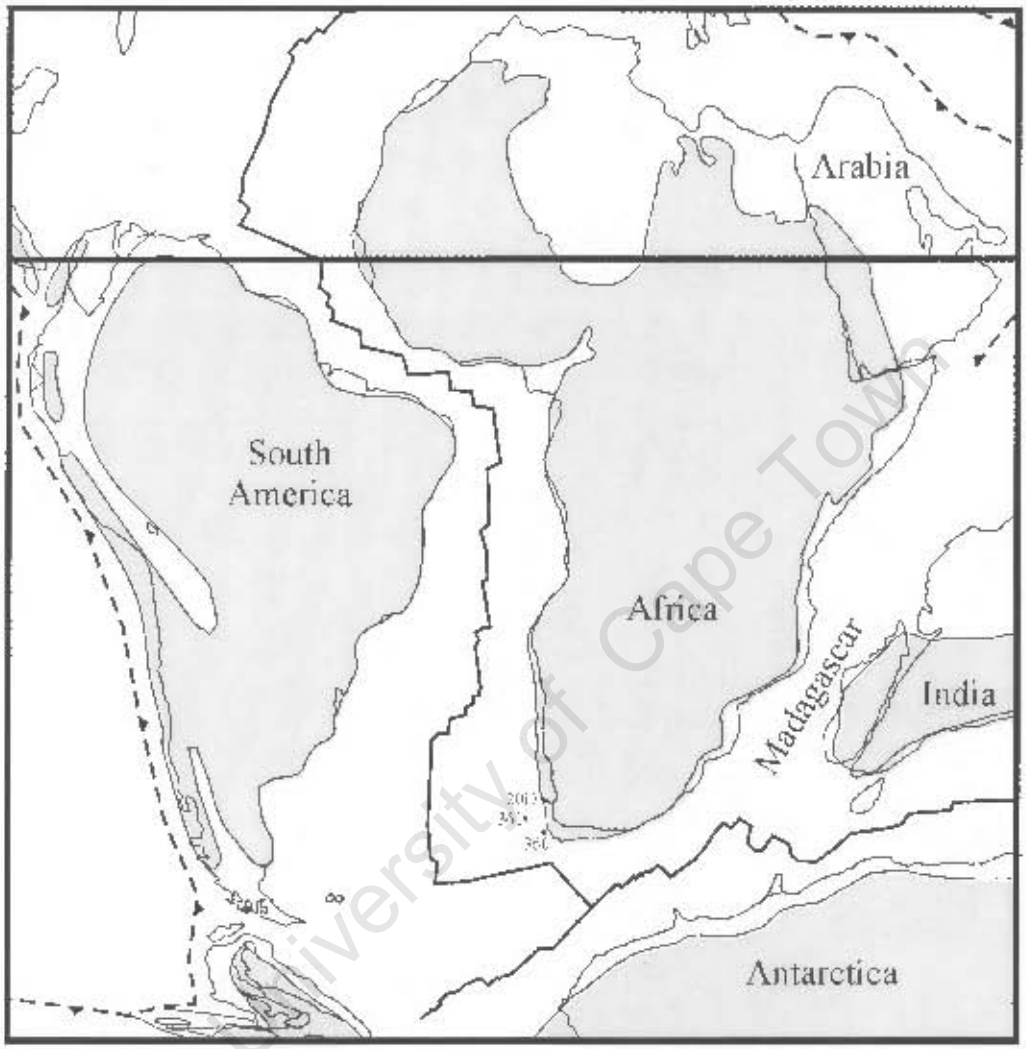


Figure 4.14 The palaeogeographic map of the continents during the mid Cretaceous (96 Ma) using the Scotese Paleomap Program, showing the approximate location of Concession 20D and the two DSDP Sites 360 and 361. The ancient landmasses are shaded grey with the modern landmasses outlined.

The interbedded sands and muds of the Woody Quartzose Sand suggest that anoxic, water-logged swamps/marshy mud flats of the mid Cretaceous coastal plain were cross cut by channel-infill quartz sands, sandbanks or sand-sheets, although insufficient information is available to define this environment in any more detail. Dale and McMillan (1998b) described similar depositional environments of the coastal regions of the West Coast of southern Africa during the late Cretaceous, which they interpreted to have included a complex interplay of subtidal channels, intratidal sand flats and mudflats. The Albian-Cenomanian quartzose sand off the West Coast is dominated by fluvial successions of alternating sand and kaolinitic clay (Dale and McMillan, 1998b). Similar sand-dominated Albian (mid Cretaceous) sediments are recovered in borehole P-A1 drilled within the study

University of Cape Town

area by SOEKOR (I. McMillan, *pers. comm.*, 2001) as additional support for a mid Cretaceous age for the Woody Quartzose Sand. Upper Cretaceous (Coniacian) non-calcareous, unconsolidated quartzose sand, mottled muddy sand and pyritic mud were recovered in two cores collected in a water depth of 122 m, offshore from Wreck Point (Figure 4.1) (Compton *et al.*, 2002). The quartzose sand is composed of very fine to medium, angular to subangular quartz with mica, sandstone clasts, wood and lignite present locally. The pyritic mud is composed of illite, kaolinite and chlorite with iron sulphide nodules and includes agglutinated foraminifera. The Cretaceous sediments are assigned a Coniacian age using seismic data and the agglutinated benthic foraminifera are, similarly, interpreted to have been deposited in a coastal environment with alternating terrestrial and marine deposition (Compton *et al.*, 2002).

Tönsing *et al.* (2002) describe the fluvial systems of the mid Cretaceous (late Aptian) 13A channel sandstones of the Bredasdorp Basin, where the provenance varied from the southwest (*i.e.* sediment supply from the Columbine-Agulhas Arch) to the northeast during a low sea level and an early transgressive period. Although slightly older than the Woody Quartzose Sand, evidence suggests that large fluvial systems draining the Columbine–Agulhas Arch were present in the mid Cretaceous, with sediments being transported to both the Orange and Bredasdorp basins. The younger units of the Bredasdorp Basin have not been studied in any detail, because of the lack of any economic hydrocarbon potential, although fluvial input from the northwest and from the northeast continues throughout the drift succession (Brown *et al.*, 1995). The condensed Cretaceous sediment record on the flanks of the Columbine-Agulhas Arch has been interpreted to reflect repeated uplift and erosion events (Brown *et al.*, 1995), which would have resulted in reactivation of fluvial activity.

The evidence used to suggest a coastal plain subaerial environment of deposition for the Woody Quartzose Sand unit, also provides information on the prevailing palaeoclimate, where the microtextures all suggest a humid tropical environment. The mud fraction of the Woody Quartzose Sand is dominated by kaolinite, whereas the overlying Cenozoic sediments of the study area (see later sections), and the West Coast, in general (Birch, 1974), are dominated by illite. Similarly, the Cretaceous sediments of the proximal Orange Basin are dominated by kaolinite (Dale and McMillan, 1998b; Bamford and Stevenson, 2002). The deeply kaolinised weathering profiles and massive duricrusts observed below remnants of the Cretaceous African Surface along the West Coast of southern Africa, reflect the humid climatic conditions that existed for most of the Cretaceous (Partridge and Maud, 1987; Partridge, 1998; Tyson and Partridge, 2000). The palynomorphs from Concession 20D, with a predominance of fern spores, supports humid climatic conditions, and the conifer pollens, including *Podocarpidites*, *Araucariapollenites*, *Inaperturopollenites*, *Taxodiaceaepollenites*, signify a forest vegetation. However, No tropical pollens were present in the Woody Quartzose Sand unit.

Sedimentological evidence, including quartz-grain dissolution and the diagenetic precipitation of haematite, observed in the Woody Quartzose Sand samples suggests a humid climate for the mid to late Cretaceous, which is in general agreement with the available literature regarding the late Cretaceous climate for southern Africa (Bamford and Stevenson, 2002; Tyson and Partridge, 2000; Pickford and

University of Cape Town

Senut, 1999). Foraminiferal and palynology studies indicate a more temperate humid climate along the West Coast of southern Africa during the mid to late Cretaceous, (I. McMillan, *pers. comm.*, 2003; S. De Villiers, *pers. comm.*, 2003). No large benthic foraminifera, typical of tropical waters, have been observed in any of the Cretaceous units (McMillan, 1990; I. McMillan, *pers. comm.*, 2003). Pollen studies undertaken on samples from the Namaqualand area have, similarly, yielded few tropical forms (S. De Villiers, *pers. comm.*, 2003).

The Late Cretaceous climate of southern Africa is described as warm and humid with high seasonal rainfall and deep weathering profiles (McLachlan and Pieterse, 1978; Partridge, 1998; Tyson and Partridge, 2000; Bamford and Stevenson, 2002). Dingle *et al.* (1983) argued that the high clay content and rapid sedimentation rates in distal parts of the basin, together with the delta-front slumps of the late Cretaceous indicate a high sediment input, which implies a wet and warm onshore climate. Additional information on palaeoclimate comes from work done on DSDP Site 361, where a warm and wet Cretaceous palaeoclimate is envisaged (McLachlan and Pieterse, 1978; Siesser, 1978). Melguen (1978) suggests that the decreasing terrigenous sand fraction, plant material and mica abundances upcore in Unit 6 of DSDP Site 361 (Figure 4.1), may reflect a possible decrease in rainfall on the continent. Many of the crater lakes associated with kimberlitic and olivine-melilitite pipes of Namaqualand and Botswana preserve palynological, wood and fossil records, which have provided some palaeoenvironmental constraints (Scholtz, 1985; Partridge, 1998; Pickford and Senut, 1999). Palynological evidence from the Arnot "Kimberlite" Pipe from Banke, Namaqualand, taken in conjunction with similar studies from the crater lakes of Botswana suggests that some zonation of the dominant forest vegetation of southern Africa existed during the Late Cretaceous (Scholtz, 1985).

Lower Cretaceous fossil woods are a common reworked component of the Pleistocene diamondiferous deposits of both the Namaqualand shelf (~100-150 mbsl) and palaeoshorelines of southern Africa (Bamford and Corbett, 1994; 1995). These woods are predominantly primitive members of the Podocarpaceae family, which grew on the extensive low-lying coastal regions in the early Cretaceous, indicating a moister climate than that of today (Bamford and Corbett, 1994). Bamford and Stevenson (2002) described an *in situ* exhumed upper Cretaceous (Coniacian ~83-88 Ma) fossil forest on the continental shelf off Buffels Bay at the mouth of the Buffels River (Figure 4.1) in a water depth of 136-140 m, which represents one of the rare examples of upper Cretaceous woods in southern Africa. Bamford and Stevenson (2002) interpreted the late Cretaceous coastal plain of southern Africa off Namaqualand, from at least as far south as the Groen River to Bogenfels in the north (Figure 4.1), to have had deeply incised valleys and dense low-canopy or riverine forest vegetation in the valleys with a humid and seasonally wet climate. The presence of wood fragments in the Woody Quartzose Sand unit, together with the conifer palynomorphs, suggests that the Columbine-Agulhas Arch was forested in the mid Cretaceous and that the extensive Cretaceous forested areas of Namaqualand (Kleinzee to the Orange River), described by Bamford and Corbett (1995), extended much farther south than originally estimated.

University of Cape Town

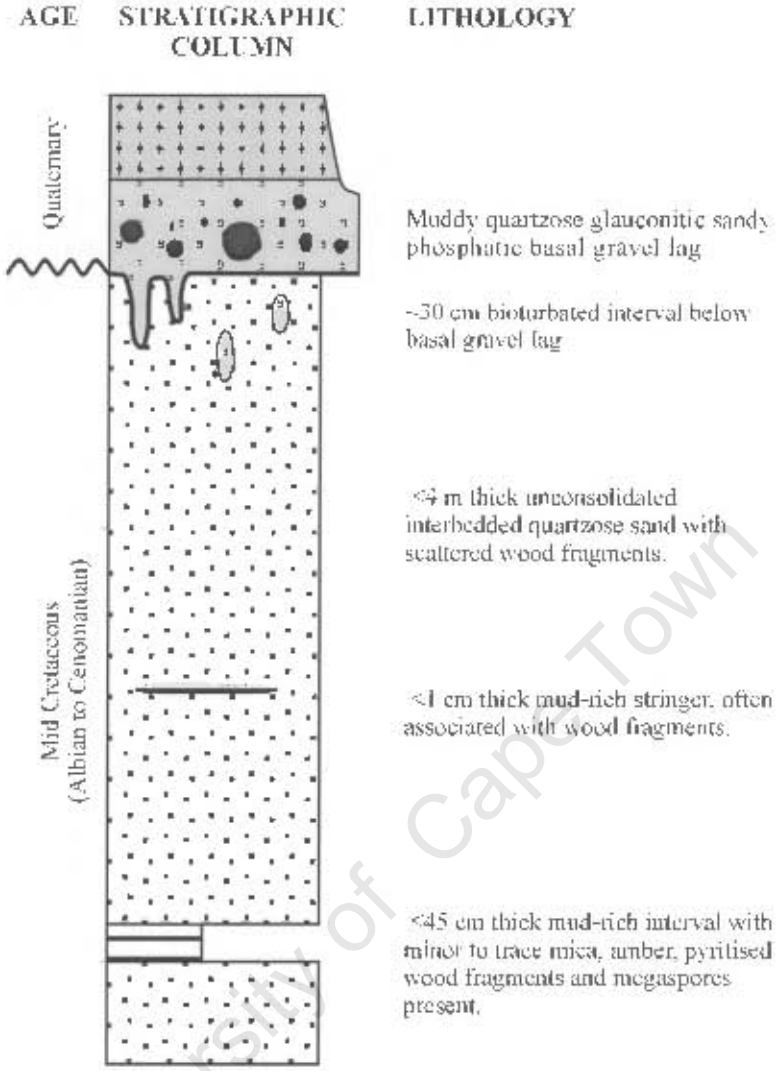


Figure 4.15. A schematic stratigraphic column for the Quartzose Woody Sand, based on Core 178A

University of Cape Town

4.7 CONCLUSIONS

The Woody Quartzose Sand unit is composed of unconsolidated interbedded brown kaolinitic mud and pink-grey coloured, well to moderately well sorted, subangular to subrounded, fine to medium grained quartzose sand (Figure 4.15). The absence of diagnostic lithic fragments prevents the possibility of identifying the provenance of these quartzose sediments. Scattered sand to small cobble-size wood fragments, partially to completely pseudomorphed by pyrite, are common and deeply etched frosted quartz grains, minor ochre-stained quartz grains with surface Fe-oxide precipitates and minor to trace amounts of muscovite are present in all samples. Trace amounts of megaspores, plant material and sand-size grains of yellow amber (>250μm <2mm) are present in the sand fraction of the mud-rich samples. The unconsolidated Woody Quartzose Sand unit is part of the extensive wedge of Cretaceous sediments, which forms the basal sediments of the western continental margin of southern Africa. The

unconsolidated sediments indicate that they were never deeply buried, with little or no evidence for post-burial diagenetic cementation observed. Dingle (1971a) noted that the only suspected outcrop of Cretaceous material on the western continental shelf occurs north of Cape Town as a small erosional inlier occurring at the bottom of the Cape Canyon.

The Woody Quartzose Sand unit is interpreted, using sedimentary evidence presented in this chapter, to have been deposited in a forested coastal wetland environment during humid wet conditions of the mid Cretaceous (Albian to Cenomanian). The depositional environment was most likely anoxic, water-logged swamp or marshy mud flats, cross cut by channel-infill quartz sand, sandbanks or sand-sheets. The presence of wood debris in the sediment, together with the pollen assemblage, implies that the extensive Cretaceous forested areas of Namaqualand (Bamford and Corbett, 1994, 1995; Bamford and Stevenson, 2002) extended much farther south than originally estimated.

This study presents a preliminary examination of the mid Cretaceous Woody Quartzose Sand unit and has concentrated on the sand-fraction. More detailed studies in the future, concentrating particularly on the organic material (wood and pollen assemblage and organic matter C/S ratio) may provide more details regarding the nature of the surrounding forested area and information on the depositional environment.

University of Cape Town

5 LATE CENOZOIC PHOSPHOGENESIS ON THE WESTERN SHELF OF SOUTH AFRICA IN THE VICINITY OF THE CAPE CANYON

Chapter 5 is a copy of a paper, of which I am second author, submitted and accepted by *Marine Geology* for publication in 2004. This paper, focusing on the late Cenozoic phosphogenesis of the western margin of southern Africa, includes the currently available Sr-isotope stratigraphy (Compton) as well as a summary of the lithostratigraphy (Wigley) and biostratigraphy (McMillan). The paper sets up the chrono- and biostratigraphy utilised in the age models for the late Cenozoic evolution discussed in the subsequent Chapters 6-8.

University of Cape Town

ELSEVIER

Marine Geology 206 (2004) 19–40

MARINE GEOLOGY
INTERNATIONAL JOURNAL OF MARINE GEOLOGY, GEOCHEMISTRY AND GEOPHYSICS

www.elsevier.com/locate/margeo

Late Cenozoic phosphogenesis on the western shelf of South Africa in the vicinity of the Cape Canyon

John S. Compton[a,*], Rochelle Wigley[a], I.K. McMillan[b]

[a] *Department of Geological Sciences, University of Cape Town, Rondebosch 7701, South Africa*
[b] *De Beers Marine (Pty) Ltd., P.O. Box 87, Cape Town 8001, South Africa*

Received 20 May 2003; received in revised form 12 November 2003; accepted 6 February 2004

UNIVERSITY OF CAPE TOWN

Abstract

The strontium isotope ($^{87}Sr/^{86}Sr$) composition of phosphorite (carbonate fluorapatite) cemented grains (PCG), phosphate-cemented limestone (PCL), skeletal phosphorite grains (SPG) and biogenic calcite (mollusc shell, benthic foraminifera and echinoid spines) from sediment on the outer continental shelf in the vicinity of the Cape Canyon ranges from 0.707981 to 0.709167 and corresponds to an age range of late early Oligocene to late Pleistocene. Most biogenic carbonate Sr ages agree with biostratigraphic ages, but some samples contain significantly older and reworked robust (>250 μm) benthic foraminifera. Although the Sr ages of biogenic and phosphorite grains indicate that sedimentation was fairly continuous, most sediment is reworked with only lower Miocene, upper Pliocene and upper Pleistocene successions generally preserved in the study area. The initial phosphogenic episode from the latest Oligocene to early early Miocene (21–26 Ma) was the largest, with additional phosphogenic episodes in the late early Miocene (16–19 Ma) and middle Miocene (10–15 Ma). Most phosphorite occurs as PCG that formed during marine transgressions and highstands from the late Oligocene warming event until the mid-Miocene climatic optimum, a period of episodic Antarctic glaciation and several positive marine $\delta^{13}C$ excursions. Upper Oligocene to lower Miocene PCG have been extensively reworked and are associated with major erosional unconformities. PCG vary from peloidal sands to gravel mollusc moulds and contain variable amounts of quartz, glauconite and pyrite inclusions. PCL formed from 9 to 17 Ma by cementation and replacement of older calcareous sediment during the middle to late Miocene marine regression. Phosphorite, as well as associated glauconite and pyrite, indicate that periods of rapid accumulation of organic-rich, terrigenous muds derived from the focusing of the suspended load of rivers and organic matter produced in areas of coastal upwelling have occurred episodically on the margin since the late Oligocene. The relative paucity of phosphorite younger than the middle Miocene may result from frequent erosional events as documented by pronounced unconformities on the shelf that reflect lowered eustatic sea level, tectonic uplift and high-frequency, high-amplitude Quaternary sea-level fluctuations.
© 2004 Elsevier B.V. All rights reserved.

Keywords: phosphorite; strontium isotopes; sea level; Cape Canyon; Miocene; continental shelf

1. Introduction

The western continental margin of southern Africa is well known as an area of present-day coastal upwelling that results in the deposition of organic-

* Corresponding author. Fax: +27-21-6503783.
E-mail address: compton@geology.uct.ac.za (J.S. Compton).

0025-3227/$ - see front matter © 2004 Elsevier B.V. All rights reserved.
doi:10.1016/j.margeo.2004.02.004

rich muds and authigenic phosphorite formation. Modern phosphorite has been documented to occur in diatomaceous ooze off Namibia (Veeh et al., 1973, Baturin, 2000) as well as perhaps in the Holocene mud belt of the Orange River Prodelta (Compton et al., 2002). Modern phosphogenesis on the western margin of southern Africa occurs in areas of upwelling and mud accumulation where phosphate released by microbial degradation of organic matter during early diagenesis results in precipitation of carbonate fluorapatite (CFA) within pore spaces of the sediment to form CFA-cemented nodules (Bentor, 1980; Birch, 1980; Rogers and Bremner, 1991; Baturin, 2000). In addition to Recent phosphorites, older phosphorites, commonly observed filling and replacing limestone, and associated with abundant glauconite, have been documented along the western margin as far south as the Agulhas Bank, with surface sediments containing between 0.5 and 20 wt.% P_2O_5 (Parker and Siesser, 1972; Summerhayes et al., 1973; Birch, 1979; Rogers and Bremner, 1991). The Cenozoic is poorly preserved on the western continental shelf where sediment successions are thin and many have been extensively reworked (Birch et al., 1991; McMillan, 1993). Lithified CFA-cemented grains, retained in reworked gravel lag deposits on the shelf, can provide a rare record of past fine-grain, organic-rich marine sedimentation (Compton et al., 1993; 2002).

The petrography and geochemistry of phosphorite from the South African margin are well documented (Parker and Siesser, 1972; Parker, 1975), but the age of these older, relict phosphorite deposits is poorly constrained (Birch, 1980). The age of phosphorites from the Agulhas Bank and the outer continental shelf off South Africa was inferred to be largely middle Miocene to Pliocene based on associated microfossils in the limestone that the phosphorite replaced (Parker and Siesser, 1972; Siesser, 1978). However, fossils can be either younger or older than associated reworked phosphorite grains, and fossils included within phosphorite grains provide only a maximum age of phosphorite formation. For example, phosphorite from the South African margin that replaces Eocene to Miocene limestone has been shown to be late Pleistocene in age (Birch et al., 1983). The age of phosphorite and biogenic carbonate grains can be determined by comparison of their Sr isotope composition with the marine Sr isotope record (DePaolo and Ingram, 1985). The utility of Sr isotope analysis is that it provides a means to date phosphorite formation directly and, depending on the steepness of the marine Sr isotope record, can provide ages with uncertainties of less than 1 Myr (Hodell et al., 1991; Farrell et al., 1995). Sr dating of phosphogenic episodes can be used to infer changes in sea level and paleoproductivity, but few studies have applied Sr isotope stratigraphy to deposits on the South African margin (Lavelle and Armstrong, 1993; Compton et al., 2002). In this paper, the Sr-derived ages of phosphorite and biogenic grains are integrated with the biostratigraphy of outer continental shelf successions at the Head of the Cape Canyon to decipher the complex depositional history of the area and its relation to sea level and climate changes.

2. Geological setting

The Orange Shelf on the western South African margin extends from the Orange Banks off the Orange River south to the Cape Canyon (Fig. 1). The Orange Shelf has a narrow inner shelf that extends to 100 m water depth and a broad outer shelf that extends to roughly 400 m water depth (Dingle et al., 1987). The broad Orange Shelf and Agulhas Bank are separated by a relatively narrow shelf defined by a basement structural high, the Columbine–Agulhas Arch, that runs southeast to northwest from offshore of Cape Agulhas to Cape Columbine. Precambrian and Paleozoic basement rocks are exposed along the coastal inner shelf and are overlain further offshore by seaward-dipping Upper Cretaceous sediments and a relatively thin (< 50 m thick) Tertiary cover extending out onto the outer shelf (Rogers, 1977; Dingle et al., 1987). The inner and outer shelf are generally starved of sediment, with only a thin veneer of Quaternary sediments that are generally focused in a band between the Precambrian bedrock along the coast and Tertiary sediments offshore (Birch et al., 1991; McMillan, 1993). River bedload sediment delivered to the coast is largely carried north by longshore drift and much of the sand fraction is blown onshore to form eolian deposits such as the Namib Sand Sea derived from Orange River sand (Rogers, 1977). The suspended load of the Orange, Olifants and Berg rivers is transported south by a poleward undercurrent

University of Cape Town

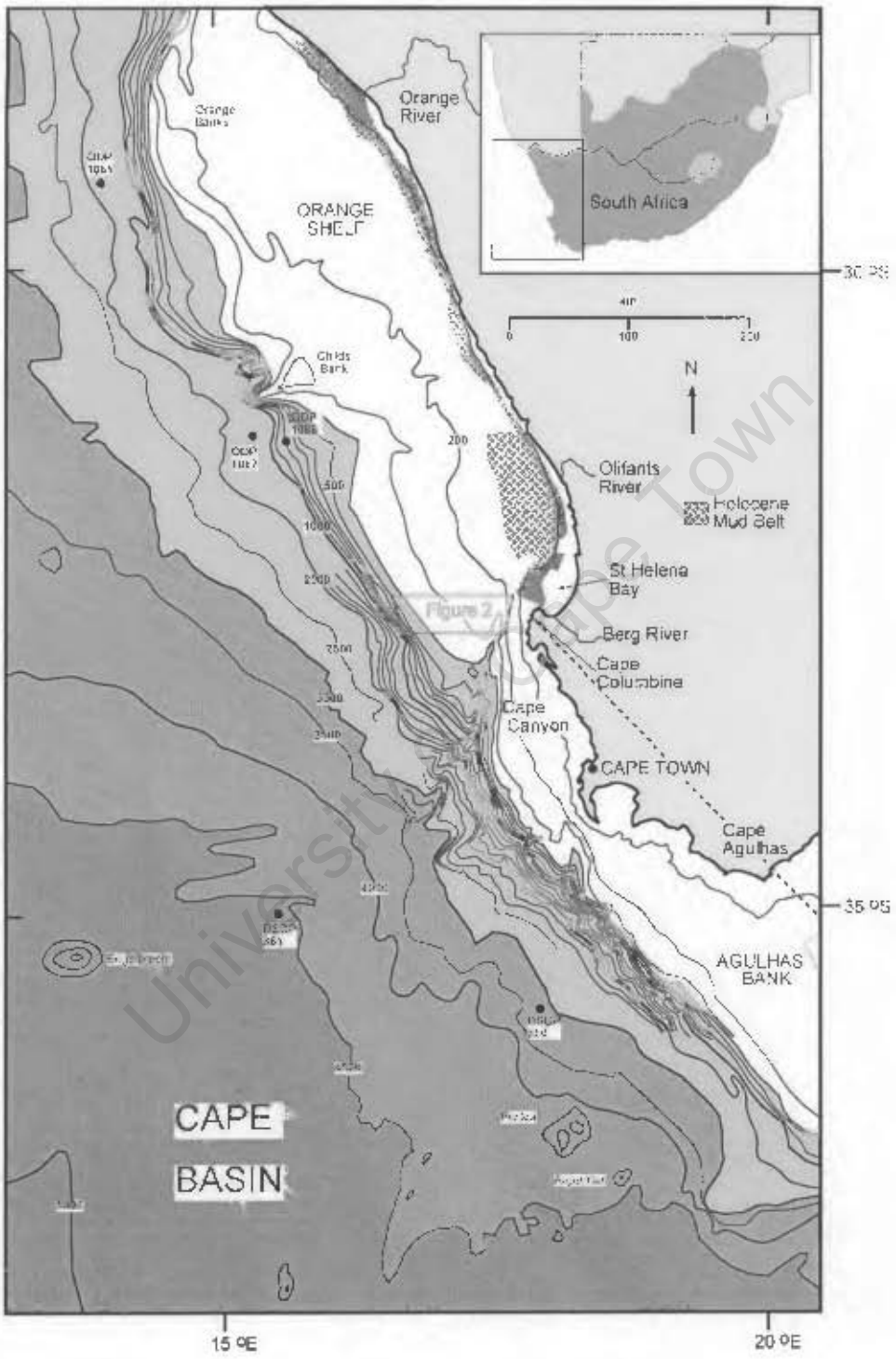


Fig. 1. Bathymetry of the western continental margin of southern Africa (Dingle et al., 1987). The study area is outlined by the rectangle (Fig. 2). Water depth in meters. Shaded area between 70 and 120 m water depth is the Holocene mud belt. Columbine–Agulhas Arch is shown by heavy dashed line and extends from Cape Columbine to offshore Cape Agulhas.

University of Cape Town

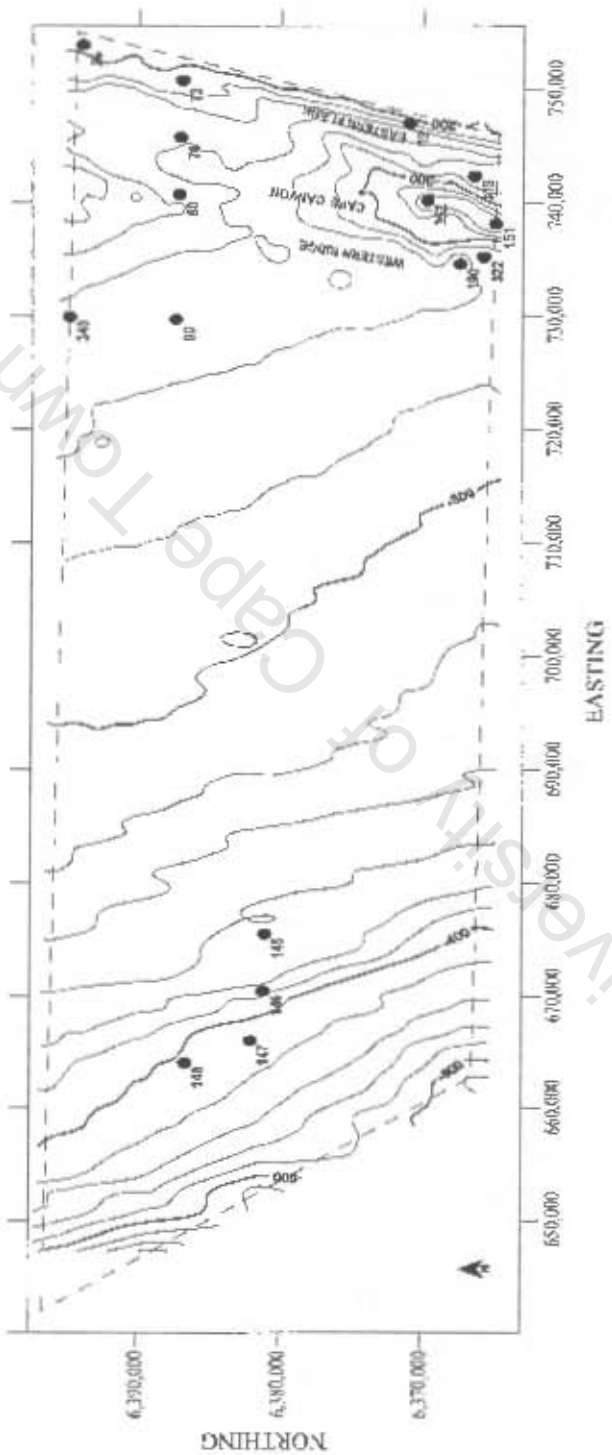


Fig. 2. Detailed bathymetry (20 m contours) of study area showing the location of vibracores (WGS 84 spheroid and UTM grid, central meridian 15°E).

University of Cape Town

that reaches velocities of 0.5 m/s off Cape Columbine (Nelson, 1989) and is deposited as a band of terrigenous-rich mud referred to as the Holocene mud belt (Mabote et al., 1997; Dale and McMillan, 1998; Meadows et al., 2002). The Cape Canyon is the only submarine canyon on the western South African margin and cuts across the southern edge of the outer shelf and extends down to the Cape Basin. The Cape Canyon may be a major conduit for sediment loss from the shelf, particularly during sea-level lowstands (Birch et al., 1991). Sediment cores for this study come from the Eastern Flank, the shallow to deeply cut submarine canyon and the Western Ridge of the Head of the Cape Canyon, as well as from the outer shelf to upper slope transition at around 400 m water depth (Fig. 2).

3. Methods

Samples for this study are from vibracores obtained by Werner Marine Research in the offshore diamond concession 20D located 50 km offshore of Cape Columbine at water depths between 190 to 450 m (Figs. 1 and 2). Grains were selected for Sr analyses on the basis of texture (Table 1). The different grain types picked include CFA-cemented phosphorite grains (PCG) with no internal structure, CFA-replaced limestone (phosphate-cemented limestone, PCL), fossil fish bones (skeletal phosphorite grains, SPG), benthic foraminifera, echinoid spines and mollusc shell. Grains of a uniform texture were handpicked from the washed sand and gravel size fractions of bulk sediment samples. Single pebbles or several coarse sand size PCG or PCL grains and up to 20 individual SPG, exclusive of teeth, with uniform color and texture were powdered for a single Sr analysis. Approximately 40 to 80 individuals of benthic foraminifera, 10 to 30 echinoid spines and single mollusc bivalves were picked of similar grain size and texture for Sr analyses. Benthic foraminifera were picked from the >250 μm sand fraction. The least altered and fragmented and morphologically similar biogenic grains were picked for Sr analysis. In some samples, several different biogenic grain types (including SPG) had to be combined to have a large enough sample for Sr analysis. In addition, the Sr isotope composition of the <38 μm fraction of calcareous sandy mud was determined for comparison with picked benthic foraminifera and mollusc shell. Biostratigraphic ages are based on the foraminiferal assemblages (Table 2) described for the Miocene (Christison, 1985; Gawlinski, 1987; McMillan, 1989), Pliocene (Dale and McMillan, 2000) and Quaternary (McMillan, 1987, 1993; Dale and McMillan, 1998). Many of the foraminifera are only known at the genus level because their exact relation to species described elsewhere has not yet been established. For these samples, any distinctive test morphology (hispid, elongate, etc.) is noted in Table 2.

The mineralogy of the samples was determined by petrography and X-ray diffraction (XRD). CFA (francolite) was the dominant mineral in the PCG, PCL and SPG analyzed. Any calcite was removed from PCG and PCL grains with buffered Na acetic acid until it was no longer detectable by XRD (<0.5 wt.%). SPG, benthic foraminifera, echinoid spines and shell were cleaned in an ultrasonic bath. Samples were dissolved at room temperature in twice-distilled 5 M glacial acetic acid for Sr analyses to minimize dissolution of other minerals. The presence of quartz, feldspar, glauconite and CFA in the insoluble residue of PCG and PCL grains indicates that dissolution of minerals other than CFA was probably minor. The amount of Sr contributed by minerals other than CFA in the PCG, PCL and SPG is considered insignificant because these samples are predominantly composed of CFA that generally has a high Sr content (2000 to 4000 ppm; Compton et al., 1993). Sr isotope ratios were measured at the University of Cape Town on a VG Instruments mass spectrometer with mass fractionation normalized to a $^{86}Sr/^{88}Sr$ ratio of 0.1194 and to a Standard Reference Material 987 $^{87}Sr/^{86}Sr$ ratio of 0.710220. Within-run precision on single measurements is $\pm 1 \times 10^{-5}$ (2σ error), whereas sample reproducibility is approximately $\pm 2 \times 10^{-5}$. The age of the samples was obtained from the Sr look-up table (V3:10/99) after adding 0.000028 to the values in Table 1 to adjust for the SRM value of 0.710248 used by McArthur et al. (2001). The range in age given in Table 1 corresponds to a $\pm 2 \times 10^{-5}$ uncertainty in the measured Sr isotope values.

The use of the Sr isotope composition to determine the age of phosphorite formation assumes that the Sr ratio reflects that of ambient seawater and that the Sr ratio has not altered since it was acquired during the

Table 1
Sr isotope analyses

Core	Depth (cm)	Grain size (μm)	Grain type	$^{87}Sr/^{86}Sr$	Age (Ma)
Northern transect					
349	005–007	250–1000	shell fragments	0.709131	0–1.1
		>250	black PCG	0.708940	5.9–7.4
	20–22	>850	shell fragments	0.709153	0–0.6
		>250	black PCG	0.708809	10.9–13.3
	40–44	>850	shell fragments	0.709100	0.7–1.5
	60–63	>850	shell fragments	0.709144	0–0.8
		>250	black PCG	0.708647	16.7–17.4
		>250	fish bones (SPG)	0.709051	1.5–4.0
	80–84	>250	black PCG	0.708656	16.6–17.3
		>2000	bivalve shell	0.709142	0–0.8
	140–144	>2000	shell fragments	0.709061	1.4–3.2
	200–204	>2000	shell fragments	0.709131	0–1.1
		250–1000	PCL	0.708824	10.4–12.6
		250–1000	fish bones (SPG)	0.709122	0.1–1.2
	245–247	>2000	shell fragments	0.709066	1.3–2.5
	300–304	>355	shell fragments	0.709069	1.3–2.4
	350–354	250–1000	PCL	0.708830	10.1–12.3
		250–1000	echinoid spines	0.709082	1.1–2.0
	388–392	>2000	PCL	0.708851	9.3–11.3
		1000–2000	shark teeth	0.708526	18.2–18.9
		250–1000	black PCG	0.708816	10.6–13.0
	425–429	>2000	PCL	0.708760	13.1–15.6
		>2000	*Pecten* shell	0.708534	18.1–18.8
	432–436	250–1000	benthic foraminifera	0.708517	18.4–19.0
		>2000	*Pecten* shell	0.708500	18.5–19.3
		1000–2000	black PCG	0.708695	15.9–16.9
	468–472	>2000	*Pecten* shell	0.708510	18.4–19.1
		250–1000	benthic foraminifera	0.708499	18.5–19.3
		1000–2000	black PCG	0.708605	17.3–17.9
90	202–206	250–500	benthic foraminifera	0.708699	15.8–16.8
		1000–2000	fish bones (SPG)	0.708731	14.8–16.3
		1000–2000	orange/black PCG	0.708544	18.0–18.6
	524–528	>2000	shell fragments	0.708161	24.6–25.6
		1000–2000	orange PCG	0.708237	23.3–24.3
80	82–86	1000–2000	fish bones (SPG)	0.708441	19.4–20.3
		>2000	black PCG	0.708183	24.3–25.2
	109–112	1000–2000	fish bones (SPG)	0.708998	4.4–5.8
		>2000	black PCG	0.708143	24.9–26.0
76	345–349	250–500	benthic foraminifera	0.709124	0.1–1.2
		>2000	black PCG	0.708782	11.9–15.0
	354–358	250–1000	BF/fish bones	0.708863	8.7–10.9
		>2000	black PCG	0.708639	16.9–17.5
73	292–296	250–1000	benthic foraminifera	0.708830	10.1–12.3
	360–364	250–1000	benthic foraminifera	0.708807	10.9–13.4
	535–539	250–1000	benthic foraminifera	0.708754	13.3–15.8
		250–1000	fish bones (SPG)	0.709062	1.3–2.8
		1000–2000	black PCG	0.708809	10.9–13.3
26	108–112	250–1000	BF/fish bones	0.708854	9.1–11.2

University of Cape Town

Table 1 (*continued*)

Core	Depth (cm)	Grain size (μm)	Grain type	$^{87}Sr/^{86}Sr$	Age (Ma)
Southern transect					
190	16–19	>2000	orange PCG	0.708135	25.0–26.1
	45–47	250–1000	BF/echinoid spines	0.709101	0.7–1.4
	45–47	>2000	orange PCG	0.708201	24.0–24.9
	86–91	250–1000	BF/shell/echinoid sp	0.709104	0.5–1.4
	86–91	>2000	orange PCG	0.708224	23.6–24.5
322	0–3	>2000	orange PCG	0.708245	23.2–24.2
	64–67	>250	benthic foraminifera	0.709167	0–0.2
	88–90	>250	benthic foraminifera	0.709167	0–0.2
	180–182	>250	benthic foraminifera	0.709104	0.5–1.4
	326–330	>2000	orange PCG	0.708294	21.9–23.3
		>500	benthic foraminifera	0.709067	1.3–2.5
	340–344	>250	benthic foraminifera	0.707981	28.6–30.1
	498–502	>355	benthic foraminifera	0.708241	23.3–24.3
	525–530	>500	benthic foraminifera	0.708313	21.4–22.9
		>2000	orange PCG	0.708256	22.9–24.0
352	0–4	1000–2000	black PCG	0.708900	6.8–9.6
	212–216	>250	BF/echinoid spines	0.709131	0–1.1
		1000–2000	black PCG	0.708808	10.9–13.4
		>1000	fish bones (SPG)	0.709002	4.1–5.7
		1000–2000	black PCG	0.708515	18.3–19.1
	493–497	>2000	shell fragments	0.709156	0–0.4
		>1000	black PCG	0.709044	1.7–4.5
151	132–136	>2000	black PCG	0.708238	23.3–24.3
	220–224	>2000	black PCG	0.708618	17.1–17.7
319	0–2	1000–2000	black PCG	0.708544	18.0–18.6
	180–184	>250	benthic foraminifera	0.708790	12.0–15.0
		1000–2000	black PCG	0.708376	20.4–21.4
		1000–2000	black PCL	0.708855	9.1–11.2
	350–354	>250	benthic foraminifera	0.708768	12.7–15.4
		1000–2000	black PCG	0.708304	21.7–23.1
		1000–2000	black PCL	0.708805	11.0–13.6
	541–545	>250	benthic foraminifera	0.708752	13.6–15.9
		1000–2000	black PCG	0.708344	20.9–22.1
	558–562	>250	benthic foraminifera	0.708633	17.0–17.6
	568–572	1000–2000	black PCG	0.708304	21.7–23.1
19	438–442	>250	BF/fish bones	0.709053	1.5–3.9
Western transect					
145	620–622	>600	shell fragments	0.708474	18.9–19.7
		300–600	benthic foraminifera	0.708407	19.9–20.8
		<38	biogenic carbonate	0.708517	18.3–19.0
146	560–562	>125	benthic foraminifera	0.708890	7.1–10.1
		>125	black PCG	0.708933	6.0–7.8
		<38	biogenic carbonate	0.708897	6.9–9.7
147	598–600	>2000	PCL	0.708674	16.3–17.1
		>300	benthic foraminifera	0.708879	7.5–10.4
		<38	biogenic carbonate	0.708913	6.4–9.0
148	620–622	250–1000	benthic foraminifera	0.708950	5.8–6.9
		<38	biogenic carbonate	0.708874	8.1–10.5

PCG: phosphate-cemented grain; BF: benthic foraminifera; PCL: phosphate-cemented limestone. Sr isotope values normalized to an SRM 987 value of 0.710220. Ages from look-up table (V3:10/99) of McArthur et al. (2001).

University of Cape Town

Table 2
Foraminiferal assemblages of selected samples

Core 73; 497–500 cm. Age: Pliocene (all brown in color). *Cancris* sp., *Sphaeroidina bulloides*, *Epistominella pulchella*, *Planulina* sp., *Vaginulina* sp. (smooth), *Uvigerina* sp. (ribbed), *Lenticulina* spp., *Pseudonodosaria* sp., *Marginulina* sp. (fat, smooth), *Amphicoryna* sp (ribbed), *Gyroidinoides* cf. *soldanii*, *Uvigerina* sp. (hispid), *Oridorsalis umbonatus*, *Pullenia subcarinata*, *Hanzawaia* sp.

Core 76; 384–386 cm. Age: Pliocene (all brown in color). *Sphaeroidina bulloides*, *Dentalina* cf. *soluta*, *Cibicidoides* sp., *Karreriella* sp., *Marginulina* sp. (fat, ribbed), *Stilostomella* sp. (hispid), *Dentalina* sp. (ribbed), *Globigerina* sp., *Amphicoryna* sp. (ribbed), *Pullenia subcarinata*, *Laticarinina paupercula*, *Lagena* sp. (smooth), *Uvigerina* sp. (ribbed), *Angulogerina* sp.

Core 90; 180–182 cm. Age: Pliocene (all brown in color). *Sphaeroidina bulloides*, *Cancris* sp., *Dentalina* sp. (smooth), *Globigerina* spp., *Uvigerina* sp. (finely ribbed), *Planulina* sp., *Marginulina* sp. (fat, smooth), *Lenticulina* sp., *Uvigerina* sp. (hispid), *Karreriella* sp., *Amphicoryna* sp. (ribbed), *Pullenia subcarinata*.

Core 90; 202–204 cm. Age: Pliocene (all brown in color; +reworked Burdigalian). *Marginulina* sp. (fat, smooth), *Sphaeroidina bulloides*, *Stilostomella* sp. (spiny), *Cibicidoides* spp., *Globigerina* sp., *Globigerinoides* spp. (reworked).

Core 90; 220–222 cm. Age: early Miocene (Burdigalian), middle to outer shelf assemblage all white in color. *Karreriella* sp., *Globigerinoides* spp., *Globigerinoides triloba*, *Uvigerina* sp. (fat, ribbed), *Cancris* sp., *Globoquadrina dehiscens*, *Globigerina praebulloides*, *Spiroplectinella* sp., *Cibicidoides* sp., *Gavelinella* sp., *Lenticulina* sp. *Globocassidulina* sp., *Cubanina* sp.

Core 90; 330–335 cm. Age: early Miocene (Burdigalian), middle to outer shelf assemblage all white in color. *Lenticulina* spp., *Martinottiella communis*, *Cubanina* sp., *Globigerinoides* spp., *Globoquadrina dehiscens*, *Cibicidoides* spp., *Spiroplectinella* sp., *Globigerina praebulloides*, *Amphicoryna* sp. (ribbed), *Globocassidulina* sp., *Karreriella* sp., *Globigerinoides triloba*, *Martinottiella* sp. (thin), *Uvigerina* sp. (ribbed), *Gavelinella* sp., *Rupertina stabilis*, *Cassigerinella chipolensis*, *Brizalina* cf. *mexicana*.

Core 90; 346–350 cm. Age: early Miocene (Burdigalian), middle to outer shelf assemblage all white in color. *Cubanina* sp., *Lenticulina* spp., *Martinottiella communis*, *Pseudopolymorphina* sp., *Spiroplectinella* sp., *Cibicidoides* spp., *Gaudryina* sp., *Globigerina praebulloides*, *Amphicoryna* sp. (ribbed), *Gavelinella* sp., *Globigerinoides* spp., *Globoquadrina dehiscens*, *Martinottiella* sp. (thin), *Globocassidulina* sp., *Cassigerinella chipolensis*, *Brizalina* cf. *mexicana*.

Core 90; 360–365 cm. Age: early Miocene (Aquitanian), inner shelf assemblage brown–yellow iron stained and/or phosphatised foraminifera, with large quartz grains. *Victoriella conoidea* (whole specimen and broken fragments), *Dentalina* spp., *Lenticulina* spp., *Vaginulina* spp., *Guttulina* sp., *Cibicidoides* spp. (abundant), *Globigerina praebulloides*, *Gyroidinoides* sp., *Cancris* sp., *Spiroplectinella* sp. (thin), *Quinqueloculina* sp., *Uvigerina* sp. (finely ribbed), echinoid spines, crinoid ossicles, *Amphicoryna* sp. (ribbed), *Quinqueloculina* cf. *horrida*, ?*Siphonaperta* sp., *Globigerina* spp., brachiopods.

Core 90; 524–527 cm. Age: early Miocene (Aquitanian), inner shelf assemblage creamy-white in colour, with large quartz grains. Brachiopods, *Victoriella conoidea* (mostly broken fragments), *Eponides* sp. (rounded margin), *Globigerina praebulloides*, *Globigerina* spp., *Globocassidulina* sp., *Dentalina* spp., *Lenticulina* spp., *Cibicidoides* spp. (abundant), *Amphicoryna* sp. (ribbed), *Gaudryina* sp., *Spiroplectinella* sp. (thin), *Martinottiella* sp. (thin), *Marginulina* sp. (hispid), *Uvigerina* sp. (finely ribbed), *Cassigerinella chipolensis*, *Planulinoides altocamerata*, *Bolivinella* sp.

Core 90; 563–566 cm. Age: early Miocene (Aquitanian), inner shelf assemblage creamy-white in colour. *Cibicidoides* spp. (abundant), *Martinottiella* sp. (thin), *Globigerina praebulloides*, *Victoriella conoidea* (rare fragments), *Globocassidulina* sp., *Dentalina* spp., *Gyroidinoides* sp., *Globigerina* spp., *Amphicoryna* sp. (ribbed), *Uvigerina* sp. (finely ribbed), *Trifarina* sp., *Spiroplectinella* sp. (thin), *Vaginulina* spp., *Gaudryina* sp., *Siphonina reticulata*, *Guttulina* sp., *Toddinella* sp. (keeled with umbilical boss), *Globigerinoides* sp. (very rare), *Epistominella* sp.

Core 145; 20–22 cm. Age: early Miocene (Burdigalian); outer shelf–upper slope assemblage. *Globigerina* spp. (abundant), *Globigerinoides* spp., *Cubanina* sp., *Globigerina praebulloides*, *Gaudryina* sp. (large, fat), *Globoquadrina dehiscens*, *Brizalina* spp., *Epistominella* sp. (flat), *Cassigerinella chipolensis*, *Oridorsalis umbonatus*, *Spiroplectinella* sp., *Cibicidoides* spp., *Globigerinoides triloba*, *Amphicoryna* sp. (ribbed).

Core 145; 620–622 cm. Age: early Miocene (Burdigalian) outer shelf–upper slope assemblage. *Karreriella* sp., *Martinottiella* sp. (thin), *Globigerina praebulloides*, *Lenticulina* spp., *Uvigerina* sp. (fat, ribbed), *Marginulina* sp. (ribbed), *Gavelinella* sp., *Dentalina* spp. (smooth), *Lenticulina* sp. (spiny), *Cibicidoides* spp., *Globigerinoides* spp., *Spiroplectinella* sp. (thin), *Pseudonodosaria* sp., *Martinottiella* cf. *communis*, *Siphonina reticulata*, *Nonion* sp. (small, rounded margin), *Pullenia bulloides*, *Globoquadrina dehiscens*, *Globocassidulina* sp., *Ramulina* sp., *Brizalina* spp., *Marginulina* sp. (hispid), *Trifarina* sp. (triangular), *Cassigerinella chipolensis*.

Core 147; 580–582 cm. Age: Pliocene. *Stilostomella* sp. (smooth), *Sphaeroidina bulloides*, *Nodogenerina* sp., *Amphicoryna* sp. (ribbed), *Lenticulina* spp., *Orbulina universa*, *Cibicidoides* spp., *Globigerina bulloides*, *Siphotextularia* sp., *Globorotalia scitula*, *Bolivina* sp., *Hanzawaia* sp., *Uvigerina* sp. (ribbed), *Angulogerina* sp. (smooth), *Gyroidinoides* cf. *soldanii*, *Uvigerina* sp. (hispid), *Bulimina* cf. *orangensis*, *Chilostomella* sp., *Neogloboquadrina pachyderma*, *Nuttallides* sp., *Epistominella pulchella*, *Globobulinina* sp., *Lagena crenata*.

Core 148; 598–600 cm. Age: no older than latest Pliocene. *Stilostomella* sp. (slightly spiny), *Pullenia* sp., *Dentalina* spp. (smooth), *Globorotalia truncatulinoides*, *Globorotalia scitula*, *Cassidulinoides normani*, *Globigerina* spp. (abundant), *Uvigerina* sp. (ribbed), *Globobulimina* cf. *turgida*, *Orbulina universa*, *Orbulina bilobata*, *Sphaeroidina bulloides*, *Cibicidoides* spp., *Angulogerina* sp. (smooth), *Uvigerina* sp. (spiny), *Nodogenerina* sp. (smooth), *Marginulina* sp. (fat, smooth), *Planulina* sp., *Globorotalia tosaensis*, *Globigerina bulloides*, *Pullenia bulloides*, *Nodosaria* cf. *longiscata*, *Oridorsalis umbonatus*, *Bolivina* sp., *Neogloboquadrina pachyderma*, *Fontbotia* cf. *wuellerstorfi*, *Frondicularia* sp., *Siphotextularia* sp., *Siphonaperta* sp., *Gyroidinoides nipponicus*.

Table 2 (*continued*)

Core 319; 16–19 cm. Age: Pleistocene (+reworked Miocene). *Globorotalia inflata*

Core 319; 88–336 cm. Age: middle Miocene (probably Langhian). *Orbulina universa, Orbulina bilobata, Gavelinella* sp., *Cibicidoides* spp., *Menardella praemenardii, Cibicides* sp., *Globocassidulina* sp., *Globoquadrina dehiscens, Uvigerina* sp. (ribbed), *Amphicoryna* sp. (ribbed), *Planularia* sp., *Sphaeroidina bulloides, Dentalina* spp. (smooth, spiny), *Quinqueloculina* sp., *Globigerina praebulloides, Globigerinoides triloba, Sigmoilina* sp., *Karreriella* sp., *Astacolus* sp.

Core 319; 541–544 cm. Age: middle Miocene (probably Langhian). *Globigerinoides* spp., *Menardella praemenardii, Globigerina praebulloides, Globoquadrina dehiscens, Cibicidoides* spp., *Brizalina* spp., *Globigerina* spp., *Globocassidulina* sp., *Globigerinoides triloba, Gavelinella* sp., *Eponides* sp. (small keeled), *Pullenia bulloides, Dentalina* spp. (smooth, thin), *Uvigerina* sp. (smooth), *Sphaeroidina bulloides.*

Core 322; 200–202 cm. Age: Pleistocene, very near littoral assemblage. *Pyrgo* sp., *Miliolinella* sp. (large, fat), *Spiroloculina communis, Dentalina* cf. *soluta* (reworked), *Cibicidoides* spp., *Lobatula lobatula.*

Core 322; 240–242 cm. Age: Pleistocene (all well preserved). *Globorotalia inflata* (abundant), *Globoquadrina dutertrei, Angulogerina angulosa, Bulimina gibba, Bulimina* cf. *aculeata, Globorotalia hirsuta, Globorotalia truncatulinoides, Globigerinella aequilateralis, Planodiscorbis rarescens, Lobatula lobatula, Cibicidoides* spp., *Globobulimina* sp., *Orbulina universa, Ehrenbergina* sp., *Sphaeroidina bulloides.*

Core 322; 340–342 cm. Age: Pliocene. *Lenticulina* sp., *Dentalina* sp. (smooth), *Nodogenerina* sp. (smooth), *Cibicidoides* sp., *Epistominella pulchella, Oridorsalis umbonatus.*

Core 322; 380–382 cm. Age: Pliocene. *Streptochilus* sp., *Brizalina* spp., *Angulogerina* sp. (smooth, thin, elongate), *Vaginulina* sp., *Heronallenia* sp., *Lenticulina* spp., *Orbulina universa, Hanzawaia* sp., *Stilostomella* sp. (slightly spiny), *Trifarina* sp. (triangular), *Cibicidoides* spp., *Gyroidinoides* cf. *soldanii, Globocassidulina* sp., *Dentalina* spp. (smooth), *Uvigerina* sp. (fat, ribbed), *Globigerina* spp., *Nonionella* sp., *Cancris* sp., *Pullenia subcarinata, Nodogenerina* sp. (smooth), *Globorotalia inflata, Ehrenbergina* sp., *Globorotalia truncatulinoides, Globorotalia hirsuta, Bulimina* cf. *aculeata, Cassidulina carinata, Angulogerina angulosa.*

Core 349; 0–62 cm. Age: Holocene, many foraminifera brilliant white, no reworked Miocene. *Globorotalia inflata, Cassidulina laevigata, Lobatula lobatula, Cassidulina carinata, Cassidulina crassa, Bulimina aculeata, Sphaeroidina bulloides, Elphidium advenum, Globoquadrina dutertrei, Angulogerina angulosa, Globorotalia truncatulinoides, Neogloboquadrina pachyderma, Orbulina universa, Gyroidina orbicularis, Hyalinea balthica, Globigerinoides ruber, Globigerinoides triloba, Uvigerina bassensis, Ammonia japonica, Cancris auriculus, Bulimina* cf. *orangensis, Lenticulina* sp., *Cibicidoides* sp., *Uvigerina peregrina, Planulina ariminensis, Globobulimina turgida, Bulimina elongata, Globigerina bulloides, Globigerinella aequilateralis, Globorotalia hirsuta, Bulimina marginata, Siphonaperta* cf. *martinae, Brizalina spathulata, Fursenkoina schreibersiana, Amphicoryna scalaris, Globigerina calida, Karreriella bradyi, Eponides* sp. (large, spiky), *Gavelinopsis* sp.

Core 349; 80–250 cm. Age: Pleistocene; few reworked Pliocene or Miocene species. *Globocassidulina pacifica, Globorotalia inflata, Cassidulina laevigata, Lobatula lobatula, Cassidulina carinata, Cassidulina crassa, Sphaeroidina bulloides, Elphidium advenum, Globoquadrina dutertrei, Angulogerina angulosa, Globorotalia truncatulinoides, Neogloboquadrina pachyderma, Orbulina universa, Gyroidina orbicularis, Hyalinea balthica, Globigerinoides ruber, Uvigerina bassensis, Ammonia japonica, Bulimina* cf. *orangensis, Lenticulina* sp., *Cibicidoides* spp. (large), *Uvigerina peregrina, Globobulimina turgida, Bulimina elongata, Globigerina bulloides, Globorotalia hirsuta, Bulimina marginata, Siphonaperta* cf. *martinae, Brizalina spathulata, Globigerina calida, Eponides* sp. (large, spiky), *Gavelinopsis* sp., *Cibicidoides pseudoungerianus, Nonionella* cf. *turgida, Pullenia subcarinata, Fontbotia* cf. *wuellerstorfi, Oolina* cf. *hexagona, Miliolinella circularis, Oolina squamososulcata, Globorotalia tumida,* bispinate *Vaginulina* sp., *Globorotalia scitula, Planodiscorbis rarescens, Orbulina bilobata, Spiroplectinella* sp., *Nonion boueanus, Quinqueloculina* sp., *Quinqueloculina dunkerquiana, Hoeglundina elegans, Siphotextularia* sp., *Saracenaria* sp., *Spiroplectinella atrata, Globorotalia menardii, Discorbinella montereyensis, Spiroplectinella wrightii, Notorotalia clathrata* (transported), *Quinqueloculina vulgaris, Spiroloculina communis, Challengerella bradyi, Oridorsalis umbonatus, Stainforthia fusiformis, Textularia conica, Lagena striata, Dentalina* sp. (smooth), *Bolivina pseudoplicata, Pyrgo* sp., *Astrononion* sp., *Amphicoryna* sp. (ribbed), *Sigmoilina* sp., *Globigerinoides sacculifer, Pyrgo* cf. *elongata, Fissurina marginata, Frondicularia* sp. (thin, long ribbed), *Hanzawaia* sp., *Rosalina* sp. (scaly), *Oolina* cf. *austroatlantica, Cassidulinoides normani, Cibicides* cf. *refulgens, Chilostomella oolina, Lagena* cf. *laevis, Gyroidinoides* cf. *soldanii, Martinottiella* sp. (thin, reworked Miocene?).

Core 349; 260–431 cm. Age: Pliocene with reworked Miocene species near base. *Fontbotia* cf. *wuellerstorfi, Cibicidoides* spp. (large), *Siphonaperta* cf. *martinae, Cancris auriculus, Globorotalia inflata, Cassidulina laevigata, Uvigerina bassensis, Lobatula lobatula, Orbulina universa, Globigerina bulloides, Globigerinoides ruber, Gyroidina orbicularis, Cibicides* cf. *refulgens, Hoeglundina elegans, Nonion boueanus, Nodosaria* cf. *longiscata, Laterostomella* sp., *Nodosaria* sp. (ribbed), *Stilostomella* sp. (spiny), *Nodogenerina* sp., *Frondicularia* sp. (ribbed), *Lenticulina* sp., *Sphaeroidina bulloides, Dentalina* sp. (smooth, thin), *Marginulina* sp. (fat, smooth), *Globocassidulina* sp., *Trifarina* sp. (spiky), *Angulogerina* sp. (ribbed), *Uvigerina* sp. (ribbed, hispid), *Stilostomella* sp. (ribbed), *Hanzawaia* sp., *Rectuvigerina* sp. (hispid), *Vaginulina* sp. (ribbed), *Globigerina calida, Neolenticulina* sp., *Neogloboquadrina pachyderma, Brizalina* sp., *Pullenia subcarinata, Amphicoryna* sp. (ribbed), *Lagena* sp. (linear, hispid), *Chilostomella oolina, Vaginulina* sp. (smooth), *Gyroidinoides* sp., *Fissurina* sp. (globular keel), *Globigerina* spp., *Karreriella* sp., *Quadrimorphina* sp., *Cibicides* sp.

Core 349; 432–436 cm. Age: early Miocene (Burdigalian), middle to outer shelf assemblage, most white in color, some phosphatized. *Globigerinoides triloba, Globigerina praebulloides, Globigerina* spp., *Cubanina* sp., *Cassigerinella chipolensis, Ehrenbergina* cf. *healyi, Globoquadrina dehiscens, Turborotalia* sp.

diagenetic precipitation of CFA. The Sr isotope composition of early diagenetic pore waters is considered equivalent to that of overlying seawater (e.g., DePaolo, 1986). CFA appears to undergo recrystallization during its evolution from friable nodules to indurated pebbles (Garrison and Kastner, 1990), but the Sr isotope ratio of CFA is not expected to change during this maturation process, primarily because the initial CFA cement has a high Sr content that is unlikely to be altered during recrystallization. Of greater concern than diagenetic alteration is the mixing of different generations of CFA cement in an individual grain or different aged phosphorite grains within the same sample. Phosphorite grains, particularly large and texturally complex phosphorite pebbles, can often have multiple generations of CFA cement or grains within the same sample that differ in age by as much as 8 Myr (Compton et al., 2002). In this study, phosphorite grains of similar texture with no evidence of multiple generations of cementation, such as included phosphorite grains or layering, were picked for Sr analyses. In addition to the analysis of different textured grains, it is necessary to analyze several grains of similar texture because different aged phosphorite grains are not always texturally distinct.

4. Results

4.1. Stratigraphy

Vibracores were selected to represent as complete a sediment succession as possible from the study area. The lithostratigraphy is briefly described here to put the Sr isotope analyses in context; a far more detailed lithofacies analysis of the entire concession area is presented elsewhere (Wigley, 2004). Cores 146–148 from the outer continental shelf (385–408 m water depth) consist of Pliocene calcareous and glauconitic fine sandy mud capped by a Pleistocene glauconitic sand (Fig. 3; Table 2). Core 145 at 368 m water depth consists of a lower Miocene (Burdigalian) foraminiferal ooze. This lower Miocene calcareous unit extends across the shelf to the edge of the Western Ridge where it was recovered in cores 90 and 349 at water depths of around 250 m (Fig. 4). The lower Miocene of cores 90 and 349 ranges from Aquitanian quartzose glauconitic calcareous sand to Burdigalian glauconitic calcareous sand (Table 2). The Miocene/Pliocene contact is marked by a phosphorite-rich gravelly sand to sandy gravel overlain by Pliocene glauconitic quartzose sands that are capped by Pleistocene glauconitic quartzose sands in cores 90 and 349. Core 80 from the Western Ridge consists of a basal Pliocene glauconitic sand capped by a meter thick, Pleistocene phosphorite-rich gravel. Core 76, in the canyon channel, consists of a Pliocene glauconitic muddy sand capped by a sandy phosphatic gravel bed that is overlain by Pleistocene fining upward units of glauconitic quartzose sand. Cores 73 and 26 on the Eastern Flank of the canyon consist of Pliocene quartzose muddy sands capped by a glauconitic and shelly Pleistocene sand that increases in thickness toward the canyon floor.

Cores from the southern transect focus on the Cape Canyon and extend from the Western Ridge across to the Eastern Flank of the canyon (Fig. 2). Core 190 from the Western Ridge is a meter thick, PCG-rich Pleistocene sandy gravel (Fig. 5). Core 322 is adjacent to Core 190 on the canyon edge of the Western Ridge and consists of Pliocene calcareous sandy mud and mud capped by a Pleistocene PCG-rich sandy gravel that is overlain by coarse glauconitic quartzose shelly sands. Core 151 was recovered from the canyon floor and consists of a basal coarse quartzose sand with up to 20% wood and pyritic muddy sands capped by a PCG-rich sandy gravel that is overlain by coarse glauconitic quartzose sand with an occasional PCG-rich pebble layer. The basal woody quartzose sands are Cretaceous (Wigley, 2004) and the overlying unit is barren of fossils except for the upper 40 cm where the presence of *Globorotalia inflata* indicates a Pleistocene age. Core 352, located slightly further up the canyon floor from Core 151, consists of Pleistocene coarse glauconitic quartzose sand capped by a PCG pebble layer that is overlain by medium to coarse glauconitic quartzose sand. Core 319 is located on a terrace feature on the Eastern Flank of the canyon and consists of a Cretaceous basal woody sandy mud that is overlain by a lower Miocene gravel that contains reworked ferricrete nodules and carbonate clasts. The gravel is overlain by a calcareous muddy sand that includes variable subordinate amounts of quartz and glauconite sand and scattered phosphorite and quartz pebbles. In the core interval from 360 to 180 cm, the calcareous muddy sand contains irregularly shaped

University of Cape Town

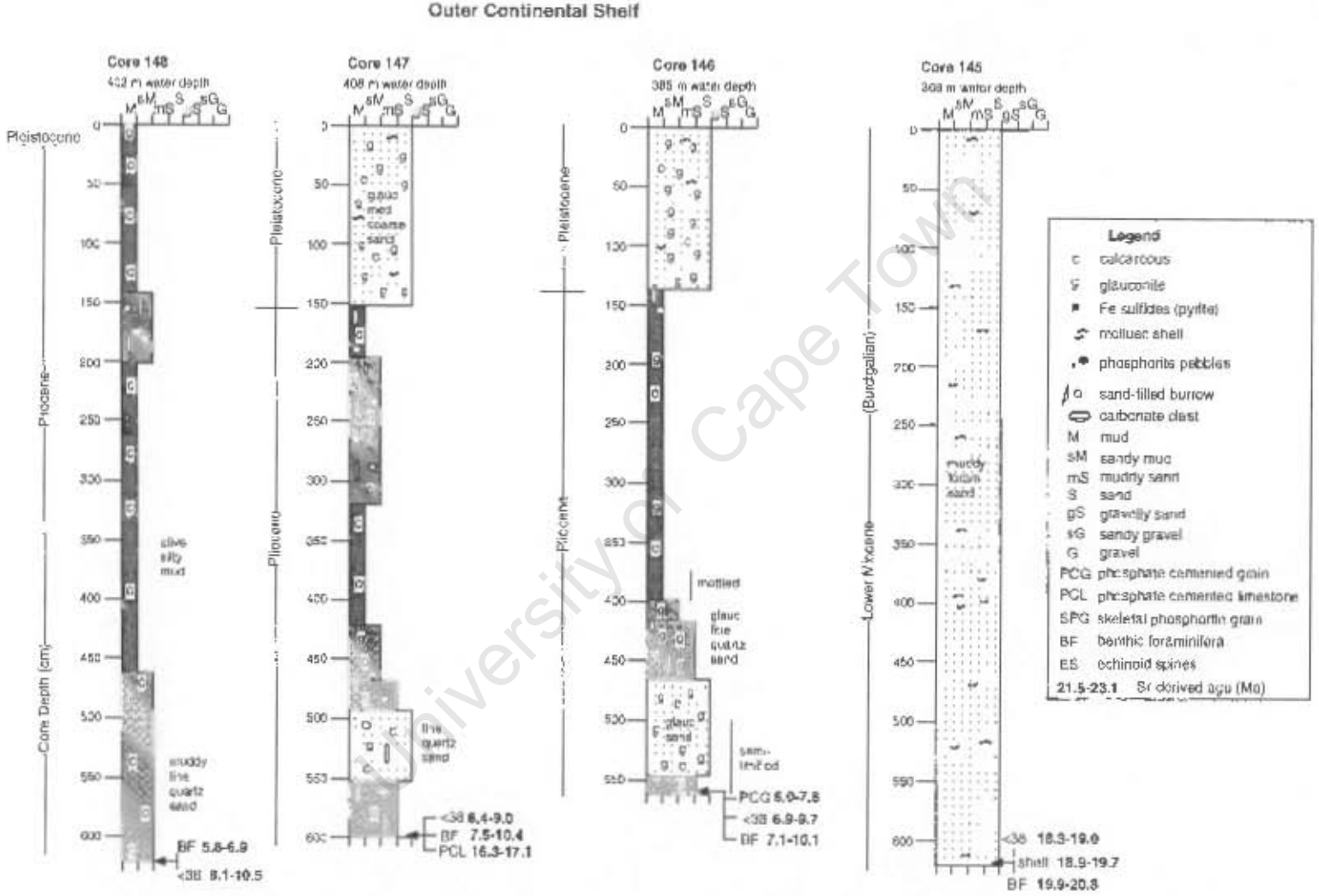


Fig. 3. Stratigraphy of vibracores of the deep water, western area of the outer shelf. Ages are derived from Sr isotope ratios (Table 1). Refer to text for discussion.

University of Cape Town

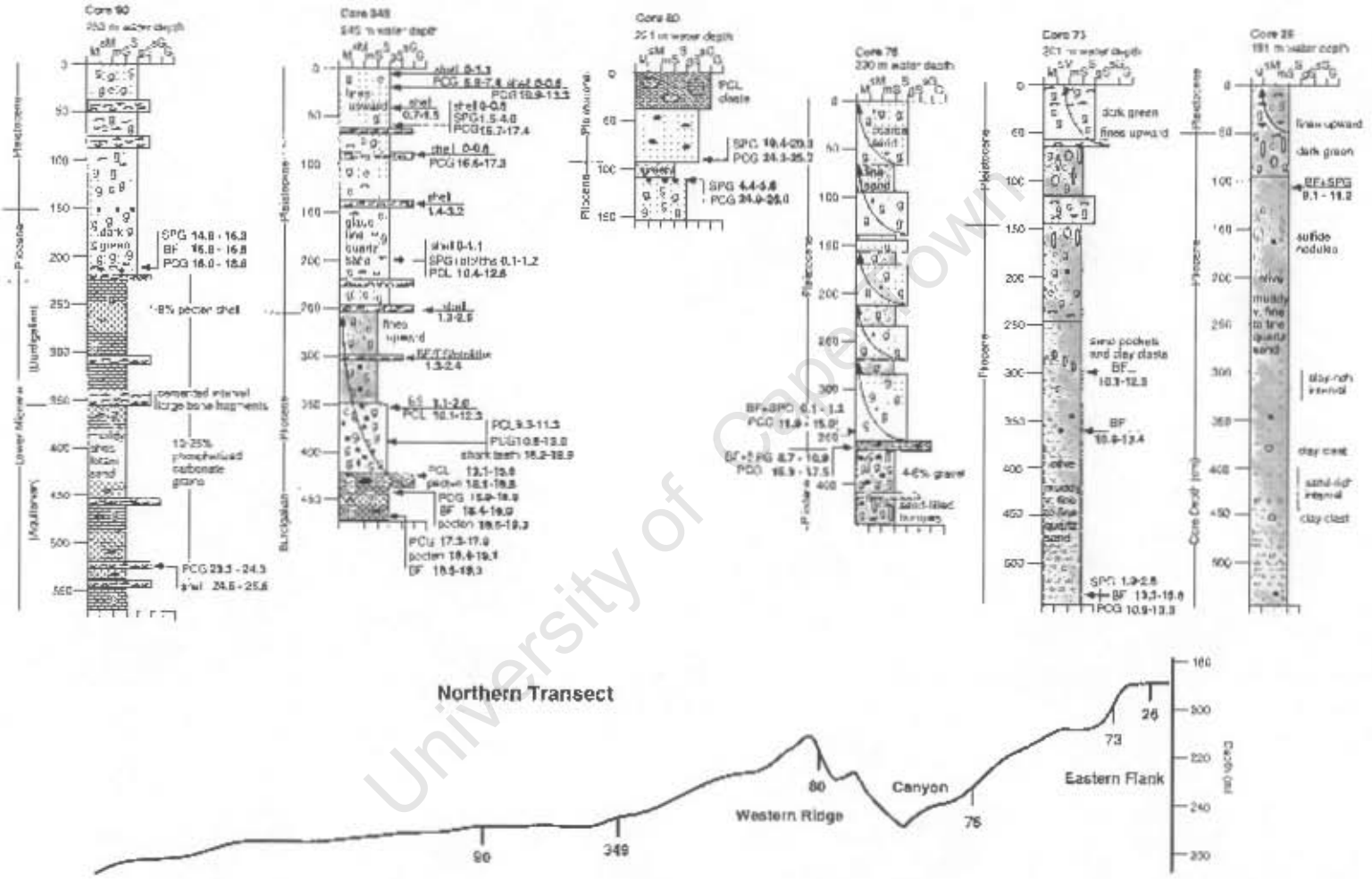


Fig. 4. Stratigraphy of vibracores of the northern end of the Head of the Cape Canyon area on the outer shelf. Ages are derived from Sr isotope ratios (Table 1). Legend in Fig. 3; refer to text for discussion.

University of Cape Town

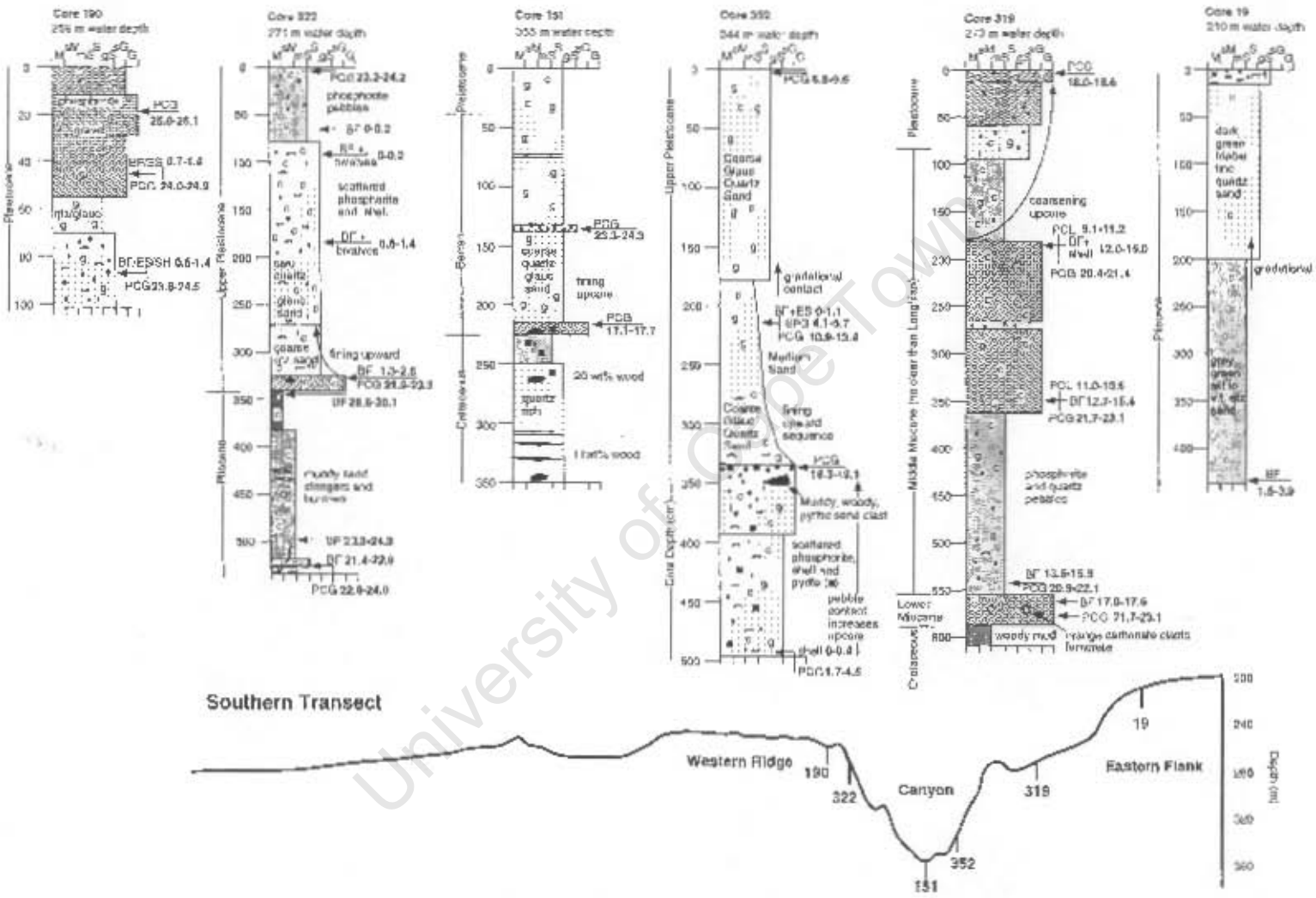


Fig. 5. Stratigraphy of vibrocores of the southern end of the Head of the Cape Canyon area on the outer shelf. Ages are derived from Sr isotope ratios (Table 1). Legend in Fig. 3; refer to text for discussion.

University of Cape Town

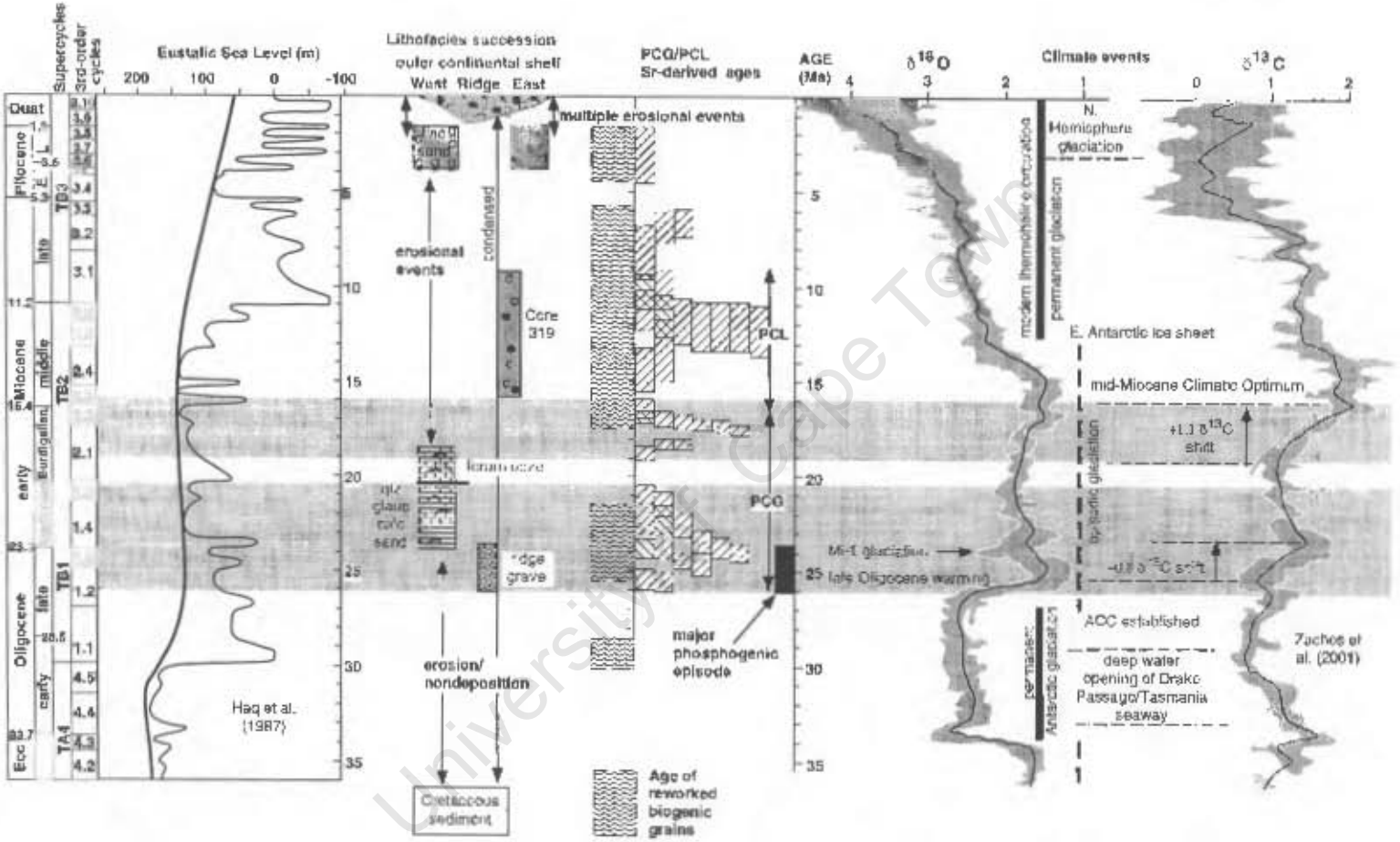


Fig. 6 Comparison of proposed sea-level fluctuations (Haq et al., 1987), simplified stratigraphy of the outer shelf successions, the age distribution of reworked biogenic grains (▩ and ▩) and phosphorite grains from this study, the marine oxygen and carbon isotope records (Zachos et al., 2001) and climate events. The range in age of phosphorite samples plotted reflects the analytical uncertainty and variations in the steepness of the marine Sr isotope record. The sea-level curve of Haq et al. (1987) has been adjusted to fit the Cande and Kent (1995) timescale after Miller et al. (1998).

University of Cape Town

PCL nodules that appear to be in place because the sediment they cement is similar to the host sediment. The foraminiferal assemblage indicates that the calcareous muddy sand unit is middle Miocene, no older than Langhian (Table 2). The calcareous muddy sand grades into an increasingly glauconitic and noncalcareous Pleistocene quartzose sand that coarsens up core into a phosphorite-rich gravel. Core 19 from the upper Eastern Flank of the canyon consists of a Pliocene quartzose muddy sand that grades up core into a fine glauconitic quartzose sand capped by a 20-cm-thick Pleistocene sandy gravel.

4.2. Phosphorite grains

Most phosphorite occurs as coarse sand to pebble size grains. CFA-cemented phosphorite grains (PCG) contain varying amounts of quartz and glauconite sand grains. Internal moulds of molluscs are common but PCG contain few, if any, foraminifera or other calcareous biogenic grains. CFA cement varies in color from orange, tan, grey and black. Phosphorite pebbles have surfaces that vary from polished and smooth to dull and irregular. Most phosphorite pebbles contain varying amounts of included quartz, feldspar, glauconite, organic matter, pyrite, mica and clay minerals, and some pebbles contain biogenic calcite. Phosphorite with significant amounts of foraminifera or micritic carbonate cement is termed phosphate-cemented limestone (PCL). Less commonly, such as in lower Miocene carbonate sands seaward of the Western Ridge (cores 90 and 349), biogenic carbonate grains have been replaced by translucent amber colored CFA. Skeletal phosphorite grains (SPG) are predominantly translucent amber color fish bone material but include fish scales, otoliths and shark teeth in some samples.

The Sr isotope composition of phosphorite samples ranges from 0.708135 to 0.709044 and corresponds to an age range of late Oligocene to Pliocene (Table 1; Figs. 3–6). The greatest percentage of samples from this study formed during the late Oligocene to early early Miocene (36%), the late early Miocene (26%) and middle to late Miocene (9–15 Ma; 28%); only 8% formed in the late Miocene and 3% in the Pliocene. However, these percentages do not reflect the actual abundance of phosphorite that formed at these times because samples were selected to provide maximum stratigraphic control of the successions studied rather than in proportion to the total amount of phosphorite present in the core. Phosphorite abundance is difficult to quantify, but on the basis of the over 400 core logs available from the Head of the Cape Canyon area, most of the phosphorite in the study area is concentrated in PCG-rich gravels on the Western Ridge of the Cape Canyon (e.g., cores 190 and 80) and pebbles focused in the regional early Miocene to Plio/Pleistocene erosional unconformity (Figs. 4 and 5). The bulk of the phosphorite from these units is late Oligocene to early Miocene in age and represents the major episode of phosphogenesis in the Head of the Cape Canyon area. In fact, most phosphorite samples from the PCG-rich gravel lag on the Western Ridge have a narrow range in Sr ages of 23.6–26.1 Ma, suggesting that this earliest phosphogenic episode was one of the largest and best preserved in the area.

5. Discussion

5.1. Depositional history based on biostratigraphy and Sr isotope ratios

A depositional age model is developed by integrating biostratigraphic and Sr isotope-derived ages. The Sr isotope composition of biogenic calcite grains ranges from 0.707981 to 0.709167 and corresponds to an age range of late early Oligocene to late Pleistocene (Table 1; Figs. 3–5). Sr analysis of biogenic grains provides independent age control to augment and enhance biostratigraphic ages (e.g., DePaolo and Finger, 1991). Sr-derived ages are maximum ages, as the final depositional age of the sediment can not be older than the age of its constituent grains. Sediment grains with Sr ages older than biostratigraphic ages indicate reworking of these grains into younger deposits. Sediment grains with Sr ages that agree with biostratigraphic ages give a final depositional age of the sediment, but these grains can also be reworked within the uncertainty of the Sr and biostratigraphic ages (generally >1 Myr). At first glance, the wide range of Sr ages obtained for different grains within the same sample as well as the number of age inversions in the cores cast doubt on the Sr isotope method. However, these Sr ages are

Property of Cape Canyon

believed to be real and to reflect the complex depositional and diagenetic history of these sediments. Because of the complex depositional history of these successions, Sr analysis of several different biogenic and authigenic grains from the same sample was obtained to increase the confidence in the age model. Biogenic grains did not appear recrystallized, and so their Sr ratio is assumed to be unaltered and represents the seawater in which they were living. This interpretation is supported by the fact that, in most cores, the Sr-derived ages of biogenic grains decrease upsection and agree with biostratigraphic ages (Figs. 3–5). In addition, Sr ages of different biogenic grain types picked from the same sample are usually similar.

A key objective of this study is to relate the diagenetic and depositional history, as inferred from the Sr ages of biogenic and phosphorite grains, to changes in sea level. The large range in Sr ages of different grain types from the same sample or lithostratigraphic unit, age inversions and major erosional unconformities attest to the extensive reworking of these sediments. In addition to changes in sea level, bottom currents (Nelson, 1989), sediment supply, slumping (Dingle, 1980) and uplift (Partridge and Maud, 1987; McMillan, 1993) were also important processes that contributed to reworking and erosional events on the margin. However, because the magnitude and timing of tectonic movements (uplift and slumping) as well as bottom currents on the margin are not well constrained, we focus here on the record of global eustatic sea-level fluctuations as proposed by the Exxon group (Haq et al., 1987). Although sea-level amplitudes appear exaggerated, a good correlation was found between proposed sequence boundaries and glacioeustatic lowstands for successions on the New Jersey margin (Miller et al., 1998).

5.1.2. Miocene successions

The oldest Cenozoic sediment succession recovered in the study area is Miocene, but Sr ages ranging from late early Oligocene (28.6–30.1) to latest Oligocene were obtained for reworked benthic foraminifera, shell and PCG. These Sr ages and the erosional contact with the underlying Cretaceous indicate that, although Oligocene deposits existed in the past, Paleogene successions were not recovered in the study area (Wigley, 2004). The lower Miocene (Aquitanian) quartzose glauconitic calcareous sand recovered in Core 90 contains abundant inner shelf warm water foraminifera (Table 2), phosphatized biogenic carbonate grains, reworked late Oligocene (24.6–25.6 Ma) shell and some medium to coarse sand quartz grains. Taken together, these observations indicate deposition during the earliest Miocene marine transgression of 3rd-order cycle 1.4 (Fig. 6). The contact with the overlying Burdigalian glauconitic calcareous sand is marked by a carbonate-cemented layer that includes large bone fragments. The Burdigalian succession contains abundant middle to outer shelf warm water foraminifera (Table 2) that indicates deposition during the marine transgression of 3rd-order cycle 2.1 (Fig. 6) between 18.4 and 20.7 Ma, based on the Sr ages of benthic foraminifera and *Pecten* shells from the base of Core 349 (Fig. 4) and from elsewhere in the study area (Wigley, 2004).

A major unconformity occurs throughout the study area between the lower Miocene calcareous unit and the overlying Plio/Pleistocene siliciclastic sediments (Fig. 6) that represents a composite of erosional events (Wigley, 2004). The transition from the early to middle Miocene is only preserved as reworked grains. The erosional contact between lower Miocene (Burdigalian) and Pliocene sediments is marked by a phosphatic, shelly sandy gravel in successions seaward of the Western Ridge (cores 90 and 349) that contains reworked foraminifera, shark teeth, *Pecten* shell, PCG, SPG and PCL that have Sr ages that range from late early Miocene (18.2–18.9 Ma) to late Miocene (9.3–11.3 Ma; Fig. 4). Although reworked benthic foraminifera of middle to late Miocene age are common in Pliocene successions, Core 319 was the only middle to upper Miocene succession recovered in the study area. Benthic foraminifera from calcareous muddy sand to sandy phosphatic gravel recovered in Core 319 on the Eastern Flank of the Cape Canyon young upsection, with overlapping Sr ages that range from 12 to 15.9 Ma (Fig. 5). These Sr ages are consistent with the middle Miocene foraminiferal assemblage of Core 319 (Table 2). The Sr ages of in place PCL nodules in core 319 range from 9.1 to 13.6 Ma and indicate that episodic sediment deposition extended into the early late Miocene. The general lack of middle, and particularly upper, Miocene successions and the presence of Miocene reworked foraminifera

University of Oregon

in upper Pliocene sediment indicate that most of the sediments deposited during the late early to late Miocene were eroded by the late Pliocene. In addition to possible margin uplift (Partridge and Maud, 1987), poor preservation of middle and upper Miocene successions corresponds to the major marine regression between the middle Miocene and early Pliocene highstands that is reflected in the Sr ages (5.8–17.6 Ma) of reworked biogenic grains (Fig. 6). The composite erosional unconformity corresponds to a transition from carbonate to siliciclastic (quartz and glauconite) dominated lithologies that indicates a more proximal depositional environment associated with the long-term shoaling of the shelf since the middle Miocene.

5.1.3. Pliocene successions

Pliocene successions consist of muddy fine quartzose sands on the Eastern Flank of the canyon, glauconite-rich sands adjacent to the Western Ridge, and calcareous muds and sandy muds on the outer shelf (Figs. 3 and 4; Birch et al., 1991). The Sr ages of SPG from the base of Core 73 (1.3–2.8 Ma) and benthic foraminifera from the base of Core 19 (1.5–3.9 Ma) are consistent with the Pliocene foraminiferal assemblage (Table 2) of muddy fine quartzose sands on the Eastern Flank. However, the Sr ages of PCG (10.9–13.3 Ma) and *Lenticulina* and *Dentalina* benthic foraminifera (9.1–15.8 Ma) of muddy fine quartzose sands on the Eastern Flank (cores 73 and 26) are considerably older than Pliocene and are interpreted to have been reworked during the Pliocene from sediment originally deposited in the middle to late Miocene (9.1 to 15.8 Ma). Basal sediment of successions at the shelf to upper slope transition (cores 146–148) has a Pliocene foraminiferal assemblage (Table 2) but contains significant amounts of reworked upper Miocene benthic foraminifera (including *Lenticulina*) with late Miocene Sr ages (5.8 to 10.5 Ma) obtained for picked benthic foraminifera and the <38 μm fraction (Fig. 3). The Sr ages of *Lenticulina* and *Dentalina* benthic foraminifera from the Pliocene succession recovered on the flank of the Western Ridge (Core 322) range from early Oligocene to early Miocene (21.4–30.1 Ma; Fig. 5). Inversion of these benthic foraminifera ages suggests erosional unroofing of lower Oligocene to Miocene deposits during the Pliocene.

Although Sr isotope analyses are limited and their uncertainty is relatively large because of the flattening out of the Pliocene marine Sr record (Farrell et al., 1995), the range in Sr ages of biogenic grains (1.1 to 3.9 Ma) indicates that most Pliocene successions were deposited in the late rather than early Pliocene. This interpretation is supported by the presence of *G. inflata*, with an age range of late Pliocene to Recent (Kennett and Srinivasan, 1983), in foraminiferal assemblages that are otherwise typical of the Pliocene in cores 322 and 349 (Table 2). The possibility that these Pliocene sediments were reworked during the Pleistocene seems unlikely because their lithologies are more typical of other Pliocene rather than Pleistocene successions in the study area and even delicate features of the Pliocene foraminifera are generally unabraded. Deposition on the shelf during the early Pliocene, perhaps associated with the highstand of 3rd-order cycle 3.4, is indicated by the Sr ages of several reworked fish bone samples (4.1–5.8 Ma) and one PCG (1.7–4.5 Ma) that occur in Pleistocene successions. Poor preservation of lower Pliocene sediments may result from significant sea-level regressions of 3rd-order cycles 3.6 and 3.7, with preservation of upper Pliocene successions associated with sea-level transgressions of 3rd-order cycles 3.7 and 3.8 (Fig. 6).

5.1.4. Pleistocene successions

The Plio/Pleistocene contact is erosional in most cores, marked by phosphatic sandy gravel (cores 322, 80 and 76), shelly sandy gravel (Core 349), phosphorite pebble layer (Core 90) or sharp lithological boundary (cores 146 and 147). Pleistocene sediment in the study area consists of fine to coarse, glauconitic quartzose sands and reworked phosphorite gravels. Pleistocene sediments are distinct from underlying Pliocene sediments by having a greater amount of medium to coarse quartz grains, less glauconite and more biogenic calcite, especially mollusc shells. Picked benthic foraminifera, echinoid spines and shell have Sr ages (0–1.4 Ma) that are consistent with their Pleistocene biostratigraphic age (Table 2). Pleistocene sediments contain Cretaceous rip-up clasts (Core 352 at 350 cm), upper Oligocene to upper Miocene PCG and PCL, and Miocene to Pleistocene SPG. These reworked grains and the common presence of fining upward cycles and shell lag layers in Pleistocene

successions indicate multiple Pleistocene erosional unconformities throughout the study area consistent with Quaternary high-amplitude and high-frequency sea-level fluctuations associated with Northern Hemisphere glaciation (Wigley, 2004). Many of the Pleistocene successions from the canyon or adjacent to the Western Ridge (cores 322, 352 and 349) have late Pleistocene Sr ages (0–0.5 Ma), consistent with their late Pleistocene foraminiferal assemblages (McMillan, 1993; Dale and McMillan, 1998), and indicate better preservation of upper rather than lower Pleistocene sediments in the study area.

5.2. Phosphogenic episodes

The range in Sr isotope ages indicates that deposition of fine-grained, organic-rich sediments necessary for phosphorite formation (Bentor, 1980; Baturin, 2000) occurred episodically since the late Oligocene in the study area. The generally low organic matter content (<0.5 wt.%) of sediments from throughout the study area demonstrates, however, that the organic-rich sediment in which the phosphorite formed has not been preserved. The organic-rich muds typical of phosphorite formation were removed while their diagenetic sand to pebble sized phosphorite grains were retained on the shelf during erosional events (Compton et al., 1993; 2002). The significantly older age of hard, tightly cemented phosphorite grains indicates that they are more likely to survive reworking than most biogenic carbonate or skeletal phosphorite grains. Phosphorite is, therefore, commonly focused within condensed successions or on erosional unconformities, such as at the contact between lower Miocene and Plio/Pleistocene sediments (cores 90 and 349), and in Pleistocene gravels on the Western Ridge (cores 80 and 190) composed primarily of phosphorite that formed in the late Oligocene.

Nonskeletal phosphorite grains from this study can be divided into two major, and somewhat overlapping, textural types that tend to have distinct Sr ages and relation to sea level. Most phosphorite occurs as CFA-cemented grains (PCG) that range from peloidal sand to gravel. The association of phosphorite with glauconite and pyrite suggests a common origin during the early diagenesis of terrigenous (Fe-rich), organic-rich reducing sediments. Phosphorite and glauconite are commonly associated with marine condensed sections and indicate periods of slow deposition during maximum rates of sea-level rise and sea-level highstands (Loutit et al., 1988; Föllmi et al., 1992). The majority of PCG have late Oligocene to early Miocene Sr ages that correspond to an overall marine transgression with superimposed 3rd-order cycles 1.2 to 1.5 (Fig. 6). In particular, the oldest and largest phosphogenic episode represented by 23.6–26.1 Ma PCG-rich gravel on the Western Ridge overlap with the late Oligocene marine transgressions and highstands of 3rd-order cycles 1.2 and 1.3. Late Oligocene to early Miocene (Aquitanian) marine transgressions and highstands are predicted to have enhanced phosphorite formation on the shelf from the deposition of organic-rich, terrigenous muds derived from coastal upwelling and the suspended load of the Orange and Olifants rivers (Compton et al., 2002). An apparent gap in PCG ages from 19 to 20.5 Ma is associated with nonphosphatic early Burdigalian foraminiferal ooze (cores 145 and 90) and suggests that the marine regression of 3rd-order cycle 2.1 was a period of reduced phosphorite formation. The late early Miocene (Burdigalian) sea-level highstands of cycles 2.1 and 2.2 correspond to significant PCG formation between 16 and 19 Ma.

PCL are less abundant than PCG in the study area with in place PCL recovered from the Eastern Flank of the Canyon in Core 319 and reworked PCL pebbles recovered seaward of the Western Ridge in Core 349. Most PCG are older, and some are younger than PCL, but few PCG and PCL Sr ages overlap. PCL Sr ages range between 9.1 and 17.1 Ma and correspond to an overall middle to late Miocene marine regression (Fig. 6). An overall marine regression would shift the focus of upwelling and terrigenous mud deposition offshore such that organic-rich, terrigenous muds mix with or cover older, middle to outer shelf calcareous deposits where PCL formation is favored by the replacement of biogenic carbonate grains and rip-up clasts (Parker and Siesser, 1972; Parker, 1975), as well as by CFA cementation of calcareous sandy mud. There are localized 3rd-order highstands (cycles 2.4, 2.5 and 2.6) superimposed on the overall middle to late Miocene marine regression, but the resolution of the Sr ages is not sufficient to determine if PCL formation was enhanced during these local highstands. Alternate depositional and erosional cycles are indicated by

Author's Proof of Offprint

PCG and PCL in Miocene sediments that are of similar or somewhat younger age than associated biogenic grains (Figs. 3–5). For example, PCG younger (15.9 to 17.9 Ma) than associated biogenic carbonate (18.4–19.3 Ma) at the base of Core 349 indicate that these PCG have been preferentially retained on down-cut, erosional surfaces of the underlying Miocene carbonate sands. In Core 319, reworked polished PCG pebbles are significantly older than associated benthic foraminifera; however, the up to 2 Myr age difference between PCL nodules and associated biogenic grains (Fig. 5) indicates that PCL nodules formed on older, exhumed erosional surfaces. Reworked PCL of similar age and texture as in place PCL nodules from Core 319 (e.g., Core 349) indicate widespread erosion of phosphatized middle Miocene calcareous deposits between the late Miocene and late Pliocene.

5.3. Phosphogenesis and climate

The Sr ages of phosphorite indicate that upwelling has occurred episodically since the late Oligocene on the continental shelf in the vicinity of the Cape Canyon. Here, we speculate on the correlation of phosphogenesis to changes in climate and ocean circulation. While it is possible that phosphorite older than the late Oligocene has since been eroded from margin uplift and long-term lowering of sea level since the Cretaceous (Haq et al., 1987), preservation of reworked 28.6–30.1 Ma benthic foraminifera in Pliocene sediment and reworked 23.6–26.1 Ma phosphorite in Pleistocene sediment indicate that significant phosphogenesis was initiated in the study area only by the late Oligocene. The major, initial late Oligocene phosphogenic episode occurs at least 3 Myr after the 31 ± 2 Ma final, deep-water opening of Drake Passage (Lawver and Gahagan, 2003) and corresponds to the late Oligocene warming event associated with a sudden decrease in benthic foraminifera $\delta^{18}O$ (Zachos et al., 2001). Permanent ice sheets were established on Antarctica by the early Oligocene but ice cover was episodic from the late Oligocene warming until a major, permanent East Antarctic ice sheet was established by 13 Ma (Shackleton and Kennett, 1975; Flower and Kennett, 1994; Miller et al., 1998; Zachos et al., 2001), a period that spans when most PCG formed in the study area (Fig. 6).

The association of phosphogenesis with periods of episodic Antarctica ice appears counterintuitive because a permanent ice sheet would be expected to produce a steeper latitudinal temperature gradient, stronger winds, and hence more intense, sustained coastal upwelling. However, isotope records from the South Atlantic indicate that the late Oligocene warming event may not reflect a reduction in ice volume (Billups et al., 2002) and significant glaciation events do occur during the period of nonpermanent ice. For example, the rapid glaciation event Mi-1 occurs at the Oligocene/Miocene boundary and a less pronounced, unnamed glaciation event occurs 0.5 Myr before, and the Mi-1a event occurs 2 Myr after the Mi-1 event (Miller et al., 1998). The unnamed, Mi-1 and Mi-1a glaciation events occur within the period of major phosphogenesis from the late Oligocene to early early Miocene and may have enhanced phosphogenesis by increasing wind-forced coastal upwelling. In addition, less intense upwelling may have been required to sustain high-productivity surface waters during the late Oligocene to early Miocene because of the accumulation of phosphate in relatively stagnant Paleogene, as well as early Miocene oceans (e.g., Sheldon, 1980). Warm, subtropical waters upwelled over the shelf during the late Oligocene and early Miocene as indicated by the microfossil assemblages (McMillan, 1986; Dingle et al., 2001). Upwelling of cool waters was clearly established by the Pliocene and, although upper Miocene sediments are lacking on the shelf, sediment from the Walvis Ridge indicate cool water upwelling by the late Miocene (Siesser, 1980).

The major late Oligocene phosphogenic episode is associated with a $+0.8$ $\delta^{13}C$ shift and high $\delta^{13}C$ values from 25.5 to 23 Ma that indicate a global increase in the burial of organic carbon that may have included increased organic carbon burial on continental shelves that enhanced phosphorite formation (Compton et al., 1990). Another significant positive $\delta^{13}C$ excursion occurs in the late early Miocene that is also associated with significant phosphorite formation between 16 and 19 Ma. During the intervening period of decreasing $\delta^{13}C$ values between 19 and 23 Ma, phosphorite formation continues from 23 to 20.5 Ma but is followed by the early Burdigalian gap in phosphorite formation associated with minimum $\delta^{13}C$ values (Fig. 6).

These observations suggest that phosphogenesis on the margin was promoted primarily during marine transgressions and highstands associated with episodic glaciation, particularly when they coincide with periods of increased organic carbon burial as indicated by positive $\delta^{13}C$ shifts.

Why are there relatively few phosphorite grains younger than middle Miocene? An overall marine regression (Haq et al., 1987), less overall organic carbon burial as indicated by the decrease in the marine $\delta^{13}C$ record (Zachos et al., 2001), tectonic uplift of the margin since the middle Miocene (Partridge and Maud, 1987; McMillan, 1993), greater bottom current erosion associated with more vigorous oceanic circulation and Quaternary sea-level fluctuations may have all acted to reduce the residence time of transgressive and highstand organic-rich, terrigenous muds on the shelf. The short residence time makes it unlikely that phosphorite will mature into sufficiently hard and large grains to survive reworking events particularly as the frequency and amplitude of sea-level fluctuations increased (Compton et al., 2002).

6. Summary

The Sr isotope composition of biogenic and phosphatic grains has proved extremely useful in documenting the complex depositional and diagenetic history of the Head of the Cape Canyon area. Sr analysis of different grain types from the same lithologic unit combined with biostratigraphy greatly increases the confidence in Sr-derived ages and their interpretation. In general, biogenic Sr ages decrease upsection, are similar among different biogenic grain types from the same sample and agree with foraminiferal biostratigraphic ages. However, relatively large (>250 μm) and robust reworked benthic foraminifera (e.g., *Lenticulina*) are significantly older than biostratigraphic ages. Skeletal phosphorite (SPG), particularly fine translucent fish bone and scales, can provide approximate final depositional ages where foraminifera are reworked or lacking. Biogenic Sr ages where integrated with biostratigraphic ages can increase stratigraphic resolution, particularly for lower Miocene sediments. Mixing of biogenic components by sediment reworking underscores the need to pick biogenic grains for Sr analysis with reference to the composition and condition of the overall biogenic assemblage.

The Sr ages of reworked phosphorite and biogenic grains indicate that deposition was fairly continuous on the margin throughout the late Cenozoic but only a small proportion of these deposits end up preserved because of episodic and extensive erosional events related to changes in sea level, tectonic movement and bottom-water currents. Major composite erosional unconformities occur in the study area between Cretaceous and lower Miocene, lower Miocene and Plio/Pleistocene, and upper Pliocene and upper Pleistocene sediments. Middle Miocene sediment is rarely preserved in the area, and the lower Miocene to upper Pliocene unconformity is marked by reworked Miocene PCG pebbles and a transition from calcareous to fine quartzose sand sediment. The Pliocene to Pleistocene unconformity is marked by a gravel composed of reworked lower Miocene PCG and a transition to medium to coarse glauconitic quartzose sands with shell gravel layers.

The Sr isotopes of phosphorite are particularly useful in determining the age of phosphogenesis, which was found to be both significantly older, as well as younger, than associated biogenic grains. Included quartz, glauconite and pyrite indicate that phosphorite formation was enhanced by deposition of organic-rich muds in response to upwelling of the Benguela system combined with accumulation of Fe-rich suspended muds from the Orange and Olifants rivers. Nonskeletal phosphorite grains occur primarily as phosphorite (CFA)-cemented grains (PCG) and to a lesser extent, as phosphate-cemented limestone (PCL). Most PCG formed during marine transgressions and highstands of the late Oligocene to early early Miocene (21–26 Ma) and late early Miocene (16–19 Ma). PCL formed between 9 and 17 Ma, primarily by replacement and cementation of older, middle to outer shelf calcareous deposits during the middle to late Miocene marine regression as upwelling and terrigenous mud deposition shifted seaward. PCG and PCL younger than associated biogenic carbonate represent lag deposits on erosional, downcut surfaces.

The initial phosphogenic episode from 23.6 to 26.1 Ma appears to be the largest and coincides with

the late Oligocene warming event and a positive shift in the marine $\delta^{13}C$ record. Phosphogenesis on the margin was enhanced by the overall late Oligocene to mid-Miocene marine transgression combined with episodic glaciation and upwelling that increased organic carbon burial on the shelf. The paucity of phosphorite formation since the middle Miocene corresponds to an overall lowering of sea level and an increased frequency in the reworking of organic-rich, terrigenous mud deposits off of the shelf.

Acknowledgements

This research was funded by the South African National Research Foundation and the University of Cape Town. Werner Marine Research kindly provided the vibracores used in this study and we thank De Beers for providing support for the Sr analyses. This paper benefited from the reviews of M. Delaney and K. Föllmi.

References

Baturin, G.N., 2000. Formation and evolution of phosphorite grains and nodules on the Namibian shelf, from Recent to Pleistocene. In: Glenn, C.R., Prévôt-Lucas, L., Lucas, J. (Eds.), Marine Authigenesis: From Global to Microbial. Spec. Publ. Soc. Econ. Paleontol. Mineral 66, 185–199.

Bentor, Y.K., 1980. Phosphorites—the unsolved problems. In: Bentor, Y.K. (Ed.), Marine Phosphorites—Geochemistry, Occurrence, Genesis. Spec. Publ. Soc. Econ. Paleontol. Mineral 29, 3–18.

Billups, K., Channel, J.E.T., Zachos, J., 2002. Late Oligocene to early Miocene geochronology and paleoceanography from the subantarctic South Atlantic. Paleoceanography 17, 4-1–4-11.

Birch, G.F., 1979. Phosphorite pellets and rock from the western continental margin and adjacent coastal terrace of South Africa. Mar. Geol. 33, 91–116.

Birch, G.F., 1980. A model of penecontemporaneous phosphatization by diagenetic and authigenic mechanisms from the western margin of southern Africa. In: Bentor, Y.K. (Ed.), Marine Phosphorites—Geochemistry, Occurrence, Genesis. Spec. Publ. Soc. Econ. Paleontol. Mineral 29, 79–100.

Birch, G.F., Thomson, J., McArthur, J.M., Burnett, W.C., 1983. Pleistocene phosphorites off the west coast of South Africa. Nature 302, 601–603.

Birch, G.F., Day, R.W., Du Plessis, A., 1991. Nearshore Quaternary sediments on the west coast of southern Africa. Geol. Surv. Bull. (S. Afr.) 101, 1–14.

Cande, S.C., Kent, D.V., 1995. Revised calibration of the geomagnetic polarity timescale for the Late Cretaceous and Cenozoic. J. Geophys. Res. 100, 6093–6095.

Christison, I.D., 1985. Foraminifera from the continental shelf of southwest Africa. Unpublished MSc thesis. University College of Wales, Aberystwyth. 174 pp.

Compton, J.S., Snyder, S.W., Hodell, D.A., 1990. Phosphogenesis and weathering of shelf sediments from the southeastern United States: implications for Miocene $\delta^{13}C$ excursions and global cooling. Geology 18, 1227–1230.

Compton, J.S., Hodell, D.A., Garrido, J.R., Mallinson, D.J., 1993. Origin and age of phosphorite from the south-central Florida platform: relation of phosphogenesis to sea-level fluctuations and $\delta^{13}C$ excursions. Geochim. Cosmochim. Acta 57, 131–146.

Compton, J.S., Mulabisana, J., McMillan, I.K., 2002. Origin and age of phosphorite from the Last Glacial Maximum to Holocene transgressive succession off the Orange River, South Africa. Mar. Geol. 186, 243–261.

Dale, D.C., McMillan, I.K., 1998. Mud belt and middle shelf benthonic and planktonic foraminiferal assemblages and sedimentation processes compared through the Holocene successions at two tropical African (Sierre Leone) and two temperate African (western offshore South Africa) sites. S. Afr. J. Sci. 94, 319–340.

Dale, D.C., McMillan, I.K., 2000. Pliocene foraminifera and biostratigraphic correlations of the Atlantic continental margin of South Africa and southern Namibia. 14th African Colloquium on Micropalaeontology, Luanda, Angola, 21–24 May 2000. Abstract.

DePaolo, D.J., 1986. Detailed record of the Neogene Sr isotopic evolution of seawater from DSDP Site 590B. Geology 14, 103–106.

DePaolo, D.J., Finger, K.L., 1991. High-resolution strontium-isotope stratigraphy and biostratigraphy of the Miocene Monterey Formation, central California. Geol. Soc. Am. Bull. 103, 112–124.

DePaolo, D.J., Ingram, B.L., 1985. High-resolution stratigraphy with strontium isotopes. Science 227, 938–941.

Dingle, R.V., 1980. Large allochthonous sediment masses and their role in the construction of the continental slope and rise off southwestern Africa. Mar. Geol. 37, 333–354.

Dingle, R.V., Birch, G.F., Bremner, J.M., De Decker, R.H., Du Plessis, A., Englebrecht, J.C., Fincham, M.J., Fitton, T., Flemming, B.W., Gentle, R.I., Goodlad, S.W., Martin, A.K., Mills, E.G., Moir, G.J., Parker, R.J., Robson, S.H., Rogers, J., Salmon, D.A., Siesser, W.G., Simpson, E.S.W., Summerhayes, C.P., Westall, F., Winter, A., Woodborne, M.W., 1987. Deep-sea sedimentary environments around southern Africa (south-east Atlantic and south-west Indian Oceans). Ann. S. Afr. Mus. 98, 1–27 (2 separate maps).

Dingle, R.V., McMillan, I.K., Majoran, S., Bisset, L., 2001. Palaeooceanographical implications of early–middle Miocene subtropical ostracod faunas from the continental shelf of the SE Atlantic Ocean. Palaeogeogr. Palaeoclimatol. Palaeoecol. 173, 43–60.

Farrell, J.W., Clemens, S.C., Gromet, L.P., 1995. Improved chronostratigraphic reference curve of late Neogene seawater $^{87}Sr/^{86}Sr$. Geology 23, 403–406.

University of Cape Town

Föllmi, K.B., Garrison, R.E., Ramirez, P.C., Zambrano-Ortiz, F., Kennedy, W.J., Lehner, B.L., 1992. Cyclic phosphate-rich successions in the Upper Cretaceous of Colombia. Palaeogeogr. Palaeoclimatol. Palaeoecol. 93, 151–182.

Flower, B.P., Kennett, J.P., 1994. The middle Miocene climatic transition: East Antarctic ice sheet development, deep ocean circulation and global carbon cycling. Palaeogeogr. Palaeoclimatol. Palaeoecol. 108, 537–555.

Garrison, R.E., Kastner, M., 1990. Phosphatic sediments and rocks recovered from the Peru margin during ODP Leg 112. Proc. Ocean Drill. Prog., Sci. Results 112, 111–134.

Gawlinski, S., 1987. Benthonic foraminifera from the continental shelf of southwest Africa. Unpublished MSc thesis. University College of Wales, Aberystwyth. 127 pp.

Haq, B.U., Hardenbol, J., Vail, P.R., 1987. Chronology of fluctuating sea-levels since the Triassic. Science 235, 1156–1166.

Hodell, D.A., Mueller, P.A., Garrido, J.R., 1991. Variations in the strontium isotopic composition of seawater during the Neogene. Geology 19, 24–27.

Kennett, J.P., Srinivasan, M.S., 1983. Neogene planktonic foraminifera. A Phylogenetic Atlas. Hutchinson Ross, Stroudsburg, Pennsylvania. 265 pp.

Lavelle, M., Armstrong, R., 1993. Strontium isotope ratios in modern biogenic and chemical marine precipitates from southern Africa. S. Afr. J. Sci. 89, 533–536.

Lawver, L.A., Gahagan, L.M., 2003. Evolution of Cenozoic seaways in the circum-Antarctic region. Palaeogeogr. Palaeoclimatol. Palaeoecol. 198, 11–37.

Loutit, T.S., Hardenbol, J., Vail, P.R., Baum, G.R., 1988. Condensed sections: the key to age determinations and correlation of continental margin sequences. In: Wilgus, C.K., Hastings, B.S., Posamentier, H., Van Wagoner, J., Ross, C.A., Kendall, C. (Eds.), Sea-Level Changes: An Integrated Approach. Spec. Publ.-Soc. Econ. Paleontol. Mineral., vol. 42, pp. 183–213.

Mabote, M.E., Rogers, J., Meadows, M.E., 1997. Sedimentology of terrigenous mud from the Orange River Delta and the inner shelf off Namaqualand, South Africa. S. Afr. Geogr. J., 108–114 (Special Edition).

McArthur, J.M., Howarth, R.J., Bailey, T.R., 2001. Strontium isotope stratigraphy: LOWESS Version 3: best fit to the marine Sr-isotope curve for 0–509 Ma and accompanying look-up table for deriving numerical age. J. Geol. 109, 155–170.

McMillan, I.K., 1986. Cainozoic planktonic and larger foraminifera distributions around southern Africa and their implications for past changes of oceanic water temperatures. S. Afr. J. Sci. 82, 66–69.

McMillan, I.K., 1987. Late Quaternary foraminifera from the southern part of offshore southwest Africa/Namibia. Unpublished PhD thesis. University College of Wales, Aberystwyth. 565 pp.

McMillan, I.K., 1989. *Victoriella conoidea* (Rutten, 1914): a guide foraminifera for the later Aquitanian (early Miocene) marine rocks of southern Africa. S. Afr. J. Geol. 92, 95–101.

McMillan, I.K., 1993. Foraminiferal biostratigraphy, sequence stratigraphy and interpreted chronostratigraphy of marine Quaternary sedimentation on the South African continental shelf. S. Afr. J. Sci. 89, 83–89.

Meadows, M.E., Rogers, J., Lee-Thorp, J.A., Bateman, M.D., Dingle, R.V., 2002. Holocene geochronology of a continental-shelf mudbelt off southwestern Africa. Holocene 12, 59–67.

Miller, K.G., Mountain, G.S., Browning, J.V., Kominz, M., Sugarman, P.J., Christie-Blick, N., Katz, M., Wright, J.D., 1998. Cenozoic global sea level, sequences, and the New Jersey transect: results from coastal plain and continental slope drilling. Rev. Geophys. 36, 569–601.

Nelson, G., 1989. Poleward motion in the Benguela area. In: Neshyba, S.J., et al. (Ed.), Poleward Flows Along Eastern Ocean Boundaries. Springer, New York, pp. 110–130.

Parker, R.J., 1975. The petrology and origin of some glauconitic and glaucoconglomeratic phosphorites from the South African continental margin. J. Sediment. Petrol. 45, 230–242.

Parker, R.J., Siesser, W.G., 1972. Petrology and origin of some phosphorites from the South Africa continental margin. J. Sediment. Petrol. 42, 434–440.

Partridge, T.C., Maud, R.R., 1987. Geomorphic evolution of southern Africa since the Mesozoic. S. Afr. J. Geol. 90, 179–208.

Rogers, J., 1977. Sedimentation on the Continental Margin off the Orange River and Namib Desert. PhD thesis, Department of Geological Sciences. University of Cape Town.

Rogers, J., Bremner, M., 1991. The Benguela ecosystem: Part VII. Marine-geological aspects. In: Barnes, M. (Ed.), Annual Review-Oceanography and Marine Biology, vol. 29. Aberdeen Univ. Press, Aberdeen, pp. 1–85.

Shackleton, N., Kennett, J., 1975. Paleotemperature history of the Cenozoic and the initiation of Antarctic glaciation: oxygen and carbon isotope analyses in DSDP Sites 277, 279 and 281. Initial Reports of the Deep Sea Drilling Project, vol. 29. US Government Printing Office, Washington, DC, pp. 743–755.

Sheldon, R.P., 1980. Episodicity of phosphate deposition and deep ocean circulation—a hypothesis. In: Bentor, Y.K. (Ed.), Marine Phosphorites—Geochemistry, Occurrence, Genesis. Spec. Publ.-SEPM, vol. 29, pp. 239–247.

Siesser, W.G., 1978. Age of phosphorites on the South African continental margin. Mar. Geol. 26, M17–M28.

Siesser, W.G., 1980. Late Miocene origin of the Benguela upwelling system off northern Namibia. Science 208, 283–285.

Summerhayes, C.P., Birch, G.F., Rogers, J., Dingle, R.V., 1973. Phosphate in sediments off south-western Africa. Nature 243, 509–511.

Veeh, H.H., Burnett, W.C., Soutar, A., 1973. Contemporary phosphorites on the continental margin off Peru. Science 181, 844–845.

Wigley, R., 2004. Sedimentary facies from the Head of the Cape Canyon: Insights into the Cenozoic evolution of the western margin of South Africa. PhD thesis, University of Cape Town.

Zachos, J., Pagani, M., Sloan, L., Thomas, E., Billups, K., 2001. Trends, rhythms, and aberrations in global climate 65 Ma to present. Science 292, 686–693.

Property of CSS Drilling

6 OLIGOCENE-MIOCENE SUCCESSION

The Upper Oligocene/Lower Miocene Calcareous Unit of Concession 20D includes four sediment facies that differ significantly in their calcareous components (Figure 6.1). The oldest facies is the Quartzose Foraminiferal Muddy Sand, which is overlain successively by the Quartzose Glauconitic Calcareous Sand, the Glauconitic Calcareous Sand and the Foraminiferal Ooze. The original WMR core logs were used in conjunction with upper Oligocene/lower Miocene sediments analysed in detail in this study and Compton *et al.* (2004) to establish the lithostratigraphy of the Upper Oligocene/Lower Miocene Calcareous Unit. The close of early Miocene deposition is marked by an abrupt change in sedimentary environment and deposition of the Gravelly Calcareous Quartzose Muddy Sand.

6.1 QUARTZOSE FORAMINIFERAL MUDDY SAND

The Quartzose Foraminiferal Muddy Sand was recovered in the lowermost 31 cm of Core 324 (Appendix A1-39). Core 324, with a total recovery of 1.58 m, was collected from a water depth of 264 m in the south of the concession area on the Southern Rocky Plateau of the Western Ridge (Figure 6.2). The Quartzose Foraminiferal Muddy Sand was only recovered from Core 324 and represents the oldest Cenozoic sediment recovered in the study area.

6.1.1 LITHOSTRATIGRAPHY OF THE QUARTZOSE FORAMINIFERAL MUDDY SAND

The basal contact of the Quartzose Foraminiferal Muddy Sand was not recovered. The Quartzose Foraminiferal Muddy Sand is an unconsolidated pink to reddish yellow (5YR 7/4 to 7/6) stained muddy sand with an abundance of larger benthic foraminifera (Figure 6.3). The two samples (Appendix A1-39) vary between a lower, slightly gravelly muddy sand and an upper gravelly muddy sand towards the top of the unit (Figure 6.4). The sediment is poorly sorted and contains very fine to very coarse sand grains. The sand fraction is composed of pink to reddish yellow-stained carbonate fragments dominated by larger benthic foraminifera (whole and broken fragments) and clear, angular very fine quartz. Phospho-glauconite grains, minor benthic and planktic foraminifera, and traces of echinoid spines and bryozoa are also present. The bryozoan zooecia commonly have a green infilling. The composition of the green infilling is shown, by EDS analysis, to vary between glauconite (phosphorite-free) and a phospho-glauconite. In addition, minor well-rounded, light-brown, phosphate-cemented quartz (and minor glauconite) grains, amber phosphorite granules and pelletal phosphorite grains are present. The relative abundance of the components of the sand fraction was determined by point-counting a minimum of 300 grains (Table 6.1), although this method may be biased towards the very fine sand-size quartz component. Shell fragments were included in the benthic foraminifera group during point-counting as the very fine to coarse sand-sized shell fragments were difficult to distinguish from the broken larger benthic foraminiferal fragments, particularly as both carbonate grain types are stained pink to reddish yellow. Trace amounts of well-rounded, medium to very coarse sand-size quartz grains are also present. A red-coating on surface hollows of these coarse quartz grains is common. The surface coating has an EDS composition that ranges from being dominated by Ca to including Ca with Fe, P and minor

University of Cape Town

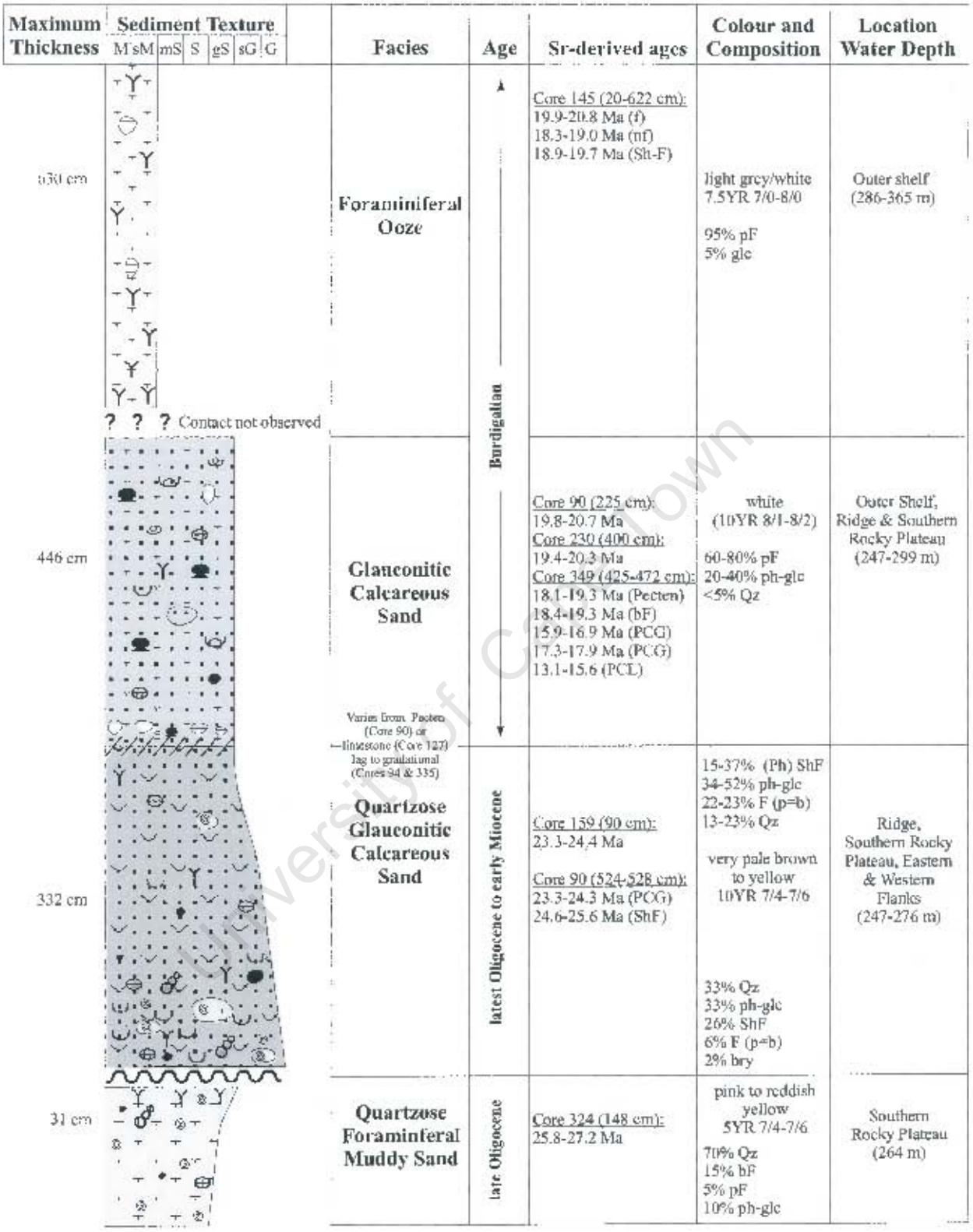


Figure 6.1. The stratigraphy of the Upper Oligocene/Lower Miocene Calcareous Unit. The legend for the symbols is included in Figure 3.11, with the grey scale reflecting the glauconite abundance.

University of Cape Town

amounts of Ti, Si, Al and Mg (Figure 6.5). The well-rounded, coated surfaces have an etched appearance similar to that described for the surfaces of quartz grains from the Cretaceous Woody Quartzose Sand (Figure 4.11). The composition of the sand fraction of the two samples is similar, although the upper Sample 324-7 includes a higher percentage of authigenic grains and benthic foraminifera at the expense of quartz and has a greater diversity in the foraminiferal assemblage. Sample, 324-7, collected from the top of the unit, also includes minor shell, predominantly bivalve and bryozoan fragments.

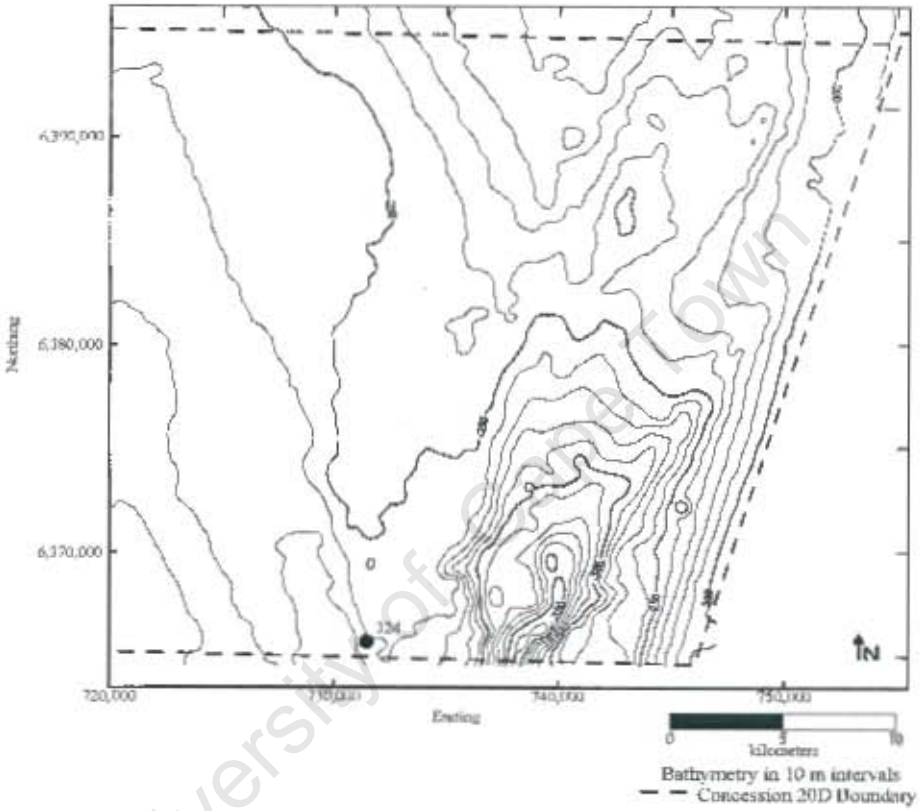


Figure 6.2. The distribution of the Quartzose Foraminiferal Muddy Sand facies on the Southern Rocky Plateau of the Western Ridge in Concession 20D (dashed line denotes concession boundary).

The benthic foraminiferal assemblage is dominated by the larger benthic foraminifera identified as *Operculina* sp. (I. McMillan, *pers. comm.*, 2002). The *Operculina* sp. is poorly preserved and rarely complete. The surfaces of the *Operculina* sp. are shown to be extensively recrystallised (Figure 6.6), with small amounts of Fe, Al and K detected by EDS. The foraminiferal assemblage, in general, of this facies shows similar macroscopic evidence of Fe-staining and recrystallisation (Figure 6.3A). The complete foraminiferal assemblage of the Quartzose Foraminiferal Muddy Sand is included in Table 6.2 and is interpreted to represent an inner shelf (50-60 m) assemblage by I. McMillan *(pers. comm.*, 2003).

Table 6.1. The relative abundance (% of grains) of the components present in the sand fraction of the Quartzose Foraminiferal Muddy Sand.

Sample (Appendix A1-39)	Quartz	Benthic Foraminifera	Planktic Foraminifera	Authigenic grains	Echinoid Spines	Bryozoa fragments
324-7	59.3	15.8	1.8	22.2	0.5	0.5
324-8	70.5	14.7	4.2	10.0	0.5	-

University of Cape Town

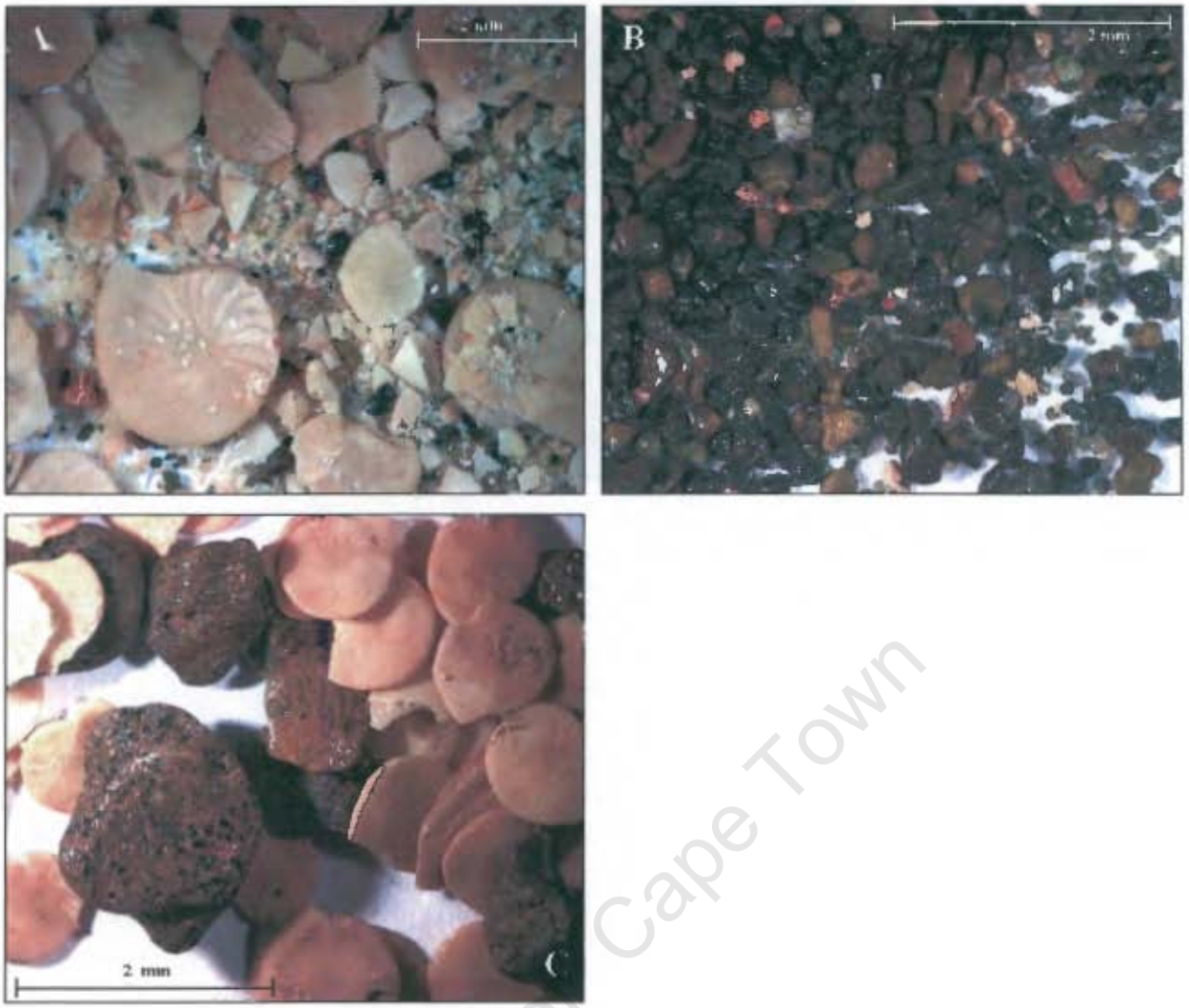


Figure 6.3. Photographs of the sand fraction (A) of the Quartzose Foraminiferal Muddy Sand from Sample 324-8. The magnetic fraction (B) is dominated by earthy brown-green phospho-glauconite grains. The gravel fraction (C) is composed of the larger benthic foraminifera *Operculina* sp., amber phosphorite pebbles and a single orange-stained bivalve fragment (not pictured).

University of Cape Town

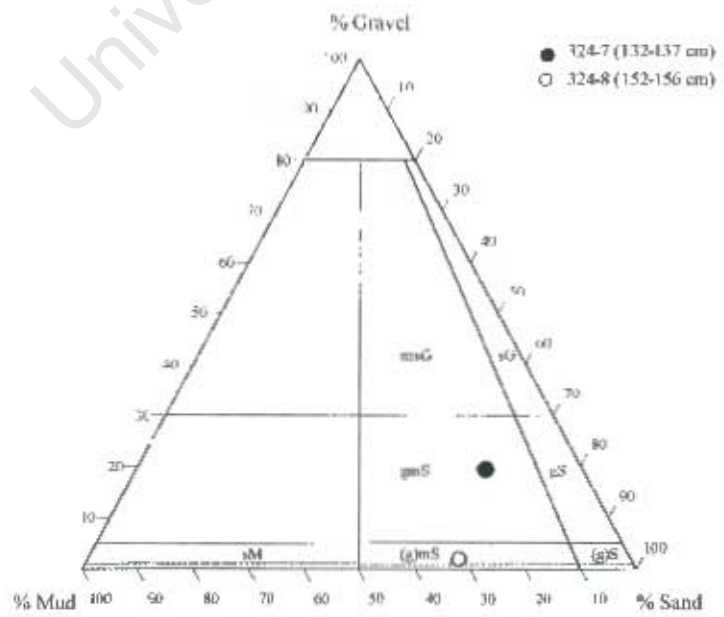


Figure 6.4. A summary of Quartzose Foraminiferal Muddy Sand grain size textures.

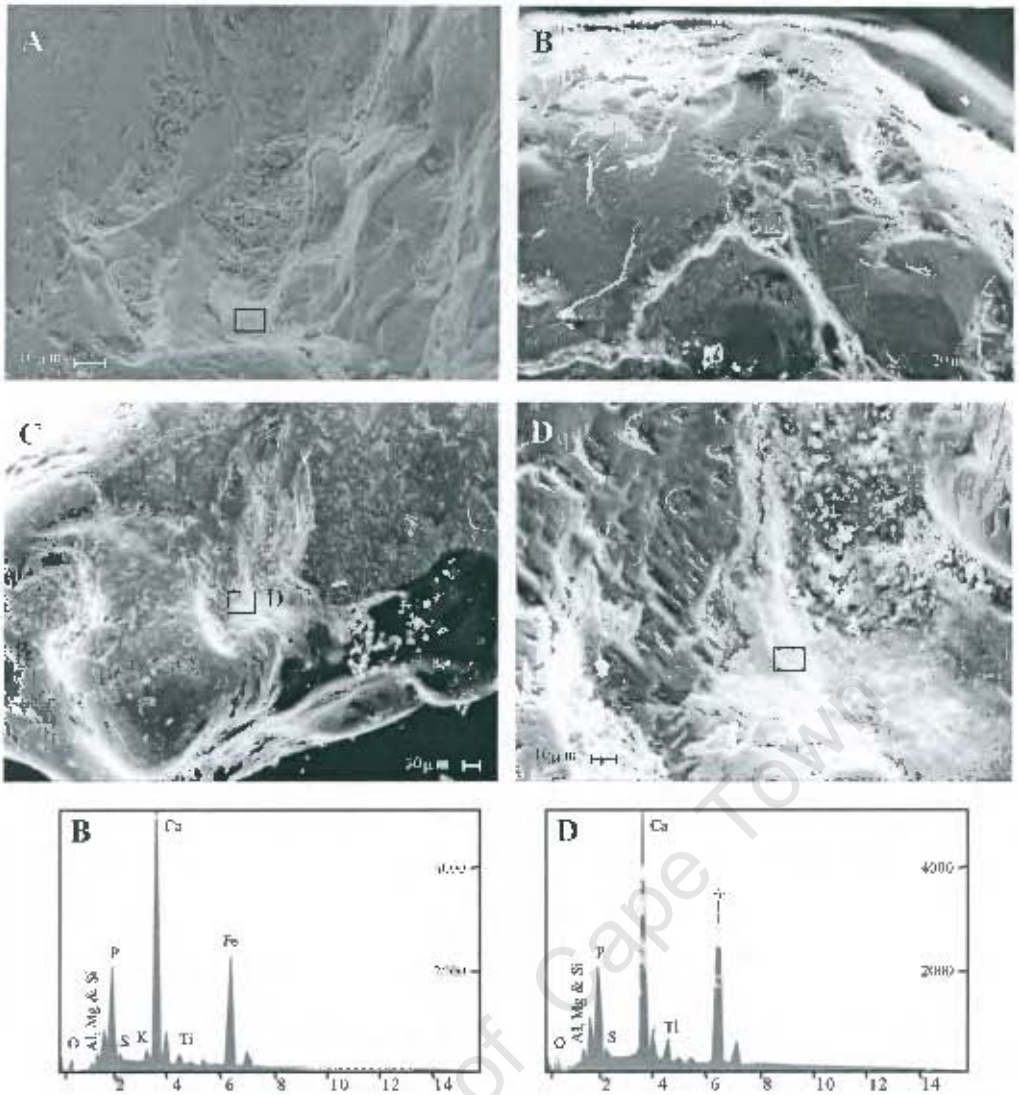


Figure 6.5. Typical coarse quartz grains from the Quartzose Foraminiferal Muddy Sand with orange surface coatings from Sample 324-8 (152-156 cm). The composition of the coating, obtained by EDS scans of the areas enclosed in the black squares, varies from calcite, composed entirely of Ca (A) (EDS spectrum not shown), to a carbonate-fluorapatite - Fe-oxide coating composed of a mixture of predominantly P, Ca and Fe (B & C→D).

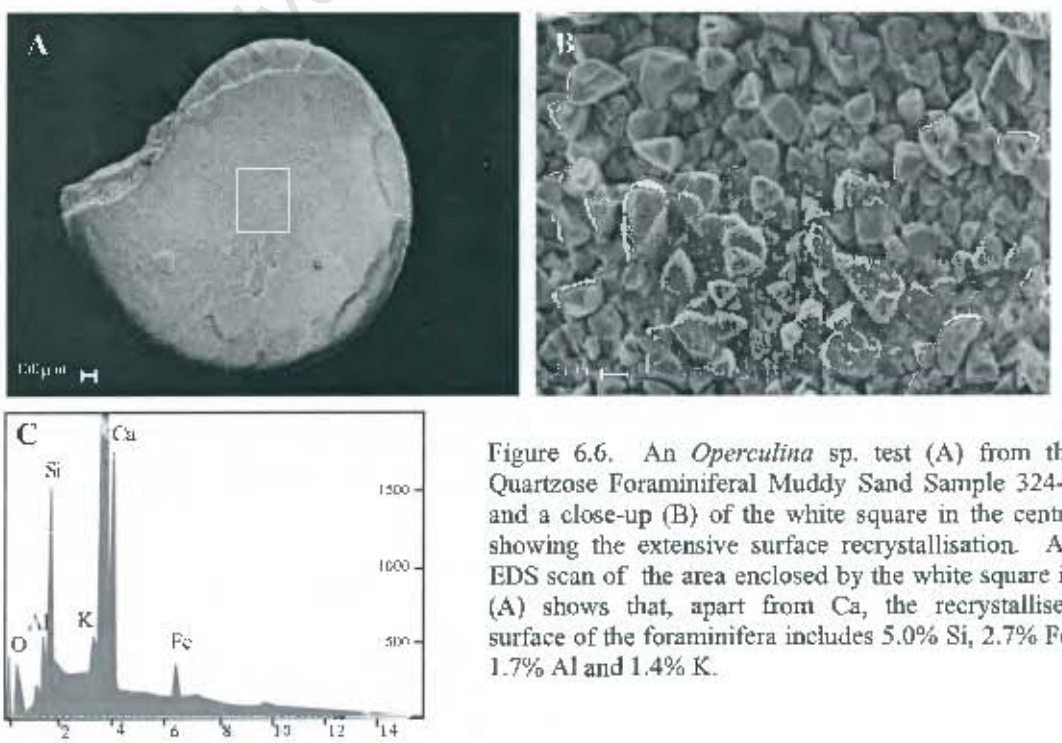


Figure 6.6. An *Operculina* sp. test (A) from the Quartzose Foraminiferal Muddy Sand Sample 324-8 and a close-up (B) of the white square in the centre showing the extensive surface recrystallisation. An EDS scan of the area enclosed by the white square in (A) shows that, apart from Ca, the recrystallised surface of the foraminifera includes 5.0% Si, 2.7% Fe, 1.7% Al and 1.4% K.

University of Cape Town

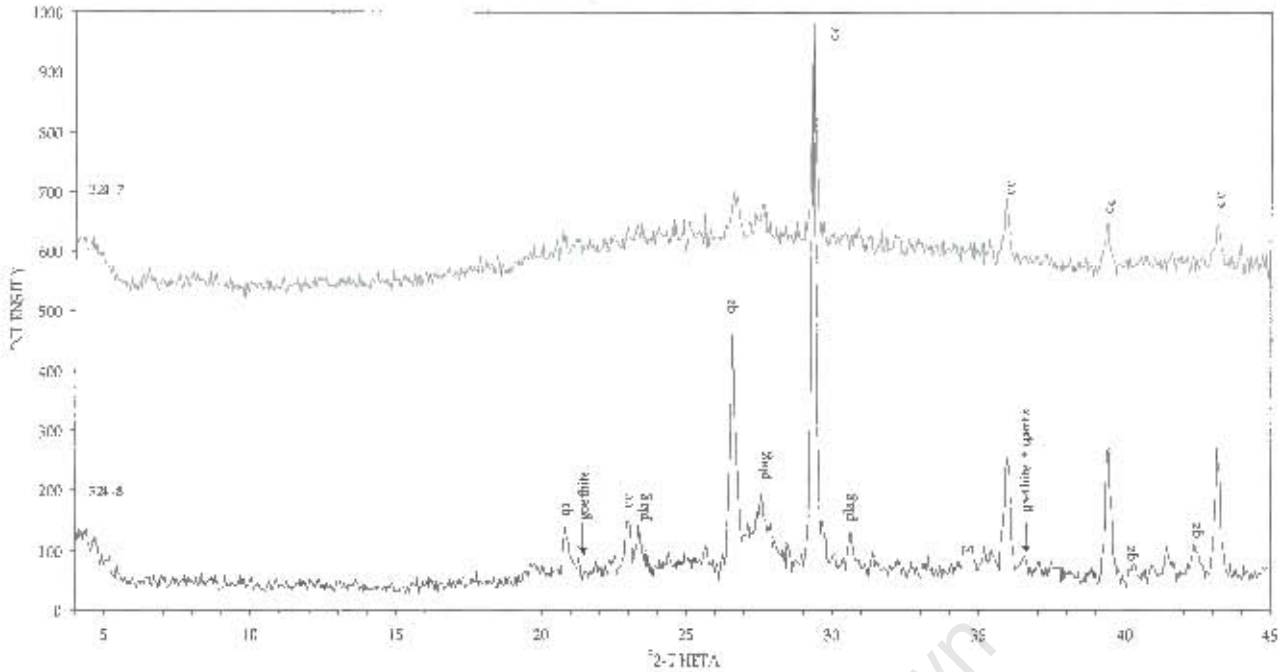


Figure 6.7. XRD records for the mud fraction (<63 μm) of the Quartzose Foraminiferal Muddy Sand composed of calcite (cc), quartz (qz), feldspar (plag) and goethite.

Table 6.2. The foraminiferal assemblage of Sample 324-8 (I. McMillan, *pers. comm.*, 2002).

Operculina sp.	*Hanzawaia sp.*	*Globigerina spp.*	*Cancris sp.*
Ribbed *Dentalina sp.*	*Karreriella cf. siphonella*	*Globigerina praebulloides*	*Globulina sp.*
Lobatula sp	*Victoriella conoidea*	Thin *Spiroplectinella sp.*	*Globobulimina sp.*
Small *Cibicidoides sp.*	*Gaudryina sp.*	*Gyroidinoides cf. soldanii*	*Pullenia bulloides*
Lenticulina spp.	Ribbed *Uvigerina sp.*	Ribbed *Hopkinsina sp.*	Ribbed *Amphicoryna sp.*
Fattish *Spiroplectinella sp.*	Smooth *Uvigerina sp.*	*Dentalina cf. communis*	*Rupertina stabilis.*

The mud fraction (<63 μm) of both samples is dominated by calcite, quartz with minor amounts of plagioclase feldspar (Figure 6.7). The lower Sample 324-8 also includes a small peak identified as goethite, although it is largely obscured by more intense quartz peaks.

The gravel fraction of both samples is dominated by the larger benthic foraminifera *Operculina* sp. (<4 mm) and by phosphorite pebbles (Figure 6.3). The light-brown to amber phosphorite pebbles coarsen up-core from very fine to fine pebbles (vfP-fP) at the base of the core, in Sample 324-8, to very fine to medium pebbles (vfP-mP) in Sample 324-7. The well-rounded phosphorite pebbles are commonly mollusc (gastropod and bivalve) casts, composed of cemented very fine quartz sand with minor to trace amounts of glauconite. Bivalve shell fragments in the gravel component increase in abundance up-core and bryozoan fragments are present towards the top of the unit.

6.1.2 AGE OF THE QUARTZOSE FORAMINIFERAL MUDDY SAND

The determination of the age of this unit is hampered by a large discrepancy between the Sr-derived age and the biostratigraphic age. A Sr-isotope age of 25.8-27.2 Ma (late Oligocene) was obtained by the Council for Geoscience on behalf of WMR for *Operculina* sp. picked from a sample taken at 148 cm (immediately above Sample 324-8). The late Oligocene Sr-derived age is considered a minimum age for this facies because the entire foraminiferal assemblage shows evidence of recrystallisation.

University of Cape Town

A late Aquitanian (early Miocene) age for deposition of the Quartzose Foraminiferal Muddy Sand was proposed by I. McMillan (*pers. comm.*, 2002), based on the foraminiferal assemblage present in Sample 324-8. In particular, the rare traces of *Victoriella conoidea* (Table 6.2) indicated a late Aquitanian age (McMillan, 1989). I. McMillan (*pers. comm.*, 2002) also indicated that the foraminiferal species present in the Quartzose Foraminiferal Muddy Sand (excluding the *Operculina* sp.) are common to the lower Neogene (Miocene) sediments of the western margin.

The younger age indicated by the *V. conoidea* and the foraminiferal assemblage, might possibly be explained if the range of *V. conoidea* (and the lower Neogene assemblage) in southern African waters extends back into the late Oligocene. An extended range is supported by the fact that McMillan (1986) indicated a hiatus in the sedimentary record for the South African margin with no upper Oligocene to early Aquitanian sediments recovered and his proposed biostratigraphic ages must therefore provide only a minimum age range. Additional support for a late Oligocene age of the Quartzose Foraminiferal Muddy Sand is supported by the fact that this facies lies unconformably below the gravel lag at the base of the latest Oligocene to early Miocene (Aquitanian) Quartzose Glauconitic Calcareous Sand (Section 6.2.2). However, an increase in bivalve fragments up-core in the Quartzose Foraminiferal Muddy Sand may indicate that the trace amounts of younger foraminifera have been reworked into the older underlying sediment by bioturbation.

Therefore, the depositional age of this facies is believed to be late Oligocene. The younger age indicated by the foraminiferal assemblage suggests an extended age range for this assemblage on the western margin, although the possibility that younger foraminifera were worked down into the sediments by bioturbation is not discounted.

University of Cape Town

6.1.3 DEPOSITIONAL ENVIRONMENT OF THE QUARTZOSE FORAMINIFERAL MUDDY SAND

A low-energy, sandy, neritic palaeo-environment is inferred for the larger benthic foraminifera species. A similar conclusion is made by Abdelghany (2002) from the presence of large benthic foraminifera in the lower Miocene sediments of the Gebel Shabrawet area in Egypt. Larger benthic foraminifera are an important element of the modern benthic community in subtropical and tropical seas and they are found from below the intertidal (subtidal) zone to the base of the euphotic zone (Hohenegger *et al.*, 1999; Haunold *et al.*, 1997; Hohenegger, 1995; McMillan, 1986). All larger benthic foraminifera are restricted to the euphotic zone, because they house diatoms as symbiotic algae (Hallock, 1985; Hohenegger, 1995), with modern taxa largely confined to <60 m water depth (Kumar and Saraswati, 1997).

Larger benthic foraminifera commonly show strong species zonation due to environmental factors, such as salinity, temperature, sediment structure, light intensity, water energy and food availability (Hohenegger *et al.*, 1999). The presence of *Operculina* sp. as the only larger benthic foraminifera in the

Quartzose Foraminiferal Muddy Sand is indicative of the narrow range in distribution of large benthic foraminiferal taxa in response to specific environmental factors (Hohenegger *et al.*, 1999). The Nummelitid family (*Operculina* sp.) prefers low-energy environments and sandy rather than rocky bottoms (Hohenegger *et al.*, 1999; Haunold *et al.*, 1997, Kumar and Saraswati, 1997). Abundant *Operculina* sp. in this facies implies a period of carbonate deposition in a shallow-water, low-energy environment some time in the late Oligocene.

In addition to large benthic foraminifera, the unit includes up to 22.2% authigenic grains of glauconite, phospho-glauconite and phosphorite. Authigenic-rich sediments are typically interpreted as condensed sections in sequence stratigraphic models, where glauconite is reported to reflect rapid increases in relative sea level of a Transgressive Systems Tract (TST) (Loutit *et al.*, 1988; Amorosi, 1995; Kelly and Webb, 1999; Harris and Whiting, 2000). Harris and Whiting (2000) cautioned that glauconite formation does not necessarily indicate a TST, although it occurs predominantly within condensed TST of low subsidence-rate passive margins, such as the western US mid-Atlantic margin. Glauconite is a reliable indicator of deeper water on the shelf and of very low sedimentation rates (Odin and Matter, 1981; Kelly and Webb, 1999; Harris and Whiting, 2000). Glauconite is recorded from water depths ranging from the mid to outer shelf (>50 m) with an optimum depth of around 200 m (Odin and Fullagar, 1988; Chaftez and Reid, 2000). Similarly, the phosphatisation of the shell fragments and molluscan casts suggest a rise in relative sea level after the deposition of the larger benthic foraminifera. Phosphorite formation is normally associated with a maximum flooding surface, where bottom-current activity and low sedimentation rates favour phosphorite formation (Föllmi, 1996). Therefore, although recovered in only a single core, the Quartzose Foraminiferal Muddy Sand provides evidence for the first recorded cycle of relative sea-level change in the Cenozoic of the study area.

University of Cape Town

6.2 QUARTZOSE GLAUCONITIC CALCAREOUS SAND

The Quartzose Glauconitic Calcareous Sand was recovered from twelve cores collected on the upper slope flank of the Western Ridge, on the Southern Rocky Plateau and from an erosional outlier on the eastern flank of the main channel (Figure 6.8). The erosional outlier lies approximately 1.5 km ESE of the Cretaceous outlier discussed in Chapter 4. The sediments were all collected from within a narrow range of water depths of 247-276 m, with the majority of samples recovered from a water depth of 252-255 m. The Quartzose Glauconitic Calcareous Sand has a maximum thickness of 332 cm in Core 286. This unit was not recovered in any of the cores sampled along the Northern, Central or Southern Transects. Cores 324 and 159, collected from the Southern Rocky Plateau, were chosen for analysis as Sr-isotope ages had been obtained by WMR for sediments recovered in these cores (Figure 6.8). In addition, sediment and Sr-age data are available for Core 90 (Compton *et al.*, 2004).

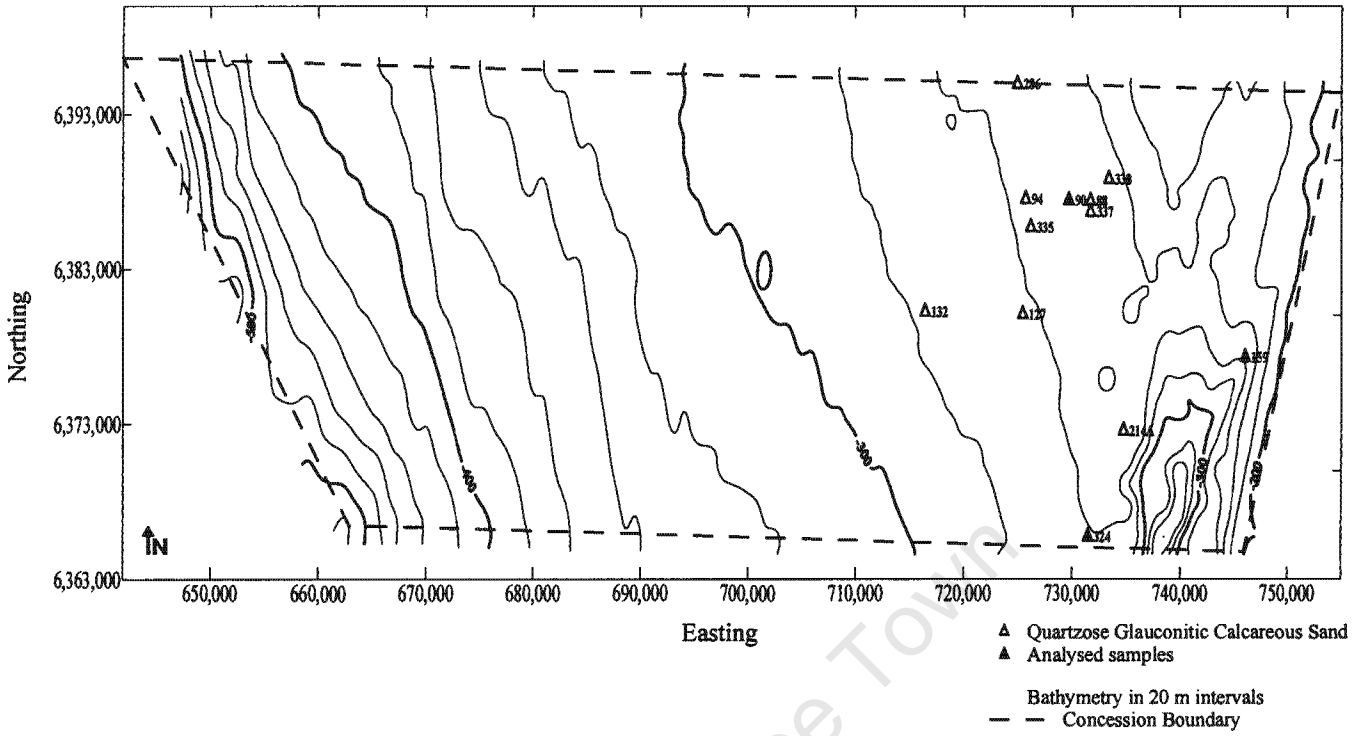


Figure 6.8. The distribution of the Quartzose Glauconitic Calcareous Sand facies in Concession 20D. Cores sampled in this study shown with a solid symbol.

University of Cape Town

6.2.1 LITHOSTRATIGRAPHY OF THE QUARTZOSE GLAUCONITIC CALCAREOUS SAND

The basal contact of the Quartzose Glauconitic Calcareous Sand above the underlying Quartzose Foraminiferal Muddy Sand is observed in Core 324 (Appendix A1-39). The sharp contact, at 157 cm below the sea-floor, reflects changes in the composition of the sediment, where the pink to reddish yellow-stained Quartzose Foraminiferal Muddy Sand is overlain by the very pale brown to yellow-coloured muddy sandy gravel at the base of the Quartzose Glauconitic Calcareous Sand (Sample 324-6). The gravel lag at the base of the Quartzose Glauconitic Calcareous sand in Core 324 is dominated by very fine to medium pebble-size light-brown phosphorite and amber phosphatised bivalve (*Pecten*) and bryozoan fragments. The phosphatic gravel, predominantly mollusc casts, are composed of very fine quartz and minor glauconite grains, cemented by a light-brown carbonate-fluorapatite (CFA) matrix. An amber-coloured CFA surface-coating on the internal casts is commonly observed. In addition, cemented *in situ* sand and cemented lithoclasts of the Quartzose Foraminiferal Muddy Sand, fine pebbles of black-brown phosphatic granules (often angular) and cemented aggregates of coarse rounded quartz grains and dark-brown phosphorite are observed. Encrusting bryozoa are a common component of the gravel fraction. The gravel fraction of the Quartzose Glauconitic Calcareous Sands (Figure 6.9D) is also variable, with shell fragments and light-brown phosphatised internal casts dominant in Cores 324 and 90, whereas the gravel fraction of Core 159 (Appendix A1-38) is composed largely of phosphate-cemented *in situ* sand.

The sand fraction of the Quartzose Glauconitic Calcareous Sand consists of unconsolidated, typically very pale brown to yellow (10YR 7/4 to 7/6) stained grains, encompassing variable proportions of shell fragments, foraminifera, phospho-glauconitic grains and quartz (Figure 6.9). The WMR core logs describe the Quartzose Glauconitic Calcareous Sand as being dominated by shell fragments (30-40%), phospho-glauconite grains (10-30%), benthic and planktic foraminifera (5-40%) with a highly variable quartz content (10-40%). The quartz varies between subangular grains of very fine sand to well-rounded coarse grains, with a greater percentage of coarser grains with increasing quartz abundance. Although the calcareous component of the Quartzose Glauconitic Calcareous Sand is usually dominated by shell fragments, occasional fine to medium foraminifera-rich samples are also observed.

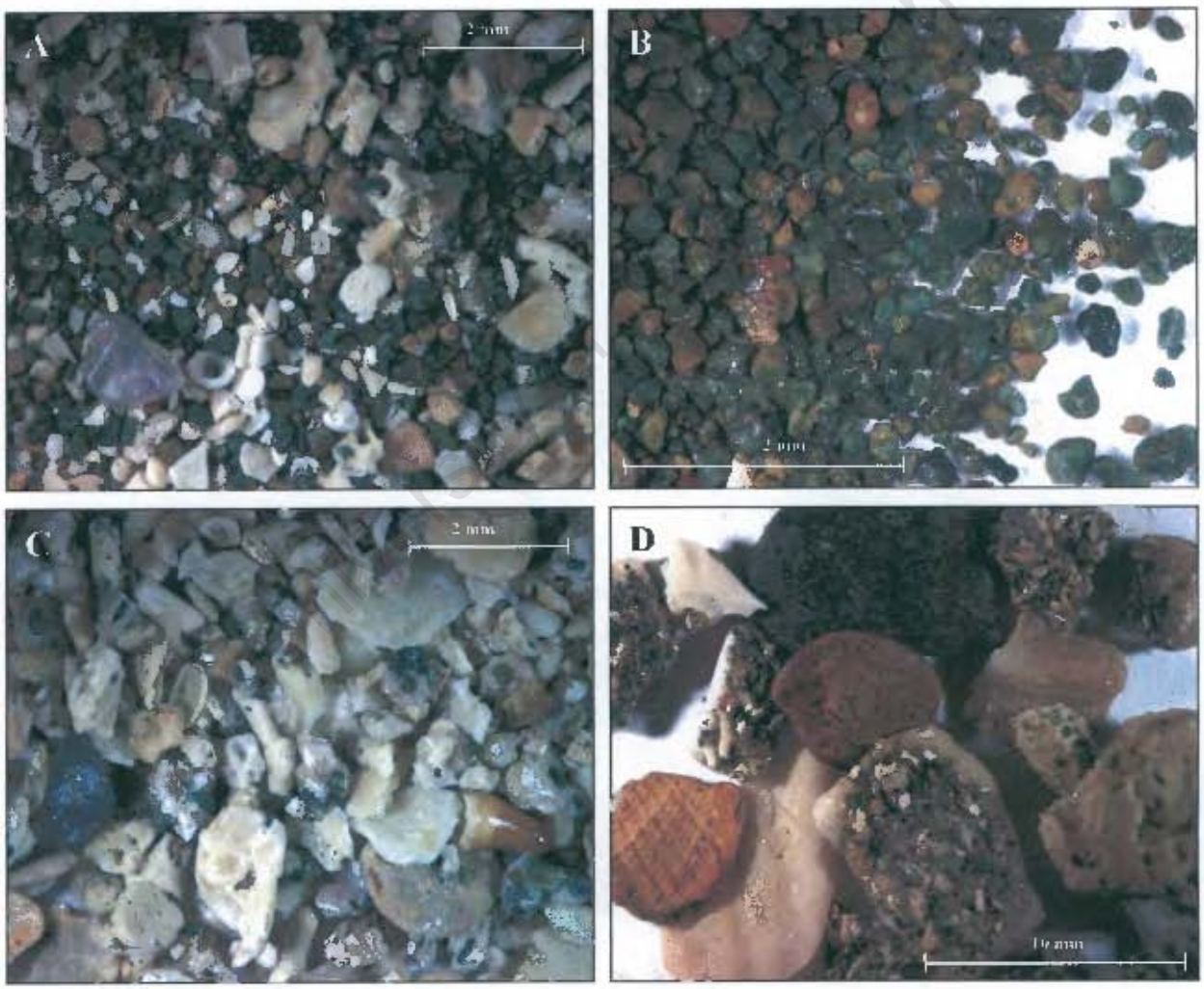


Figure 6.9. Photographs of the sand fraction (A) of the Quartzose Glauconitic Calcareous Sand of Sample 324-5 (77-82 cm) with coarse polished quartz grains and bryozoan fragments. The magnetic fraction (B) is dominated by earthy green-brown phospho-glauconite grains. The non-magnetic fraction (C) is composed of shell fragments, quartz and foraminifera. Rare phosphatised fish teeth are present. The gravel fraction (D) includes bivalve fragments, often phosphatised, light brown phosphorite casts, dark-brown phosphorite and cemented Quartzose Foraminiferal Muddy Sand aggregates (not shown).

Table 6.3. The relative percent grain types of the sand fraction of the Quartzose Glauconitic Calcareous Sand determined by point-counting a minimum of 300 grains. Foraminifera include only those species not replaced or infilled by phospho-glauconite.

Sample	Shell fragments	Bryozoa	Foraminifera (benthic+planktic)	Phospho-glauconite	Phosphorite	Quartz
159-5	36.7	0.8	5.2	33.9	0.0	23.4
324-4	33.5	0.0	2.0	51.6	0.0	12.6
324-5	29.6	0.9	4.0	48.7	0.9	15.9
324-6	26.0	2.3	5.5	32.9	0.5	32.9
90-504	15.4	0	22.7	42.7	3.1	16.1

The Quartzose Glauconitic Calcareous Sand shows considerable textural variation, both within and between cores (Figure 6.10), varying between a slightly gravelly sand to a muddy sandy gravel. The texture shows no consistent within-core trend in either Core 324 or Core 90. The phospho-glauconitic and foraminiferal components are predominantly fine sand–size (±200-250 µm), whereas the shell fragments and quartzose components vary from very coarse to very fine sand. The shell fragments, foraminifera and quartzose non-magnetic fraction, in particular, show considerable variations in abundance (Table 6.3 and Figure 6.11). In Core 159, the surfaces of all sand and gravel-size grains have tiny (20-50 µm) red precipitates that are composed predominantly of Fe and Ca (Figure 6.12).

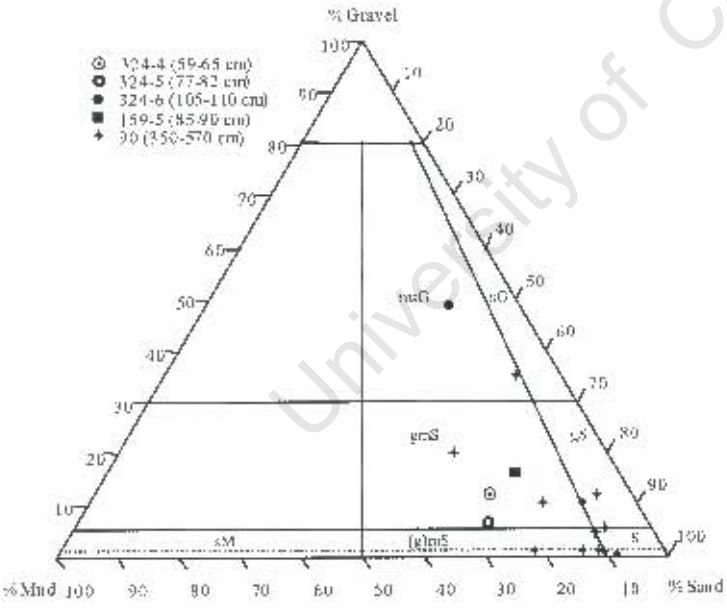


Figure 6.10. A summary of Quartzose Glauconitic Calcareous Sand grain size textures.

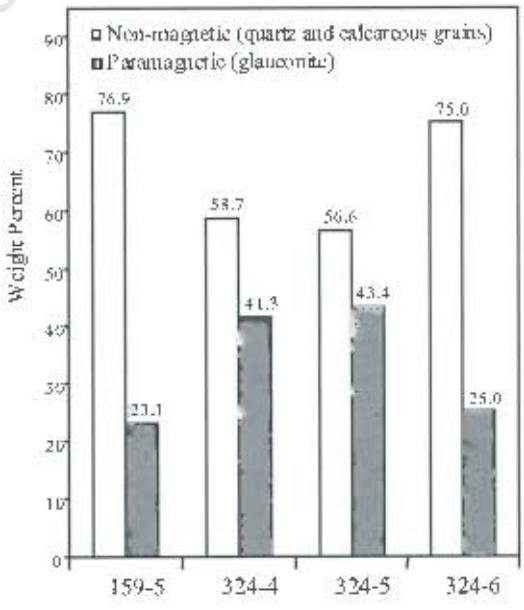


Figure 6.11. The weight percent non-magnetic and paramagnetic fractions for the Quartzose Glauconitic Calcareous Sand.

Traces of jasper were seen in the sample taken from 504 cm in Core 90 and the WMR core logs describe the presence of trace amounts of jasper in cores 337 and 214A. The quartz component includes both clear, angular to subrounded, very fine to fine sand-size grains and well-rounded, often frosted, predominantly medium (to very coarse) sand-size quartz grains. The coarse quartz population becomes dominant as the abundance of quartz increases. The abundance of quartz decreases from 32.9% at the

University of Cape Town

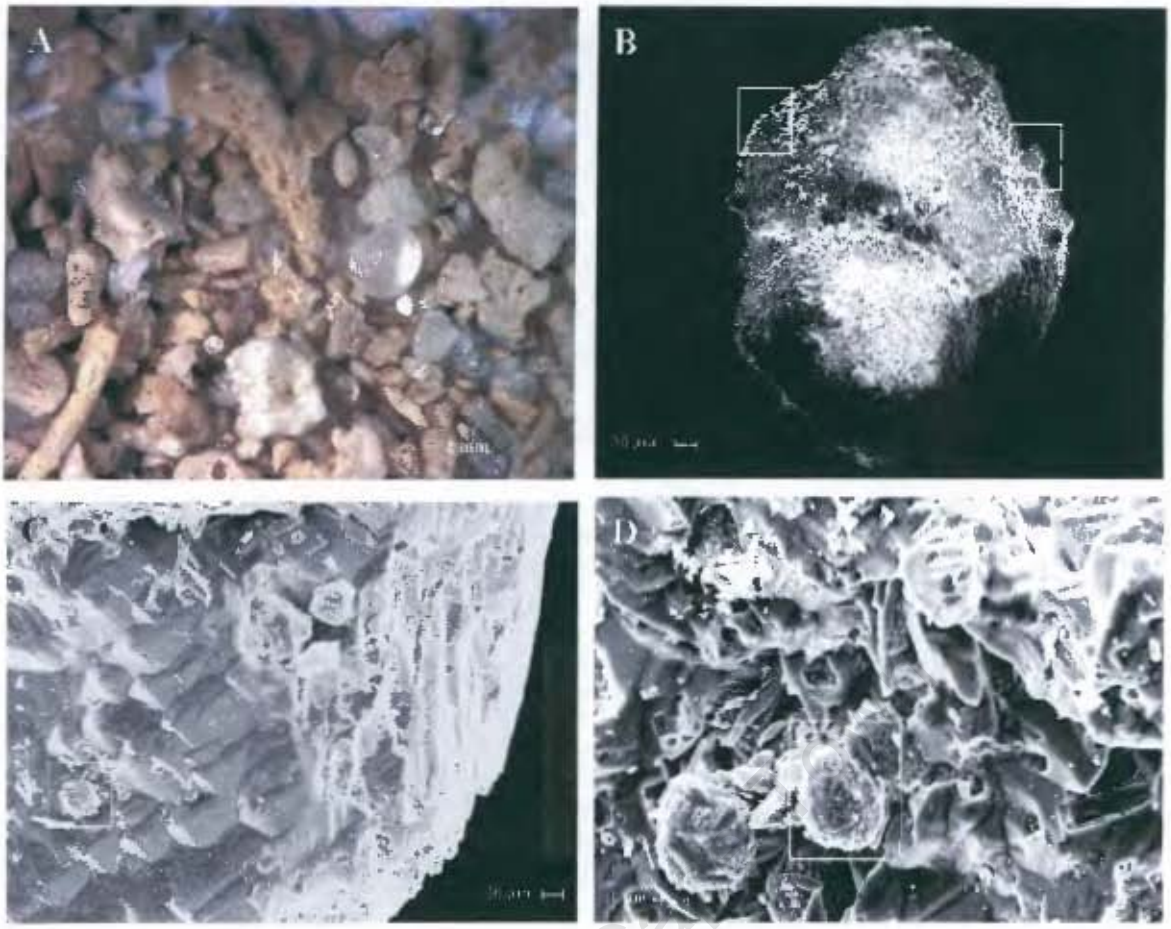


Figure 6.12. (A) A photograph of the sand fraction of the Quartzose Glauconitic Calcareous Sand Sample 159-5 (Appendix A1-38) with red surface precipitates visible on all of the sand grains. SEM images of the red precipitate (marked with white squares) on the surface of a foraminifera test (B) and quartz grains (C & D). The result of the EDS scans of the precipitates in the white squares show that they are composed predominantly of Fe (55.2-74.1%) and Ca (31.5-11.9%) with minor Si (3.4-5.5%) and Al (1.2-1.7%).

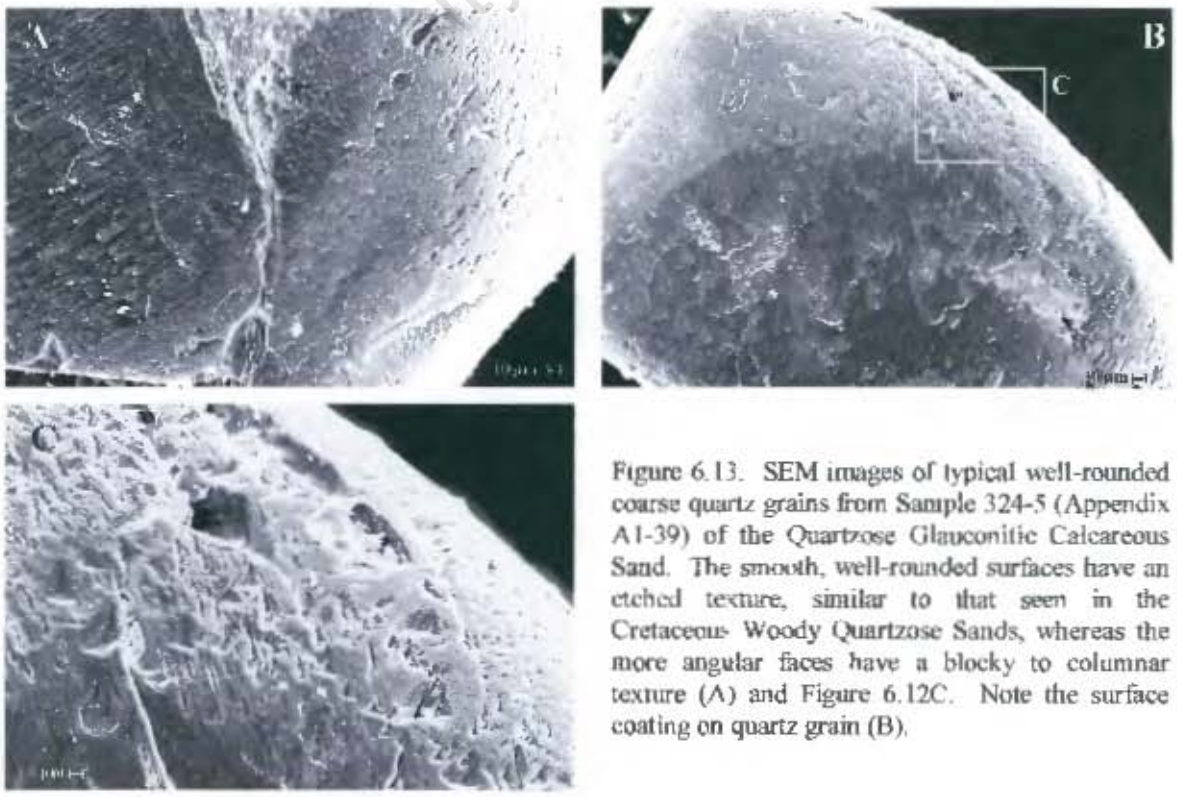


Figure 6.13. SEM images of typical well-rounded coarse quartz grains from Sample 324-5 (Appendix A1-39) of the Quartzose Glauconitic Calcareous Sand. The smooth, well-rounded surfaces have an etched texture, similar to that seen in the Cretaceous Woody Quartzose Sands, whereas the more angular faces have a blocky to columnar texture (A) and Figure 6.12C. Note the surface coating on quartz grain (B).

base of the Quartzose Glauconitic Calcareous Sand, with an up-core decrease from 16% at the base of Core 90 to 3-5% at the contact with the Glauconitic Calcareous Sand, showing an overall decrease in abundance of quartz with continued deposition of the Quartzose Glauconitic Calcareous Sand.

The rounded, coarse quartz grains often have a red-brown surface coating, particularly within irregularities on the grain surface (Figure 6.13). The composition of this coating is similar to that observed for the Quartzose Foraminiferal Muddy Sand (Figure 6.5) and EDS analyses show that it is dominated by Fe (43.0-72.7 wt%), with varying proportions of Si, Ca, K, Al, Ti, P, Mg and O (Figure 6.13B). The smooth, often milky to frosted, surfaces of the rounded quartz grains are often deeply etched with linked etch pits similar to those seen in the Quartzose Foraminiferal and Cretaceous Woody Quartzose Sands (Figure 4.11). However, a distinctive blocky or columnar surface texture (Figures 6.12 and 6.13) was also observed, particularly on less rounded, apparently fractured, surfaces.

The authigenic component of the Quartzose Glauconitic Calcareous Sand is dominated by an earthy green-brown phospho-glauconite (Figures 6.9B and 6.14). The phospho-glauconite grains are predominantly infilled and replaced foraminifera, where the test of the glauconite-infilled foraminifera is replaced by phosphorite. Although dark green glauconite is present, the sutures of the glauconite grains commonly include green-brown phospho-glauconite. Minor phosphorite is present in the sand fraction, typically as well-rounded, light-brown CFA-cemented aggregates of very fine quartz grains with minor glauconite, amber shell fragments and calcareous material. The authigenic grains are discussed in detail in Chapter 9.

The shell fragments vary from a very fine to a very coarse sand-size and are dominated by *Pecten* and bryozoan fragments. Some shell fragments are phosphatised and have a translucent amber colour, similar to onshore phosphorite of the Varswater Quarry and Bomgat that are also believed to have formed by replacement of carbonate precursors (Middleton, 2003). The zooecia of the bryozoa fragments are typically filled with dark-green phospho-glauconite (Figure 6.15). The foraminiferal assemblage includes a diversity of benthic and planktic species present in approximately equal proportions. In Core 90, the shell fragments show a decrease in abundance up-core coupled with an increase in foraminiferal abundance, such that the calcareous component of the Quartzose Glauconitic Calcareous Sand is predominantly foraminiferal below the contact with the overlying Glauconitic Calcareous Sand at ±340 cm. This up-core decrease in shell fragments is associated with the decrease in quartz abundance. The entire foraminiferal assemblage was picked from a sub-sample of Samples 159-5 and 324-5, and submitted to I. McMillan for identification (Table 6.4).

The composition of the mud fraction (<63 μm fraction) was not studied in any detail, but XRD analyses showed that it was dominated by quartz, calcite, glauconite and carbonate fluorapatite in two samples from Core 324.

University of Cape Town

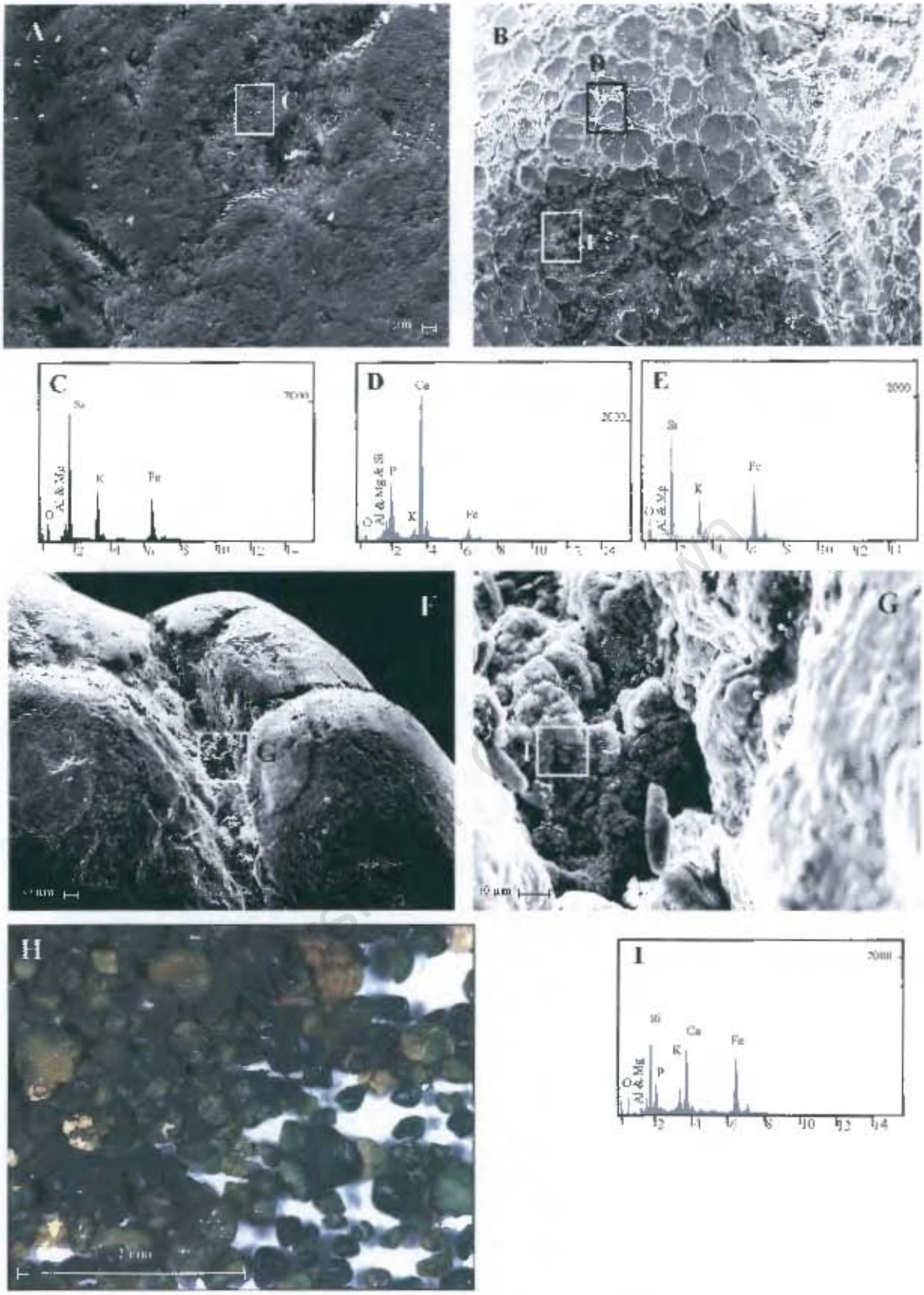


Figure 6.14. The magnetic fraction of Sample 159-5 (Quartzose Glauconitic Calcareous Sand) is dominated by earthy, green-brown, phospho-glauconite grains (H). An EDS scan of a dark green/black grain (A) shows a glauconite composition (C) with 13.27 wt% Fe, 8.5 wt% K, 28.18 wt% Si, 4.54 wt% Al, 3.31 wt% Mg and 42.19 wt% O.) A rounded, light green to brown mottled authigenic grain is shown in (B). The EDS scan of the grain surface (black block D) shows a phospho-glauconite composition (D) whereas, below the surface (white block E), glauconite is dominant. A dark green, rounded, glauconite grain with well-defined sutures is shown in (F). A close up (G) shows brown, immature glauconite rosette structures in the suture. The EDS scan (I) of suture material in white box (G) shows a phospho-glauconite composition with 16.0 wt% Fe, 10.5 wt% Ca, 3.7 wt% K, 6.9 wt% P, 15.0 wt% Si, 4.2 wt% Al, 2.6 wt% Mg and 40.0 wt% O.

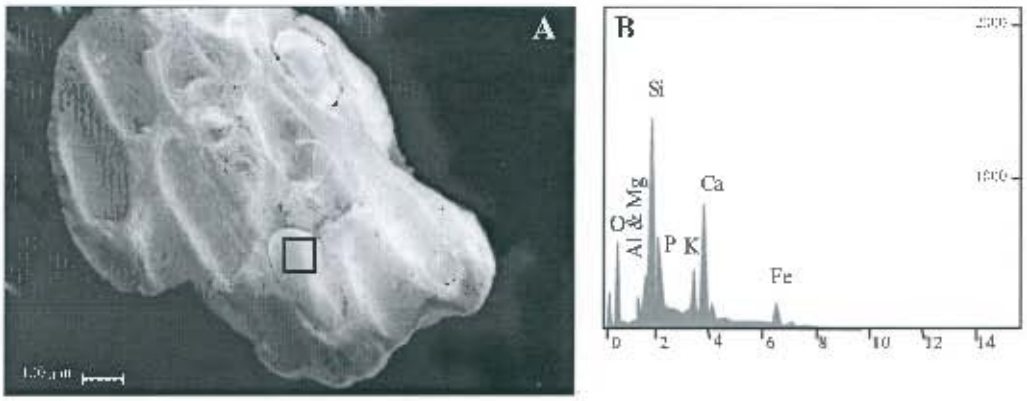


Figure 6.15. A dark green glauconite grain *in situ* in a zooecium of a bryozoan fragment of the Quartzose Glauconitic Calcareous Sand Sample 324-6. The EDS scan (B) of the grain inside the black box (B) shows a phospho-glauconite composition with 16.4 wt% Si, 10.9 wt% Ca, 8.5 wt% P, 4.6 wt% Fe, 4.0 wt% K, 3.9 wt% Al, 2.5 wt% Mg and 49.3 wt% O.

Table 6.4. The foraminiferal assemblage of the Quartzose Glauconitic Calcareous Sand

324-5	159-5
Finely ribbed *Uvigerina* sp.	*Victoriella conoidea*
Globocassidulina sp.	*Gaudryina* sp.
Cancris sp.	*Quinqueloculina* cf. *vulgaris* *
Lenticulina spp.	*Spiroplectinella* sp.
Cibicides spp.	Flat *Spiroplectinella* sp.
Guttulina sp.	*Cibicidoides* spp.
Small *Cibicidoides* sp.	*Globigerina* spp.
Hanzawaia sp.	Flat *Nonion* sp.
Eponides "miocenica"	Small rounded margin *Nonion* sp.
Lobatula sp.	*Lenticulina* sp.
Globigerina sp.	*Quinqueloculina* spp. *
Gyroidinoides soldanii	*Pyrgo* sp.
Sphaerogypsina globulus	*Globulina* sp.
Baggina sp.	*Eponides "miocenica"*
Globigerina cf. *ouachitaensis*	*Triloculina* cf. *tricarinata* *
	Siphonaperta sp.
	Sigmoilina sp. *
Aquitanian/Burdigalian ?inner shelf environment (approximately 50-60 m)	Aquitanian innermost shelf deposit with some hypersaline indicators (*)

University of Cape Town

6.2.2 AGE OF THE QUARTZOSE GLAUCONITIC CALCAREOUS SAND

Latest Oligocene to earliest Miocene (Aquitanian: 23.8-20.5 Ma) Sr-isotope ages of 23.3-24.4 Ma were obtained for duplicate picked bulk foraminiferal assemblages of samples collected from 90 cm (6 cm above the base of core) in Core 159 by the Council of Geoscience for WMR (Table 3.1). Sr-ages of 24.6-25.6 Ma (shell fragments) and 23.3-24.3 Ma (orange phosphorite) were obtained from the Quartzose Glauconitic Calcareous Sand at 524-528 cm in Core 90 (Compton *et al.*, 2004). The older ages of the shell fragments may suggest inclusion of reworked material into the facies. The foraminiferal assemblage from the Sample 159-5 (85-90 cm) includes a large number of the indicator species *Victoriella conoidea* (Figure 6.16), where *V. conoidea* is confined to the late Aquitanian in the marine rocks of southern Africa according to McMillan (1989). Further work is required to sort out the discrepancy between the latest Oligocene to earliest Aquitanian Sr-derived age of the bulk foraminiferal assemblage and the reported late Aquitanian distribution of *V. conoidea* in marine units of southern Africa (Section 6.1.2). A latest Oligocene to early Miocene (Aquitanian) age is assigned to the Quartzose Glauconitic Calcareous Sand using the foraminiferal assemblage and Sr-isotope ages.

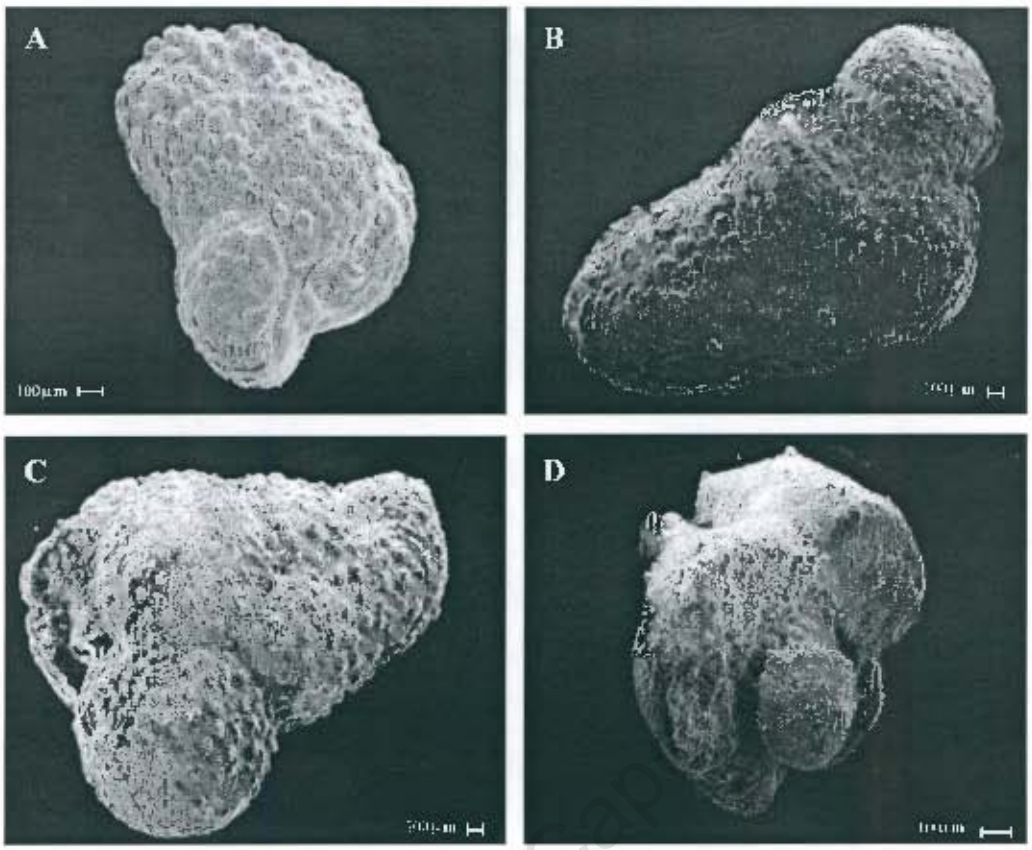


Figure 6.16. *Victoriella conoidea* (A-C) and *Rupertina stabilis* (D) from Sample 159-5. The foraminiferal indicator species, *V. conoidea* is confined to the late Aquitanian in marine sediments of southern Africa (McMillan, 1989).

University of Cape Town

6.2.3 DEPOSITIONAL ENVIRONMENT OF THE QUARTZOSE GLAUCONITIC CALCAREOUS SAND

Sediments of the Quartzose Glauconitic Calcareous Sand were recovered from a narrow range in water depth on the Western Ridge and the Southern Rocky Plateau of Concession 20D. However, the presence of this facies in Core 159, on the eastern flank of the Cape Canyon, implies a more widespread distribution prior to erosion of the Cape Canyon. The environment of deposition indicated by the foraminiferal assemblage from two select samples within this facies varies from innermost shelf in Core 159, in the east, to inner shelf in Core 324, on the Southern Rocky Plateau (Figure 6.8).

Erosion and winnowing of the Quartzose Foraminiferal Muddy Sand resulted in formation of the Quartzose Glauconitic Calcareous Sand basal gravel lag composed predominantly of reworked mollusc casts and phosphatised shell fragments from the underlying Quartzose Foraminiferal Muddy Sand. This gravel lag suggests a high-energy (wave or current eroded) abrasional shelf environment (Coffey and Read, 2004; McLaughlin *et al.*, 2004), which may correspond to a drop in relative sea level. The innermost to inner shelf foraminiferal assemblage of the Quartzose Glauconitic Calcareous Sand facies supports this interpreted drop in relative sea level. The erosional surface represents a sequence

boundary demarcating a new cycle of change in relative sea level with the final relatively deeper water environment interpreted for the Quartzose Foraminiferal Muddy Sand overlain by a shallower water basal gravel of the Quartzose Glauconitic Calcareous Sand facies (*eg.* Van Wagoner, 1988; McLaughlin *et al.*, 2004). This erosional surface or forced regressive surface is interpreted to indicate a fall in relative sea level, which is commonly interpreted to be responsible for the greatest amount of erosion within a depositional sequence (Brachert *et al.*, 2003).

The Quartzose Glauconitic Calcareous Sand facies, which lies above this forced regressive surface gravel lag is interpreted as a latest Oligocene/early Miocene (Aquitanian) sequence recording a rising relative sea level. The facies shows many characteristics of transgressive-system tracts, such as an overall upcore trend of increasing water depth indicated by decreasing terrigenous input and increasing pelagic deposition initiating the formation of a condensed section (Loutit *et al.*, 1988). A mixed carbonate-siliciclastic composition is commonly interpreted to represent high-energy pulses of fluvio-deltaic material onto carbonate platforms (Einsele, 1996, Duncan *et al.*, 2003) followed by reworking by marine processes, often resulting in lateral depositional heterogeneities. The medium to coarse quartz sand is interpreted to be eroded and reworked from underlying terrigenous Cretaceous sediments (Chapter 4) during a relative sea-level lowstand. A Cretaceous source of the quartz grains is supported by their similar surface microtextures. The trace amounts of jasper observed in these sediments could possibly be from a Cretaceous source, where jasper is commonly interpreted to imply the presence of a Karoo River draining the central interior (Dingle and Hendey, 1984). Alternatively erosion of the Dwyka Tillites on the adjacent coastal platform could be a possible secondary source for jasper (Moore and Moore, 2004). A rise in relative sea level and the maximum flooding surface is again associated with extensive phosphatisation and glauconite formation as described earlier for the Quartzose Foraminiferal Muddy Sand facies. The micro-environments provided by the interior chambers of increasingly abundant foraminiferal tests favours glauconite formation (Odin and Matter, 1981; Kelly and Webb, 1999), where the preservation of terrigenous mud in a low-energy outer shelf environment would be more likely during relatively high sea levels. The compositional and textural variability observed within this facies may indicate that the Quartzose Glauconitic Calcareous Sand facies does not represent a single relative sea-level cycle, but rather a complex signature of two or more relative sea-level cycles. In addition, the variation within this mixed siliciclastic-carbonate sediment may reflect changes in the depositional environment across the inner to middle shelf.

6.3 GLAUCONITIC CALCAREOUS SAND

The Glauconitic Calcareous Sand was recovered in thirty-one cores from water depths ranging between 247 and 299 m from the seaward flank of the Western Ridge and from the Southern Rocky Plateau (Figure 6.17). The Glauconitic Calcareous Sand with an average thickness of approximately 200 cm, has a maximum thickness of 446 cm in Core 315A. This facies was recovered from cores along both the Central (Cores 128 and 129) and Southern (Core 187) Transects (Figure 6.17). In addition, sediment data were available for Core 90 (Compton *et al.*, 2004).

University of Cape Town

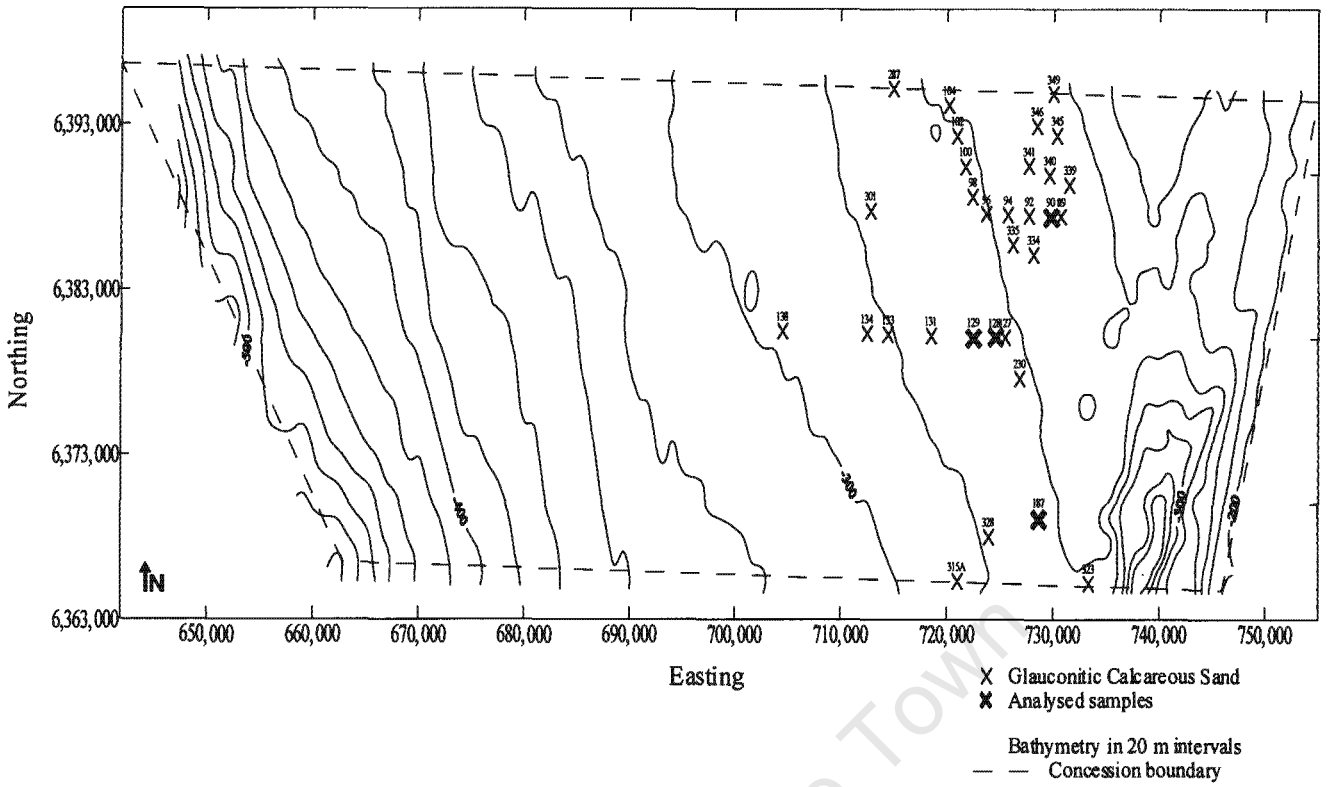


Figure 6.17. The distribution of the Glauconitic Calcareous Sand facies in Concession 20D. Cores sampled in this study shown in bold.

6.3.1 LITHOSTRATIGRAPHY OF THE GLAUCONITIC CALCAREOUS SAND

The basal contact between the Glauconitic Calcareous Sand and underlying Quartzose Glauconitic Calcareous Sand is poorly defined and is gradational in Cores 94 and 335, but is defined by a cemented interval with large bone fragments at 350 cm in Core 90 and a 15 cm thick lag dominated by carbonate clasts in Core 127.

The Glauconitic Calcareous Sand varies between a slightly gravelly muddy sand to a gravelly muddy sand (Figure 6.18). In comparison to the underlying Quartzose Glauconitic Calcareous Sand, this facies has a more uniform composition (Table 6.5, Figure 6.19 and 6.20), texture (Figure 6.18), sorting and grain size. The predominantly fine-grained sand (200-250 μm) is composed of white (10YR 8/1 to 8/2) foraminiferal tests and shell fragments, authigenic grains with minor amounts of quartz and ostracods (Figure 6.19).

Table 6.5. The relative percent grain types of the sand fraction of the Glauconitic Calcareous Sand as determined by point-counting a minimum of 300 grains.

Sample	Foraminifera* (benthic≈planktic)	Shell fragments	Authigenic Grains	Quartz
128-11	33.2	21.6	42.6	2.6
128-13	34.0	17.7	43.5	4.8
129-5	43.8	13.9	38.4	3.9
187-3	33.5	8.7	56.1	1.6

*foraminifera are not replaced or infilled by authigenic minerals and are very white

University of Cape Town

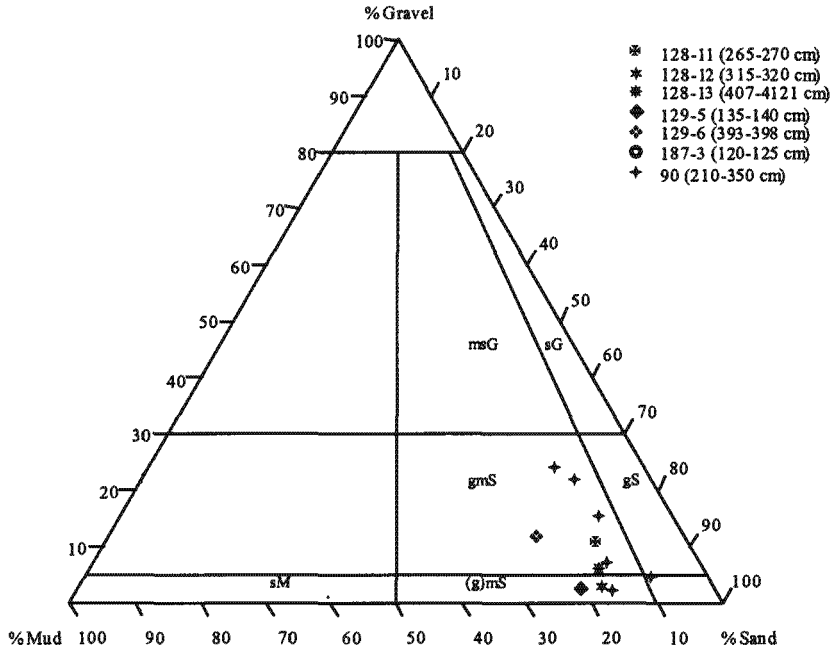


Figure 6.18. A summary of the Glauconitic Calcareous Sand grain size textures.

The foraminiferal assemblage includes a diversity of often well-preserved, benthic and planktic species and includes minor medium to coarse sand-size benthic foraminifera (including agglutinated species and *Dentalina* sp.). The fine sand-size calcareous fragments include foraminiferal, bivalve, echinoid and bryozoan fragments. Quartz grains are present in much lower concentrations than in the underlying Quartzose Glauconitic Calcareous sediment, and quartz grains are predominantly fine to very fine sand. Well-rounded coarse quartz grains are either absent or are only very rarely observed. The authigenic component, similar to that observed in the underlying Quartzose Glauconitic Calcareous Sand, is predominantly an earthy green-brown phospho-glauconite (Figure 6.19F). The phospho-glauconite grains are predominantly infilled and replaced foraminifera, where the test of the glauconite-infilled foraminifera has been replaced by CFA (discussed in detail in Chapter 9). The sutures of the glauconite grains also commonly include green-brown phospho-glauconite. Minor amber-coloured phosphatised foraminiferal tests, calcareous fragments and fish teeth are present in the sand fraction. The original WMR core logs describe a much higher foraminiferal abundance for this facies, but they noted that up to approximately 40% of the calcareous material may be replaced by phospho-glauconite.

The gravel-fraction includes medium pebble-sized *Pecten*, bryozoa (with glauconite-filled zooecia), phosphatised shell fragments, light-brown phosphatic gravel, often as molluscan internal casts, and occasional shark teeth. Fine to very fine pebble-size articulated brachiopods (Figure 6.19H), and cemented coarse quartz and dark-brown phosphatised aggregates are present. The gravel fraction of Sample 187-3 is dominated by coarse pebble-size cemented aggregates of *in situ* cemented sand. The gravel fraction of the Glauconitic Calcareous Sand is described in the WMR core logs as including phosphorite and limestone gravel, shell fragments (often partially phosphatised to brown-stained) dominated by *Pecten*, brachiopods, bryozoa, calcareous algae and at least two different types of oysters. The oyster assemblage includes a true *Neopycnodonte cochlear* species and a transitional species, which is neither a classic *Pycnodonte* (Cretaceous to Miocene), nor a classic *Neopycnodonte* (Miocene to Recent) species (J. Pether, *pers. comm., 2003)*. Cemented layers, up to 15 cm thick (Core 323) and concentrations of cemented pebbles are common (Core 328).

University of Cape Town

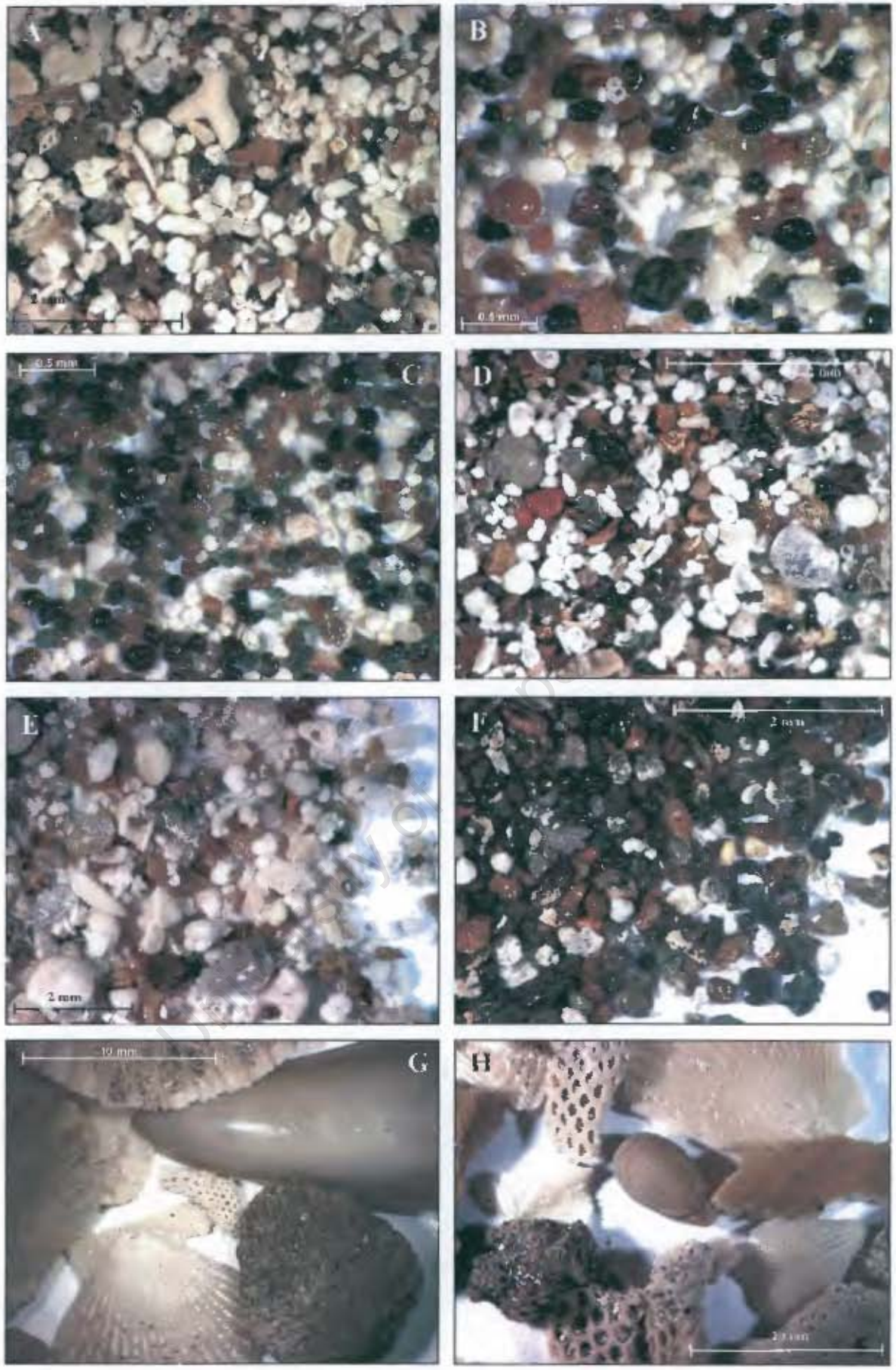


Figure 6.19. Photographs of the sand fraction (A-D) of the Glauconitic Calcareous Sand (Samples 187-3; 129-6, 128-11 and 128-13, respectively). The non-magnetic fraction (E) is dominated by foraminifera (often partially phosphatised). The magnetic fraction (F) is composed of earthy brown-green phospho-glauconite. The gravel fraction (G: Sample 128-11 and H: Sample 128-13) includes *Pecten* and bryozoan fragments, brachiopods, sharks teeth and PCG fine pebbles.

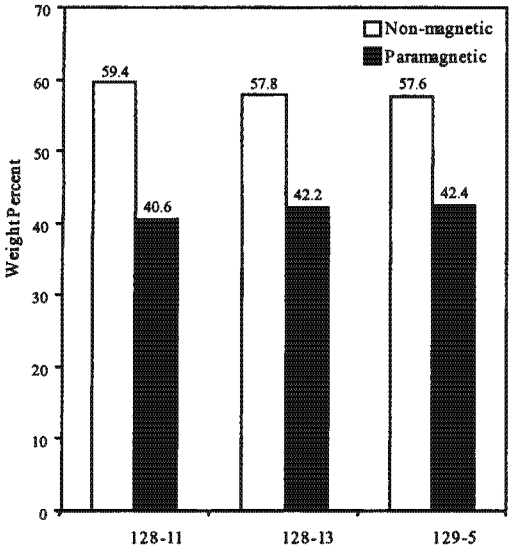


Figure 6.20. The weight percent non-magnetic (quartz and calcareous grains) and paramagnetic (glauconite) fractions for the Glauconitic Calcareous Sand facies. (Sample locations in Appendix A1-28 and -29)

6.3.2 AGE OF THE GLAUCONITIC CALCAREOUS SAND

The Glauconitic Calcareous Sand is interpreted to have been deposited in the late Aquitanian to Burdigalian, with Sr-isotope ages varying from 18.4-20.7 Ma. Sr-isotope ages of 19.8-20.7 Ma (Core 90: 225 cm) and 19.4-20.3 Ma (Core 230: 400 cm) for the Glauconitic Calcareous Sand were obtained for a picked bulk foraminiferal assemblage by the Council of Geoscience for WMR. Sr-isotope ages of 18.4-19.3 Ma (benthic foraminifera and shell (*Pecten*) fragments) were obtained from the Glauconitic Calcareous Sand of Core 349 (Compton *et al.*, 2004). In addition, Sr-isotope ages of 15.8-16.8 Ma (benthic foraminifera), 14.8-16.3 Ma (fish bones) and 18.0-18.6 Ma (orange/black phosphorite) were obtained from the basal gravel lag of the overlying Glauconitic Sand Unit in Core 90 at 200-202 cm. A similar early Miocene (Burdigalian) age of deposition is indicated by the foraminiferal assemblage of the Glauconitic Calcareous Sand in Core 128, which includes neither the older Aquitanian *Victoriella conoidea* nor the younger Langhian *Orbulina universa* species (McMillan, 1989; Table 6.6). A similar Burdigalian deep-water foraminiferal assemblage was described for the sample taken at 220 cm in Core 90 (Compton *et al.*, 2004). The slightly younger Sr-ages obtained from Core 349 may reflect some downward bioturbation of younger foraminifera into the Glauconitic Calcareous Sand as only the upper ~40 cm of this facies was recovered from below a 12 cm thick phosphorite gravel lag at the base of the Pliocene Glauconite Sand Unit. The upper Oligocene/Lower Miocene Calcareous Unit is commonly bioturbated where it occurs below the basal phosphorite gravel of the Glauconitic Sand Unit (Chapter 7).

6.3.3 DEPOSITIONAL ENVIRONMENT OF THE GLAUCONITIC CALCAREOUS SAND

The Burdigalian Glauconitic Calcareous Sand facies was recovered from a relatively narrow range of water depths (247-299 m), in slightly deeper water than the Quartzose Glauconitic Calcareous Sand (247-276 m). However, in contrast to the innermost to inner-shelf environment recorded in the underlying Quartzose Glauconitic Calcareous Sand, the Glauconitic Calcareous Sand foraminiferal assemblage from Core 90 suggests a deeper-water, outer shelf to upper slope depositional environment for this facies (Compton *et al.*, 2004). These deeper water depths imply a significant relative rise in sea level, following the deposition of the underlying Quartzose Glauconitic Calcareous Sand facies. The

University of Cape Town

winnowed nature of this facies signifies that episodic bottom-current activity was active over this part of the western margin during the Burdigalian.

Although the contact between the Glauconitic Calcareous Sand and the underlying Quartzose Glauconitic Calcareous Sand facies is poorly represented within the sample set, the basal gravel lag in Core 127 and a cemented interval in Core 90 may represent erosional unconformity surfaces and the basal sequence boundary of the Glauconitic Calcareous Sand. The transitional contact described in the WMR records for Cores 94 and 335 may record this inferred depositional hiatus.

The presence of primary phospho-glauconite grains replacing the foraminiferal assemblage provides additional support for low sedimentation rates indicative of rising relative sea levels, as suggested by the foraminiferal assemblage, during the Burdigalian (Loutit *et al.*, 1988; Amorosi, 1995; Kelly and Webb, 1999; Harris and Whiting, 2000). Siliciclastic material is present only in minor amounts (<5%) in the Glauconitic Calcareous Sand, indicating minimal reworking of the underlying quartz-rich sediments as well as minor fluvial input. The gravel fraction of these authigenic-carbonate-rich sediments is dominated by phosphatised mollusc casts and shell fragments, including *Pecten*, bryozoa and brachiopods. Further research into this macrofaunal assemblage may provide additional palaeo-environmental constraints.

University of Cape Town

6.4 FORAMINIFERAL OOZE

Up to 630 cm of the Foraminiferal Ooze facies were recovered on the outer shelf at water depths between 286-365m (Figure 6.21). The lower contact of the Foraminiferal Ooze was not intersected in any of the cores recovered from Concession 20D and the relationship with the Glauconitic Calcareous Sand is therefore not apparent. The Foraminiferal Ooze is composed almost entirely (95-99%) of biogenic calcareous material. The light grey to white (7.5YR 7/0-8/0) Foraminiferal Ooze is very uniform in appearance, but varies between a muddy sand and a sandy mud (Figure 6.22). The sand fraction is dominated by planktic foraminifera with minor glauconite grains (<5%). Quartz is either absent or present in only trace amounts. Scattered *Pecten* shells, thin-shelled oysters (Core 144) and medium pebble-size *in situ* cemented aggregates are scattered within the sediment. Bryozoa (and calcareous algae) are a dominant component of the sand fraction in Cores 137, 304 and 140, with bryozoa-rich intervals recognized in Core 139 and at the base (532-635 cm) of Core 140. In addition, bryozoan and calcareous algal fragments are present in minor amounts in most of the recovered Foraminiferal Ooze, with bryozoan concentration decreasing seawards in the cores across the outer shelf, bryozoa being absent from Core 145, the most seaward core (Figure 6.21)

The foraminiferal assemblage is assigned a Burdigalian age (Table 6.6) as argued for the Glauconitic Calcareous Sand (Compton *et al.*, 2004). This age is in agreement with Sr-isotope ages of 19.9-20.8 Ma (benthic foraminifera) and 18.9-19.7 Ma (shell fragments) (Compton *et al.*, 2004).

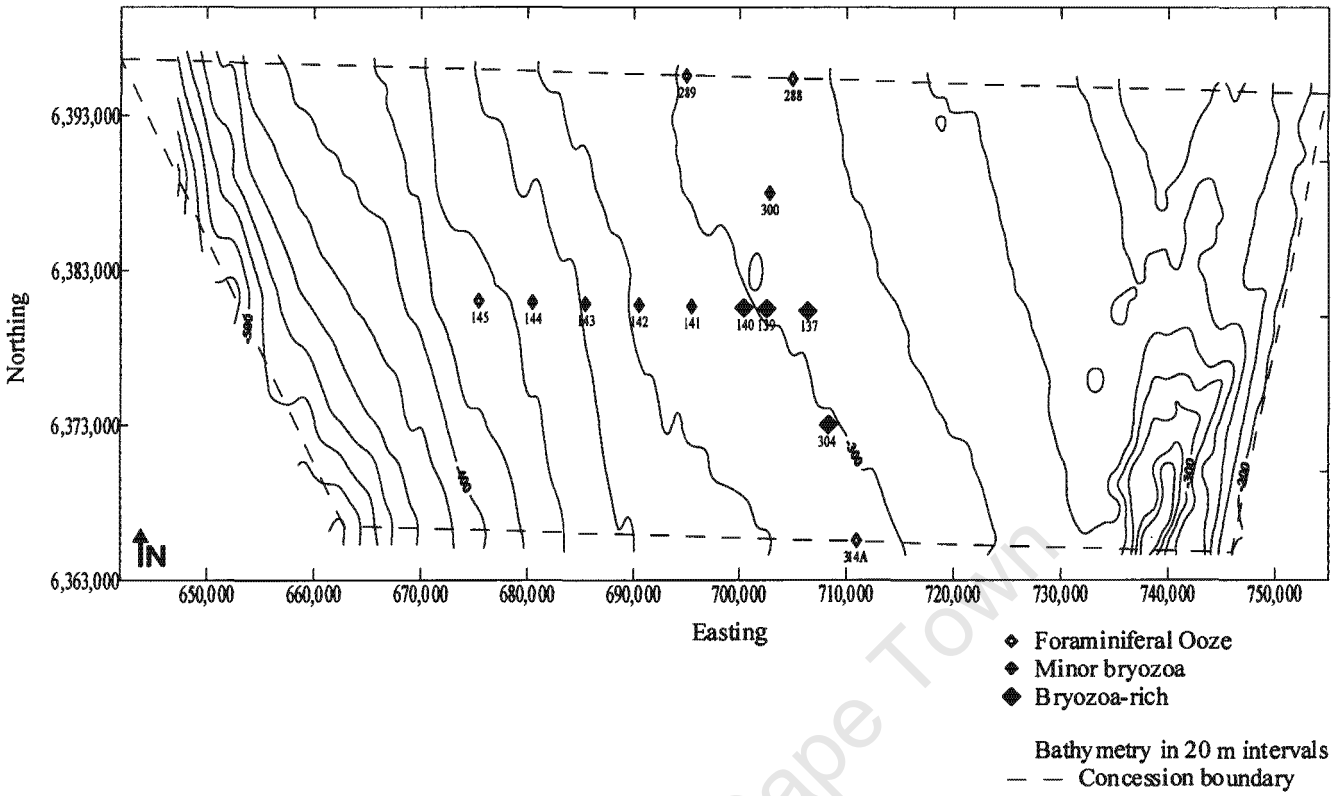


Figure 6.21. The distribution of the Foraminiferal Ooze facies in Concession 20D, where the symbol size increases with increasing bryozoan abundance.

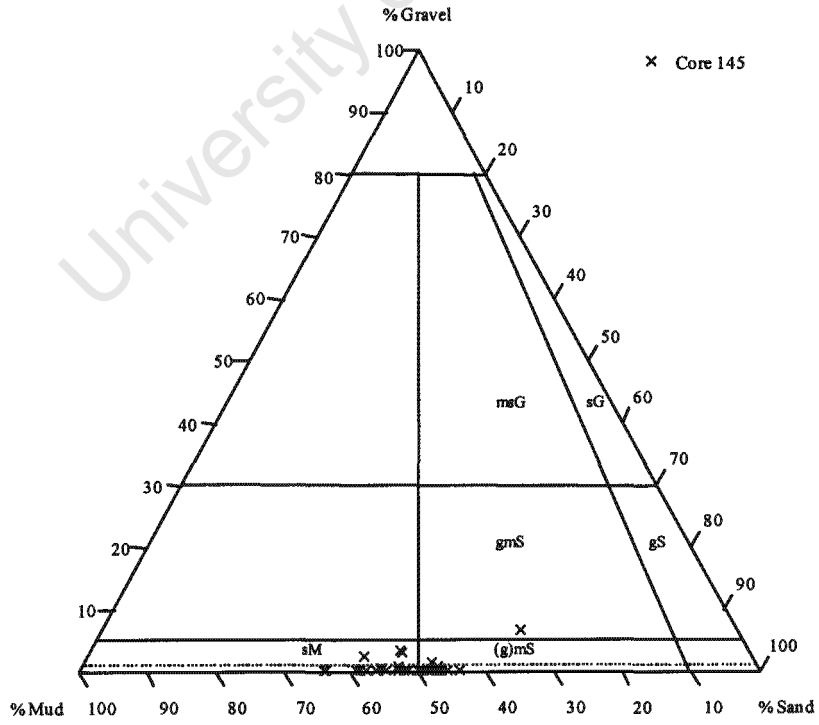


Figure 6.22. A summary of Foraminiferal Ooze grain size textures.

University of Cape Town

The deep-marine foraminiferal assemblage of the Foraminiferal Ooze, dominated by planktic species, indicates deposition in an outer shelf to upper slope environment (Compton *et al.*, 2004). The abundance of bryozoan fragments in some of the cores, particularly those collected from the shallower water depths, suggests that bryozoan "forests" covered portions of the outer shelf sea-floor during the Burdigalian. Bryozoa are filter feeders, implying low terrigenous sediment input onto the outer shelf region, supported by the absence of a terrigenous component in this facies. Bryomols (bryozoan molluscan oozes) are common on parts of the modern high-energy open shelves of New Zealand and Australia (Hayton *et al.*, 1995). A similar high-energy shelf is likely for the Foraminiferal Ooze.

The Sr-derived ages of the Foraminiferal Ooze are similar to those of the Glauconitic Calcareous Sand facies (18.4-20.7 Ma) that was recovered from shallower water depths on the outer shelf. Similarly, the foraminiferal assemblages of both sediments are interpreted to have been deposited in an outer shelf environment. The overlapping ages and similar depositional environments suggest that the Foraminiferal Ooze, recovered on the outer shelf only, may be a deeper water stratigraphic equivalent of the Glauconitic Calcareous Sand. More detailed analyses of the foraminiferal assemblages from the two facies would help clarify this relationship. However, the Foraminiferal Ooze is a uniform muddy sand dominated by planktic foraminifera, with only minor amounts of glauconite present. The absence of any sediment compositions gradational between the Glauconitic Calcareous Sand and the Foraminiferal Ooze may counter the argument that the two facies are syndepositional. Glauconitic Calcareous Sand was recovered in Core 138, yet the Foraminiferal Ooze facies was recovered from the adjacent cores 137 and 139 located only 2 km to either side of Core 138. This would represent a dramatic facies change over a short distance, which is unlikely considering the uniformity of the two facies. The Foraminiferal Ooze is therefore interpreted to be slightly younger than the Glauconitic Calcareous Sand (Figure 6.1).

6.5 MIOCENE SEDIMENTS OF THE SOUTHERN AFRICAN MARGIN

Unfortunately very little sedimentological data are available for the Miocene carbonate successions of southern Africa, hindering correlation with facies defined in the present study. However, in addition to the early studies by Siesser (1971, 1972), Rogers (1977) and Dingle *et al.* (1983), a limited amount of information has been made available more recently by marine mining companies, who have largely focused on the siliciclastic sediment successions, with their interest in the inner to middle shelf dictated by diamond distribution (McMillan, 1990; Corbett, 1996; Dale and McMillan, 2003b).

The unconsolidated surface sediments of the middle to outer shelf of the west and south coast of southern Africa are predominantly a foraminiferal muddy sand to sandy mud (Figures 2.7 and 2.9; Rogers and Bremner, 1991). The shelf and upper slope of the western (Figure 2.8 and 2.9) and south continental margins of southern Africa are underlain by flat-lying to gently seaward dipping lower Miocene (T_3) sediments (Dingle, 1971a, 1973c; Dingle *et al.*, 1983) with a maximum thickness of ~180-200 m preserved on the outer shelf (McMillan, 1990; Dale and McMillan, 2003b). The unconsolidated outer-shelf Miocene sediments of the western margin are composed of white to creamy nannofossil and

University of Cape Town

foraminiferal ooze, locally consisting almost exclusively of foraminiferal tests (McMillan, 1990). Bryozoa, *Pectens* and calcareous algae are also locally abundant. Glauconite pellets and quartz grains are usually absent, but inshore, and in the south, can be locally abundant (McMillan, 1990; Corbett, 1996; Dale and McMillan, 2003b; I. McMillan, *pers. comm.*, 2003). Cementing is generally poor, and these deposits can be considered to be a stiff clay or compacted biogenic ooze (I. McMillan, *pers. comm.*, 2003). Rogers (1977) dredged a variety of limestones from the Orange Shelf, suggesting partial lithification, at least locally, within the Miocene unit and a 10-20 cm thick surface carbonate or phosphate-cemented hardground crust is commonly observed on the sea-floor (Compton *et al.*, 2002; McMillan, 1989; I. McMillan, *pers. comm.*, 2003; Rogers, 1977). Three distinct sedimentary units are recognised in lower to middle Miocene successions of the western margin, namely the Aquitanian, the Burdigalian and the Langhian, where the units are separated by erosional surfaces (McMillan, 1989, 1990; Dingle *et al.*, 2001).

Siesser (1971, 1972) identified the Planktic Foraminiferal Lime Packstone as the most widespread Miocene lithofacies of the Agulhas Bank (southern continental margin), where it is recovered from water depths ranging between 85 and 800 m with the majority recovered from between 110 and 400 m. This lithofacies is composed of variable proportions of sand-size bryozoa and/or planktic foraminifera in a micrite matrix (Siesser, 1971). Trace amounts of non-carbonate components present include quartz and phospho-glauconite infilled foraminifera. The microspar matrix formed by *in situ* dissolution and re-precipitation of lime mud winnowed from the inner shelf, with this matrix occasionally replaced by CFA. The Planktic Foraminiferal Lime Packstone sediments are interpreted to have been deposited in an open-ocean outer shelf to upper slope environment during the early to late middle Miocene from the microfaunal content of seven samples (Siesser, 1971). The foraminiferal ooze of the south coast is largely cemented, whereas only a thin surface hardground capping the Miocene succession is common on the western margin. The cemented character of the Agulhas Bank limestones may reflect a bias in dredging, because most early work was undertaken using dredges on a fairly coarse grid, where the sediments below the surface hardground may not have been sampled.

Although the lower Miocene sediments of the southern and western margin have been interpreted to have been deposited in environments varying from littoral to outer shelf/upper slope (Table 6.6), all of these sediments are described as being predominantly a biogenic (foraminiferal) ooze (McMillan, 1990; Corbett, 1996; Dale and McMillan, 2003b; I. McMillan, *pers. comm.*, 2003). However, Rogers (1977) describes micrite-cemented foraminiferal limestones, dominated by phospho-glauconite infilling of the foraminifera, on the western margin of southern Africa. In contrast, although a similar range in depostional environments is interpreted for the sediments of the Upper Oligocene/Lower Miocene Calcareous Unit of Concession 20D, a much more variable sediment composition is recorded.

University of Cape Town

Table 6.6. The stratigraphy of lower Miocene sediments found on the outer shelf and upper slope (seawards of 120 m) of the western margin of southern Africa (after Dale and McMillan, 2003b; McMillan, 1989, 1990; Corbett, 1996).

Age	Foraminiferal indicator species of the lower Miocene stratigraphy	Lithology
(Serravalian to) Langhian (14.8-16.4 Ma)	*Orbulina universa*	• Distal inner shelf mud and chalk with abundant planktic foraminifera. Very rare outcrops on Orange Banks and Childs Bank.
Burdigalian (16.4-20.5 Ma)	*Miogypsina* sp. and *Globigerinoides* spp.	• Off the Orange River: Inner shelf-offshore bar sand and silt (Dingle *et al.*, 2001). • Varies from littoral to inner shelf foraminiferal assemblage (Corbett, 1996) • Clastic shoreline facies through biogenic "lagoonal" and offshore bar facies to outer shelf-upper slope biogenic clay (Dale and McMillan, 2003b). • Kudu 9A-boreholes: Cream to off white foraminiferal-rich limey clay with bryozoans and other shell fragments deposited in middle to outer shelf (McMillan, 1989, 1990).
Aquitanian (20.5-23.8 Ma)	*Victoriella conoidea* & *Globigerinoides* spp.	• Inner-middle shelf mud and chalk • Varies from littoral, through middle to inner shelf to outer shelf foraminiferal/carbonate assemblages (Corbett, 1996, Dale and McMillan, 2003b).

University of Cape Town

Siesser (1971) described the Infralittoral Skeletal Lime Packstone of the Agulhas Bank, typically found in water depths less than 130 m, which is composed of micrite-cemented skeletal fragments with 5% quartz, occasionally red-stained, 3% medium sand-size glauconite and minor phosphorite granules. The phosphorite granules are typically composed of either CFA-cemented silt to very-fine sand size quartz grains or planktic foraminifera (and glauconite). The Infralittoral Skeletal Lime Packstone is the only lithofacies of the Agulhas Bank that includes phosphorite pebbles (Siesser, 1971). The lithofacies is interpreted to have been deposited during a marine transgression with highstand lime mud settling onto reworked inner shelf sediments (Siesser, 1971). The age of this lithofacies is poorly constrained, but Siesser (1971) suggested a late Pleistocene age. However, comparison with new data from Concession 20D suggests that it may be worth re-examining this unit to ascertain whether at least some of the samples assigned to this lithofacies may not in fact be considerably older (late Oligocene) and lateral equivalents to the Quartzose Glauconitic Calcareous Sand of Concession 20D.

Incision by the Cape Canyon appears to have exposed older condensed calcareous sediments seldom seen elsewhere along the western margin. Reference to more diverse carbonates present on the western margin (Table 6.6; Siesser, 1971, 1972; Rogers, 1977; McMillan 2003b) suggests that the Oligocene-Miocene condensed succession, preserved in the Cape Canyon, may be representative of the carbonate platforms of both the southern and western margins of southern Africa, where the thick prograding Burdigalian Foraminiferal Ooze has been best preserved on the outer shelf and upper slope of the southern African margin. The condensed sediment record of Concession 20D is therefore important, because it allows the evolution of the southern African margin during the late Oligocene to early Miocene to be described in detail for the first time.

6.6 GRAVELLY CALCAREOUS QUARTZOSE MUDDY SAND (CORE 319)

The western margin of Concession 20D and southern Africa in general, is dominated by the widespread occurrence of lower Miocene sediments, with no upper middle to upper Miocene sediments recovered from the western (and southern) margin of southern Africa (Dale and McMillan, 2003b). A single core from Concession 20D, Core 319, in which an *in situ* lower to upper Miocene unit was recovered, is described by Compton *et al.* (2004). Core 319 was collected from the seaward (eastern) flank of the Canyon at a water depth of 274 m (Figure 6.23). The Miocene sediments are found stratigraphically above the Cretaceous Woody Quartzose Sand in Core 319, where a 40 cm basal gravel lag occurs on this major erosional unconformity (Figure 6.24). The basal gravel lag is overlain by approximately 500 cm of calcareous muddy sand (Compton *et al.*, 2004). This unit contains abundant light grey (5Y 7/2) mud, which dominates the appearance of the sediment.

The basal gravel lag varies between a gravel and a muddy gravel up-core (Figure 6.24). The gravel component of the two samples collected from within the basal lag are very different. The lower sample includes a number of phosphorite/ferricrete very coarse pebbles together with minor fine to very fine pebbles. The coarse pebbles are dominated by brown phosphorite composed of coarse to very coarse, often brown-stained quartz (and agates) and varying amounts of glauconitic medium sand, together with mollusc casts and phosphatised shell fragments. The pebbles commonly have a thin, polished surface coating. Occasional clasts show bedding with an iron-rich phosphorite erosional surface above the phosphatised coarse quartz overlain by a phosphate-cemented quartz-glauconite-foraminiferal medium sand. The fine to very fine gravel fraction includes angular to subrounded brown-stained quartz, rounded mollusc casts, SPG (teeth), Fe-rich carbonate clasts and minor amounts of rounded black phosphorite pebbles. The mollusc casts are typically CFA-cemented very fine quartz sand with trace amounts of glauconite. These layered phosphorite clasts are similar in composition and appearance to some of the phosphorite pebbles described for the Pliocene Glauconitic Sand Unit (Chapter 7). The benthic foraminifera yield a Sr-isotopic age of 17.0-17.7 Ma (Compton *et al.*, 2004). A black phosphorite from the same samples has a Sr-isotopic age of 21.7-23.1 Ma. In contrast, the gravel collected from the upper sample of the basal lag (558-567 cm), is composed entirely of very coarse to very fine Fe-rich carbonate pebbles that have an iron-phosphate-rich polished outer surface. The clasts react vigorously with dilute HCl leaving a residue of very fine sand to silty quartz, glauconite and Fe-rich colloidal aggregates.

University of Cape Town

Table 6.7. The composition of the basal gravel (568-572 cm) and overlying sands (520-524 cm) of the Gravelly Calcareous Quartzose Muddy Sand determined by point-counting a minimum of 300 grains.

Sampling interval	Quartz mS	Quartz vcS	Glauconite	Fe-rich carbonate	Foraminifera	vfS calcareous fragments	Phosphorite
520-524 cm	30.5	1.3	21.3	0.3	19.7	26.2	0.7
568-572 cm	48.6	1.1	34.4	9.4		5.1	1.4

The sand fraction of the gravel lag is composed of medium to coarse quartz, green glauconite and carbonate fragments together with Fe-rich carbonate and ferricrete/phosphorite (Table 6.7) aggregates. Rare phosphatised shell fragments and teeth are present. The sand has a bimodal grain-size distribution (Figure 6.24), where the coarse sand component is dominated by coarse (to very coarse) quartz grains. The coarse quartz varies between angular to rounded grains, commonly brown-stained or frosted, with glauconite present as a surface coating within hollows on irregular grain surfaces. The medium sand is dominated by subangular to subrounded quartz and green glauconite, which often has an oxidised appearance (Birch, 1971) with sutures infilled with the Fe-rich carbonate material abundant in the sand and gravel fractions. Calcareous fragments are a minor component (3.5% by weight of non-magnetic fraction) and are predominantly fragments of thick-shelled, white benthic foraminifera.

The Gravelly Calcareous Quartzose Muddy Sand facies lies between a basal gravel lag and a Pleistocene reworked lag in the upper ~90 cm of the core and shows considerable textural variation, with up to 58.6% gravel. The gravel fraction of the lower part of the facies (441-384 cm) is dominated by very fine to medium pebbles of quartz (subangular to rounded and brown-stained), phosphatised mollusc casts (bivalves, gastropods and scaphopods), ferricrete/Fe-rich phosphorite fragments, SPG (teeth) and minor black phosphorite. In contrast, abundant irregular-shaped phosphorite (micrite) nodules of cemented *in situ* sand, up to very coarse pebbles in size, are present in the interval between 180-360 cm, with the first evidence of *in situ* cementation seen at 384 cm. The phosphorite nodules typically include the very fine to medium gravel components present in the lower part of the facies. The upper part of the unit is reworked and coarsens up-core into a reworked Pleistocene phosphorite lag (where the quartz commonly has a characteristic green-stained appearance).

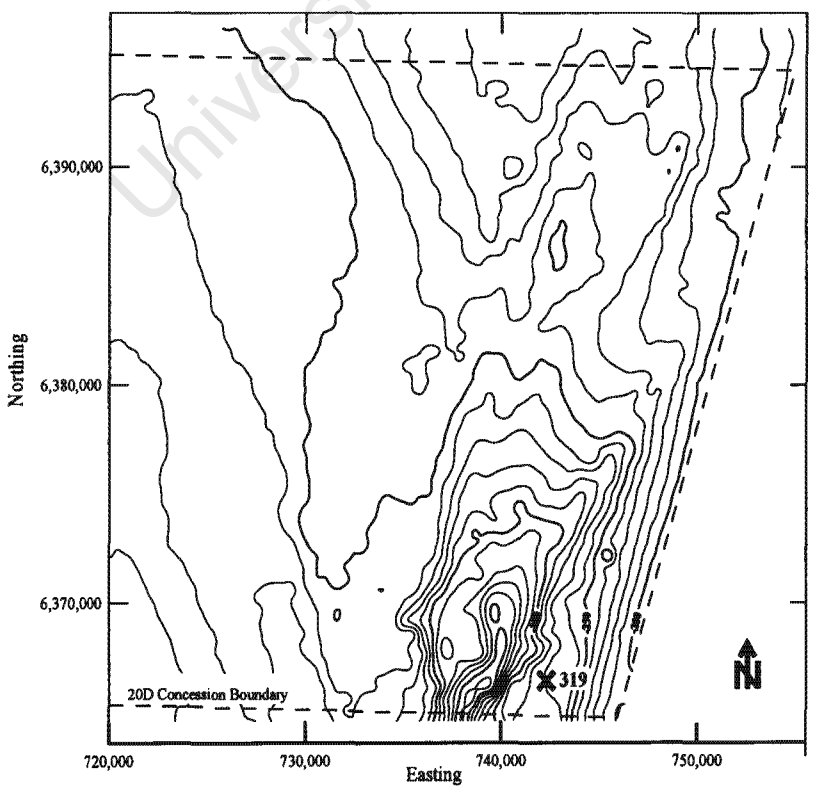


Figure 6.23. Distribution of the Gravelly Calcareous Quartzose Muddy Sand.

University of Cape Town

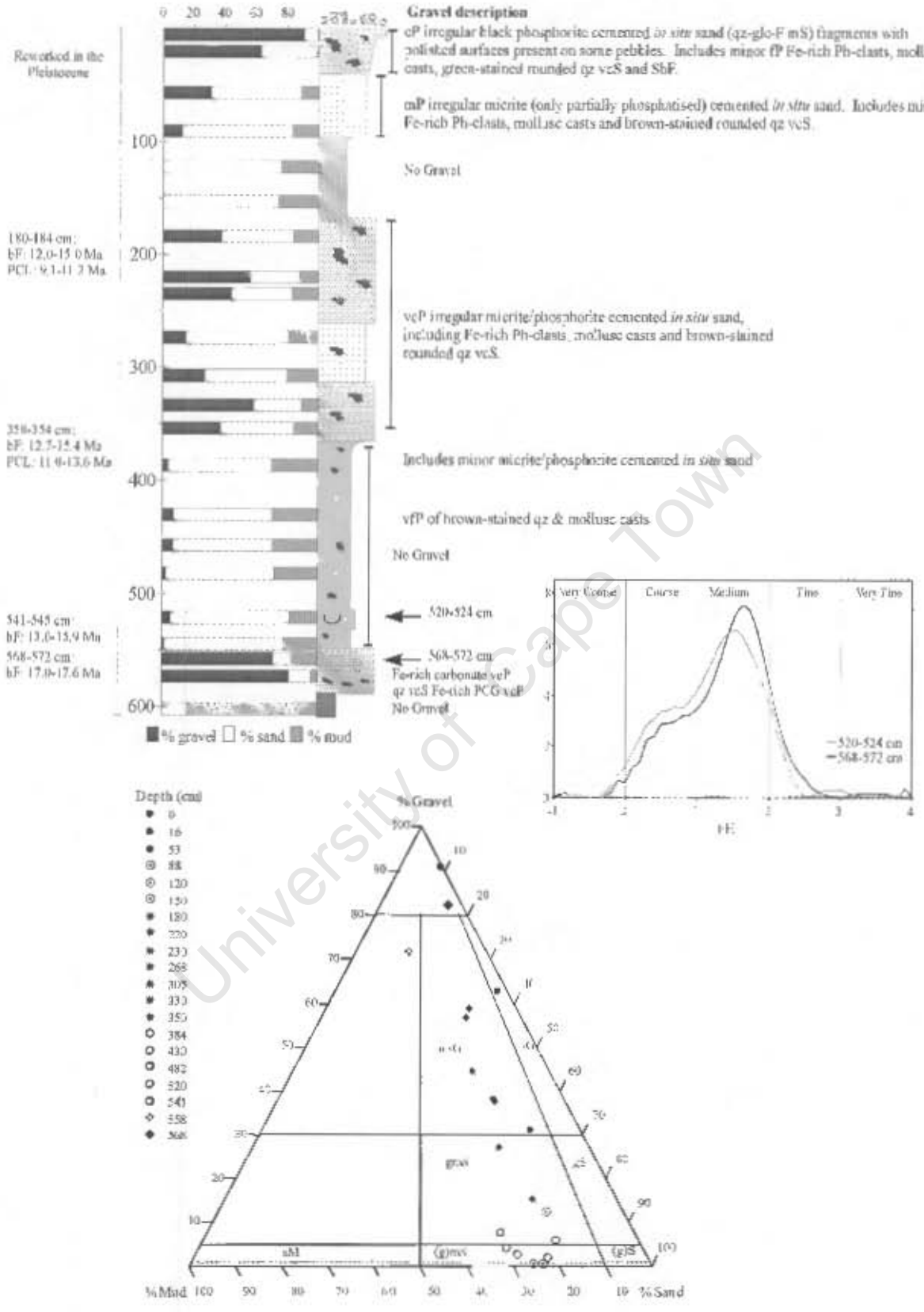


Figure 6.24. A summary of the Gravelly Calcareous Quartzose Muddy Sand stratigraphy in Core 319 (modified after Compton *et al.*, 2004) including the frequency curves showing the particle-size distribution of the sand fraction and grain size textures of Gravelly Calcareous Quartzose Muddy Sand.

University of Cape Town

The sand fraction of the Gravelly Calcareous Quartzose Muddy Sand facies is very similar to that of the gravel lag (Figure 6.24) and has a similar bimodal grain size distribution, where the two grain size populations are compositionally similar to those described above, although the Fe-rich carbonate and ferricrete grains are absent. The coarse quartz population varies between brown-stained, often subangular, grains to green-stained grains with a glauconitic surface coating. However, this sediment includes a calcareous component, dominated by foraminifera (planktic>benthic) and very fine sand-size calcareous (foraminiferal) fragments (Table 6.6). The composition of the sand determined by point-counting shows a bias towards the finest grain size, where the sand fraction is composed of 72.7% quartz, 19.5% glauconite and 7.8% foraminifera and calcareous fragments by weight. The foraminiferal assemblage indicates an age no older than Langhian (middle Miocene), which supports the Sr-ages of 12.0-15.9 Ma obtained for benthic foraminifera (Compton *et al.*, 2004).

6.6.1 DEPOSITIONAL ENVIRONMENT OF THE GRAVELLY CALCAREOUS QUARTZOSE MUDDY SAND

The gravel lag at the base of the Gravelly Calcareous Quartzose Muddy Sand facies lies above the erosional surface marking the end of the deposition of the deep water Upper Oligocene/Lower Miocene Calcareous Unit. This basal sequence boundary indicates the onset of the Langhian sediment depositional cycle. . The lower part of the basal gravel lag of the Gravelly Calcareous Quartzose Muddy Sand facies is dominated by winnowed late Oligocene to Aquitanian phosphorite gravels (Compton *et al.*, 2004), implying a high-energy erosion of the entire Upper Oligocene/Lower Miocene Calcareous Unit. The Gravelly Calcareous Quartzose Muddy Sand, recovered in deeper water than the uppermost Oligocene to Aquitanian sediments recovered predominantly at ~252-255 m, indicates that the middle Miocene (Langhian) erosional event cut down through the upper Oligocene/lower Miocene sediments into the Cretaceous sediments in places. The location of Core 319 on the eastern flank of the Canyon, at a water depth of 274 m, supports the argument for an earlier more widespread distribution of the Upper Oligocene/Lower Miocene Calcareous Unit. The Fe-rich carbonate clasts and the oxidised appearance of the glauconite grains in the upper part of the basal lag imply highly oxidising conditions existed at times during the erosional winnowing process during this relative sea-level lowstand. The brown-stained quartz sand grains, together with the Fe-rich composition of the basal gravel sediments, indicates that the Fe-rich siliciclastic component of this facies is most likely to have been derived by reworking of the underlying Cretaceous sediments (Chapter 4). A shallow-water, high-energy environment is proposed for this erosional event, implying a significant drop in the relative sea level from the upper slope/outer shelf environment of the Burdigalian Foraminiferal Ooze.

The middle Miocene marine sediments of the Gravelly Calcareous Quartzose Muddy Sand facies, deposited above the basal lag, were probably deposited in a deeper water environment, with low sedimentation rates indicated by the presence of glauconite and *in situ* phosphorite. The similarity in appearance, grain size and composition of the quartzose sand fraction of the basal lag and the overlying sediments of the middle Miocene unit, suggests a similar Cretaceous sediment source for this quartz.

University of Cape Town

6.7 OLIGOCENE-MIOCENE GEOLOGICAL EVOLUTION OF THE MARGIN

The geological evolution of passive margins is largely governed by changes in relative sea level. Relative sea level records both changes in global (eustatic) sea level and the local effects of subsidence (due to thermal subsidence and sediment and water loading), tectonic movement and sediment supply (Section 3.4). The individual contributions of factors influencing the recovered sequence stratigraphy of the upper Oligocene/lower Miocene succession in this study need to be assessed in order to distinguish between local and global events (Miller *et al.*, 1998; Lavier *et al.*, 2001).

The geological history of the western margin of southern Africa is still poorly constrained (Chapter 2), and there is almost no consensus in the literature regarding the Tertiary strata. The available seismic-stratigraphic studies concentrate on the oil-bearing Cretaceous record with no detailed analyses of the Tertiary sequence stratigraphy. Although post-rift subsidence of a passive margin is primarily driven by conductive heat loss, many margins show substantial deviations from the expected thermal subsidence rates (Müller *et al.*, 2000). Deviations in the post-rift tectonic history of southern Africa (Section 2.1) are poorly known, although it is recognised that Tertiary out-building is associated with seaward tilting of the western margin (Du Plessis *et al.*, 1971). The majority of recent work indicates that the high elevation of the rifted margin has a Cretaceous origin and that the Tertiary history of the coastal plain along the western margin is dominated by minor uplift (<200 m), with peak periods of uplift in the middle Miocene and late Pliocene, with greatest amount of uplift along a line generally corresponding to the Great Escarpment (Figures 2.1 and 2.2). These uplift events of the continental interior are associated with downwarping of the western margin (Partridge and Maud, 1987, 2000; Partridge, 1998; Spönemann and Hagedorn, 2000; Pickford, 1998, 2000; Pether *et al.*, 2000; Brown *et al.*, 2000). In contrast, Burke (1996) indicates a late Oligocene uplift of a previously low-elevation margin. The post-rift buoyancy of the southern African margin is often argued to be related to thermal anomalies associated with the African Superswell (Burke, 1996; Partridge, 1998). In addition, the study area lies adjacent to the relatively buoyant basement block, the Columbine-Agulhas Arch, composed predominantly of Cape Granite Suite granitoids, which defines the southern extent of the Orange Basin (Scrutton and Dingle, 1976; Dingle *et al.*, 1983). Partridge and Maud (1987) proposed that reactivation of the Columbine-Agulhas Axis during the Tertiary was associated with downwarping of the continental margin to the southwest.

In the absence of any well-constrained local tectonic records, the following discussion on the geological evolution of the study area considers the possible contribution of tectonics and sediment supply rates (productivity and terrigenous input) in the context of major mid-Tertiary global oceanographic and climatic changes as recorded in the modified Haq *et al.* (1987) eustatic sea-level curve recalibrated to the Berggren *et al.* (1995) time scale and the marine oxygen isotopic record (Zachos *et al.*, 2001) (Figure 3.10). However, without these local constraints, the amplitude of the relative sea level change, reflecting in part eustatic changes, cannot be resolved and the following arguments consider only the cycles of sea-level change and not the amplitude of these changes (Kendall and Lerche, 1988; Miller *et al.*, 1998). The arguments for and against the interpretive value of a global sea-level curve are discussed

University of Cape Town

Figure 6.25. A summary of the Sr-derived ages of the upper Oligocene to Miocene sedimentary facies and relevant global climatic and tectonic events plotted against the Haq *et al.* (1987, 1988) eustatic curve re-calibrated to the Berggren *et al.* (1995) time scale after Miller *et al.* (1997; 1998) (Figure 3.10). See Figure 6.1 for stratigraphy.

University of Cape Town

in detail in Section 3.4. The available age data for the four facies of the Upper Oligocene/Lower Miocene Calcareous Unit are plotted against the proposed eustatic sea-level curve (Figure 6.25). The detailed analysis of the sediments of the Upper Oligocene/Lower Miocene Calcareous Unit presented here is the first such study published for the western margin of southern Africa.

The Cenozoic sediments recovered from Concession 20D (Figure 6.1) were deposited after the opening of the Drake Passage to deep water circulation and the establishment of the Antarctic Circumpolar Current (ACC). Initiation of the ACC, the resultant thermal isolation of Antarctica and the development of ice-sheets played a major role in Neogene climate evolution. Although the timing for the opening of the Drake Passage is poorly constrained, recent research has suggested an older age than the late Oligocene opening proposed by Shackleton and Kennett (1975). Palaeoproductivity proxies have suggested an initial opening of Drake Passage by 37 Ma (Diester-Haass and Zahn, 1996), geochemical proxies supported a deep-water opening by 32.8 Ma (Latimer and Filippelli, 2002) and tectonic reconstructions indicated that the Drake Passage was open to deep-water circulation by ~31±2 Ma (Lawver and Gahagan, 2003). Although the Circum-Antarctic seaway opened in the early Oligocene, there is little evidence supporting a vigorous ACC until the Miocene (Rack, 1993).

It has been argued that the variation in the size of ice sheets has been a primary control on the formation of sequence boundaries on passive margins since ~42 Ma (Miller *et al.*, 1998), implying the presence of ice on Antarctica, at least intermittently, since the late Eocene. The late Oligocene to the Oligocene to Miocene transition is a period of global importance in that it is at this time that periods of major growth and decay of the Antarctic ice sheets occurred (Figure 6.25; Miller *et al.*, 1991). The early Oligocene (~33 Ma) is associated with major continental glaciation in East Antarctica and a pronounced rise in the marine $\delta^{18}O$ record (Zachos *et al.*, 2001), which persisted until around 26 Ma (Gallagher *et al.*, 2001; Lawver and Gahagan, 2003). The late Oligocene is a period of global warming, where the increase in water temperature is reflected in a major drop in the $\delta^{18}O$ of benthic foraminifera after 26 Ma (Zachos *et al.*, 2001). The late Oligocene warming is associated with an overall decrease in size of the East Antarctic ice-sheet and glaciation that lasted until ~ 14 Ma (Abreu and Anderson, 1998; Lawver and Gahagan, 2003). The long-term global trend to a warm early to middle Miocene climate is well documented (Flower and Kennett, 1994; Gallagher *et al.*, 2001 and references therein). However, a number of cycles of ice sheet growth and cooling are identified within the late Oligocene to Miocene period, with considerable ice-sheet expansion and global cooling occurring around 32.5 and at 23.7 Ma (Miller *et al.*, 1991; Naish *et al.*, 2001).

The absence of marine sediments older than late Oligocene in Concession 20D favours arguments for non-deposition and erosional events along the western and southern African margin in the later part of the Palaeogene, where erosion removed sediments younger than mid Cretaceous (Albian to Cenomanian) and older than upper Oligocene from the study area. Laminated Fe-rich siltstones from the base of Core 223A (250-288 cm), recovered from the western flank of the Cape Canyon suggest that rare lower Turonian or upper Coniacian Red Bed Successions (Chapter 4) are preserved during this

University of Cape Town

major erosional event. Coniacian-aged sediments were similarly recovered off Wreck Point (Figure 2.2), south of the Orange River mouth, in water depths of 122 m (Compton *et al.*, 2002). Siesser and Dingle (1981) described a mid-Cenozoic erosional unconformity in Tertiary seismic records collected along the western and southern African margin, which occurs at a remarkably constant maximum depth out to ~500 m below present sea level. They interpreted this erosional unconformity as evidence for a ~500 m drop in relative sea level in the Oligocene. A mid-Oligocene unconformity in the sediment record is a global occurrence, resulting from a major sea-level regression associated with the onset of major glaciation in eastern Antarctica (Gallagher *et al.*, 2001; Zachos *et al.*, 2001; Lawver and Gahagan, 2003). However, the amplitude of sea-level variation is only on the order of tens of metres (Miller *et al.*, 1998), rather than 150 m (Haq *et al.*, 1987, 1988). The erosional event resulting in the regional unconformity along the southern African margin cannot therefore simply be a result of a drop in eustatic sea level alone. Many authors have argued for a mid-Tertiary tectonic event along the western margin of Africa (Partridge and Maud, 1987; McMillan, 1989; Burke, 1996; Cramez and Jackson, 2000; Lavier *et al.*, 2001). However, the timing and the amount of uplift and the processes involved are open to debate (Chapter 2). The major erosional unconformities recognized in the marine seismic records of the western African margin have been variously attributed to a major drop in sea level (Siesser and Dingle, 1981), 2-3 km of vertical displacement (Cramez and Jackson, 2000) and a major erosional event associated with changes in ocean currents and the initiation of upwelling (Lavier *et al.*, 2001). The recovery of the 25.8-27.2 Ma Quartzose Foraminiferal Muddy Sand at a water depth of 264 m in Concession 20D and the presence of reworked Oligocene to Miocene (21.4-30.1 Ma) benthic foraminifera in Core 322 (Compton *et al.*, 2004) suggest that the palaeo-shoreline never dropped much lower than the modern ~200 m isobath in the late Oligocene. The late Oligocene palaeo-shoreline would therefore have been located near the modern middle to outer shelf break. Alternate processes for the formation of the 500 m unconformity must therefore be examined, where the proposed mass wasting and erosion associated with the changes in ocean currents and the initiation of upwelling along the Angolan Shelf are likely possibilities (Lavier *et al.*, 2001).

The Upper Oligocene/Lower Miocene Calcareous Unit of Concession 20D is composed of four facies (Figure 6.25) that record a complex, discontinuous and condensed depositional history. The Upper Oligocene/Lower Miocene Calcareous Unit has a diverse range in composition with the calcareous sands including variable amounts of phospho-glauconite and quartz grains. The oldest upper Oligocene sediments are recovered on the seaward edge of the Western Ridge and within the Cape Canyon Head region. The Upper Oligocene/Lower Miocene Calcareous Unit youngs seawards, indicating erosion of the seaward-dipping facies as observed elsewhere for Tertiary sediments on the southern African margin (Dingle *et al.*, 1983). In general, the Upper Oligocene/Lower Miocene Calcareous Unit becomes increasingly more marine (calcareous) up section with quartz only being a significant component in the oldest sediment facies (Figure 6.1). The overall increase in planktic foraminifera and the decrease in the siliciclastic component with time reflect deposition of the sediments at progressively greater water depths. The interpreted depositional environments of the foraminiferal assemblage from the four facies supports this overall long-term increase in water depth from the late Oligocene to early Miocene.

University of Cape Town

The interpreted sequence stratigraphy of the Upper Oligocene/Lower Miocene Calcareous Unit facies discussed in earlier sections indicate that these facies record at least four complete relative sea-level cycles (rise and fall) as defined in the literature (Vail *et al.*, 1977; Loutit *et al.*, 1988; Posamentier, 1988; Posamentier and Vail, 1988; Van Wagoner *et al.*, 1988; Helland-Hansen and Gjelberg, 1994). The erosional gravel lag observed between the Quartzose Foraminiferal Muddy Sand and the Quartzose Glauconitic Calcareous Sand towards the base of Core 324 is a well-defined sequence boundary. The variability of the Quartzose Glauconitic Calcareous Sand is interpreted to indicate at least two cycles of changing sea level, although no clearly defined sequence boundary is recognised. The presence of a sequence boundary between the Quartzose Glauconitic Calcareous Sand and the overlying Glauconitic Calcareous Sand is indicated by the presence of a basal gravel lag and a cemented interval within Core 127 and Core 90 respectively (Section 6.3.3). In contrast, the contact between the Glauconitic Calcareous Sand and the Foraminiferal Ooze was not recovered and the relative stratigraphic position of these two is therefore equivocal.

Following the major early to middle Oligocene erosional event, the sediments of the Upper Oligocene/Lower Miocene Calcareous Unit of Concession 20D record the initiation of deposition on the carbonate platform along the southern African margin (Section 6.5). The Cenozoic depositional history commenced with the deposition of the large benthic foraminifera *Operculina* sp. of the late Oligocene Quartzose Foraminiferal Muddy Sand in a low-energy, sandy subtropical to tropical palaeo-environment in a palaeo-water depth most likely less than 60 m (Section 6.1.3). This facies is interpreted to have been deposited in the late Oligocene with Sr-ages of 25.8-27.2 Ma obtained for the large benthic foraminifera *Operculina* sp. This facies lies below the basal gravel lag of the overlying Quartzose Glauconitic Calcareous Sand, where latest Oligocene to earliest Miocene Sr-ages are recorded for the gravel fraction of Core 90. Shallow-water deposition of the larger benthic foraminifera was followed by authigenic phosphorite (phosphatised shell fragments and mollusc casts) and glauconite formation. The presence of authigenic minerals, characteristic of condensed sequences, are interpreted to indicate a relatively rapid rise in relative sea level and low sedimentation rates on the western margin in the late Oligocene. The available Sr-isotopic ages suggest that the phosphatisation event is post-depositional, because no phosphorite ages older than late Oligocene to earliest Miocene have yet been recorded on the western margin (Compton *et al.*, 2004).

The available Sr-ages suggest that the Quartzose Foraminiferal Muddy Sand records a cycle of relative sea-level change that coincides with the TB1.2/Oi2b third-order cycle with the lowstand at 27.0-27.3 Ma (Figure 6.25: Haq *et al.*, 1987; Miller *et al.*, 1991, 1997, 1998). The large benthic foraminifera in these samples indicate deposition in a water depth of less than 60 m (Section 6.1.3), which implies a relative drop in sea level in the order of ~200 m. However, this required drop in sea level is much greater than can be supported by the changing eustatic sea level alone, particularly as the western margin of southern Africa is reported to have been uplifted by 90-100 m in the mid-Miocene (Section 2.1.1). Two possible explanations for the presence of shallow-water foraminifera in these sediments are 1) that this facies is a

University of Cape Town

prograding lowstand wedge with inner-shelf foraminifera reworked out into deeper water or 2) that a local tectonic contribution of margin subsidence occurred after deposition of these sediments. These possibilities are discussed in more detail later in this section.

The well-defined erosional sequence boundary at the base of the Quartzose Glauconitic Calcareous Sand (Section 6.2.3) indicates a drop in relative sea level, following the higher relative sea level interpreted for the authigenic mineral formation of the Quartzose Foraminiferal Muddy Sand facies. The gravel lag at the base of the Quartzose Glauconite Calcareous Sand facies is composed of reworked phosphatised mollusc casts and shell fragments, winnowed from the Quartzose Foraminiferal Muddy Sand. The foraminiferal assemblage from two samples collected above the basal lag indicate that deposition occurred in the innermost to inner shelf environment, with broken sand-size shell fragments suggesting reworking in a relatively high-energy environment. In addition, the abundance of medium to coarse quartz sand indicates an increase in energy that may reflect proximity to the palaeo-shoreline. The medium to coarse quartz sand of this sediment is interpreted to have been eroded and reworked from the underlying Cretaceous sediments (Section 6.2.3). The available information from the interpreted high-energy inner shelf (in close proximity to a palaeo-shoreline) depositional environment of the Quartzose Glauconite Calcareous Sand facies suggests that the latest Oligocene relative sea-level drop, associated with the erosional surface at the base of this facies, was similar to the ~200 m drop interpreted for the late Oligocene depositional environment indicated by *Operculina* sp. Again this drop in relative sea level is at odds with the proposed eustatic sea-level record. However, the elevation of Core 159 with an innermost shelf foraminiferal assemblage, has clearly been influenced by post-Miocene down-faulting (Figures 3.5 and 3.6) and the original elevation of the palaeo-shoreline cannot be determined.

Additional support for a latest Oligocene drop in relative sea level is recorded in the post-depositional alteration of the underlying Quartzose Foraminiferal Muddy Sand. The pink to reddish yellow colouration of the recrystallised carbonate fragments and the oxidized appearance of the earthy green-brown glauconite (Birch, 1971) of the Quartzose Foraminiferal Muddy Sand suggests either oxygenated bottom water or subaerial exposure of this underlying unit during the relative sea-level lowstand. The recrystallisation of the large benthic *Operculina* sp. foraminiferal tests may be associated with the formation of the Ca-Fe coating on many of the coarse quartz grains. Similarly, the presence of goethite in XRD scans of the mud (<63 μm) fraction of the Quartzose Foraminiferal Muddy Sand may indicate either oxidation or terrigenous input.

The Quartzose Glauconitic Calcareous Sand sediments record a deepening of relative sea level above the basal lag. Evidence for rising sea level is provided by the decrease, up-facies, of the quartzose sand and reworked calcareous fragments associated with a progressive increase in planktic foraminiferal abundance. However, the extreme variability of the calcareous component, dominated by shell fragments and foraminifera, is interpreted to indicate either changes in depositional environment across the inner to middle shelf and/or a complex history of more than one cycle of relative sea-level change (Section 6.2.3). Phosphatic gravels collected predominantly from the overlying lag at the base of the

University of Cape Town

Glauconitic Sand Unit (Chapter 7), show that phosphatisation and possible formation of complex hardground horizons occurred between 26.1-20.1 Ma, with a peak in phosphogenesis around 26.1-23.6 Ma in the Oligocene (Compton *et al.*, 2004). A similar peak in phosphogenesis during a late Oligocene/early Miocene sea-level highstand is recorded in the Cenozoic sediments of north Patagonia, Argentina (Scasso and Castro, 1999). The maximum flooding surfaces appear again to be associated with enhanced phosphatisation and glauconite formation, where the micro-environment provided by the increasingly abundant foraminiferal test favours glauconite formation (Odin and Matter, 1981). The abundance of upper Oligocene/lower Miocene authigenic minerals indicates low sedimentation rates and deepening relative sea level at this time. The available Sr-data suggest the recorded cycles of changing relative sea level may be coincident with the TB 1.3 and 1.4 third-order cycles of the late Oligocene to early Miocene (Figure 6.25) and major Mi1-glaciation event of Miller *et al.* (1998) (Figure 6.25). As argued for the Quartzose Foraminiferal Muddy Sand the interpreted drop of ~200 m in relative sea level is much greater than can be supported by the eustatic sea-level curve alone.

Distinctly different foraminiferal assemblages and sediment compositions are recovered from the upper Oligocene Quartzose Foraminiferal Muddy Sand and the uppermost Oligocene to lower Miocene Quartzose Glauconitic Calcareous Sand facies. These differences most likely reflect circulation changes in the Southern Ocean resulting in the global warming of the late Oligocene and the subsequent major Mi-1 glaciation event at around 23.5 Ma (Abrey and Anderson, 1998; Zachos *et al.*, 2001; Lawver and Gahagan, 2003). The Mi-1 glaciation event indicates major global cooling and ice-sheet expansion (Miller *et al.*, 1998; Gallagher *et al.*, 2001; Naish *et al.*, 2001; Zachos *et al.*, 2001). The ice-sheet expansion would most likely have resulted in an increased latitudinal temperature gradient and a consequent increase in wind-driven coastal upwelling along the western margin of southern Africa. The Quartz Foraminiferal Muddy Sand is interpreted to have been deposited in a low-energy environment, whereas the overlying basal lag and mixed sediments of the Quartzose Glauconitic Calcareous Sand facies indicate a significant increase in bottom water activity, possibly associated with increased upwelling. Compton *et al.* (2004) similarly argued that the late Oligocene phosphogenesis episode (26.1-23.6 Ma) indicated increased upwelling and organic burial along the western margin of southern Africa. Siesser (1978b) described the weak spasmodic introduction of upwelled water into the northern Namibian coastal system from the middle to Late Oligocene until the middle Miocene based on sedimentological, palaeontological and geochemical studies of the DSDP sites 362 and 363 on the Walvis Ridge off northern Namibia (Figure 2.1). The change in the depositional environment, recorded in the lower two facies of the Upper Oligocene/Lower Miocene Calcareous Unit, provide evidence for a significant change in oceanographic conditions in the later Oligocene along the western margin of southern Africa, particularly as changes in interpreted water depth for the two facies are apparently not significantly different.

The uppermost Oligocene to lower Miocene Quartzose Glauconitic Calcareous Sand is unconformably overlain by the Burdigalian Glauconitic Calcareous Sand. The relationship between these two units is poorly understood as it varies from gradational in appearance to being defined by a gravel lag (*e.g.*

University of Cape Town

Cores 127 and 90) dominated by cemented carbonate clasts and bone. Although the contact between these two facies is variable, the presence of the basal lag is interpreted to reflect a drop in relative sea level following the final stages of relatively deep-water deposition of the underlying Quartzose Glauconitic Calcareous Sand. The absence of a well-defined basal lag in the Burdigalian Glauconitic Calcareous Sand facies suggests that most of the recovered shelf deposits were at water depths below an energy regime sufficient for the development of a winnowed gravel lag during this inferred relative sea-level lowstand. The deep-water foraminiferal assemblage of the Glauconitic Calcareous Sand indicates deposition in an outer-shelf to upper-slope environment. The abundance of glauconite in the Burdigalian Glauconitic Calcareous Sand is, similarly, interpreted to indicate rising relative sea levels and low sedimentation rates. The relative highstand is associated with a phosphatisation event recorded by the formation of phosphatic gravels with a range of Sr-ages from 18.8-15.4 Ma. Seismic studies by De Beers Marine (Pty) Ltd (I. McMillan, *pers. comm.*, 2003) show that the Burdigalian sequence off Namaqualand is not a simple transgressive sequence, but records a complex layering of progradational wedges implying a complex history of changing relative sea level for the area. Comparison of Sr-isotopic data from the Glauconitic Calcareous Sand also suggests deposition during the proposed third-order eustatic sea-level cycle TB2.1 of the modified Haq *et al.* (1988) curve (Figure 6.25).

Increasing water depths associated with the late Burdigalian rising relative sea level resulted in deposition of the deep-water Foraminiferal Ooze, and compositionally similar sediments all along the southern and western margin (Section 6.5). Carbonate production is often greatest during rising and high sea levels (Gonzales, 1996) and the increased foraminiferal production may have resulted from a warming global climate (Miocene Climatic Optimum at ~16 Ma of Flower and Kennett, 1994; Gallagher *et al.*, 2001). The increased accumulation of foraminifera and lime mud may reflect a general lowering of the bottom water energy with increasing water depth, but reduced upwelling may also play a role if the climate optimum is associated with decreased latitudinal temperature gradients and a reduction in upwelling strength. The absence of phospho-glauconite from the Foraminiferal Ooze has implications on the changing depositional environment, with an absence of a terrigenous component likely related to the increased water depth and regression of the coastline. In addition, the increased carbonate production and accumulation rates may also have prevented glauconite formation. Recent work has suggested that most prolific carbonate production may not necessarily be in the shallow euphotic zone, as traditionally interpreted for both recent and ancient carbonate platforms, but that significant carbonate production can occur in the aphotic zone (Corda and Brandano, 2003). The lower Miocene sediment record of southern Africa margin is dominated by planktic foraminiferal muddy sands with a significant bryozoan component (McMillan, 1989, 1990). The prevalence of bryozoa in the outer-shelf lower Miocene sediments may indicate a component of significant aphotic carbonate production on the southern African margin during the early Miocene (Burdigalian).

The interpreted sequence stratigraphy of the Upper Oligocene/Lower Miocene Calcareous Unit shows an apparent correlation with the modified Haq *et al.* (1988) sea-level curve (Figure 6.25), suggesting a correlation between eustasy and the observed sequence boundaries. This proposed correlation does not

University of Cape Town

take into account any of the uncertainties in the ages of the facies within the Upper Oligocene/Lower Miocene Calcareous Unit or the inherent uncertainty of the ages of the modified Haq *et al.* (1988) curve and therefore no unequivocal causal link can be demonstrated (Miller *et al.*, 1998). However, a number of studies of sequence stratigraphy from passive margins of both the northern and southern Hemisphere similarly argue for a close causal relationship between sequence boundaries and the eustatic sea-level curve (Section 3.4.3; Sugarman and Miller, 1997; Miller *et al.*, 1997, 1998; Gallagher and Holdgate, 2000; Harris and Whiting, 2000; Monteverde *et al.*, 2000; Gallagher *et al.*, 2001; Rossetti, 2001; McHugh *et al.*, 2002; Brachert *et al.*, 2003; Caron *et al.*, 2004; Holbourn *et al.*, 2004; Li *et al*, 2004).

The lower three facies of the Upper Oligocene/Lower Miocene Calcareous Unit all indicate the presence of a palaeo-shoreline approximately 200 m below the modern sea level in the vicinity of the present-day middle to outer shelf-break. Dale and McMillan (2003b) proposed an early Miocene (Aquitanian) clastic shorelines at around 140 m water depth for the Namaqualand coast. This approximately ~60 m difference in elevation of the interpreted palaeo-shoreline most likely reflects the post-depositional differential uplift in the middle Miocene along the western margin of southern Africa (Section 2.1.1). As argued previously, this required drop in sea level is much greater than can be supported by the eustatic sea level alone. The most important factors governing relative sea level on a passive margin are commonly reported to be eustasy, margin subsidence, tectonics, sediment supply and compaction. The late Oligocene to early Miocene depositional environment, as recorded in the condensed sections of the oldest three facies, is clearly sediment-starved indicating a negligible contribution to margin evolution by sediment supply and compaction. These condensed sedimentary sequences suggest that sediment loading also played a minor role in margin evolution during the deposition of the oldest three facies. In contrast, the Burdigalian Foraminiferal Ooze is interpreted to be representative of the thick succession of lower Miocene sediments described along the western and southern margin of southern Africa. The lower Miocene sediments form a coast-parallel lens along the southern and western continental margin, with the thickest and most extensive deposits found on the outer shelf (180-200 m) and slope (~300 m in Kudu 9A boreholes) (Dingle *et al.*, 1983; McMillan, 1990; Corbet, 1996; Dale and McMillan, 2003b). The sediment (and water) loading associated with deposition of this carbonate unit during the long-term middle Miocene eustatic highstand would have contributed towards increased rates of margin subsidence, whereas previously margin subsidence was dominated simply by post-rift subsidence associated with conductive heat loss. Although the local tectonic regime along the western coastal platform is one of uplift, with both an underlying buoyant pre-Cretaceous basement and Tertiary uplift events (Section 2.1.1) no significant late Oligocene to early Miocene active tectonic contribution to accommodation space is recognised within the sediment succession of the Upper Oligocene/Lower Miocene Calcareous Unit. This is consistent with the mid Miocene age assigned, in the available literature, to tectonic activity along the western margin of southern Africa.

The deposition of the Upper Oligocene/Lower Miocene Calcareous Sand Unit came to an abrupt end around 18 Ma, where the lower Miocene sediments include no foraminifera younger than 18.3 Ma. These carbonate-rich sediments were probably down-cut during the later erosional events such that

University of Cape Town

deposition of this facies may have extended past 18.3 Ma. However, a dramatic change in the depositional environment is observed between the deep-water outer-shelf marine-dominated Foraminiferal Ooze and the quartz-rich sediments of the Gravelly Calcareous Quartzose Muddy Sand. The lithofacies change reflects increased energy and sediment input, which may have resulted from a relative lowering of the sea level, in addition to reworking by bottom currents. The high-energy shallow-water environment interpreted for this erosional event cannot simply reflect a eustatic sea-level lowstand, as the required change in water depth is far greater than can be accounted for by any rise in eustatic sea level (Miller *et al.*, 1998). In addition, the 17.0-17.7 Ma Sr-ages obtained from the benthic foraminifera of the gravel lag in Core 319 are slightly older than the oldest major eustatic sea-level lowstand of the middle Miocene (recalibrated TB2.3 of Haq *et al.*, 1987; Figure 6.25). Therefore, a tectonic contribution of margin uplift is required to account for the interpreted rapid shallowing of the water depth after 18.3 Ma.

An early Miocene uplift of southern Africa is suggested by many authors, with the greatest amount of movement (100-200 m) on the West Coast along a line roughly coincident with the Great Escarpment (Partridge and Maud, 1987; Partridge, 1998; Pickford, 1998; Lavier *et al.*, 2001). The uplift resulted in the elevation of marine and coastal deposits, with the Columbine-Agulhas Axis reactivated/developed during this time with seaward downwarping to the southwest (Partridge and Maud, 1987). This proposed seaward downwarping may be argued to represent a tectonic contribution to the described post early Miocene subsidence of the margin recorded in the Upper Oligocene/Lower Miocene Calcareous Unit. The overall asymmetry of the Miocene uplift resulted in a slight westward tilt to the sub-continent (Partridge and Maud, 1987). The timing of this uplift event along the southern African margin is poorly constrained. Dale and McMillan (2003b) indicated uplift at ~16.5 Ma, whereas Partridge (1988) suggested a timing for uplift at around 16-19 Ma as evidenced by minor increases in terrestrial input in the Orange Basin (Dingle *et al.*, 1983). Similarly Lavier *et al.* (2001) argued that ~230 m of uplift of the Angolan margin reflects Miocene uplift with a major peak of increased rate of uplift at 16 Ma. Anderson *et al.* (2000) argued that the turbidites of the Angolan slope, aged 17.5-15.5 Ma, formed in response to uplift.

The Sr-ages of benthic foraminifera from the lower Miocene Foraminiferal Ooze indicate that initiation/reactivation of increased rates of uplift of the western margin of southern Africa occurred after 18.3-20.8 Ma, but prior to the deposition at 12.0-15.9 Ma of the middle Miocene sediments recovered in Core 319. The available Sr-age data therefore indicate a marked change in environment and uplift that occurred towards the end of the Burdigalian. The presence onshore of a Langhian (~16 Ma) marine green silty clay and white carbonate unit at +65 m (Dale and McMillan, 2003b) or somewhat lower than +40 m (Pether *et al.*, 2000) in the Hondeklip Bay area (Figure 2.2) supports arguments for increased uplift at this time.

Following the climatic optimum at ~16 Ma, rapid expansion of the East Antarctica ice-sheets is associated with the abrupt end to the Miocene Climatic Optimum and the mid to late Miocene cooling

University of Cape Town

(Flower and Kennett, 1994; Gallagher *et al.*, 2001; Zachos *et al.*, 2001). The expansion of the ice sheets is associated with the intensification of Southern Ocean circulation and rapid cooling of deep waters (Pagani *et al.*, 1999). These changes in global climate resulted in the formation of a well-developed thermocline and ocean stratification (Gallagher *et al.*, 2001). This change in climate is well documented along the SE Australian coast (Gallagher *et al.*, 2001), where the sediment record shows an abrupt change at ~14.5 Ma from warm water to cold water foraminifera species and increased upwelling over the shelf break. McMillan (1986) argued, using the foraminiferal assemblage, that similar warm water conditions prevailed from the early Oligocene to at least the Langhian on the western margin of southern Africa. The ostracod assemblage of these southern African sediments also supports a subtropical/tropical climate until at least the Langhian, when changes in the faunal assemblage are observed between 16-13 Ma (and ~3.5 Ma) in ODP Site 1087 drilled on the continental slope of the Orange Shelf (Dingle *et al.*, 2001). This is in agreement with onshore evidence provided by kaolinisation below the lower Miocene deposits of the Namaqualand coast (Pether, 1994; Pickford and Senut, 1999) and the Cape Peninsula (Rogers, 1982; Partridge and Maud, 1987). The middle Miocene (12.0-15.9 Ma) sand to gravelly sand overlying the basal lag of Core 319, includes a significant amount of reworked (Cretaceous) medium to coarse quartz and *in situ* glauconite, indicating a significant decrease in carbonate productivity relative to the thickness of the underlying Burdigalian calcareous sediments. This significant decrease in carbonate productivity may reflect the changes in oceanographic conditions and cooling of the shelf waters along the margin of southern Africa as a result of mid to late Miocene ice sheet expansion.

The four facies defined within the Upper Oligocene/Lower Miocene Calcareous Unit of Concession 20D provide some constraints on the development of carbonate platforms of the southern and western margin of southern Africa. The upper Oligocene/lower Miocene carbonate platform is constructed and modified by depositional and erosional processes, where changes in relative sea level appear to play a dominant role although these required changes in sea level are not necessarily of a large amplitude. The timing of the recognised sequence boundaries correlates well with the modified Haq *et al.* (1987) global sea-level curve (Miller *et al.*, 1998) attesting to the apparent importance of eustasy, in conjunction with margin subsidence, in the evolution of this passive margin. The influence on the depositional environment by additional factors such as changing oceanographic conditions, sediment production, dominant biota and decreasing siliciclastic input is also recognised. The distribution of upper Oligocene to lower Miocene facies on both flanks of the Canyon Head region, suggests an earlier more widespread distribution of the Upper Oligocene/Lower Miocene Calcareous Unit. Although the Miocene sediment record of the southern and western margin is dominated by foraminiferal-rich sediments, a variety of calcareous and authigenic-rich Miocene-aged sediments are briefly mentioned in the literature (Section 6.5). The interpretation of the geological history of these upper Oligocene/Lower Miocene Calcareous Unit may therefore have a widespread relevance to the evolution of the southern African margin during the late Oligocene to early Miocene as a whole.

University of Cape Town

7 PLIOCENE SUCCESSION

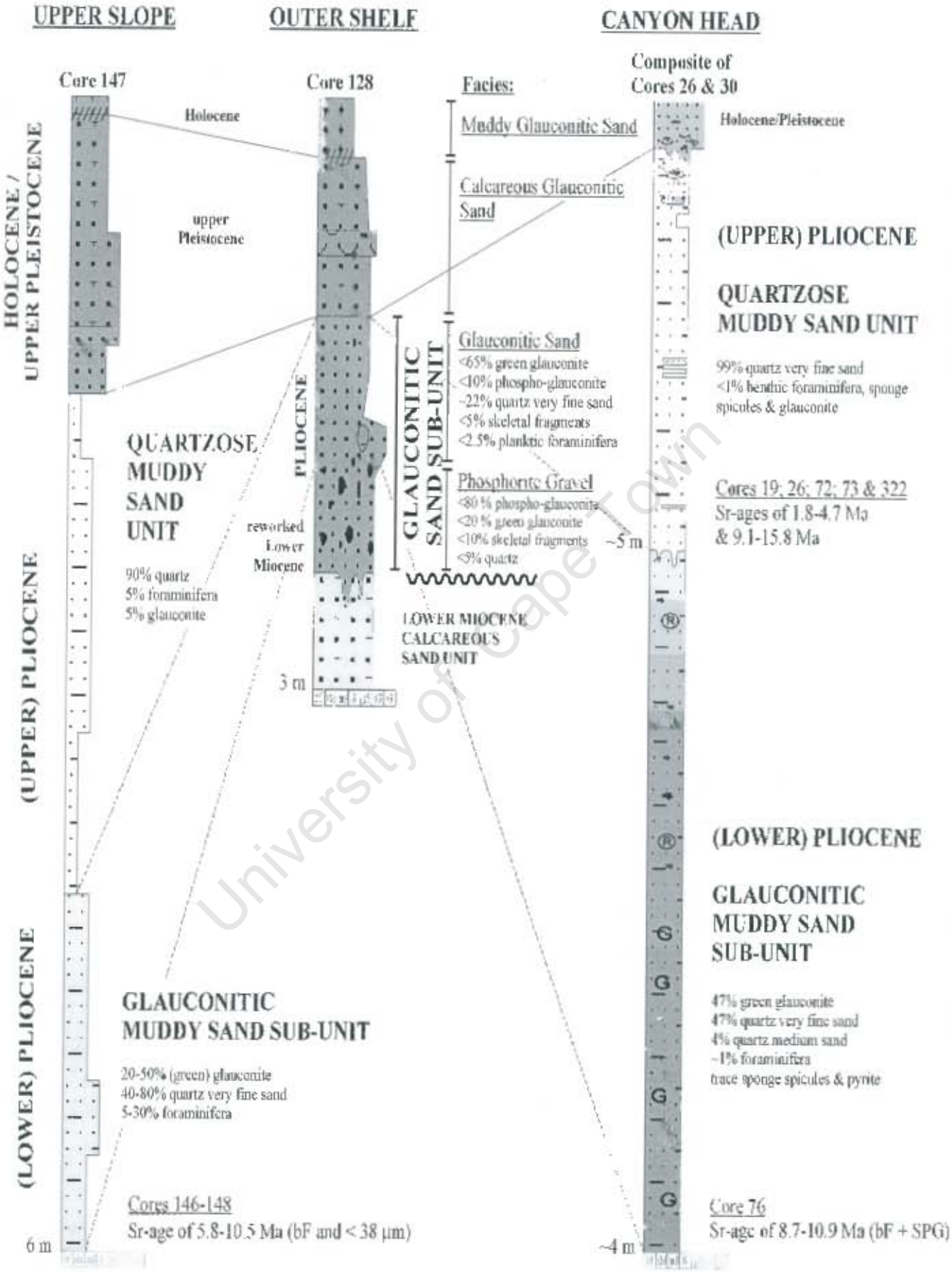
A complex succession of Pliocene sediments was recovered from Concession 20D. The Pliocene sediments are subdivided into two lithologic units, which differ significantly in quartz and glauconite abundance (Figure 7.1), with the Glauconitic Sand Unit overlain by the Quartzose Muddy Sand Unit. The Pliocene sediments differ markedly from the underlying Miocene sediments in composition. The Glauconitic Sand Unit contains abundant glauconite and only minor calcareous grains. The Quartzose Muddy Sand Unit is dominated by a very fine quartzose sand with a grain size distribution that is unique in the study area. The Glauconitic Sand Sub-unit of the outer shelf is overlain by the Quaternary Calcareous Glauconitic Sand facies (Figure 7.1; Appendix A1-14). The Pliocene and Quaternary glauconitic sediments are similar in macroscopic appearance and where therefore not differentiated in the original WMR core logs. The term, *glauconite-rich sediments*, is used to refer to these Pliocene to Quaternary glauconitic sands. The original WMR core logs and the data of Compton *et al.* (2004) were used in conjunction with the cores logged and sampled during this study to establish the lithostratigraphy of the Glauconitic Sand and Quartzose Muddy Sand Units of Concession 20D.

University of Cape Town

7.1 GLAUCONITIC SAND UNIT

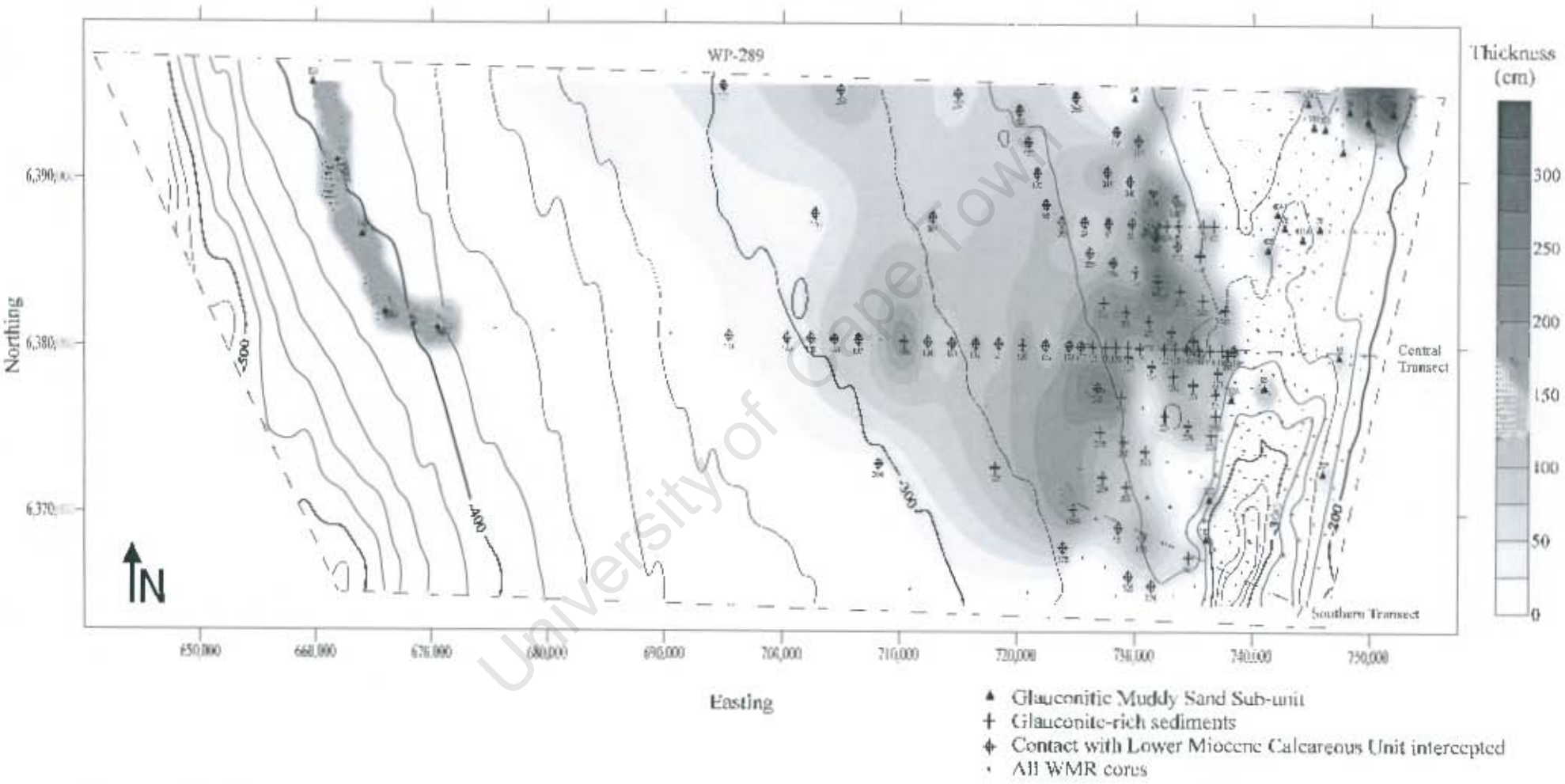
The Glauconitic Sand Unit is subdivided into the Glauconitic Muddy Sand and the Glauconitic Sand Sub-units, on the basis of sediment texture and the abundance of very fine quartz sand (Figure 7.1). The Glauconitic Muddy Sand Sub-unit is found in both the Cape Canyon Head Area and on the upper slope, whereas the Glauconitic Sand Sub-unit dominates the outer shelf area (Figure 7.1 and 7.2).

The Glauconitic Sand Sub-unit of the outer shelf is recovered seaward of the Western Ridge and the Main Channel of the Cape Canyon and is restricted to water depths of between 233 m and 312 m (Figure 7.2). Seaward of the ~300 m isobath, the Upper Oligocene/Lower Miocene Calcareous Unit crops out on the sea-floor. The sediment isopach map reflects the total thickness of the Tertiary glauconite-rich sediments because the WMR core descriptions are insufficient to differentiate between the Pliocene and Quaternary units with any degree of confidence. The glauconite-rich sediments vary in thickness between 7 cm and 388 cm, with an average recovery of 147 cm from all of the WMR cores. The glauconite-rich sediments are thickest adjacent to the Western Ridge and thin both seawards and southwards towards the Southern Rocky Plateau (Figure 7.2). The contact between the Pliocene Glauconitic Sand Sub-unit and the underlying Upper Oligocene/Lower Miocene Calcareous Unit was intercepted in the majority of cores collected west of the ~250 m isobath (Figure 7.2). The sediment facies of the Glauconitic Sand Sub-unit are defined and described using Core 128 as a type section (Figure 7.3; Appendix A1-28), because this core includes the unconformable contact with the underlying Upper Oligocene/Lower Miocene Calcareous Unit. The glauconite-rich sediments of the outer shelf display a remarkably consistent internal stratigraphy and can be subdivided into two Pliocene facies and two Quaternary facies (Figures 7.1 and 7.3). The two Pliocene facies are defined as the Phosphorite Gravel facies and the Glauconitic Sand facies (together referred to as the Glauconitic Sand Sub-unit).



University of Cape Town

Figure 7.1. Pliocene stratigraphy of the study area. The legend for the symbols is included in Figure 3.11; glauconite abundance is shown as a grey scale.



University of Cape Town

Figure 7.2. The sediment isopachs for the glauconite-rich sediments from Concession 20D. Core 289 (295 cm recovered) was excluded from the dataset to prevent edge effects resulting from the lack of data on the outer shelf. The vibrocores with no recovery were excluded from the WMR dataset, as most of these are located on the Southern Rocky Plateau where refusal reflects the gravelly nature of the surface sediments.

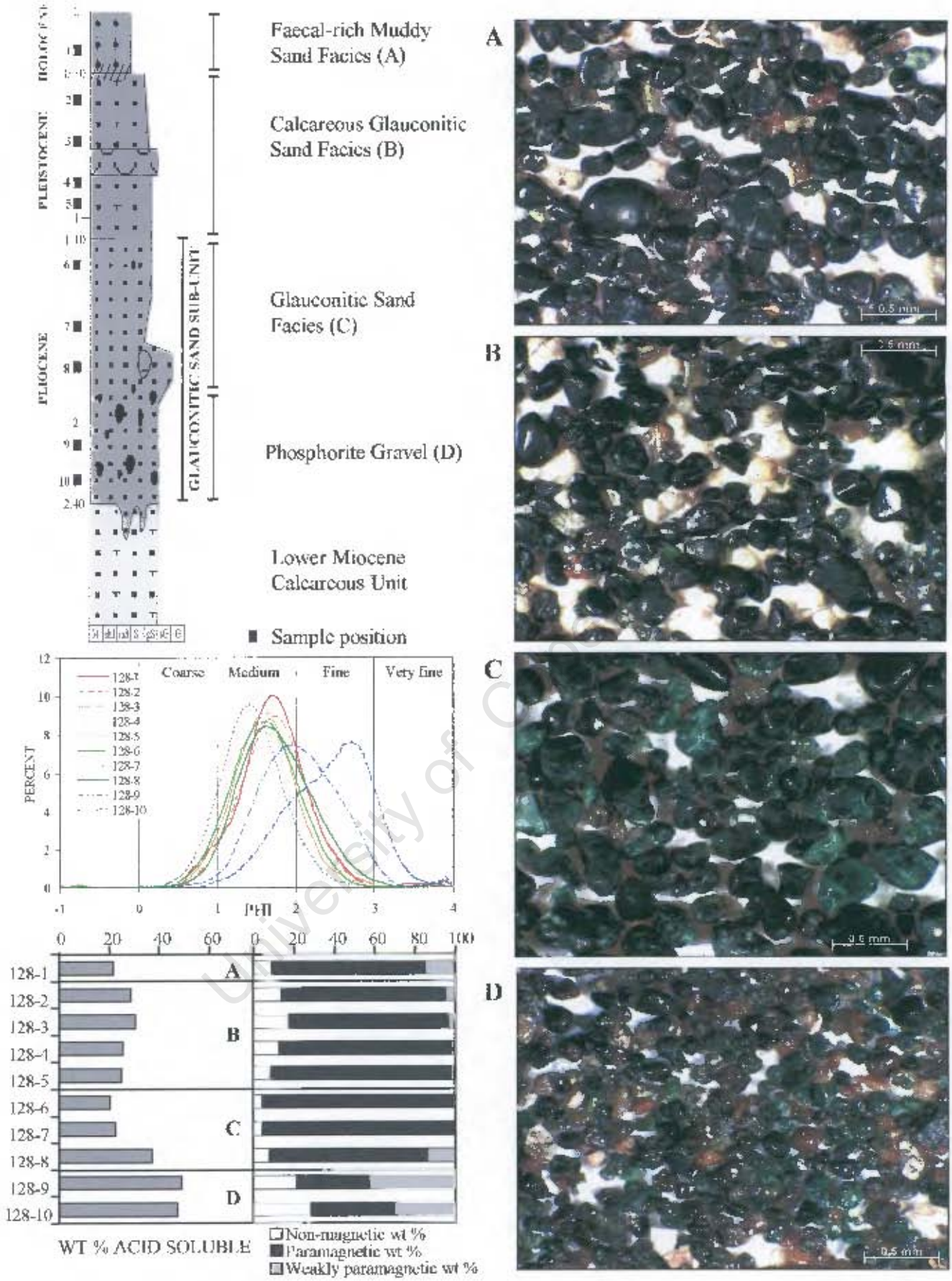


Figure 7.3. Stratigraphy of the glauconite-rich sediments of the Outer Shelf in Core 128 (Figure 7.2). The legend for the symbols is included in Figure 1.1; glauconite abundance is shown as a grey scale. The photomicrographs (A: 128-1; B: 128-3; C: 128-7 and D: 128-10) show the sand fractions of the four facies. Frequency curves showing the particle size distribution, the weight percent acid-soluble components ($CaCO_3$ and phosphorite) and the weight percent non-magnetic (quartz, biogenic and phosphorite), paramagnetic (glauconite) and weakly paramagnetic (phospho-glauconite) of the sand-fractions from the four facies are included.

University of Cape Town

The basal phosphatic gravel lag lies unconformably above the Upper Oligocene/Lower Miocene Calcareous Unit and grades up-core into the Glauconitic Sand facies. The lithology of these facies is described in more detail in subsequent sections.

The Pliocene and Quaternary glauconite-rich sediments were recovered in all of the analysed outer shelf cores, with the exception of Cores 114-116 where only the Quaternary facies was recovered (Appendix A1-14). The subdivision into Pliocene and Quaternary glauconite-rich sediments is based largely on the variations in the texture and composition of the glauconite/phospho-glauconite and the abundance of subordinate components in the sand fraction, where the Pliocene is characterised by the dominance of glauconite (Figure 7.4). The glauconite-rich sediments include a variety of glauconite grain types, including phospho-glauconite foraminiferal infillings, green glauconite and black lobate to deeply sutured grains (Figure 7.3). The lobate to deeply sutured glauconite grains, throughout the succession, typically have abundant coccoliths on the suture surface (Figure 7.5). Pebbles are found scattered throughout the glauconite-rich sediments and are not associated with erosional lag deposits. These pebbles are relatively rare and they tend to occur primarily in the Glauconitic Sand facies and the Quaternary Calcareous Glauconitic Sand facies (Table 7.1). These scattered pebbles include both pink and white granite up to very coarse pebble size, quartzite coarse pebbles and quartz and phosphorite up to small cobble size. An example of a scattered pebble was recovered in Sample 129-3 where the angular ~2 cm coarse pebble of pink granite is petrographically similar to metamorphosed Cape Granite Suite (Frimmel *et al.*, 2001).

University of Cape Town

Table 7.1. A summary of the scattered pebbles and small cobbles found within the glauconite-rich sediments of the outer shelf.

Core	Isolated pebbles
86	very coarse granite pebble (4 cm) at 145 cm
90	very coarse phosphorite pebble (4 cm) at 152 cm
92	coarse phosphorite pebble (3 cm) at 83 cm
96	two well rounded oval quartzite pebbles (<4 cm) at 62 & 123 cm
115	phosphorite pebble at 122 cm
116	layered phosphorite small cobble pebble (7 cm) near base of core at ~120 cm
129	pink granite pebble (2 cm) at 86 cm
131	very coarse phosphorite pebble (6 cm) at 90 cm
203	very coarse granite pebble (5 cm) at ~60 cm
204	quartz medium pebble (1.5 cm) at 120 cm
229	angular elongated quartzite (5 cm) at 153 cm
230	coarse phosphorite pebble (3 cm) at 187 cm
234	phosphorite pebbles (<7cm) and quartz (no size) at 91 cm
245	coarse granite pebble (2 cm) at 212 cm
248	very coarse phosphorite pebble (6 cm) at 177 cm
289	very coarse granite pebble (4 cm) at 240 cm
324	small phosphorite cobble (8 cm) above Phosphorite Gravel at 35 cm
334	white granite (no size) at 86 cm
339	very coarse phosphorite pebble (5 cm) at 272 cm
373	quartz pebble (no size) at 65 cm.
189A	phosphorite cobble (10 cm) at 80 cm; quartzite cobble (9 cm) at 104 cm and phosphorite pebble at 242 cm
368A	two phosphorite pebbles (no size) at 60 cm

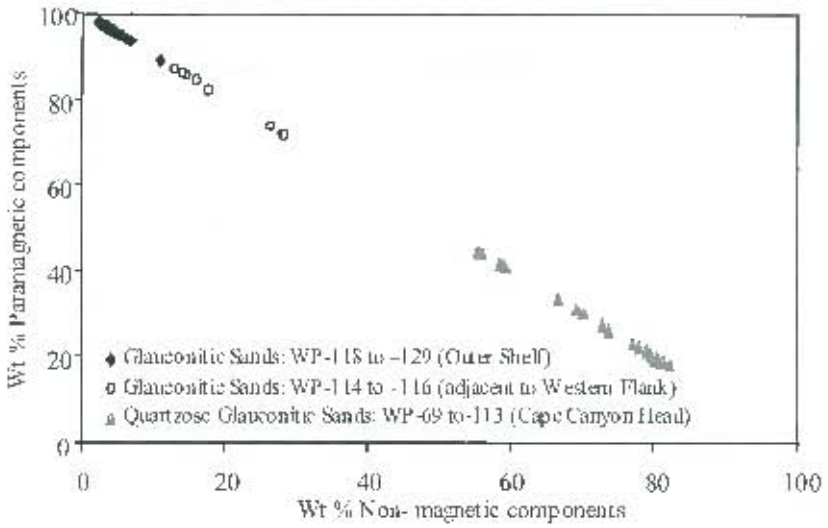


Figure 7.4. The wt % non-magnetic *vs* paramagnetic components of the sand fractions from the Central Transect. The magnetic separation was undertaken on acid-leached samples so that the non-magnetic fraction represents quartz and the paramagnetic fraction glauconite and phospho-glauconite.

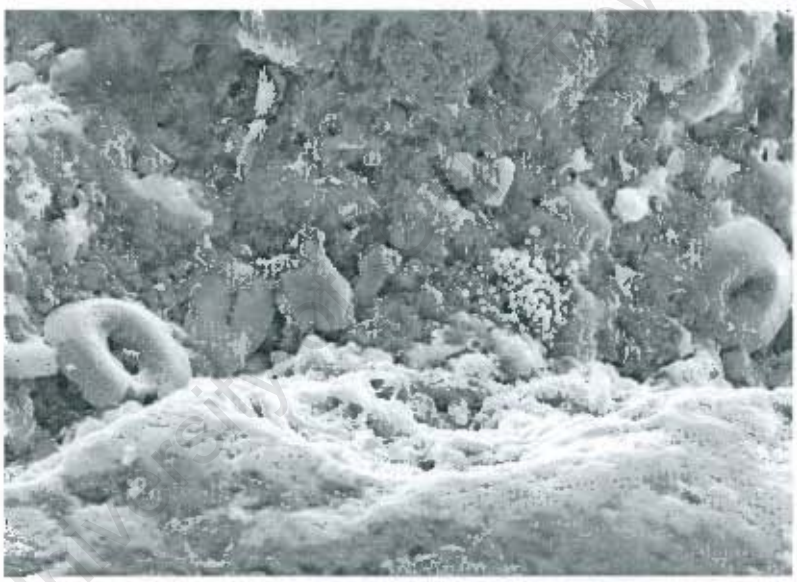


Figure 7.5. A SEM image showing coccoliths in a suture of a typical lobate glauconite grain (Figure 7.3)

The Glauconitic Muddy Sand Sub-unit is recovered from the upper slope and the Cape Canyon Head region (Figure 7.2). A similar sediment succession is recovered from both areas (Figure 7.1) with the Glauconitic Muddy Sand overlain by the Quartzose Muddy Sand Unit. The Glauconitic Muddy Sand was recovered from nineteen cores, collected over a range in water depths varying between 223 and 307 m, with cores recovered from both flanks of the Main Channel and from within the Northern Depression of the Cape Canyon Head Area (Figure 7.2). The lower contact with the Miocene sediments was not recovered. A single outlier, Core 349, was collected from the seaward edge of the Western Ridge. The Glauconitic Muddy Sand was not recovered in any of the cores sampled along the Northern, Central or Southern Transects. Cores 30 and 281, from the Northern Depression were selected for analysis, because these cores include both the Glauconitic Sand Sub-Unit and the Quartzose Muddy Sand Unit (Figure 7.1 and 7.2). In addition, sediment and Sr-age data are available for Cores 76, 146-148 and 349 (Compton *et al.*, 2004).

7.1.1 LITHOSTRATIGRAPHY OF THE GLAUCONITIC SAND SUB-UNIT

As the basal contact of the Glauconitic Muddy Sand Sub-unit is not recovered in any of the WMR cores, the lithostratigraphy of the Glauconitic Sand Sub-unit, which unconformably overlies the Upper Oligocene/Lower Miocene Calcareous Unit is described first.

The Glauconitic Sand Sub-unit lies unconformably above the Quartzose Glauconitic Calcareous Sand, the Glauconitic Calcareous Sand and the Foraminiferal Ooze of the Upper Oligocene/Lower Miocene Calcareous Sand Unit. The erosional contact between the Upper Oligocene/Lower Miocene Calcareous Unit sediments and overlying Glauconitic Sand Sub-unit, is marked by the well-defined Phosphorite Gravel facies. However, the contact between the Foraminiferal Ooze and the Glauconitic Sand on the outer shelf is described as gradational in the WMR core logs. The Phosphorite Gravel facies occurs at, on average, 190 cm below the sea-floor for the Quartzose Glauconitic Calcareous Sand and 170 cm below the sea-floor for the Glauconitic Calcareous Sand. The Upper Oligocene/Lower Miocene Calcareous Sand Unit may be bioturbated below the Phosphorite Gravel facies, with burrows observed 100 cm below the contact between theses two units in Core 129 (Appendix A1-29). The contact with the Upper Oligocene/Lower Miocene Calcareous Unit was only recovered in this study in two cores from the Central Transect (Cores 128 and 129), in a single core (Core 187) from the Southern Transect and in Core 324 from the Southern Rocky Plateau (Appendix A1-28, 29, 37 and 39, respectively).

7.1.1.1 PHOSPHORITE GRAVEL FACIES OF THE OUTER SHELF

The Phosphorite Gravel facies of the Central Transect varies from a slightly gravelly sand at the base of Core 129 to ~40 cm thick gravelly muddy sand lag in Core 128 (Figure 7.6). In contrast, a ~70 cm thick gravelly sand was recovered from the base of the Glauconitic Sand Unit in Core 187 from the Southern Transect and a ~20 cm muddy sandy gravel was recovered from the base of the glauconitic sand at ~37-57 cm in Core 324 (Figures 7.2 and 7.6). The thickness of the Phosphorite Gravel facies varies from a couple of centimetres to over 1 m according to the WMR core logs, with an average recorded thickness of 20-30 cm.

Although the Phosphorite Gravel facies is, on average, 170-190 m below the sediment surface, the Glauconitic Sand Unit thins out to the south (Figure 7.2) and is more condensed and gravelly over the Southern Rocky Plateau as demonstrated by the gravelly muddy sand and sandy muddy gravel of Cores 190 and 187 (Figure 7.7). In addition, many of the WMR logs record gravelly glauconitic sediments from the Southern Rocky Plateau. A number of dredges were carried out on this Southern Rocky Plateau because of the poor core recovery. The >2 mm jigged gravel-fraction of the dredge samples were examined in order to complement the available core data.

University of Cape Town

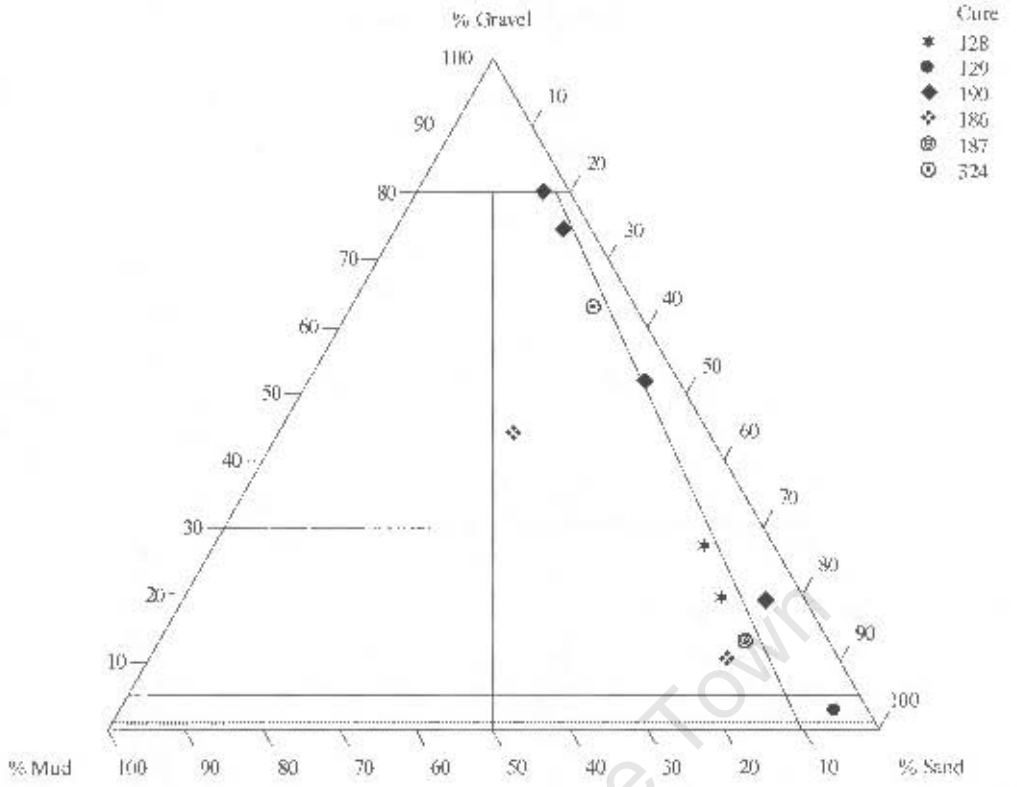


Figure 7.6. A summary of the grain size textures for the Phosphorite Gravel facies of the Glauconitic Sand Sub-unit.

University of Cape Town

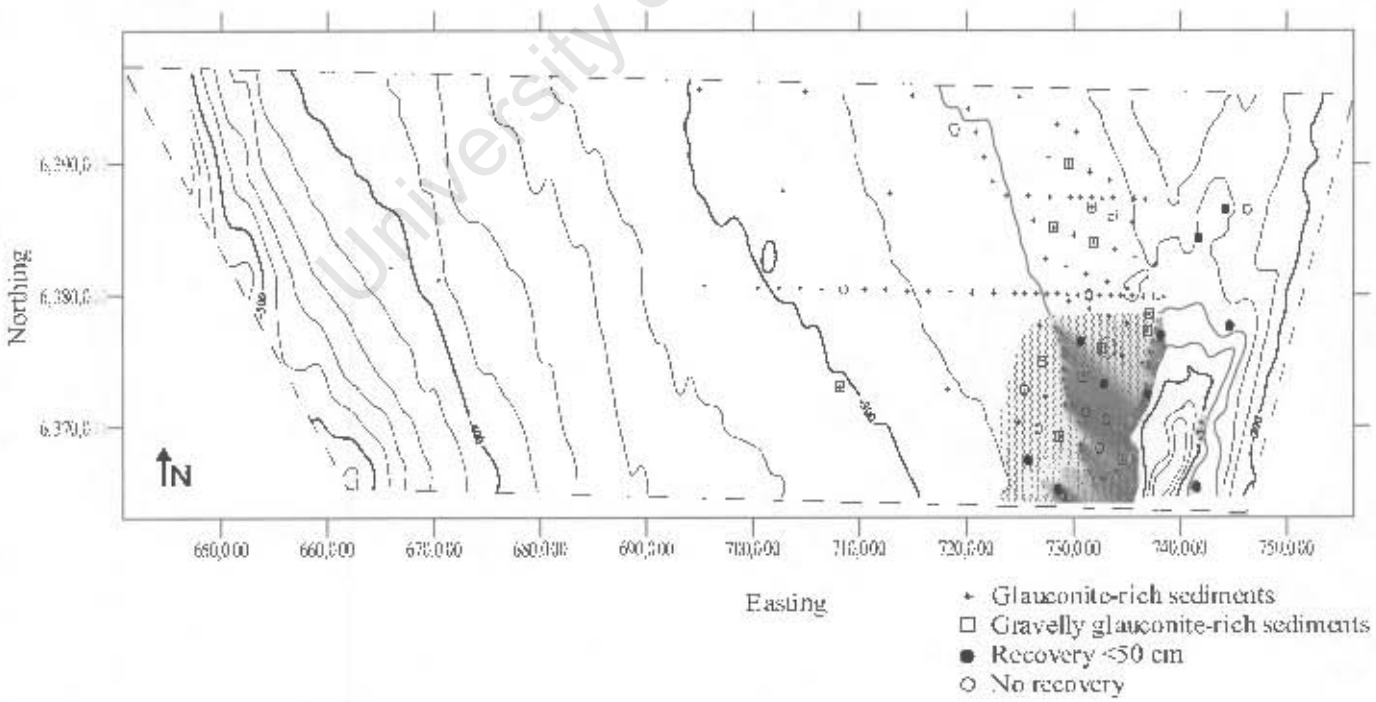


Figure 7.7. The recovery of vibrocores from the Southern Rocky Plateau (shaded area) was poor and a number of vibrocore attempts failed. The Glauconitic Sand Unit recovered from this area is gravel rich.

The gravel-fraction from the recovered Phosphorite Gravel facies is dominated by an irregularly shaped, dark brown to black phosphorite with polished surfaces and phosphatised mollusc casts. The phosphorite varies in size from granules to small cobbles, although small boulders were recovered during dredging. The irregular polished phosphorite is commonly composed of carbonate-fluorapatite (CFA)-cemented medium glauconite or phospho-glauconite sand grains with subordinate to minor amounts of very fine to coarse rounded quartz and biogenic (foraminifera) grains. The Phosphorite Gravel facies is often clast-rich with micritic limestone (partially replaced by CFA), phosphatised mollusc casts and shell fragments and quartz granules commonly observed. The phosphatised mollusc casts are predominantly bivalves, with gastropods, scaphopods, solitary coral and brachiopods also present. The mollusc casts are composed of CFA-cemented very fine quartz sand with variable amounts of foraminifera and very fine glauconite, where the phosphatised carbonate shell, enclosing the cemented casts, may also be preserved. The mollusc casts vary from being well preserved to rounded and reworked (Core 190). Quartz is the most common accessory mineral in the Phosphorite Gravel lag, although it is present in minor amounts. Quartz pebbles (and clasts) tend to be rounded and very fine to fine pebble-size and commonly have a green to brown surface coating. Rare medium quartz pebbles are present in Core 190. The gravel-fraction of the Phosphorite Gravel facies also includes variable amounts of *Pecten* and other bivalve fragments, bryozoa, brachiopod, echinoid and other shell fragments (Sample 187-3). Additional minor components of phosphorite include rare goethite-rich, micrite-cemented clasts, including medium to coarse sand-size rounded quartzose and (bivalve) shelly sands, phosphorite and Fe-rich cemented *in situ* sands, medium pebbles of pink and white granite (Core 190) and a phosphorite including an oblate Malmesbury Group shale clast (Core 190). In addition, fish and shark teeth are recovered in the gravel fraction. The Gravel Lag described in the WMR core logs also includes traces of jasper (<1 mm in Core 88 & 337), granite (<30 mm in Core 53), agate (Core 337), limestone (Core 338), sandstone and pyrite (Core 94). According to the WMR logs, the Phosphorite Gravel may occasionally be composed entirely of reworked limestone clasts of the Upper Oligocene/Lower Miocene Calcareous Unit (Cores 88 & 92). The majority of the dredge samples are dominated by irregularly shaped phosphorite pebbles and cobbles, with only minor amounts of mollusc casts present. However, mollusc casts are a subordinate component of Core 190 and Dredge Samples 4 and 5 (adjacent to Core 214 in Figure 7.2) are dominated by phosphatised mollusc casts.

Occasional bedded or layered phosphorite pebbles and small cobbles are recovered (Figure 7.8). The phosphorite layer from Core 228A is described in detail, because it summarises the features seen in all of the other layered phosphorites recovered. The photomicrograph of the thin-section of Core 228A and the close-up photomicrographs of Figure 7.9 and 7.10 clearly illustrate the characteristics of the different intervals recognised within the layered phosphorites. Micrite-cemented Quartzose Glauconitic Calcareous Sand of the Upper Oligocene/Lower Miocene Calcareous Unit, is overlain by micrite-cemented Coarse Quartz Shelly Sand, which is in turn, overlain by a CFA-cemented clast-rich Glauconitic Foraminiferal Sand. The layers are clearly separated by well-defined erosional contacts, with truncated quartz and glauconite grains preserved.

University of Cape Town

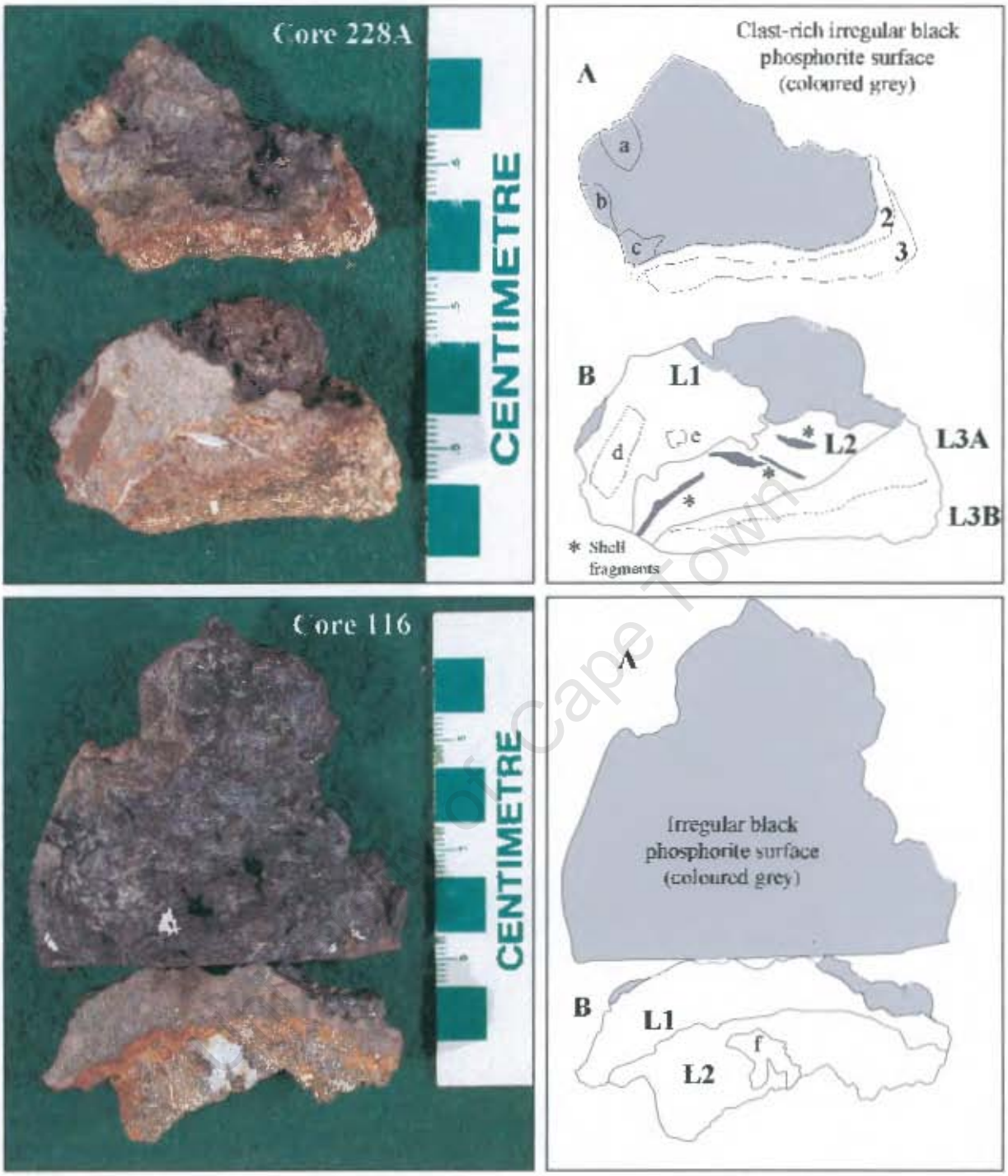


Figure 7.8. Photographs of layered phosphorite pebbles from the shoe of Core 228A and a small cobble recovered from the Glauconitic Sand facies at the base of Core 116 (Figure 7.2). The sketch on the right summarises the main features, with A showing the oblique and top views, respectively, of the black polished phosphorite surface. The cross-section (B) clearly shows the upward-younging layers, L1 (clast-rich phosphorite), L2 (Coarse Quartz Shelly Sand) and L3A (glauconite-rich) and L3B (shell and quartz -rich) limestone. The clasts include phosphatised mollusc casts (a & b) with phosphatised shell preserved (a), micrite cemented aggregates (e & f with shell fragments), laminated Fe-rich clasts (d) and a rip-up clast of B2 (e).

University of Cape Town

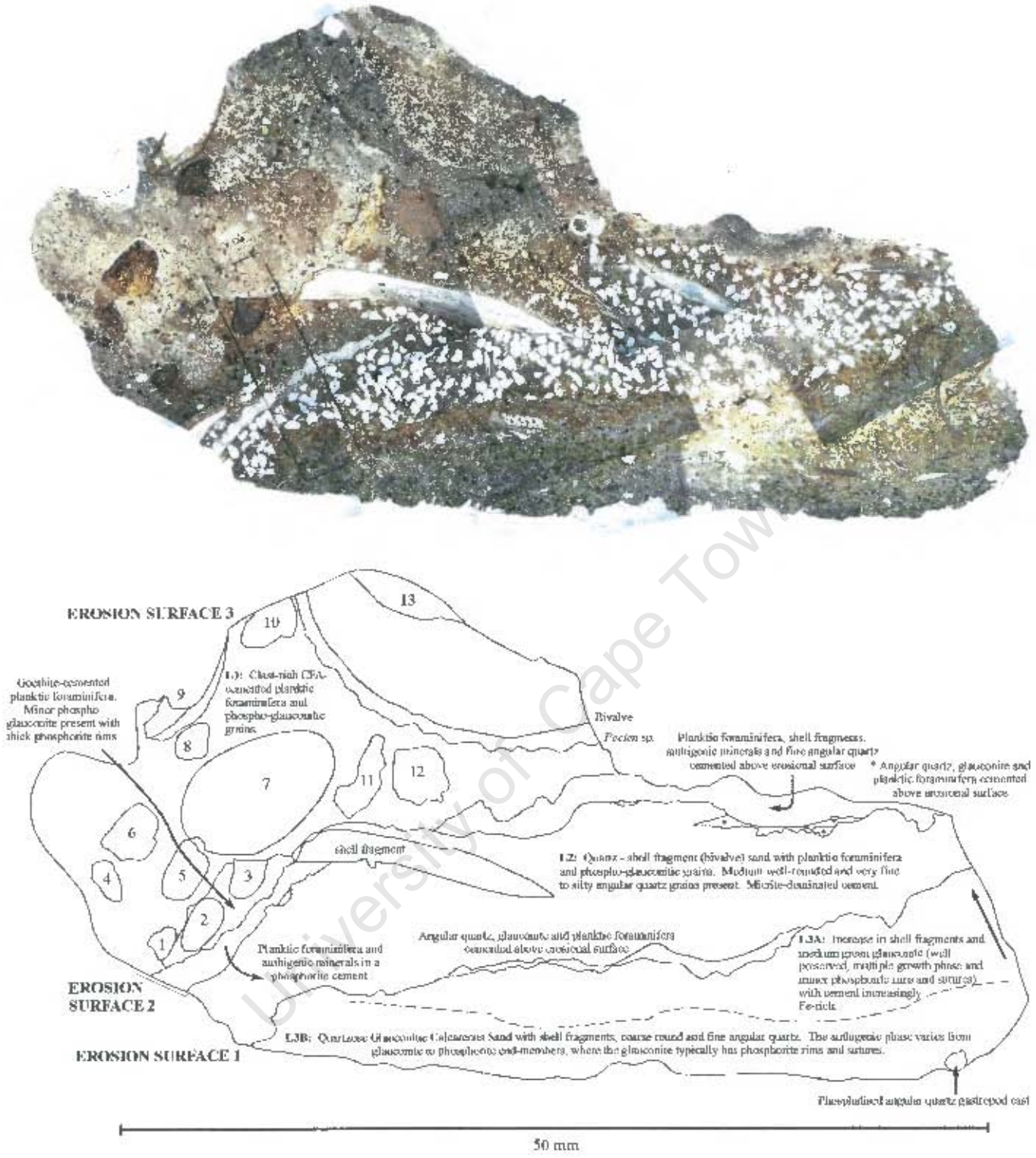


Figure 7.9. A photomicrograph of a thin-section from the layered phosphorite of Core 228A with the identified intervals and surfaces identified on the schematic sketch. A close-up of the black box is shown in Figure 7.10

A variety of rounded to well rounded clasts are present in L1, including 1, 4) Goethite-cemented planktic foraminifera (infilled with goethite), glauconite (with phosphorite rims) and minor angular very fine quartz; 2) CFA-cemented silty angular quartz, feldspar and zircon; 3) Phosphatised bone fragment; 5) Intraclasts composed of CFA-cemented medium glauconite and minor very fine quartz; 6) Laminated Fe-rich clast with angular silty quartz and trace glauconite; 7, 8) CFA-cemented planktic foraminifera (phosphatised) and minor phospho-glauconitic grains, with glauconite rimmed with phosphorite. (Clast 8 has an goethite-rich rim); 9) Bedded clast with Fe-rich rim. Medium round glauconite and quartz above phosphatised shell fragment; 10) CFA-cemented planktic foraminifera and rare silty angular quartz; 11) Phosphatised bryozoa fragment; 12) Fe-rich clast and 13) Micrite-cemented Glauconitic Calcareous limestone clast.

University of Cape Town

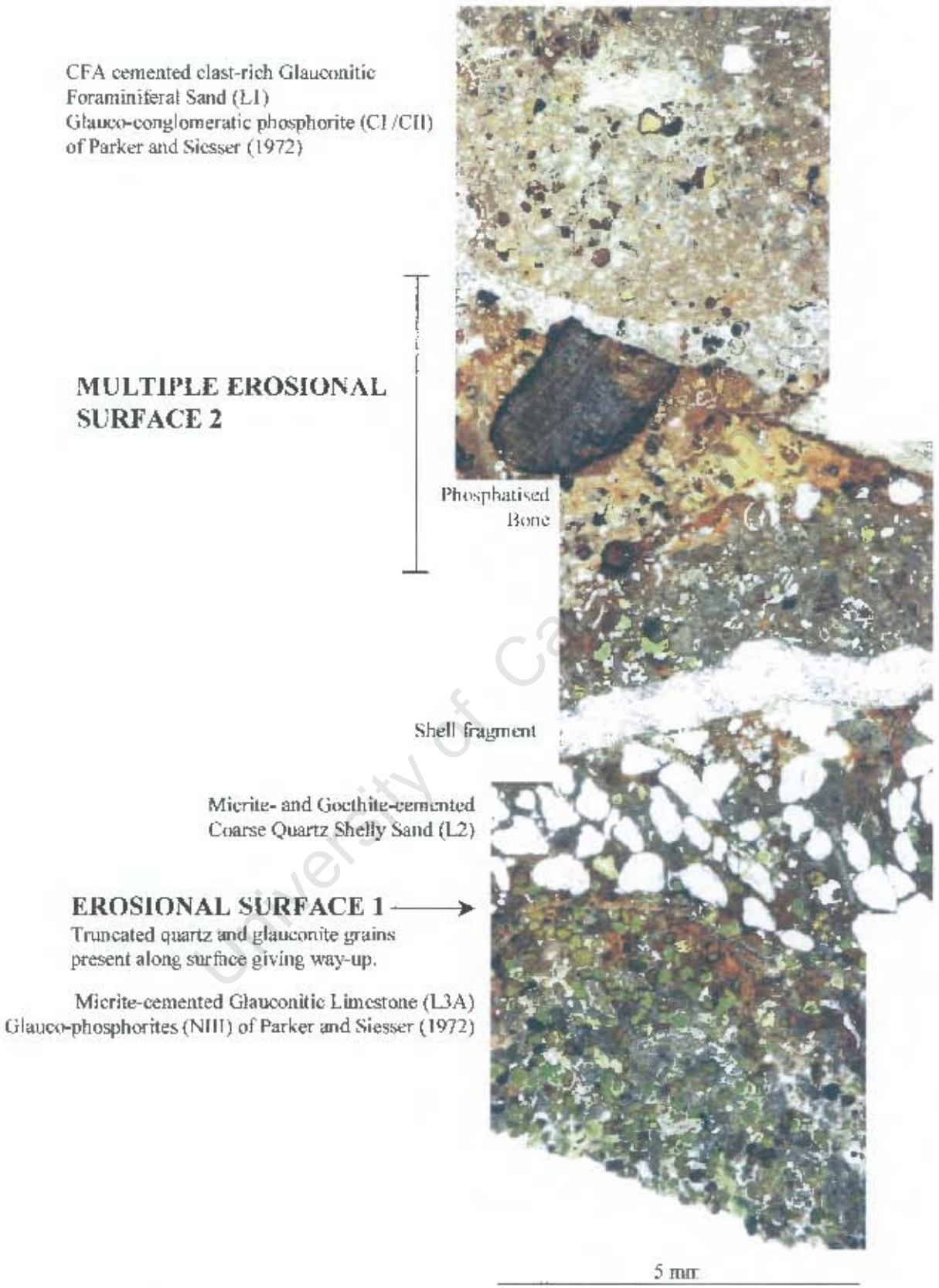


Figure 7.10. A close-up photomicrograph of the area shown as a black box in Figure 7.9 clearly illustrating the differences in compositions between erosional surfaces in the layered phosphorite of Core 228A.

University of Ca

The oldest interval (L3) can be further subdivided into two layers. The lower limestone (L3B) is composed of phospho-glauconite, foraminifera, shell fragments, coarse rounded and fine angular quartz, which closely resembles the uppermost Oligocene to Lower Miocene (Aquitanian) Quartzose Glauconitic Calcareous Sand and includes a phosphatised mollusc cast. The authigenic phase varies from glauconite to phosphorite end-members, the glauconite typically having phosphatic rims and sutures. An increase in shell fragments and medium green glauconite (well preserved, multiple growth phase and minor phosphorite rims and sutures) occurs within the upper interval L3A, where the cement becomes increasingly Fe-rich towards the contact with the Coarse Quartz Shelly Sand (layer L2).

The Coarse Quartz Shelly Sand (layer L2) interval lies above the well-defined Erosion Surface 1. This erosional surface is defined by a light-brown Fe-stained/CFA-cement and includes only minor secondary cemented surfaces (L1b in Figure 7.9), with angular quartz, glauconite and planktic foraminifera cemented above the initial erosional surface. Truncated burrows and fractured clasts, glauconite and quartz grains on the erosional surface indicate way up. The Coarse Quartz Shelly Sand (layer L2) is composed of micrite-cemented medium to coarse well-rounded to very fine silty angular quartz grains, together with bivalve shell fragments, foraminifera and authigenic grains. Although the Coarse Quartz Shelly Sand is typically micrite-cemented, phosphorite-and goethite-rich cements are observed. The Coarse Quartz Shelly Sand (L2) interval fines upwards with an increasing abundance of foraminifera, glauconite and very fine quartz.

University of Cape Town

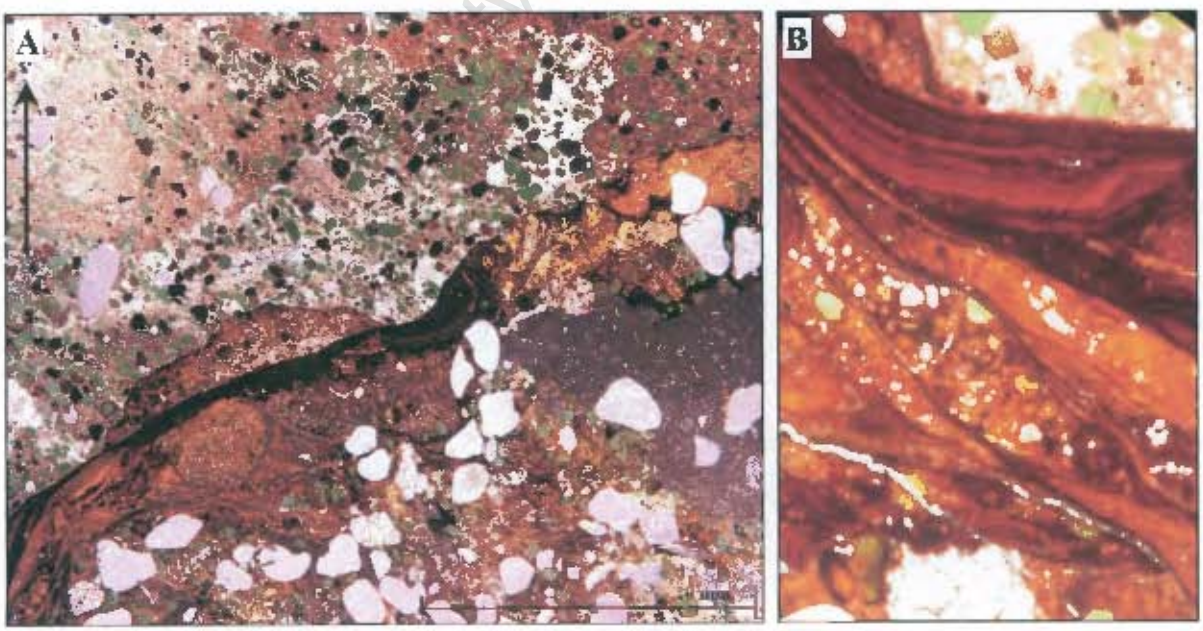


Figure 7.11. A photomicrograph of the upper erosional surface (2) above the Coarse Quartz Shelly Sand interval of the layered phosphorite from Core 116 (Figure 7.10). The younging direction is marked with a black arrow in A. The complexity of this surface is shown, with the laminations within the goethite-rich surface clearly visible in the close-up (Horizontal field of view: 1.75 mm) from elsewhere along the erosional surface (B).

The contact between the CFA-cemented clast-rich Glauconitic Foraminiferal Sand (layer L1) and the Coarse Quartz Shelly Sand (L2) is a more complex and displays a variety of small-scale internal boundaries, typical of condensed phosphates, which have undergone multiple Baturin cycles (Föllmi, 1996). The surface varies from a series of cemented, condensed, clast-rich sediments (Figures 7.9 and 7.10) to a goethite-rich laminated interval layer (Erosion Surface 2 in Figure 7.9 and 7.11), which is often associated with well-developed epibiont (trace) fossils, dominated by goethite-filled worm-tubes.

The youngest layer (L1) includes a variety of rounded to well-rounded phosphorite-cemented clasts (Figure 7.9). Planktic foraminifera (infilled with glauconite, phosphorite or rarely Fe-oxides), shell fragments (bivalves), glauconite grains, coarse and fine angular quartz are cemented in a CFA-cement with variable amounts of goethite adjacent to Erosion Surface 2. The polished surface of the phosphorite clast interval represents the third erosional surface (Figure 7.9). This clast-rich phosphorite (L1) is the most abundant phosphorite type recognised in the study area, with the sand fraction often dominated by medium glauconite.

Parker and Siesser (1972) described the phosphorites from the continental margin of southern Africa, the term *phosphorite* being defined using a convention outlined in Parker (1971), which includes all phosphate-rich rocks (>5% P_2O_5 after Birch, 1979). Parker (1971) and Parker & Siesser (1972) described conglomeratic and non-conglomeratic phosphorites dredged from the Agulhas Bank between Cape Town and Cape St. Francis. Three non-conglomeratic varieties are recognised, namely the phosphatised limestone (NI and NII – goethite-rich) and the glauco-phosphorites (NIII) and two conglomeratic phosphorites, namely the glauco-conglomeratic phosphorite (CI - NI clasts in NIII matrix) and CII (goethite-and cast-rich and glauconite-poor) conglomeratic phosphorites (Parker, 1971, 1975; Parker and Siesser, 1972). Birch (1979) noted that the phosphorites off Saldanha are compositionally similar to those of the Agulhas Bank, although they tend to be more glauconite-rich. Occasional bedded glauco-conglomeratic phosphorites are recognized on the Agulhas Bank (Parker, 1971,1975) and on the middle shelf west of Cape Town (Ndwamise, 1995). The full suite of phosphorites from the Cape Canyon closely resembles those described by Parker and Siesser (1975) and any processes invoked for the formation of the phosphorites of the southwestern Cape is most likely to be a large-scale process, involving both the southern and western margin. The layered Phosphorites of Concession 20D and elsewhere point to the importance of middle Tertiary hardground formation along the southern Africa continental margin.

The sand fraction of the Phosphorite Gravel facies is typically a moderately well-sorted fine to medium sand (Figure 7.3D). The sand fraction is composed predominantly of phospho-glauconite grains (Table 7.2), with up to 87% phospho-glauconite grains, as determined by point-counting. Subordinate to minor amounts of glauconite, very fine angular quartz and shell fragments are present. The phospho-glauconite grains are predominantly foraminiferal infillings (Chapter 9). The abundance of foraminiferal infillings is reflected in the high weight percent of the acid-soluble and semi-magnetic fractions in the samples from the Phosphorite Gravel facies of Core 128 (Figure 7.3).

University of Cape Town

Table 7.2. The composition of the Pliocene Glauconitic Sand Sub-unit and, for comparison, the Quaternary glauconite-rich sediments (in italics) of the outer shelf as determined by point-counting a minimum of 300 grains (Sample numbers in Appendix A1-28 and A1-36).

	Glauconite	Phospho-glauconite	Very fine quartz sand	Medium quartz sand	Planktic foraminifera	Calcareous fragments	Echinoid Spines	Other	
128-1	*40.5*	*11.3*	*25.8*	*0.3*	*4.9*	*16.9*	*0.3*		
128-2	*31.6*	*17.7*	*23.4*	*0.4*	*11.0*	*15.6*	*0.4*		
128-3	*37.9*	*15.8*	*15.1*	*0.3*	*18.6*	*11.3*	*0.6*	*0.3*	*Ostracods*
128-4	*33.2*	*9.0*	*20.2*	*0.4*	*12.3*	*24.5*	*0.4*		
128-5	*46.8*	*18.2*	*16.7*	*0.3*	*7.3*	*9.1*	*0.3*	*1.2*	
128-6	65.1	4.7	23.0		2.5	4.7			
128-7	65.0	10.5	21.1		0.8	2.5			
128-8	34.5	48.1	9.5	0.4		2.3		5.3	*in situ* cement
128-9	21.0	62.7	5.4			10.8			
128-10	7.9	86.6	3.1		1.4	1.0			
186-9	56.8	30.0	10.8	0.5	1.9				

The Phosphorite Gravel facies typically grades up-core into the Glauconitic Sand facies, with a decrease in amount and size of the gravel-fraction present. The decrease in the gravel component is associated with an increase in green glauconite at the expense of the phospho-glauconite foraminiferal infillings (see Sample 128-8). The increase in glauconite up-core is associated with an increase in the paramagnetic component and a decrease in the acid soluble weight percent (Figure 7.3). The grain size grades from a fine sand in the Phosphorite Gravel facies to medium sand in the Glauconitic Sand facies.

7.1.1.2 GLAUCONITIC SAND FACIES OF THE OUTER SHELF

The Glauconitic Sand facies is composed predominantly (average of 95.8 wt%) of medium grained green glauconite with subordinate amounts of very fine quartz sand and only minor biogenic grains (Figure 7.3). The glauconite grains have a distinctive appearance, with the polished grain surfaces typically fractured, with the fractured polished surfaces are partially broken off and the sugary texture of the inside of the glauconite grain is exposed (Figure 7.12).

The Glauconitic Sand facies shows considerable variation in grain size texture from a sand to a muddy sandy gravel (Figure 7.13). The composition of the sand fraction of the Glauconitic Sand facies in Core 128, as determined by point-counting, is summarised in Table 7.2. The sand fraction of the Glauconitic Sand facies is composed of approximately 65-75% glauconite, 5-10% phospho-glauconite (foraminiferal infillings), 20-25% very fine quartz and 2-5% biogenic grains. The glauconite is predominantly green, with a decrease in phospho-glauconite foraminiferal infillings up-core and an increase in black lobate glauconite grains associated with an increase in the biogenic component in the gradational contact with the overlying Calcareous Glauconitic Sand facies. The ~20% of very fine

University of Cape Town

quartz sand is subangular to angular. The biogenic component is composed of a mixture of fragmented benthic foraminifera and whole, delicate planktic foraminifera. The relatively low weight percent of acid-soluble components, with an average of 17.8% (range: 13.0-26.9%), in the Glauconitic Sand facies, reflects the low abundances of both biogenic grains and phospho-glauconite foraminiferal infillings.

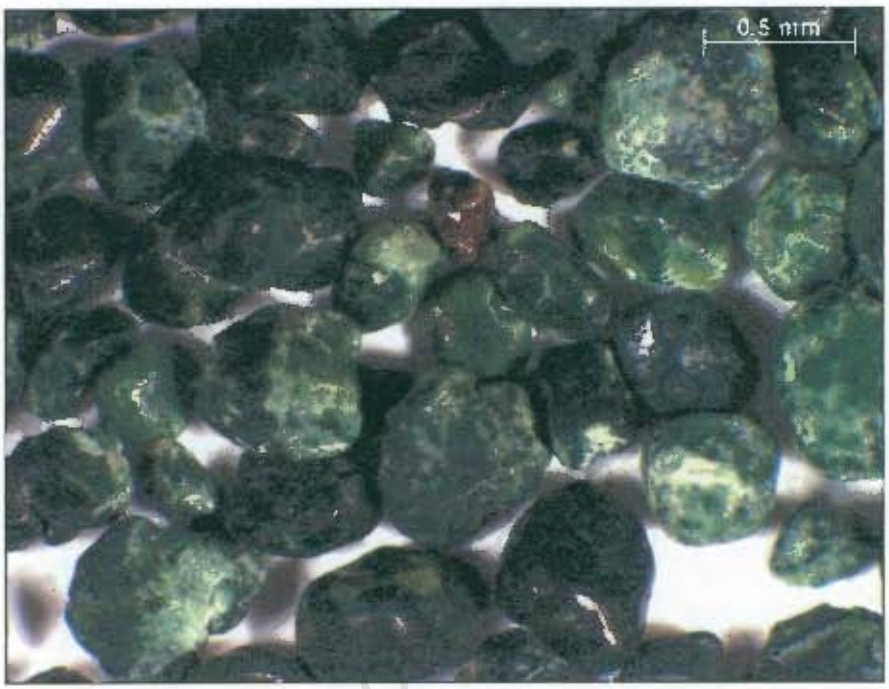


Figure 7.12. Green glauconite grains (paramagnetic fraction) of the Glauconitic Sand facies.

The Glauconitic Sand facies is typically a slightly gravelly sand (Figure 7.13), with the gravel-fraction predominantly composed of a variety of very fine to fine phosphorite and green-stained quartz pebbles. The phosphorite pebbles include CFA-cemented glauconite medium sand, cemented coarse rounded quartz grains with minor amounts of glauconite and mollusc casts of cemented very fine quartz, biogenic grains and minor glauconite. In addition, rare medium phosphorite pebbles are present, with coarse to very coarse phosphorite pebbles recovered from Samples 119-4 and 120-5. However, the gravel-fraction of the gravelly muddy sand (gmS) and sandy muddy gravel (smG) in Figure 7.13 are predominantly *in situ* cemented sand aggregates up to small cobbles in size. The medium grained glauconite sand is cemented by a light-brown cement, the sand grains being coated in a brown cement and pyrite-rich muddy aggregates are present (Figure 7.14 and 7.15). The sand fraction of Cores 119 and 120 shows typical evidence of *in situ* cementation, where the glauconite sand grains also have surface precipitates of gypsum and prismatic gypsum cemented aggregates are observed (Figure 7.14D). A SEM study of the cemented aggregates, summarised in Figures 7.14 and 7.15, shows that the cement is predominantly composed of Fe, with deeply etched pyrite cubes being common. Early diagenetic formation of siderite in marine glauconitic sediments from Alaska is common and usually occurs in suboxic (Fe-reducing) conditions associated with organic matter decomposition (Mozley and Carothers, 1992), where oxygen and carbon isotope studies of the New Jersey shelf suggest that siderites formed

within the zone of methanogenesis (Malone *et al.*, 2002). The abundance of deeply etched pyrite cubes implies a secondary post-coring oxidation reaction, resulting in gypsum formation. These Fe-rich cements need to be studied in more detail, because the presence of pyrite and siderite both imply high organic material concentrations during deposition.

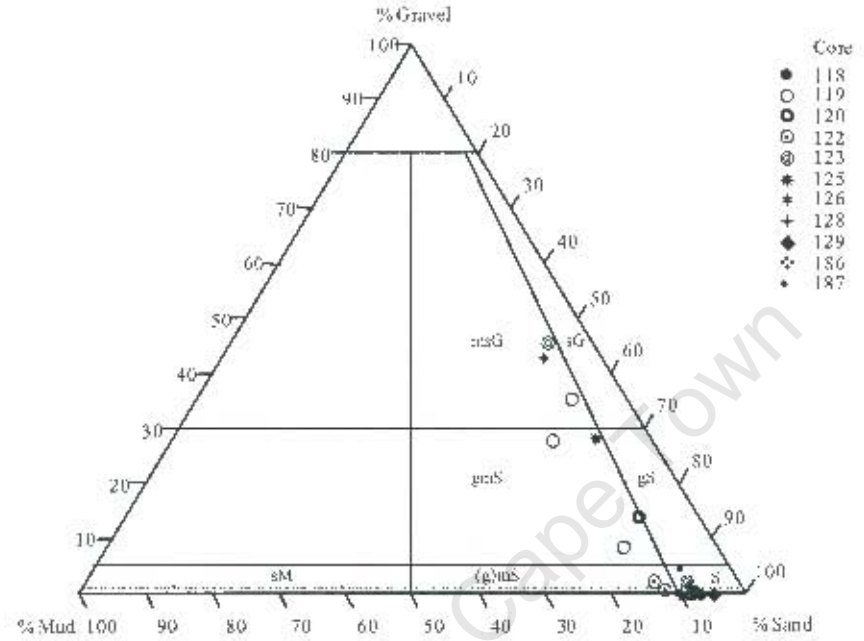


Figure 7.13. A summary of the grain size textures for the Glauconitic Sand facies.

University of Cape Town

7.1.2 LITHOSTRATIGRAPHY OF THE GLAUCONITIC MUDDY SAND SUB-UNIT

The Glauconitic Muddy Sand Sub-unit is recovered from within the Cape Canyon Head region and on the upper slope, rather than on the outer shelf, where the Glauconitic Sand Sub-unit occurs (Figure 7.2). The base of the Glauconitic Muddy Sand was not recovered and a maximum thickness of 386 cm of Glauconitic Muddy Sand was recovered from Core 28 in the Cape Canyon Head region (Figure 7.2). However, a minimum thickness of the sub-unit is estimated to be 17.5 m, where the upper contacts of the Glauconitic Muddy Sand in two adjacent Cores 404 and 78, located less than 1000 m apart, were recovered at 236.10 m and 253.62 m, respectively. The Glauconitic Muddy Sand reaches a maximum thickness of <2 m in the upper slope cores.

The Glauconitic Muddy Sand Sub-unit shows some textural and compositional variation from the proximal Cape Canyon Head region to the more distal upper slope. The Glauconitic Muddy Sand of the Cape Canyon Head region is an olive grey (5Y 4/2) muddy sand with a highly variable gravel content (Figure 7.16). The sand fraction of the proximal sub-unit is composed of variable proportions of medium green glauconite and quartz. The basal part of the Glauconitic Muddy Sand is composed predominantly of medium green glauconite sand, with approximately 77-88 wt% glauconite (paramagnetic component) in the lowermost samples from Core 30 (Figure 7.16). Trace amounts of

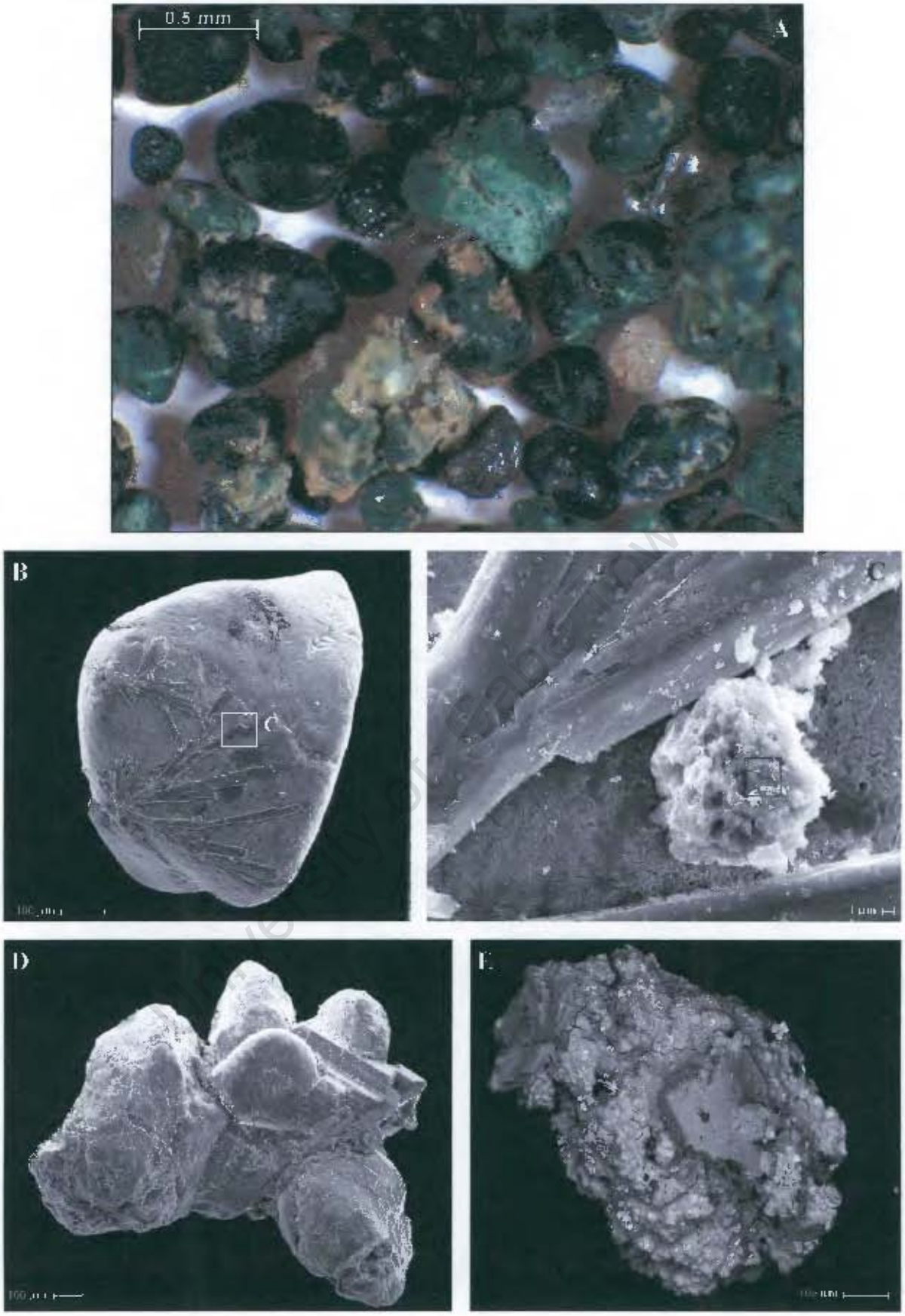


Figure 7.14. The Glauconitic Sand facies commonly has *in situ* cemented aggregates of sand, which are common near the base of Core 119. The sand fraction of Sample 119-6 (A) shows a variety of surface precipitates, dominated by bladed gypsym, on the glauconite (B & and close-up of white square in C) and commonly includes a number of prismatic gypsum-cemented grains (D) and pyrite-rich blebs (E). An EDS scan of the surface aggregate (black block in C) shows pyrite together with lesser amounts of glauconite and phosphorite between gypsum blades. The back-scatter image (E) shows the distribution of pyrite in a cemented aggregate.

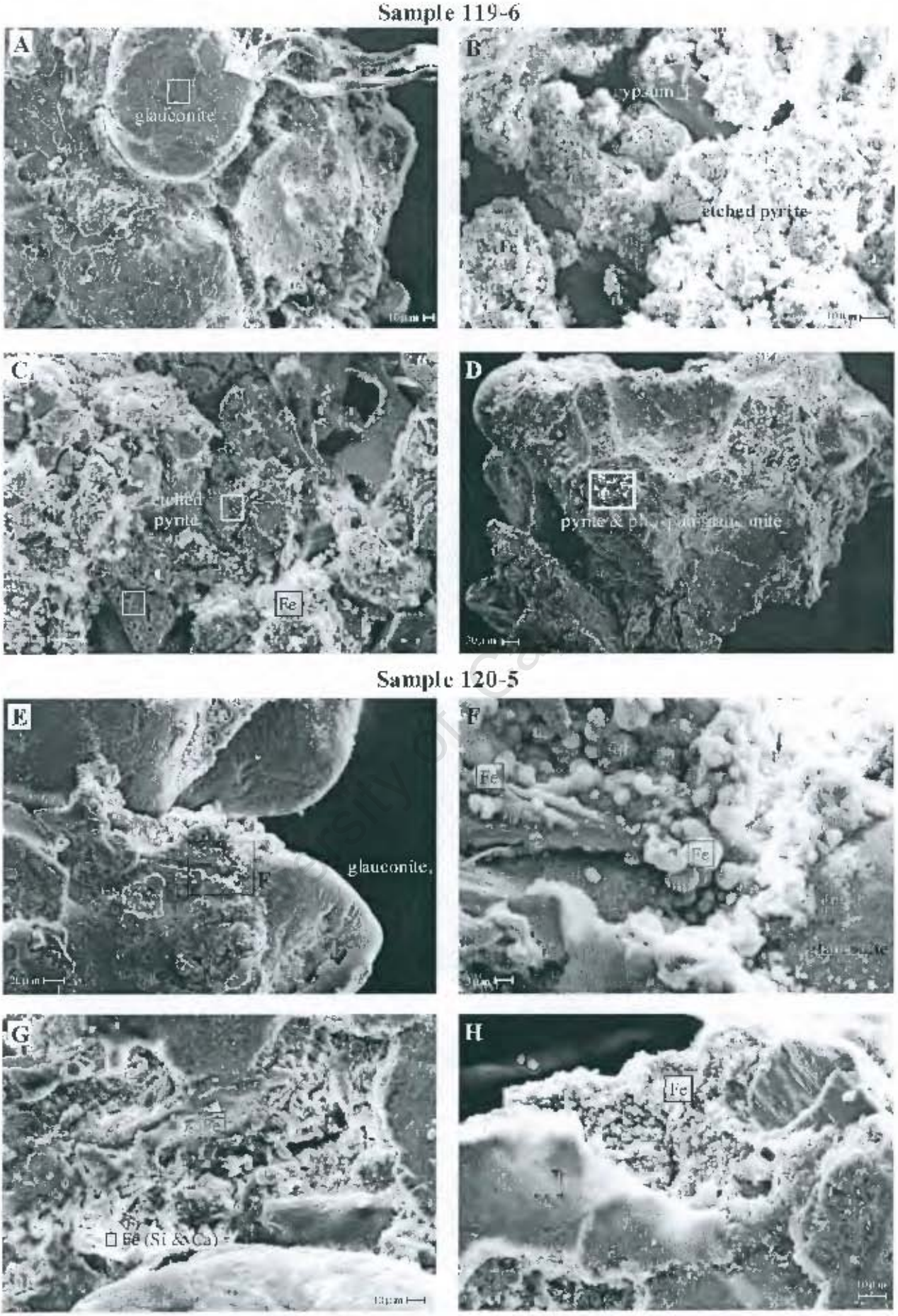
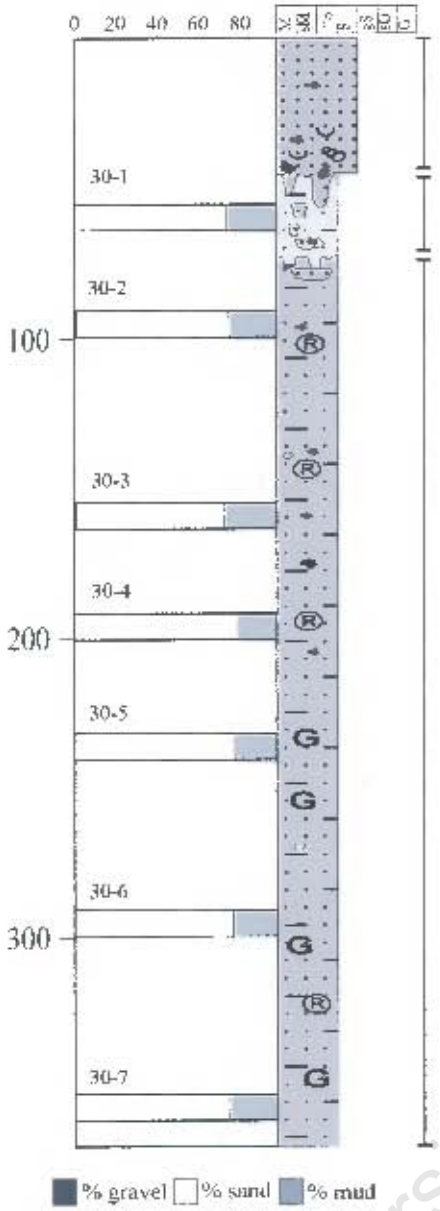


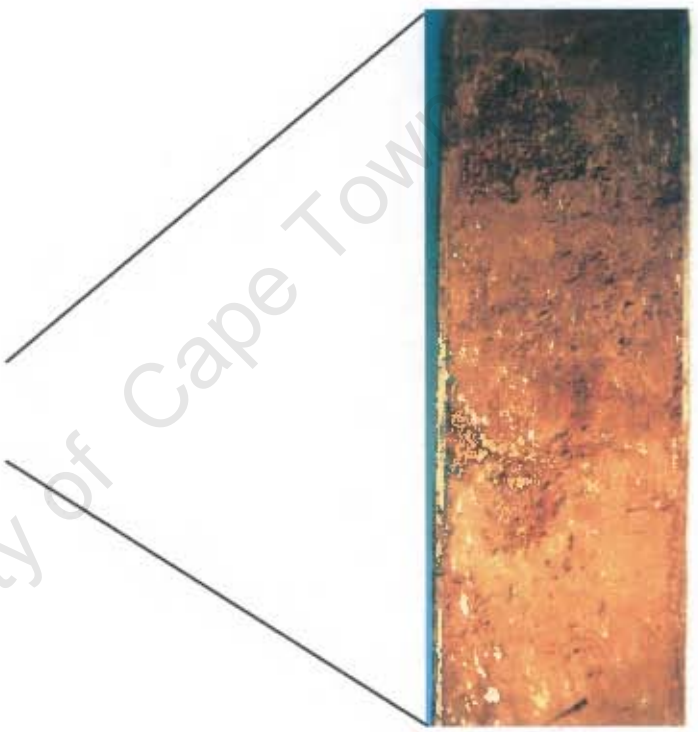
Figure 7.15. SEM images of cemented aggregates from the Glauconitic Sand facies of Cores 119 (A-D) and 120 (E-H). The composition, determined by EDS, of various demarcated components (small squares) is shown.

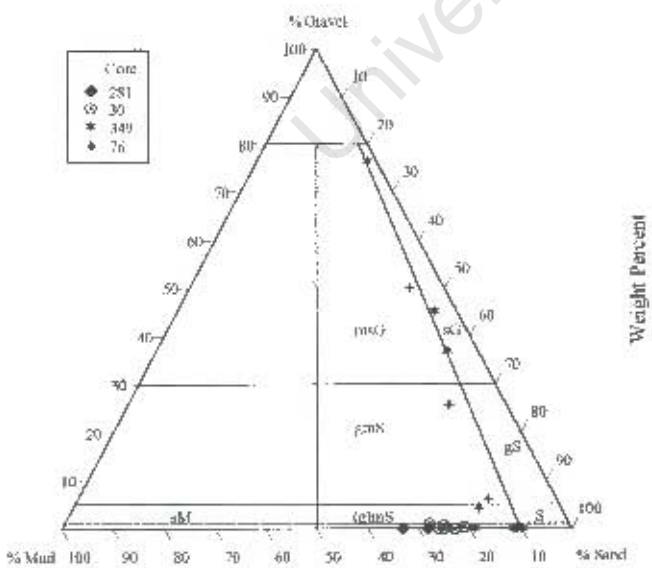


Holocene/Pleistocene veneer

Upper Pliocene extensively burrowed Quartzose Muddy Sand Unit.
99% very fine quartz
Trace sponge spicules, SPG, and gypsum

Glauconitic Muddy Sand facies
Bimodal sand composed predominantly (by weight) of green medium glauconite grains with very fine angular and medium to coarse rounded quartz and 5% gypsum. Minor components include brown-stained, poorly preserved coarse foraminifera (often associated with gypsum aggregates), pyritised wood and shell fragments, phospho-glauconite foraminiferal infillings, sponge spicules and PCG. Trace Fe-rich cemented aggregates present. Very coarse angular feldspar in Sample 30-6.





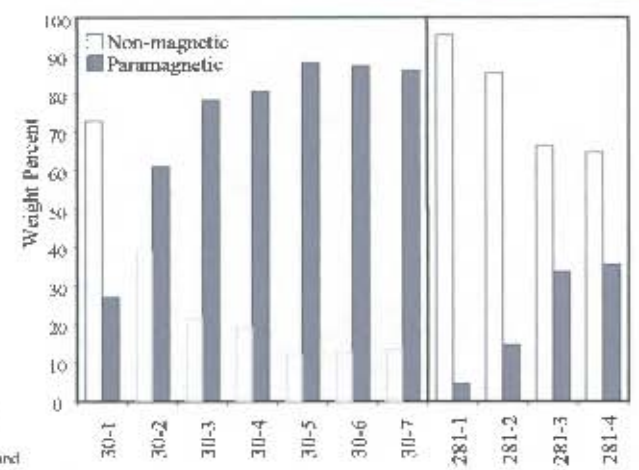


Figure 7.16. The stratigraphy of the Pliocene Glauconitic Muddy Sand Unit in Core 30. The legend for the symbols is included in Figure 3.11; glauconite abundance is shown as a grey scale. The reduced pockets and abundant post-recovery gypsum mineralization is illustrated by the white blebs in the photograph of the cut core section. The grain size textures and the weight percent non-magnetic (quartz, biogenic and phosphorite) and paramagnetic (glauconite) components of the sand fraction of the Glauconitic Muddy Sand are included.

University of Cape Town

framboidal pyrite and pyritised wood/shell fragments are included in the non-magnetic fraction. EDS analyses (not shown) of glauconite grains from Sample 30-7 show that the randomly selected glauconite grains included no CFA component (Ca- and P-free) nor evidence of foraminiferal infilling. Although the facies is dominated by glauconite, the non-magnetic components present include quartz, biogenic grains, phosphorite (including pelletal grains and SPG) and gypsum. Point-counting of Samples 30-6 and 30-7 (Table 7.3), collected towards the base of Core 30, shows that, in addition to the abundant very fine angular quartz sand component, medium to coarse quartz sand grains represent up to 3.7% of the sand fraction. Minor amounts of benthic and planktic foraminifera are present and two foraminiferal assemblages are observed. Benthic foraminiferal tests tend to be present as poorly preserved, brown-stained, etched, medium to coarse sand grains, often associated with gypsum aggregates and trace amounts of better-preserved benthic and planktic medium to fine sand size Pliocene foraminifera are also present. The gypsum in these samples is present as a white, prismatic cement of *in situ* sand grains, similar to those observed in the Glauconitic Sand facies (Figure 7.14D). Rare phospho-glauconitic foraminiferal infillings are observed in Sample 30-7, similar to those described for the lowermost parts of the Glauconitic Sand facies of the outer shelf succession.

The Glauconitic Muddy Sand facies has well-defined reduced pockets, up to 5 cm across (Figure 7.16), which tend to decrease in abundance up-core. The reduced pockets commonly include very fine to fine phosphorite pebbles. The abundance of blocky white gypsum tends to increase adjacent to the reduced pockets. The sand fraction within the reduced pockets (Sample 30-4), although similar to that described above, includes an abundance of a Fe-rich (siderite) cement coating and cementing the sand grains. The loosely cemented aggregates are associated with two types of gypsum, with both gypsum-cemented aggregates and bladed gypsum surface precipitates observed. This association of pyrite, gypsum and siderite-rich cementation of *in situ* sand is very similar to that described in the Glauconitic Sand facies of the outer shelf succession (Section 7.1.1.2).

Table 7.3. The composition (reported as the percent grain types by number) of the Glauconitic Muddy Sand and Glauconite Sand facies as determined by point-counting a minimum of 300 grains. The weight percent of the paramagnetic and non-magnetic fractions (in italics) are included for comparison.

Sample	Glauconite	Very fine quartz sand	Medium quartz sand	Foraminifera	Calcareous fragments	Sponge Spicules	Other	
Glauconitic Muddy Sand Sub-unit (% by point counting)								
30-2	23.8	75.4	0.3				0.5	gypsum
	61.0 wt% paramagnetic and 39.0 wt% non-magnetic							
30-6	45.9	48.5	3.7	0.8	0.3	0.8		
	87.2 wt% paramagnetic and 12.8 wt% non-magnetic							
30-7	47.0	47.0	3.6	1.3 (pF)	0.3	0.3	0.3	pyrite
	86.1 wt% paramagnetic and 13.9 wt% non-magnetic							
Glauconitic Sand facies of Glauconitic Sand Sub-unit (% by point counting)								
128-6	69.8	23.0		2.5	4.7			
	94.7 wt% paramagnetic; 4.4 wt % non-magnetic and 0.9 wt% semi-magnetic							
128-7	75.5	21.1		0.8	2.5			
	94.5 wt% paramagnetic; 4.6 wt % non-magnetic and 0.9 wt% semi-magnetic							

University of Cape Town

In contrast to the basal samples, the upper parts of this facies (Samples 30-2 and 30-1, 281-1 and 281-2) include significantly more quartz (Figure 7.16). The quartz is predominantly very fine sand with only traces (~1%) of medium to coarse quartz. The glauconite in the upper parts (Samples 30-2 and 30-1) is fine grained, and fractured, with a sugary internal texture and a distinct Pliocene foraminiferal assemblage (subsequent section). Although worn, etched, brown-stained larger benthic foraminifera are present, planktic foraminifera are absent or present in only trace amounts. Sample 30-1 also includes abundant and varied Pleistocene microfossils downworked by bioturbation of the overlying Pleistocene sediment (Figure 7.16). Phosphatised fish bone fragments are present in minor to trace amounts.

Very fine to fine pebbles of phosphorite and quartz are scattered throughout the proximal sub-unit. The gravelly texture of the samples from Cores 76 and 349 reflects a bias in sampling, with a focus on these scattered phosphorite pebbles, where the gravelly nature of Core 76 may, in part, be due to Pleistocene bioturbation (Compton *et al.*, 2004). The gravel-fraction of the samples analyzed included a variety of phosphorite granules, including mollusc casts and CFA-cemented glauconite medium sands, with traces of coarse rounded quartz and Fe-rich-/micrite-cemented *in situ* sand. The WMR core logs describe a 3 cm granite pebble at 360 cm in Core 349 and a 5 cm wood fragment at 207 cm in Core 232A. The mud-fraction (<63 µm) of the proximal Glauconitic Muddy Sand is dominated by quartz, calcite, and feldspar with kaolinite, glauconite/illite (a non-expandable 10 Å sheet silicate) and minor gypsum present (Figure 7.17). Sample 30-4, collected from within a reduced pocket, has a significantly different mud composition with pyrite, but not calcite, present. A number of small peaks around 15-18 °2-Theta are interpreted as oxidation products including Fe-chloride and -sulphate salts.

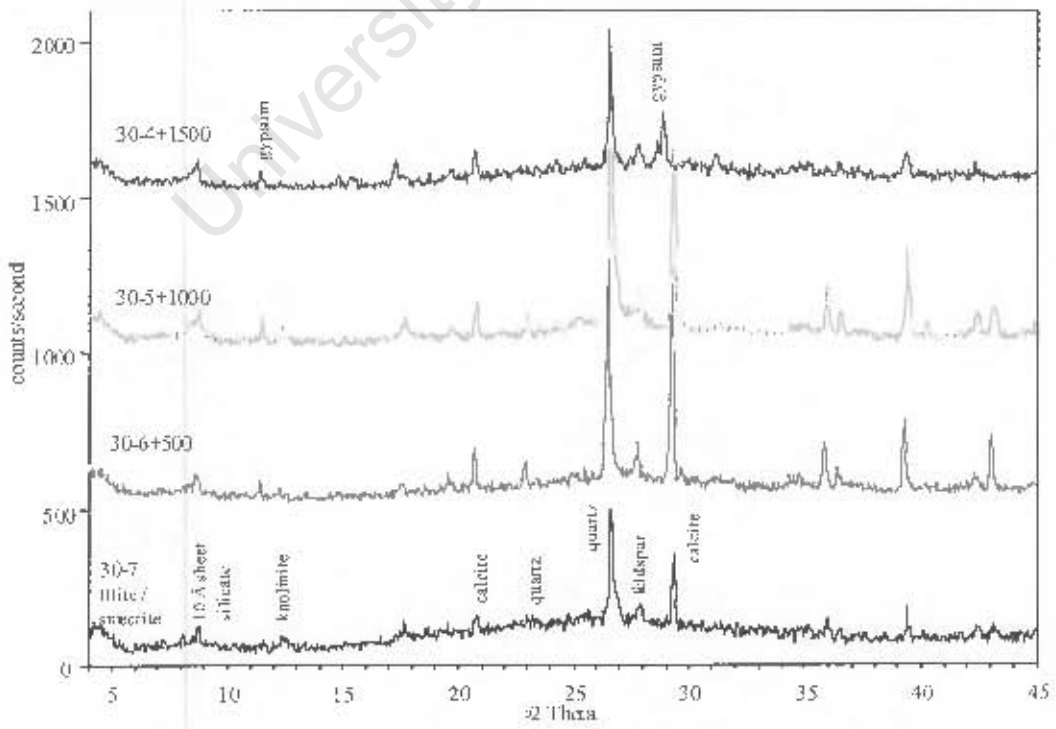


Figure 7.17. A summary of the XRD records for the mud fraction (<63 µm) of the Glauconitic Muddy Sand facies of Core 30.

University of Cape Town

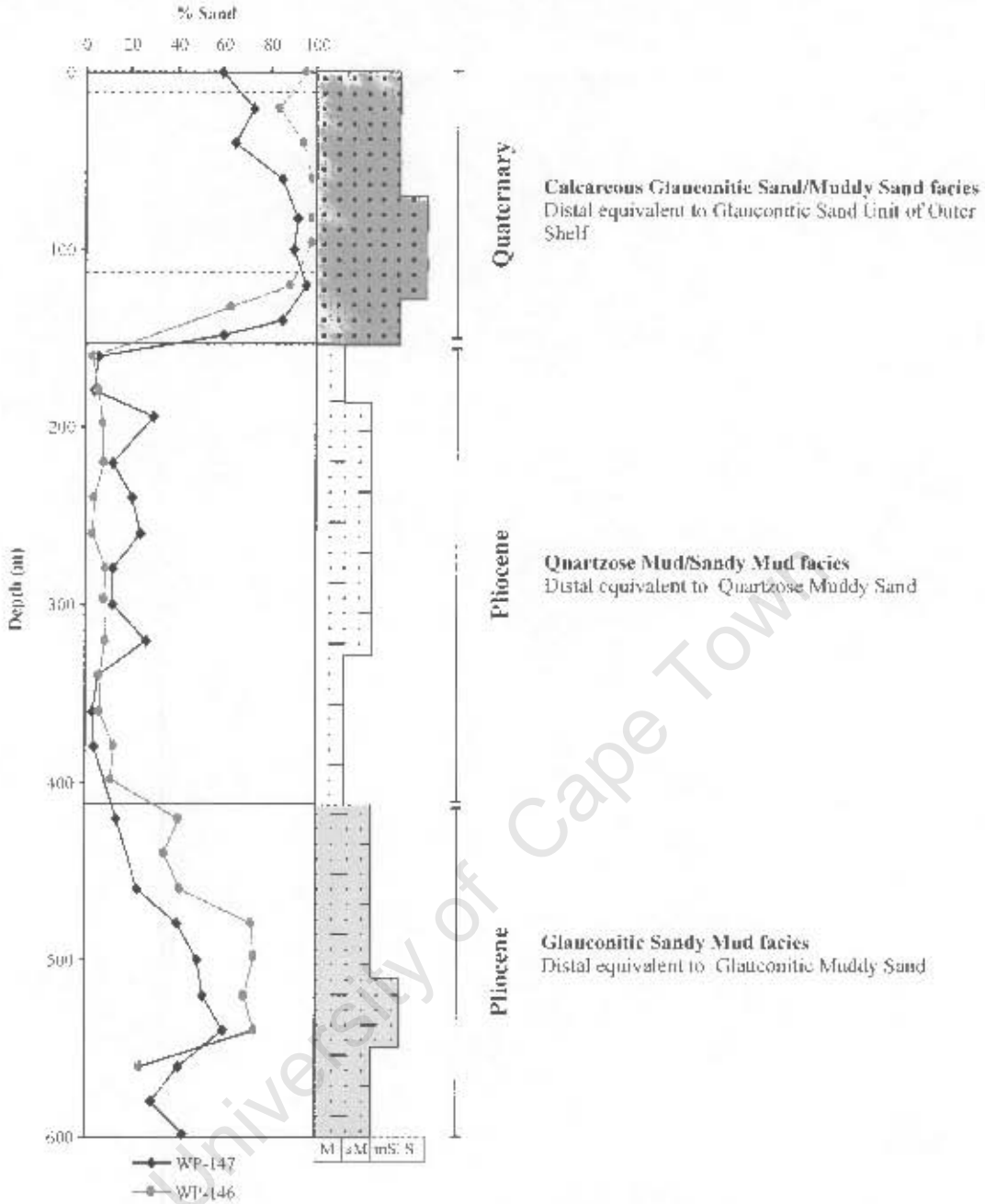


Figure 7.18. The percent sand and stratigraphy of the two upper slope Cores 146 and 147.

The basal Glauconitic Muddy Sand Sub-unit recovered from the upper slope cores (Figure 7.2) varies between a sandy mud and muddy sand (Cores 146 and 147) (Figure 7.18). The sand fraction of this distal sub-unit is composed of variable amounts of quartz and glauconite together with a typical Pliocene foraminiferal assemblage (Figure 7.18). The base of the distal Glauconitic Muddy Sand of Core 146 is composed of approximately 50% green glauconite, 40% very fine angular quartz, 5% foraminifera, 3% mixed phospho-glauconite and 2% phosphorite. The foraminifera include delicate and well-preserved Pliocene benthic species, some of which are brown-stained and broken from 480-540 cm core depth. An increase in quartz up-core is associated with a decrease in glauconite abundance and by the top of the lower Glauconitic Muddy Sand Sub-unit, the sand fraction is dominated by quartz (50%) with subordinate foraminifera (30%) and glauconite (20%). The Glauconitic Muddy Sand Sub-unit of Core 147 is dominated by 80% very fine angular quartz with 15% fine authigenic grains (green to black

University of Cape Town

glauconite and phosphorite in approximately equal proportions) and 5% foraminifera, including broken Pliocene species. The relatively high quartz content of the upper slope Glauconitic Muddy Sand Sub-unit suggests that these sediments are distal equivalents of the uppermost gradational interval of the more proximal sediments.

7.2 QUARTZOSE MUDDY SAND UNIT

The Quartzose Muddy Sand Unit was recovered from ninety cores collected from the Cape Canyon Head region in water depths ranging from 192 to 357 m and was also recovered in the five upper slope cores (Figure 7.2). The Quartzose Muddy Sand has a widespread distribution in the landwards (eastern) parts of Concession 20D and is found on the Western Ridge and Southern Rocky Plateau, on the Eastern and Western Flanks of the Cape Canyon Head Area and from within the Northern Depression and the Main Channel of the Cape Canyon (Figure 7.19). The interpreted CHIRP high-resolution seismic section (Chapter 3) shows that the Pliocene Quartzose Muddy Sand crops out seawards of the unlithified Cretaceous sedimentary basement high below the Western Ridge. The Quartzose Muddy Sand was recovered in the cores sampled along the Northern, Central or Southern Transects as well as in Cores 30, 279, 281 and 284 from the Northern Depression of the Cape Canyon Head. In addition, sediment and Sr-age data were available for Cores 19, 26, 73, 146-148 and 322 (Compton *et al.*, 2004).

7.2.1 Lithostratigraphy of the Quartzose Muddy Sand Unit

The basal contact of the Quartzose Muddy Sand Unit with the underlying Glauconitic Muddy Sand Sub-unit was recovered in Cores 30, 52, 174, 281 and 391 in the Cape Canyon Head and in the upper slope cores. The contact between the two facies is poorly defined and varies from sharp to gradational. The contact in Cores 30 and 281 is bioturbated with fine (mm scale) burrows of quartz-rich sand included into the upper 10-15 cm of the underlying Glauconitic Muddy Sand Sub-unit, although the contact in Core 30 is obscured by coarser late Pleistocene large-scale burrows filled with Glauconitic Quartzose Sand (Figure 7.16). In Cores 174, 52 and 392 and the upper slope Cores 146-148 the contact is gradational. The upper boundary of the Glauconitic Muddy Sand facies was taken where quartz rather than glauconite is the dominant component of the sand fraction and by the absence of reduced patches and associated gypsum surface precipitates.

The Quartzose Muddy Sand Unit shows some textural variation from the proximal Cape Canyon Head region to the more distal upper slope, similar to that described for the Glauconitic Muddy Sand Sub-unit. The proximal Quartzose Muddy Sand is a light olive grey to pale olive coloured (5Y 6/2 to 5Y 6/3) sediment that varies in thickness from 10 to 495 cm. The Quartzose Muddy Sand Unit generally lacks primary or secondary sedimentary structures. However, laminae of clean quartz sand occur in places (Figure 7.20A) although they are more commonly poorly developed (Figure 7.20B) or obscured by fine-scale to wispy bioturbation (Figure 7.20C). The proximal Quartzose Muddy Sand Unit varies from a sand to a sandy mud, but muddy sand is dominant (Figure 7.21). The sand fraction is composed predominantly of angular to subangular very fine quartz with an average of 91.5 wt% non-magnetic

University of Cape Town

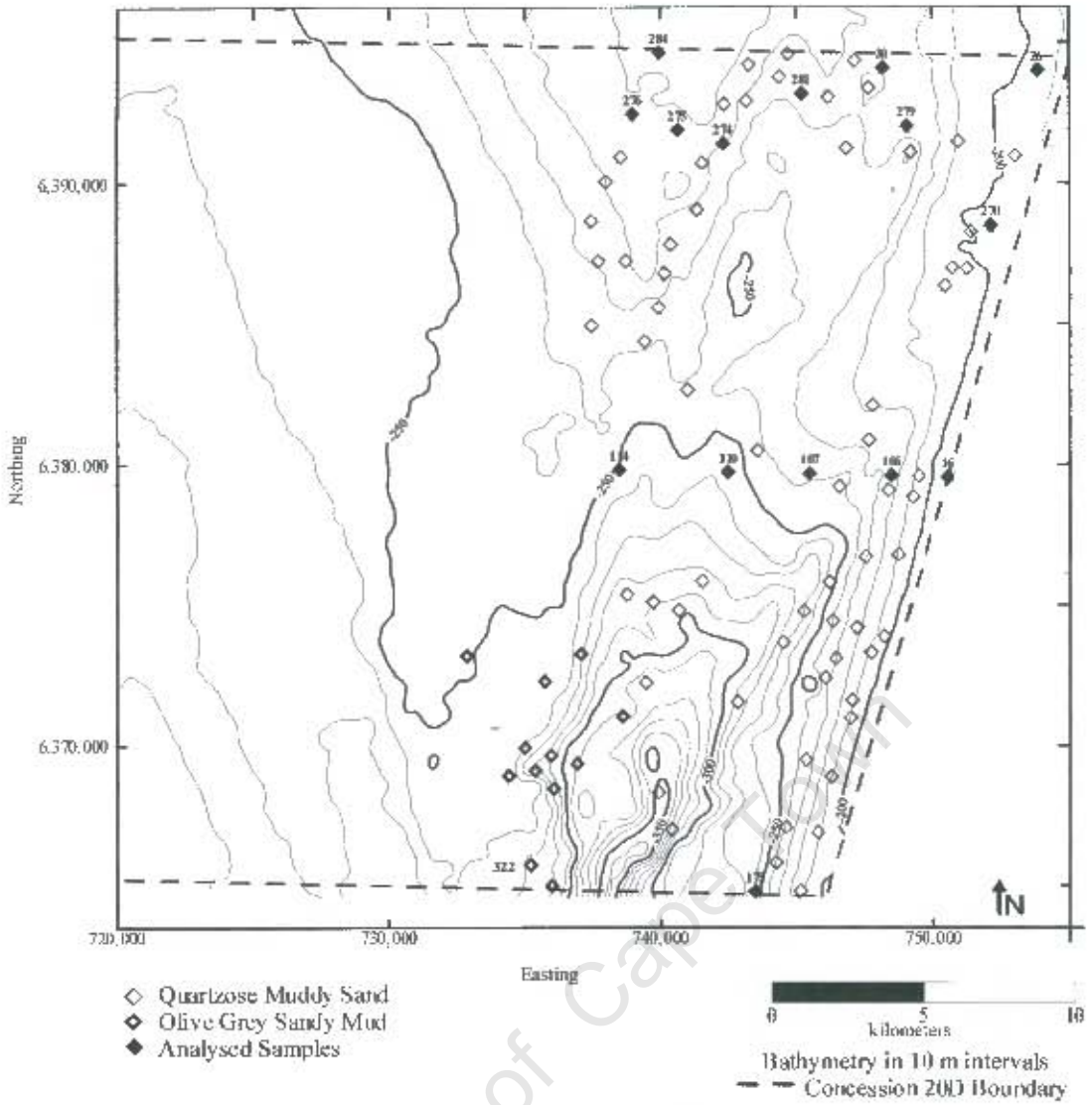


Figure 7.19. The distribution of the Quartzose Muddy Sand Unit in the Cape Canyon Head Area.

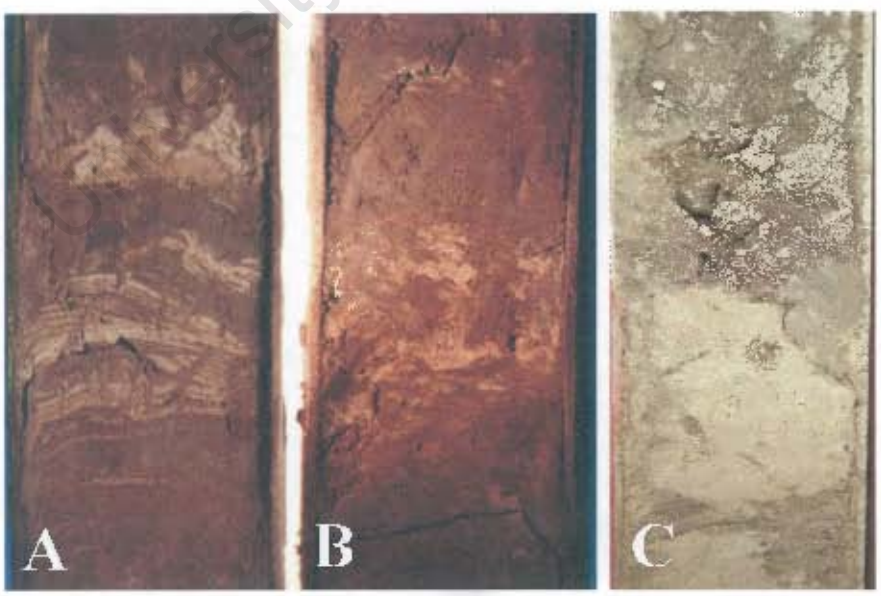


Figure 7.20. Core photographs of the Quartzose Muddy Sand Unit (core width ± 8.25 cm).
A: Well developed laminations, which are slightly bioturbated, reflecting variations in the mud content at ~100 -115 cm in Core 279.
B: Unusually well-defined example of the bioturbated texture observed in the Quartzose Muddy Sand Unit at ~45-60 cm in Core 279.
C: The bioturbated contact at 31 cm between the Quartzose Muddy Sand Unit and basal gravel lag of the overlying Pleistocene Glauconitic Quartzose Sand in Core 274.

University of Cape Town

fraction, which for the majority of analysed samples is composed of >95 wt% quartz (Figures 7.22 and 7.23). Grain-size analysis of the acid-leached sand fraction of a number of samples from across the concession area (Figure 7.24) shows that the quartz sand is a remarkably uniform, well to very well sorted, very fine sand with a bimodal grain size distribution. The dominant population has a mean mode of 3.19 ϕ (110 µm), the second smaller population having a mean of ±3.8 ϕ (72 µm) (Figure 7.24). Minor to trace components include very fine to medium glauconite, medium to very coarse, often glauconite-coated, sub- to well-rounded quartz grains, sponge spicules (often pyritised), foraminifera (predominantly benthic), echinoid spines and white gypsum cemented aggregates. Trace amounts of sand-size SPG (bones and teeth) are also present. The low wt% $CaCO_3$ of <5% (Figure 7.25) in this facies reflects the low abundance of calcareous microfossils and shows no consistent variation within or between cores. Sample 270-6 was submitted to S. de Villiers for palynological analysis, but it contained no palynomorphs. In contrast to the proximal Quartzose Muddy Sand Unit of the Cape Canyon Head region, the distal Quartzose Muddy Sandy Unit of the upper slope cores varies between a mud and a sandy mud (Figure 7.18). The sand fraction is similarly dominated by very fine angular quartz (90%) with minor foraminifera and glauconite.

The mud-fraction (<63 µm) is predominantly a quartzose silt, with feldspar (plagioclase more abundant than alkali feldspar), calcite, a non-expandable 10 Å sheet silicate and kaolinite (Figure 7.26). The XRD patterns show little variation either up-core or among cores in the composition of the mud-fraction from the three transects. The Quartzose Muddy Sand is typically gravel-free, but vertebrate bone fragments up to ±2 cm in size were recovered from Cores 274 and 284 and rarely preserved fine pebble-sized articulated brachiopod shells were recovered from Core 175 (species unknown; J. Pether, *pers. comm.*, 2003). The Quartzose Muddy Sand Unit varies from being barren of macrofauna to having very fragile, worn and bleached bivalve fragments sparsely scattered throughout according to the WMR core logs. A 4 cm-thick shell layer, composed of small worn and partially dissolved bivalves, is described in the WMR core logs at 146 cm in Core 71.

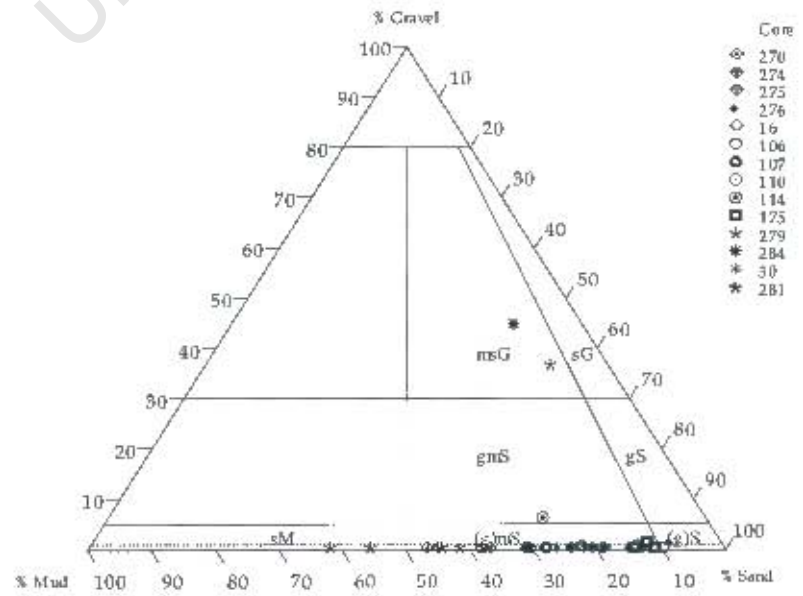


Figure 7.21. A summary of the Quartzose Muddy Sand grain size textures.

University of Cape Town

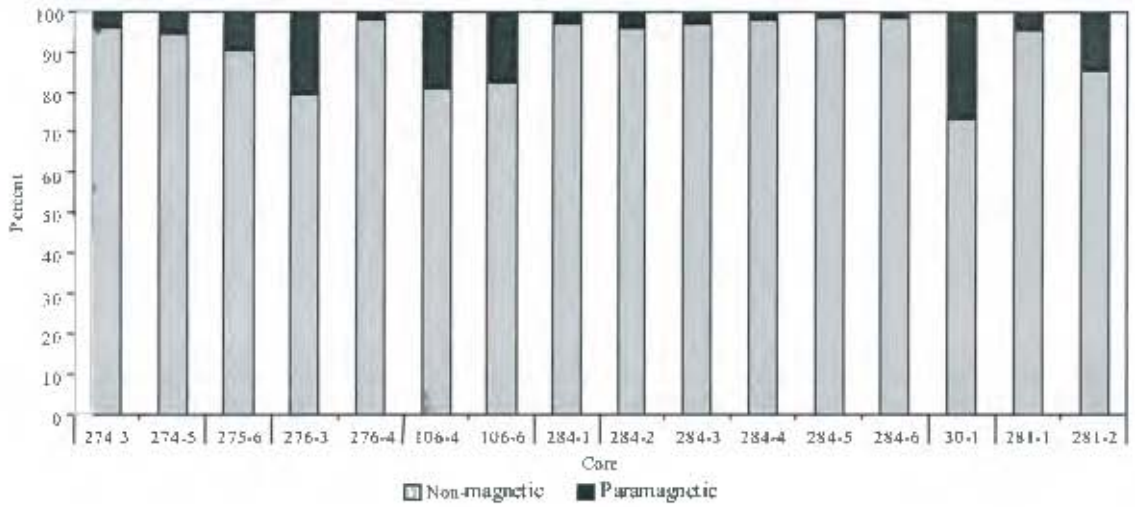


Figure 7.22. A summary of the paramagnetic (glauconite) and non-magnetic (quartz, phosphorite and foraminifera) weight percent present in the sand fraction of the Quartzose Muddy Sand.

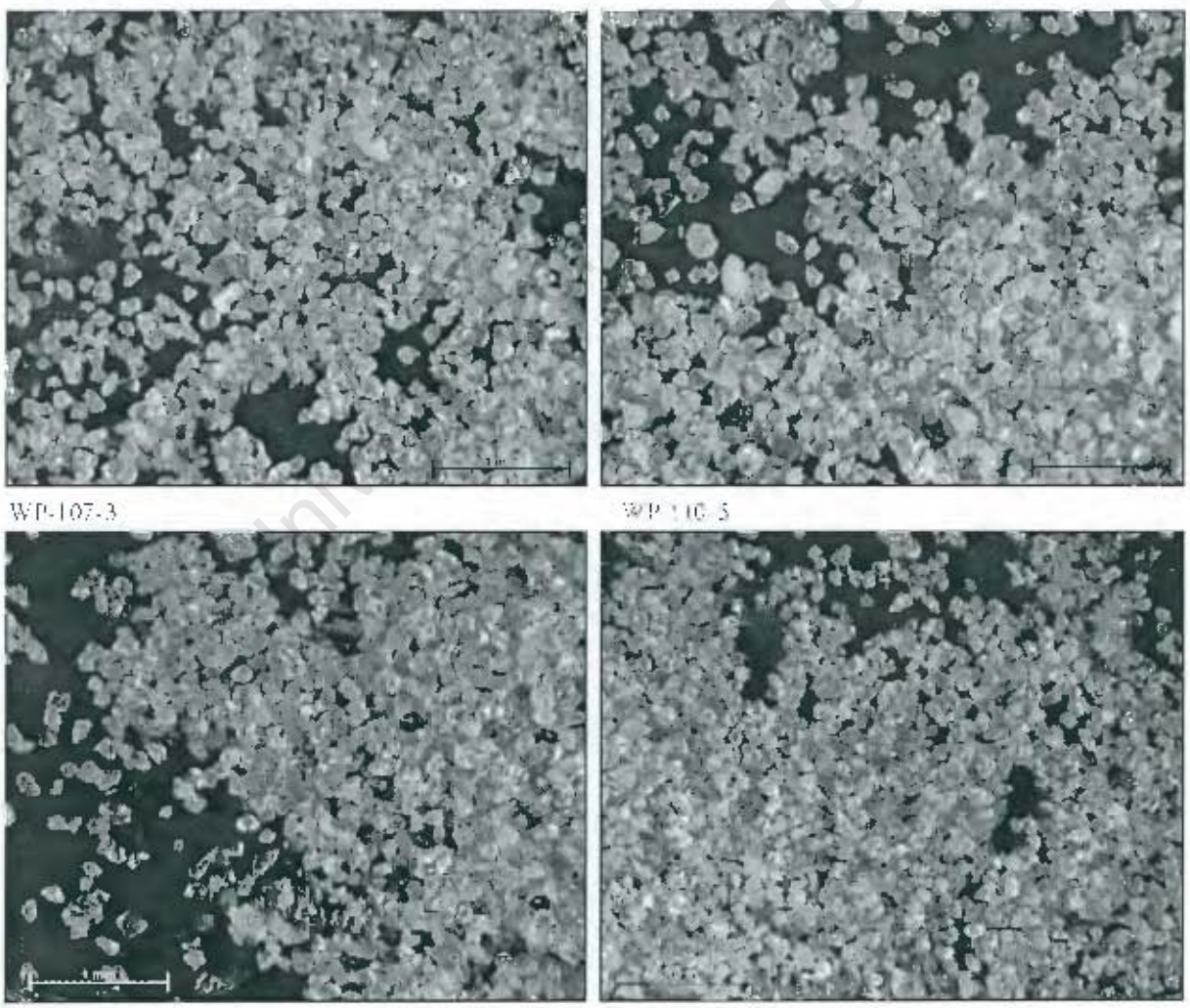


Figure 7.23. The sand fraction of the Quartzose Muddy Sand, composed primarily of very fine grained quartz.

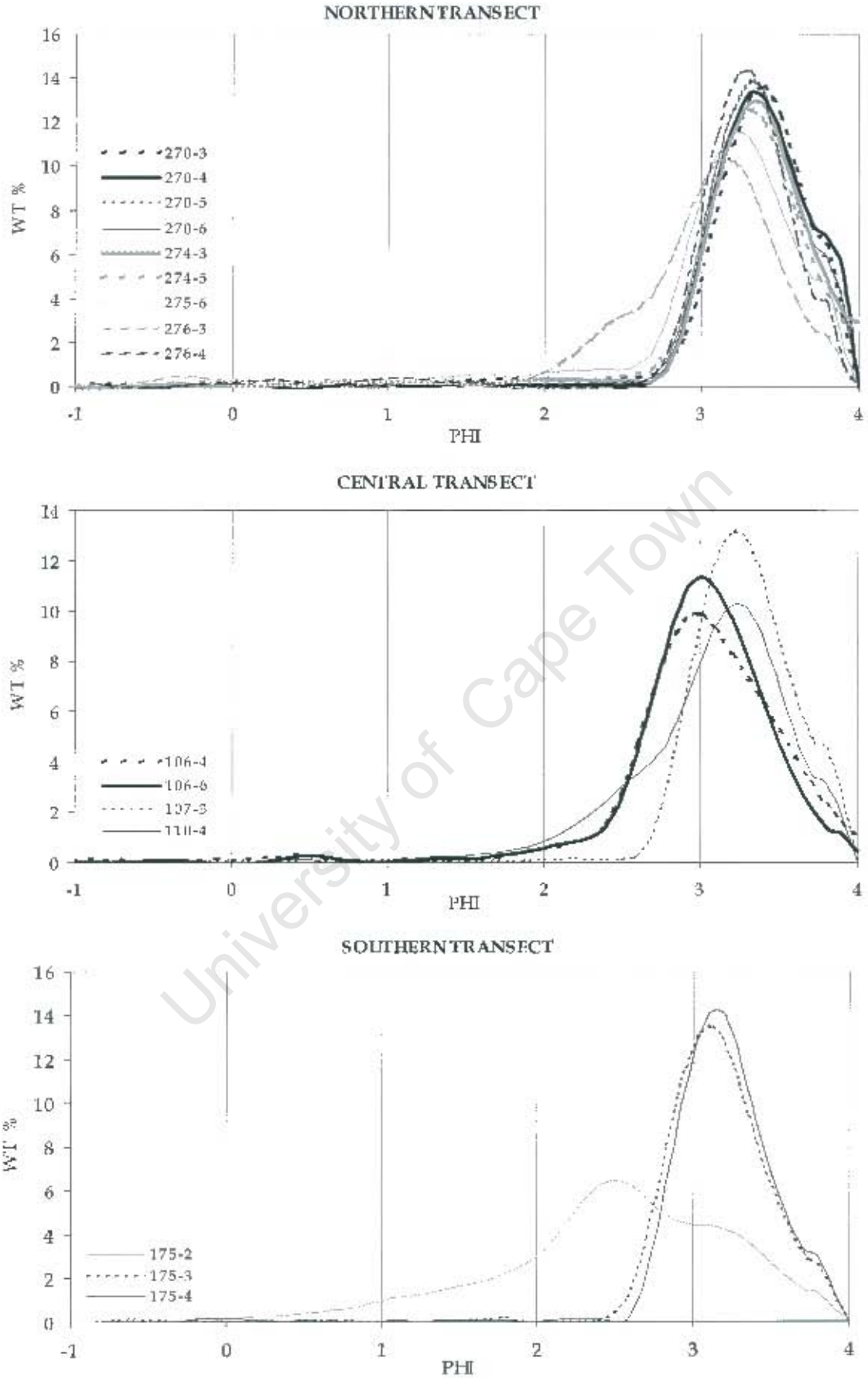


Figure 7.24. Frequency curves showing the particle-size distribution of the sand fractions of the Quartzose Muddy Sand Unit from the Northern, Central and Southern Transects. Sample locations indicated on Figure 7.19.

University of Cape Town

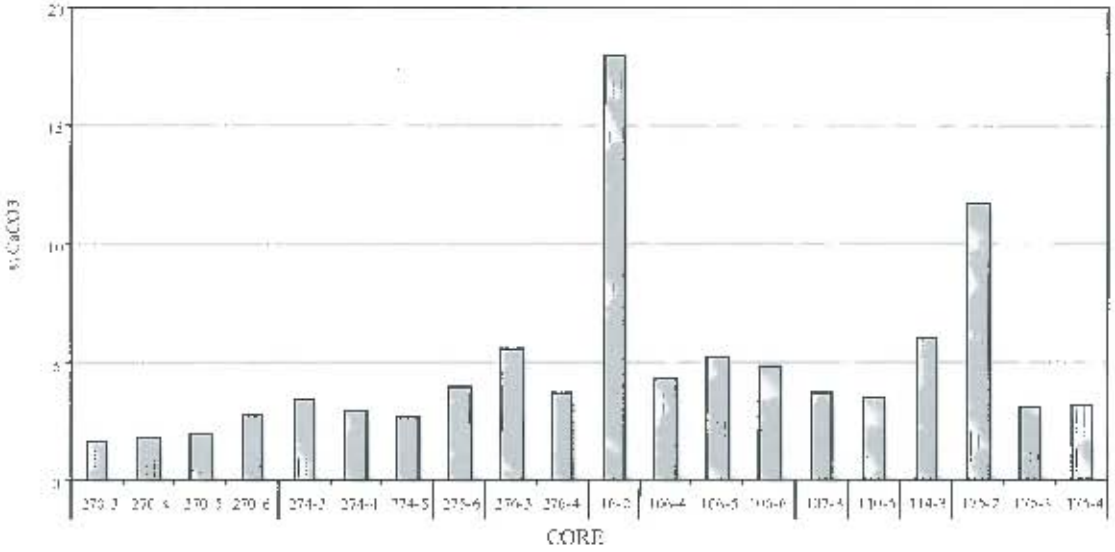
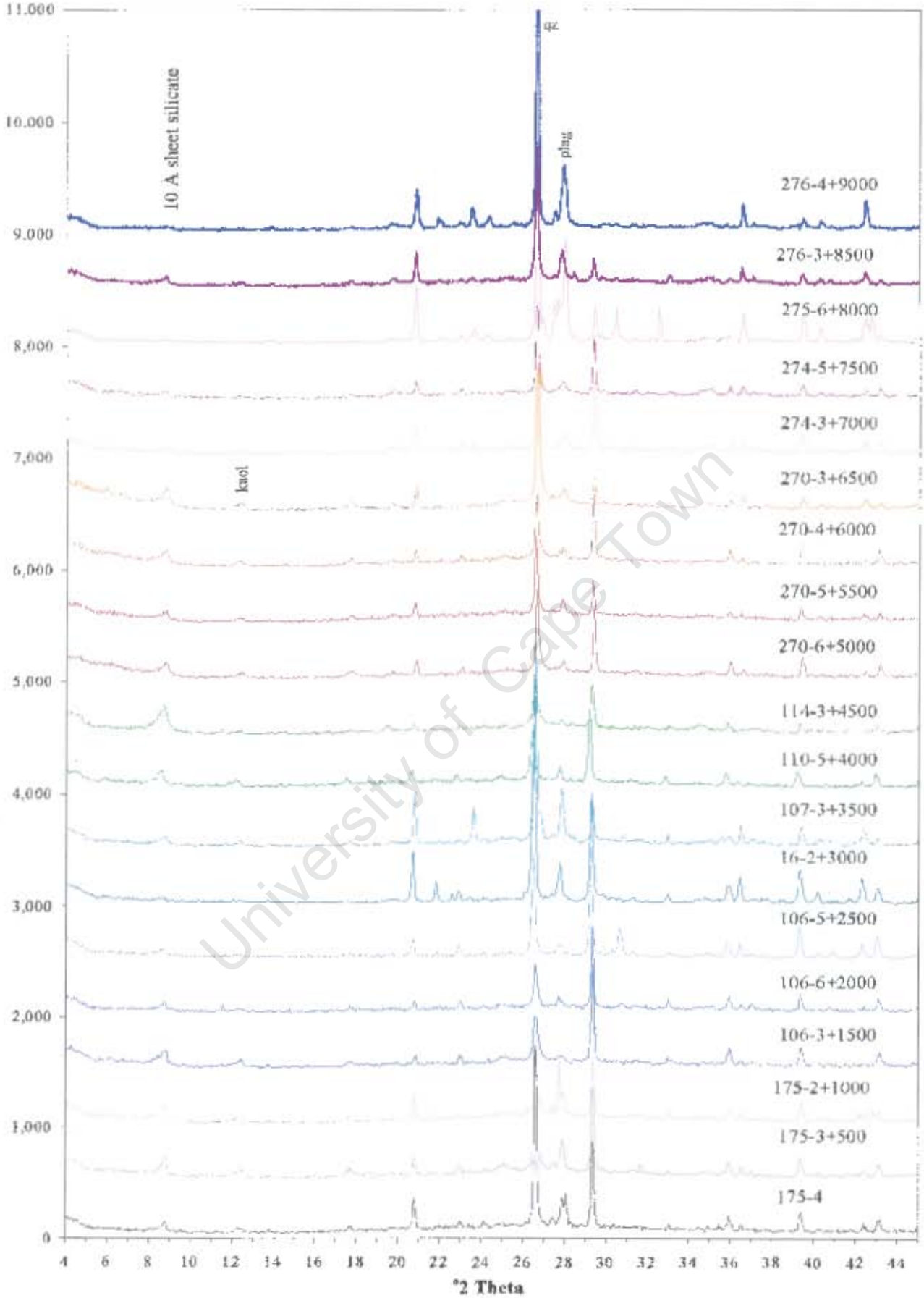


Figure 7.25. Weight % $CaCO_3$ determined by acid leaching, using dilute (10%) HCl, of the sand fraction (63 µm - 2mm) of the Quartzose Muddy Sand. The high $CaCO_3$ of Samples 16-2 and 175-2 reflect the abundance of Pleistocene microfauna bioturbated into the upper parts of these cores.

A group of twelve cores collected on the Western Flank and Southern Rocky Plateau in the south of the Cape Canyon Head Area (Figure 7.19) are all described as recovering an olive grey sandy mud to mud, which is considerably finer grained than the typical Pliocene Quartzose Muddy Sand Unit. The following brief description of the Olive Grey Sandy Mud sub-facies is based on the sediment data available from Core 322 (Compton *et al.*, 2004) and the WMR core logs, as this sediment was not intercepted in any of the cores sampled on the selected transects. The grain size of Core 322 fines upwards from a sandy mud near the base (with a single muddy sand sample) to a mud at the top of the Pliocene succession. However, the Olive Grey Sandy Mud is included, as a sub-facies, with the Quartzose Muddy Sand Unit for the following reasons. It is recovered in the stratigraphically equivalent position overlying, with a gradational contact, the Glauconitic Muddy Sand (at ± 275 cm in Core 317). It is overlain either by a phosphorite gravel lag at the base of the Pleistocene Glauconitic Quartzose Sand facies or only by a thin (<20 cm) Holocene Faecal–rich Muddy Sand drape, although a thick (=1.2 m) gradational contact with the Holocene muddy sand is observed in Core 200. In addition, the sub-facies is similarly interpreted to have been affected by late Pleistocene slumping (*e.g.* Core 213A). The foraminiferal assemblage of the Olive Grey Sandy Mud sub-facies is typically Pliocene (Compton *et al.*, 2004), but includes the oldest reworked foraminifera of the study area with Sr-ages ranging from 21.4-30.1 Ma (Compton *et al.*, 2004). A preliminary description of this unit was included, because it may represent a possible equivalent to the typical Pliocene "brown clay" units (no reported compositions) preserved along the Orange Shelf as described by Dale and McMillan (1999).

Although the Quartzose Muddy Sand Unit is a uniform, very fine quartzose sand, a number of analysed samples do show higher than average $CaCO_3$ wt% (Samples 16-2 and 175-2 in Figure 7.25) and increased glauconite abundances (Samples 275-6, 276-3, 106-4, 106-6, 30-1 and 281-2 in Figure 7.22). The variations in sediment composition may also be associated with variations in grain size (Figure 7.24). However, many of these compositional variations are shown to be due to post-depositional

University of Cape Town



University of Cape Town

Figure 7.26. XRD records for the mud fraction (<63 μm) of the Quartzose Muddy Sand Unit composed of calcite (cc), quartz (quartz), feldspar (plag) with a non-expandable 10 Å sheet-silicate and kaolinite (kaol) present.

bioturbation and slumping or to reflect the gradational contact with the underlying Glauconitic Muddy Sand (Samples 30-1 and 281-2). The Quartzose Muddy Sand, below the upper sequence boundary, is almost always extensively bioturbated with evidence of centimeter-scale burrows as deep as 1 m (Core 281) below the upper contact of the Quartzose Muddy Sand (Figure 7.27). The overlying Pleistocene sediments (together with any shell fragments and phosphorite gravel) are mixed by bioturbation down into the Quartzose Muddy Sand. The effect of bioturbation and inclusion of the overlying coarser grained sediment is clearly observed in the bimodality of the frequency curves showing the grain-size distribution for Samples 275-6, 276-3, 175-2 and 114-3 (not shown). Samples collected adjacent to the bioturbated upper contact of the Quartzose Muddy Sand often show increased glauconite abundances. These sediments also include echinoid spines, shell fragments and the distinct uppermost Pleistocene diverse microfaunal assemblage (Chapter 8 and Compton *et al.*, 2004). The increased glauconite abundances may be associated with a higher wt% of $CaCO_3$ with 11.7 wt% $CaCO_3$ in Sample 175-2.

In addition to bioturbation, late Quaternary slumping plays a role in modifying the composition of the Quartzose Muddy Sand Unit. The reworked Pliocene Quartzose Muddy Sand (see Section 7.3.1) of Core 16 was recovered between two upper Pleistocene Glauconitic Quartzose Sand intervals (Figure 7.27). The delicate laminae preserved at the base of the Quartzose Muddy Sand suggest that re-entry during coring is not responsible for the repeated stratigraphy. The underlying Pleistocene unit is composed of 50% quartz, 30% glauconite and 20% biogenic grains. The biogenic fraction includes a typical later Pleistocene assemblage with bivalve shell fragments, diverse planktic and benthic foraminifera, including an agglutinated miliolid species (*Siphonaperta martinae*), ostracods, holothurian sclerites (Dale and McMillan, 1998a) and echinoid spines. The sand fraction of the overlying Pleistocene unit has a similar composition, although it includes only ~10% biogenic grains. The age of this Pleistocene lag is unknown, but is assumed to be latest Pleistocene based on the foraminiferal assemblage. This assumption is based on the interpreted foraminiferal assemblage age for the shell- and gravel-rich near surface lag present across most of the Concession area. The abundant bioturbation present in the Quartzose Muddy Sand and the latest Pleistocene age for the gravel lag below the Holocene sediments imply an older than latest Pleistocene age for the slumping event. The higher wt% $CaCO_3$ of Sample 16-2 (18.0%) reflects the inclusion of micro-and macrofaunal-rich overlying Pleistocene Quartz Glauconite Sand during slumping. Similarly, Core 106 has unusually high glauconite abundances (17.9-19.5%), which is reflected in the slightly coarser mean grain size of 2.99 ϕ (Figure 7.24). The sand fraction of Core 106, in addition to more abundant glauconite, includes subordinate fine to medium quartz grains with minor to trace shell fragments, ostracods, echinoid spines and planktic and benthic foraminifera. The composition of Core 106 is similarly interpreted to have been altered by late Pleistocene slumping or reworking. The WMR core logs describe inverted or repeated stratigraphic sequences for eleven of the ninety cores in which Quartzose Muddy Sand is recovered. These slumped successions are always recovered on the steepened flanks above the Main Channel, where local slumping is interpreted to have occurred in response to slope failure. The recognition of these post-depositional late stage processes is important when attempting to establish the overall lithostratigraphy of the area.

University of Cape Town

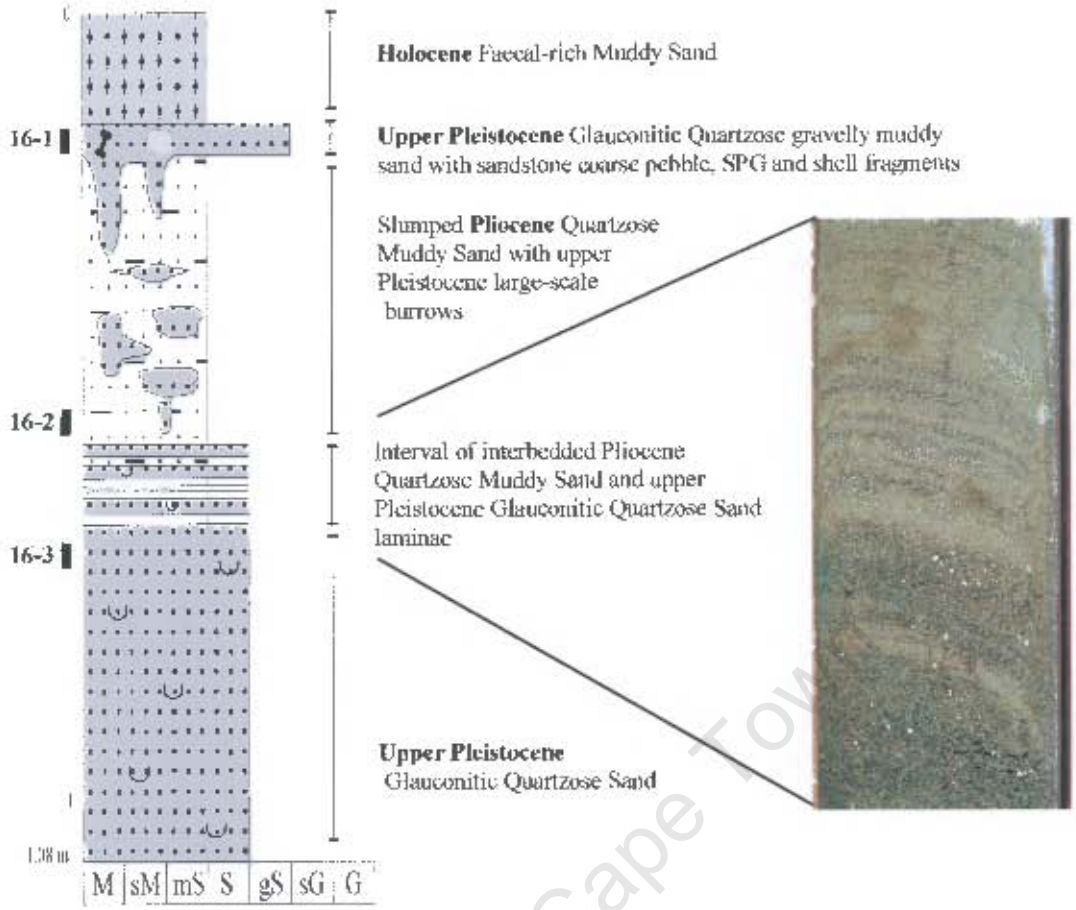


Figure 7.27. The slumped stratigraphy of the Pliocene Quartzose Muddy Sand and Pleistocene Glauconitic Quartzose Sand in Core 16 (Appendix A1-15), located on the steep Eastern Flank of the Cape Canyon (Appendix A1-14). The legend for the symbols is included in Figure 1.1, where the glauconite abundance is shown as a grey scale.

University of Cape Town

7.3 DEPOSITIONAL HISTORY OF PLIOCENE SUCCESSION

The Pliocene Succession of Concession 20D includes two sedimentary units of very different composition, with the Glauconite Sand Unit overlain by the Quartzose Muddy Sand Unit. These compositional and textural variations imply significant changes in the depositional environment on the western margin during the Pliocene.

7.3.1 AGE OF THE PLIOCENE SUCCESSION

This complex suite of sediments, dominated by either glauconite or quartz, summarised in the previous sections, is interpreted to have a predominantly Pliocene depositional age with some minor reworking during the Quaternary, particularly on the Western Ridge and the Southern Rocky Plateau. This interpretation is based on the available lithostratigraphic data, foraminiferal assemblages and Sr-ages for the various facies. The foraminiferal assemblage from a number of samples, including picked assemblages and SEM images, were submitted to I. McMillan for identification in order to determine the depositional age and environment of the selected samples. This biostratigraphic interpretation was then utilised to provide age control for additional samples. The Sr-age data are presented in Chapter 3

(WMR data) and Compton *et al.* (2004) (Chapter 5). The following section outlines the complexity of the age data and provides a summary for the interpreted sequence of depositional events recorded in the Pliocene Succession.

The Glauconitic Sand Sub-unit, the Glauconitic Muddy Sand Sub-unit and the Quartzose Muddy Sand Unit of the Pliocene Successions were deposited above the Upper Oligocene/Lower Miocene Calcareous Unit, following the uplift of the western margin in the mid Miocene (Chapter 6). Data from Core 319 indicates that since the middle Miocene (12.0-15.9 Ma) the sedimentary record of the study area has been dominated by reworked quartz and glauconite (and authigenic minerals) with only minor foraminifera and other calcareous grains present. The formation of glauconite and the presence of reworked quartzose sand in Core 319 and the sediments of the Pliocene Succession indicates that low sedimentation rates have dominated on the western margin since the middle Miocene.

Table 7.4. The available Sr-age data of the Quartzose Muddy Sand (Compton *et al.*, 2004)

Core	Depth	Grain Type	Age
19	438-442 cm	Benthic foraminifera and fish bones	1.5-3.9 Ma
26	108-112 cm	Benthic foraminifera and fish bones	9.1-11.2 Ma
73	292-296 cm	Benthic foraminifera	10.1-12.3 Ma
	360-364 cm	Benthic foraminifera	10.9-13.4 Ma
	535-539 cm	Benthic foraminifera	13.3-15.8 Ma
		Fish bones	1.3-2.8 Ma
		Black phosphorite	10.9-13.3 Ma
322	340-344 cm	Benthic foraminifera	28.6-30.1 Ma
	498-502 cm	Benthic foraminifera	23.3-24.3 Ma
	525-530 cm	Benthic foraminifera	21.4-22.9 Ma
		Orange phosphorite	22.9-24.0 Ma
72 (WMR)	1.00 m	Benthic foraminifera	1.8-4.7 Ma

The following discussion on the relative ages of the Pliocene Succession starts with the youngest sediments, because the age of the Quartzose Muddy Sand is relatively well constrained with a general agreement between the biostratigraphic and Sr-age data. The Quartzose Muddy Sand contains only a few, predominantly benthic, foraminifera. The foraminiferal assemblage of the Cape Canyon Head region is very similar to that recovered from the upper slope cores. The available Sr-ages were obtained from a number of different Quartzose Muddy Sand samples and from different grain types within these samples (Table 7.4; Compton et al., 2004). The Sr-isotope age of the picked benthic foraminifera bracket two time intervals, namely a middle Miocene age (9.1-15.8 Ma) and an upper Pliocene/lower Pleistocene (1.3-3.9 Ma) age. A bulk foraminiferal sample, dated for WMR, gave an age of 1.8-4.7 Ma, which is in general agreement with the results of Compton *et al.* (2004). Two distinct foraminiferal assemblages are commonly present in the Quartzose Muddy Sand Unit, namely the medium to very coarse (>250 μm), often elongated, robust, brown-stained (ferruginised) foraminifera and the very fine (63–125 μm), often delicately ornamented, benthic assemblage (Figure 7.28). The very fine sand assemblage shows low species diversity, and is commonly dominated by species such as *Epistomella pulchella*, *Nodogenerina* sp., *Hanzawaia* sp., *Frondicularia* sp. *Nuttallides* sp. and ribbed *Uvigerina* sp.

University of Cape Town

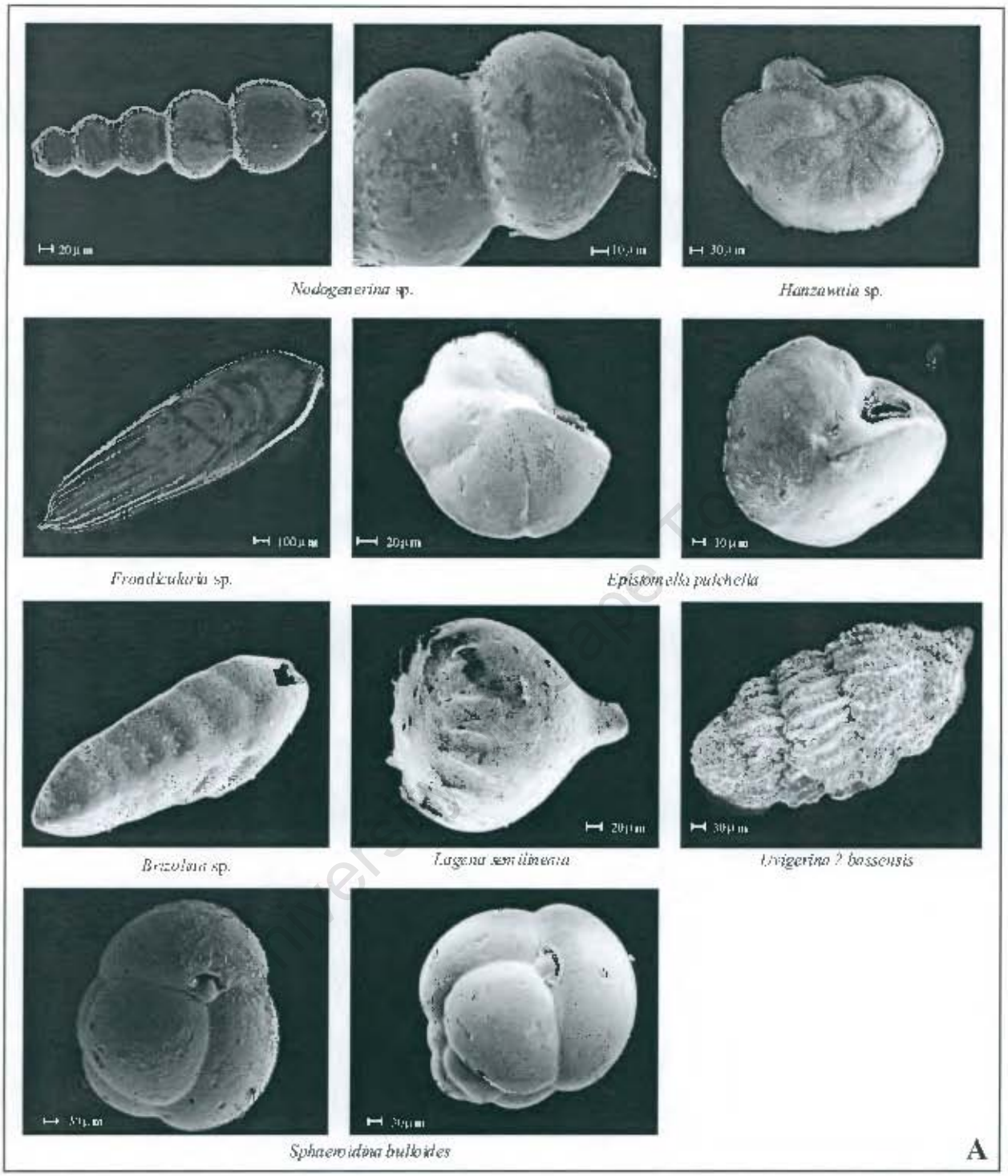
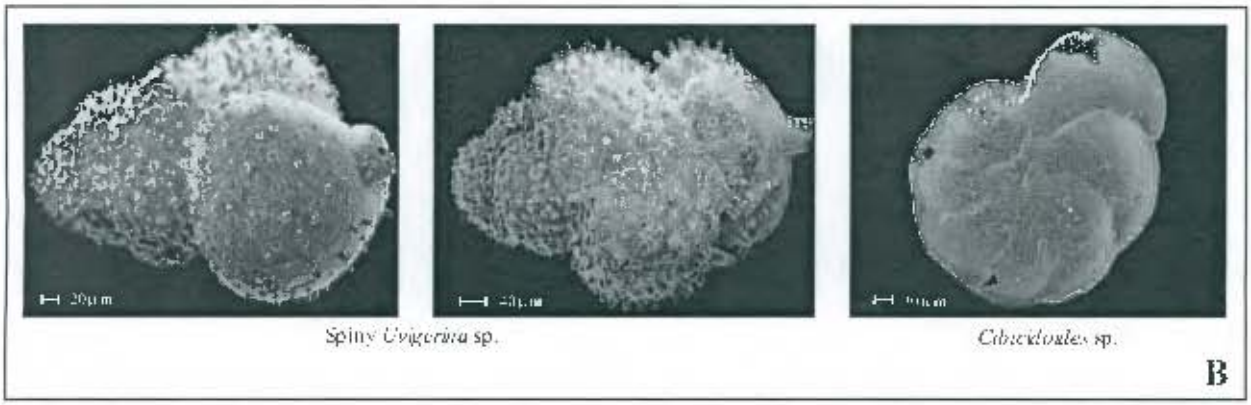


Figure 7.28. The foraminiferal assemblage of the Pliocene Quartzose Muddy Sand Unit, which includes the distinct Pliocene assemblage (A), together with Miocene to Pliocene species (B) and a reworked Miocene assemblage (C). Identification and age determinations according to I. McMillan, *pers. comm.*, 2002.



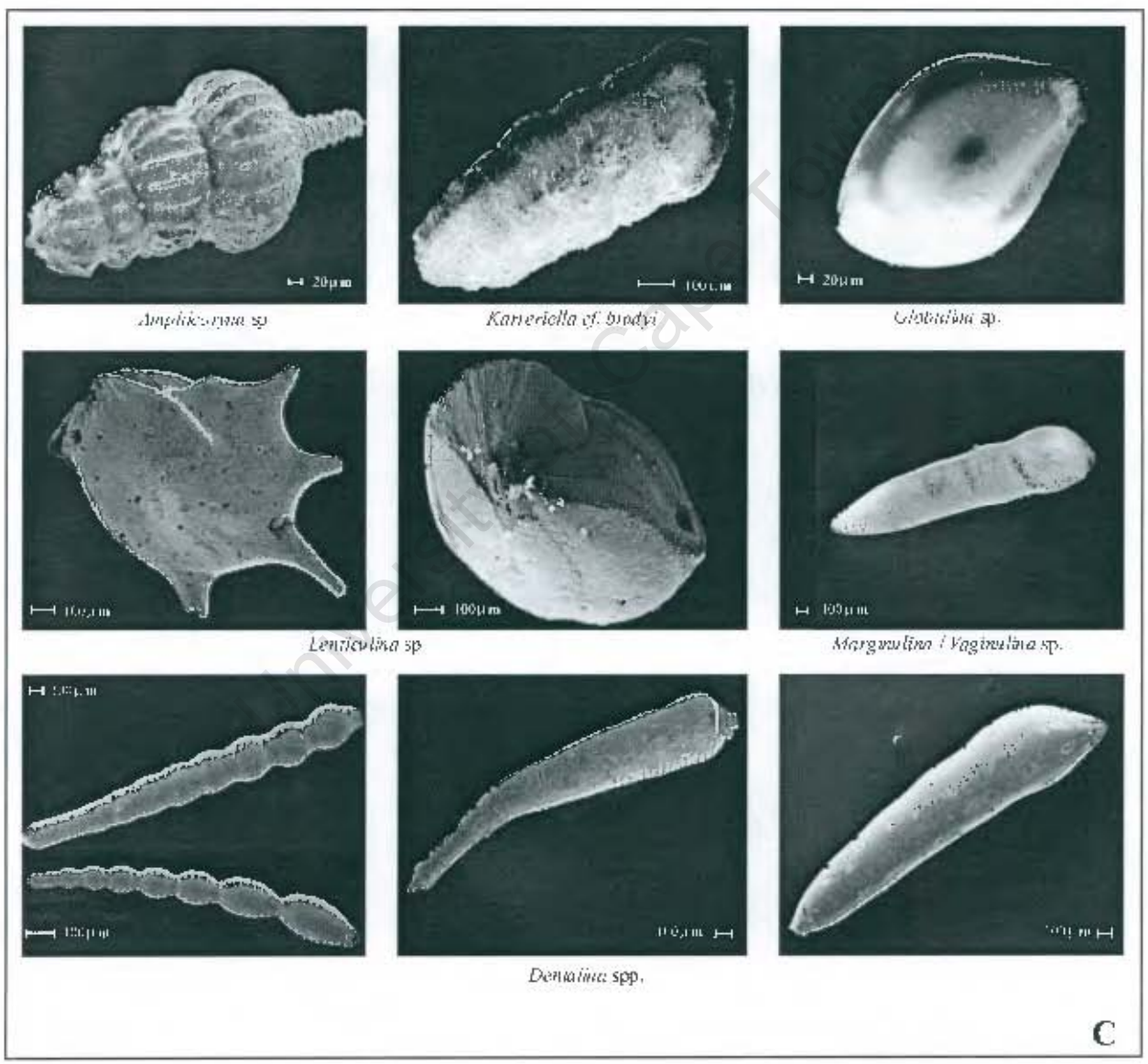


Figure 7.28 continued.

This assemblage collected from within the Cape Canyon Head Area and from the upper slope closely resembles the typical benthic foraminiferal assemblage observed in the Pliocene sediments of the Orange Shelf (Dale and McMillan, 2000, 2003a). Dale and McMillan (2003a) assigned a late early to early late Pliocene age for the Pliocene sediments of the West Coast using the planktic foraminifera of the slope assemblage. The larger (>250 μm) robust benthic foraminifera (e.g. *Lenticulina*, *Marginulina/Vaginulina* sp., *Dentalina* spp. in Figure 7.28), which were selectively picked for Sr analysis because of their larger size, typically give a middle to late Miocene age (Table 7.4; Compton *et al.*, 2004). Although no biostratigraphic marker species were identified within the coarser foraminiferal assemblage, *Amphicoryna* sp. (Figure 7.28) is a common Miocene species off the West Coast of southern Africa (I. McMillan, *pers. comm.*, 2002). In contradiction to the apparent uniformity of the Quartzose Muddy Sand Unit sediments, the foraminiferal assemblage is variable, both within and between cores. Discrete intervals show marked variations in abundance of the Miocene and Pliocene assemblages. For example, Sample 270-5 has a typical mixed Miocene-Pliocene assemblage, whereas only the Pliocene assemblage is present in Sample 270-4. The Sr-derived ages are in agreement with the biostratigraphic data available for the Quartzose Muddy Sand Unit, which indicates a final uppermost lower Pliocene to lowermost upper Pliocene depositional age for this unit, although a component of older mid Miocene (15.8-9.1 Ma) reworked foraminiferal species are present in the sediment (Figure 7.29). Unfortunately, the age resolution of Sr-isotopes is diminished in the Plio/Pleistocene, because the marine Sr-record flattens out at the start of the Pliocene (McArthur *et al.*, 2001). The large uncertainty on Sr-derived Pliocene ages is reflected in the poor Sr-age control within the Pliocene for the Quartzose Muddy Sand Unit.

The stratigraphic relationship between the glauconite- and quartz-rich units is best preserved in the upper slope Cores 146 and 147 (Figure 7.18). In these distal sediments, as well as in the more proximal Core 30 (Figure 7.16), the Glauconitic Muddy Sand Sub-unit is overlain by the Quartzose Muddy Sand Unit, suggesting that the Glauconitic Muddy Sand Sub-unit is older. Sr-ages from 5.8-10.5 Ma were obtained from biogenic carbonate (<38μm), benthic foraminifera and black phosphorite from the base of Cores 146-148 (Compton *et al.*, 2004). In addition, Sr-isotope ages ranging from 8.7-10.9 Ma were obtained for picked benthic foraminifera and fish bones from Core 76 (Compton *et al.*, 2004). However, the foraminiferal assemblage of the Glauconitic Muddy Sand Sub-unit from samples at the base of the distal Cores 147 and 148 are interpreted by I.McMillan, using the presence of typical delicate foraminifera to indicate a Pliocene age of deposition (Compton *et al.*, 2004). Similarly, McMillan *pers. comm.* (2003) interpreted a possible Pliocene age for Sample 30-7 collected towards the base of the proximal Core 30. The foraminiferal assemblage of Sample 30-7 includes smooth *Angulogerina* sp., fat *Fissurina* sp., *Lenticulina* sp., *Nuttallides* sp., ribbed and smooth *Uvigerina* spp., *Brizalina* sp.; *Sphaeroidina bulloides*, *Neogloboquadrina pachyderma* and *Cibicidoides* sp. (McMillan *pers comm.*, 2003). The discrepancy between the Pliocene biostratigraphic and upper Miocene Sr-derived age of the Glauconitic Muddy Sand indicates that the selectively picked upper Miocene robust foraminifera (>125 μm) were reworked during the Pliocene (Figure 7.29).

University of Cape Town

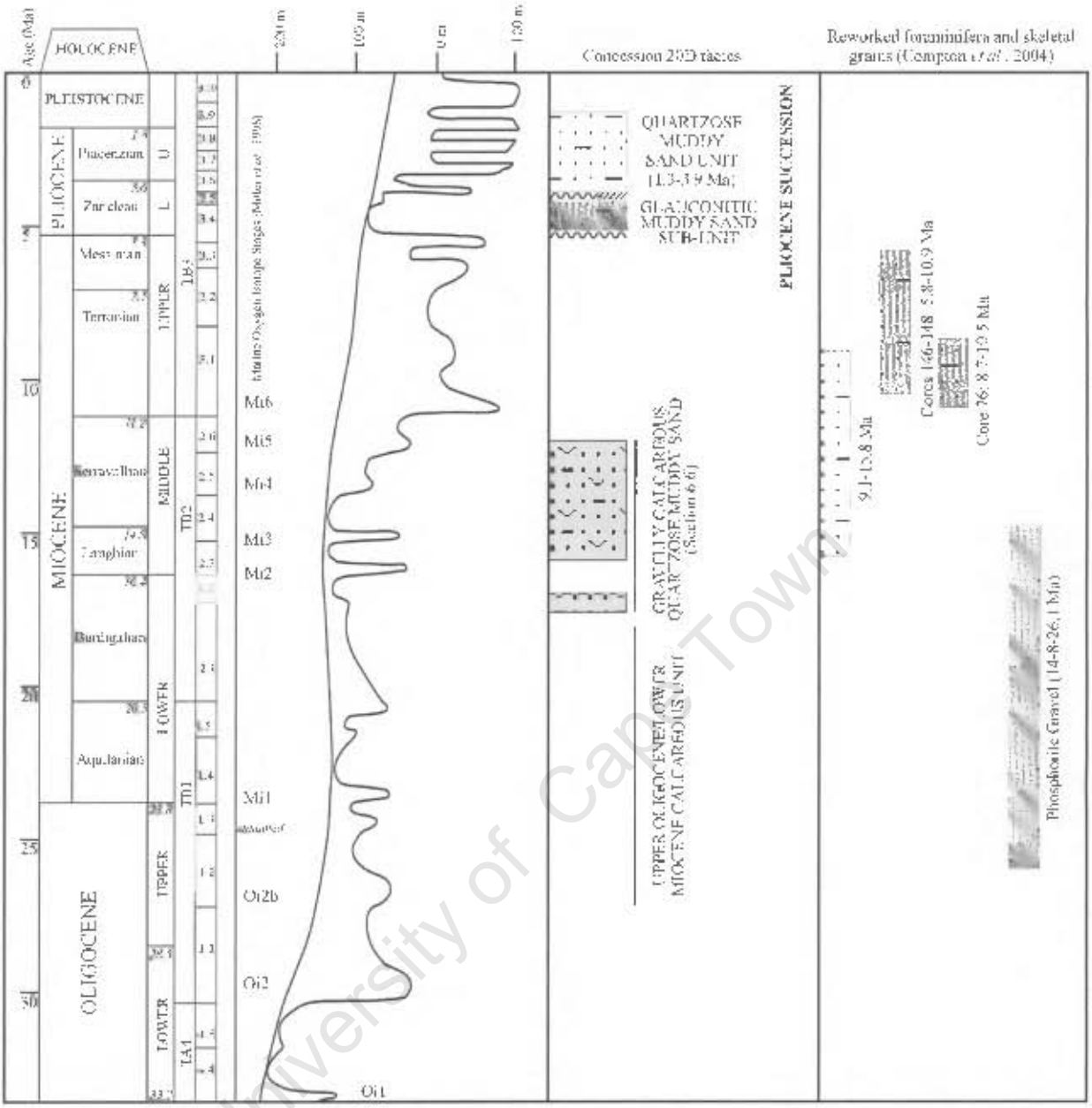


Figure 7.29. The Pliocene Succession and the middle Miocene Gravelly Calcareous Quartzose Muddy Sand together with the Sr-ages of reworked foraminifera, skeletal phosphorite grains and phosphorite gravels recovered from the Pliocene Succession are plotted against the proposed Haq *et al.* (1987, 1988) eustatic sea-level curve recalibrated to the Berggren *et al.* (1995) time scale after Miller *et al.* (1997; 1998).

The age of the Glauconitic Sand Unit of the outer shelf is similarly poorly constrained, and these sediments typically include less than 2.5% foraminifera (Table 7.2). The foraminiferal assemblage clearly differentiates between the upper Pleistocene Calcareous Glauconitic Sand and the underlying predominantly Pliocene Glauconitic Sand Sub-unit (Figure 7.1; Chapter 8). The minor foraminiferal assemblage of the Glauconitic Sand facies includes both Pliocene and Pleistocene foraminifera (Table 7.5). The characteristic appearance of the green glauconite of the Glauconitic Sand facies (Figure 7.12) is very similar to the glauconite of the Glauconitic Muddy Sand unit, suggesting a lateral facies variation and a possible Pliocene age for this Glauconitic Sand facies. The well-preserved, delicate, and often spiny Pliocene foraminifera present in the Glauconitic Sand facies are most likely not

University of Cape Town

extensively re-worked and support a Pliocene-age for this facies (Figure 7.29). However, a number of Pleistocene and Holocene foraminifera are identified, suggesting post-depositional reworking of this unit must have occurred in the Quaternary, most likely by bioturbation (see Section 7.3.2).

Table 7.5. A summary of the interpretation of the foraminiferal assemblage (I. McMillan *pers. comm.*, 2003).

Sample	Age	Environment	Comments
128-7 **Glauconitic Sand facies**	Upper Pleistocene	Deep water	Dominated by planktics and includes a more typical upwelling assemblage. Possibly represents a maximum flooding surface.
	Globorotalia inflata, Orbulina universa, Globorotalia truncatulinoides, Neogloboquadrina pachyderma, Cassidulina laevigata, Uvigerina bassensis, Globorotalia hirsuta, Bulimina aculeata, Oolina sp., smooth *Angulogerina* sp. and few *Globigerinoides ruber*		
128-10 **Phosphorite Gravel facies**	Miocene/Pliocene Includes Pleistocene and Holocene species	Inner to middle shelf	Considerable reworking of Lower Miocene species observed.
	Globigerina cf. *ouachitaensis, Brizalina* sp., flat *Epistominella* sp., flat, faintly ribbed *Uvigerina* sp., *Globigerina* spp., *Sphaeroidina bulloides,* small rounded margin *Nonion,* sp., fat smooth Angulogerina sp., *Hanzawaia* sp., *Neogloboquadrina pachyderma,* fat ribbed *Uvigerina* sp., *Gyroidinoides soldanii,* smooth *Marginulina* sp., *Oridorsalis umbonatus* and small *Cibicidoides* spp.		
120-5 **Glauconitic Sand facies**	Pliocene Includes Pleistocene species	Deep water	Pliocene species well preserved and not reworked. Includes the Pliocene deep-water species *Latero stimela.*
	Finely ribbed *Uvigerina* sp., *Planulina ariminensis* (reworked), *Neogloboquadrina pachyderma, Globigerina calida, Globorotalia inflata, Lobatula lobatula, Cassidulina laevigata, Cassidulina* cf. *minuta, Globigerina bulloides* and the Pliocene species *Bolivina* cf. *variabilis,* ribbed *Siphouvigerina* sp., fat ribbed *Uvigerina* sp. and *Lenticulina* sp.		
186-9 **Glauconitic Sand facies**	Pliocene, contaminated by Pleistocene species	Deep water	Includes both Pliocene and abundant Pleistocene species, including typical upwelling species.
	Globorotalia inflata, Globigerina spp., *Cibicidoides pseudoungerianus, Globocassidulina pacifica,* finely ribbed *Angulogerina* sp., *Cassidulina laevigata, Neogloboquadrina pachyderma and Sphaerogypsina globulus* (Miocene sp.).		
190-4 **Phosphorite Gravel facies**	Pliocene Includes Pleistocene and Holocene species	Complex mixture of deep water to littoral	Very mixed assemblage with little evidence for reworking, including rare Pliocene species and abundant Pleistocene foraminifera. The latest Pleistocene assemblage includes some littoral species, deposited not far from the shoreline.

The basal Phosphorite Gravel facies records a complex history dominated by winnowing and erosion since the Middle Miocene. The foraminiferal assemblage of the basal gravel is commonly dominated by reworked Lower Miocene foraminifera, but is assigned a final Pliocene depositional age in Cores 90, 190 and 128 although Pleistocene and Holocene species are recognised (I. McMillan *pers. comm.*, 2003; Compton *et al.*, 2004). The Quaternary foraminifera are similarly argued to be due to a later bioturbation down into these condensed sediments. The Sr-ages from benthic foraminifera (15.8-16.8 Ma) and fish bones (14.8-16.3 Ma) from the base of the Glauconitic Sand facies (202-207 cm) in Core 90 indicate a younger than middle Miocene age for this lag. Core 190, collected along the Southern Transect, includes a similar complex foraminiferal assemblage, reflecting the highly condensed nature of the sediments preserved on the Southern Rocky Plateau, where Quaternary foraminifera (0.5-1.4 Ma) and Oligocene to Miocene phosphorites (23.6-26.1 Ma) are recovered (Compton *et al.*, 2004).

7.3.2 DEPOSITIONAL HISTORY OF THE PLIOCENE SUCCESSION

Following deposition of the upper Oligocene to lower Miocene sediments, the outer shelf of Concession 20D was subjected to uplift, tilting and erosion (Chapter 6). Multiple erosional events resulted in an outer shelf-wide unconformity and a planing off of the seaward-dipping Upper Oligocene/Lower Miocene Calcareous Sand Unit. The basal Phosphorite Gravel facies, predominantly composed of upper Oligocene to middle Miocene phosphorites, lies above this erosional unconformity and forms the lower sequence boundary of the Pliocene Succession. The foraminiferal assemblage suggests a final Pliocene age for the deposition of this erosional gravel lag (Table 7.5). Quaternary foraminifera appear to have been introduced into the Phosphorite Gravel facies by extensive late Quaternary bioturbation. This interpretation is supported by the observation that Quaternary sediment-filled burrows extend to depths greater than 1 m into the Quartzose Muddy Sand Unit in Core 281. In some cores, Quaternary sediments may have been introduced during vibrocoring or as a result of reworking/winnowing in the Pleistocene (see later in this discussion).

The gravel-rich lag is only recovered at water depths shallower than approximately 280 m, and tends to occur above the gravelly uppermost Oligocene to lower Miocene Quartzose Glauconitic Calcareous Sand and the lower Miocene Glauconitic Calcareous Sand facies. The observed variation in the composition of the Phosphorite Gravel facies across the study area, particularly the relative abundance of phosphorite gravel and phosphatised mollusc casts, reflects variations in the underlying eroded sediments. This implies that *in situ* winnowing, rather than redeposition, was the dominant factor in the formation of the Phosphorite Gravel facies. The presence of phospho-glauconite and reworked lower Miocene foraminifera (Table 7.5) in the sand fraction of the basal Phosphorite Gravel facies indicates a selective winnowing of the biogenic component from the Upper Oligocene/Lower Miocene Calcareous Unit by bottom-water currents.

The amount of phosphorite and phospho-glauconite decreases significantly above the Phosphorite Gravel facies and the most distinguishing characteristic of the Glauconitic Sand Unit, including both the Glauconitic Muddy Sand Sub-Unit and the Glauconitic Sand Sub-unit, is the predominance of glauconite sand (85-96 wt%). Glauconite-rich sediments are generally associated with condensed sections, unconformities, transgressive system tracts or maximum flooding surfaces (Odin and Matter, 1981; Loutit *et al.*, 1988; Kelly and Webb, 1999; Harris and Whiting, 2000). Abundant glauconite in a stratigraphic succession indicates low sediment accumulation rates to sediment-starvation in water depths ranging from 50-500 m, with significant concentrations of modern glauconite usually occurring on the outer shelf/upper slope (Amorosi, 1995; Kitamura, 1998; Chafetz and Reid, 2000; Harris and Whiting, 2000; Hesselbo and Huggett, 2001). The formation of glauconite typically occurs at the shelf edge where the required balance between fluvial detrital input and redistribution of sediments onto the slope by bottom water current winnowing occurs, such that there is very little net accumulation (Odin and Matter, 1981; Stille and Clauer, 1994). Odin and Matter (1981) noted that a rising sea level provides favourable conditions for widespread glauconitization, where shallower water deposits, rich in

University of Cape Town

both detritus (providing the necessary semi-confined microenvironment) and clastic components, are subjected to an increasingly low-energy environment.

Two sub-units are defined in the Glauconitic Sand Unit. The Glauconitic Muddy Sand Sub-unit, recovered from the Canyon Head region and the upper slope, has a Pliocene age. The Glauconitic Muddy Sand Sub-unit is largely unaffected by the post-depositional reworking recorded in the outer shelf Glauconitic Sand Sub-unit. Deposition of the overlying Pliocene Quartzose Muddy Sand Unit appears to have protected the Glauconitic Muddy Sand from Quaternary reworking (Figures 7.29 and 7.30). In contrast, the Glauconitic Sand Sub-unit is best developed on the outer shelf and Southern Rocky Plateau. The Glauconitic Sand Sub-unit has a low mud content and decreased very fine quartz sand relative to the Glauconitic Muddy Sand Sub-unit and includes Pleistocene foraminifera that indicate reworking. Later Pleistocene reworking of the Glauconitic Sand Unit occurred when removal of the overlying Quartzose Muddy Sand resulted in its exposure on the sea-floor. The following interpretation of the Pliocene depositional environment does not include this late Pliocene to Pleistocene reworking event.

The abundance of glauconite recovered from these Pliocene sediments indicates post-early Miocene glauconitization. Zonation and multiple growth stages observed in thin-section of the green glauconite (discussed in detail in Chapter 9) imply multiple periods of glauconitization. The complex zonation of the glauconite grains resembles the interpreted history of reworking indicated by the foraminiferal assemblage, where the final stage of reworking and deposition for the bulk of these glauconitic sediments occurred sometime during the early Pliocene, assuming an latest early Pliocene to earliest late Pliocene depositional age of the Quartzose Muddy Sand Unit (Figures 7.29 and 7.30; Dale and McMillan, 2003a). The delicate spinose tests of several of the Pliocene foraminifera, the absence of Pleistocene species in the Glauconitic Sandy Mud Sub-unit (Figure 7.28) and the greater mud content suggests that the Glauconitic Muddy Sand Sub-unit was not reworked, but preserves the early Pliocene depositional environment. Although the Glauconitic Sand Unit is dominated by glauconite, it also includes a significant but minor amount of pyrite and possibly siderite, consistent with an organic matter-rich reducing depositional environment having abundant Fe. The muds in which the fine to medium sand size authigenic glauconite grains grew still contain abundant illite, illite/smectite and kaolinite clay minerals. The silty to very fine quartz component of the Glauconitic Muddy Sand is similar to that observed in the modern mudbelt (Rogers, 1977; Meadows *et al.*,1997; Gray *et al.*, 1999; Williamson and Stevenson, 1999) and indicates a similar depositional environment on the shelf. The high organic matter content of a mudbelt would provide the redox conditions required for glauconitization (Odin and Matter, 1981). The delicate Pliocene foraminifera of the glauconitic sediments indicate a final low-energy, deep-water depositional environment during a relative rise in sea level or highstand.

The Holocene transgressive system tract along the West Coast of southern Africa is associated with a mudbelt, which runs roughly parallel to the coastline, from north of the Orange River to St Helena Bay

University of Cape Town

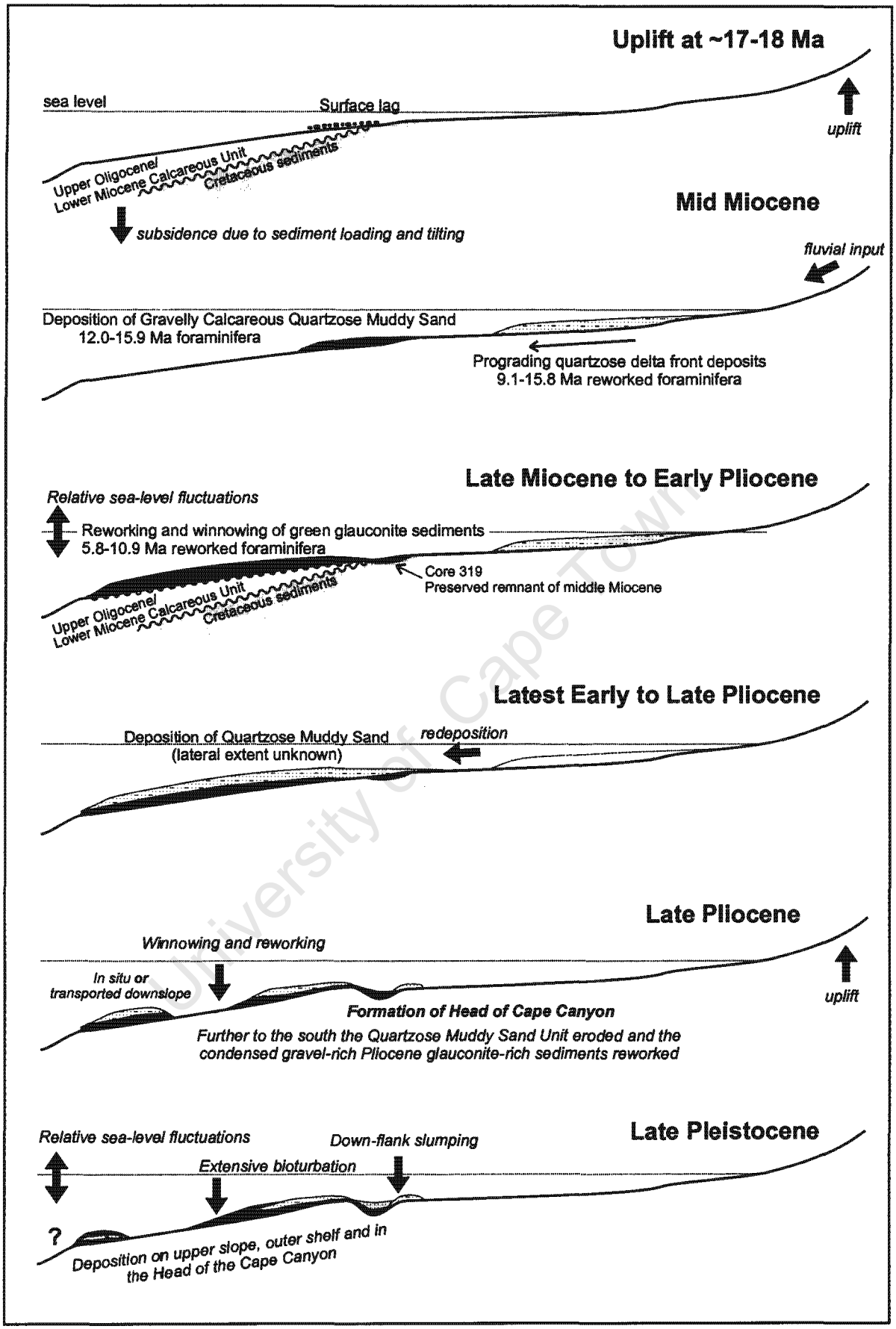


Figure 7.30. A sketch of the proposed mid Miocene to Plio/Pleistocene geological history of the western margin in the vicinity of the Northern Transect in Concession 20D as interpreted using a combination of *in situ* and reworked foraminiferal assemblages in conjunction with sediment compositions and textures of the Pliocene Succession.

University of Cape Town

in the south at water depths between 40 and 140 m in the north and deepening to 70-140 m to the south (Gray *et al.*, 1999; Williamson and Stevenson, 1999; Rogers, 1977). The large river input of terrigenous sediment onto the wave-dominated submarine Orange Delta is redistributed parallel to the coastline. Littoral drift, resulting from southwesterly swells (De Decker, 1988) transports the gravel and sand fractions northwards, while a poleward undercurrent transports the mud fraction in suspension southwards (De Decker, 1970; Rogers, 1977; Nelson, 1985; Birch *et al.*, 1986; Dingle *et al.*, 1987; Bremner *et al.*, 1990; Rogers and Bremner, 1991). The mudbelt lies below the influence of wave-induced currents (Meadows *et al.*, 1997). The composition of the mudbelt is variable, with a poleward increase in organic matter south of the Orange River accompanied by an increase in benthic faecal pellets (Rogers and Bremner, 1991). There is a similar increase seawards off the Orange River. Both trends are partly ascribed to less dilution by terrigenous material with increasing distance from the Orange River mouth. Although predominantly a fine silt, the mudbelt includes subordinate amounts of silty to very fine angular quartz sand (MacHutchon, 2003). SEM images of a mudbelt bulk sample show 1-2 μm spheres, which have a typical glauconite composition determined by EDS analysis (J. Compton, *pers. comm.*, 2003), indicating active glauconitization in the modern mudbelt. A pilot study on clay mineralogy (≤2 μm) of surface samples from the West Coast, from south of Cape Town to the Swartlintjies River in Namaqualand, was undertaken by Birch (1974). His results revealed that the clay minerals in the marine sediments, and in the alluvium being supplied to the shelf appear to be kaolinite and illite with illite (65-75%) more dominant than kaolinite (25-37%) in marine sediments. In contrast, the rivers show a more varied distribution of clay compositions reflecting the very variable geology of adjacent continental bedrock.

The transition from the underlying Glauconitic Sand Unit to quartz-rich sediments of the Pliocene Quartzose Muddy Sand Unit marks the end of clayey mud deposition and the beginning of quartzose silty very fine sand deposition. The contact between the Quartzose Muddy Sand Unit and the underlying Glauconitic Sand Unit varies from transitional on the upper slope to sharp and bioturbated in Core 30 in the Canyon Head region (Figure 7.29). The deposition of the Quartzose Muddy Sand Unit indicates a major change in depositional environment and sediment input into the Concession 20D area.

The presence of two distinct foraminiferal assemblages in the Quartzose Muddy Sand (Figure 7.29), *i.e.* the coarser, robust mid-Miocene assemblage and the finer, more delicate Pliocene assemblage is indicative of the complex sedimentary history of these quartzose sediments, and implies reworking of an older middle Miocene (9.1-15.8 Ma) sediment during the latest early to earliest late Pliocene (Figure 7.30). The Quartzose Muddy Sand Unit was most likely reworked out onto the outer shelf during the earliest late Pliocene, as the quartz abundance increases rapidly from the underlying glauconitic sand until very well sorted, very fine quartzose muddy sands dominate outer shelf deposition. The subtle variations in the microfaunal assemblage, as well as the rare, but well preserved fine-scale laminated sand in the Quartzose Muddy Sand, suggest that a single massive slumping event is an unlikely process for the origin of these quartzose sediments, although the distribution, uniform quartzose composition and thickness of these sediments suggest rapid deposition relative to other deposits on the western

University of Cape Town

margin. The rapid deposition of the Quartzose Muddy Sand Unit indicates a change from the depositional environment recorded by the low-energy, mudbelt type deposit of the Glauconitic Sand Unit. The presence of the Pliocene benthic foraminifera *Epistominella pulchella* indicates that dysoxic sea-floor conditions dominated during the Pliocene, as has been described for Pliocene deposits on the western margin in general (Dale and McMillan, 2003a). Pyrite, usually as pyritised sponge spicules, are a trace but ubiquitous component of the sand fraction. The mechanisms behind this rapid change in sediment composition on the outer shelf are most likely linked to either 1) increased fluvial input, where the increased bedload may reflect a more humid climate; 2) increased uplift-driven erosion or 3) reworking of marginal-marine sediments by fluctuations in relative sea level reflecting eustatic changes, margin subsidence, tectonic uplift or a combination of these factors.

Although still open to debate (Spönemann and Hagedorn, 2000; Van der Wateren and Dunai, 2001), many authors have argued for Pliocene uplift of the southern African continent producing the Post-African II Surface. Uplift occurred along the same axes as the Miocene uplift event, in which ±100 m of uplift is estimated along the western margin of southern Africa (Section 2.3.1; Partridge and Maud, 1987; Partridge, 1998; Gallagher and Brown, 1999; Brown *et al.*, 2000). Differential rates of uplift are proposed to explain the differences in heights above sea level of the marine terraces along the West Coast of Southern Africa, where apatite fission-track analyses show a general decrease in age northwards between Cape Town and Lüderitz, supporting the asymmetric tilting of the sub-continent (Gallagher and Brown, 1999). Unfortunately, the age of this proposed uplift event is poorly constrained within the late Pliocene (Dale and McMillan, 2003b), although an estimated age of 2.5 Ma is proposed by Partridge and Maud (1987). Christensen *et al.* (2002) noted that the foraminiferal assemblage suggests a significant component of downslope transport during the Pliocene at ODP Site 1085. The Pliocene uplift event may have triggered the dramatic increase in the output of very fine quartz sand onto the outer shelf. However, Dale and McMillan (2003a), assigned an uppermost lower to upper Pliocene age for the Pliocene sediments of the western margin using the planktic foraminifera of the slope assemblage. The foraminiferal assemblage of the Quartzose Muddy Sand is apparently very similar to other outer shelf deposits of the western margin (Dale and McMillan, 2003a), suggesting that the deposition of the Quartzose Muddy Sand predates the Pliocene uplift. In addition, the comparable age and composition of the Pliocene Quartzose Muddy Sand of the Cape Canyon Head and the upper slope implies a uniform drape of Pliocene sediment across the study area. The deposition of these quartzose sediments was clearly not controlled by present-day canyon bathymetry and indicates that the Plio/Pleistocene uplift associated with the formation of the Head of the Cape Canyon (to be discussed in Chapter 8) must have occurred after the final deposition of the Quartzose Muddy Sand in the Pliocene.

Although the distribution of the Quartzose Muddy Sand Unit does not appear to be related to the late Pliocene uplift event associated with the formation of the Head of the Cape Canyon, it is proposed that a combination of concurrent processes are related to the reworking of inner to middle shelf deposits in the Pliocene. The quartzose sediments of the inner shelf would have become increasingly unstable with continued late Miocene margin subsidence, possibly heightened by the renewed tilting associated with

University of Cape Town

uplift of the Columbine-Agulhas Arch basement high. The late Pliocene is a time of ice-sheet expansion and the onset of Northern Hemisphere glaciation (Haug and Tiedemann, 1998). The termination of the long-term late Miocene to Pliocene eustatic trangression is associated with a dramatic increase in a very fine quartz sand component in the glauconitic sediments. The proposed mid Pliocene eustatic sea-level fluctuations could have been an additional factor involved in the rapid progradation of the quartzose sediments onto the outer shelf at this time. The narrowness of the shelf off St Helena Bay in the south, relative to the wide shallow inner shelf to the north may have played a further role in the rapid margin progradation off the south-western Cape. Murray *et al.* (2002) noted two peaks at 3.03 Ma and 2.25 Ma of increased terrigenous input onto the Orange Shelf at Site 1085 (ODP Leg 175) and suggest that sea-level fluctuations and associated variations in fluvial input were important transport mechanisms.

The distal, upper slope succession is clearly a lateral equivalent of the Cape Canyon Head sediments, although this sediment is not recovered on the outer shelf, where the underlying Glauconitic Sand Unit and Upper Oligocene/Lower Miocene Calcareous Sands units erosionally crop out on the sea-floor. The Pliocene quartzose sediments may never have been deposited within this erosional zone, but were rather continuously winnowed off the shelf onto the upper slope as a clinoform wedge. However, it is possible that the sediment succession slid downslope as a coherent package in response to uplift of the Western Ridge during the Plio/Pleistocene. However, the absence of an inverted succession in these upper slope cores argues against a later-stage erosion and down-slope redistribution, but it has been proposed that the massive Pliocene slumps on the continental slope were triggered by the Pliocene uplift event (Dingle, 1980b; Partridge and Maud, 1987; Dingle and Robson, 1992). Either winnowing or mass-movement of the distal parts of the Quartzose Muddy Sand unit would explain the sea-floor surface exposure of the underlying Pliocene Glauconite Sand facies by the latest Pliocene-early Pleistocene. The presence of Pleistocene species within the predominantly Pliocene foraminiferal assemblage of the distal Olive Grey Sandy Mud sub-facies (*e.g.* Core 322) of the Southern Rocky Plateau may suggest that this very muddy sediment represents the final stage of shelf progradation during the latest Pliocene. The southern distal cohesive clay-rich sediments may not have been affected by continued uplift of the Western Ridge and are *in situ*.

Following the removal of the Quartzose Muddy Sand Unit from the outer shelf, the Pliocene Glauconitic Sand facies was subjected to winnowing of the mud fraction and a significant proportion of the very fine quartz sand (Figure 7.30). The winnowing process did not destroy the delicate Pliocene microfauna and Fe-cemented grains. Winnowing seems to have been more pronounced to the south, with extensive condensed sections on the Southern Rocky Plateau. Similarly, Berger *et al.* (2002) suggest strong winnowing on the Olifants River Slope throughout the entire Quaternary succession from ODP Site 1086 (Leg 175). The Pliocene sediment was bioturbated during the Pleistocene as indicated by the presence of Pleistocene upwelling or cold-water foraminifera.

Pliocene sediments of the western margin are preserved as perched outliers on the middle to outer shelf (Dingle, 1971a, 1973c; Dingle *et al.*, 1983) with an up to 1200 m thick Pliocene sediment succession

University of Cape Town

preserved along the upper continental slope at water depths greater than 500 m, from Cape Town to Lüderitz (Figure 2.8; Dale and McMillan, 2003a). The reported composition of Pliocene sediments along the western margin of southern Africa is predominantly calcareous. The Neogene succession of the ODP Sites 1085, 1086 and 1087 (Figure 7.29) is predominantly a nannofossil ooze, increasing slightly up-core in grain size to a nannofossil-foraminiferal ooze and a foraminiferal ooze at Site 1087 only, where the sand fraction is dominated by foraminifera (Berger *et al.*, 2002). The scarce compositional data for the shelf sediments (Section 2.7.3.4.2) suggest that calcareous clays dominate, where the green, brown or brown-green clay may include a proportion of glauconite and little terrigenous material (Dingle *et al.*, 1983; Dale and McMillan, 2003a). Therefore, this study suggests that there is far more terrigenous material in Pliocene sediments of the western margin than has been reported or inferred in the literature. The rapid progradation of quartzose sediments across the narrow steep inner to middle shelf onto the broad outer shelf followed by the incision of the Head of the Cape Canyon (Chapter 8) may account for the unusual preservation of the Pliocene succession in Concession 20D. The incision of a cross-cutting canyon would have had important implications on the hydrodynamics of the area with the canyon acting as a preferential transport pathway, thereby protecting the outer shelf from regional erosion (Granata *et al.*, 1999).

7.3.3 REWORKED MIOCENE IN THE PLIOCENE SUCCESSION

The mid Miocene depositional environment is interpreted using the single Core 319, recovered on the Eastern Flank of the Cape Canyon (Chapter 6). No upper Miocene (to lower Pliocene) sediments were recovered during this study or elsewhere along the western continental shelf of southern Africa (Chapter 2). However, the reworked middle to upper Miocene foraminifera recovered from the Pliocene Succession allow for some speculation on the geological history of the western margin during this time period (Figure 7.30).

7.3.3.1 QUARTZOSE DELTA FRONT DEPOSITS

The distribution of the Pliocene Quartzose Muddy Sand within Concession 20D is part of a far more extensive deposit that extends across the inner to outer shelf west of St. Helena Bay (Birch, 1975) (Figure 2.8). The surficial Holocene samples are texturally similar to the Quartzose Muddy Sand Unit and are composed of very fine quartz sand to muddy sand (Birch, 1975; Rogers and Bremner, 1991). However, faecal pellet-rich quartz sand dominates the inner-shelf north of the Berg River, reflecting the increased productivity associated with the modern Columbine upwelling cell (Shannon and Nelson, 1996). Birch (1975) proposed that the terrigenous sediments of the western margin were reworked out onto the outer shelf during the major Pliocene regressive/transgressive cycle (T_4) of Dingle (1970b, 1971a, 1973c). Further to the north, Rogers (1977) noted the presence of well-sorted, very fine quartzose sand across the shelf and slope west of Lüderitz, deposited during the Late Miocene regression and reworked and winnowed during the late Pliocene regression. Therefore, it appears that the observed deposition of the Quartzose Muddy Sand in the study area was part of a widespread process on the western margin of southern Africa.

University of Cape Town

The deposition of these Pliocene siliciclastic sediments on the continental shelf of southern Africa is poorly constrained. The Pliocene Succession quartzose sediments include a reworked middle to late Miocene (9.1-15.8 Ma) foraminiferal assemblage, suggesting a major input of well-sorted very fine quartzose muddy sand onto the inner to middle shelf along the entire southern African margin (Figure 7.30). What is the source for this widespread well-sorted, very fine quartzose muddy sand? The most likely source is fluvial and so the Orange and Olifants river sediments are examined as modern analogues. The Pleistocene and Holocene Orange River delta fronts (Rogers, 1977) and the Holocene Olifants River delta front (Birch, 1975) are characterised by well-sorted, very fine quartz sand, indicating that modern deltas are very effective at sediment fractionation. Therefore, the well-sorted, very fine quartzose sand of the western margin, typified by the Quartzose Muddy Sand Unit, may indicate a period of widespread siliciclastic input onto the western continental margin during the middle to late Miocene, where the grain size and sorting along with distribution on the margin sediments indicates a series of delta front-type depositional environments.

Fluvial deposits, preserved from palaeo-drainage systems of southern Africa, consistently show increased activity during the Miocene, Pliocene/Pleistocene and late Pleistocene/Holocene (De Wit *et al.*, 2000). A number of onshore diamond-bearing placer deposits indicate widespread fluvial activity during the lower to middle Miocene, *i.e.* the Bosluispan/Geelvloer fluvial phase of De Wit (1993, 1999). The fossil record preserved in the fluvial grits and gravels at Bosluispan within the Koa/Geelvloer palaeo-river valley of the Northern Cape are interpreted to represent a riparian woodland environment and a more tropical climate, with the main depositional event at 15-16 Ma (Senut and Pickford, 1996). A similar environment and age (± 17-19 Ma) are suggested for the Arrisdrift sediments of southern Namibia (Jacob *et al.*, 2000; De Wit *et al.*, 2000). Similarly, Smith and Mason (2002) described the mid-Miocene (±16-10 Ma) Karpfenkliff Conglomerate Formation in the central Namib Desert, which are alluvial fan deposits related to increased rainfall during the mid-Miocene.

The onshore record of increased fluvial activity in the middle Miocene is related to the mid-Miocene Climatic Optimum (Flower and Kennett, 1994; Gallagher *et al.*, 2001; Zachos *et al.*, 2001), where the interval from ~16-14.8 Ma is marked by major short-term variations in global sea level and climate. (Flower and Kennett, 1994). This wetter phase occurred immediately after the (~18 Ma) middle Miocene uplift event (Chapter 6). The consequence of these environmental changes would have resulted in an increased fluvial erosion of the uplifted continental margin with an increased sediment supply to the palaeo-drainage systems. Following the increased fluvial activity of the middle Miocene, the climate of the west coast of southern Africa became more arid (De Wit *et al.*, 2000), with the fluvial source of sediments becoming considerably reduced. Aridification of the western margin is interpreted to reflect the initiation (intensification) of upwelling of the Benguela system during the late Miocene (Section 2.4; Siesser, 1978b; Ward and Corbett, 1990; Diester-Haass *et al.*, 1992; Berger and Wefer, 1996a; Wefer *et al.*, 1998; Diester-Haass *et al.*, 2002).

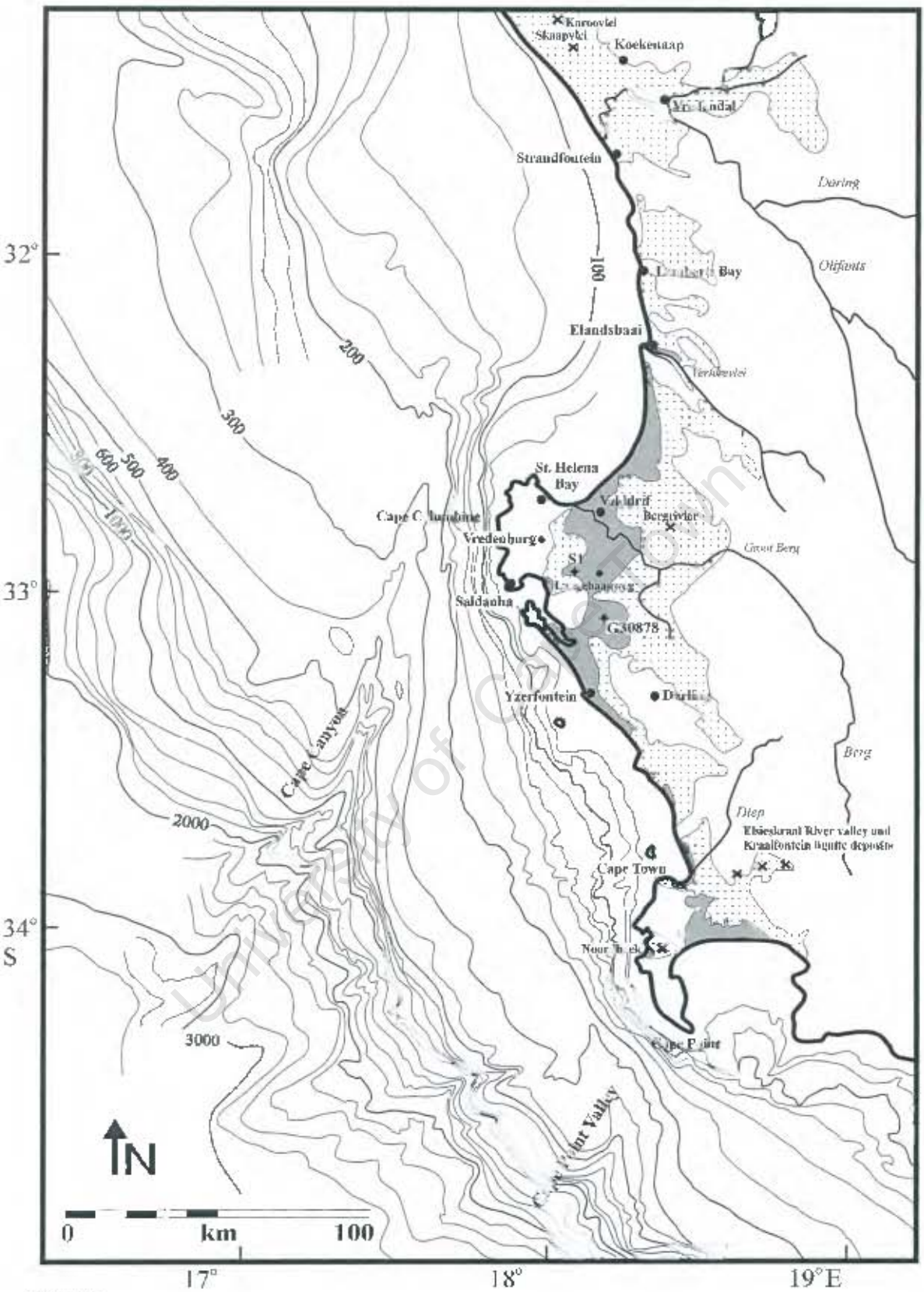
University of Cape Town

THE ELANDSFONTYN FORMATION

The onshore sediment record for the southwestern Cape was examined in order to ascertain whether the fluvial source for the Pliocene quartzose sediments of Concession 20D could be identified. The Elandsfontyn Formation is interpreted as the sediments of a meandering river system and is therefore a possible source for the delta-front quartzose muddy sands. The age of the Elandsfontyn Formation has been the subject of considerable debate in the literature (Section 2.5.2), although there is general agreement on an early to middle Miocene age, based largely on palynology (*e.g.* Coetzee and Rogers, 1982; Coetzee, 1986; Cole and Roberts, 1996; Roberts and Brink, 2002). If it is middle Miocene in age, then the Elandsfontyn Formation is the most likely palaeo-fluvial source for these reworked quartzose sediments of the Quartzose Muddy Sand. A number of Elandsfontyn Formation samples were collected as very little sedimentological data are available in the literature. The only other reported middle Miocene deposits preserved along the West Coast are the marine terrace deposits preserved as the 90 m package along the Namaqualand coast. The 90 m package has a basal gravel, with abundant silcrete clasts, overlain by a coarse to medium red sand with laminated heavy mineral sand deposited on the wave cut platform during falling sea levels (Rogers *et al.*, 1990; Pether, 1994a).

Although the Elandsfontyn Formation (Rogers, 1980) is referred to extensively in the literature, it is not yet recognised as a lithostratigraphic unit by the South African Committee for Stratigraphy (SACS). The Elandsfontyn Formation, the lowermost unit of the Tertiary Sandveld Group, is described from borehole core material with the holostratotype being borehole G30878 (Figure 7.31) drilled on the farm Elandsfontyn 349 (Rogers, 1980; 1982). The Elandsfontyn Formation is found below the coastal plains between Darling and the Elandsbaai area (Rogers, 1982). However, similar peaty angular quartzose sand is intercepted in boreholes drilled in the Noordhoek-Fishhoek Valley and in the Cape Flats area (Rogers, 1980, 1982; Theron et al., 1992). Cole and Roberts (1996) correlated the informally named "Channel Clay" successions of the Karoovlei and Skaapvlei palaeo-channels in the Koekenaap region with the Elandsfontyn Formation, on the basis of similar palynomorph assemblages (Figure 7.31). The Elandsfontyn Formation rests unconformably on deeply weathered Late Precambrian bedrock (Pether, 1994a) and reaches thicknesses of up to 60 m (Cole and Roberts, 1996). It is characterised by angular, quartzose fining-upward cycles, varying from gravelly sand to peaty clay, where the upward fining cycles are interpreted as deposits of tropical meandering rivers (Rogers, 1982; Theron et al., 1992). The quartz sands are carbonate- and phosphorite-free and diagenetic marcasite is common in the clay-rich intervals (Rogers, 1982). The overall upward fining of the Elandsfontyn Formation has been ascribed to the rise in the base level associated with rising sea levels of the mid-Miocene (Cole and Roberts, 1996). Palynology of the clay units suggests middle to late Miocene ages, based on the presence of Asteraceae palynomorphs, and a warm and humid palaeo-climate (Coetzee and Rogers, 1982; Cole and Roberts, 1996) with the sediments aggrading during a middle Miocene transgression (Cole and Roberts, 1996). The kaolinite-rich and lignitic succession of the Koekenaap region were deposited in palaeo-channels that linked up with the palaeo-Olifants River, under similar climatic conditions to those ascribed to the Elandsfontyn Formation (Cole and Roberts, 1996).

University of Cape Town



LEGEND:

- Cenozoic sediments (Cole and Roberts, 1996)
- Bedrock topography <-20 to 0 m for areas south of Elandsbaai (Rogers, 1980)
- Known lignite deposits of Elandsfontyn Formation (Cole and Roberts, 1996)
- Various boreholes penetrating the Elandsfontyn Formation (Rogers, 1980)
- Bathymetry (60-300 m in 20 m intervals; 1000-3000 m in 200 m intervals) after Dingle (1971b) and Dingle *et al.* (1987)

Figure 7.31. The distribution of Cenozoic sediments in the western Cape.

University of Cape Town

Several remnants of widespread fluvial systems are present along the Namaqualand coast between the Olifants River and Kleinzee (Figure 2.2; Pether, 1994a; Pether *et al.*, 2000; De Villiers and Cadman, 2001), where the palaeo-fluvial channels are infilled with arkosic gravels and sands in a poorly sorted sandy kaolinitic matrix and include significant diamond content (Pether, 1994a). The sand fraction of the predominant conglomeratic portions include coarse to very coarse angular to subangular quartz grains (Pether, 1994a). The latter suggests that the high-energy, arkosic, fluvial channel fill deposits overlain by clayey sand, clay and carbonaceous material (Rogers *et al.*, 1990), were subsequently kaolinised (decomposition of feldspar) and locally silicified in humid conditions in the Hondeklipbaai area (*in situ* chemical weathering). The presence of organic material in the sediments supports a humid climate (Pether, 1994a). The age of these channels is poorly constrained and proposed ages vary from the Palaeocene to pre-later Middle Miocene (De Villiers and Cadman, 2001) and Neogene (Lower Miocene pollen assemblage in Pether, 1994a). Pether (1994a) acknowledged that these channel deposits may not be coeval, although the Namaqualand fluvial deposits have tentatively been correlated with the Elandsfontyn Formation because both units are contained in channels incised into the bedrock during the Oligocene lowstand (Rogers *et al.*, 1990; Cole and Roberts, 1996). Pether (1994a) has suggested that the correlation may be problematical because the Elandsfontyn Formation shows no evidence of *in situ* weathering (kaolinitisation or silicification).

Ten representative samples were collected from the holostratotype borehole G30878 at Elandsfontyn using the sediment summary core log of Rogers (1980) to ensure that a representative suite of samples were collected (Figure 7.31). Two additional samples were collected from the S1 borehole at Langebaanweg, which was used for palynology studies (Coetzee and Rogers, 1982) although, unfortunately, the mud-rich samples were not available for sampling. The samples (typically ~50 g) were collected from the bulk reserve samples, stored in plastic containers at the core store of the Council for Geoscience in Belville. Four additional samples were collected from the three incomplete Saldanha Steel boreholes (9/14, 9/11 and 9/12) collected from the general vicinity of 32°58.648' S and 18°01.378' E and stored at the West Coast Fossil Park at Langebaanweg (Figure 7.31).

The sediments show a general increase in mud up-core in agreement with the core log of Rogers (1980) (Figure 7.32). The textures of the Elandsfontyn Formation sediments, which vary from mud to sand end-members, with varying amounts of gravel, are shown. The Elandsfontyn Formation sand (and gravel) studied is composed predominantly of angular to subangular quartz grains showing considerable variation in grain size. The sand fraction is characterised by a bimodal (to multi-modal) grain size distribution, where most samples include a distinct very fine sand population (Figure 7.32). The sand fraction from the sandy mud of G30878-9 has a grain size distribution that closely resembles the Pliocene Quartzose Muddy Sand Unit. A minor to trace iron-sulphide phase is ubiquitous in the sediments, although it is present in higher proportions in the muddier and more peaty intervals, where the sulphides appear to have replaced organic matter (Figure 7.33). The sulphide phase in these samples is characterised by a blue tarnish, which suggests that pyrrhotite dominates (Deer *et al.*, 1966), with only minor amounts of pyrite present.

University of Cape Town

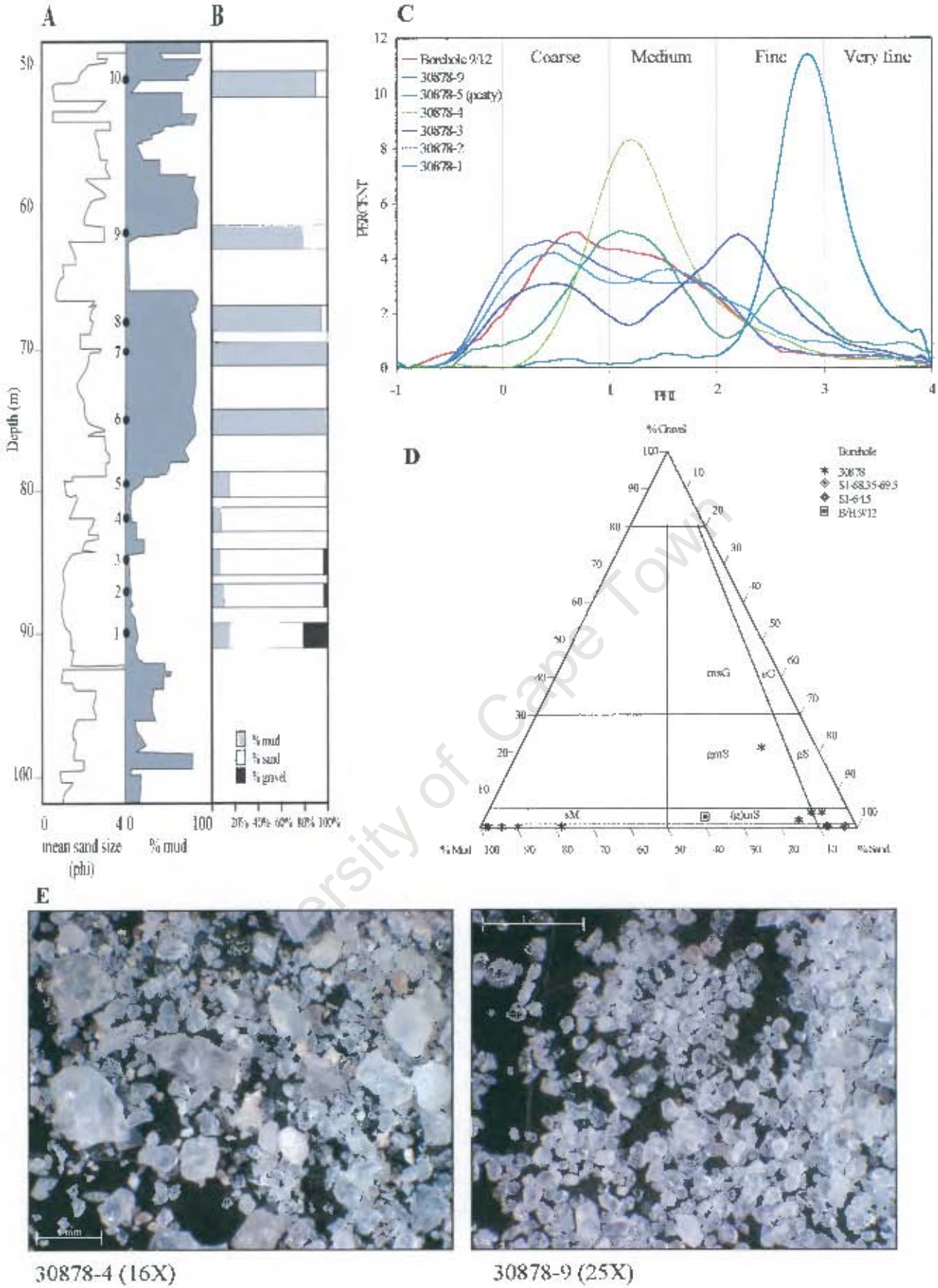


Figure 7.32. A: The section of the core log for G30878, the holostratotype core of the Elandsfontyn Formation after Rogers (1980) with samples locations for this study superimposed.
B: The sediment textures obtained for the samples collected
C: Frequency curves showing the particle-size distribution of the sand fraction of selected samples.
D: Grains size textures for all samples.
E: Photomicrographs of the sand fraction from selected samples from borehole G30878

University of Cape Town

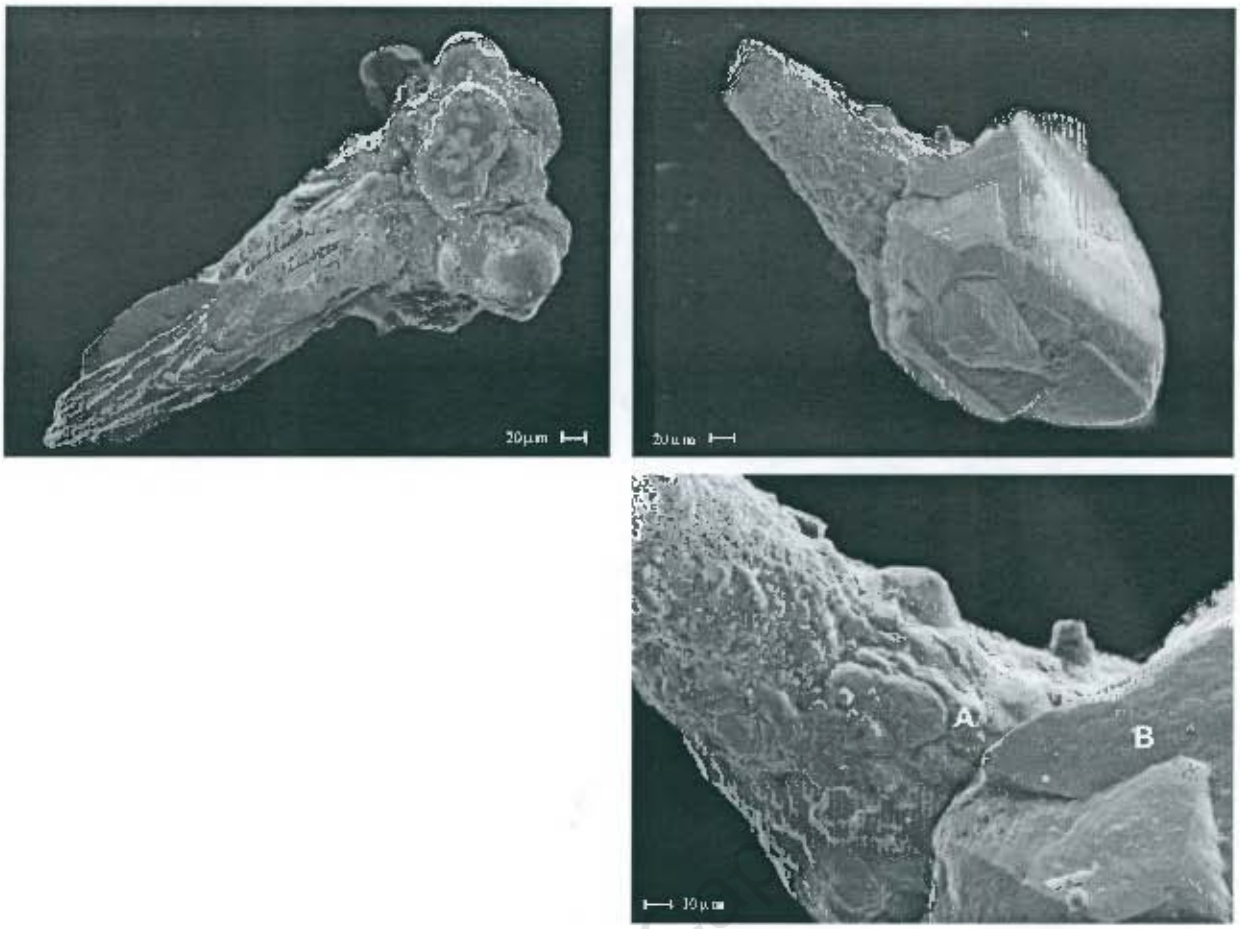
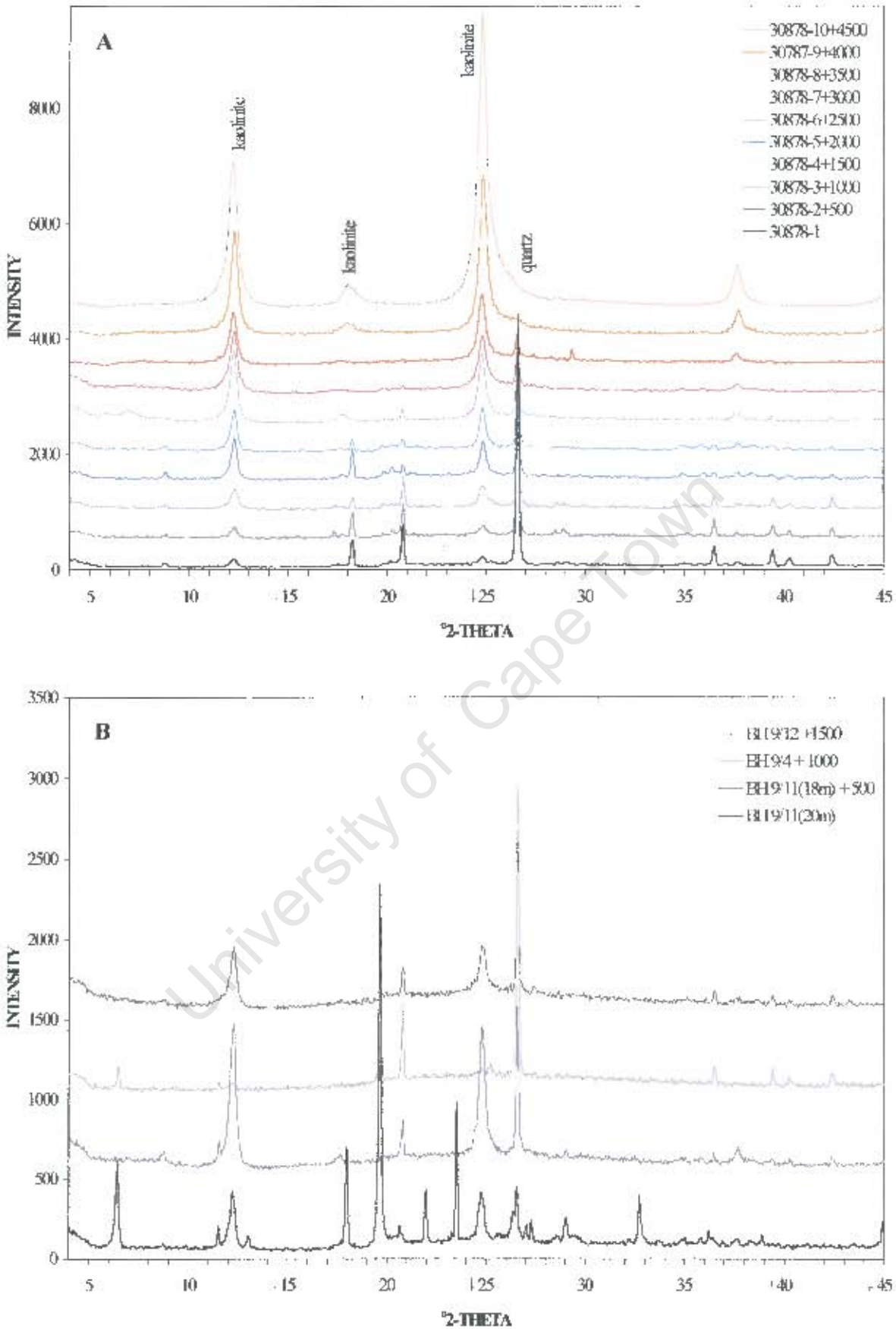


Figure 7.33. SEM images of the blue-tarnished iron sulphides from G30878-7. EDS scans show considerable variation in the weight % Fe : S ratio between points A & B, with the ratio at A: 43.93:52.92 (FeS / Pyrrhotite) and at B: 33.54: 62.43 (FeS_2 / Pyrite). Pyrrhotite tarnishes easily to iridescent colours, which suggests that the bulk of the sulphides in the samples are Pyrrhotite.

Traces of sand-size feldspar grains and lithic fragments, typically, sandstone (cemented quartz) and Malmesbury Group shale were observed. Occasional well-rounded frosted quartz grains are present. These grains are very similar in appearance to the Cretaceous quartz from the Woody Quartzose Sand unit of this study, suggesting that re-worked Cretaceous sand may be included in this unit.

XRD analyses show that the mud fraction is dominated by kaolinite, although a non-expandable 10 Å sheet-silicate (illite/mica) is present (Figure 7.34). Some of the samples include gibbsite, a common soil-forming mineral and jarosite is also present in sample 9/11-20 m (see discussion in Woody Quartzose Sand in Chapter 4). Birch (1974) studied the clay fraction of a large number of Holocene surficial marine sediments as well as the Holocene alluvium being supplied to the shelf by the major rivers of the West Coast. He found that the clay fraction of the entire West Coast continental shelf is dominated by illite (63-75%) with lesser amounts of kaolinite (25-37%). Kaolinite and illite are the only clay minerals being delivered by the modern fluvial systems (Birch, 1974) south of 30°S, with the clay compositions of the river samples being more variable and dependent largely on the bedrock composition. Therefore, the high kaolinite content of the Elandsfontyn Formation suggests that the quartz is locally derived from the Cape Granite and Table Mountain Group (Birch, 1974).

University of Cape Town



University of Cape Town

Figure 7.34. XRD records for the mud fraction (<63 µm) of the Elandsfontyn Formation from A) G30878 and B) the Saldanha Steel boreholes.

The close proximity of the Pliocene Quartzose Muddy Sand Unit offshore in Concession 20D and the Elandsfontyn Formation suggests that the offshore and onshore sediments might be syndepositional. However, until the age of the Elandsfontyn Formation is better constrained, any correlation between the onshore and offshore sediments, is at best, tentative. The much coarser grain size of the Elandsfontyn Formation compared to that of the Quartzose Muddy Sand Unit argues against correlation of the onshore and offshore sediments. However, the modern Orange and Olifants River deltas are very effective at sediment fractionation with their delta fronts composed almost entirely of a similar well-sorted, very fine quartzose sand. The coarser sand being retained in the littoral zone and transported northwards by longshore drift (Rogers, 1977). The absence of any lithic fragments in the Pliocene Quartzose Muddy Sand Unit prevents any interpretation on the possible source region for these quartzose sediments.

Although further work is clearly required, enhanced fluvial activity during the middle to late Miocene resulted in the deposition of siliciclastic, delta-front deposits along the inner to middle shelf of the western coast of southern Africa between Cape Columbine and Lüderitz. Deposition of the prograding wedge of siliciclastic sediments would correspond to the proposed overall fall in eustatic sea level during the middle Miocene (Figure 7.29). The middle to late Miocene age proposed for the Elandsfontyn Formation (Coetzee and Rogers, 1982; Cole and Roberts, 1996) and for many of the other fluvial sediments of the Namaqualand coast are similar to those recovered in the reworked foraminiferal assemblage of the Quartzose Muddy Sand. The quartzose sand deposition is interpreted to reflect increased climate and uplift-driven fluvial activity in the middle Miocene. Whether this fluvial activity is preserved as the Elandsfontyn Formation cannot definitely be established, but it seems likely. The medium to coarse sand of the early to basal Middle Miocene (Pickford and Senut, 1999) ~16 Ma (Pether *et al.*, 2000) (Section 2.7.2) 90 m Marine Terrace deposits at Hondeklipbaai may reflect the northward movement by longshore drift of the coarse fraction of these fluvial sediments, as has similarly been argued for the Orange River (Rogers, 1977).

University of Cape Town

7.3.3.2 GLAUCONITIZATION

While these quartzose silty delta-front sands were being deposited on the inner to middle shelf during the mid to late Miocene, the Gravelly Calcareous Quartzose Muddy Sand, recovered in Core 319, was being deposited in deeper water (Figure 7.30). The Sr-derived ages of 15.8-16.8 Ma (benthic foraminifera) and 14.8-16.3 Ma (SPG), recovered from the basal lag in Core 90 (Compton *et al.*, 2004), suggest that this sedimentary facies was later largely reworked, with the gravel fraction preserved in the very condensed Phosphorite Gravel lag. Erosion of the outer shelf is interpreted to reflect, in part, the proposed uplift of the western margin in the mid Miocene (Section 6.7), when the long-term middle to late Miocene eustatic regression (Figure 7.29) and increased oceanic circulation of the Neogene oceans (Kennett, 1982) may have further enhanced winnowing on the shelf.

The 5.8-10.9 Ma Sr-ages of reworked benthic foraminifera and SPGs recovered from the Glauconitic Sand unit indicate that the largely absent (apart from the single Middle Miocene Unit in Core 319)

middle to late Miocene complex geological history of Concession 20D is preserved in the condensed Glauconitic Sand Unit (Figure 7.29). The green glauconite of the Gravelly Calcareous Quartzose Muddy Sand of Core 319 is very similar in appearance to the green glauconite of the Pliocene Succession, suggesting that glauconitization in largely similar depositional environments must have occurred throughout the middle to late Miocene and into the Pliocene. K/Ar-ages ranging from 6.5-17.7 Ma reported by Birch (1975), support this long history of glauconitization on the western margin. The intensification of upwelling in the mid to late Miocene is associated with aridification of the western margin of southern Africa (Siesser, 1978b; Ward and Corbett, 1990), with the change to a more arid temperate climate occurring at ~15 Ma (De Wit *et al.,* 2000; Pickford and Senut, 1999). The late Miocene aridification would have resulted in a sediment-starved western margin following termination of the fluvial activity recorded in the reworked foraminifera of the Quartzose Muddy Sands. The much reduced fluvial sediment input onto the western margin would have favoured glauconitization. Recent work (Vidal *et al.*, 2002; Diester-Haass *et al.* 2002) on ODP Site 1085 (Figure 2.1 and 2.2), located to the north of Concession 20D, on the slope off the Orange River, shows that the late Miocene (6.9-9.1 Ma) was a period of low sediment-accumulation rates (<5 cm/kyr) indicating low carbonate productivity and low accumulation rates on the continental slope, conditions favorable for glauconite formation.

Many of the foraminifera preserved in the lower parts of the Glauconitic Muddy Sand have a robust appearance, similar to those recovered from the Holocene sediments to the north of the study area (McHutchon, 2003). The Holocene mudbelt is generally low in foraminiferal abundance and biodiversity (Dale and McMillan, 1998a) similar to the Glauconitic Sand Unit. Sancetta *et al.* (1992) and Diester-Haass *et al.* (1986) argued that the poor correlation between biogenic opal and carbonate (as indicators of primary productivity) at DSDP Site 532 on the Walvis Ridge suggests variable calcite preservation, where calcite fragmentation and dissolution is highest during glacials. They argued that the correlation between mud content and the carbonate record suggests that organic-rich mud belts existed during highstands of the Pliocene. These reworked condensed glauconite sediments are interpreted to indicate that organic-rich mudbelts were present along the western margin during middle to upper Miocene relative highstands. The repeated lowering of relative sea level would result in the re-suspension and winnowing of the mudbelt. Lowstand erosional events would result in the oxidation of organic matter and sulphides, removal of clay and fine silt and the concentration of authigenic glauconite sand grains. However, the upcore fining of the quartz sand in the Glauconitic Muddy Sand Sub-unit of Core 30 favours an overall increase in water depth with time, which would reflect a combination of increased margin subsidence and the overall latest Miocene to early Pliocene rise in the eustatic sea level (Figure 7.29). A final Pliocene depositional age is inferred from the foraminiferal assemblage from the base of Core 30, although the Glauconitic Muddy Sand Sub-unit includes none of the typical Pliocene species (Figure 7.28). The glauconite in the upper parts of Core 30 (Samples 30-2 and 30-1) is finer grained and fractured, with a sugary internal texture. This reworked interval also records the first appearance of the distinct Pliocene foraminiferal assemblage (Figure 7.28A). The upper parts of the underlying Glauconitic Muddy Sand are interpreted to have been reworked, supporting the interpreted later Pliocene reworking of the Glauconite Sand Unit. The presence of scattered isolated

University of Cape Town

pebbles to cobbles throughout the glauconite-rich sediments of the outer shelf (Table 7.1) are interpreted as kelp-rafted debris (Woodborne *et al.*, 1989), possibly providing evidence of kelp forestation, which requires upwelled cold water, of the West Coast since the late Miocene/early Pliocene.

The late Miocene was a time of global cooling, prior to the early Pliocene climatic warmth, although a late Miocene increase in global ice volume is still being debated because it is not ubiquitously recorded in late Miocene benthic foraminiferal $\delta^{18}O$ records (Billups, 2002). This early Pliocene global warming, as deduced from warming of deep-water temperatures in the South Atlantic, might be linked to the gradual closure of the Isthmus of Panama (Vidal *et al.* 2002). Haug and Tiedmann (1998) argued that the closure of the Isthmus of Panama caused a marked reorganisation of ocean circulation starting only 4.6 million years ago, where they compare the stable-isotope and carbonate sand fraction records of Caribbean sediments to the Atlantic and Pacific sediment records. Vidal *et al.* (2002) argued that the late Miocene sedimentary sequences throughout the world record a long-term eustatic drop in sea level, with significant lowstands at 6.1 Ma and 6.8 Ma, where this overall drop in sea level is associated with an increased Antarctica ice volume. The high-resolution sediment record from ODP Site 1085 on the slope off the Orange River shows a dramatic increase in sedimentation rate from the late Miocene (6.5-6.7 Ma) to the early Pliocene (4.8 Ma) with a maximum at 5.3 Ma (12 cm/kyr). Similarly, the percentage of terrigenous material and glauconite present is low until about 6.5 Ma and increases after 5.7 Ma with maxima at 5.3-5.6 Ma and at 4.8 Ma. The sediment accumulation rates of ODP Site 1085 are highly variable, where cooler intervals are associated with greater productivity (Diester-Haass *et al.*, 2002), whereas the increased terrigenous sedimentation rates could be linked to enhanced fluvial supply during interglacial periods (Vidal *et al.*, 2002).

The Pliocene Glauconitic Sand Unit is interpreted to record alternating relative transgressive periods of increased productivity and terrigenous input in an environment similar to that of the Holocene Namaqualand mudbelt, followed by winnowing of the fine fraction during the lowering of the relative sea level. These interpreted fluctuations in sea level may simply reflect changes in the eustatic sea level (Figure 7.29). However, the changes in relative sea level along the western margin may simply reflect changes in accommodation space recording changes in subsidence rate *vs.* uplift rate. Although Amorosi (1997) notes that glauconites of superimposed third-order cycles are generally distinguishable on a geochemical and mineralogical basis, this is apparently not true for glauconite of the western margin. The upper Miocene–Pliocene transgressive sequence of the New Jersey outer shelf is similarly interpreted by Metzger *et al.* (2000) to have formed by high-frequency eustatic cycles (1–2 Myr) superimposed on a longer-term eustatic rise (~5 Myr).

University of Cape Town

8 QUATERNARY SUCCESSION

Three compositionally distinct Pleistocene facies are recognised in Concession 20D. The Pleistocene sediment record shows a well-defined correlation between sediment composition and bathymetry of the study area. The outer shelf sediments are dominated by glauconite, but include a subordinate biogenic component. Calcareous Quartzose Very Fine Sand crops out on the seaward flank of the Western Ridge. The sediments of the Canyon Head area are composed of varying abundances of quartz and glauconite, with a fine to medium glauconitic quartzose sand present in the Northern Depression and a bimodal medium to very coarse quartzose sand present in the southern Main Channel area. The three Pleistocene sediment facies are described, starting on the outer shelf, in the subsequent sections. Holocene faecal-rich sediments are recovered as a uniform thin veneer less than 20-30 cm thick, across most of Concession 20D.

8.1 CALCAREOUS GLAUCONITIC SAND OF THE OUTER SHELF SUCCESSION

The stratigraphy of the Glauconitic Sand Unit of the outer shelf was introduced in Chapter 7, where the Phosphorite Gravel and Pliocene Glauconitic Sand facies are overlain by the Pleistocene Calcareous Glauconitic Sand facies (Figure 8.1). The contact between the Calcareous Glauconitic Sand and the underlying Pliocene Glauconitic Sand is poorly defined and appears gradational. However, the Pleistocene Calcareous Glauconitic Sand is recognised by the speckled appearance of the sand, reflecting the abundance of calcareous grains, in contrast to the dark green to black colour of the underlying Glauconitic Sand facies. The distribution of the glauconite-rich sediments is shown in Figure 7.2. The Calcareous Glauconitic Sand facies was recovered from all of the WMR cores present in the study area in which the glauconite-rich sediments was recovered.

The Calcareous Glauconitic Sand, recovered from the Central Transect, is approximately 75 cm thick, but varies in thickness from >2 m, thinning seawards of the Western Ridge to less than 30 cm in Core 129 (Appendix A1-29). The Calcareous Glauconitic Sand recovered from Core 186 of the Southern Transect is similar in thickness and appearance to the Calcareous Glauconitic Sand of the Central Transect. However, the sediments recovered from the remaining gravel-rich cores collected from the Southern Rocky Plateau (Cores 187, 190 and 324), record a complex condensed sequence, which includes Pliocene foraminifera near the base of the core and abundant Pleistocene species throughout. However, in all three cores, a distinct Calcareous Glauconitic Sand facies sand fraction is present below the Holocene drape, with a shell-rich layer recovered in Core 187 from 20-24 cm.

A shell-rich interval is commonly recovered towards the very top of the Calcareous Glauconitic Sand facies. This shell-rich interval, although not well represented in Core 128 (Figure 8.1), is laterally continuous throughout the Glauconitic Sand Unit and defines the upper contact of this Pleistocene unit. The shell-rich interval is most commonly recovered as an approximately 5-50 cm thick shell-rich lag layer. However, a number of discrete shelly layers, rather than a single shell-rich layer, may be

University of Cape Town

recovered towards the top of the facies (Core 122), whereas in other cores only a gravelly sand with scattered shell fragments was recovered (Core 118). The abundance of shelly material in the Calcareous Glauconitic Sand is reflected in the sediment grain-size textures, which vary from a sand to a sandy gravel (Figure 8.2), with a uniformly low mud content of less than 10%.

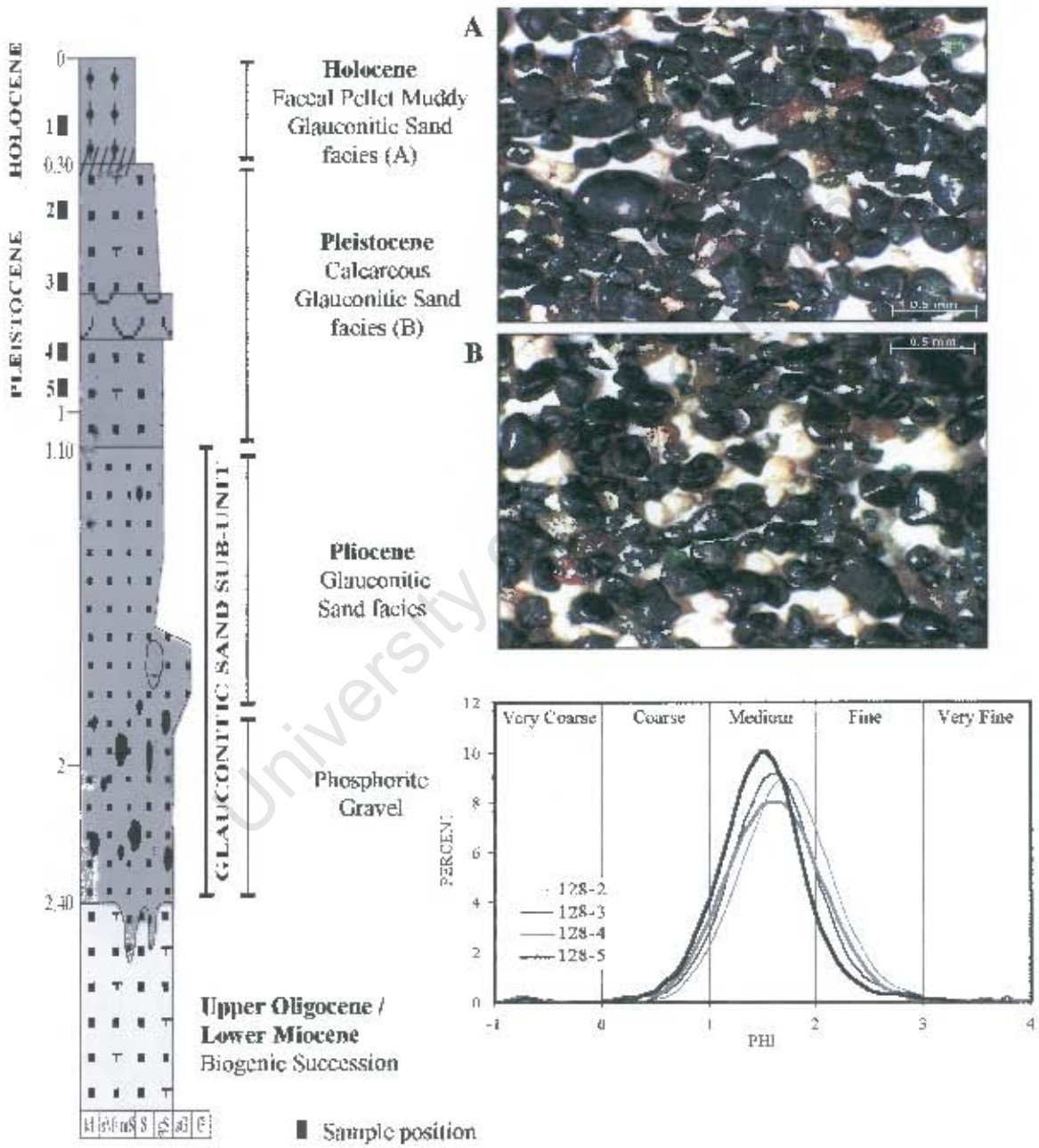


Figure 8.1. The stratigraphy of the glauconite-rich sediments of Core 128 (see Figure 7. 3). The legend for the symbols is included in Figure 1.1 with the grey scale reflecting the glauconite abundance. The photomicrographs (A : 128-1 and B: 128-3) show the main characteristics of the sand fraction of the Quaternary glauconitic sediments of the outer shelf. The frequency curve shows particle size distribution of the sand fraction of the Calcareous Glauconitic Sand facies.

University of Wollongong

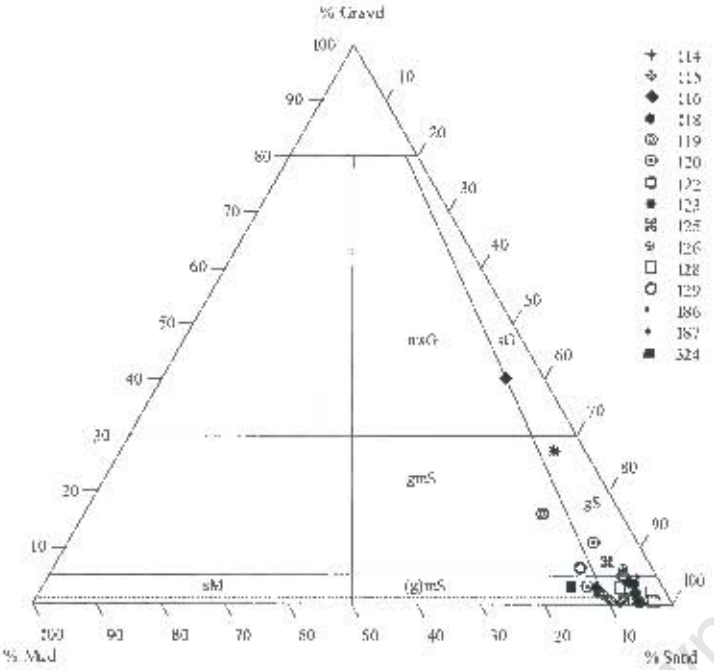


Figure 8.2. A summary of the grain size textures for the Calcareous Glauconitic Sand.

Mollusc shells were identified with the assistance of J. Pether (De Beers Marine) using the macrofaunal reference collection at UCT, Branch and Branch (1981) and Kilburn and Rippey (1982). The shell layer is dominated by the bivalve *Limopsis chuni*, which varies from articulated to worn, leached and bored fragments, together with varying numbers of the gastropods *Turritella declivis*, *T. sanguinea*, *Amalda bulloides*, *Volutocorbis abyssicola*, *Cylichna tubulosa* and *Nassarius vinctus*. Other bivalve species present include *Anomia* sp, *Tawera philomela*, *Lucinoma capensis*, *Pitar abbreviatus*, *Cardiatella* spp., *Hiatella* sp., a small hooked *Patella* sp., *Pecten* sp., with the brachiopod *Megerlina pisum*, scaphopods, solitary coral, echinoid plates, bryozoa, fish otoliths, phosphatised bone, subrounded quartz (often green-stained) and phosphorite very fine to fine pebbles present. The above assemblage includes only the most abundant and commonly observed species and is not a comprehensive list of the macrofaunal assemblage. The shell assemblage of this layer is a typical Pleistocene assemblage, seen in the sediments of the west coast shelf (J. Pether, *pers. comm.*, 2003). The thin-shelled, often fragmented, bivalve, *Anomia* sp, forms a 7 cm thick articulated shell layer in Core 119. The upper shell layer includes only a minor lithic gravel component with granules of phosphorite, quartz and phosphatised shell fragments occasionally present. However, the shell layer in Cores 120 to 123 includes phosphatic pebbles (CFA-cemented glauconitic medium sand) and phosphatised mollusc casts finer than medium pebbles. A small cobble-sized phosphorite (CFA-cemented glauconitic medium sand) is also present in the shell layer of Core 123.

The well-sorted, medium sand fraction of the Calcareous Glauconitic Sand is composed of 40-50% black lobate polished glauconite, 15-20% authigenic grains (including sand-sized phosphorite fragments, pelletal phosphorite and phospho-glauconite foraminiferal infillings), 15-25% microfauna, 5-10% shell fragments and 10-15% very fine quartz (Figure 8.1; Table 8.1). Although minor amounts of

University of Cape Town

subrounded, medium sand-sized quartz is present in all of the Calcareous Glauconitic Sand, the Cores 114 to 116 also include up to 15% medium to coarse quartz sand. The abundance of the micro- and macrofaunal assemblage is reflected in the high average acid-soluble weight percent determined for the Calcareous Glauconitic Sand, with an average of 20.9 wt% and a maximum of 39.7 wt% recorded. The microfaunal component includes a diverse assemblage of thin-shelled, delicate planktic and benthic foraminifera with agglutinated miliolid foraminifera (*Siphonaperta martinae*) and ostracods present (Table 8.2). The Calcareous Glauconitic Sand also includes approximately 1-2% echinoid spines and traces of holothurian sclerites (Dale and McMillan, 1998a) and subordinate amounts of sand-size mollusc shell fragments (bivalve, gastropod), solitary coral, echinoid plates and scaphopods.

Table 8.1. The composition of the Glauconitic Sand Unit was determined by point-counting a minimum of 300 grains.

Sample	Glauconite	Phospho-glauconite	Very fine quartz sand	Medium quartz sand	Foraminifera	Calcareous fragments	Echinoid Spines	Other	
128-2	31.6	17.7	23.4	0.4	11.0	15.6	0.4		
128-3	37.9	15.8	15.1	0.3	18.6	11.3	0.6	0.3	Ostracods
128-4	33.2	9.0	20.2	0.4	12.3	24.5	0.4		
128-5	46.8	18.2	16.7	0.3	7.3	9.1	0.3	1.2	Ostracods

8.1.1 AGE OF THE CALCAREOUS GLAUCONITIC SAND

The foraminiferal assemblage from Samples 128-3 and 128-5 was picked and submitted to I. McMillan for identification (Table 8.2). The foraminiferal assemblage indicates a latest Pleistocene depositional age for the Calcareous Glauconitic Sand facies. The diverse outer-shelf planktic foraminiferal assemblage is dominated by the transitional species *Globorotalia inflata* and includes warm to temperate-water species such as *Globorotalia menardii*, *Globigerinoides ruber* and *Globigerinoides sacculifer* and lacks typical modern Benguela upwelling species such as *Neogloboquadrina pachyderma* (s), *Globigerina bulloides* and *Globorotalia truncatulinoides* (s).

University of Cape Town

Table 8.2. A summary of the foraminiferal assemblage of Samples 128-3 & 128-5 from the Calcareous Glauconitic Sand (I. McMillan *pers. comm.*, 2003).

Samples	Age	Assemblage
128-3 and 128-5	Upper Pleistocene (Eemian to Weichselian)	Dominated by *Globorotalia inflata*, *Siphonaperta martinae* (agglutinated) *and Cassidulina laevigata*. Includes *Globorotalia menardii*, *Globigerinoides sacculifer*, *Globigerinoides ruber*, *Amphicoryna scalaris*, large *Cibicidoides* sp. *Lobatula lobatula*, smooth *Amphicoryna* sp., *Hoeglundina elegans*, *Orbulina universa*, *Globoquadrina dutertrei*. *Bulimina orangensis*, *Bulimina marginata*, *Bulimina aculeata*, *Uvigerina bassensis*, *Uvigerina peregrina*, *Globigerinella aequilateralis*, *Pyrgo* spp., *Elphidium advenum*, *Quinqueloculina dunkerquiana*, *?Fontbotia wuellerstorfi*, small *Nonion* sp., *Lenticulina sp.*, spiny *Ehrenbergina* sp., a few *Globorotalia truncatulinoides* and *Spiroloculina* cf. *communis* (a littoral species). (Sample 128-5 also includes *Planulina ariminensis* and *Pullenia subcarinata*.)

A Sr-age of 0.5-1.4 Ma was obtained from benthic foraminifera, echinoid spines and shell fragments collected at 45-47 and 86-91cm from Core 190 recovered on the southern Rocky Plateau (Chapter 7; Compton *et al.*, 2004). The presence of upper Pleistocene microfauna in the sediments of Core 190 indicates that the Pliocene sediment (interpreted using the microfaunal assemblage) was reworked during the late Pleistocene.

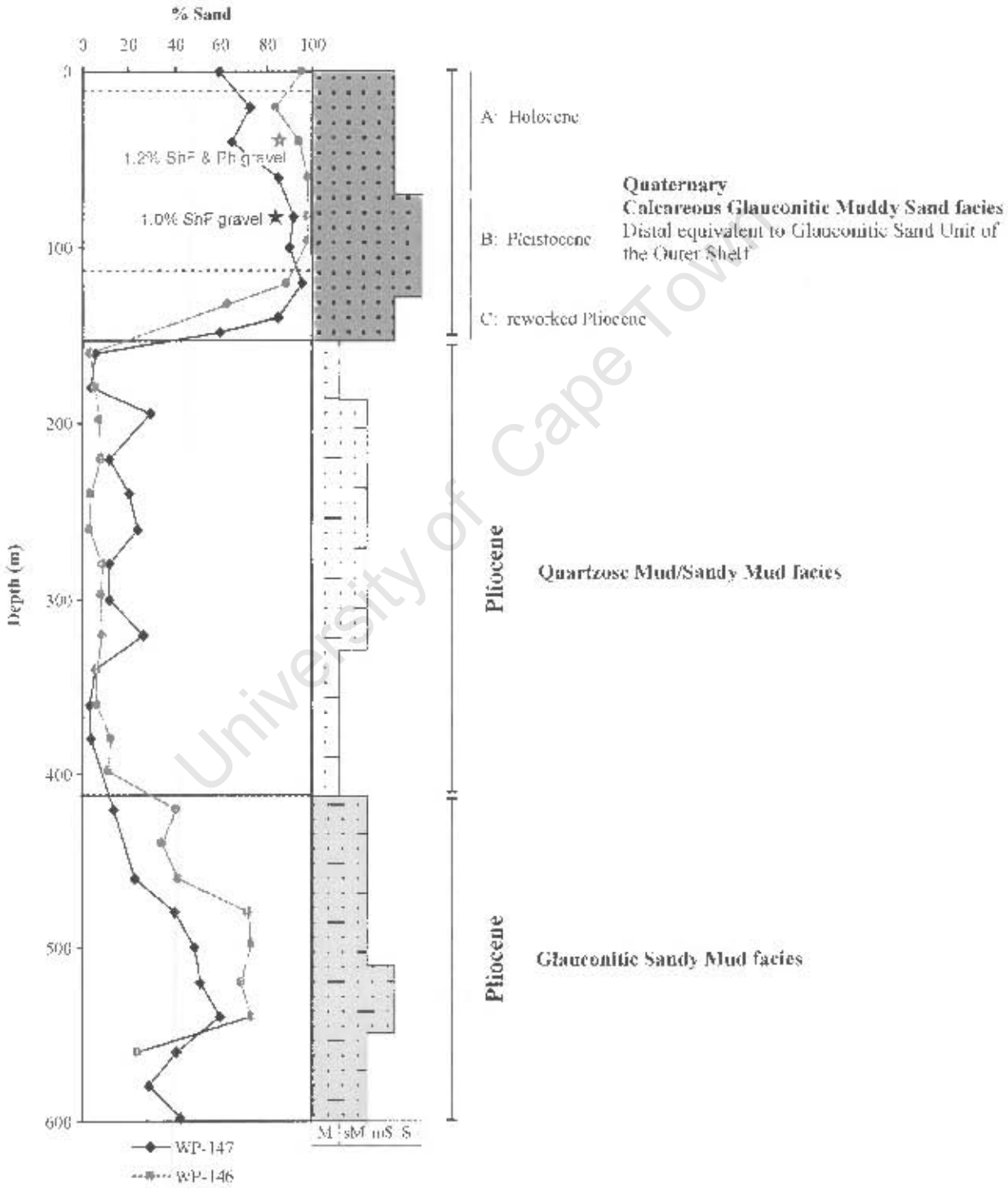


Figure 8.3. The percent sand and stratigraphy for the two upper slope Cores 146 and 147. A gravel fraction is present in the two samples indicated with a star.

University of Cape Town

8.1.2 UPPER SLOPE CORES

The outer shelf below 312 m is eroded so that the Upper Oligocene/Lower Miocene Calcareous sediments crop out on the sea-floor surface. However, Quaternary Glauconitic Sand to Muddy Sand are present in Cores 146 and 147, collected on the upper slope (Figure 7.1). The ~150 cm thick Quaternary sediments are recovered overlying a distal equivalent to the Pliocene Quartzose Muddy Sand and Glauconitic Muddy Sand Units, described in Chapter 7 (Figure 8.3). The fine to medium glauconite-rich Quaternary sediments of the upper slope cores reveal a stratigraphic succession of glauconite-rich sediments identical to that seen on the outer shelf (Chapter 7). The Pliocene Glauconite Sand overlain by a Pleistocene Calcareous Sand, which is in turn, overlain by a Holocene Faecal-rich Glauconitic Muddy Sand.

The base of the Quaternary unit is composed of >95% green earthy glauconite, 2% phosphorite and 2% foraminifera and closely resembles the Glauconitic Sand facies, although Holocene, Pleistocene and Pliocene foraminifera are present in these upper slope core (I. McMillan, *pers. comm.*, 2003). The Pliocene foraminiferal assemblage varies from fragments in Core 147 to delicate and well-preserved predominantly benthic species, including *Nodogenerina* and *Stilostomella* sp., in Core 146. Evidence suggests that the outer shelf Pliocene Glauconitic Sand was reworked onto the upper slope prior to the latest Pleistocene, therefore indicating a Pleistocene depositional age for the sample from 120-122 cm (near the base of the Calcareous Glauconitic Sand) in Core 147 (I. McMillan, *pers. comm.* 2003).

The basal glauconite-rich sand is overlain, from approximately 20-100 cm, by a typical upper Pleistocene sand composed of ~60% polished black lobate glauconite, 35% foraminifera (diverse planktic and benthic, often agglutinated, foraminiferal assemblage), 5% very fine angular quartz with traces of medium, subrounded, quartz grains, echinoid spines, ostracods and holothurian sclerites (Figure 8.3). Bivalve shell fragments, including rare gravel-size fragments, are occasionally present. The foraminiferal assemblage of the sample from 100-102cm in Core 147 indicates a latest Pleistocene age (I. McMillan, *pers. comm.* 2003). I. McMillan notes that the assemblage also includes temperate planktic species as seen in the Calcareous Glauconitic Sand Unit. The Pleistocene Sand is overlain by a veneer of typical Holocene Sand composed of ~60% polished black lobate glauconite; 10% phosphorite, 15% foraminifera (planktic dominated); 10% very fine angular quartz with traces of sponge spicules and echinoid spines.

8.1.3 DEPOSITIONAL ENVIRONMENT OF THE CALCAREOUS GLAUCONITIC SAND

The sediments of the Calcareous Glauconitic Sand are composed largely of glauconite with a significant biogenic component together with reworked PCG and very fine quartz sand. The biogenic fraction includes a diverse late Pleistocene macro-and microfaunal assemblage, which provides some insights into the depositional environment.

University of Cape Town

The Calcareous Glauconitic Sand is characterised by the presence of the well-preserved, widespread, capping shell layer, which is overlain by the Holocene Faecal-rich Muddy Sand. In addition, the WMR core logs describe the presence of multiple shell layers in many of the Calcareous Glauconitic cores from the outer shelf. Although not looked at in any detail, the shelly layer assemblage usually includes a combination of reworked, broken, bored shells together with articulated bivalves. The shell lag layers usually include a phosphorite component and quartz granules. Shell layers in marine sediments are typically interpreted to indicate condensed sediment surfaces where biological, sedimentological and diagenetic factors may play a role in concentration of shelly material (Kidwell *et al.*, 1986). The use of shell beds in sequence stratigraphic analysis is well established with shell concentrations representing discontinuity surfaces (Di Celma *et al.*, 2002; Abbot and Carter, 1994). Shelly layers in marine sediments are commonly interpreted to indicate the low sediment accumulations of transgressive systems tracts or the condensed surface corresponding to maximum transgressions (Kondo *et al.*, 1998). An understanding of the macrofaunal assemblage in association with the fauna of the intervening less shelly layers may be used to provide constraints on the changing environments of deposition associated with the fluctuating glacio-eustatic sea-levels of the late Pleistocene (Di Celma *et al.*, 2002). Recent work has shown that an understanding of the benthic assemblage as well as the taphonomy or mode of fossil occurrence allows inferences to be made about the characteristics of the condensed surface and the associated systems tract it is likely to be associated with (Kondo *et al.*, 1998). However, the Pleistocene shell assemblage was not examined in enough detail to make any such deductions.

During the Last Glacial Maximum (LGM) sea level dropped ±125 m along the west coast of southern Africa (Cutler *et al.*, 2003; Dale and McMillan, 2003b; Ramsay and Cooper, 2002; Compton *et al.*, 2002) and the study area would have been more proximal. Christie (1974) showed that the modern mollusc species diversity and abundance is greatest on the inner to middle shelf (20-150 m) on a transect west of Lamberts Bay (Figure 2.2), with very low gastropod and bivalve abundances recovered on the outer shelf at water depths greater than 200 m. The presence of the shelly layers in the Pleistocene sediments suggest that shallower, higher-energy oxygen-rich environments during relative lowstands supported a more abundant benthic community in the study area. The high biodiversity of benthic foraminifera of shelly layers in the Calcareous Glauconitic Sand indicates the increased availability of nutrients associated with upwelling. Glacial periods tend to be associated with increased upwelling and an associated increase in productivity along the western margin of southern Africa (Berger and Wefer, 2002). Martin (1981) also noted an increased biomass associated with upwelling in the benthic assemblage and showed a maximum biodiversity in the benthic foraminiferal population on the middle to outer Orange-Lüderitz shelf of southern Africa. The processes involved in the formation of these shelly layers on the outer shelf, whether due to erosion or non-deposition, is uncertain, although evidence does suggest a lowstand origin for these lag layers. The presence of multiple shell layers below the capping shell layer in some cores of the Calcareous Glauconitic Sand reflects the preservation of repeated late Pleistocene glacial-interglacial cycles.

University of Cape Town

The Pliocene Glauconitic Sand facies below the contact with the Pleistocene Calcareous Glauconitic Sand contain bioturbated cold-water or upwelling Pleistocene microfossils (Chapter 7), whereas the uppermost Pleistocene assemblage includes abundant transitional to temperate-water species. The Pleistocene foraminiferal assemblage shows a general increase in surface water temperatures up-core, and this warming of surface waters through the Pleistocene has been observed elsewhere along the western slope of southern Africa (Rau, 2002; Rau *et al.*, 2002). Rau *et al.* (2002) indicated that the coldest-surface water temperatures are recorded during the glacial MIS 12 (~430-470 ka) and noted that a profound change to overall warmer conditions and more pronounced glacial-interglacial fluctuations in surface water conditions occurs at MIS 7 (200-250 ka). The planktic assemblage of the latest Pleistocene of the outer shelf in Concession 20D is dominated by *G. inflata* and other transitional species and does not have a typical modern west coast Benguela upwelling cold-water assemblage (Rau, 2002), which may reflect warming of the surface water. In addition, Rau *et al.* (2002) noted that maximum leakage of warm Indian Ocean water via the Agulhas Current into the Atlantic Ocean occurs at glacial terminations. *G. bulloides* (cold-water) and *G. inflata* (transitional) dominated assemblages show high-frequency abundance changes through the last 600 ka in the IMAGES II core MD962085 (offshore the Orange River mouth). These are not parallel to the glacial–interglacial changes, and may be a response to rapid oceanic frontal movements from the south or changes in the upwelling signature (Chen *et al.*, 2002). Although further work is clearly required, it is proposed that the abundance of transitional species in the microfaunal assemblage may indicate that the shell-lag records the transition into the LGM deglaciation cycle.

The Calcareous Glauconitic Sand of the outer shelf of Concession 20D is interpreted to record the rapidly changing environments associated with changes in water depth during glacial-interglacial eustatic sea-level fluctuations. The uppermost Pleistocene Calcareous Glauconitic Sand is characterised by the presence of black, polished, lobate glauconite grains, in contrast to the green glauconite of the underlying Pliocene Glauconitic Muddy Sand. The differences in the appearance and geochemistry (Chapter 9) and similarities in grain size suggest Pleistocene glauconitization. Pleistocene glauconitization implies that relative rising sea level and highstands were periods of low accumulation and sub-oxic conditions on the outer shelf of Concession 20D (Odin and Matter, 1981; Amorosi, 1997; Harris and Whiting, 2000). This is consistent with the organic, mud-rich Holocene transgressive sediment that blankets the study area and the outer shelf of the western margin as a whole (Dale and McMillan, 1998a). The formation of glauconite on passive margins reflects a balance between detrital influx and winnowing by marine currents (Odin and Matter, 1981), where the transgressive system tract would provide an opportunity for the accumulation of the mud providing the lithophile elements required for glauconitization.

The highstand muddy sands would be winnowed and reworked to deeper water sites as sea level falls, where this winnowing is associated with the concentration of any macrofauna present. The chemistry of the Pleistocene glauconite will be shown in Chapter 9 to be typically little-evolved to evolved, thereby only requiring 10^4-10^5 years for the formation of the glauconite (Odin and Matter, 1981). The less

University of Cape Town

evolved nature of the glauconite favours rapidly changing depositional environments associated with fluctuating sea levels (Odin and Matter, 1981). The low mud content of the Calcareous Glauconitic Sand facies relative to the Holocene drape indicates that fine material must have been winnowed during relative sea-level lowstands. Recent work on the Core GeoB8307, collected on the upper slope to the southwest of the study area, shows a remarkable correlation between sea-level lowstands and an increased quartz and glauconite abundance, suggesting that off-shelf transport increased during glacial periods (J. Wiltshire, *pers. comm.,* 2004). The processes involved in the winnowing and off-shelf transport are likely to be related to the increased bottom current velocities, which are thought to occur during the glacial–interglacial transitions (Gröger *et al.*, 2003).

Compton *et al.* (2002) have similarly argued that gravel lags observed in cores recovered in water depths of ~120 m from the shelf offshore the Orange River were formed by increased winnowing and erosion during the LGM lowstand. A study on cores collected from 130-150 m on the southeastern Australian margin record a similar late Quaternary depositional history. The outer-shelf sediments are dominated by relict biogenic material deposited during glacial maxima with finer-grained sediments deposited during interglacials, where the sediment records indicates that lowstand deposits of MIS stages 2, 6 and 8 are preserved (Ferland *et al.*, 1995).

University of Cape Town

8.2 CALCAREOUS QUARTZOSE VERY FINE SAND

Landward of the outer shelf Calcareous Glauconitic Sand, the Calcareous Quartzose Very Fine Sand was recovered on the seaward slope of the Western Ridge in nine cores collected from a water depth ranging from 220 to 247 m (Figure 8.4). The Calcareous Quartzose Very Fine Sand is composed of a very fine quartz sand and subordinate biogenic grains (Figure 8.5). The quartz component closely resembles that of the Pliocene Quartzose Muddy Sand. However, the weight percent $CaCO_3$ ranging from 5.6 and 29.5% (average of 12.8%) is considerably higher than the <5% $CaCO_3$ of the Pliocene Quartzose Muddy Sand. Macro- and microfauna are abundant, with shell-rich intervals and numerous shell lag layers are present.

The Calcareous Quartzose Very Fine Sand varies in thickness from 1.92 to 3.33 m. The contact with the underlying Pliocene sediments was only recovered in Core 349 (Figure 8.4). This lower contact is gradational, with the Calcareous Quartzose Very Fine Sand recovered above the Pliocene Glauconitic Muddy Sand facies (Compton *et al.*, 2004). The upper ~100 cm of the Pliocene Glauconitic Muddy Sand facies has been reworked during the late Pliocene/early Pleistocene as Sr-ages ranging from 1.1-2.5 Ma were obtained from shell fragments, benthic foraminifera and echinoid spines from this upper interval. The first shell layer at 295-305 cm occurs within this reworked interval.

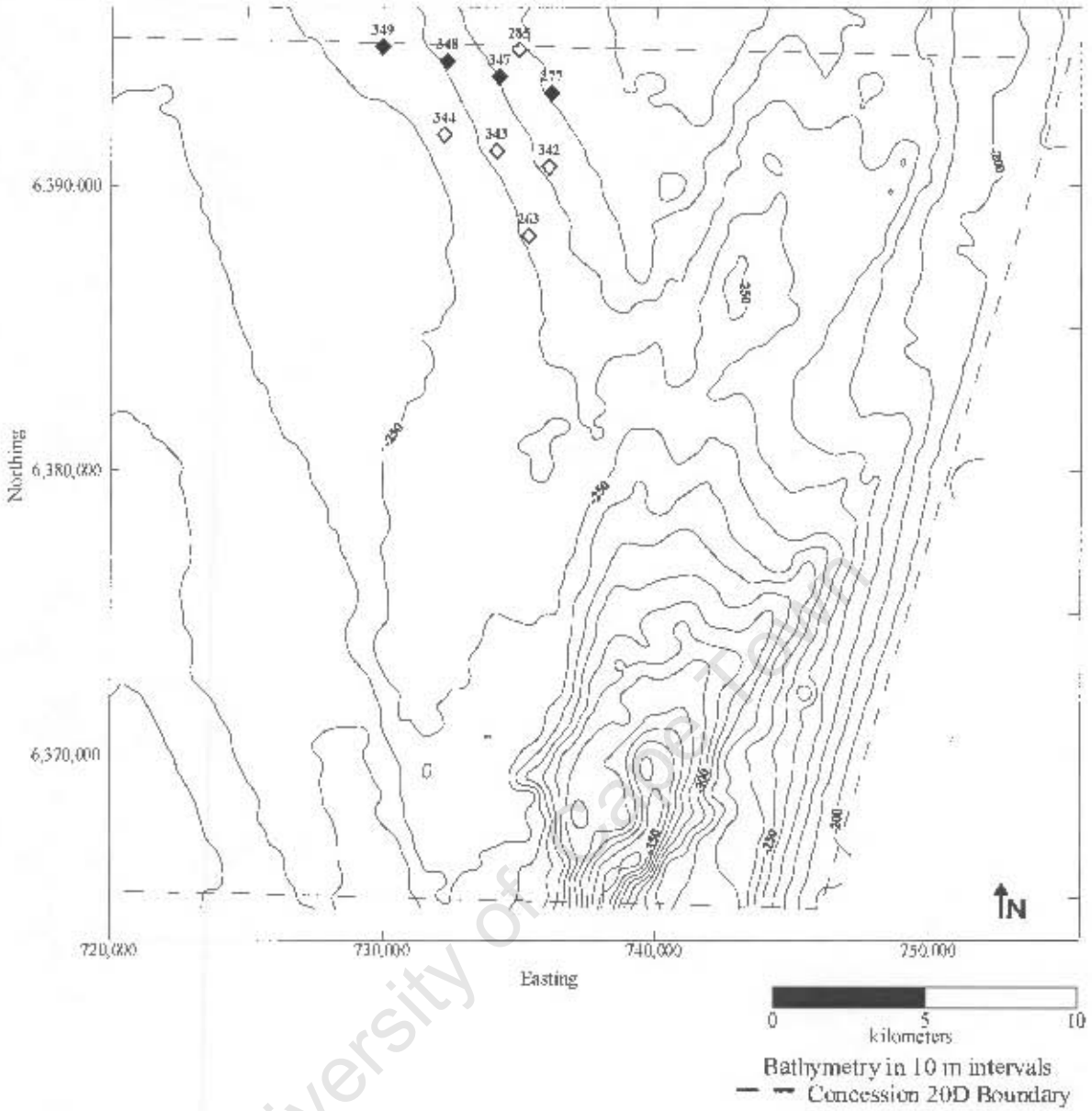


Figure 8.4. The distribution of the Calcareous Quartzose Very Fine Sand facies in the Canyon Head Area of Concession 20D (dashed line denotes concession boundary). Bold symbols indicate samples analysed in this study and Compton *et al.* (2004.)

The Calcareous Quartzose Very Fine Sand is light olive grey to pale olive (5Y 6/2 to 6/3) in colour and varies between a muddy sand to sand and a muddy sandy gravel sediment texture, but always contains <14 % mud (Figure 8.6). The very well to moderately well sorted, very fine quartz sand has a slightly bimodal grain size distribution (with very fine sand mean modes of 3.11-3.24 ϕ (major) and ~3.8 ϕ (minor)) (Figure 8.7). Although dominated by quartz (60-90%), the sand-size fraction includes biogenic grains (5-30%) (Figure 8.8) and glauconite (5.0-32.8 wt%) (Figure 8.9). Core 277 includes 9.9-32.8 wt% glauconite, with abundances increasing up-core, whereas Cores 347 and 348 contain only 5.0-7.2 wt% glauconite (Figure 8.9). The biogenic grains include a diverse planktic and benthic (including agglutinated) foraminiferal assemblage (Figure 8.10), ostracods, echinoid spines (<1%), holothurian sclerites, and <2% bivalve and minor gastropod shell fragments. The planktic foraminiferal assemblage

is dominated by the upwelling species *G. bulloides* and *N. pachyderma*, but shows a slightly increasing *G. inflata* (transitional species) abundance up-core. In addition, minor fragmented (Miocene?) brown-stained benthic foraminifera (*Dentalina* spp.) are preserved near the base of Core 277. The mud (<63 µm) fraction is dominated by calcite, quartz and feldspar, with only a minor 10 Å illite/glauconite peak in Sample 348-7 and Core 277 (Figure 8.11).

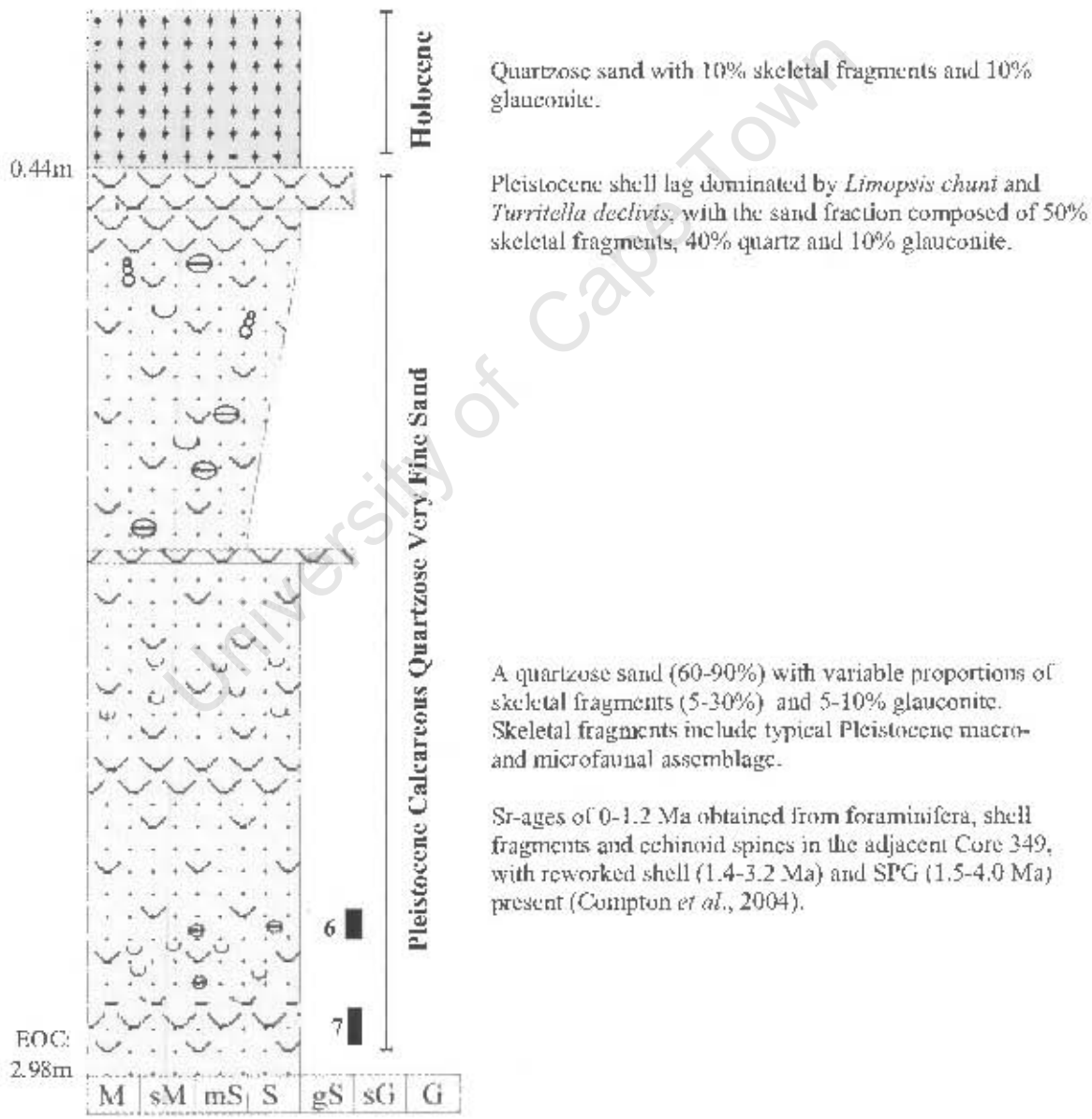


Figure 8.5. The stratigraphy of the Calcareous Quartzose Very Fine Sand facies of Core 348. Sample positions referred to in the text are included.

University of Cape Town

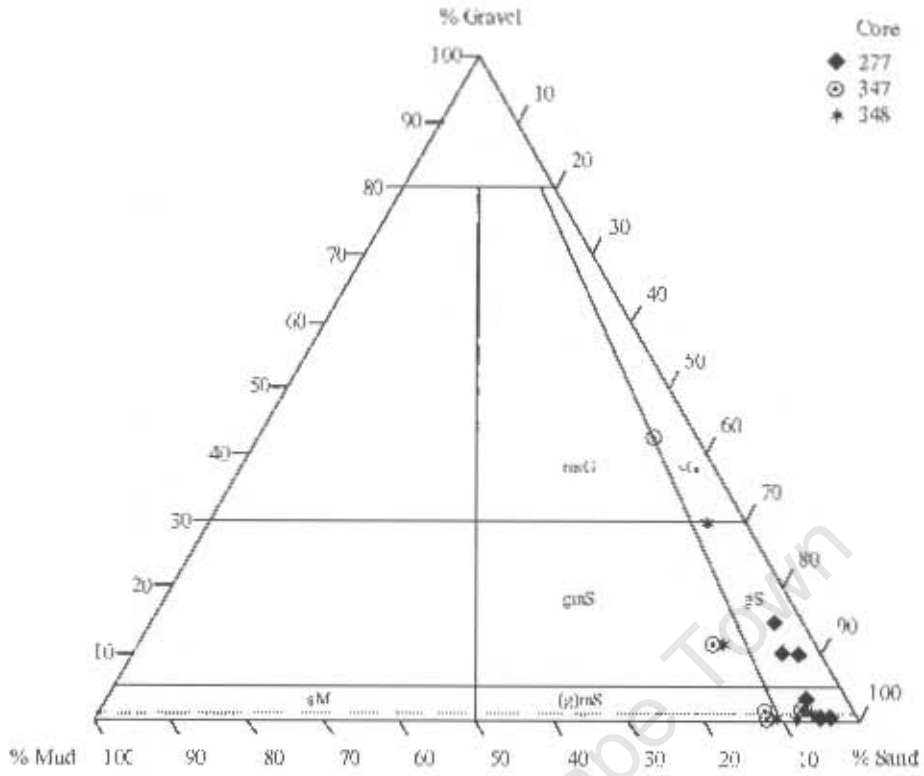


Figure 8.6. A summary of the textural nomenclature of the Calcareous Quartzose Very Fine Sand after Folk (1954).

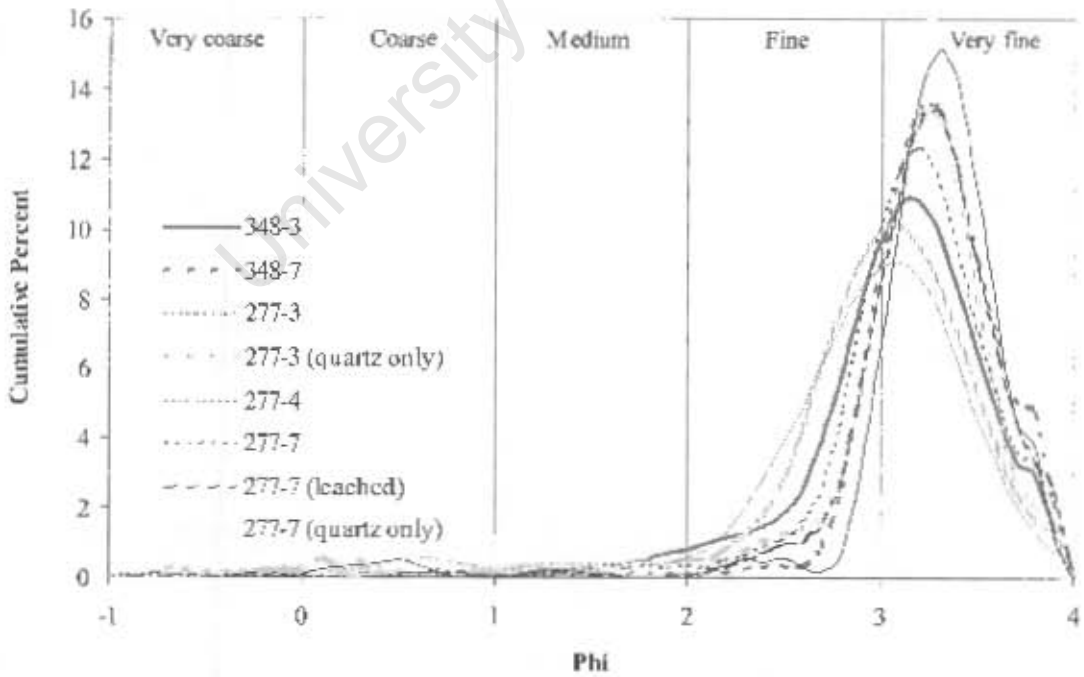


Figure 8.7. Frequency curves showing the particle-size distribution of the sand fractions of the Calcareous Quartzose Very Fine Sand. Note the presence of a medium to coarse tail not observed in the Quartzose Muddy Sand sediments. Sample locations indicated on Figure 8.4.

University of Cape Town

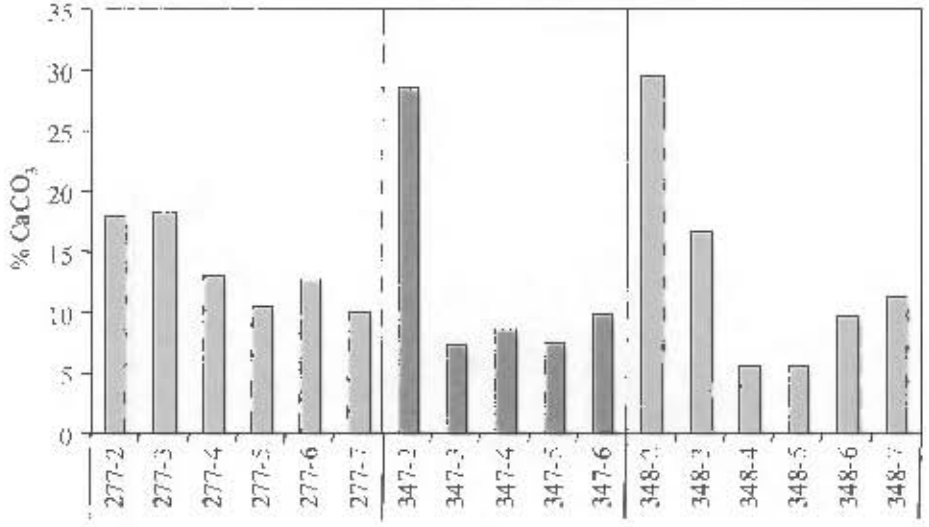


Figure 8.8. Weight percent $CaCO_3$ of the sand fraction of the Calcareous Quartzose Very Fine Sand facies. (See Appendix 1 for sample numbers)

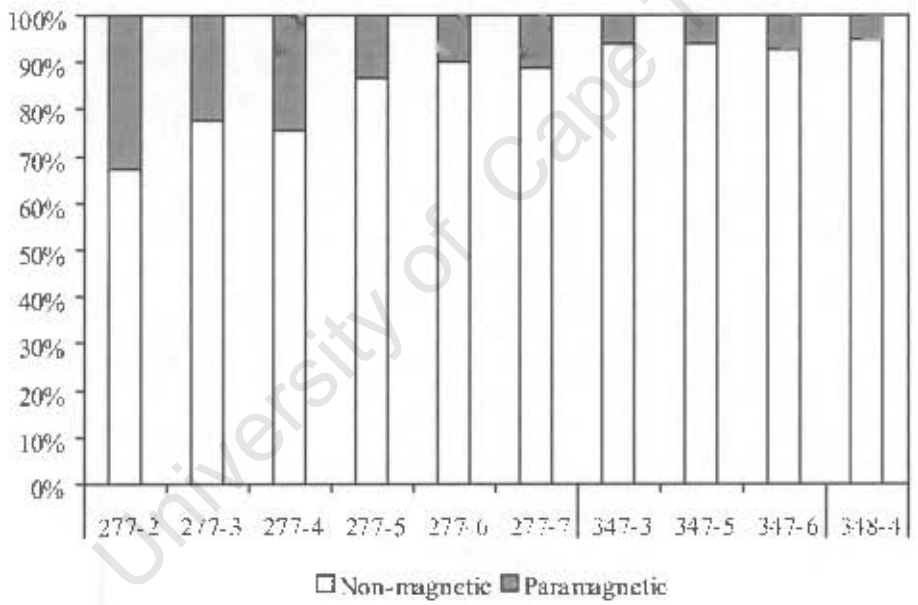


Figure 8.9. The weight percent non-magnetic (quartz) and paramagnetic (glauconite) components of the acid leached sand fraction of the Calcareous Quartzose Very Fine Sand. (See Appendix 1 for sample numbers)

The gravel-fraction is dominated by well-preserved, bored, mollusc shells, including *Limopsis chuni*, with *Turritella declivis* common in the capping shell lag layer. In addition, *Anomia* sp., *Carditella* sp., *Megerlina pisum*, *Hiatella* sp., hooked *Patella* sp., *Volutocorbis abyssicola*, *Nassarius vinctus*, *Polinices* sp. *Conus* sp., scaphopods, fish otoliths, SPG (teeth and bone) and echinoid spines and plates, are present in varying proportions in the gravel fraction. The articulated *L. chuni* of the uppermost capping shell lag often include internal casts. Reworked worn and leached *L. chuni* and *Amalda bulloides* are also present in the capping shell lag. Trace amounts of grey and pink granite and phosphorite granules are present in many of the shell lag layers.

University of Cape Town

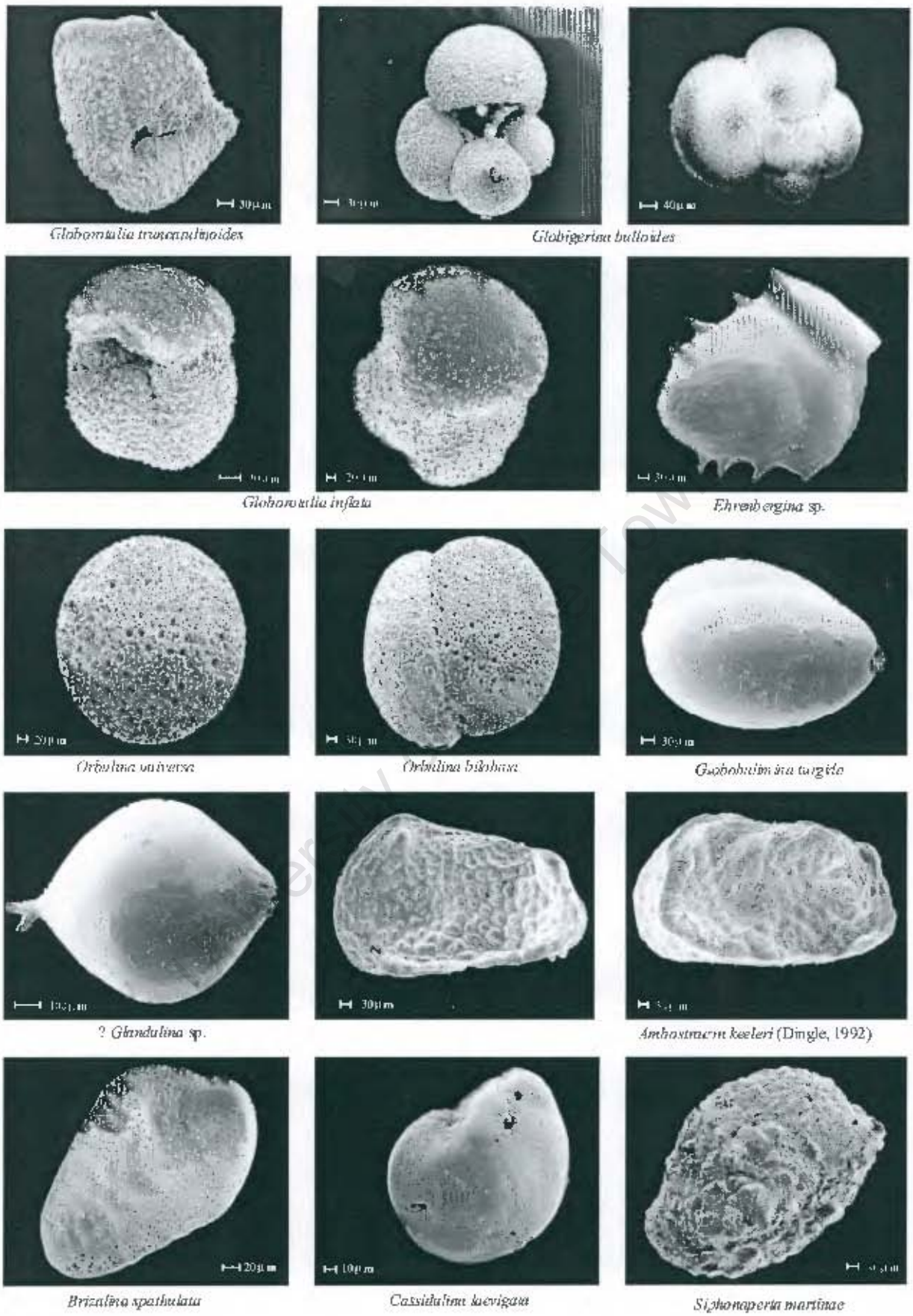


Figure 8.10. The predominantly cold water (upwelling) late Pleistocene assemblage of the Calcareous Quartzose Very Fine Sand facies, although the transitional species *G. inflata* is usually present in varying proportions.

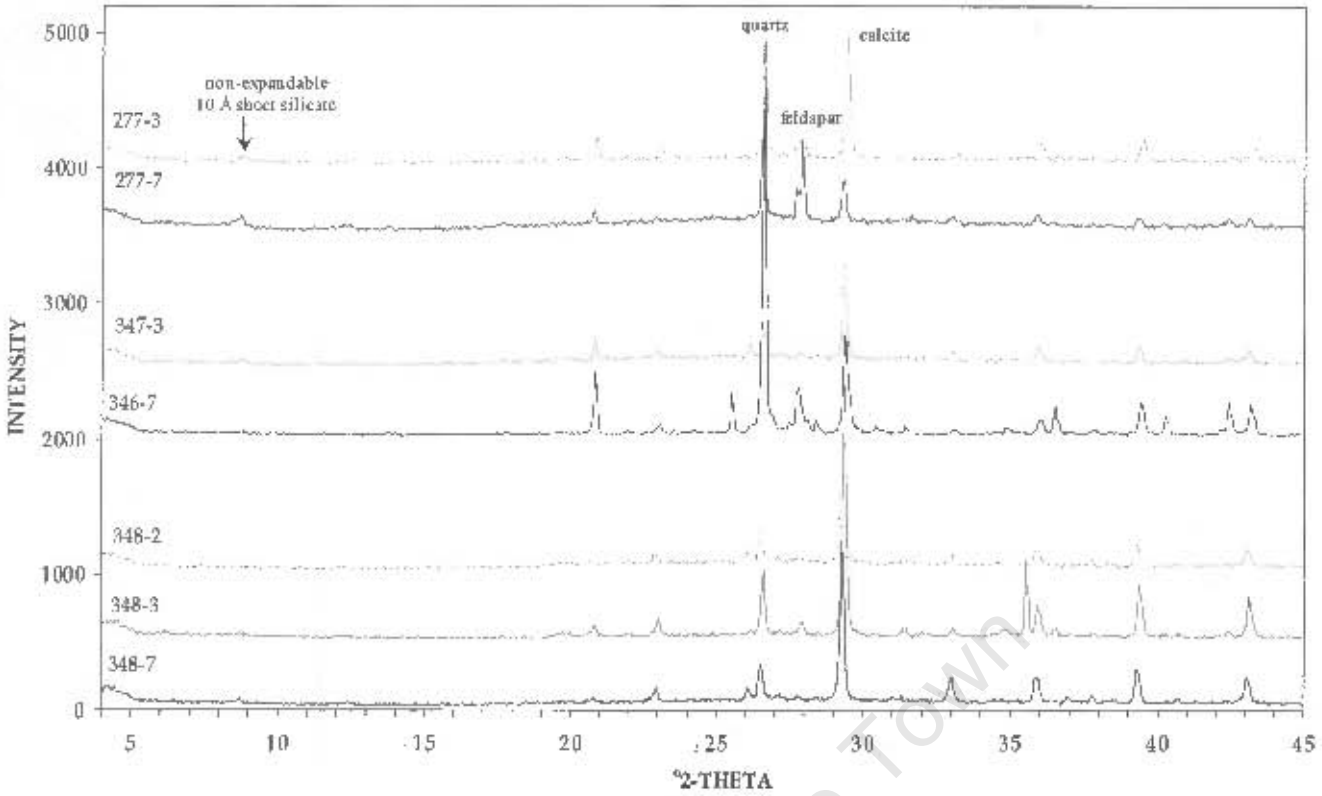


Figure 8.11. The XRD records for the mud fraction (<63 μm) of the Calcareous Quartzose Very Fine Sand facies is dominated by calcite, quartz and feldspar, with only minor clay peaks present.

University of Cape Town

8.2.1 AGE OF THE CALCAREOUS QUARTZOSE VERY FINE SAND

The deposition of the Calcareous Quartzose Very Fine Sand facies is interpreted to have occurred during the late Pleistocene, based on the microfossil assemblage from Samples 348-6 and 348-7 collected from the base of Core 348 (Figure 8.5). This is in agreement with the Sr-derived ages of 0-1.2 Ma obtained on benthic foraminifera, echinoid spines and shell fragments picked from Core 349 (Compton *et al.*, 2004). The dominance of cold-water species in the planktic assemblage indicates an older than latest Pleistocene age for the Calcareous Quartzose Very Fine Sand as the uppermost Pleistocene sediments of the outer shelf are dominated by a more transitional planktic assemblage.

8.2.2 DEPOSITIONAL ENVIRONMENT OF THE CALCAREOUS QUARTZOSE VERY FINE SAND

The Calcareous Quartzose Very Fine Sand shows an almost identical grain-size distribution to that described for the Quartzose Muddy Sand facies (average of 3.2 and 3.8 ϕ). However, the Calcareous Quartzose Very Fine Sand tends to be less well sorted and includes minor medium to coarse grains not present in the Pliocene Quartzose Muddy Sand facies. The coarser fraction (>125 μm) is dominated by shell fragments and larger foraminifera, but also includes traces of phosphorite and quartz grains. The Calcareous Quartzose Very Fine Sand facies is interpreted as reworked Pliocene Quartzose Muddy

Sand, owing to the close resemblance of the quartz population. Additional evidence for reworking of the Pliocene Quartzose Muddy Sand is provided by the presence of brown-stained robust Miocene benthic foraminifera in Core 277, and the Sr-derived ages of 1.4-3.2 Ma (shell fragments) and 1.5-4.0 Ma (SPG) in the shell layers of Core 349 (Compton *et al.*, 2004). The lower mud content of the Calcareous Quartzose Very Fine Sand implies winnowing of the mud fraction during reworking of the Pliocene Quartzose Muddy Sand.

The foraminiferal assemblage from the base of Core 348 is a typical upwelling cold-water assemblage. The abundance of micro- and macrofauna suggests that well-oxygenated bottom-water conditions, associated with high productivity, dominated on the Western Ridge during the deposition of these sediments during glacial sea-level lowstands. The presence of shell layers in the Calcareous Glauconitic Sand are proposed to represent winnowed lowstand/stillstand lag layers, as argued for the Calcareous Glauconitic Sand. The reworking of the Pliocene Quartzose Muddy Sand during the Pleistocene implies that the erosion of the more widespread Pliocene Quartzose Muddy Sand, which resulted in their approximate present-day distribution, must have occurred before the latest Pleistocene. The biodiversity of the micro-and macrofauna imply well-oxygenated bottom water and nutrient-rich conditions occurred above the Western Ridge at some time in the late Pleistocene prior to the LGM.

8.3 THE GLAUCONITIC QUARTZOSE SAND

The Glauconitic Quartzose Sand is found only within the Cape Canyon Head area (Figure 8.12) and was recovered in 210 cores from water depths ranging between 192 and 365 m. The distribution of the Glauconitic Quartzose Sand is restricted to within the Main Channel in the south, but is more widespread to the north with Pleistocene sediments recovered from the eastern flank of the Western Ridge. However, the distribution is, for the most part, restricted to within the Cape Canyon Head region, as defined by the Cretaceous sediment high observed, below the Western Ridge in the interpreted seismic sections (Chapter 4). The Glauconitic Quartzose Sand, recovered from Core 276, which is located to the west of the Cretaceous high in the Northern Transect, occurs only as latest Pleistocene burrows in the upper metre of the Pliocene Quartzose Muddy Sand. The isopach contours of the Glauconitic Quartzose Sand show a maximum recovered thickness towards the central parts of the Canyon Head region, with up to 497 cm of sand recovered in Core 352 (Figure 8.12). The isopach contours show that the Glauconitic Quartzose Sand Unit thins towards the Central Transect. The Central Transect occurs on an east-west bathymetric high that separates the two main Pleistocene facies of the Cape Canyon Head region.

The Pleistocene Cape Canyon Head sediments were recovered in cores from the Northern, Central and Southern Transects. Representative core logs from each of the transects show some of the variability observed in the Pleistocene Succession (Figure 8.13). The Pleistocene sediments vary in composition and texture within individual cores, between adjacent cores along the sampled transects and in a north-south direction along the canyon axis. Pleistocene sediment range between a fine to medium sand,

University of Cape Town

composed of approximately equal proportions of quartz and glauconite in the Northern Depression, to a quartz-rich medium sand with a bimodal coarse to very coarse sand population in the southern Main Channel of the Cape Canyon (Figure 8.14). The sediment facies in the Northern Depression is highly variable with the quartz content varying between 28.6 to 81.3 wt% in the analysed samples (Figure 8.15). The Pleistocene sediments of the southern Main Channel of the Cape Canyon consist of exceptionally clean bimodal quartzose sand and contain minor mud and calcareous biogenic grains.

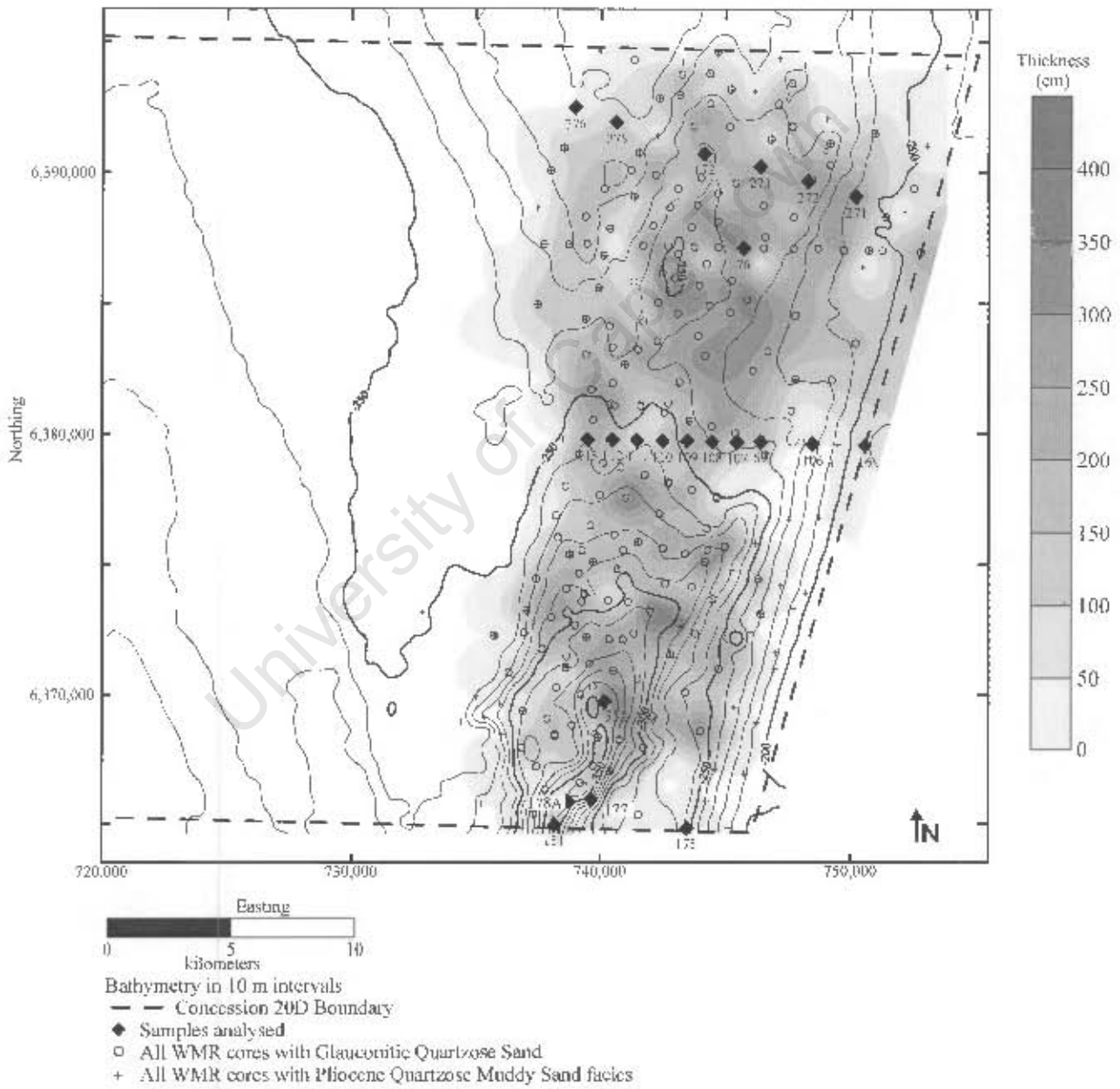


Figure 8.12. The sediment isopachs for the Glauconite Quartzose Sand Unit. The true thickness is only known for those cores in which the underlying Pliocene Quartzose Muddy Sand is intersected. The analysed samples include data from Compton *et al.* (2004).

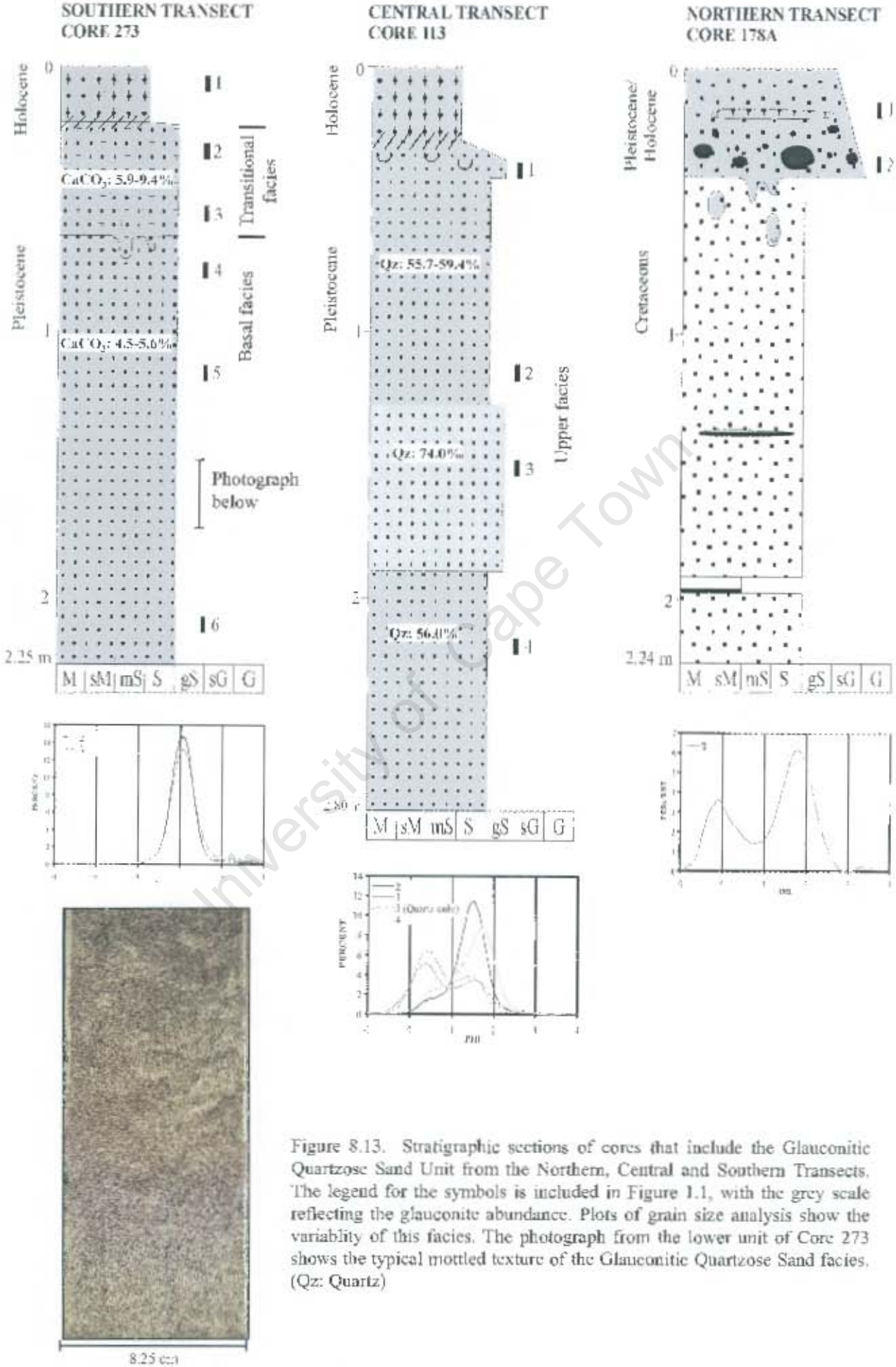


Figure 8.13. Stratigraphic sections of cores that include the Glauconitic Quartzose Sand Unit from the Northern, Central and Southern Transects. The legend for the symbols is included in Figure 1.1, with the grey scale reflecting the glauconite abundance. Plots of grain size analysis show the variability of this facies. The photograph from the lower unit of Core 273 shows the typical mottled texture of the Glauconitic Quartzose Sand facies. (Qz: Quartz)

University of Cape Town

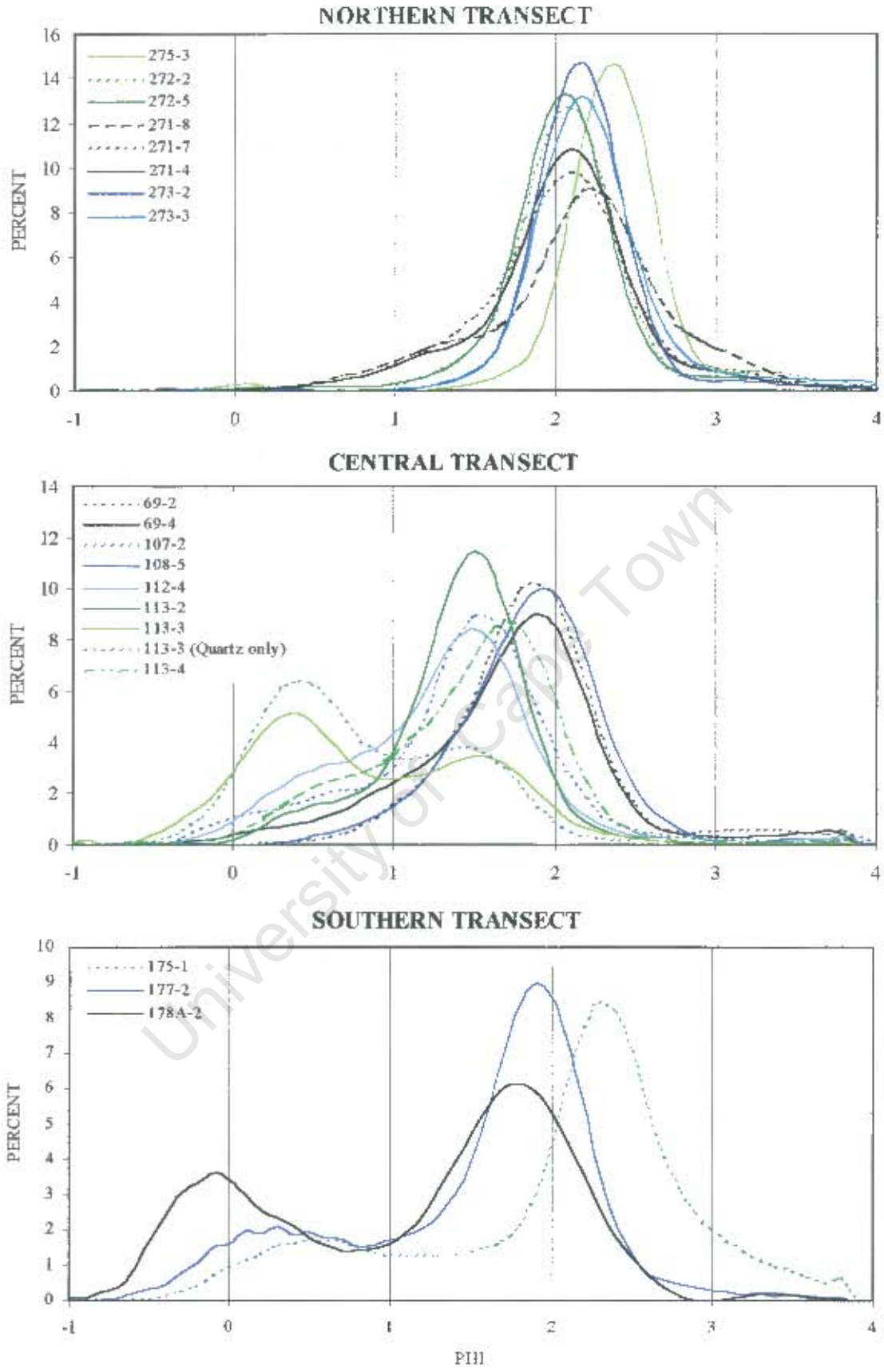


Figure 8.14. Frequency curves showing the particle-size distribution of the sand fractions of the Glauconitic Quartzose Sand. Sample locations indicated on Figure 8.12.

University of Cape Town

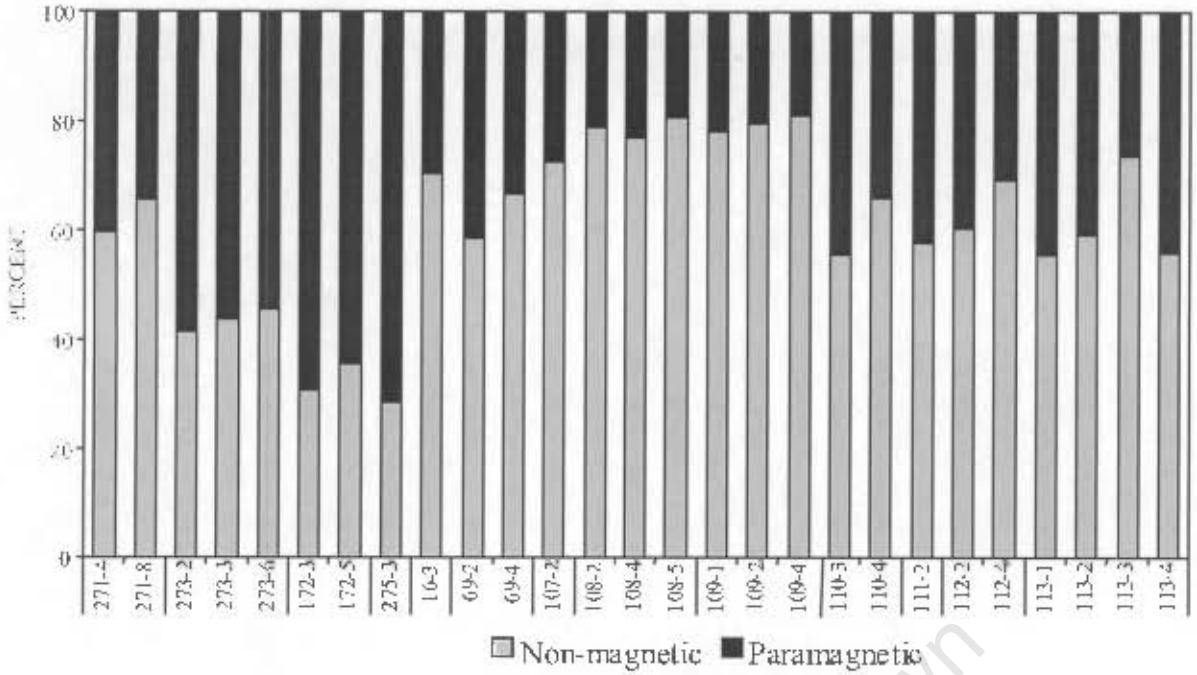


Figure 8.15. A summary of the non-magnetic (quartz) and paramagnetic (glauconite) weight percent present in the acid-leached (carbonate-free) sand fraction of the Glauconitic Quartzose Sand. (Refer to Appendix 1 for Core and sample numbers)

The Pleistocene Glauconitic Quartzose Sand is found unconformably overlying the Pliocene Quartzose Muddy Sand. This contact is recovered predominantly in cores from the flanks of the Cape Canyon Head Area, although the contact with the Pliocene was also recovered at 93 cm in Core 107 and at 200 cm in Core 110 along the Central Transect. The contact between the Glauconitic Quartzose Sand and the Pliocene Quartzose Muddy Sand is usually sharp, typically with latest Pleistocene bioturbation observed for up to one metre into the Pliocene Succession. A basal lag may (Cores 275; 175, 177 and 178A) or may not (Cores 107 and 110) be present. The slightly gravelly sand from the base of Core 275, recovered from the Northern Transect, includes medium pebble-size mollusc and lithic fragments together with phosphorite and quartz granules. The macrofaunal assemblage includes well-preserved and bored *L. chuni*, *Cardiella* sp., *Anomia* sp., *M. pisum*, *A. bulloides* and bivalve fragments, SPGs and coralline algae. The lithic fragments include a single angular, equant, pink granite medium pebble and grey granite granules with a sandstone fine pebble present in Core 175. The WMR core logs describe a <10 cm thick basal lag, where present, that includes *L. chuni*, *T. declivis*, *A. bulloides*, *N. vinctus*, *V. abbysicola*, *Patella sp.* and scaphopods together with phosphorite (<6 cm) and quartz pebbles to granules. Occasional granite, quartzite and sandstone lithic fragments (<4 cm), wood and phosphatised bone fragments are also described. The basal lag becomes thicker and better developed further to the south, down-canyon within the Main Channel and a sandy gravel is preserved at the base of the Glauconitic Quartzose Sand in Cores 177 and 178A of the Southern Transect. The gravel in these cores is dominated by irregular phosphorite up to coarse pebble size. The phosphorite is predominantly a CFA-cemented glauconitic medium sand, with minor SPGs and phosphatised casts of molluscs and calcareous algae. In addition, minor shell fragments and rounded medium to fine quartz pebbles, angular to subangular quartz granules, trace amounts of jasper and fine pebbles of sandstone are present. The shell fragments include *Dosinia lupinus*, *Turritella declivis* and *Nuculana bicuspidata*.

University of Cape Town

The Glauconitic Quartzose Sand Unit is predominantly a sand with <5% gravel (Figure 8.16), although gravel-rich samples are recovered from all three transects. The $CaCO_3$ content of the sand fraction is slightly higher (4.5-13.5 wt %) in the cores recovered along the Northern Transect, than that recorded for the Central Transect (2.6-7.1%) (Figure 8.17). The high $CaCO_3$ content of Cores 16, 106, 175 and 177 reflects a marked increase in abundance of upper Pleistocene micro- and macrofauna in the sand fraction (possibly related to their position in the very east of the study area). The Pleistocene sediments from the three transects are described separately, starting in the north, because they are sufficiently different in composition. The Pleistocene Glauconitic Quartzose sediments usually display a slight mottled texture (Figure 8.13) in the interval between shell layers. Scattered shells are occasionally present, including *L. chuni*, *Hiatella* sp., *Carditella* sp., *T. philomela*, *T. declivis*, *A. bulloides*, *N. vinctus*, *V. abyssicola*, *M. pisum*, *T. abyssicola*, juvenile *Ancilla marmata*, *N. bicuspidata*, scaphopods and fish otoliths.

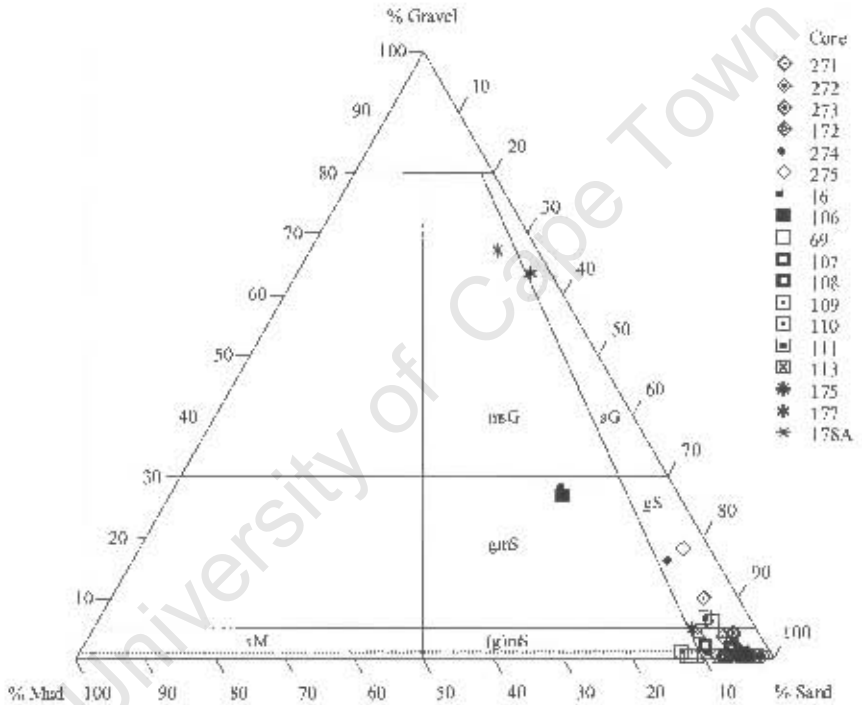


Figure 8.16. A summary of the Glauconitic Quartzose Sand grain size textures.

Three distinct sediment packages can be recognised within the Glauconitic Quartzose Sand collected from the Northern Transect. The oldest facies is found within the channels of the Northern Depression and only uppermost Pleistocene sediments are recovered from the canyon flanks and Western Ridge. The basal facies is recovered in Core 172 and from below 65 cm in Core 273 (Figure 8.13). The sediments of the basal facies are a uniform, well-sorted, medium sand (no grain size analyses available) composed of approximately 60% glauconite and 40% quartz with less than 2% biogenic grains. The glauconite tends to be predominantly green, fractured grains with a distinct sugary texture, similar in appearance to the glauconite in Pliocene sediments and only subordinate to minor black, polished, lobate grains are present. The quartz grains are angular to subrounded with traces of red-stained and coarse frosted grains present. The biogenic component includes traces of echinoid spines and a low biodiversity benthic foraminiferal assemblage dominated by spiny *Uvigerina* sp. and other fragments.

University of Cape Town

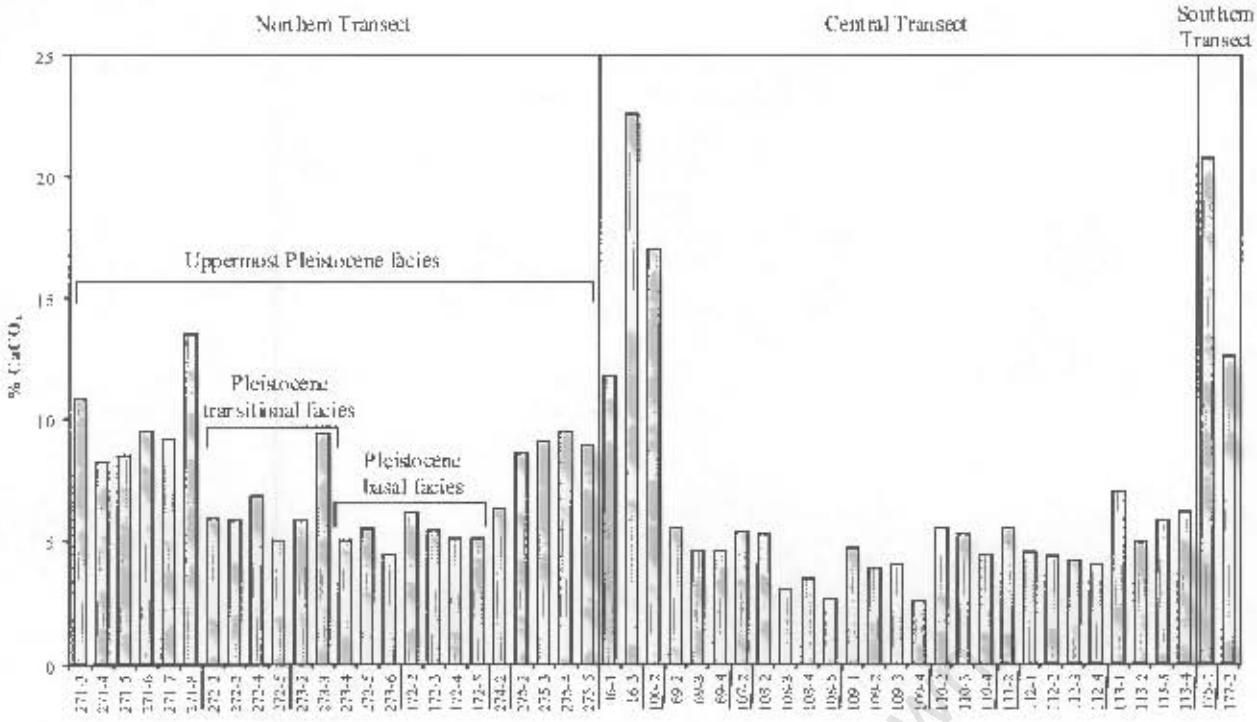


Figure 8.17. Weight percent $CaCO_3$ of the sand fraction of the Glauconitic Quartzose Sand. (Refer to Appendix 1 for Core and samples numbers)

This basal Glauconitic Quartzose Sand is unconformably overlain by a fine to medium sand of a similar composition, but containing up to 10% calcareous fragments. The basal facies has 4.5-6.2 wt% $CaCO_3$, in contrast to the slightly increased values of 5.0-9.4 wt% $CaCO_3$ recovered from the overlying Pleistocene transitional facies (Figure 8.17). The contact between the two sediment types is slightly bioturbated in Core 273. The biogenic component includes ~1% echinoid spines and a slightly more diverse foraminiferal assemblage, which is dominated by planktic species including *G. bulloides, N. pachyderma, O. universa, Bulimina* sp. *etc.* A thin shell layer near the base of Core 272 is dominated by brachiopods (cf. *Terebratulina abyssicola*) and worn gastropods (*A. bulloides* and *N. vinctus*) fragments. Fine pebble-size *N. vinctus*, *Polinices* sp. and other gastropods are present in the gravel-fraction towards the top of Core 272.

The third sedimentary package from the Northern Depression contains greater than 10 wt% biogenic grains and is a quartz-dominated sand on the eastern flank (59.7-65.8 wt% quartz) and a glauconite-dominated sand on the Western Ridge (71.4 wt% glauconite). The WMR core logs for the Glauconitic Quartzose Sand sediments recovered from the western flank of the Western Ridge are all composed of 60% glauconite, 30% quartz and 10% biogenic grains, with shell layers abundant. The biogenic assemblage is typical of the latest Pleistocene (see previous sections) and includes 2-3% mollusc (largely bivalve) fragments, 1-2% echinoid spines, <1% ostracods, traces of holothurian sclerites and an extremely diverse planktic and benthic foraminiferal assemblage. The benthic assemblage is typically dominated by *C. laevigata* and the agglutinated miliolid species *S. martinae* is present in all samples. The planktic assemblage tends to be dominated by *G. inflata* relative to *G. bulloides*. The foraminiferal species abundances of the northern Glauconitic Quartzose Sand show a similar trend to that observed for the Calcareous Quartzose Very Fine Sand. A shell layer is present towards the top of this unit, which

University of Cape Town

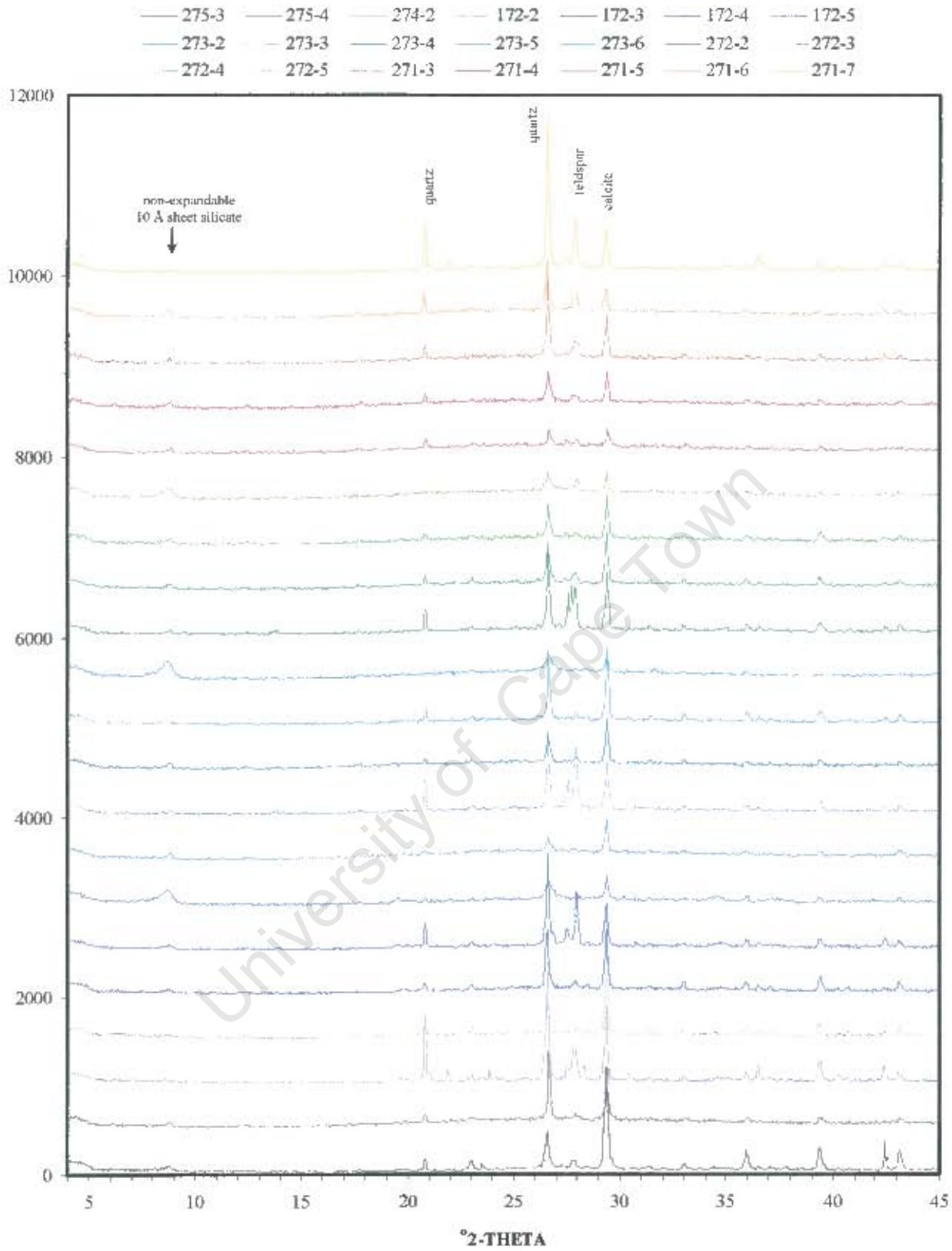
includes the same macrofaunal assemblage described for Calcareous Quartzose Very Fine Sand. The mud-fraction of the samples collected the Northern Transect are dominated by quartz, feldspar and calcite with only minor glauconite/illite (non-expandable 10 Å sheet silicate) present (Figure 8.18). Unlike the underlying Pliocene Quartzose Muddy Sand sediments, kaolinite is almost entirely absent.

In contrast to the Northern Transect, the Pleistocene Glauconitic Quartzose Sand of the Central Transect is dominated by quartz (55.4-81.3 wt%), where Cores 107 to 113, recovered within the interpreted main channel of the Cretaceous sediment (Chapter 3) represent a single sedimentary package. The quartz abundance is highest in the east (81.3 wt%) and decreases westwards across the Main Channel (55.7 wt%). The quartz-rich sediments (Figure 8.19) typically show a bimodal grain size distribution (Figure 8.14), with a coarse to very coarse component, dominated by quartz and lesser amounts of phosphorite. The coarse to very coarse quartz varies from subangular to well rounded, with milky, clear and frosted grains commonly present. A green glauconite surface-coating on these quartz grains is common (Figure 8.20 A & B). Similar glauconite-coatings are observed on the medium quartz population, which also includes rare red-stained quartz grains. The quartz-rich sand, which is occasionally barren (base of Core 109 and 112), seldom includes more than 2% biogenic grains, where traces of echinoid spines and shell fragments occur with a moderate to low diversity foraminiferal assemblage. The foraminiferal assemblage is dominated by planktic species with abundant transitional species including *G. inflata* (with *N. pachyderma*, *G. dutertrei*, *O. universa* and less abundant *G. bulloides* commonly present). The quartzose sand shows considerable variation, within core, in grain size where very coarse sand intervals and fining-upward sequences are observed. The coarser sand appears to include a slightly more abundant and diverse foraminiferal assemblage, where the coarse sand interval from 127-190 cm in Core 113 (Figure 8.13) includes a typical uppermost Pleistocene foraminiferal assemblage. Traces of lithic fragments are present, with feldspar (Core 108), agate (Core 111) and jasper (Core 109, 112) recognised. The gravel-fraction of gravelly sand and gravel layers are dominated by phosphorite with lesser amounts of quartz. Fine pebbles of pink granite and agate (Core 107, 109) together with fish otoliths and bivalve shell fragments are also present. A typical uppermost Pleistocene shell layer caps the Glauconitic Quartzose Sand in Core 113.

In contrast, Core 69, recovered from a side channel in the east, landward of the faulted (uplifted) Cretaceous sediment, is a muddy sand (10.9-12.5% mud). The Pleistocene sand is slightly more glauconitic (33.1-41.3% paramagnetic fraction) than the adjacent sediments and is a moderately well sorted fine to medium (slightly coarsely skewed) sand, with no distinctive bimodal grain size distribution (Figure 8.14). This sediment most closely resembles the lower facies of the Northern Transect, with green fractured glauconite and ~2% biogenic grains, which similarly show a low species diversity, although benthic foraminifera, including the agglutinated miliolid, *S. martinae*, are present.

The Pleistocene units of the Southern Transect are present only as condensed gravel-lags, dominated by coarse to very fine phosphorite pebbles. The sand fraction of Glauconitic Quartzose Sand from the Southern Transect shows a similar bimodal grain size distribution. The fine to medium sand is

University of Cape Town



University of Cape Town

Figure 8.18. The XRD records show that the mud fraction (<63 μm) of the Glauconitic Quartzose Sand Unit from the Northern Transect is composed of quartz, feldspar and calcite, usually with only minor amounts of glauconite/illite (a non-expandable 10 Å sheet silicate) present.
(Refer to Appendix 1 for Core and sample numbers)

dominated by quartz (>70% visually) with 20% black polished glauconite, 5% phosphorite and 5% uppermost Pleistocene biogenic grains. Core 175, collected on the eastern flank, is a typical uppermost Pleistocene sediment composed of 60% quartz, 20% biogenic grains and 20% glauconite (visually). The sediment data of Core 352 and 151, collected from the very southern end of the Main Channel (Figure 8.12) are presented in Compton *et al.* (2004), where 497 cm of sand to sandy gravels were recovered in Core 352. Both cores show considerable variation in texture and grain size, with fining-upward cycles recovered, similar to those described for the sediments of the Central Transect. The gravel-fraction of the entire working half of cores 152 and 352, collected from the southern end of the Main Cape Canyon, is dominated by phosphorite pebbles. However, minor to subordinate, very fine to medium, typically well-rounded, quartz pebbles with trace amounts of agate, yellow quartz and jasper are present. In addition, phosphatised fish and sharks teeth, pyritised wood fragments, pyritic mud clasts and manganese-ferricrete nodules (up to small cobbles in size) are present in the gravel-fraction. The pyritic mud clast are assumed to be reworked Cretaceous sediments because of the similar appearance to the underlying Cretaceous mud of the Woody Quartzose Sand unit. The manganese-ferricrete nodules are also likely to be upper Cretaceous in age, where many authors have described similar cementation in the upper Cretaceous sediments of the Namaqualand and Namibian middle shelf (Section 4.2; Rogers, 1977; Kuhns, 1995; Corbett, 1996; Barnford and Stevenson, 2002).

University of Cape Town

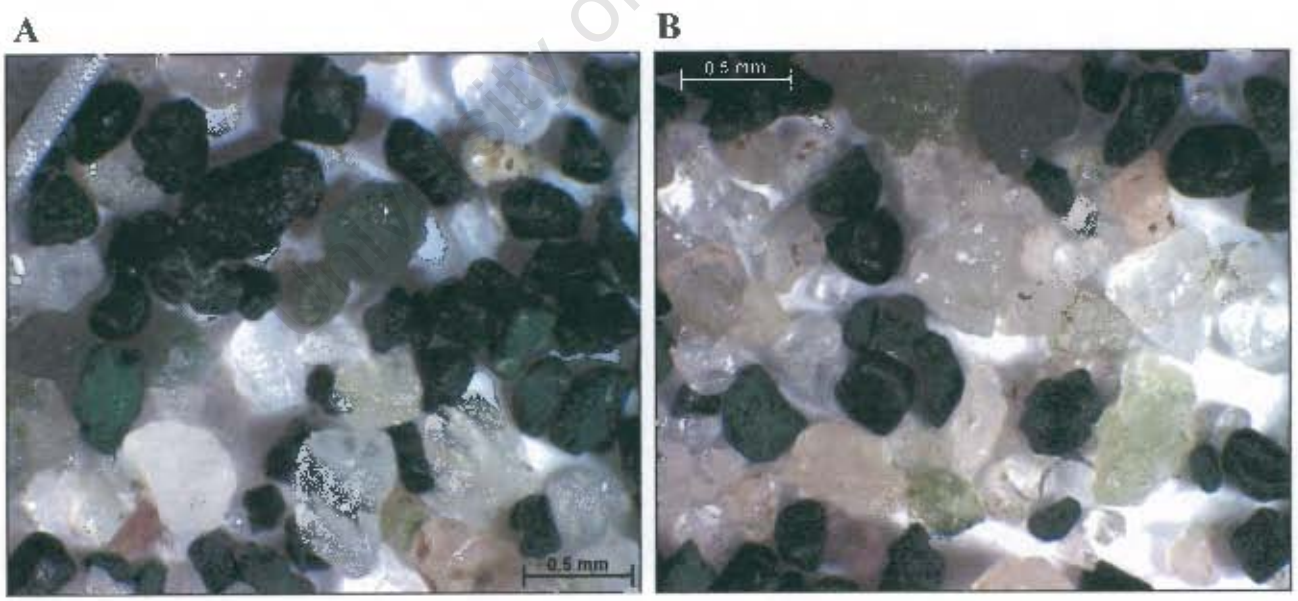


Figure 8.19. The sand fraction of the Glauconitic Quartzose Sand of Samples 107-2 (A) and 110-4 (B) recovered along the Central Transect. Note that quartz grains range from clear to partially glauconite-coated (green).

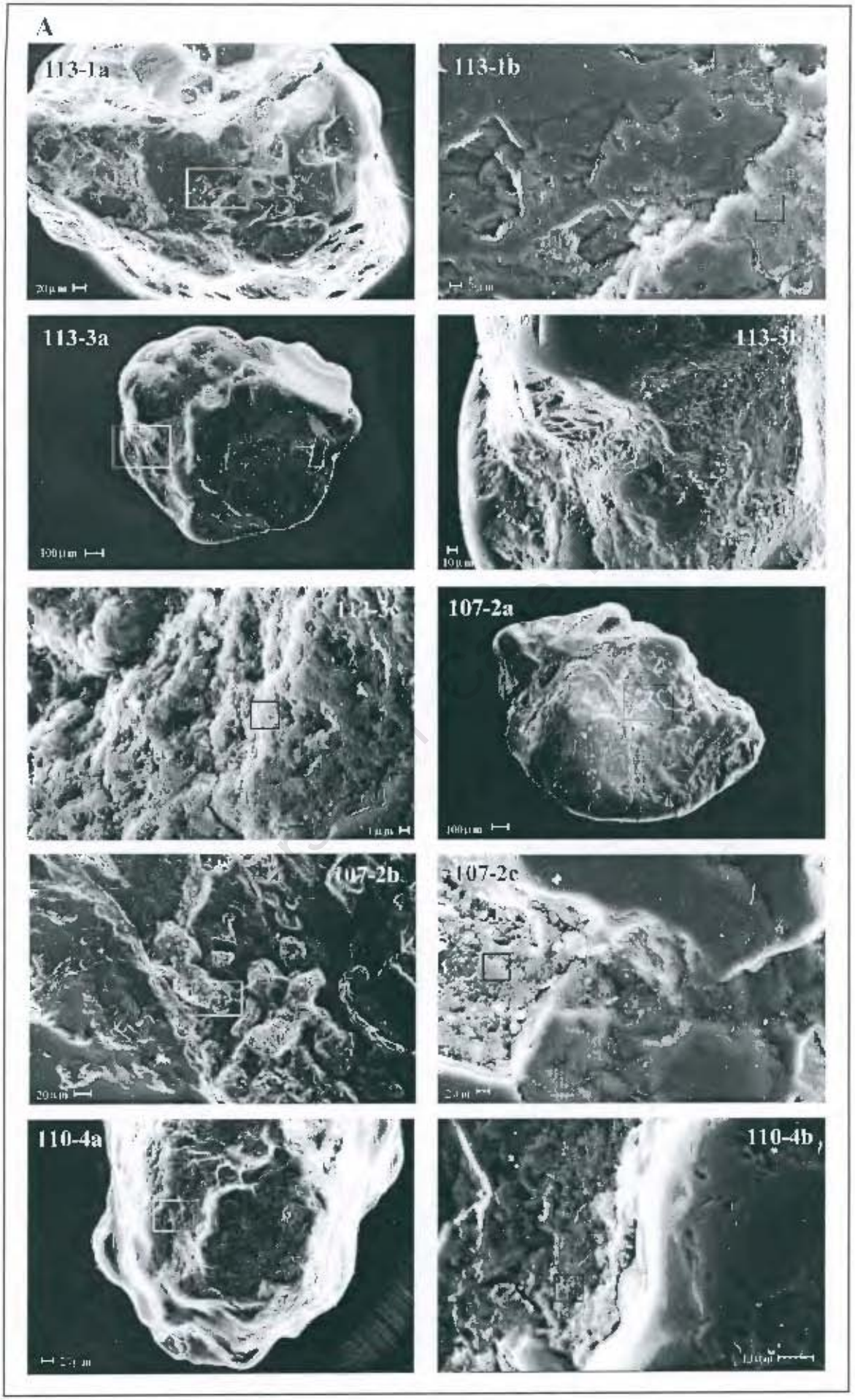


Figure 8.20A. Legend on page 8-27

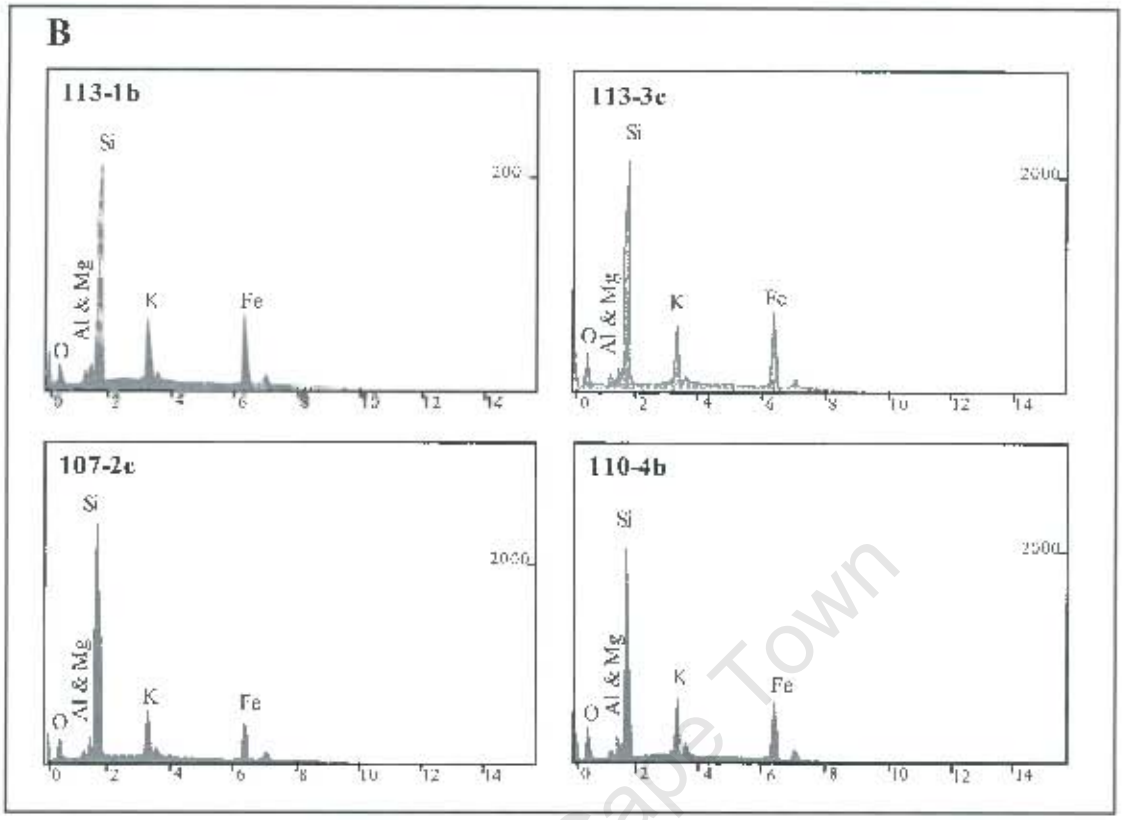


Figure 8.20. SEM images (A) and the EDS determined composition (B) of the glauconitic surface coating of green-stained quartz with no obvious glauconite-rich areas (Sample 113-1) and with well-defined glauconitic patches (Samples 113-3, 107-2 and 110-4). EDS analyses were undertaken on areas demarcated with a black box in relevant SEM image in (B).

University of Cape Town

8.3.1 AGE OF THE GLAUCONITIC QUARTZOSE SAND

The Glauconitic Quartzose Sand Unit is interpreted as an upper Pleistocene deposit, based on both the foraminiferal assemblage and the available Sr-isotopic ages. The Sr-derived ages from Core 76 from the Northern Depression and Core 352 from the Main Channel vary between 0-1.2 Ma (Compton *et al.*, 2004). At least three phases of deposition within the Glauconitic Quartzose Sand facies are indicated by the stratigraphy recovered in the Northern Depression. The basal facies of the Northern Depression is Pleistocene in age, based on the stratigraphy. The basal sedimentary package of the Northern facies, dominated by spiny *Uvigerina* sp., shows low foraminiferal abundance and biodiversity, similar to that observed within the underlying Pliocene Quartzose Muddy Sand, and suggests that this facies is a rarely preserved lower Pleistocene sediment. The overlying transitional facies is dominated by a planktic foraminiferal assemblage dominated by *G. bulloides* and *N. pachyderma*. This facies show a trend of decreasing *G. bulloides* and *N. pachyderma* (both cold-water species) and increasing *G. inflata* (transitional species) up-core as seen in the outer shelf Calcareous Glauconitic Sand (Section 8.1.3), where *G. inflata* is the dominant planktic species in the uppermost Pleistocene facies. The youngest of

these facies is interpreted as an uppermost Pleistocene sediment, on the basis of the faunal assemblage described for the Glauconitic Calcareous Sand in Section 8.1.1.

The dominance of *G. inflata* in the quartz-rich sediments of the Central Transect, together with an uppermost Pleistocene foraminiferal assemblage in the coarse interval near the base of Core 113, indicates that the quartzose sand recovered from within the southern Main Channel are latest Pleistocene in age. Similarly, the sediments of the Southern Transect are dominated by uppermost Pleistocene fauna, and correlate in age with the sediments of the Central Transect. Core 69, collected from a side channel on the Central Transect on the eastern flank, is distinctly different from the adjacent sediments and may represent a rare outlier of older Pleistocene sediments preserved in the southern Main Channel region.

8.3.2 DEPOSITIONAL ENVIRONMENT OF THE GLAUCONITIC QUARTZOSE SAND

The sediment succession of the Cape Canyon Head of Concession 20D provides a rare opportunity to study the changing Pleistocene depositional environment on the middle to outer shelf. In particular, the variations in the biogenic fraction, from a low-diversity, low-abundance foraminiferal assemblage in the basal sub-facies to the diverse macro-and microfaunal uppermost Pleistocene assemblage, provide insights into the Pleistocene depositional environment.

The basal facies includes only a small foraminiferal population, which shows low species biodiversity. The low biodiversity and dominance of spiny *Uvigerina* sp. most likely reflects low bottom-water oxygen conditions during deposition (Berger *et al.*, 2002). The latter also argued that the foraminiferal content and assemblage indicate strong winnowing on the Olifants River Slope throughout the entire Quaternary succession of Site 1086 (ODP Leg 175). Giraudeau *et al.* (2002) observed that the late Pliocene in Site 1087 (ODP Leg 175), recovered from water depths of 1371 m on the slope off the Olifants River, has a decreased rate of organic material burial. This is interpreted as having resulted from reduced upwelling intensity and nutrient-depleted thermocline waters in the southern Benguela region, in response to intensification of the Northern Hemisphere glaciation. Giraudeau *et al.* (2002) noted that this pattern of decreasing accumulation rates continues through to the Pleistocene with the progressive isolation of the southernmost Benguela region from coastal upwelling.

The late Quaternary, since 0.9 Ma, was a time of high-amplitude (100+ m) and high-frequency (±100 kyr) sea-level fluctuations (Shackleton, 1987). The transitional subfacies within the Northern Depression most likely represents the influence of increased upwelling during glacial periods prior to the latest Pleistocene LGM (Berger and Wefer, 2002). However, diatoms, radiolaria, and other opaline fossils are not observed, indicating the lack of a strong upwelling signal in these sediments (Berger *et al.*, 2002.). The early late Pleistocene sea-level fluctuations, at least, are associated with slightly reduced variations in sea level (Imbrie *et al.* 1984, Cutler *et al.*, 2003). The earlier lowstand drops in sea

University of Cape Town

level may have been insufficient to reproduce the well-oxygenated and organic matter-rich depositional environment of the LGM. The uppermost Pleistocene sediments of the Northern Depression shows a similar faunal assemblage to that observed on the Western Ridge and outer shelf. The abundance and diversity of molluscs and benthic foraminifera indicate deposition of organic matter under well-oxygenated bottom water conditions. The presence of the well-preserved, widespread, capping shell layer of the Calcareous Glauconitic Sand is interpreted to represent the winnowed LGM lowstand-lag described in detail for the Calcareous Glauconitic Sand. The Pleistocene foraminiferal assemblage of the transitional and uppermost Pleistocene sub-facies clearly demonstrates the same general trend of an increase in surface water temperatures up-core, as described for the Calcareous Glauconitic Sand.

The sedimentary environment of the southern Main Channel is completely different in that it is predominantly erosional. The absence of microfauna and mud indicate higher-energy conditions prevailed, resulting in the winnowing of the fine fraction. Similarly, the absence of molluscs in these medium to coarse sediments indicates that winnowing has produced very clean (mud and organic matter-free) sand.

8.4 HOLOCENE FAECAL–RICH MUDDY SAND

A thin veneer of Holocene sediments is distributed across most of the study area. The Holocene drape has an average thickness of 33 cm, where the thickest sediment succession is recovered from both flanks of the Cape Canyon (95 to 100 cm in Cores 271 and 114). The Holocene drape thins out across the outer shelf and is only 1-2 cm thick in Cores 142-144 (water depths from 317-357 m) and it is absent in Core 145 at a water depth of 365 m. Holocene sediments are absent, or present only as a ≤10 cm thin veneer in the cores recovered from the Central and Southern Transects of the Main Channel of the Cape Canyon Head. Additional evidence for Holocene erosion in the Cape Canyon Head region is observed in Cores 274 and 276, collected on the Western Ridge, where Pleistocene sediments are preserved only as burrows in the underlying Pliocene Quartzose Muddy Sand.

The contact between the Holocene Faecal-rich Muddy Sand facies and the underlying sediment is typically poorly defined and is marked by a gradual increase in an olive mud component in the sediment above the uppermost Pleistocene shell layers (Figures 8.1, 8.3, 8.5 and 8.13). In contrast, the contact between the Holocene sediments and the underlying Upper Oligocene/Lower Miocene Calcareous Unit of the outer shelf is sharp. The sediment texture of the Holocene Faecal–rich Muddy Sand varies between a sand in the Northern Depression to a muddy sand on the outer shelf (Figure 8.21). The composition of the Holocene sediment is strongly influenced by the underlying Pleistocene sediments and typically includes a significant reworked component.

The Holocene sediments of the Northern Depression of the Cape Canyon Head region tend to be a well to moderately well sorted fine to medium sand composed of quartz, phospho-glauconite, ≤2% foraminifera (cold water planktic dominate) and ~5% faecal mud/pellets with minor to trace amounts of

University of Cape Town

sponge spicules always present. The foraminiferal assemblage is dominated by *G. bulloides* and *O. universa* with robust thick-shelled planktics such as *Quinqueloculina* sp., *Sphaeroidina bulloides, Globobulimina sp. and Globulina sp.* common. Benthic species present are typical of the Holocene west coast "condensed section" settings (Dale and McMillan, 1998a) and include *Ammonia japonica, Nonion boueanus, Planulina ariminensis, Lobatula lobatula, Uvigerina* sp. and *Brizalina spathulata*. The Holocene sediments show a similar seawards decrease in quartz abundance from 58.9% in Core 271 to 31.5% Core 275. The Holocene drape from the Western Ridge is dominated by very fine quartz, but includes subordinate glauconite with minor biogenic grains, faecal mud and 1-2% sponge spicules. The medium sand of the outer shelf Faecal-rich Muddy Sand has a higher glauconite and phospho-glauconite (phospho-glauconite foraminiferal infillings) abundance and a decreased abundance and biodiversity of the biogenic components relative to the underlying Pleistocene Calcareous Glauconitic Sand (Figure 8.1A & B). The composition of the sand fraction is shown in Table 8.3, where ≤5% faecal pellets and cohesive mud aggregates are also present in the sand fraction (Figure 8.22).

University of Cape Town

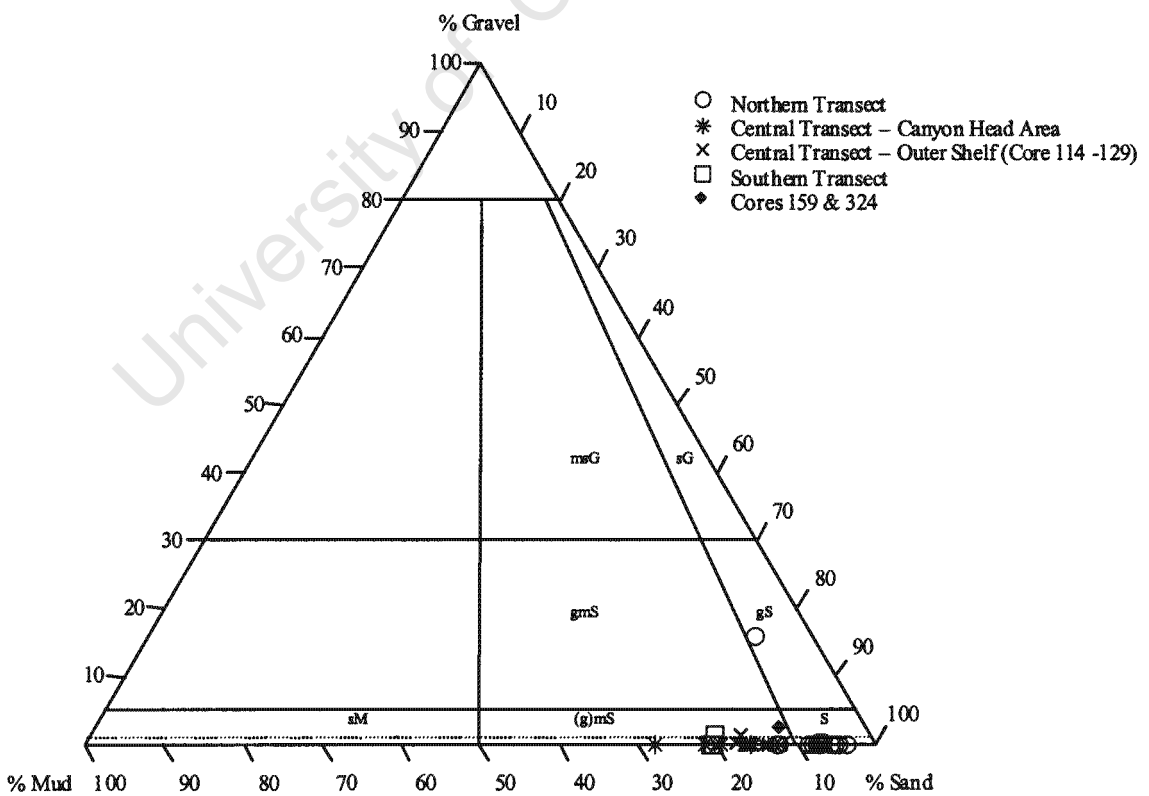


Figure 8.21. A summary of the grain size textures of the Holocene Faecal-rich Muddy Sand.

Table 8.3. The composition of the Holocene Faecal-rich Muddy Sand of the outer shelf unit as determined by point-counting a minimum of 300 grains.

	Glauconite	Phospho-glauconite	Very fine quartz sand	Medium quartz sand	Foraminifera	Calcareous fragments	Echinoid Spines	Sponge Spicules
128-1	40.5	11.3	25.8	0.3	4.9	16.6	0.3	0.2
115-1	48.0	5.9	12.5	7.9+ 2% cS	11.2	10.5	1.3	0.7

Gravel constitutes less than 1% of the bulk sample and is commonly quartz and brown phosphorite (CFA-cemented glauconite medium sand) very fine pebbles. No modern molluscs were recovered from the Holocene sediments during this study. Sample 116-1 contains a single coarse phosphorite (CFA-cemented glauconite medium sand) pebble. Traces of soft, thin, polychaete worm tubes are present in the gravel fraction of Core 273. The mud (<63 μm) fraction is dominated by calcite, quartz and feldspar, with a broad flattened peak reflecting the presence of amorphous organic matter in these sediments. Minor 10 Å illite/glauconite and kaolinite peaks are present in some samples within the Northern Depression, where the terrigenous clay abundance decreases seawards and is absent from the Western Ridge.

Sediment textures indicate differences in the Holocene depositional environment of the outer shelf and Cape Canyon Head areas. The relative abundance of organic faecal-rich mud in outer shelf sediments indicates quiet-water conditions, where the biogenic component, dominated by cold-water planktic foraminifera and sponge spicules, indicates continued upwelling. However, the absence of benthic fauna suggests that dysaerobic bottom-water conditions prevailed during the Holocene deglaciation. Dale and McMillan (1998a) described similar conditions for the Holocene sediments along the inner and middle shelf of the western margin of southern Africa.

The increased abundance of phospho-glauconite in the Holocene sediments suggests that, besides possible reworking of the underlying Plio/Pleistocene Glauconitic Sand Unit, additional material appears to have been transported across the shelf. Phospho-glauconite dominates the upper Oligocene/lower Miocene, suggesting that active erosion of upper Oligocene to lower Miocene sediments occurred during the Holocene. The Holocene sediments from the Northern Depression are sandier than those of the outer shelf (Figure 8.21), indicating increased bottom-water activity in the Cape Canyon Head region. To the south, the Holocene is a period of active erosion within the Main Channel, where Holocene sediments are absent from many of the cores and, where present, occur only as a <10 cm thick drape.

University of Cape Town

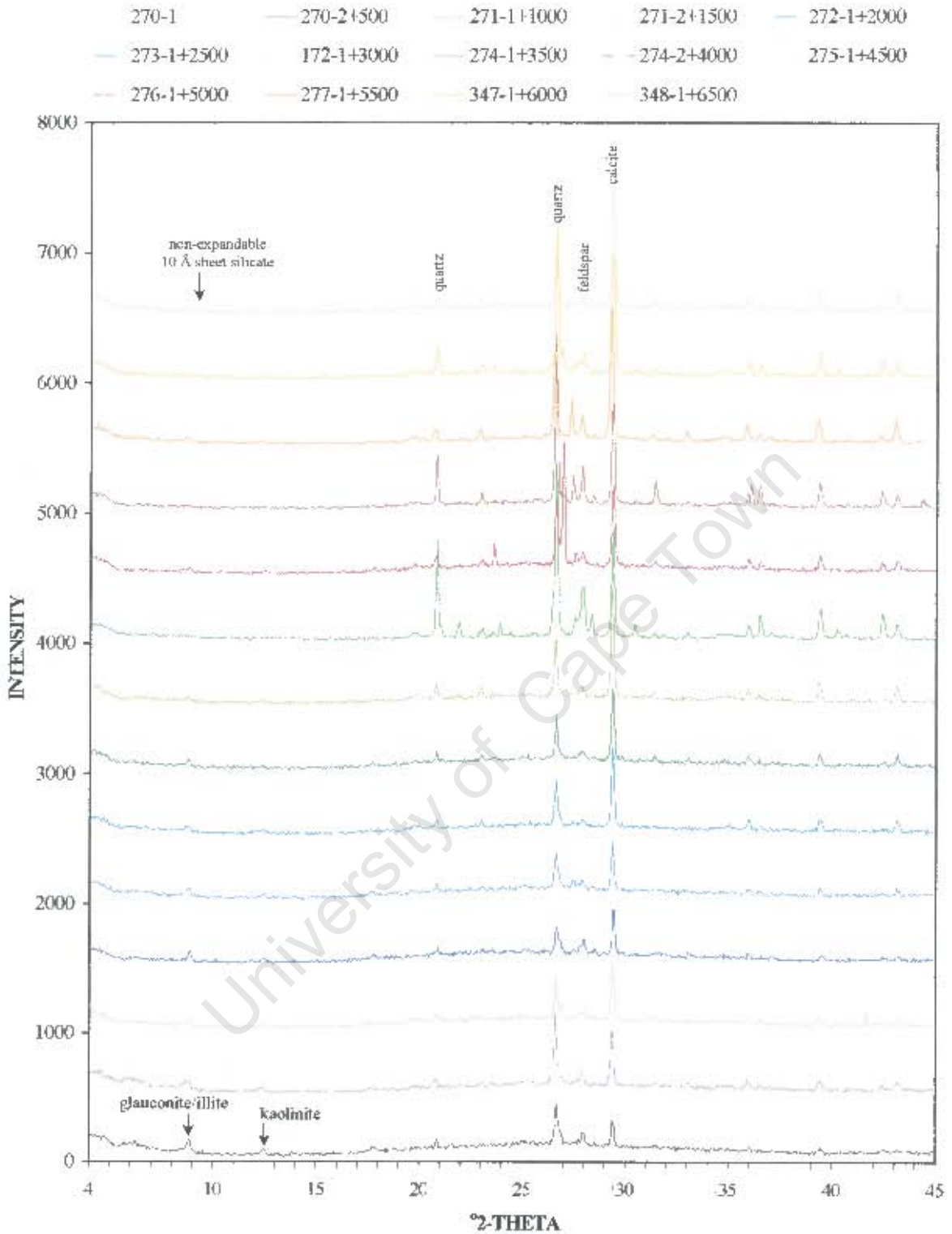


Figure 8.22. The XRD records show that the mud fraction (<63 μm) of the Holocene sediments from the Northern Transect is composed of quartz, feldspar and calcite, usually with only minor amounts of glauconite/illite (a non-expandable 10 Å sheet silicate) and kaolinite occasionally present.
(Refer to Appendix 1 for Core and Sample numbers)

University of Cape Town

8.5 QUATERNARY EVOLUTION OF CONCESSION 20D

The available seismic records, interpreted in conjunction with the sediment facies data, indicate that incision (significant reactivation) of the Cape Canyon Head region of Concession 20D occurred after the widespread deposition of the Pliocene Quartzose Muddy Sand sometime during the late Pliocene/early Pleistocene. The Tertiary sediments of Concession 20D show no variation in composition across the concession area and display no apparent relationship between bathymetry and deposition, suggesting that the canyon was not yet a significant bathymetric feature. Furthermore, only marine sediments and no obvious fluvial sediments were recovered within the Tertiary Succession, although erosion into the Cretaceous sedimentary basement had occurred. In contrast to the Tertiary succession, the very variable Quaternary sediments display an intimate relationship between composition and the modern bathymetric features, implying that the incision of the Cape Canyon had occurred before Pleistocene deposition occurred. The interpreted mini-gun seismic profile (Figure 8.23) shows that the change in quartz-glauconite ratio observed between cores 113 and 114 of the Central Transect (Chapter 7) occurs above the location of the major western boundary fault of the incised Cape Canyon. In addition, the distribution of the Pleistocene quartzose sediments of the Cape Canyon Head region is largely restricted to within the Cretaceous sediment high indicated in the CHIRP record from the Northern Transect (Chapter 3). This implies that the Cape Canyon Head region was a trap site during the Pleistocene.

University of Cape Town

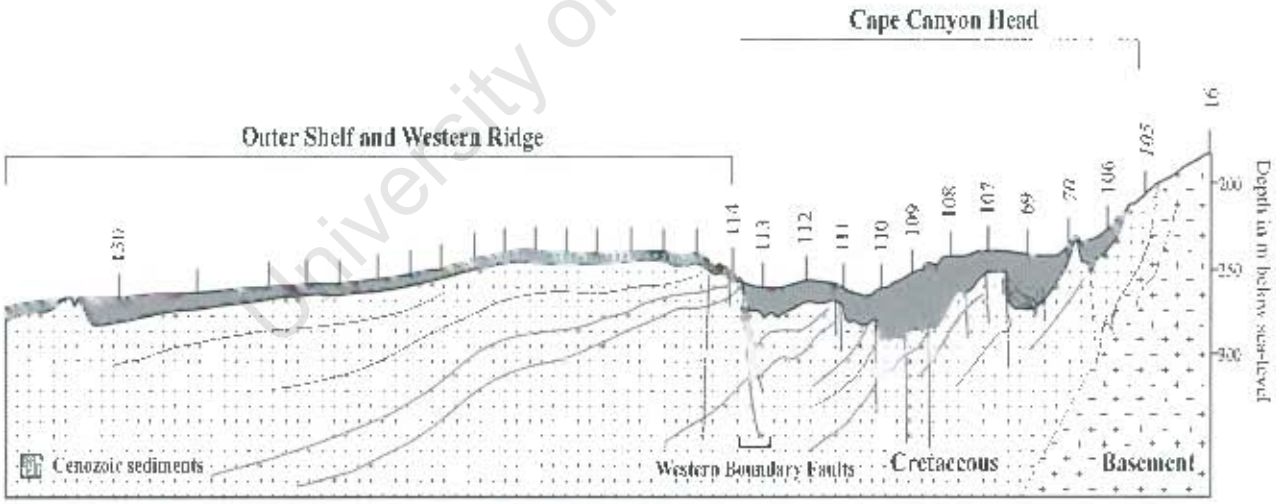


Figure 8.23. The interpreted mini-gun seismic record along the Central Transect of Concession 20D, showing location of cores (See Figure 3.6). (Cores in italics not studied.)

The late Pliocene is a period of tectonic activity and uplift along the continental margin of southern Africa (Partridge and Maud, 1987; Andreoli *et al.*, 1996; Partridge, 1998; Gallagher and Brown, 1999; Brown *et al.*, 2000; Roberts and Brink, 2002; Dale and McMillan, 2003b), where the amount and timing of the uplift event is still poorly understood (Section 2.3.1). The incision of the Head of the Cape Canyon during the late Pliocene/early Pleistocene is consistent with flexural processes related to the late Pliocene tectonic regime of the western continental margin. The tectonic activity in the southwestern

Cape indicates the existence of an extensional regime during the late Neogene (Andreoli *et al.*, 1996). The western boundary faults of the Cape Canyon, as observed in the interpreted seismic line of Figure 8.23, are antithetic faults related to normal faulting along the rifted margin of the underlying Columbine-Agulhas Arch. The presence of low-angle rotated slump masses on the outer margin of the west coast of southern Africa (Section 2.7.3) favours increased tectonic activity, where slumping is post-Early Pliocene in age as evidenced by the sediment succession in borehole DSDP Site 360 (Bolli *et al.*, 1978; Dingle, 1980b; Dingle and Robson, 1992). Dingle (1980b) suggested that the margin-oblique orientation of the Cape Canyon may be in some way controlled by slump glide planes. Although poorly constrained, evidence from this study suggests that uplift of the Columbine-Agulhas Arch in later Pliocene times is associated with the faulting of the Cape Canyon Head region by downwards rotation along antithetic listric faults.

The abundance of fine to coarse quartz sand in the Pleistocene Canyon Head sediments clearly marks a major change in the Quaternary depositional environment on the western margin. The Glauconitic Quartzose Sand facies includes significant amounts of fine to medium quartz sand, as well as coarse to very coarse quartz sand and occasional lithic pebbles in the southern Main Channel of the Cape Canyon Head area. The coarser quartz sand cannot have been derived from reworking of the underlying Pliocene deposits, because Pliocene sediments consist of a uniform very fine quartzose sand. This very fine Pliocene quartz sand is not included in the Pleistocene Glauconitic Quartzose Sand, except in cores recording slump events. The published information on the surface sediments to the north of the study area (Figure 2.8) suggests that the Pliocene Quartzose Muddy Sand of Concession 20D is at the southern end of a more widespread muddy sand deposit (Birch, 1975; Rogers and Bremner, 1991). The fine to medium and coarse quartz sand components are therefore unlikely to result from erosion of older units upslope. The fine to medium quartz sand of the Northern Depression, in particular, requires a Pleistocene source for the quartz sand. Although the Cretaceous and Middle Miocene Units are both quartz-rich, the Northern Depression does not appear to be eroded sufficiently deeply through the Pliocene succession to intersect the Cretaceous sediments, where the Cretaceous sediments are only recovered below 250 m water depth in the southern Main Channel (see bathymetic contour in Figure 8.24). The Middle Miocene unit is only recovered in a single core in the very south of the concession area, on an unusually preserved, less steeply dipping, portion of the Eastern Flank. Therefore, neither the Cretaceous nor Middle Miocene sedimentary units are likely sources of coarser quartz sand to the Northern Depression.

A rejuvenation of fluvial activity along 2000 km of the Namibian coast starting at 2.8 ±0.11 Ma (late Pliocene) is indicated by cosmogenic dating of surface pediments and river terraces in Namibia (Van der Wateren and Dunai, 2001), where the increased incision of river channels is interpreted to indicate a wetter climate. Peizhen *et al.* (2001) noted that the period between 2-4 Ma ago was a time of increased erosion rates on a global scale and argued that this is in response to a transition from early Pliocene climate stability to the rapid climate degeneration resulting from intensification of Northern Hemisphere glaciation. De Wit (1993, 1999) interprets the late Pliocene as being more humid (Section 2.3.1),

University of Cape Town

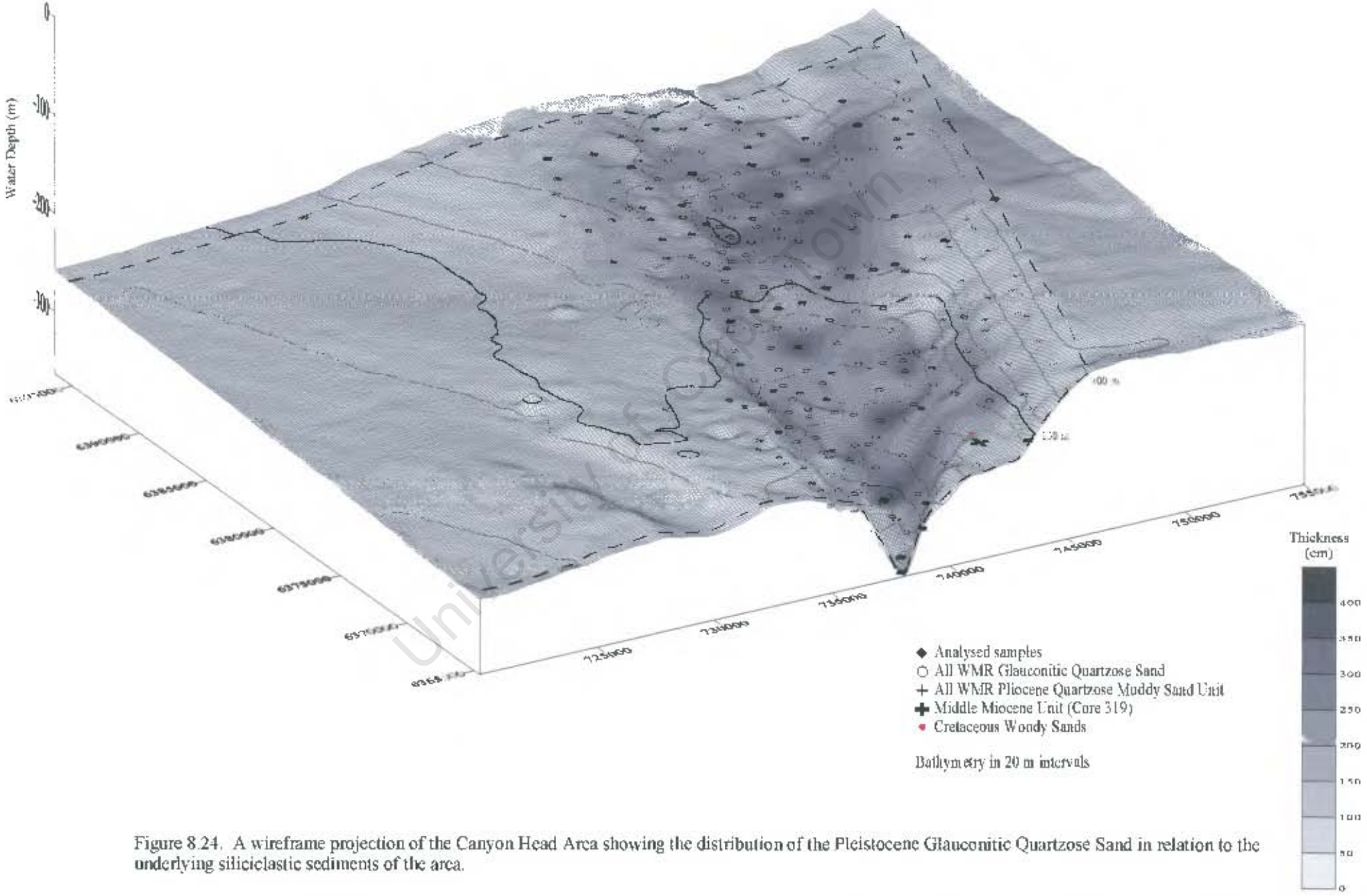


Figure 8.24. A wireframe projection of the Canyon Head Area showing the distribution of the Pleistocene Glauconitic Quartzose Sand in relation to the underlying siliciclastic sediments of the area.

University of Cape Town

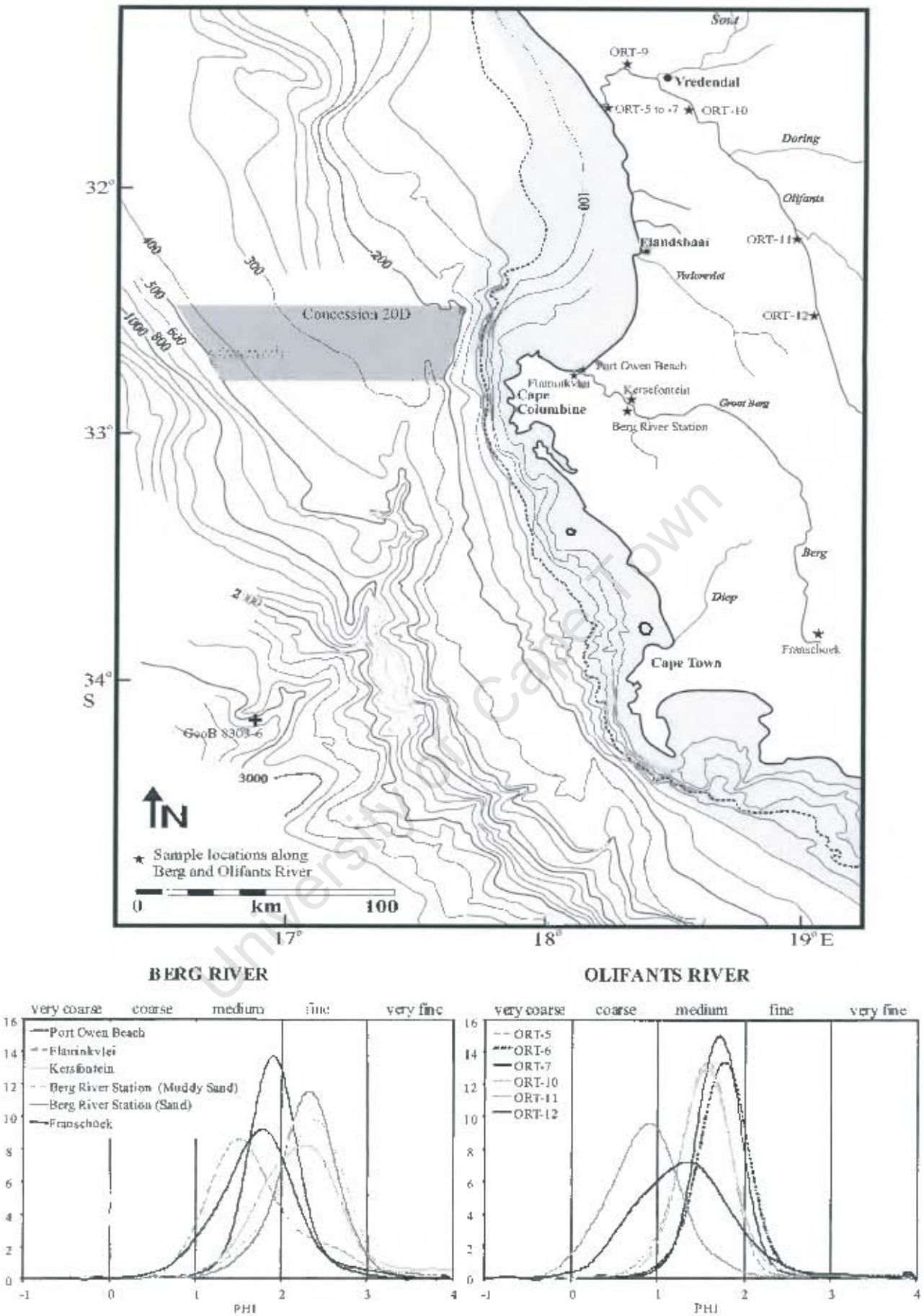


Figure 8.25. The location of Concession 20D in relation to the modern rivers, where the shaded area shows the extent of the pre-Cretaceous basement high of Brown *et al.* (1995). The frequency curves showing the particle size distribution of the sand fraction of river bank sediments sampled along the Berg and Olifants Rivers. Bathymetry after Dingle (1971b, 1986), with the approximate position of the LGM palaeo-shoreline at –120 m drawn as a dashed line. The location of core GeoB 8303-6 of Botha (2003) shown.

University of Cape Town

whereas Giraudeau *et al.* (2002) and references therein, describe a mid-Pliocene warm period from 3-3.5 Ma. Increased fluvial output in the late Pliocene/early Pleistocene, whether due to wetter climates, increased uplift or lowered sea levels, or due to a combination of these factors, is anticipated in context of the current understanding of the western margin of southern Africa. Therefore a fluvial origin for the fine to medium coarse quartz of the Northern Depression is considered likely.

The available bathymetric data from Dingle (1986), particularly the 60 m isobath, shows a suggestion of a palaeo-Berg River delta in St. Helena Bay (Figure 8.25). This sediment wedge is inshore of the clearly defined "bulge" of the eastern flank, which separates the Northern Depression from the southern Main Channel in Concession 20D. Furthermore, the increase in quartz abundance from east to west across the Canyon area supports an easterly landward input of quartzose sand into the newly formed canyon. This bulge appears to have controlled deposition in the area and limited erosion in the Northern Depression. Because no published sediment data are available for the modern major rivers of the west coast, reconnaissance sampling of river sand was undertaken (Figure 8.25). The Berg River samples are a fine to medium quartzose sands, composed almost entirely of quartz (Figure 8.25).

In contrast, the slightly coarser and better rounded Olifants River sands, particularly those collected from the river mouth, include a significant heavy mineral and garnet component not seen anywhere in Concession 20D. The garnet appears to be restricted to the river mouth area, but sand from the Olifants River downstream of the Doring confluence (Figure 8.25) show a marked increase in lithic fragments that are largely absent from the Berg River and from Pleistocene sediments of Concession 20D. Most of the lithic clasts present in the Cape Canyon Head region are either granite or quartz, derived from Cape Granite intrusions and Table Mountain Group outcrops exposed in the Berg River catchment, indicating a local Berg River origin.

In contrast to the Northern Depression, the southern Main Channel of the Cape Canyon Head cuts deeply into the unconsolidated Cretaceous sediments. The bimodal quartz sand, as well as all of the exotic components in this southern Pleistocene unit, record the condensed coarse-fraction of sediments extending as far back as the mid-Cretaceous (Chapter 4). Fining-upward cycles and gravelly layers suggest that bottom currents, whether turbidity currents or mass-transport processes (*eg.* slumps, slides, grain and debris flows), were important in the downcutting of the southern part of the Canyon during the late Pleistocene and the Holocene (Damuth, 1994; Shanmugam, 2002, 2003). The preservation of Cretaceous mud clasts and pyritised wood suggests rapid erosion and deposition of the steep canyon walls, with little reworking of these sediments. Mass-wasting processes, associated with increased across shelf/slope sediment transport, occur more often within submarine canyons than in other location on the continental shelf, as these submarine canyons are associated with complex and dynamic hydrography (Okey, 1997; Granata *et al.*, 1999; Boyer *et al.*, 2000; Liu *et al.*, 2002) and incision of submarine canyons becomes self-propagating. The absence of very fine sand from the Cape Canyon may reflect its removal down canyon, because very fine glauconitic quartzose sand is a common constituent of the minor non-carbonate fraction of deep-water (3445 m) Pleistocene sediments recovered

University of Cape Town

from the distal Cape Canyon Core GeoB 8303-6 in Figure 8.25 (Botha, 2003). This down canyon transport of shelf sediments is typical of submarine canyons, which act as a natural conduit for the transport of sediments to the deep ocean basins (Liu *et al.*, 2002; Puig *et al.*, 2003). Recent work by Wåhlin (2002, 2004) proposed that dense bottom-water geostrophic flow may be redirected off-shelf by bathymetric irregularities, such as the fault-controlled incision of the Head of the Cape Canyon. The increased downward transport (and erosion) of the dense water occurs as a consequence of canyon incision and Wåhlin (2004) argued that available information points to the formation of narrow canyons on steep slopes. Although speculative, this does provide a possible mechanism for the Quaternary incision of the Cape Canyon. However, although this study proposes a much younger incision of the Head of the Cape Canyon than the Oligocene age previously suggested (Dingle, 1971a, 1992/1993; Dingle and Hendey, 1984; Dingle and Robson, 1992), it is possible that the deeper water portion of the deeply incised Cape Canyon that transects the upper slope was incised earlier.

The late Pleistocene was a time of major sea-level fluctuations related to Northern Hemisphere glaciation and deglaciation, where the mean sea level fluctuated between +10 and –125 m along the west coast of southern Africa (Cutler *et al.*, 2003; Dale and McMillan, 2003b; Ramsay and Cooper, 2002; Compton *et al.*, 2002). On average, the palaeo-shoreline lay tens of kilometres seawards of its present Holocene location. The continental shelf between Concession 20D and the modern shoreline is relatively steep, so that, during the lowstands of the late Pleistocene, the newly formed (reactivated) Cape Canyon would have been immediately downslope of the very steeply dipping inner shelf (Figure 8.25). Pulses of terrigenous sand would have been delivered to the shelf edge during sea-level lowstands and deposited in the Cape Canyon Head region.

Sediment cover on the middle to outer shelf of the western continental margin is very thin (< 50 cm) above the lower Miocene calcareous sediments (Rogers, 1977; Dingle *et al.*, 1983; Corbett, 1996). Evidence suggests that late Pleistocene sea level fluctuations and shoreface migration were effective in scouring and transporting sediment off the continental shelf and most of the fine-grained shelf sediments deposited prior to the Last Glacial Maximum (LGM) have been removed from the continental shelf by erosion (Compton *et al.*, 2002). The increased accommodation space, associated with the downfaulting of the Cape Canyon Head area, resulted in the rare preservation of a Pleistocene sediment succession on the western margin.

The basal sub-facies of the Glauconitic Quartzose Sand in the Northern Depression indicates that similar anoxic bottom water conditions existed before and after incision of the Cape Canyon. As described for the western continental margin, glacio-eustatic sea level lowstands are associated with reworking of the underlying sediments across the whole of Concession 20D. The Pliocene Glauconitic Sand of the outer shelf and Southern Rocky Plateau include cold-water (older than latest Pleistocene) foraminifera, with a similar foraminiferal assemblages indicating reworking and deposition on the Western Ridge. The lowstand of the LGM is preserved as a shell lag layer from the Northern Depression to the outer shelf of Concession 20D, where the macrofaunal assemblage of all three Pleistocene sediment facies is similar,

University of Cape Town

although the bivalves show a decrease in biodiversity seawards. Following the LGM, deglaciation is associated with increasing water depths and a return to quieter water and dysaerobic conditions over most of the concession area. The sediment succession of the upper slope cores indicates Recent renewed mass movement of sediments off the shelf.

University of Cape Town

9 TEXTURE AND GEOCHEMISTRY OF GLAUCONITE GRAINS

Authigenic glauconite and phosphorite are present in varying proportions in all of the Cenozoic sediments of Concession 20D. This chapter focuses primarily on the glauconite pellets as phosphorite is dealt with in detail in Chapter 5 (Compton *et al.*, 2004). Glauconite, rather than the proposed facies name glaucony (Odin and Matter, 1981; Odin, 1988), is used throughout this thesis in the broadest sense to include all of the green pellets and is not intended to imply that a glauconitic mica mineral dominates. The descriptions of the lithostratigraphic units in Chapters 6-8 indicate that at least three morphological glauconite varieties can be recognised within the Cenozoic sediments of Concession 20D. Phospho-glauconite infilled foraminifera dominate the Upper Oligocene/Lower Miocene Calcareous Unit and the Pliocene Phosphorite Gravel facies, whereas green glauconite pellets dominate the Pliocene and a black to very dark green lobate glauconite dominates the Quaternary sediments. The glauconite pellets were looked at in more detail to determine whether morphological and textural variations correspond to geochemical or mineralogical differences. In addition, Eocene and Cretaceous glauconite from southern Namibia are compared to the glauconite of Concession 20D off South Africa to determine whether glauconite texture and composition vary with age and if younger glauconite is derived from reworking of older deposits.

Phosphorite and glauconitic sediments were first recovered from the South African coast during the Challenger Expedition under Murray and Renard (1891). A number of authors have described the extensive phosphorite and glauconite deposits of the western and southern margins (Birch, 1971, 1975; Parker, 1971; Parker and Siesser, 1972; Rogers, 1977; Bremner, 1981). Birch (1971, 1975, 1979a, 1979b, 1980) has described, in detail, the glauconite deposits of the southern African margin and the terminology and classification schemes he defined are referred to throughout this discussion. Birch subdivided glauconite into Holocene and pre-Holocene subgroups and estimated that ≤5% of Agulhas glauconite is Holocene where the distribution of this glauconite (blue-green glauconite foraminiferal infillings and coatings), is confined to the western margin off the Cape Peninsula. Pre-Holocene glauconites are subdivided into authigenic and detrital grains. Authigenic grains include all primary morphologies, whereas detrital grains tend to be fragmented, abraded, rounded and occasionally oxidised. Although Birch (1971) indicated that the surficial glauconite deposits off the Cape Columbine area were dominated by detrital ancient glauconite, both authigenic and detrital glauconite were recovered from Concession 20D during this study. Birch (1971, 1975) noted that surficial glauconite-rich sediments of the Agulhas Bank and western margin areas are concentrated in elongated belts. The richest belt extends for over 400 km from south of Cape Agulhas to north of Saldanha Bay on the inner shelf to the mid-slope region (200-400m water depths). Parts of Concession 20D therefore fall within this Agulhas-Columbine glauconite belt. Birch (1971, 1975) argued that the Agulhas-Columbine glauconite belt is a late Cenozoic winnowed (lag) deposit, composed largely of reworked glauconite from Cretaceous and Miocene sediments, where the

University of Cape Town

preservation of the deposit reflects low, late Tertiary, sedimentation rates. Birch (1971) suggested that low glauconite concentrations in surface sediments on the mid shelf region to the northwest of Cape Columbine most likely reflect burial by prograding Holocene sediments.

9.1 GLAUCONITE MORPHOLOGY

Authigenic glauconite pellets dominate the Upper Oligocene/Lower Miocene Calcareous Unit and the Phosphorite Gravel facies at the base of the Pliocene Glauconitic Sand Unit. The predominantly fine sand-size authigenic pellets of these units are referred to in the previous chapters because phospho-glauconite grains and occur predominantly as infilled and replaced benthic and planktic foraminifera (Figure 9.1). The test of the infilled foraminifera consists of a phospho-glauconite mixed-mineral (Birch, 1975, 1979b), whereas EDS analyses of the infilling show considerable variation from a relatively insignificant to a dominant CFA component. Birch (1971) described similar "proto-glauconite" infillings of a diverse benthic and planktic foraminiferal assemblage from elsewhere on the southern African margin. Future studies on the infilled foraminiferal assemblage may provide some information on the oxygen, organic matter and phosphate content at the sediment-water interface (Rao *et al.*, 1993).

Medium sand-size glauconite pellets dominate the remaining Cenozoic lithostratigraphic units of Concession 20D, where two macroscopic glauconite varieties are present in the glauconite-rich sediments of the outer shelf. The morphology of the black and green glauconite pellet varieties are described below, where the microstructures of whole pellets as well as freshly broken glauconite grain surfaces were examined by SEM (Figures 9.2 to 9.5). Holocene and Pleistocene sediments from the concession area are dominated by black to very dark green glauconite (Figure 9.2A and B, respectively). The black glauconite occurs as rounded to lobate pellets, which commonly show a distinctive suture pattern comprised of one to two wide and deep radial triangular sutures (Birch, 1971). Birch (1971) defines the black to very dark green glauconite, either non-sutured or slightly sutured as mature, containing >8 wt% K_2O. This black glauconite is the dominant glauconite on the western continental margin. Grain surfaces are normally smooth and highly polished and the grains are usually well consolidated. The very distinctive rounded green glauconite of the Pliocene Glauconite Sand facies (Figure 9.2 C and D) appears to be both texturally and compositionally similar to the Quaternary black glauconite (Figure 9.2), although the compacted polished surface layer may be partially lost from the Pliocene green glauconite (Figure 9.2C). Birch (1971) described similar frosted black glauconite grains, which have lost the thin outer layer of well-polished glauconite, resulting in the exposure of the irregular inner glauconite.

University of Cape Town

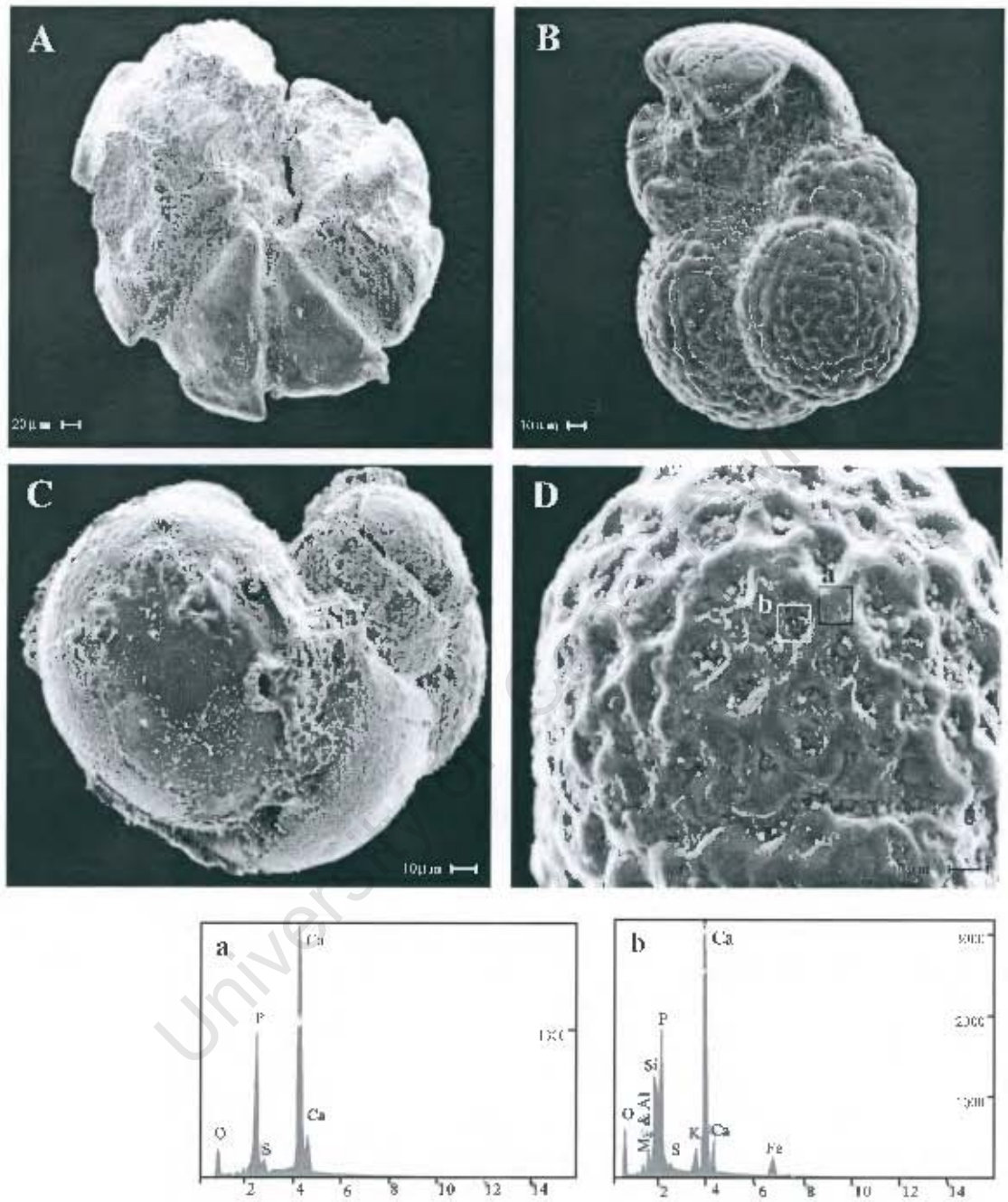
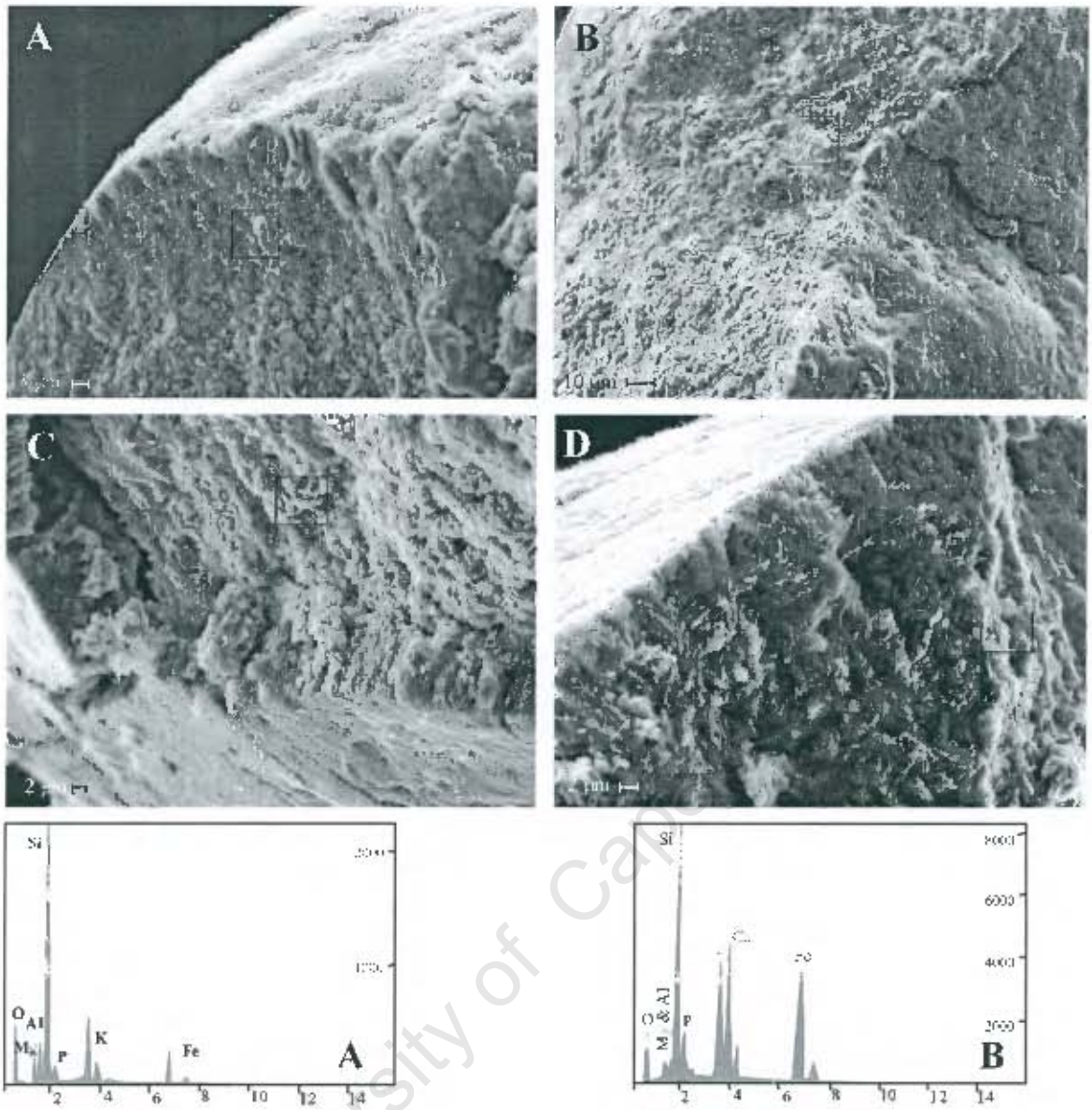
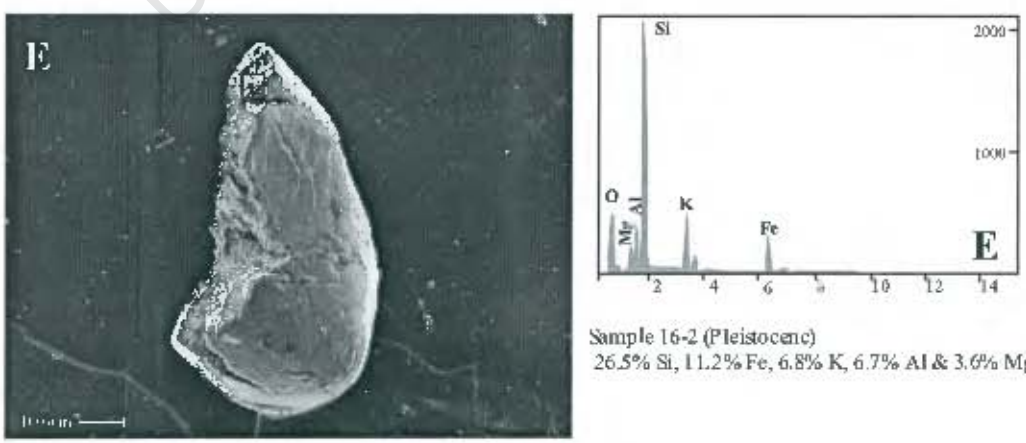


Figure 9.1. SEM images of infilled benthic (A) and planktic (B-D) foraminifera from the Pliocene Phosphorite Gravel facies (Samples 128-7 and 129-4). Representative EDS analyses show that the foraminiferal test is replaced by phosphorite with 36.5% Ca, 15.7% P, 1.2% S and <1% Si, Al, K and Fe (black square in D), whereas the foraminiferal infilling (white square in D) has a mixed-mineral phospho-glauconitic composition of 28.4% Ca, 14.3% P and 1.5% S with 5.7% Si, 2,5% Fe, 2.0% K, 1.5% Al and 1.2% Mg (Birch, 1975, 1979b).



A: Sample 128-1 (Holocene)
26.0% Si, 11.2% Fe, 8.8% K, 5.5% Al, 3.8% Mg & 2.6% P
C: Sample 128-7 (Pliocene)
15.0% Si, 11.1% Fe, 6.7% K, 3.4% Al, 1.4% Mg , 21.8%Ca & 9.1% P

B: Sample 128-3 (Pleistocene)
25.1% Si, 29.3% Fe, 11.0% K, 1.7% Al & Mg, 13.8%, Ca & 4.1% P
D: Sample 128-7 (Pliocene)
20.6% Si, 9.9% Fe, 6.7% K, 3.0% Al & 2.3% Mg, 9.3%, Ca & 5.1% P



Sample 16-2 (Pleistocene)
26.5% Si, 11.2% Fe, 6.8% K, 6.7% Al & 3.6% Mg

Figure 9.2. Representative SEM images of broken Pliocene, Pleistocene and Holocene glauconite pellets from Concession 20D. The results of EDS analyses, within the respective black boxes, emphasize the compositional variability of the phospho-glauconite mixed-mineral.

University of Cape

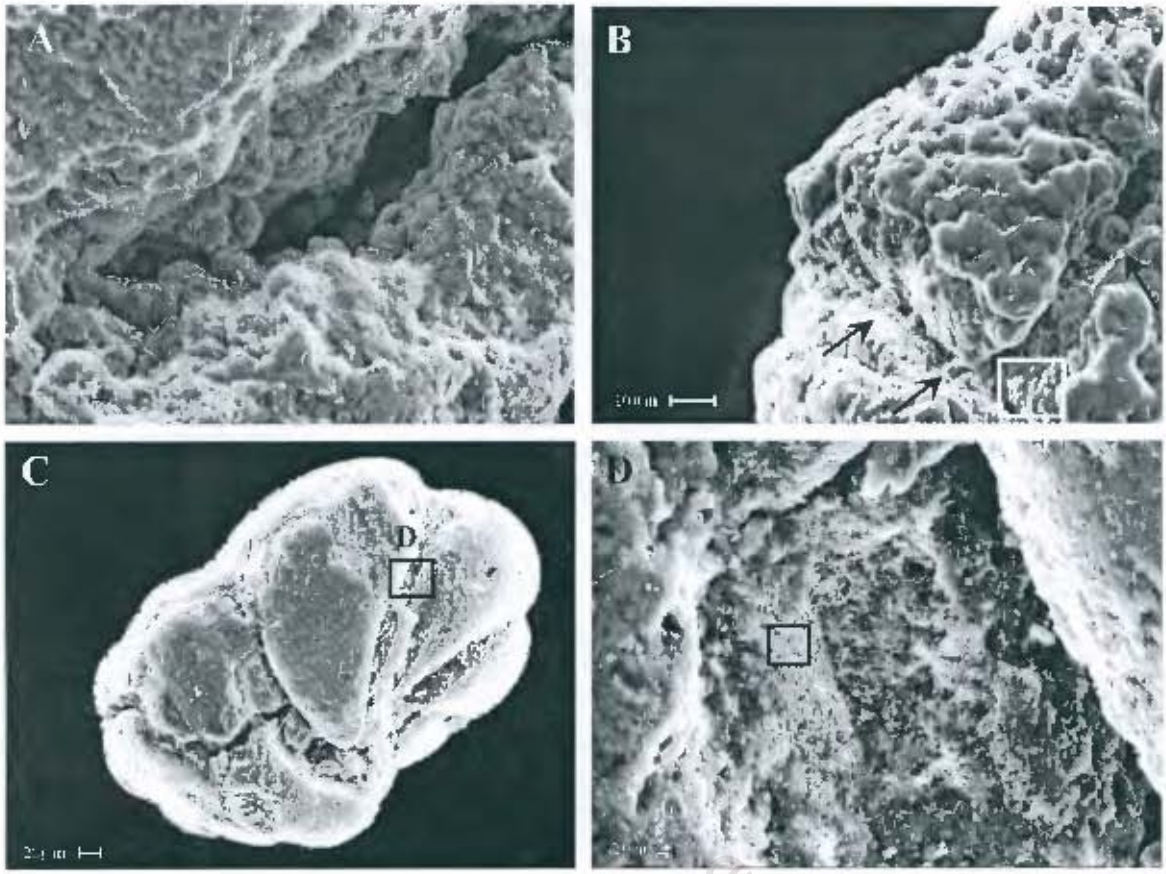


Figure 9.3. Sutures in glauconite pellets (A) and foraminiferal infills (B-D), where rosette (A and B) and box-work (D) textures typical of evolved glauconite (>6.5% K_2O) are common (Odin and Matter, 1981). The globular texture towards the bottom left of the suture in (D) shows the typical appearance of ill-defined globules of nascent glauconite (Odin and Matter, 1981). Coccoliths (indicated with arrows in B) are commonly abundant in the sutures. The boxed areas in the sutures (B: 129-5; C/D: 129-6) show phospho-glauconitic compositions. The EDS scan of the black box in (D) shows a phospho-glauconite composition of 26.0% Si, 14.2% Fe, 8.6% K, 4.9% Al and 2.6% Mg with 7.2% Ca and 3.4% P, whereas the blebs are predominantly CFA (33.1% Ca and 15.3 % P).

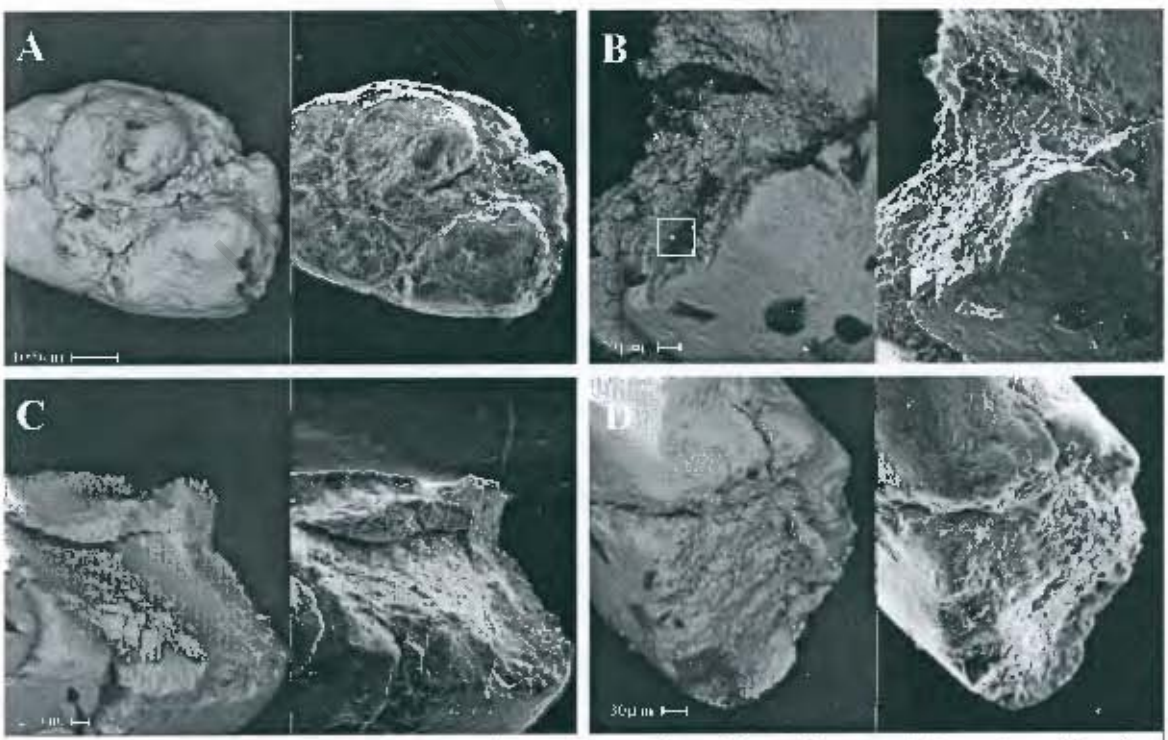


Figure 9.4. Representative SEM backscatter and normal secondary collector images of glauconite pellets from the Pliocene Sample 128-7 (A), Pleistocene Samples 110-4 (B) and 112-4 (C) and Holocene Sample 112-1 (D). The glauconite of Concession 20D includes very rare high reflectivity spots, with pyrite (in the white box) only identified by EDS analysis in the single Sample 110-4 (B).

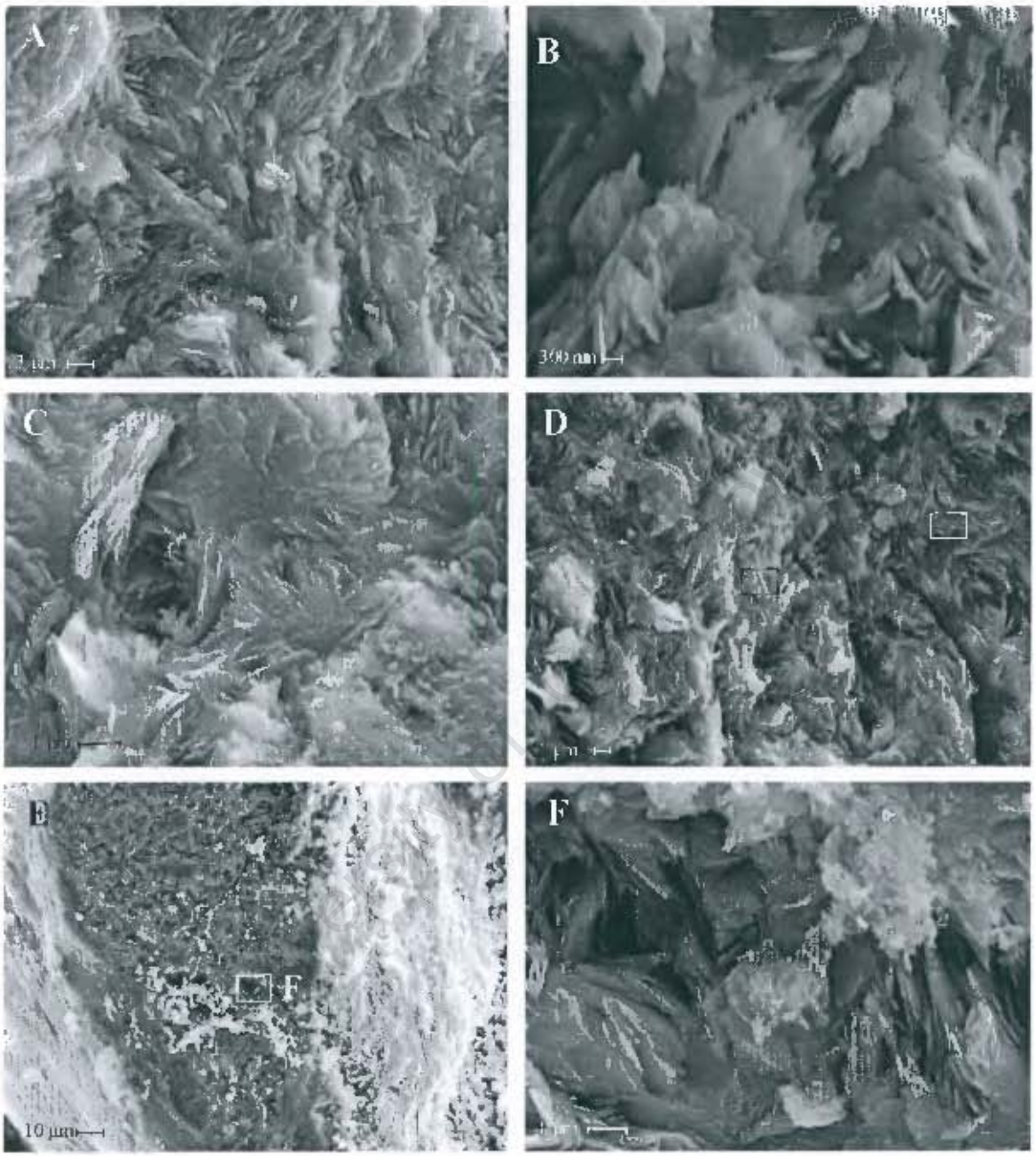


Figure 9.5. High-resolution SEM images of glauconite pellets from Concession 20D shows the complex relationship between lamellar textured glauconite and CFA. The CFA component is present either as tiny globules/rods (well-developed in A) to a irregular surface coating (C-F). EDS analyses of the white square in D show a glauconitic composition, whereas a phospho-glauconitic mixed-mineral is present within the black box.

The glauconite pellets from the Pliocene, Pleistocene and Holocene lithostratigraphic units have similar microstructures and compositional variation as determined by EDS analysis. These glauconite pellets all show a homogeneous internal lamellar texture typical of mature glauconite (Odin and Matter, 1981; Amouric and Parron, 1985). The freshly broken glauconite surface in Figure 9.2A and D and the naturally fragmented surface in Figure 9.2C clearly show the lamellar internal structure that becomes increasingly compact towards the polished pellet surface. In contrast to the internal lamellar glauconite, the sutures in glauconite pellets commonly show more varied textures (Figure 9.3) with a number of nanostructures that are more typical of nascent to evolved glauconite (Odin and Matter, 1981). No internal lithic or biogenic components were recognized within any of the glauconite grains analysed (Figure 9.2). Odin and Fullagar (1988) showed that detrital remnants may be preserved until a relatively late stage in glauconite evolution (6-8% K_2O). The absence of detritus in the glauconite pellets of Concession 20D may imply an absence of these components in the original mud-rich depositional environment. The relative absence of internal impurities within the Cenozoic glauconites is emphasized in the backscatter images of Figure 9.4, where the only obvious high-reflectivity areas are present in the glauconite suture of Figure 9.4B. However, coccoliths are commonly abundant in the glauconite sutures (Figures 9.3B and 7.5). The Pliocene to Recent glauconites show considerable compositional variation. The composition of the glauconite pellets is shown, by EDS analysis in Figure 9.2, to vary between a relatively pure glauconite end-member (Figure 9.2E) and a CFA-glauconite mixed-mineral (Figure 9.2B and C). However, this compositional variability is not reflected in the age, colour, morphology or internal textures of the glauconite pellets. However, both the Pliocene green glauconite and Quaternary black lobate grains, are compared to the black to dark green glauconite type of Birch (1971). The differences in macroscopic morphology, and colour in particular, may be related to the increasingly compacted internal lamellar structure towards the well-polished grain surfaces. The Quaternary glauconite pellets tend to be more compacted and have a more polished smooth surface than the underlying Pliocene green glauconite, which commonly shows fractured surfaces, where the compacted surface layer is often partially lost, revealing the internal sugary texture of the glauconite. It is most likely that continued glauconitization and abrasion during sea-level fluctuations of the late Pleistocene resulted in this morphological change.

The EDS analyses of the glauconite pellets showed that the glauconite grains almost always include a CFA component. The SEM images in Figure 9.5 illustrate the complex relationship between glauconite and CFA. The CFA-component is observed to vary from globular to a more complex apparent intergrowth of CFA blebs and glauconite blades. Rao *et al.* (1993) argued that similar globular CFA aggregates and glauconite-CFA intergrowth textures observed in the mixed-mineral phosphorite-glauconite pellets of the southwestern Indian margin indicate the importance of microbial processes in their origin.

Photomicrographs of thin-sections of glauconite grains from the different glauconite-rich facies of Core 128 from the outer shelf are shown in Figure 9.6. The black to green lobate to rounded Pliocene

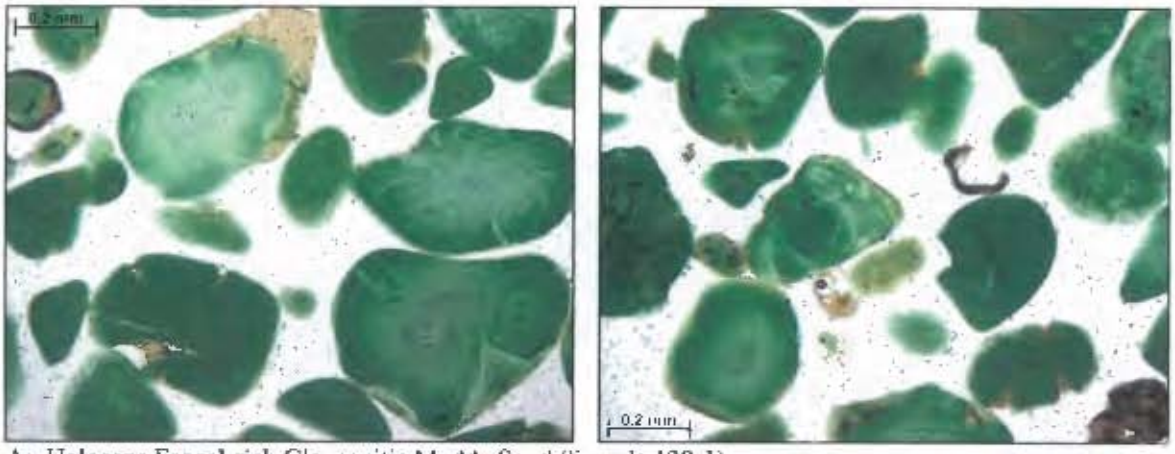
University of Cape Town

to Holocene glauconite pellets are similar and all have either a mottled/variegated appearance or show a complex internal zonation. Primary sutures, varying from inconspicuous to prominent, are commonly infilled by later glauconitization events. Concentric zonation patterns reflected in changes in the colour of the glauconite are commonly observed, similarly suggesting multiple growth phases. Birch (1980) noted that the mixed-mineral pellets of the southern African margin have usually undergone a secondary glauconitization with an increasing maturity towards grain surface commonly observed. Grains frequently show evidence of exsolution or zones enriched in either an opaque ore mineral, probably pyrite, or of an amorphous dull brown oxide, where these hydrated Fe-oxides are referred to as limonite or goethite (Birch, 1975). Exsolution blebs, similar to those described by Birch (1975), occur randomly scattered throughout the pellet, concentrated in central or peripheral zones, or concentrated along sutures. In addition, oxidized abraded pellets, with or without subsequent glauconite layers are present (Birch, 1971). Composite grains of glauconite and phosphorite are present and grain coatings by a secondary fluorapatite (probably francolite) as described by Birch (1975) are observed. The complex internal structures and zoned textures of the glauconite pellets are very similar in all aspects to those described by Birch (1975) for the southern African black glauconite type, where the glauconite is sufficiently evolved that it is difficult to identify the original mineralogy and morphology of the precursor material. In contrast to the above facies, the Phosphorite Gravel and Upper Oligocene/Lower Miocene Calcareous Unit is clearly dominated by foraminiferal infillings and phosphorite sand-sized fragments, although rounded glauconite pellets are present (Figure 9.6D).

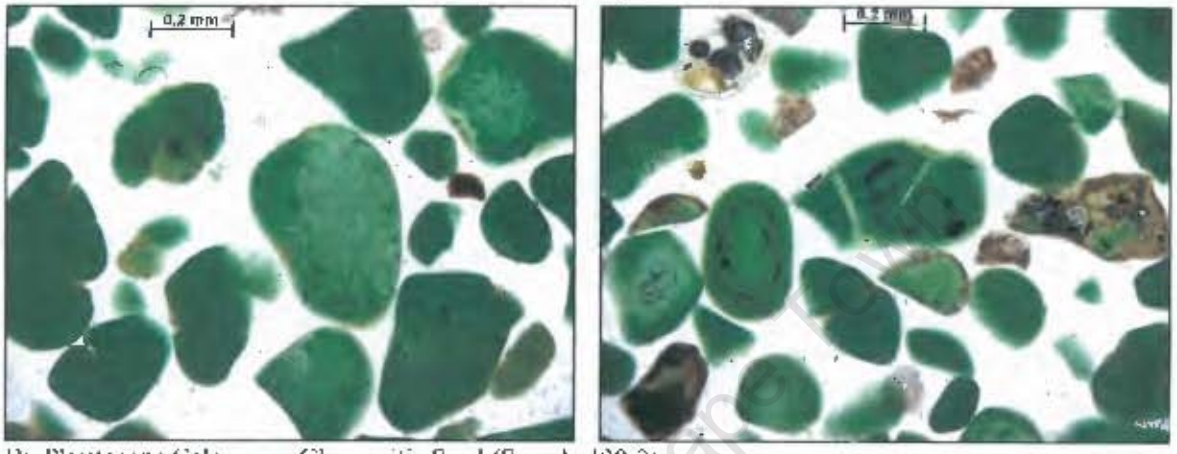
9.2 MAJOR ELEMENT GEOCHEMISTRY

Birch (1971, 1975, 1979a, b, 1980) noted that the close spatial association of glauconite and phosphorite in the surficial shelf sediments off southern Africa is mimicked by an intimate association of these minerals within all of the Agulhas Bank authigenic pellets, similar to those described above. The glauconite and phosphorite association was recognized in thin sections (Figure 9.6) and from XRD and wet-chemistry analyses. Birch (1979a) recognised five mixed-mineral types from the southern African margin, namely phosphorite fragments, altered glauconite pellets, foraminiferal infillings, altered faecal pellets and the most abundant mottled or variegated pellets. Random CFA-segregations within mottled pellets vary from <1 μm to 50 μm in size. Microprobe analyses of the glauconite from the Holocene, Pleistocene and Pliocene facies from Core 128 were undertaken in order to allow comparison to the earlier studies of Birch (1975, 1979b) and to determine whether the differences in morphology of glauconite from different lithostratigraphic units is reflected in the mineral chemistry (Figure 9.7). The total Fe is presented as FeO, although glauconite tends to include iron in a ferric (Fe^{III}) rather than a ferrous (Fe^{II}) valence state (Ireland *et al.*, 1983). The compositional variability of the glauconite grains from the three glauconite-rich facies is as great as that shown among the facies. In addition, the range in composition of individual grains is similar to that of multiple grains from the same sample (Figure 9.8). The microprobe analyses clearly show that the glauconite grains from all three stratigraphic units include a carbonate-fluorapatite (CFA) component,

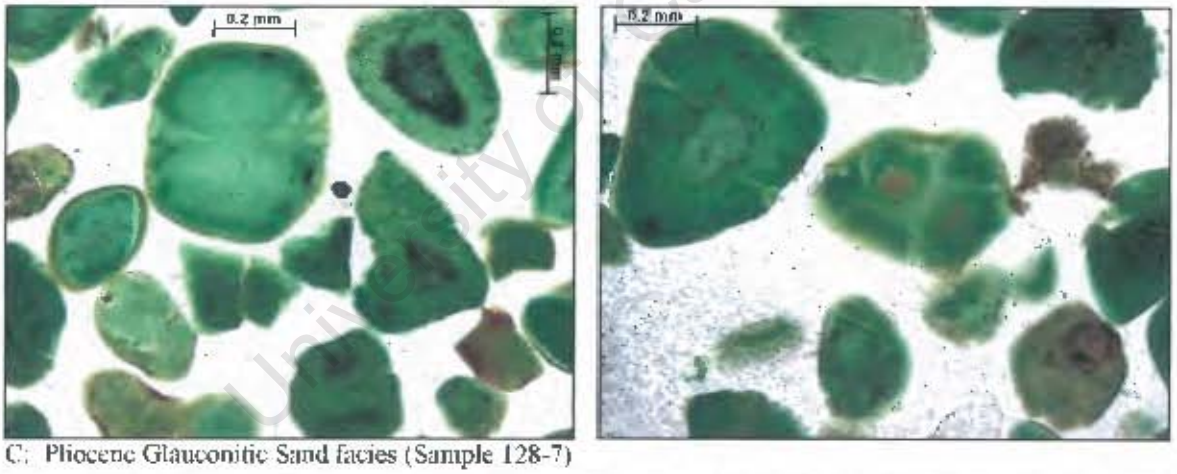
University of Cape Town



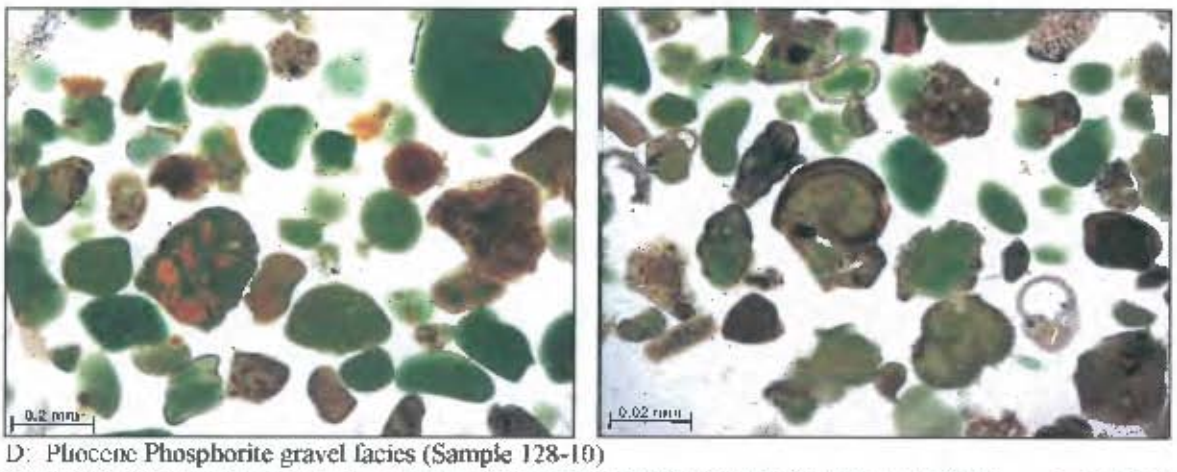
A: Holocene Faecal-rich Glauconitic Muddy Sand (Sample 128-1)



B: Pleistocene Calcareous Glauconitic Sand (Sample 128-3)



C: Pliocene Glauconitic Sand facies (Sample 128-7)



D: Pliocene Phosphorite gravel facies (Sample 128-10)

Figure 9.6. Thin section photomicrographs of glauconite pellets from the four outer shelf glauconite-rich facies.

University of Cape Town

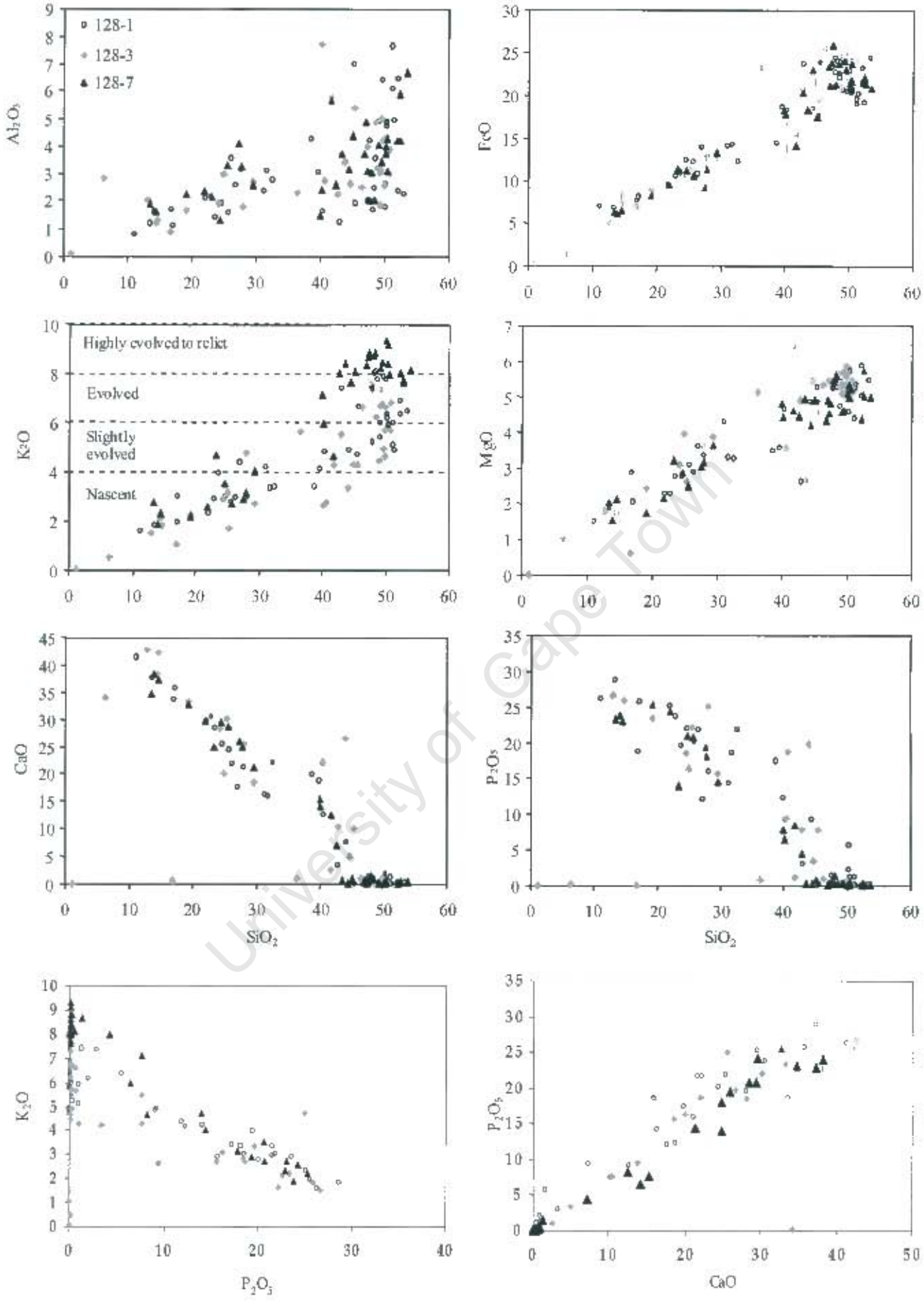


Figure 9.7. The glauconite compositions from Core 128 as determined by microprobe analysis.

University of Cape Town

with all three facies showing a range from 0-<28.8 wt% P_2O_5. Microprobe analyses of mixed glauconite/apatite with the phosphorites of the Agulhas Bank (Birch, 1975, 1979b), showed a very similar range in composition from an apatite end-member (~32% P_2O_5) to a glauconite end-member with an average of 8.7 wt% K_2O (Figures 9.7 and 9.8). The low totals recovered in the microprobe analyses are due to a high volatile content, with a similar range in volatile content of between 8-16 wt% recorded by Birch (1971).

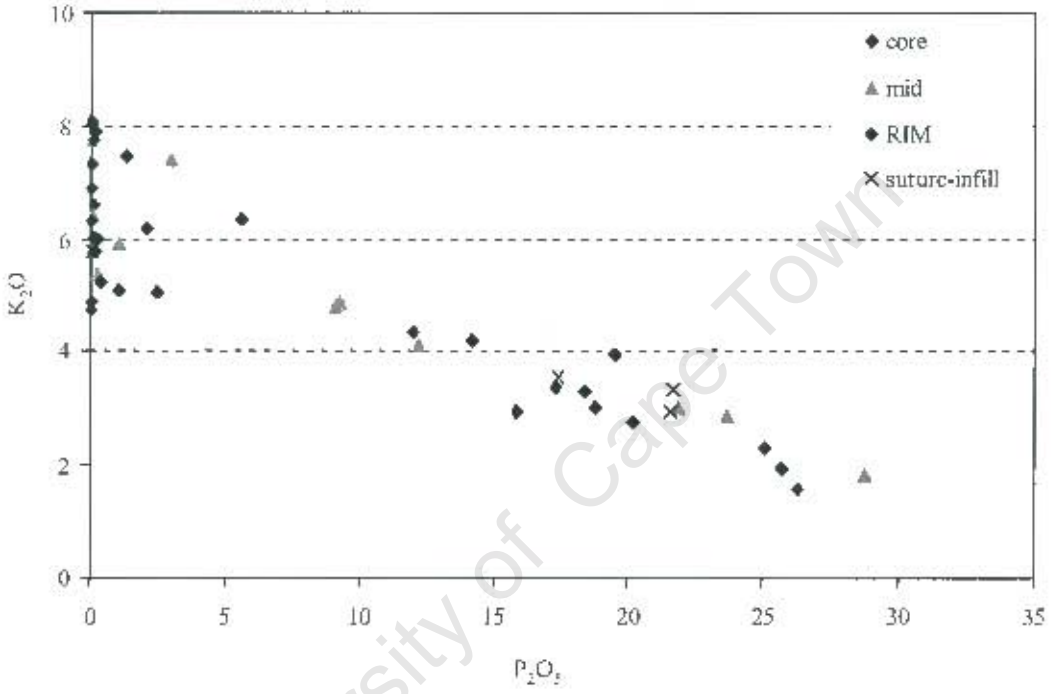


Figure 9.8. The glauconite compositions from Sample 128-1 showing the within-grain range in compositions determined by microprobe analysis.

University of Cape Town

In order to estimate the maturity of the glauconite, the microprobe data were recalculated whenever CaO was >1 wt%. The calculation assumed that negligible Ca or P is included in the glauconite mineral, and excess Ca and P were excluded from the analysis total. The CFA-enriched glauconite compositions were recalculated using the average CaO, P_2O_5 and Total of the analyses with <1 wt% CaO from that sample (Figures 9.9 to 9.11). The glauconite compositions from all three facies show a similar range in K_2O concentrations of 3.2 to 9.3 wt%. The glauconite compositions fall predominantly within the slightly evolved to evolved categories of Odin and Matter (1981), where the deeply sutured nature of the pellets in thin-section supports an evolved stage of glauconitization. Although poorly constrained, the microprobe data suggest that the glauconite from the Pliocene unit is, on average, more evolved than the Quaternary glauconite. However, the glauconite composition clearly cannot be used to differentiate between lithostratigraphic units.

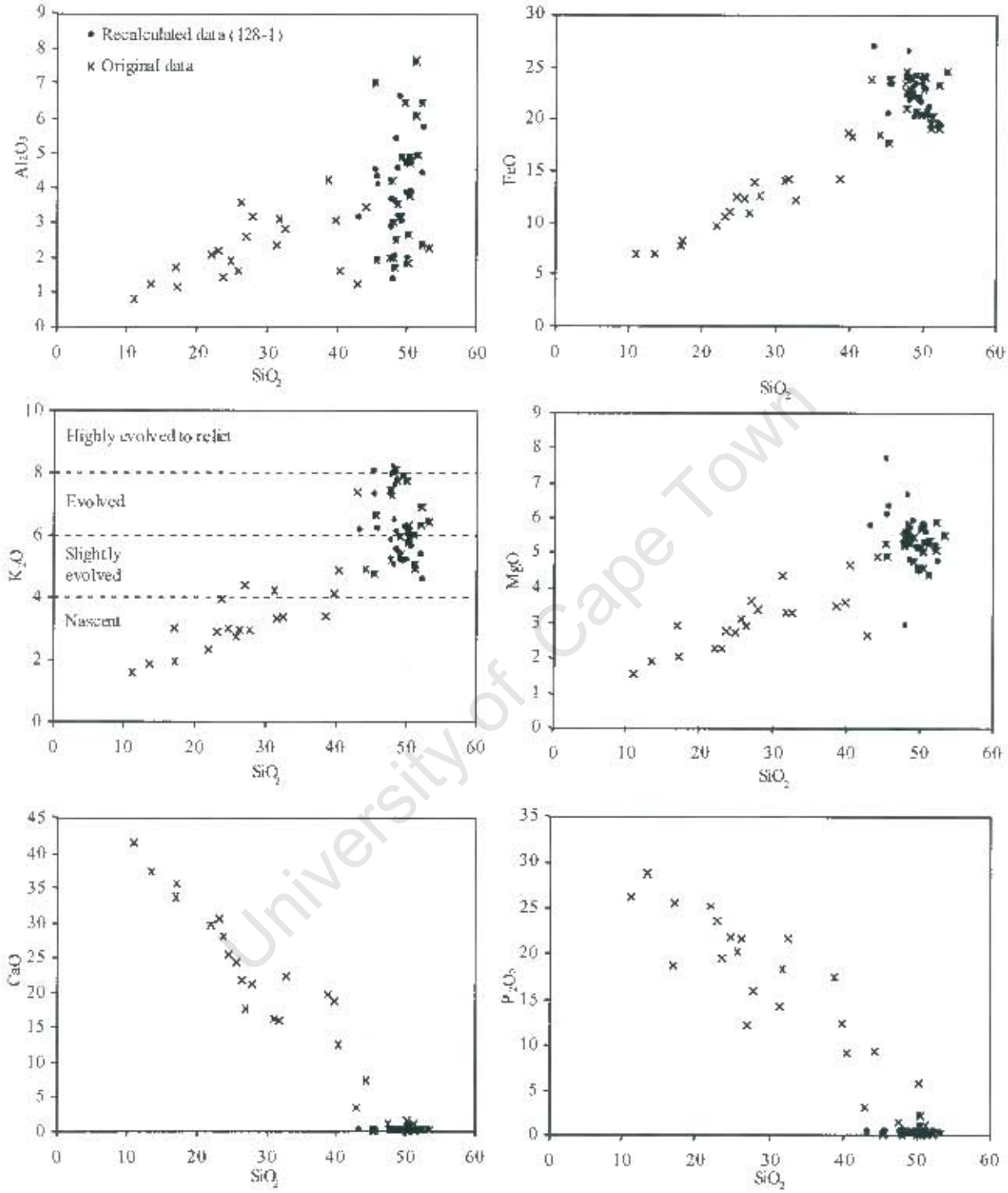
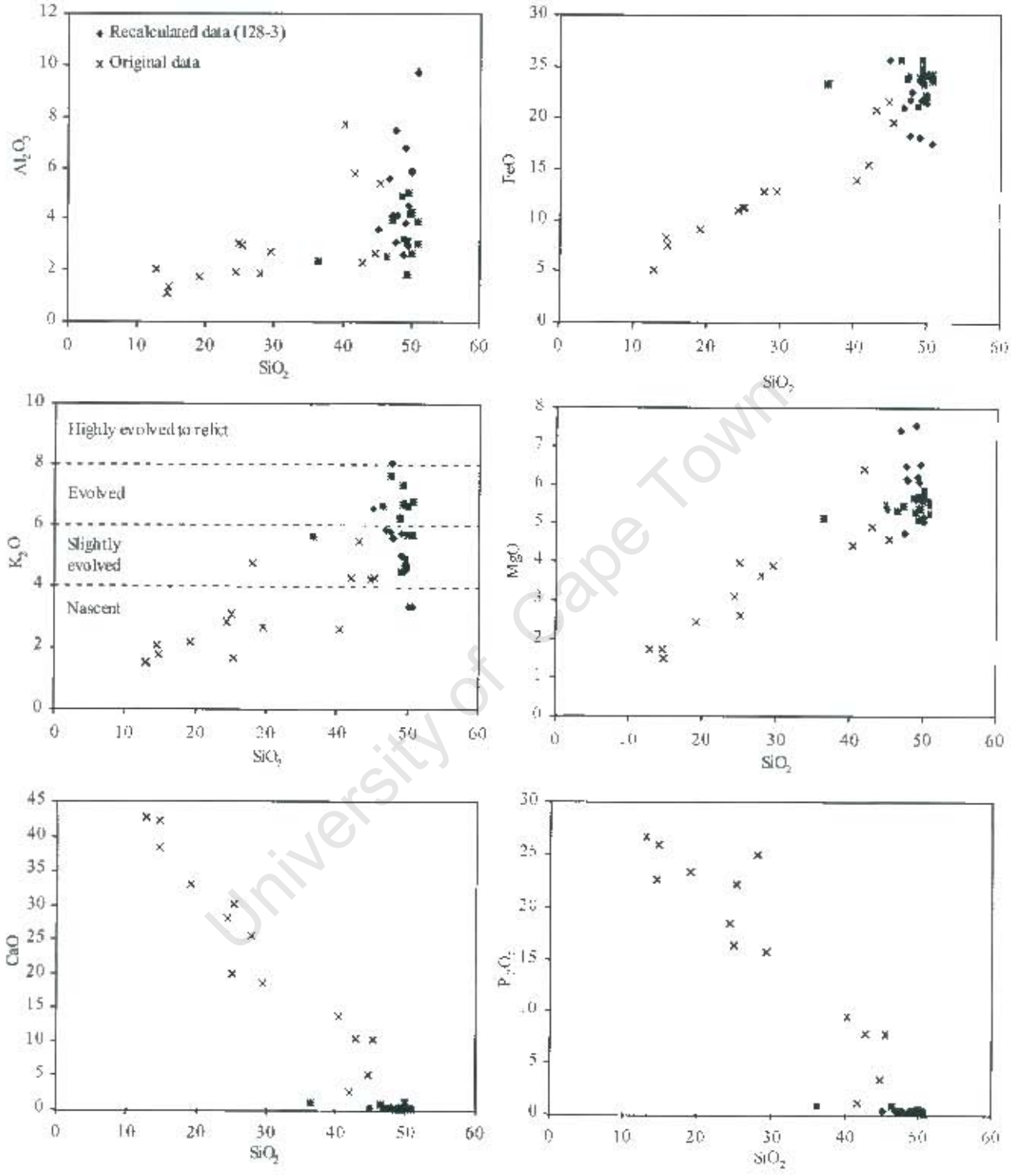


Figure 9.9. Holocene glauconite (Sample 128-1) compositions determined by microprobe analysis.

University of Cape Town



University of Cape Town

Figure 9.10. Pleistocene glauconite (Sample 128-3) compositions determined by microprobe analysis.

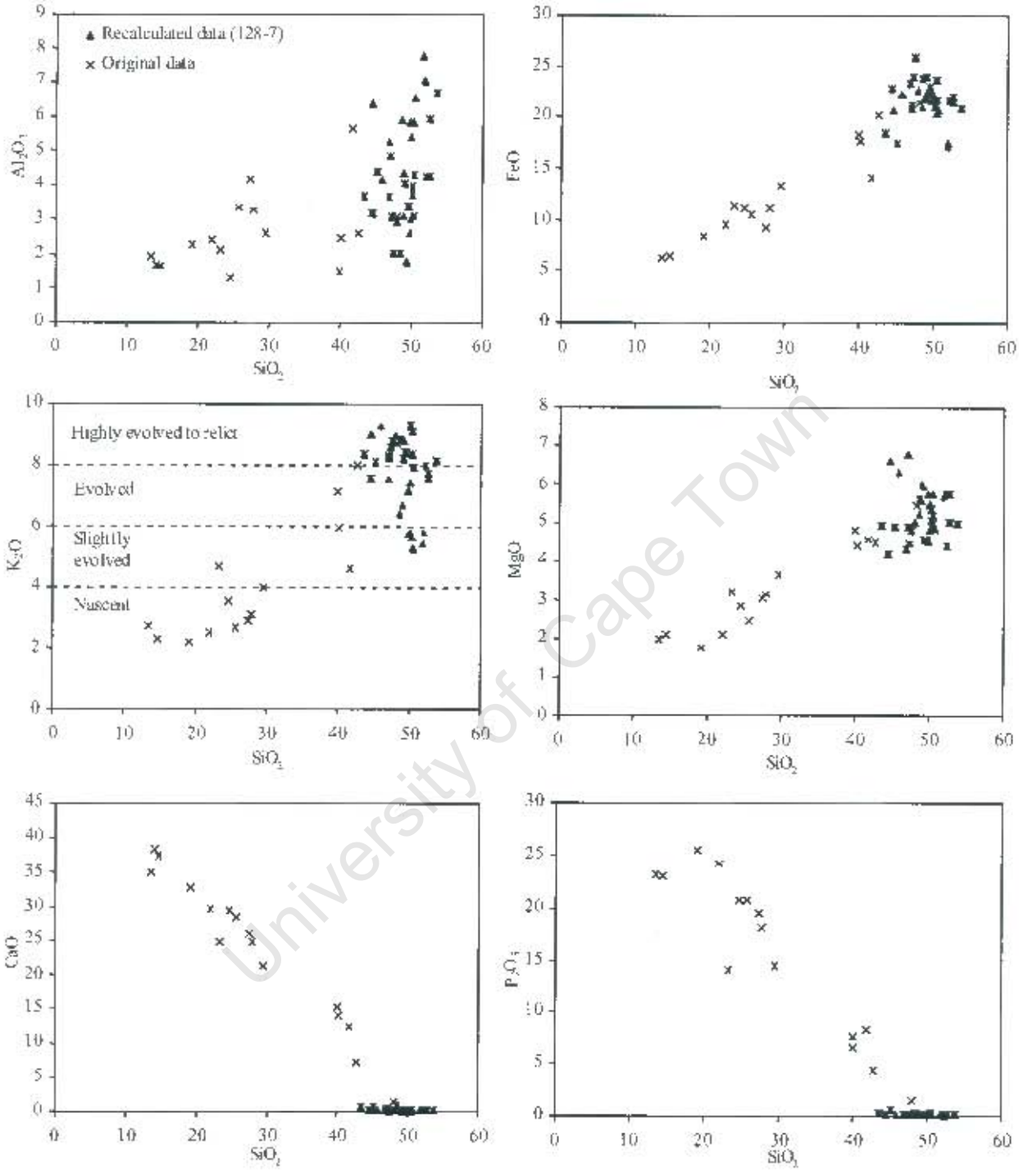


Figure 9.11. Pliocene glauconite (Sample 128-7) compositions determined by microprobe analysis.

University of Cape Town

Birch (1971, 1975) suggested that the Agulhas-Columbine glauconite belt is composed of reworked older glauconite pellets. Therefore, four Eocene glauconite-rich samples from southern Namibian margin provided by I. McMillan, were analysed to compare to the younger late Cenozoic glauconite samples from Concession 20D (Table 9.1), although these glauconite-rich sediments were collected at some distance from the study area. However, no information is available on the depositional environment of the south-western continental shelf in the vicinity of the study area during this time and therefore the comparison between the samples, which may have been deposited under different environmental conditions, is only speculative. The three Eocene olive green glauconite sandy-clay samples and the Cretaceous laminated shelly glauconitic sandstone and grey clay were all collected from approximately 2-3 m below the surface in a water depth of between 120-140 m offshore of Chamais Bay, southern Namibia (Figure 2.2). The ±500 m thick later middle Eocene (Bartonian) sediments overlie the nearshore Cretaceous package and are overstepped by Miocene marine sediments. The surface exposure of the Eocene package is discontinuous, and crops out only where surficial Miocene sediments are eroded. I. McMillan (*pers. comm.*, 2003) noted that Eocene and occasional fine glauconite clays of the Cretaceous typically have large light green glauconite pellets, whereas glauconite from the Pliocene and younger units tends to be blacker and has more distinct grain morphologies.

Table 9.1. The age and location of Eocene and Cretaceous glauconitic sediments analysed in this study from the southern Namibian margin.

Age	Sample No.	Latitude	Longitude
Later middle Eocene (Bartonian)	DN1407	27°52'50" S	15°19'18" E
	DN1418	28°02'12" S	15°15'51" E
	No. 3949	28°11'03" S	15°19'49" E
Late Cretaceous (±90 Ma Coniacian)	DN 4396	28°02'55" S	15°32'52" E

The Eocene and Cretaceous glauconite have variable textures similar to those described for Pliocene to Recent glauconite pellets (Figure 9.12). SEM micrographs show that the Eocene glauconite pellets display a similar lamellar internal texture, although the rosette texture of the glauconite indicates a decrease in maturity towards the grain boundary, which is a common feature of glauconite pellets in general (Odin and Fullagar, 1988). EDS analyses of the Eocene glauconite pellets indicate that a significant CFA component is present (Figure 9.13). However, in contrast to glauconite grains of Concession 20D, the Eocene glauconite includes a relative abundance of well-formed pyrite crystals, which are clearly visible in the back-scatter images of Figure 9.13.

University of Cape Town

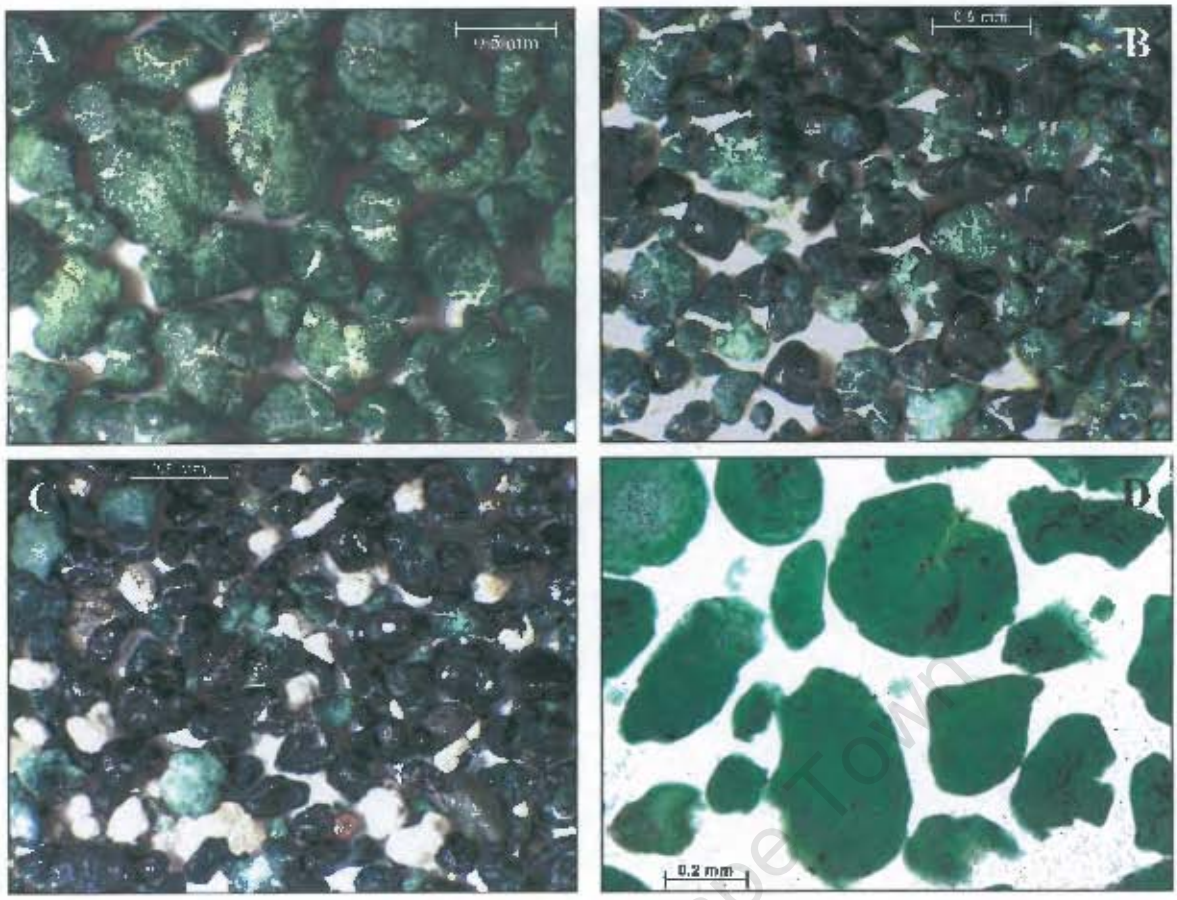


Figure 9.12. Photomicrographs of southern Namibian Eocene glauconite grains from samples DN 1418 (A), DN 1407 (B) and No. 3949 (C) and thin-section of glauconite pellets from DN 1418.

University of Cape Town

9.3 RARE-EARTH ELEMENT GEOCHEMISTRY

The rare-earth element (REE) geochemistry of a range of glauconite and phospho-glauconite grains were examined in order to establish whether the REE patterns could be used to distinguish between glauconite types from the different lithostratigraphic units. The REE data were obtained by laser ablation ICP-MS of mounted grains, where multiple analyses were obtained from some grains. The glauconite pellets of Concession 20D, and the southern African margin in general (Birch, 1975, 1979a, b, 1980), almost always include a CFA-component. Similarly, almost all of the laser-ablation ICP-MS analyses indicate the presence of a CFA component with variable, but significant Ca. The representative results of the ICP-MS analysis of the Pliocene glauconite grains are shown in Figure 9.14. Increased Ca abundances are correlated with high Sr, Y, REE, Th and U concentrations, indicating that most of the REE are associated with the CFA-component of the CFA-glauconite mixed-mineral grains. The rare analyses with low Ca and Sr show very low REE abundances, often near or below detection limits. Although a low degree of confidence is attached to the absolute values for the REE concentrations of the "end-member" glauconite composition, these data are included in subsequent plots because they emphasise the scatter in the glauconite composition. All of the REE data (Appendix 3) are normalized to Post-Archaean Average Australian Shale (PAAS) of Taylor and McLennan (1985) (Table 9.2) and the normalised plots are presented in Figure 9.15. The very

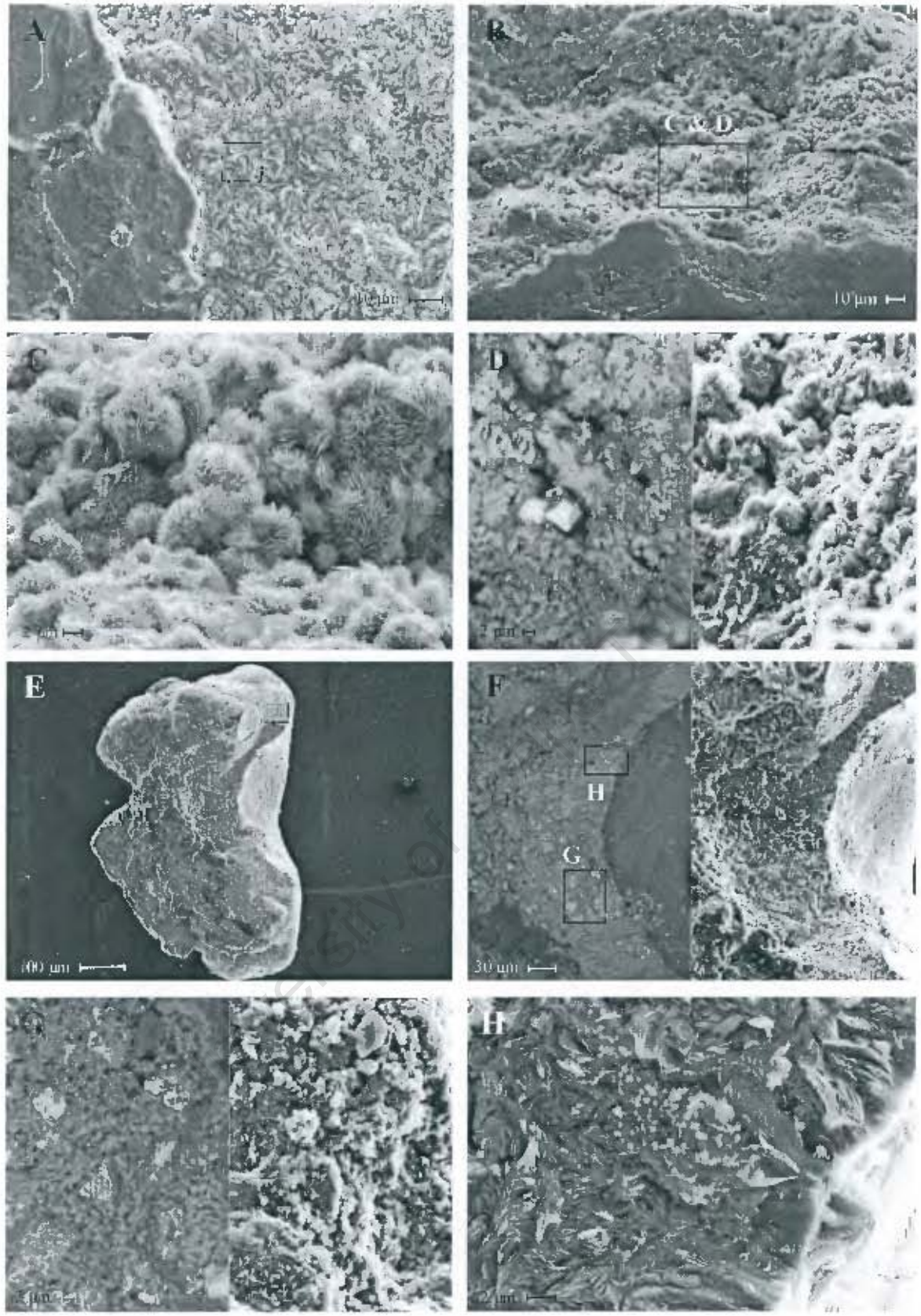


Figure 9.13. SEM images of southern Namibian Eocene glauconite pellets.
A: No. 3949. EDS analysis shows a typical glauconite lamellar texture and composition with 8.8 wt% K, but includes 2.4 wt% P and 3.7 wt% Ca.
B-D: DN 1418. EDS analysis of the broken surface away from steep edge of the broken surface indicates a glauconite composition with 7.8% K. Two close-up images from within the black box in B show typical glauconite rosette structures in C (Odin and Matter, 1981) and cubic pyrite (more clearly visible in the back scatter image on the left) in D.
E-H: DN 1407. E: EDS analysis of the broken surface in the black box shows a typical glauconite composition with 11.8 wt% K, but includes 1.7 wt% P and 5.5 wt% Ca. Close-up images in F-H show the relative abundance of pyrite (G) and Fe (H) in these glauconite grains.

depleted compositions of the glauconite "end-member" mineral is best represented in the Pliocene and Eocene/Cretaceous normalised plots, where the apparent anomalies in this depleted data set are interpreted to reflect the errors associated with the proximity of the REE abundances to the detection limit of the ICP-MS.

Table 9.2. The PAAS REE abundance (in ppm) used in all normalization calculations (Taylor and McLennan, 1985).

La	Ce	Pr	Nd	Sm	Eu	Gd	Tb	Dy	Ho	Er	Tm	Yb	Lu
38.2	79.6	8.8	33.9	5.6	1.1	4.7	0.8	4.7	1	2.9	0.4	2.8	0.4

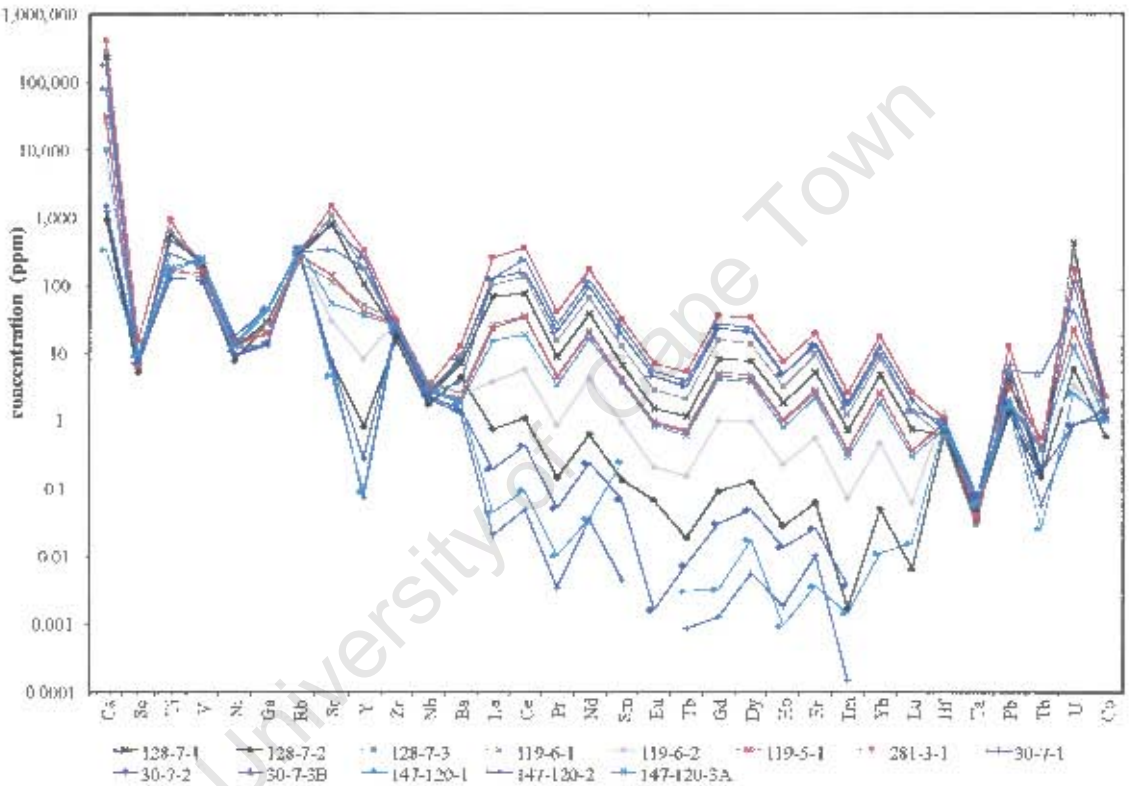


Figure 9.14. The absolute trace and REE compositions for CFA-glauconite mixed-mineral pellets from the Pliocene glauconite-rich sediment units.

The REE patterns show a range in normalised ratios from <0.001 to >10, where the range within samples is similar to that between samples. In addition, individual grains show considerable heterogeneity (*e.g.* grain 128-1-5 from the Holocene). The relatively low abundance and normalized patterns of REE in the CFA-glauconite mixed-mineral grains is very similar to that described by Watkins *et al.* (1995) and Middleton (2003) for phosphorites of the western margin of southern Africa. The range in PAAS-normalized data from the various lithostratigraphic groups of Figure 9.15 clearly shows three different REE patterns (Figure 9.16). The Pliocene to Holocene glauconite pellets (including glauconite grains and not infilled-foraminifera from the basal Phosphorite Gravel facies) show a flat REE pattern with a slight HREE enrichment and a strong negative Ce-anomaly. This is a typical seawater pattern (German *et al.*, 1995; Shields and Stille, 2001.), indicating formation of the

University of Cape Town

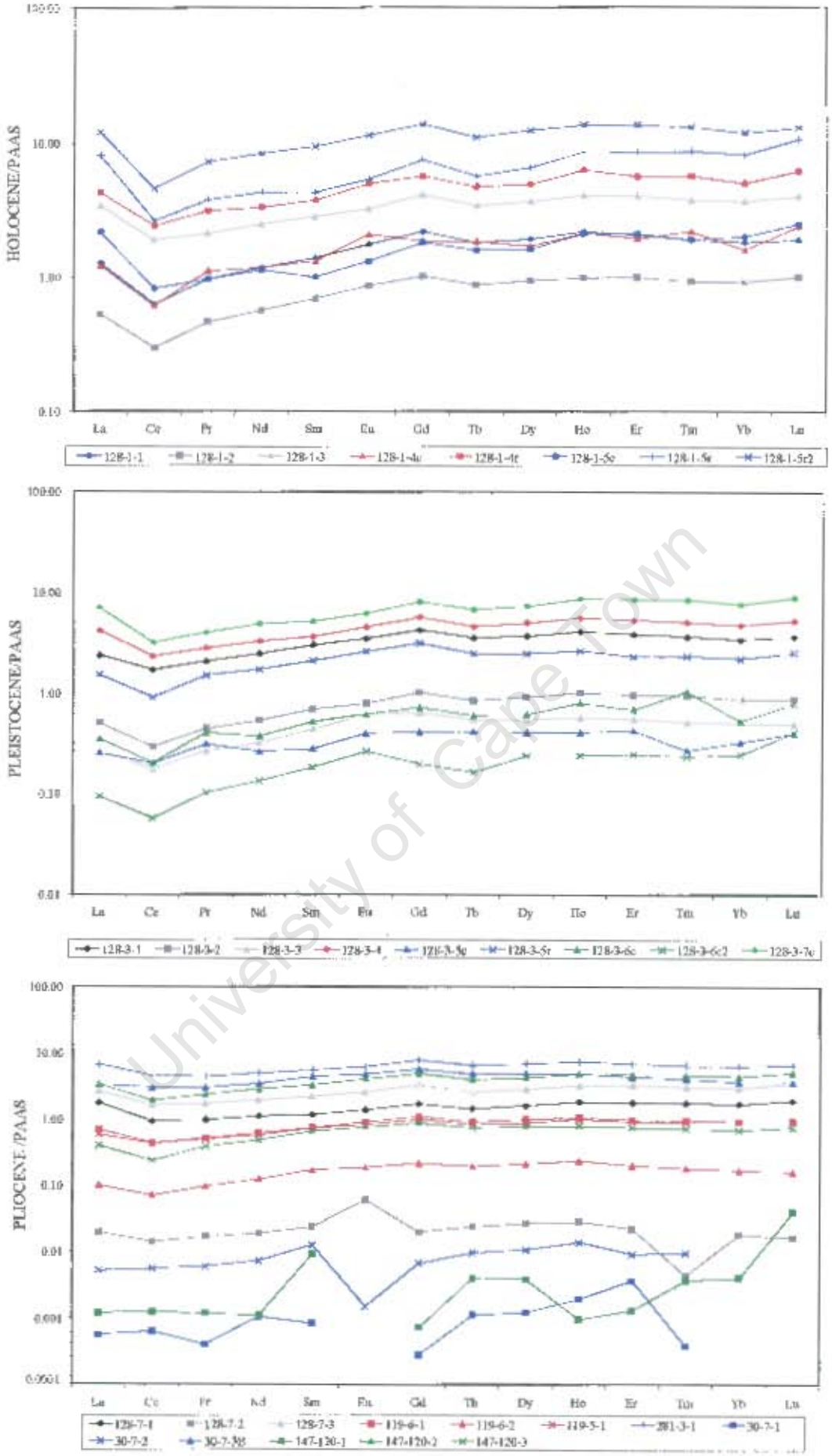


Figure 9.15. PAAS-normalized REE diagrams for CFA-glauconite mixed-mineral pellets from the Holocene (Sample 128-1), Pleistocene (128-3) and Pliocene (sample numbers in legend) glauconite-rich facies. (Abbreviations in legend: c=core, and r=rim)

University of Cape Town

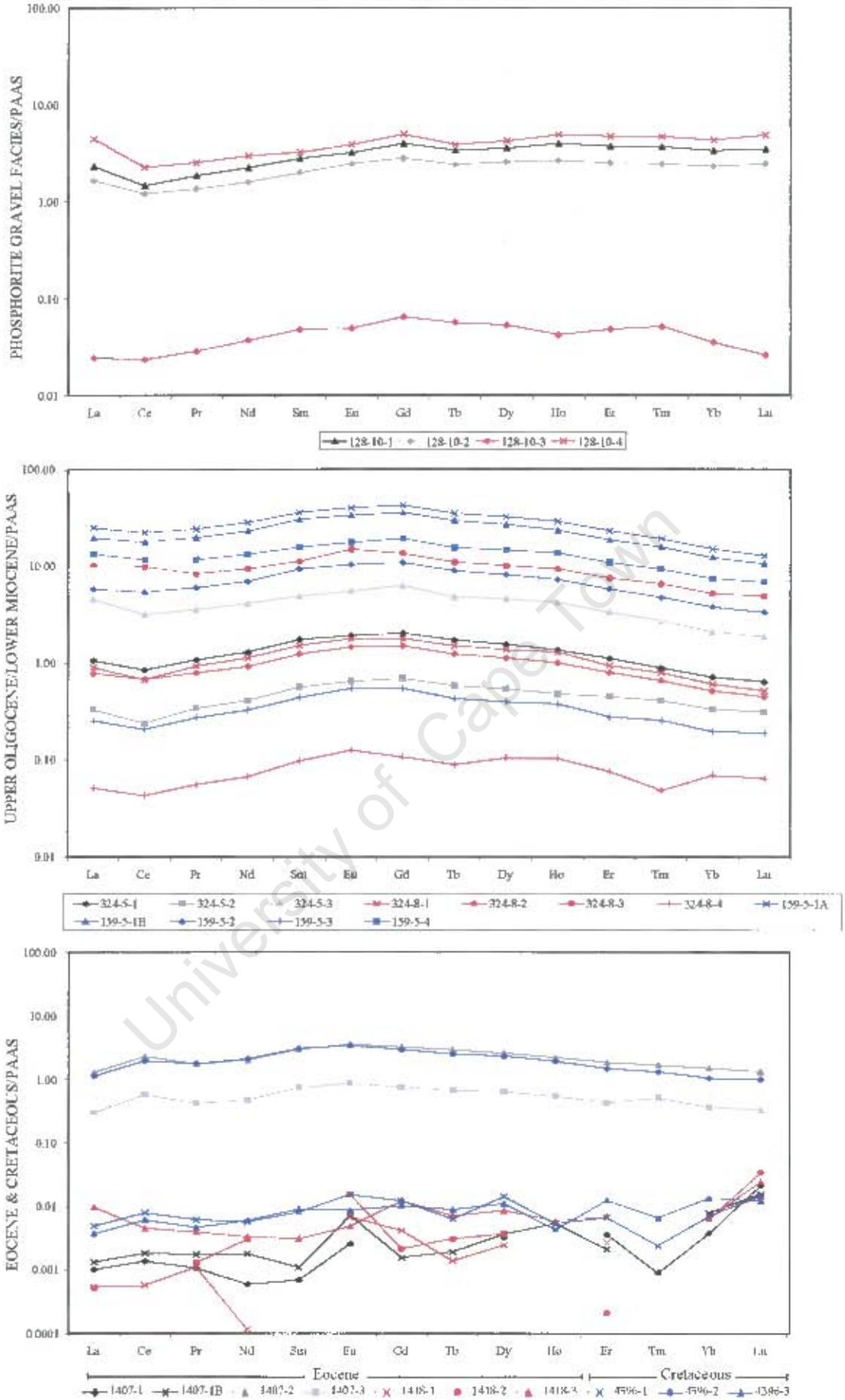


Figure 9.15 continued. PAAS-normalized REE diagrams for CFA-glauconite mixed-mineral pellets from the Pliocene basal lag (Sample 128-10) and upper Oligocene/lower Miocene (sample numbers in legend) glauconite-rich facies and from Eocene and Cretaceous samples.

University of Cape Town

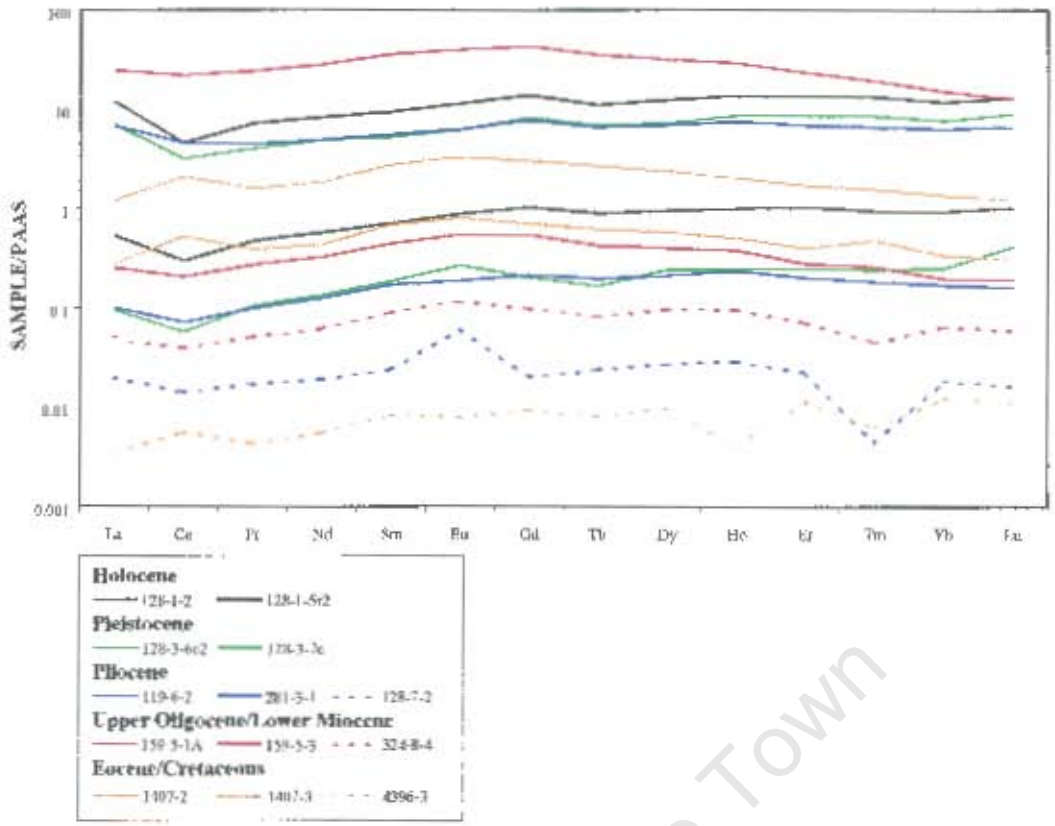


Figure 9.16. A summary of the range in PAAS-normalised REE abundances from Figure 9.14 for CFA-glauconite mixed-mineral pellets from the major lithostratigraphic units of Concession 20D.

University of Cape Town

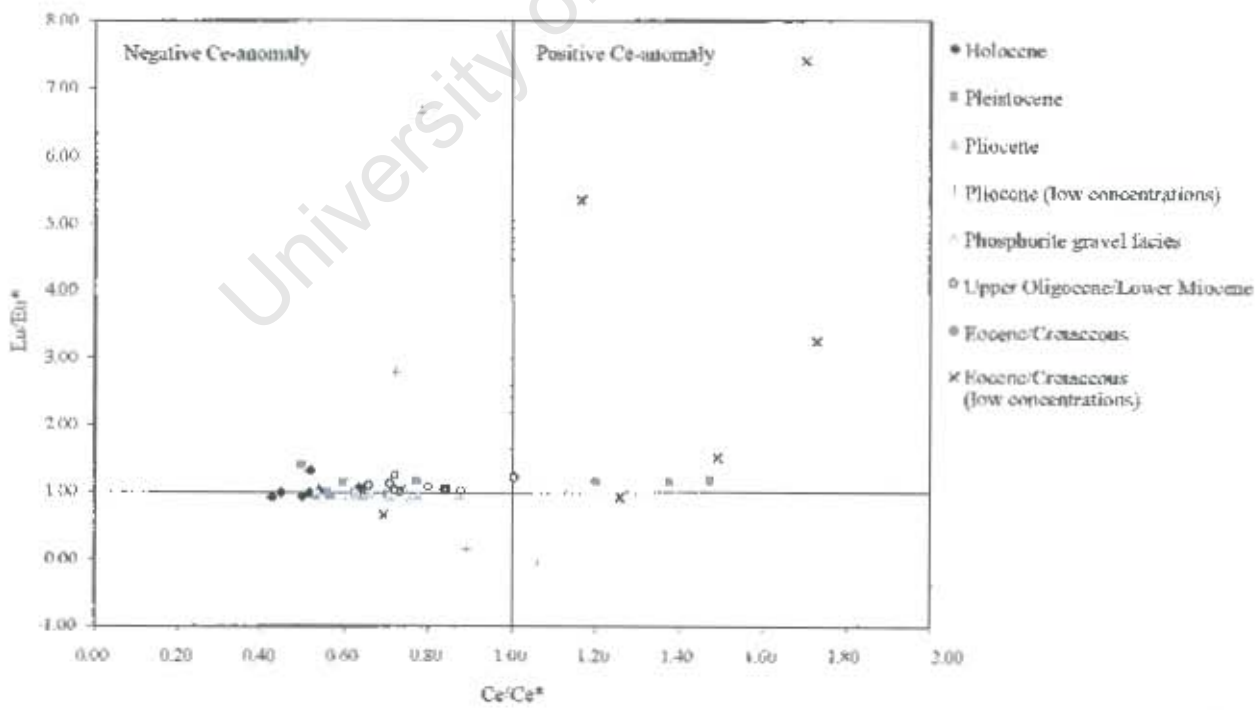


Figure 9.17. The relationship between the Ce- and Eu-anomalies for various CFA-glauconite mixed-mineral pellets. Note that all of the scatter in the data is from samples with the low REE abundances near or below the detection limits of the ICP-MS.

authigenic minerals in an open-ocean environment. The glauconite from the Upper Oligocene/Lower Miocene Calcareous Unit shows a normalized REE pattern slightly depleted in HREE, with a "MREE bulge" and a reduced negative Ce-anomaly. The upper Oligocene/lower Miocene glauconite shows the lowest normalised Lu/La ratio (average of 0.64) resulting from the relative HREE depletion. The Eocene to Cretaceous glauconites show a similar REE pattern of HREE depletion and a distinct "MREE bulge", but these glauconite samples have a positive Ce-anomaly. Haley and Klinkhammer (2003) suggested that a "MREE bulge" reflects the input of REE from dissolving Fe-hydroxides in more reducing conditions. Goethite-cementing and Fe-hydroxides form a significant component of the layered upper Oligocene/lower Miocene phosphorite "hardground" gravels from Concession 20D, implying that scavenging and dissolution of Fe-hydroxides is a likely process to result in this "MREE bulge". Shields and Stille (2001) similarly argued that diagenetic scavenging of the LREE results in a preferential enrichment of MREE and weakening of the Ce-anomaly.

Ce-anomalies are commonly used as an indicator of palaeoredox conditions and the Ce-and Eu anomalies were determined by the calculations $Ce/Ce^*=(2*Ce/Ce_{PAAS})/(La/La_{PAAS} + Nd/Nd_{PAAS})$ and $Eu/Eu^*=(2*Eu/Eu_{PAAS})/(Sm/Sm_{PAAS} + Gd/Gd_{PAAS})$ used by Middleton (2003), where Shields and Stille (2001) noted that either of the LREE Pr or Nd can be used in this calculation. Ce/Ce* is plotted against Eu/Eu* in Figure 9.17, where the samples consistently show little to no Eu/Eu* anomalies. However, the Ce/Ce* ratio varies from positive in the Cretaceous, through slightly negative (sub-oxic) in the upper Oligocene/lower Miocene to strongly negative in the Pliocene to Holocene. Haley and Klinkhammer (2003) suggested that the magnitude of the Ce-anomaly may not reflect simply the oxygen conditions, but may reflect changes in the LREE abundance related to Fe-hydroxide scavenging (Sarkar *et al.*, 2003) or organic LREE-complexes. The increased magnitude of the Pliocene to Holocene Ce-anomaly relative to that of the upper Oligocene/lower Miocene samples may therefore reflect either increased oxidation of Ce in progressively more oxic surface waters (Kidder *et al.*, 2003) or may result from increased organic LREE-complexing or a combination of both processes. The positive Ce-anomaly of the Eocene/Cretaceous CFA-glauconite mixed-minerals suggests anoxic diagenesis in shallow oceans (Sarkar *et al.*, 2003), where Dale and McMillan (1999b) similarly argued that middle Eocene (42-40 Ma) green clays were deposited in poorly oxygenated waters.

The morphological and geochemical data presented above indicate that the glauconite recovered from Concession 20D represents an intimate intergrowth of glauconite and CFA. Previously, Birch (1979a, b, 1980) argued that the mixed-mineral nature of the authigenic pellets must indicate contemporaneous transformation of micritic mud to CFA and illitic clay particles to glauconite. He suggested that a change in depositional conditions following the authigenic growth of glauconite and CFA must have resulted in the disaggregation of the semi-lithified surface "hardground" and the formation of the mixed-mineral pellets. Although many of the earlier arguments favoured a transformation of a precursor clay mineral (Burst, 1958a, b), recent research favours a 2-fold evolutionary process for glauconitization. The glauconitization process involves an initial formation of a ferric (glauconitic)

University of Cape Town

smectite (Odin, 1988) or "gel" phase (Amouric and Parron, 1985) by dissolution-crystallization processes in equilibrium with a detrital precursor in a semi-confined environment. The second step involves destabilization of the precursor and crystallization of glauconite *sensu stricto* (Odin and Matter, 1981; Odin and Lamboy, 1988; Clauer *et al.*, 1992; Stille and Clauer, 1994). Individual glauconite pellets appear to be a mixture of authigenic layered minerals evolving towards glauconitic mica (Amouric and Parron, 1985). Rao *et al.* (1993) described a similar intimate association of glauconite and phosphate in foraminiferal infillings from the southwest Indian continental margin. They argued that the coexistence of these minerals reflects a combination of low-oxygen conditions, low terrigenous input and a seasonal upwelling resulting in the accumulation of organic-rich sediments as a source for P, and supplying the required low-oxygen conditions required for glauconitization. They propose that glauconitization occurs within semi-confined local microenvironments and that glauconite growth slows down as the environment becomes more confined, at which point microbially mediated CFA/phosphate growth is favoured. The compositions and textures observed within the glauconite pellets of Concession 20D imply that multiple glauconitization events must have occurred, suggesting an episodic depositional history, tending towards conditions favouring glauconite and CFA formation. Low terrigenous input and possibly low carbonate productivity dominated the late Miocene to Pliocene (Chapter 7) and no lithic fragments are identified within the glauconite pellets. Birch (1979b, 1980) also proposed that the intimate association of CFA and glauconite indicated repeated slight changes in reducing to oxidising conditions of the micro- environment favoured either glauconite or phosphorite formation, where sea level fluctuations and variations in upwelling-related productivity may have played a role in the formation of the authigenic minerals.

The REE patterns suggest changes in the depositional environment through time since the Cretaceous, with little to no change recorded in the Pliocene to Holocene glauconites. The upper Oligocene/lower Miocene sediments of Concession 20D are carbonate-rich warm-water deposits, associated with abundant phospho-glauconitic infilled foraminifera. In contrast, green to black CFA-glauconite mixed-mineral pellets dominate the Pliocene to Holocene sediments, which are interpreted to reflect the influence of cold-water upwelling along the western margin since the middle Miocene. The change in the REE patterns from the Upper Oligocene/Lower Miocene to the Pliocene-Holocene may reflect changes in the depositional environment linked to changes in water temperature and carbonate abundances, where the Ce-anomaly indicates possible changes in the bottom water oxygen content. The observed differences in the microscopic appearance and REE patterns for the later Neogene and the upper Oligocene/lower Miocene glauconite pellets indicate that the upper Miocene to Pliocene glauconite-rich deposits of the western margin are not reworked older upper Oligocene/lower Miocene glauconite pellets, favouring post mid Miocene glauconitization events. The positive Ce-anomaly of the Eocene and Cretaceous glauconite may only reflect local environmental conditions off southern Namibia, where the geochemistry of Eocene or older glauconites from the south-western margin need to be studied before the possibility of a pre-Late Oligocene age for the glauconite from Concession 20D can be excluded.

University of Cape Town

10 SYNOPSIS

10.1 STRATIGRAPHY

The complex and very condensed late Cenozoic sediment succession recovered from Concession 20D is separated from the underlying middle Cretaceous strata by a post-Cretaceous unconformity. The unlithified interbedded quartzose sands and kaolinitic clays of the Cretaceous Woody Quartzose Sand underlie the Cenozoic Succession of Concession 20D. This Cretaceous unit includes scattered sand-size to small cobble-size carbonised wood fragments, which are often pyritised. The kaolinitic mud-rich intervals include minor to trace amounts of mica, amber and pyritised organic material, including megaspores. The quartz sand grains are deeply etched and Fe-oxide precipitates on the quartz grain surfaces are observed in sandy intervals. The Woody Quartzose Sand is interpreted to have been deposited during the middle Albian to early Cenomanian (mid-Cretaceous) based on the ages obtained from wood and palynological analyses and a lithostratigraphic comparison with the reported Cretaceous sediments of the western margin, especially DSDP Site 361, southwest of the Cape Canyon (Figure 2.1). The Cretaceous/Tertiary contact (22At1 or Davie unconformity) is only intersected within the Main Channel of the Cape Canyon Head region, where the contact is defined by a phosphorite-rich gravel lag at the base of either the Quaternary Succession within the Main Channel (Appendix A1-30) or at the base of the middle Miocene Gravelly Calcareous Quartzose Muddy Sand Unit of Core 319 located on the eastern (landward) flank of the Cape Canyon

The oldest Cenozoic sediments recovered from Concession 20D are the carbonate-rich sediments of the Upper Oligocene/Lower Miocene Calcareous Unit. The unit is recovered predominantly on the Outer Shelf, although the location of Core 159 on the eastern (landward) flank of the Main Channel, and the widespread presence of phosphorite gravels, indicates an earlier, more widespread, distribution of this unit. Four lithostratigraphic facies are defined within the Upper Oligocene/Lower Miocene Calcareous Unit (Figure 6.1). The upper Oligocene (25.8-27.2 Ma) Quartzose Foraminiferal Muddy Sand, recovered from a single core, is a poorly sorted muddy sand composed of pink to reddish yellow-stained carbonate fragments, dominated by the larger benthic foraminifera *Operculina* sp. and very fine angular quartz sand. Minor amounts of phospho-glauconite and foraminifera (benthic and planktic) with traces of bryozoa, echinoid spines and well-rounded medium to very coarse quartz sand are present. A red surface-coating of the calcareous grain and coarser quartz sand is common. The gravel fraction is dominated by *Operculina* sp. and light-brown to amber phosphatised mollusc casts, composed predominantly of CFA-cemented very fine quartz sand. The Quartzose Foraminiferal Muddy Sand is unconformably overlain by a gravel lag, dominated by winnowed phosphatised mollusc casts at the base of the latest Oligocene to early Miocene (23.3-25.6 Ma) Quartzose Glauconitic Calcareous Sand. The Quartzose Glauconitic Calcareous Sand is a very variable slightly gravelly sand to muddy sandy gravel, composed of variable amounts of shell fragments, foraminifera, quartz and phospho-glauconite foraminiferal infillings. The quartz grains are interpreted, on the basis of surface textures, to be reworked from the underlying Cretaceous sediment. The facies shows an upward decrease in quartz

University of Cape Town

sand and shell fragments associated with an increase in foraminifera. The Quartzose Glauconitic Calcareous Sand is overlain by the Burdigalian (18.3-20.7 Ma) Glauconitic Calcareous Sand. The poorly defined lower contact of the Burdigalian facies varies from gradational to a cemented interval with large bone fragments. The uniform Glauconitic Calcareous Sand is composed predominantly of fine sand-size foraminifera and phospho-glauconite foraminiferal infillings, with subordinate fine sand-size shell fragments and minor amounts of fine to very fine quartz sand. Both the Quartzose Glauconitic Calcareous Sand and the overlying Glauconitic Calcareous Sand facies include a significant gravel component, dominated by phosphatised mollusc casts, shell fragments and micrite- and phosphorite-cemented *in situ* aggregates. The Glauconitic Calcareous Sand facies shows a more varied shell assemblage that includes brachiopods, bryozoa, *Pecten* and a range of oyster species. The Glauconitic Calcareous Sand is interpreted to be overlain by the deep-marine Burdigalian (18.3-20.8 Ma) Foraminiferal Ooze, although the relationship between these two facies is unclear. No foraminifera younger than 18.3 Ma were recovered from the Upper Oligocene/Lower Miocene Calcareous Unit.

Middle Miocene sediments were only recovered from Core 319, located on the eastern flank of the Main Channel. The 17.0-17.7 Ma basal lag of the Gravelly Calcareous Quartzose Muddy Sand Unit lies unconformably above Cretaceous sediments. This basal lag, dominated by phosphorite to Fe-rich carbonate clasts, is overlain by the *in situ* 12.0-15.9 Ma muddy sand interval of the Gravelly Calcareous Quartzose Muddy Sand Unit. The medium to coarse calcareous quartzose sand includes ~20% green glauconite pellets.

Elsewhere the Upper Oligocene/Lower Miocene Calcareous Sand Unit is unconformably overlain by a complex condensed sediment succession, which records a final Pliocene depositional age. These Pliocene sediments differ significantly in glauconite and quartz abundance. The depositional history of many of the glauconite-rich sediments is further complicated by subsequent Quaternary bioturbation and reworking events. The Pliocene sediments are found across most of Concession 20D and show no apparent relationship between distribution and modern bathymetry, except for a fining offshore. The unconformable contact with the underlying Upper Oligocene/Lower Miocene Calcareous Unit is only recovered on the outer shelf, where it is defined by the Phosphorite Gravel facies of the Glauconitic Sand Unit. The basal lag is overlain, with a gradational contact, by the Glauconitic Sand facies, which is composed predominantly (average of 95 wt%) of green glauconite pellets. Minor amounts of very fine quartz sand and biogenic grains are present, where the biogenic grains indicate a Pleistocene reworking of the Glauconitic Sand facies. The laterally equivalent Glauconitic Muddy Sand Sub-unit is recovered from the upper slope and from the Cape Canyon Head region. Although similar to the Glauconitic Sand, this sub-unit includes a significant mud-fraction. Reduced pockets, up to 5 cm across, are dominated by Fe-rich cementation. Late Miocene (5.8-10.9 Ma) Sr-ages are obtained from the more robust foraminifera of the Glauconitic Muddy Sand Sub-unit, although the foraminiferal assemblage indicates a uppermost lower to lowermost upper Pliocene depositional age. The Glauconitic Muddy Sand shows a marked increase in very fine quartz sand upcore and is overlain by the Pliocene Quartzose Muddy Sand, which prevented later reworking of these glauconite-rich sediments. The sand-fraction of the uniform

University of Cape Town

Quartzose Muddy Sand is composed of 99% very fine quartz sand and trace amounts of two distinct foraminiferal assemblages, which indicate a latest early to earliest late Pliocene reworking of a middle Miocene (9.1-15.8 Ma) quartzose sediment.

Pleistocene sediments unconformably overlie the Pliocene units and show a well-defined correlation between distribution and composition. The outer shelf and upper slope Calcareous Glauconitic Sand facies is composed largely of black (to very dark green) glauconite with subordinate late Pleistocene foraminifera, shell fragments and very fine quartz sand. Shell-rich intervals are common, with a laterally continuous 5-50 cm thick shell-rich lag, recovered towards the top of this unit. The microfaunal assemblage includes diverse planktic and benthic foraminifera, ostracods and holothurian sclerites, and transitional planktic foraminiferal species predominate. The Calcareous Quartzose Very Fine Sand, recovered from the Western Ridge, is composed of well-sorted, very fine quartz sand with variable amounts of subordinate biogenic grains and glauconite, with shell lag layers common. The biogenic assemblage is very similar to that recovered on the outer shelf. The Glauconitic Quartzose Sand Unit is recovered only within the Cape Canyon Head region, as defined by a Cretaceous sediment high in the seismic records. Three distinct fine to medium grained facies of the Glauconitic Quartzose Sand Unit are recognised within the Northern Depression, with a basal quartzose green glauconitic sand overlain by a transitional facies, which includes up to 10% calcareous grains. The third facies varies from being quartz-rich in the east (landwards), to glauconite-rich in the west (seawards), and includes >10% biogenic grains, with a similar varied faunal assemblage as described for the Western Ridge and the outer shelf. In contrast, the Pleistocene unit from the Main Channel, to the south, is dominated by medium to coarse, often green-stained quartz (although increasingly glauconite-rich to the west) and biogenic grains are absent or present in trace to minor amounts. The quartzose sands show considerable grain-size variation, with coarse-grained intervals and (stacked) fining-upward sequences. Traces of jasper, agate and feldspar are recognised. These quartzose sands are typically recovered above a phosphorite gravel lag overlying the Cretaceous Quartzose Woody Sand unit. The gravel lag includes minor quartz pebbles and other lithic fragments. A ~30 cm veneer of Holocene Faecal-rich Muddy Sand drapes most of the study area, where active erosion or non-deposition occurs on the outermost shelf and within the Main Channel of the Cape Canyon. The composition of the Holocene sediment is similar to the underlying Pleistocene unit, but includes only minor robust cold-water planktic foraminifera with sponge spicules and faecal pellets (or faecal mud) always present.

University of Cape Town

10.2 GEOLOGICAL EVOLUTION OF THE WESTERN MARGIN (FIGURE 10.1)

Mid Cretaceous (Albian to Cenomanian) deposition on the coastal plain of the western margin in water-logged, brackish swamps or marshy mud flats, crosscut by channel-infill quartz sand, sand-banks and sand-sheets is preserved as the Woody Quartzose Sand Unit. Similar Cretaceous environments have been described for the west coast in general (Dale and McMillan, 1998b). The palynology indicates that humid temperate conditions prevailed, which is supported by an abundance of kaolinite, the severe etching of the quartz grains and the diagenetic precipitation of Fe-oxides on the quartz grain surfaces.

Figure 10.1. Caption on following page

University of Cape Town

The late Cenozoic evolution of the western margin of southern Africa is characterized, in general, by very low sedimentation rates and repeated reworking of sediments on the continental shelf. The observed changes in depositional environment, recorded in the sediments of Concession 20D throughout the late Cenozoic, are attributed to changes in relative sea level. This study has shown that the fluctuations in this relative sea level are largely coincident with the proposed third-order glacio-eustatic sea-level fluctuations of the modified Haq *et al.* (1987, 1988) sea-level model. However, the importance of additional factors such as margin subsidence, uplift of the western interior, changing oceanographic and climatic conditions and periods of increased terrigenous input are also recognized (Figure 10.1). This study has revealed the power of an integrated stratigraphic interpretation, as a means to sort out the depositional environments and margin evolution recorded in the complex, condensed, reworked and bioturbated sedimentary package recovered from the Head of the Cape Canyon. Although very little detailed information is available for the stratigraphic succession of the western margin as a whole, the age and depositional model developed for Concession 20D is consistent with the existing published data. This indicates that the interpreted geological evolution of Concession 20D may be extrapolated to the regional evolution of the passive western margin of South Africa

University of Cape Town

sediment infill observed in this profile. Furthermore, the Sr- and biostratigraphic ages obtained from foraminifera in all the samples studied and the Sr-ages from all analysed phosphorites from a number of different lag deposits within the study area (Compton *et al.*, 2004) are all younger than late Oligocene, even where the lag layers lie directly above Cretaceous sediments. These gravel lag layers are composed predominantly of phosphorite and include no lithic fragments, beyond those recovered from the overlying upper Cenozoic succession. The absence of any lower Cenozoic or exotic material within any of the sediment recovered from the Canyon Head region implies an absence of older sediments within the observed canyon infill succession and implies a shelf-wide erosion of these sediments prior to deposition of the post-upper Oligocene succession in the study area.

The fine to medium quartz sand of the Northern Depression is interpreted to have a fluvial origin, where a rejuvenation of fluvial activity in the late Pliocene is widely accepted along the western margin (De Wit, 1993, 1999; Peizhen *et al.*, 2001; Van der Wateren and Dunai, 2001). This input of siliciclastic material onto the outer shelf reflects a combination of increased uplift rates of the coastal platform and fluvial activity in the late Pliocene in association with fluctuating eustatic sea levels. The available bathymetric and sedimentary data suggest that the palaeo-Berg River is the most likely source of the fine to medium quartz sand of the Pleistocene sediments of the Cape Canyon Head. The point source of these palaeo-Berg River sediments into Concession 20D results in the formation of the bathymetric high that separates the Northern Depression from the Southern Main Channel region. This wedge of fluvial sediments appears to have prevented extensive erosion and incision of the Canyon to the north. The coarse to very coarse quartz sand and other traces of residual reworked components of the quartzose Pleistocene sands within the Main Channel of the Cape Canyon record incision into the underlying unconsolidated quartzose Cretaceous strata. Active erosion and downcutting of the Cape Canyon, by mass wasting processes, has occurred throughout the late Pleistocene and Holocene, as the last 25 kyr of the sediment record has been eroded from the distal Cape Canyon fan (Botha, 2003). Mass-wasting processes and the rapid erosion and redeposition, with little reworking of the sediment, is recorded in the late Pleistocene slumping of the canyon walls, preserved in inverted stratigraphic sequences, and by the presence of Cretaceous mud-clasts and pyritised wood fragments in the gravel fraction of Pleistocene quartzose sands. The presence of very fine quartzose sand and glauconite in the Pleistocene sediments in the distal Cape Canyon suggests that the Cape Canyon has acted as a pathway for sediment transport off the continental shelf throughout the Quaternary (Okey, 1997; Granata *et al.*, 1999).

It is well established in the literature that the late Quaternary glacio-eustatic sea-level, which fluctuated between +10 and –125 m along the western margin of southern Africa, has effectively eroded much of the sediments of the western margin, so that only a ~50 cm veneer of Quaternary sediments is preserved above lower Miocene calcareous sediments (Rogers, 1977; Dingle *et al.*, 1983; Corbett, 1996; Compton *et al.*, 2002). The uplift of the buoyant Agulhas-Columbine Arch and the associated fault-controlled incision of the Head of the Cape Canyon resulted in the preservation of the *in situ* late Neogene sedimentary succession of Concession 20D.

University of Cape Town

responsible for the unusual preservation of the Pliocene Glauconitic Muddy Sand Sub-unit in Concession 20D.

The increased rate of uplift of the western coastal platform in the late Pliocene is argued here to be associated with the formation of the Head of the Cape Canyon. The incision of the upper reaches of the Cape Canyon are interpreted to be due to downthrow of the western margin along a reactivated steeply dipping fault at the seaward boundary of the buoyant pre-Cretaceous Columbine-Agulhas Arch, with a number of down-faulted blocks of unconsolidated Cretaceous strata recognised seaward of the buoyant basement (Figure 3.6). The unconsolidated character of the Cretaceous Woody Quartzose Sand and the preservation of the observed fault scarps in these strata imply the presence of a protective drape of Neogene sediments prior to faulting.

Additional support for a late Pliocene incision of the Head of the Cape Canoyon is provided by the sediment facies distribution. The recovered Upper Oligocene/Lower Miocene through to the uppermost lower to lowermost upper Pliocene sediments show no distinct lateral variations across the study area indicating no changes in the depositional environment besides an increase in water depth seawards. In contrast, the Pleistocene Succession shows lateral facies changes clearly related to the modern canyon bathymetric features. It is therefore proposed that the timing of the tectonic event leading to the formation of the Head of the Cape Canyon must post-date the deposition of the middle to upper Pliocene Quartzose Muddy Sand, but pre-date the deposition of bathymetric-controlled Pleistocene sediments. A more detailed bio-and chronostratigraphic study of the Pleistocene facies may tighten the age controls of this tectonic event. The proposed tectonic origin for the Head of the Cape Canyon in the late Pliocene to early Pleistocene, opposes earlier suggestions that the Cape Canyon, in general, was cut by the proto-Olifants River during the Oligocene lowstand (Dingle, 1971a; Dingle and Hendey, 1984; Dingle, 1992/1993). However, this study is confined to the uppermost reaches of the Cape Canyon and it is possible that the deeper water portion of the canyon was incised earlier.

University of Cape Town

The seismic mini-airgun profile (Figure 3.6) reveals the presence of at least 50 m of post-Cretaceous sediment fill. The available sediment cores intercept, at most, only the upper few metres of this canyon infill. However, the density of core coverage allows the minimum thickness of the recovered units to be estimated. The estimated minimum composite thickness of the recovered Neogene succession is ±30 m, with a minimum thickness of 3 m of the Upper Oligocene/Lower Miocene Calcareous Unit, 18 m of the Glauconitic Muddy Sand, 5 m of the Quartzose Muddy Sand and a minimum thickness 5 m of the Glauconitic Quartzose Sand. The seismic mini-airgun profile (Figure 3.6) is the only one available indicating the thickness of the post-Cretaceous sediment infill in the study area. This profile is located directly above the central seaward bulge in the eastern flank, which separates the Northern Depression from the southern Central Channel (Figures 3.4 and 3.5). This seaward bulge is interpreted as a Quaternary delta fan-type deposit associated with a palaeo-Berg River, and suggests an unusually thick Quaternary succession in this area. The estimated total sediment thickness may therefore be on the order of 50 m with no additional pre-upper Oligocene units necessary to produce the late Cenozoic

environment encountered off the western margin of southern Africa. The broad similarities in this proposed depositional environment, dominated by outer shelf cold water upwelling and an associated inner to middle shelf mudbelt, suggest that similar hydrographic conditions would have existed (*e.g.* Rogers, 1977; De Decker, 1988). The expected northward movement by longshore drift of the coarse fraction of the fluvial sediments, with the fine mud fraction carried offshore and to the south for glauconite formation, has therefore occurred since the mid Miocene. The abundance of very fine quartz sand in the St. Helena Bay area (Figure 2.8) may indicate increased output of the palaeo-Olifants River at this time. Increased aridification during the late Miocene resulted in a decrease in river flow (Malherbe *et al.*, 1986; Pickford and Senut, 1999; De Wit *et al.*, 2000) and the formation of glauconite throughout the late Miocene indicates overall low sediment accumulation rates for this period.

Fluctuations in the middle to late Miocene relative sea level would have resulted in a shifting distribution of the proposed inner to middle shelf terrigenous organic matter-rich mudbelt, providing a widespread area of favourable conditions for glauconitization over time. The REE patterns of the Upper Oligocene/Lower Miocene glauconite pellets are sufficiently different from those of the Pliocene to Holocene glauconite grains to discount a reworking and redeposition of the older glauconite grains. An initial investigation of glauconite grains from southern Namibia, suggests that reworking of Palaeogene glauconite grains is also an unlikely source for the Pliocene to Holocene glauconite-rich deposits of Concession 20D. The glauconite pellets from the Pliocene to Holocene facies have similar major element compositions and all show a typical flat seawater REE pattern with a slight HREE enrichment and a strong negative Ce-anomaly, although textures of the glauconite pellets imply that multiple glauconitization events occurred. The overall similarity in morphology and the geochemistry of the late Neogene glauconite pellets favours a cyclical return to similar depositional conditions over time, with each successive relative sea-level cycle lowstand responsible for the winnowing of the mud-fraction, possible rounding of relict glauconite pellets and oxidation of organic matter and sulphides. The glauconitization and phosphatisation events would be then associated with the subsequent transgressive system tracts or maximum flooding surfaces (Odin and Matter, 1981; Loutit *et al.*, 1988; Kelly and Webb, 1999; Harris and Whiting, 2000). Sancetta *et al.* (1992) and Diester-Haass *et al.* (1986) have suggested that the correlation between mud content and the carbonate record suggests that organic-rich mud belts existed during sea-level highstands of the Pliocene along the western margin.

The extended history of glauconitization on the western margin was brought to an end by the deposition of the Pliocene Quartzose Muddy Sand Unit, which forms a quartzose muddy sand drape across the entire study area. Many authors have argued for Pliocene uplift of the southern African continent (Section 2.3.1; Partridge and Maud, 1987; Partridge, 1998; Gallagher and Brown, 1999; Brown *et al.*, 2000), which is generally accepted to have occurred towards the end of the Pliocene. It is therefore argued that the rapid eustatic sea-level fluctuations of the middle Pliocene (Abreu and Anderson, 1998), associated with the general lowering of eustatic sea level, rather than margin uplift, are responsible for the rapid progradation of very fine quartz sand across the outer shelf. Rapid progradation of quartzose sands across the relatively narrow inner to middle shelf off Cape Columbine (Figure 2.1) may be

University of Cape Town

water upwelling along the western margin is associated with a rapid decrease in biogenic accumulation, an increase in organic matter and the authigenesis of green glauconite pellets. The presence of green glauconite pellets in middle Miocene sediments of Core 319, suggests that intermittent cold water upwelling occurred by 15.7 Ma, although Sr-ages of reworked foraminifera in the Glauconite Muddy Sand facies range only between 5.8-10.9 Ma. The K/Ar-ages, ranging from 6.5-17.7 Ma, reported for glauconite grains of the western margin by Birch (1975), are in agreement with these Sr-derived ages. Uenzelmann-Neben *et al.* (2002) also argued that the presence of numerous slide scarps and channels, observed in the sediments of the upper slope of the Orange Shelf in water depths of 500-2500 m, result from upwelling-related slope instabilities. The scarps are found exclusively in their seismic units CB-1 and CB-2 (Table 2.4), where all of the scarps observed are younger than ~14 Ma. Scarps observed in the lower part of CB-2 in the south (8-10 Ma), but higher up and into CB-1 in the north (2-6 Ma), suggest two steps in the northward migration of the Benguela upwelling system. The change in the normalized REE patterns, between the Upper Oligocene/Lower Miocene to the Pliocene to Holocene glauconite pellets, supports a change in the depositional environment linked to changes in water temperature and the related carbonate abundances.

The reworked middle Miocene (9.1-15.8 Ma) robust benthic foraminiferal assemblage, recovered from the Pliocene Quartzose Muddy Sand, indicates a middle Miocene peak in siliciclastic deposition. A brief mention is made in the literature of other possibly similar-aged quartzose sediments as far north as southern Namibia (Dingle, 1970b; 1971a; Rogers, 1977), implying that the middle Miocene was a time of increased terrigenous output onto the western continental shelf. Uplift of the western margin at around 16-18 Ma (this study and Partridge, 1998, Anderson *et al.*, 2000, Dale and McMillan, 2003b) occurred simultaneously with the middle Miocene Climatic Optimum. The resultant increased onshore denudation and fluvial activity is recorded offshore as the prograding, delta-front, quartzose very fine sands, associated with the long-term middle to late Miocene eustatic regression. The very fine muddy sands, redeposited as the Pliocene Quartzose Muddy Sand, have a very similar texture and appearance to the modern Orange and Olifants rivers inner shelf delta front sands (0-40 m) (Birch, 1975; Rogers, 1977) although very little information is available for these sediments. The well-sorted, fine quartzose muddy sands are therefore interpreted as delta-front deposits, associated with the increased climatic- and tectonic-driven mid Miocene fluvial activity.

The Elandsfontyn Formation, recovered from the southwestern Cape coastal platform, is generally assigned a mid Miocene age, although there is little agreement about the age of this unit in the literature. These sediments were examined as a possible fluvial source of the siliciclastic material onto the inner shelf, landward, of Concession 20D. Evidence from this study indicates that it is likely that the Elandsfontyn Formation represents the onshore record of the middle to late Miocene fluvial activity. However, more work is required to constrain the age of the Elandsfontyn Formation. These delta front sands appear to have been tightly constrained to the inner shelf. The depositional environment must have graded rapidly seawards into an organic-rich mudbelt, indicated by the syndepostional glauconite accumulation on the outer shelf. This envisaged inner to outer shelf separation is similar to the modern

University of Cape Town

reduced bottom water winnowing may imply reduced wind-driven upwelling. The increased planktic foraminiferal accumulation and reduced terrigenous input with increasing water depth prevented the formation of phospho-glauconite in the Foraminiferal Ooze.

The Sr-derived ages of the interpreted lithostratigraphic facies of the Upper Oligocene/Lower Miocene Calcareous Unit sediments show a remarkable correlation with the proposed eustatic sea-level curve (Figure 10.1). However, the amplitude of changing relative sea level, indicated by the late Oligocene palaeoshorelines at approximately –200 m, attests to the importance of post-depositional downwarping of the western margin. This downwarping most likely records the influence of sediment (and water) loading, associated with a margin-wide Burdigalian carbonate productivity peak, preserved as the Foraminiferal Ooze in Concession 20D, in conjunction with the rising mid Miocene eustatic sea level. The later mid Miocene uplift event, which has been argued to be associated with seaward tilting of the margin, would have heightened this loading influenced downwarping.

The gravel lag at the base of the Gravelly Quartzose Muddy Sand in Core 319, with benthic foraminifera ranging in age between 17.0-17.7 Ma, marks the end of the carbonate-dominated upper Oligocene to lower Miocene depositional cycle. The gravel lag is interpreted as a condensed relative lowstand deposit, reflecting increased erosion, due to an increased rate of uplift of the western margin between ~16-18 Ma. The uplift event is estimated to have resulted in 100-200 m of uplift because an Aquitanian shoreline is reported at –140 m along the Namaqualand coast and a post-uplift Langhian shoreline occurs landwards of the +50 m marine terraces at Hondeklipbaai (Pether *et al.*, 2000; Dale and McMillan, 2003b). The marine package is recovered from two localities (Lanklip and Ryskop) within 10 km of Hondeklipbaai, with elevations quoted as +40 m and at +65 m (Pether *et al.*, 2000; Dale and McMillan, 2003b, respectively). The Sr-ages of the Gravelly Quartzose Muddy Sand provide the first well-constrained ages for the middle Miocene uplift event from the offshore record (Partridge and Maud, 1987; Partridge, 1998; Pickford, 1998; Lavier *et al.*, 2001).

The uplift of the western coastal platform occured just prior to the Miocene Climatic Optimum at ~16 Ma (Flower and Kennett, 1994; Gallagher *et al.*, 2001; Zachos *et al.*, 2001), after which major changes in the global oceanographic and climatic systems are recorded. Rapid expansion of the East Antarctic ice-sheet was associated with the intensification of Southern Ocean circulation and rapid cooling of deep waters (Pagani *et al.*, 1999; Lawver and Gahagan, 2003) and the establishment of ocean stratification associated with the mid to late Miocene cooling (Gallagher *et al.*, 2001). These changes in global conditions are mirrored by a change in the dominant component of the sediments of Concession 20D, with the formation and preservation of phospho-glauconite on the middle to outer shelf of southern Africa dominating the middle to late Miocene. The onset of cold-water upwelling along the western margin reflects the stratification of the Southern Ocean (Pagani *et al.*, 1999). The ostracod assemblage of sediments from ODP Site 1087 of the Orange Slope indicate a subtropical/tropical climate until at least the Langhian, where changes in the fauna to a cold-water assemblage are observed between 16-13 Ma (Dingle *et al.*, 2001). The sediment record of Concession 20D suggests that the initiation of cold

University of Cape Town

proposed that much of the phosphorite gravels, preserved in the Pliocene and Quaternary winnowed lags, consists of reworked fragments of these Oligocene/Miocene condensed phosphatised hardgrounds. Hardgrounds, indicative of maximum flooding surfaces, are typically formed by a synsedimentary lithification process occurring during markedly reduced sedimentation rates and may be mineralised with iron hydroxides (goethite-limonite), phosphorite and glauconite (Eren and Tasli, 2002 and references therein). Hardgrounds are typically cemented limestone, although carbonate-cemented quartz sandstones do occur and hardgrounds are typically, but not exclusively, found in tropical and subtropical, shallow carbonate environments (Taylor and Wilson, 2003). The erosional surfaces of the layered phosphorites are often goethite-rich. Microbial iron-oxidation processes are invoked to explain marine ferruginisation, where these fossilised iron-encrusted bacterial and fungal mats may serve as an indicator of, at least local, anoxic to dysaerobic conditions (Préat *et al.*, 2000). The normalized REE pattern of phospho-glauconites from the Upper Oligocene/Lower Miocene Calcareous Unit are slightly depleted in HREE, shows a "MREE bulge" and a reduced negative Ce-anomaly, which all favour the importance of diagenetic Fe-oxyhydroxide scavenging of LREE. In addition, Fe-Mn crusts, although only a minor to trace component of the gravel fraction, are also recognised as clasts in the youngest CFA-cemented horizon (L1 in Figure 7.9). Although not studied in any detail, these ferromanganese oxyhydroxide crusts are also typically found in areas where currents have kept a hardground clean of sediments for considerable periods of time (Koschinsky and Hein, 2003 and references therein).

The larger benthic foraminfera *Operculina* sp. of the Quartz Foraminiferal Muddy Sand are interpreted to have been deposited in a low-energy tropical to sub-tropical environment. In contrast, the overlying Quartzose Glauconitic Calcareous Sand facies provides evidence of significant upwelling and bottom water activity associated with a major phosphogenesis event as hardground surfaces imply winnowing by a bottom current. These recorded differences in the depositional environments, particularly as the inferred lowstand water depths are apparently not significantly different, are interpreted to indicate a major change in oceanographic conditions along the western margin of southern Africa in the late Oligocene. The increased wind-driven coastal upwelling may be related to ice sheet expansion of the major Mi-1 glaciation event at 23.5 Ma (Figure 10.1; Zachos *et al.*, 2001; Lawver and Gahagan, 2003). Additional Sr-isotope analyses of the layered phosphorites may provide more information on the timing of hardground formation associated with the initiation of upwelling along the western margin.

The Quartzose Glauconitic Calcareous Sand is unconformably overlain by the outer shelf Burdigalian Glauconitic Calcareous Sand. The poorly defined basal contact is interpreted to indicate a lowering of the relative sea level such that the palaeo-shoreface was located on the modern middle shelf. The abundance of phospho-glauconite in some of these Burdigalian sediments indicates low sediment accumulation rates during a rising relative sea level, where glauconite-rich sediments are typical of transgressive systems tract deposits. The long-term late early Miocene eustatic sea-level transgression is also associated with the deposition of the Foraminiferal Ooze. It is proposed that the Burdigalian carbonate productivity peak reflects more favourable conditions associated with the mid Miocene Climatic Optimum (Flower and Kennett, 1994; Zachos *et al.*, 2001; Gallagher *et al.*, 2001), because

University of Cape Town

mid Oligocene sea-level lowstand (Miller *et* al., 1998; Gallagher *et al.*, 2001; Zachos *et al.*, 2001; Lawver and Gahagan, 2003).

The early to middle Oligocene erosional event is followed by the deposition of the Upper Oligocene/Lower Miocene Calcareous Unit, forming part of the coast-parallel lens of reported Lower Miocene sediments of the western margin. The four stratigraphic sequences recognized with the Upper Oligocene/Lower Miocene Calcareous Unit record at least three cycles of relative sea-level change superimposed on a long-term increase in water depth. The long-term deepening, evidenced, in part, by an increasingly marine (calcareous) sediment up-unit, is interpreted to reflect a combination of the lower Miocene marine eustatic transgression (Figure 10.1) and increased margin subsidence, associated with sediment loading following the Burdigalian carbonate productivity peak.

The larger benthic foraminifera of the upper Oligocene Quartzose Foraminiferal Muddy Sand were deposited in a low-energy, sandy, inner shelf, subtropical to tropical environment during a relative sea-level lowstand. The larger benthic foraminiferal assemblage indicates that the late Oligocene palaeoshoreline would have been at around -200 m, in the vicinity of the inner shelf break of the present-day isobaths. The presence of phosphatised shell fragments and glauconite in the Quartzose Foraminiferal Muddy Sand is interpreted to indicate a rising relative sea level associated with low sediment accumulation rates. The available Sr-ages suggest that deposition (and recrystallisation) of the complete foraminiferal assemblage occurred at the same time as the eustatic sea-level lowstand of TB1.2 at around 26.5 Ma (Figure 10.1). The erosional surface, defined by the basal gravel lag of the overlying Quartzose Glauconitic Calcareous Sand, marks the start of a new cycle of changing relative sea level. This latest Oligocene to early Miocene (Aquitanian) lowstand is associated with winnowing of the underlying Quartzose Foraminiferal Muddy Sand and the underlying unconsolidated Cretaceous Quartzose Woody Sand. The complexity of the variable sand composition recovered from the Quartzose Glauconitic Calcareous Sand facies is interpreted to possibly represent more than one cycle of changing sea level. The interpreted cycles of changing sea level are again coincident with a series of third-order eustatic cycles (TB1.3 and 1.4) at the Oligocene/Miocene transition (Figure 10.1). The foraminiferal assemblage, recovered from above the basal lag of the Quartzose Glauconitic Calcareous Sand facies, indicates deposition in an innermost shelf (Core 159 on the eastern flank) to inner shelf (Core 324 on the Western Ridge) environment, suggesting that the latest Oligocene to Aquitanian lowstand palaeoshoreline is slightly deeper in Concession 20D, at ~-200 m modern isobath, than the -140 m proposed by Dale and McMillan (2003b) for the Namaqualand margin. The reported difference is believed to indicate greater post-depositional uplift in the north (Figure 10.1).

The maximum flooding surfaces recorded by the Quartzose Glauconitic Calcareous Sand are associated with extensive phosphatisation. Although no Sr-ages are available for the layered phosphorites, the Sr-ages available for the phosphorite gravels show an initial phosphogenesis event around 23.6-26.1 Ma associated with the late Oligocene warming event (Compton *et al.*, 2004), which coincide with the recorded age of deposition of the 23.3-25.6 Ma Quartzose Glauconitic Calcareous Sand facies. It is

University of Cape Town

Figure 10.1. A summary of the Cenozoic geological evolution of the western margin from analyses of the sediment succession of Concession 20D. The most important factors influencing sediment accumulation are considered, including eustasy, tectonic activity, palaeoceanographic and palaeoclimate. The resultant facies evolution is summarised in the far right column. The proposed Haq *et al.* (1987) eustatic sea-level curve was replotted to the Berggren *et al.* (1995) time scale after Miller *et al.* (1997; 1998).

- The highly condensed Cenozoic record reveals a complex history or deposition, erosion and redeposition.
- Four major Cenozoic lithostratigraphic units are recovered unconformably above the unconsolidated mid Cretaceous Quartzose Woody Sand.
- The Upper Oligocene/Lower Miocene Calcareous Unit includes four facies, which record a number of cycles of changing relative sea level. These changes in relative sea level largely correspond to eustatic sea-level fluctuations, although a contribution of increased margin subsidence and palaeoceanographic changes are also recognised. A major phosphogenesis episode occurred during the latest Oligocene-earliest Micene.
- Uplift of the western continental margin occurred around 16-18 Ma. This uplift and the later onset of cold water upwelling, brought about a major change in the evolution of the western margin. There was an increased terrigenous input, in the form of prograding delta front deposits, largely restricted to the inner shelf. Low sediment accumulation rates and glauconite formation in highstand mudbelt depositional environments occurred from the middle to late Miocene and into the early Pliocene.
- Redeposition of the delta front deposits occurred in response to sea-level fluctuations during a mid Pliocene long-term lowstand. These quartzose sediments of the Quartzose Muddy Sand form a relatively uniform drape across the study area.
- Renewed uplift of the western continental margin occurred in the late Pliocene/early Pleistocene. This uplift is associated with the incision of the Head of the Cape Canyon. Renewed terrigenous input followed uplift.
- The Pleistocene Succession shows a distinct bathymetry-controlled distribution of sediments. The sea-level fluctuations of the late Pleistocene resulted in erosion and incision of the Main Channel as well as the large scale reworking, slumping, erosion and bioturbation of the condensed Tertiary sediment succession.

Abbreviations: QFmS-Quartzose Foraminiferal Muddy Sand facies, QGCS-Quartzose Glauconitic Calcareous Sand facies, GCS-Glauconitic Calcareous Sand facies, FO-Foraminiferal Ooze facies, GS-Glauconitic Sand Unit, GmS-Glauconitic Muddy Sand Sub-unit, QmS-Quartzose Muddy Sand Unit.

The presence of wood fragments and conifer palynomorphs indicates the presence of an extensive mid Cretaceous forested area, which probably extended from the Cape Columbine area northwards to the Orange River (Bamford and Corbett, 1995). The unconsolidated nature of these sediments indicates that they were never deeply buried, with no evidence for post-burial diagenetic cementation observed.

The western margin of southern Africa is a high-elevation passive rifted margin. The timing of the margin uplift and the formation of the associated Great Escarpment is open to debate. It has been argued that uplift occurred from prior to Early Cretaceous rifting (Gallagher and Brown, 1999) to the Oligocene (Burke, 1996). Recent fission-track data indicated that massive denudation had ceased by the earliest Palaeogene and that minimal escarpment retreat has occurred since the Eocene (Cockburn *et al.*, 2000). The Agulhas-Columbine Arch has been buoyant since rifting and the condensed post-rifting succession preserved on flanks of the pre-Cretaceous basement suggest repeated uplift and erosion events (Scrutton and Dingle, 1976; Dingle *et al.*, 1983; Brown *et al.*, 1995). The presence of ferricrete gravel in the basal lag, unconformably overlying the mid Cretaceous Woody Quartzose Sand Unit, suggests that the ferricrete horizons reported off the Namaqualand coast had an earlier more widespread distribution. Sediments younger than mid-Cretaceous and older than upper Oligocene have been eroded from the western continental shelf in the vicinity of Concession 20D. This erosion most likely reflects increased erosion, associated with both Tertiary tectonic uplift of the western interior (Partridge and Maud, 1987; McMillan, 1989; Burke, 1996; Cramez and Jackson, 2000; Lavier *et al.*, 2001) and a major

University of Cape Town

REFERENCES

Abbott, S.T. and Carter, R.M., 1994. The sequence architecture of mid-Pleistocene (c.1.1–0.4 Ma) cyclothems from New Zealand: facies development during a period of orbital control on sea-level cyclicity. *In*: de Boer, P.L and Smith, D.G, (eds). *Special Publication of the International Association of Sedimentologists Volume 19*, pp. 367–394.

Abdelghany, O., 2002. Lower Miocene stratigraphy of the Gebel Shabrawet area, north Eastern desert Egypt. *Journal of African Earth Sciences*, **34**, 203-212.

Abreu, V.S. and Anderson, J.B., 1998. Glacial eustasy during the Cenozoic: sequence stratigraphic implications. *American Association of Petroleum Geologists Bulletin*, **82 (7)**, 1385-1400.

Aizawa, M., Bluck, B., Cartwright, J., Milner, S., Swart, R. and Ward, J., 2000. Constraints on the geomorphological evolution of Namibia from the offshore stratigraphic record. *Communications of the Geological Survey of Namibia*, **12**, 337-346.

Amorosi, A., 1995. Glaucony and sequence stratigraphy: a conceptual framework of distribution in siliciclastic sequences. *Journal of Sedimentary Research*, **B65 (4)**, 419-425.

Amorosi, A., 1997. Detecting compositional, spatial, and temporal attributes of glaucony: a tool for provenance research, *Sedimentary Geology*, **109**, 135-153.

Amouric, M. and Parron, C., 1985. Structure and growth mechanism of glauconite as seen by high-resolution transmission electron microscopy. *Clay and Clay Minerals.* **33**, 473-482.

Anderson, J. E., Cartwright, J., Drysdall, S.J. and Vivian, N., 2000. Controls on turbidite sand deposition during gravity-driven extension of a passive margin: examples from Miocene sediments in Block 4, Angola. *Marine and Petroleum Geology*, **17**, 1165-1203.

Andreoli, M.A.G., Doucouré, M., Van Bever Donker, J., Brandt, D. and Anderson, N.J.B., 1996. Neotectonics of southern Africa – a review. *Africa Geoscience Review*, **3**, 1-16.

Austin, J.A. and Uchupi, E., 1982. Continental-oceanic crustal transition off southwest Africa. *The American Association of Petroleum Geologists Bulletin*, **66 (9)**, 1328-1347.

Bamford M.K. and Corbett I.B., 1994. Fossil wood of Cretaceous age from the Namaqualand continental shelf, South Africa. *Palaeontologia Africana,* **31**, 83-95.

Bamford M.K. and Corbett I.B., 1995. More fossil wood from the Namaqualand coast, South Africa; on-shore material. *Palaeontologia Africana,* **32**, 67-74.

Bamford, M.K. and Stevenson, I.R., 2002. A submerged Late Cretaceous podocarpaceous forest, west coast, South Africa. *South African Journal of Science*, **98**, 181-185.

Bard, E., Hamelin, B., Arnold, M., Montaggioni, L., Cabioch, G., Faure, G. and Rougerie, F., 1996. Deglacial sea-level record from Tahiti corals and the timing of global meltwater discharge. *Nature*, **382**, 241-244.

Berger, W.H. and Wefer, G., 1996a. Central Themes of South Atlantic Circulation. *In:* Wefer, G., Berger, W.H., Siedler, G. and Webb, D.J. (*eds*). *The South Atlantic: Present and Past Circulation.* Springer-Verlag, Berlin, pp. 1-11.

Berger, W.H. and Wefer, G., 1996b. Expeditions into the past: Paleoceanographic studies in the South Atlantic. *In:* Wefer, G., Berger, W.H., Siedler, G. and Webb, D.J. (*eds*). *The South Atlantic: Present and Past Circulation.* Springer-Verlag, Berlin, pp. 363-410.

Berger, W.H. and Wefer, G., 2002. On the reconstruction of upwelling history: Namibia upwelling in context, *Marine Geology*, 180, 3-28.

Berger, W.H., Lange, C.B., and Wefer, G., 2002. Upwelling history of the Benguela-Namibia system: a synthesis of Leg 175 results. *In*: Wefer, G., Berger, W.H., and Richter, C. (*eds.*), *Proceedings of the Ocean Drilling Program, Scientific Results*, **175** [Online]. Available from World Wide Web: http://www-odp.tamu.edu/publications/175_SR/synth/synth.htm [Cited 2002-12-06]

Berggren, W.A., Kent, D.V., Swisher, C.C. and Aubry, M.P., 1995. A revised Cenozoic geochronology and chronostratigraphy. *In*: Berggren, W.A., Kent, D.V., Aubrey, M.-P., and Hardenbol, J. (*eds.*). Geochronology, time scales and global stratigraphic correlation, *SEPM Special Publication*, **54**, pp. 129-212.

Berner, R.A., 1984. Sedimentary pyrite formation: An update. *Geochimica et Cosmochimica Acta,* **48**, 605-615.

Billups, K., 2002. Late Miocene through early Pliocene deep water circulation and climate change viewed from the sub-Antarctic South Atlantic. *Palaeogeography, Palaeoclimatology, Palaeoecology*, **185 (3-4)**, 287-307.

Birch, G.F., 1971. The glauconite deposits on the Agulhas Bank, South Africa. *Bulletin of the Joint Geological Survey/University of Cape Town Marine Geoscience Group,* **4**, 1-134.

University of Cape Town

Birch, G.F., 1974. Mineralogy and geochemistry of the fine sediments (<63μm) on the shelf off the south-western Cape coast and in the adjacent source area. *Technical Report of the Joint Geological Survey/University of Cape Town Marine Geology Program,* **6**, 47-51.

Birch, G.F., 1975. Sediments on the continental margin off the west coast of South Africa. *Bulletin of the Joint Geological Survey/University of Cape Town Marine Geoscience Group,* **6**, 1-142.

Birch, G.F., 1979a. The nature and origin of mixed apatite/glauconite pellets from the continental shelf off South Africa. *Marine Geology,* **29**, 313-334.

Birch, G.F., 1979b. The association of glauconite and apatite minerals in phosphatic rocks from the South African continental margin. *Transactions of the Geological Society of South Africa,* **82**, 43-53.

Birch, G.F., 1980. A model of penecontemporaneous phosphatization by diagenetic and authigenic mechanisms from the western margin of southern Africa. *The Society of Economic Palaeontologists and Mineralogists Special Publication,* **29**, 79-100.

Birch, G.F., Day, R.W. and Du Plessis, A., 1991. Nearshore Quaternary sediments on the west coast of southern Africa. *Bulletin Geological Survey of South Africa,* **101**, 1-14.

Bolli, H.M., Ryan, W.B.F., Foresman, J.B, Hottman, W.E., Kagami, H., Longoria, J.F., McKnight, B.K., Melguen, M., Natland, J.H., Proto-Decima, F. and Siesser, W.G., 1978. Cape Basin continental rise; Sites 360 and 361. *Initial Reports of the Deep Sea Drilling Project,* **40**, 29-182.

Botha, K.A. 2003. *Calibration of Reflectance Data with Carbonate Measurements from the Cape Canyon Submarine Fan: Correlation with the Late Quaternary Glacial/Interglacial Cycles.* Unpublished Honours Project, Department of Geological Sciences, University of Cape Town, 56pp.

Boyer, D.L., Zhang., X. and Pérenne, N., 2000. Laboratory observations of rotating, stratified flow in the vicinity of a submarine canyon. *Dynamics of Atmospheres and Oceans,* **31**, 47-72.

Brachert, T. C., Forst, M. H., Pais, J. J., Legoinha, P. and Reijmer, J. J. G., 2003. Lowstand carbonates, highstand sandstones? *Sedimentary Geology,* **155 (1-2)**, 1-12

Branch, G. and Branch, M., 1981. *The Living Shores of Southern Africa.* Struik Publishers (Pty) Ltd, Cape Town, 272 pp.

Bremner, J.M., 1981. Sediments on the continental margin off South West Africa between latitudes 17° and 25° South. *Bulletin of the Joint Geological Survey/University of Cape Town Marine Geoscience Group,* **10**, 1-233.

Bremner, J.M., Rogers, J. and Willis, J.P., 1990. Sedimentological aspects of the 1988 Orange River floods. *Transactions of the Royal Society of South Africa,* **47**, 247-294.

Brown, L.F., Benson, J.M., Brink, G.J., Doherty, S., Jollands, A., Jungslager, E.H.A., Keenan, J.H.G., Muntingh, A. and van Wyk, N.J.S., 1995. Sequence stratigraphy in offshore South African divergent basins: An atlas on exploration for Cretaceous lowstand traps by SOEKOR (Pty) Ltd. *American Association for Petroleum Geologists: Studies in Geology,* **41**, 1-184.

Brown, R.W., Gallagher, K, D.J., Gleadow A.J.W and Summerfield, M.A., 2000. Morphotectonic evolution of the South Atlantic margins of Africa and South America. *In:* Summerfield, M.A. (*ed*). *Geomorphology and Global Tectonics.* John Wiley & Sons, Chichester, pp. 256-281.

Brown, R.W., Rust, D.J., Summerfield, M.A., Gleadow A.J.W. and De Wit, M.J.C., 1990. An early Cretaceous phase of accelerated erosion on the south-western margin of Africa: Evidence from apatite fission-track analysis and the offshore sedimentary record. *International Journal of Radiation Applications and Instrumentation. Part D. Nuclear Tracks and Radiation Measurements,* **17**, 339-350.

Broquet, C.A.M., 1992. The sedimentary record of the Cape Supergroup: A review. *In:* De Wit, M.J. and Ransome, I.G.D. (*eds*). *Inversion Tectonics of the Cape Fold Belt, Karoo and Cretaceous Basins of Southern Africa.* A.A. Balkema, Rotterdam, pp. 159-183.

Burke, K., 1996. The African Plate. *South African Journal of Geology,* **99**, 339-409.

Burst. J.F., 1958a. "Glauconite" pellets: their mineral nature and applications to stratigraphic interpretations. *Bulletin of the American Association of Petroleum Geologists,* **42 (2)**, 310-337.

Burst, J.F., 1958b. Mineral heterogeneity in "glauconite" pellets. *American Mineralogist,* **43**, 481-497.

Caron, V., Nelson, C.S. and Kamp, P.J.J, 2004. Transgressive surfaces of erosion as sequence boundary markers in cool-water shelf carbonates. *Sedimentary Geology,* **164 (3-4)**, 179-189.

Carter, R.M., 1998. Two models: global sea-level change and sequence stratigraphic architecture. *Sedimentary Geology,* **122**, 23-36.

Catuneanu, O., Willis, A.J. and Miall, A.D., 1998. Temporal significance of sequence boundaries. *Sedimentary Geology,* **121**, 157-178.

Chafetz, H. S. and Reid, A., 2000. Syndepositional shallow-water precipitation of glauconitic minerals. *Sedimentary Geology,* **136**, 29-42.

University of Cape Town

Chappell, J. and Shackleton, N.J., 1986. Oxygen isotopes and sea level. *Nature*, **324**,137-140.

Chen, M-T., Chang, Y-P., Chang, C-C., Wang, L-W., Wang, C-H. and Yu, E-F., 2002. Late Quaternary sea-surface temperature variations in the southeast Atlantic: a planktic foraminifer faunal record of the past 600 000 yr (IMAGES II MD962085). *Marine Geology*, **180**, 163-181.

Christensen, B.A., Kalbas, J.L., Maslin, M and Murray, R.W., 2002. Paleoclimatic changes in southern Africa during the intensification of Northern Hemisphere glaciation: evidence from ODP Leg 175 Site 1085. *Marine Geology*, **180**, 117-131.

Christie, N.D., 1974. *Distribution Patterns of the Benthic Fauna Along a Transect Across the Continental Shelf off Lamberts Bay, South Africa*. Unpublished PhD thesis, Department of Zoology, University of Cape Town, South Africa, 110pp.

Christison, I.D. 1985. *Foraminifera from the continental shelf of South West Africa*. Unpublished MSc thesis, University College of Wales, Aberystwyth, 174 pp.

Church, K.D. and Coe, A.L., 2003b. Processes controlling relative sea-level change and sediment supply. *In:* Coe, A.L. (*ed*). *The Sedimentary Record of Sea-Level Change*. Cambridge University Press, Cambridge, pp. 99-117.

Clauer, N., Keppens, E. and Stille, P., 1992. Sr isotopic constraints on the process of glauconitization. *Geology*, **20**, 133-136.

Clemson, J., Cartwright, J.A. and Booth, J., 1997. Structural segmentation and the influence of basement structure on the Namibia passive margin. *Journal of the Geological Society of London*, **154**, 477-482.

Cockburn, H. A. P., Brown, R. W., Summerfield, M.A. and Seidl, M. A., 2000. Quantifying passive margin denudation and landscape development using a combined fission-track thermochronology and cosmogenic isotope analysis approach. *Earth and Planetary Science Letters*, **179**, 429-435.

Coe, A.L. and Church, K.D., 2003a. Sea-level change. *In:* Coe, A.L. (*ed*). *The Sedimentary Record of Sea-Level Change*. Cambridge University Press, Cambridge, pp. 34-55.

Coe, A.L. and Church, K.D., 2003b. Sequence Stratigraphy. *In:* Coe, A.L. (*ed*). *The Sedimentary Record of Sea-Level Change*. Cambridge University Press, Cambridge, pp. 57-98.

Coetzee, J.A., 1986. Palynological evidence for major vegetation and climatic change in the Miocene and Pliocene of the south-western Cape. *South African Journal of Science*, **82**, 71–72.

Coetzee, J.A. and Rogers, J., 1982. Palynological and lithological evidence for the Miocene palaeoenvironment in the Saldanha region (South Africa). *Palaeogeography Palaeoclimatology Palaeoecology*, **39**, 71-85.

Coffey, B.P. and Read, J.F., 2004. Mixed carbonate–siliciclastic sequence stratigraphy of a Paleogene transition zone continental shelf, southeastern USA *Sedimentary Geology*, **166 (1-2)**, 21-57.

Cole, D.I., 1992. Karoo and related basins. *In:* De Wit, M.J. and Ransome, I.G.D. (*eds*). *Inversion Tectonics of the Cape Fold Belt, Karoo and Cretaceous Basins of Southern Africa.* A.A. Balkema, Rotterdam, pp. 87-99.

Cole, D.I. and Roberts, D.L., 1996. Lignite from the western coastal plain of South Africa. *Journal of African Earth Sciences*, **23 (1)**, 95-117.

Compton, J.S., Mulabisana, J. and McMillan, I.K., 2002. Origin and age of phosphorite from the Last Glacial Maximum to Holocene transgressive succession off the Orange River, South Africa. *Marine Geology*, **186**, 243-261.

Compton, J.S., Wigley, R.A. and McMillan, I.K., 2004. Late Cenozoic phosphogenesis on the western shelf of South Africa in the vicinity of the Cape Canyon. *Marine Geology*, **206**, 19-40.

Corbett, I.B., 1996. A review of diamondiferous marine deposits of western southern Africa. *Africa Geoscience Review*, **3 (2)**, 157-174.

Corbett, I. and Burrell, B., 2001. The earliest Pleistocene (?) Orange River fan delta: an example of successful exploration delivery aided by applied Quaternary research in diamond placer sedimentology and palaeontology. *Quaternary International*, **82**, 63-73.

Corda, L. and Brandano, M., 2003. Aphotic zone carbonate production on a Miocene ramp, Central Apennines, Italy. *Sedimentary Geology*, **161**, 55-70.

Cox, K.G., 1989. The role of mantle plumes in the development of continental drainage patterns. *Nature*, **342**, 973-877.

Cramez, C. and Jackson, M.P.A., 2000. Superposed deformation straddling the continental-oceanic transition in deep-water Angola. *Marine and Petroleum Geology*, **17**, 1095-1109.

Cutler, K.B., Edwards, R.L., Taylor, F.W., Cheng, H., Adkins, J., Gallup, C.D., Cutler, P.M., Burr, G.S. and Bloom, A.L., 2003. Rapid sea-level fall and deep-ocean temperature change since the last interglacial period. *Earth and Planetary Science Letters*, **206** (3-4), 253-271.

University of Cape Town

Dale, D.C. and McMillan, I.K., 1997. *Late Cretaceous (Early Turonian to Late Coniacian) Hyposaline Agglutinating Foraminiferal Biostratigraphy of the Proximal Orange Basin, Western Offshore. South Africa and southernmost offshore Namibia.* Abstract. 3rd Colloquium on the Stratigraphy and Paleogeography of the South Atlantic, Yaounde, Cameroon.

Dale, D.C. and McMillan, I.K., 1998a. Mud belt and middle shelf benthonic and planktonic foraminiferal assemblages and sedimentation processes compared through the Holocene successions at two tropical African (Sierra Leone) and two temperate African (western offshore, South Africa) sites. *South African Journal of Science*, **94**, 319-340.

Dale, D.C. and McMillan, I.K., 1998b. A coast of giant rivers: The west coast in the time of the dinosaurs. *Earthyear: The Essential Environmental Guide*, **18**, 92-93.

Dale, D.C. and McMillan, I.K., 1999a. *On the Beach. A Field Guide to the Late Cainozoic Micropalaeontological History, Saldanha Region, South Africa.* Earthyear Environmental Communications (Pty) Ltd. 127pp.

Dale, D.C. and McMillan, I.K., 1999b. How do Microfossils help Diamond Exploration? *Earthyear: The Essential Environmental Guide*, **20**, 114-115.

Dale, D.C. and McMillan, I.K., 2000. *Pliocene Foraminifera and Biostratigraphic Correlations of the Atlantic Continental Margin of South Africa and Southern Namibia.* Abstract of 14th African Colloquium on Micropalaeontology, Luanda, Angola, 21-24 May 2000.

Dale, D.C. and McMillan, I.K., 2003a. The Pliocene. Or, how to correlate sediments using microfossils. *Earthyear: The Essential Environmental Guide*, **26**, 18-19.

Dale, D.C. and McMillan, I.K., 2003b. The rising and falling of the African continent, the rising and falling of global sea-level, and changing shoreline positions through time. *Earthyear: Journal for Sustainable Development*, **3**, 58-59.

Dale, D.C. and McMillan, I.K., in prep. Aspects of the Cainozoic foraminiferal biostratigraphy of the western continental margin of South Africa. (Submitted to *South African Journal of Geology* in December 2003)

Damuth, J.E., 1994. Neogene gravity tectonics and depositional processes on the deep Niger Delta continental margin. *Marine and Petroleum Geology*, **11 (3)**, 320

Da Silva. L.C., McNaughton, N.J., Hartmann, L.A., Fletcher, I.R., Gresse, P.G., and Scheepers, R., 1997. *U-Pb (SHRIMP) Isotopic Constraints for the Evolution of Southern Brazilian Granitic Province, and Some Correlated South African, Pan-African Plutons.* Abstracts of 2nd International Symposium on Granites and Associated Mineralizations, Salvador, 24-29 August, 276-277.

Day, R.W., Franzsen, A.J. and Rogers, J., 1992. Coast-parallel palaeochannels off southern Namibia. *Marine Geology*, **105**, 299-304.

De Decker, A.H.B., 1970. Notes on an oxygen-depleted subsurface current off the west coast of South Africa. *Investigative Reports of the Division of Sea Fisheries of South Africa*, **84**, 24pp.

De Decker, R.H., 1988. The wave regime on the inner shelf of the Orange River and its implications for sediment transport. *South African Journal of Geology*, **91**, 358-371.

De Decker, R.H. and Woodborne, M.W., 1996. *Geological and Technical Aspects of Marine Diamond Exploration in Southern Africa.* Abstracts of Offshore Technology Conference 8018, Houston, Texas, 6-9 May 1996.

Deer, W.A., Howie, R.A. and Zussman, J., 1966. *An Introduction to Rock Forming Minerals*. Longman Group Limited, Harlow. 628pp.

De Villiers, S. E. and Cadman, A., 2001. An analysis of the palynomorphs obtained from Tertiary sediments at Koingnaas, Namaqualand, South Africa. *Journal of African Earth Sciences*, **33 (1)**, 17-47.

De Villiers, S. and Wigley, R.A., *in prep.* Palaeopalynological evidence for the Cupressaceae *sensu lato* in the Cretaceous of South Africa.

De Wit, M.C.J., 1993. *Cainozoic Evolution of Drainage Systems in the North-Western Cape.* Unpublished PhD thesis, Department of Geological Sciences, University of Cape Town, 371pp.

De Wit, M.C.J., 1999. Post-Gondwana drainage and the development of diamond placers in western South Africa. *Economic Geology*, **94**, 721-740.

De Wit, M.C.J., Marshall, T.R. and Partridge, T.C., 2000. Fluvial deposits and drainage evolution. *In:* Partridge, T.C. and Maud, R.R. (*eds*). *The Cenozoic of Southern Africa.* Oxford University Press, Inc., New York, pp. 3-18.

Di Celma, C., Ragaini, L., Cantalamessa, G. and Curzio, P., 2002. Shell concentrations as tools in characterizing sedimentary dynamics at sequence-bounding unconformities: examples from the lower unit of the Canoa Formation (Late Pliocene, Ecuador). *Geobios*, **35 (1)**, 72-85.

University of Cape Town

Diekmann, B., Falker, M. and Kuhn, G., 2003. Environmental history of the south-eastern South Atlantic since the Middle Miocene: evidence from the sedimentological records of ODP Sites 1088 and 1092. *Sedimentology*, **50**, 511-529.

Diester-Haass, L. and Zahn, R., 1996. Eocene-Oligocene transition in the Southern Ocean; history of water mass circulation and biological productivity. *Geology*, **24**, 163-166.

Diester-Haass, L., Meyers, P.A. and Rothe, P., 1986. Light-dark cycles in opal-rich sediments near the Plio-Pleistocene boundary, DSDP Site 532, Walvis Ridge continental terrace. *Marine Geology*, **73**, 1-2.

Diester-Haass, L., Meyers, P.A. and Rothe, P., 1992. The Benguela Current and associated upwelling on the southwest African margin: a synthesis of the Neogene-Quaternary sedimentary record at DSDP sites 362 and 532. *In:* Summerhayes, C.P., Prell, W.L., Emeis, K.C. (*eds*). Upwelling Systems: Evolution since the Early Miocene. *Geological Society of London Special Publication*, **64**, 331-342.

Diester-Haass, L., Meyers, P.A. and Vidal, L., 2002. The late Miocene onset of high productivity in the Benguela Current upwelling system as part of a global pattern. *Marine Geology*, **180**, 87-103.

Dingle, R.V., 1970a. Bathymetry. *Technical Report of the Joint Geological Survey/University of Cape Town Marine Geology Program*, **3**, 11-12.

Dingle, R.V., 1970b. Mesozoic and Tertiary sedimentary history of the continental shelf between Cape Columbine and Cape Seal. *Technical Report of the Joint Geological Survey/University of Cape Town Marine Geology Program*, **3**, 28-37.

Dingle, R.V., 1971a. Tertiary sedimentary history of the continental shelf off southern Cape Province, South Africa. *Transactions of the Geological Society of South Africa*, 74, 173-186.

Dingle, R.V., 1971b. Bathymetry: west coast. *Technical Report of the Joint Geological Survey/University of Cape Town Marine Geoscience Unit*, **3**, 11-12.

Dingle, R.V., 1973a. Mesozoic palaeogeography of the southern Cape, South Africa. *Palaeogeography, Palaeoclimatology, Palaeoecology*, **13**, 203-213.

Dingle, R.V., 1973b. Regional distribution and thickness of post-Palaeozoic sediments on the continental margin of southern Africa. *Geological Magazine*, **110 (2)**, 97-102.

Dingle, R.V., 1973c. The geology of the continental shelf between Luderitz and Cape Town (Southwest Africa), with special reference to Tertiary strata. *Journal of the Geological Society London*, **129**, 337-363.

Dingle, R.V., 1979. Sedimentary basins and basement structures on the continental margin of southern Africa. *Bulletin of the Geological Survey of South Africa*, **63**, 29-43.

Dingle, R.V., 1980a. Sedimentary basins on the continental margins of Southern Africa: An assessment of their hydrocarbon potential. *Erdöl und Kohle Erdgas Petrochemie*, **33 (10)**, 457-463.

Dingle, R.V., 1980b. Large allochthonous sediment masses and their role in the construction of the continental slope and rise off southwestern Africa. *Marine Geology*, **37**, 333-354.

Dingle, R.V., 1986. Revised bathymetric map of the Cape Canyon. *Technical Report of the Joint Geological Survey/University of Cape Town Marine Geoscience Unit*, **16**, 20-33.

Dingle, R.V., 1992/1993. Structural and sedimentary development of the continental margin off southwestern Africa. *Communications of the Geological Survey of Namibia*, **8**, 35-43.

Dingle, R.V., 1995. Continental shelf upwelling and benthic Ostracoda in the Benguela System (south-eastern Atlantic Ocean). *Marine Geology*, **122**, 207-225.

Dingle, R.V. and Scrutton, R.W., 1974. Continental breakup and the development of post-Palaeozoic sedimentary basins around southern Africa. *Bulletin of the Geological Society of America*, **85**, 1467-1474.

Dingle, R.V. and Hendey, Q.B., 1984. Late Mesozoic and Tertiary sediment supply to the eastern Cape Basin (SE Atlantic) and palaeo-drainage systems in southwestern Africa. *Marine Geology*, **56**, 13-26.

Dingle, R.V. and Robson, S.H., 1992. Southwestern Africa continental rise: Structural and SEDIMENTARY evolution. *In:* Poag, C.W. and de Graciansky, P.C. (*eds*). *Geologic Evolution of Atlantic Continental Rises*, New York, Von Nostrand Reinhold, pp. 62-76.

Dingle, R.V., Siesser, W.G. and Newton, A.R., 1983. *Mesozoic and Tertiary Geology of Southern Africa*. A.A. Balkema, Rotterdam, 375pp.

Dingle, R.V., Birch, G.F., Bremner, J.M., De Decker, R.H., Du Plessis, A., Engelbrecht, J.C., Finchham, M.J., Fitton, T., Flemming, B.W., Gentle, R.I., Goodlad, S.W., Martin, A.K., Mills, E.G., Moir, G.J., Parker, R.J., Robson, S.H., Rogers, J., Salmon, D.A., Siesser, W.G., Simpson, E.S.W., Summerhayes, C.P., Westall, F., Winter, A. and Woodborne, M.W., 1987. Deep-sea sedimentary environments around southern Africa (south-east Atlantic and south-west Indian Oceans). *Annals of the South African Museum*, **98**, 1-27 (2 separate maps)..

University of Cape Town

Dingle, R.V., McMillan, I.K., Majoran, S. and Bisset, L., 2001. Palaeo-oceanographic implications of Early-Middle Miocene subtropical ostracod faunas from the continental shelf of SE Atlantic Ocean. *Palaeogeography, Palaeoclimatology, Palaeoecology*, **173**, 43-60.

Doher, I., 1980. Palynomorph preparation procedures currently used in the Palaeontology and Stratigraphy Laboratories, U.S. Geological Survey. *Geological Survey Circular*, 830, *United States Department of the Interior*, 29pp.

Duncan, D.S., Locker, S.D., Brooks, G.R., Hine, A.C. and. Doyle, L.J., 2003. Mixed carbonate-siliciclastic infilling of a Neogene carbonate shelf-valley system: Tampa Bay, West-Central Florida, *Marine Geology*, **200**, 125-156.

Du Plessis, A., Scrutton, R.A., Barnaby, A.M. and Simpson, E.S.W., 1972. Shallow structures of the continental margin of south-western Africa. *Marine Geology*, **13**, 77-89.

Du Toit, A.L., 1910. The evolution of the river system of Griqualand West. *Transactions of the Royal Society of South Africa*, **1**, 347-362.

Du Toit, A.L., 1954. *Geology of South Africa 3rd Edition*. Oliver and Boyd, Edinburgh and London, 611pp.

Eckardt, F.D. and Spiro, B., 1999. The origin of sulphur in gypsum and dissolved sulphate in the Central Namib Desert, Namibia. *Sedimentary Geology*, **123**, 255-273.

Einsele, G., 1996. Event deposits: the role of sediment supply and relative sea-level changes – a review. *Sedimentary Geology*, **104**, 11-37.

Emery. K.O., Uchupi, E., Bowin, C.O., Phillips, J. and Simpson, E.S.W., 1975. Continental margin off Western Africa: Cape St Francis (South Africa) to Walvis Bay (South West Africa). *Bulletin of the American Association of Petroleum Geologists*, **59**, 3-59.

Eren, M. and Tasli, K., 2002. Kilop Cretaceous Hardground (Kale, Gümüshane, NE Turkey): description and origin. *Journal of Asian Earth Sciences*, **20 (5)**, 433-448.

Eschard, R., 2001. Geological factors controlling sediment transport from platform to deep basin: a review. *Marine and Petroleum Geology*, **18**, 487-490.

Eswaran, H and Stoops, G., 1979. Surface textures of quartz in tropical soils. *Soil Science Society of America Journal*, **43 (2)**, 420-424.

Ferland, M.A., Roy, P.S. and Murray-Wallace, C.V., 1995. Glacial lowstand deposits on the outer continental shelf of southeastern Australia, *Quaternary Research*, **44** (2), 294-299.

Flemming B.W., 1976. Construction and calibration of an automatically recording settling tube systems for the hydraulic grain-size analysis of sand. *Technical Report of the Joint Geological Survey/University of Cape Town Marine Geology Program*, **8**, 47-59.

Flemming, B.W. and Thum, A.B., 1978. The settling tube – a hydraulic method for grain size analysis of sands. *Kieler Meeresforchungen*, 4, 82-95

Flower, B.P. and Kennett, J.P., 1994. The middle Miocene climatic transition: East Antarctic ice sheet development, deep ocean circulation and global carbon cycling. *Palaeogeography, Palaeoclimatology, Palaeoecology*, **108**, 537-555.

Folk, R.L., 1965. *Petrology of Sedimentary Rocks*. Hemphill's, Austin, Texas, 159pp.

Föllmi, K.B., 1996. The phosphorus cycle, phosphogenesis and marine phosphate-rich deposits. *Earth-Science Reviews*, **40**, 55-124.

Fouché, J., Bate, K.J and Van der Merwe, R., 1992. Plate tectonic setting of the Mesozoic basins, southern offshore, South Africa: a review. *In:* De Wit, M.J. and Ransome, I.G.D. (*eds*). *Inversion Tectonics of the Cape Fold Belt, Karoo and Cretaceous Basins of Southern Africa.* A.A. Balkema, Rotterdam, pp. 33-45.

Franceschini, G., 2003. *Geology of Aeolian and Marine Deposits in the Saldanha Bay Region – Western Cape, South Africa.* Unpublished PhD thesis, Department of Geological Sciences, University of Cape Town, South Africa, 276pp.

Frimmel, H.E. and Frank, W., 1998. Neoproterozoic tectono-thermal evolution of the Gariep Belt and its basement, Namibia and South Africa, *Precambrian Research*, **90**, 1-28.

Frimmel, H.E., Fölling, P.G and Diamond, R., 2001. Metamorphism of the Permo-Triassic Cape Fold Belt and its basement, South Africa. *Mineralogy and Petrology*. **73**, 325–346.

Galehouse J.S., 1971. Point counting. *In*: Carver, R.E., (*ed*). *Procedures in Sedimentary Petrology*. Wiley-Interscience, New York, pp. 385-407.

Gallagher, K. and Brown, R., 1999. Denudation and uplift at passive margins: the record on the Atlantic Margin of southern Africa. *Philosophical Transactions of the Royal Society of London*, **357**, 835-859.

University of Cape Town

Gallagher, S.J. and Holdgate, G., 2000. The palaeogeographic and palaeoenvironmental evolution of a Palaeogene mixed carbonate–siliciclastic cool-water succession in the Otway Basin, Southeast Australia. *Palaeogeography, Palaeoclimatology, Palaeoecology*, **156**,19-50.

Gallagher, S.J., Smith, A. J., Jonasson, K., Wallace, M.W., Holdgate, G.R., Daniels, J. and Taylor, D., 2001. The Miocene palaeoenvironmental and palaeoceanographic evolution of the Gippsland Basin, Southeast Australia: a record of Southern Ocean change. *Palaeogeography, Palaeoclimatology, Palaeoecology*, **172**, 53-80.

German, C.R., Masuzawa, T., Greaves, M.J., Elderfield, H. and Edmond J.M., 1995. Dissolved rare earth elements in the Southern Ocean: Cerium oxidation and the influence of hydrography. *Geochimica et Cosmochimica Acta*, **59 (8)**, 1551-1558.

Gerrard, I. and Smith, G.C., 1982. Post-Palaeozoic succession and structure of the southwestern African continental margin. *In:* Watkins, J. S. and Drake, C.L. (*eds*). Studies in Continental Margin Geology. *Memoir of the American Association of Petroleum Geologists*, **34**, pp. 49-74.

Giblin, A.E. and Wieder, R.K., 1992. Sulphur cycling in marine and freshwater wetlands. *In:* Howarth, R.W., Stewart, J.W.B. and Ivanov, M.V. (*eds*). *Sulphur Cycling on the Continents*. John Wiley and Sons Ltd, pp. 85-124.

Gilchrist, A. R. and Summerfield, M. A., 1990. Differential denudation and flexural isostasy in formation of rifted-margin upwarps. *Nature*, **346**, 739-742.

Giraudeau, J., 1993. Planktonic foraminiferal assemblages in surface sediments from the southwest African continental margin, *Marine Geology*, **110**, 47-62.

Giraudeau, J., Meyers, P.A. and Christensen, B.A., 2002. Accumulation of organic and inorganic carbon in the Pliocene-Pleistocene sediments along the SW African margin. *Marine Geology*, **180**, 49-69.

Gomez, B., Bamford, M. and Martínez-Delclòs, X., 2002. Lower Cretaceous plant cuticles and amber (Kirkwood Formation, South Africa). *Comptes Rendus Palevol*, **1**, 83-87.

Gonzales, R., 1996. Response of shallow-marine carbonate facies to third-order and high-frequency sea-level fluctuations: Hauptrogenstein Formation, northern Switzerland. *Sedimentary Geology*, **102**, 111-130.

Granata, T.C., Vidondo, B., Duarte, C.M., Satta, M.P. and Garcia, M., 1999. Hydrodynamics and particle transport associated with a submarine canyon off Blanes (Spain), NW Mediterranean Sea. *Continental Shelf Research*, **19**, 1249-1263.

Gray, C., Meadows, M.E., Lee-Thorp, J.A., Rogers, J. and Jouanneau, J., 1999. *A Record of Terrestrial Environmental Change from Marine Cores off the Namaqualand Mudbelt in Southern Africa.* Abstracts of the International Geological Correlation Programme Project No. 396, 4th annual conference 'Continental shelves in the Quaternary", Cape Town, South Africa, 18.

Gröger, M., Henrich, R. and Bickert, T., 2003. Glacial–interglacial variability in lower North Atlantic deep water: inference from silt grain-size analysis and carbonate preservation in the western equatorial Atlantic. *Marine Geology*, **201 (4)**, 321-332.

Haley, B.A. and Klinkhammer, G.P., 2003. Complete separation of rare earth elements from small volume seawater samples by automated ion chromatography: method development and application to benthic flux. *Marine Chemistry*, **82 (3-4)**, 197-220.

Hallock, P., 1985. Why are larger Foraminifera large? *Paleobiology*, **11**,195-208.

Hammerbeck, E.C.I. and Allcock, R.J.I., 1985. Geological Map of Southern Africa. *Geological Survey of South Africa, Pretoria.*

Haq, B.U., Hardenbol, J. and Vail, P.R., 1987. Chronology of fluctuating Sea Levels since the Triassic. *Science*, **235**, 1156-1167.

Haq, B.U., Hardenbol, J. and Vail, P.R., 1988. Mesozoic and Cenozoic chronostratigraphy and cycles of sea-level change. *In:* Wilgus, C.K., Hastings, B.S., Kendall, C.G.St.C., Posamentier, H.W., Ross, C.A. and Van Wagoner, J.C. (*eds*). *Sea-Level Changes - An Integrated Approach.* Society of Economic Palaeontologists and Mineralogists Special Publication, **42**, 71-108.

Harris, L. C. and Whiting, B. M., 2000. Sequence-stratigraphic significance of Miocene to Pliocene glauconite-rich layers, on- and offshore of the US Mid-Atlantic margin. *Sedimentary Geology*, **134**, 129-147.

Haug G.H. and Tiedemann, R. 1998. Effect of the formation of the Isthmus of Panama on Atlantic Ocean thermohaline circulation. *Nature*, **393** (6686), 673-676.

Haunold, T.G., Baal, C. and Piller, W.E., 1997. Benthic foraminiferal associations in the Northern Bay of Safaga, Red Sea, Egypt. *Marine Micropaleontology*, **29**, 185-210.

Hayton, S., Nelson, C.S. and Hood, S. D., 1995. A skeletal assemblage classification system for non-tropical carbonate deposits based on New Zealand Cenozoic limestones. *Sedimentary Geology*, **100**, 123-141.

University of Cape Town

Helland-Hansen, W. and Gjelberg, J.G., 1994. Conceptual basis and variability in sequence stratigraphy: a different perspective. *Sedimentary Geology*, **92**, 31-52.

Hendey, Q.B., 1982. *Langebaanweg: A Record of Past Life*. South African Museum, Cape Town, 71pp.

Hesselbo, S.P. and Huggett, J.M., 2001. Glaucony in ocean-margin sequence stratigraphy (Oligocene-Pliocene, offshore New Jersey, U.S.A.; ODP Leg 174A). *Journal of Sedimentary Research*, **71 (4)**, 599-607.

Hinz, K., Neben, S., Schreckenberger, B., Roeser, H.A., Block, M., Goncalves de Souza, K. and Meyer, H., 1999. The Argentine continental margin north of 48°S: sedimentary successions, volcanic activity during breakup. *Marine and Petroleum Geology*, **16 (1)**, 1-25.

Hohenegger, J. 1995. Depth estimation by proportions of living larger foraminifera. *Marine Micropaleontology*, **26**, 31-47.

Hohenegger, J., Yordanova, E., Nakano, Y. and Tatzreiter, F., 1999. Habitats of larger foraminifera on the upper reef slope of Sesoko Island, Okinawa, Japan, *Marine Micropalaeontology*, **36**, 109-168.

Holbourn, A., Kuhnt, W., Simo, J.A. and Li, Q., 2004. Middle Miocene isotope stratigraphy and paleoceanographic evolution of the northwest and southwest Australian margins (Wombat Plateau and Great Australian Bight). *Palaeogeography, Palaeoclimatology, Palaeoecology*, **208 (1-2)**, 1-22.

Holdgate, G.R., Kershaw, A. P. and Sluiter, I. R. K., 1995. Sequence stratigraphic analysis and the origins of Tertiary brown coal lithotypes, Latrobe Valley, Gippsland Basin, Australia. *International Journal of Coal Geology*, **28**, 249-275

Howard, J.L., Amos, D.F. and Daniels, W.L., 1995. Micromorphology and dissolution of quartz sand in some exceptionally ancient soils. *Sedimentary Geology*, **105**, 51-62.

Imbrie, J., Hays, J.D., Martinson, D.G., McIntyre, A., Mix, A.C., Morley, J.J., Pisias, N.G., Prell, W.L., Shackleton, N.J., 1984. The orbital theory of Pleistocene climate: Support from a revised chronology of the marine $\delta^{18}O$ record. *In*: Berger, A.L. *et al.* (*eds.*), *Milankovitch and Climate*. Reidel, Dordrecht, pp. 269–305.

Ireland, B.J., Curtis, C.D. and Whiteman, J.A, 1983. Compositional variation within some glauconites and illites and implications for their stability and origins. *Sedimentology*, **30 (6)**, 769-786.

Jacob, R.J., Bluck, B.J and Ward, J.D., 1999. Tertiary-age diamondiferous fluvial deposits of the lower Orange River Valley, southwestern Africa. *Economic Geology*, **94 (5)**, 749-758.

John, C.M., Karner, G.D and Mutti, M., 2004. $\delta^{18}O$ and Marion Plateau backstripping: Combining two approaches to constrain late middle Miocene eustatic amplitude. *Geology*, **32 (9)**, 829-832.

Karner, G.D., Driscoll, N.W., McGinnis, J.P., Brumbaugh, W.D. and Cameron, N.R., 1997. Tectonic significance of syn-rift sediment packages across the Gabon-Cabinda continental margin. *Marine and Petroleum Geology*, **14 (7-8)**, 973-1000.

Kelly, J.C. and Webb, J.A., 1999. The genesis of glaucony in the Oligo–Miocene Torquay Group, southeastern Australia: petrographic and geochemical evidence, *Sedimentary Geology*, **125**, 99-114.

Kendall, C,G.St.C. and Lerche, I., 1988. The rise and fall of eustasy. *In*: Wilgus, C.K., Hastings, B.S., Kendall, C.G.St.C., Posamentier, H.W., Ross, C.A. and Van Wagoner, J.C. (*eds*). *Sea-level Changes: An Integrated Approach*, SEPM Special Publication, **42**, 155-181.

Kennett, J.P., 1982. *Marine Geology*. Prentice-Hall, Inc. Englewood Cliffs, 813pp.

Kidder, D.L., Krishnaswamy, R. and Mapes, R.H., 2003. Elemental mobility in phosphatic shales during concretion growth and implications for provenance studies. *Chemical Geology*, **198**, 335-353.

Kidwell, S.M.; Fursich, F.T. and Aigner, H., 1986. Conceptual framework for the analysis and classification of fossil concentrations. *Palaios*, **1 (3)**, 228-238.

Kilburn, R and Rippey, E., 1982. *Sea Shells of Southern Africa*. McMillan South Africa (Pty) Ltd, Johannesburg, 249pp.

King, L.C. and King, L.A., 1959. A reappraisal of the Natal monocline. *South African Geographical Journal*, **41**, 15-30.

Kitamura, A., 1998. Glaucony and carbonate grains as indicators of the condensed section: Omma Formation, Japan. *Sedimentary Geology*, **122**, 151-163.

Klinger, H.C., 1977. Cretaceous deposits near Bogenfels, South West Africa. *Annals of the South African Museum*, **73**. 81-92.

Kondo, Y., Abbott, S.T., Kitamura, A., Kamp, P.J.J., Naish, T., Kamataky, T. and Sau, G., 1998. The relationship between shell bed type and sequence architecture: examples from Japan and New Zealand. *Sedimentary Geology*, **122**, 109–127.

Koschinsky, A. and Hein, J.R., 2003. Uptake of elements from seawater by ferromanganese crusts: solid-phase associations and seawater speciation. *Marine Geology*, **198 (3-4)**, 331-351.

University of Cape Town

Kraus, M.J., 1998. Development of potential acid sulfate paleosols in Paleocene floodplains, Bighorn Basin, Wyoming, USA. *Palaeogeography, Palaeoclimatology, Palaeoecology*, **144**, 203-224.

Krinsley, D.H. and Doornkamp, J.C., 1973. *Atlas of Quartz Sand Surface Textures*. Cambridge University Press, 91pp.

Kuhns, R., 1995. *Sedimentological and Geomorphological Environment of the Western South African Continental Shelf and Its Control on Distribution of Alluvial/Fluvial and Marine Diamonds.* Proceedings of the Annual Meeting of the Society Mining, Metallurgy and Exploration Inc.

Kumar, A. and Saraswati, P.K., 1997. Response of larger foraminifera to mixed carbonate-siliciclastic environments: an example from the Oligocene-Miocene sequence of Kutch, India. *Palaeogeography, Palaeoclimatology, Palaeoecology*, **136**, 53-65.

Latimer, J.C. and Filippelli, G.M. Eocene to Miocene terrigenous inputs and export production; geochemical evidence from ODP Leg 177, Site 1090. *Palaeogeography, Palaeoclimatology, Palaeoecology*, **182**, 151-164.

Lavier, L.L., Steckler, M.S. and Brigaud, F., 2001. Climatic and tectonic control on the Cenozoic evolution of the West African margin. *Marine Geology*, **178**, 63-80.

Lawver, L.A. and Gahagan, 2003. Evolution of Cenozoic seaways in the circum-Antarctic region. *Palaeogeography, Palaeoclimatology, Palaeoecology*, **198**, 11-37.

Li, Q., Simo, J. A., McGowran, B. and Holbourn, A., 2004. The eustatic and tectonic origin of Neogene unconformities from the Great Australian Bight. *Marine Geology*, **203 (1-2)**, 57-81.

Liu, J.T., Liu, K. and Huang, J.C., 2002. The effect of a submarine canyon on the river sediment dispersal and inner shelf sediment movements in southern Taiwan. *Marine Geology*, **181**, 357-386.

Loutit, T.S., Hardenbol, J. Vail, P.R and Baum, G.R., 1988. Condensed sections: the key to age determination and correlation of continental margin sequences. *In*: Wilgus, C.K., Hastings, B.S., Kendall, C.G.St.C., Posamentier, H.W., Ross, C.A. and Van Wagoner, J.C. (*eds). Sea-level Changes: An Integrated Approach*, SEPM Special Publication, **42**, 183-213.

Lutjeharms, J.R.E. and Meeuwis, J.M., 1987. The extent and variability of south-east Atlantic upwelling. *South African Journal of Marine Science*, **5**, 51-62.

MacHutchon, M., 2003. *Depositional History of the Holocene Mudbelt Offshore of the Buffels River, South Africa.* Unpublished Honours Project, Department of Geological Sciences, University of Cape Town, 36pp.

Malengreau, N and Sposito, G., 1997. Short-time dissolution mechanism of kaolinitic tropical soils. *Geochemica et Cosmochemica Acta*, **61 (20)**, 4297-4307.

Malherbe, S.J., Keyser, A.W., Botha, B.J.V., Cornelissen, A., Slabbert, M.J. and Prinsloo, M.C., 1986. The Tertiary Koa River and the development of the Orange River drainage. *Annals of the Geological Survey of South Africa*, **20**, 12-23.

Malone, M.J., Claypool, G., Martin, J. and Dickens, G.R., 2002. Variable methane fluxes in shallow marine systems over geologic time: The composition and origin of pore waters and authigenic carbonates on the New Jersey shelf. *Marine Geology*, **189 (3-4)**, 175-196.

Martin, H., 1973. The Atlantic margin of southern Africa between latitude 17° south and the Cape of Good Hope. *In*: Nairn, A.E.M. and Stehli, F.G. (*eds*). *The Ocean Basins and Margins, Volume 1: The South Atlantic.* Plenum Press, New York, pp. 277-300.

Martin, R.A., 1981. *Benthic Foraminifera from the Orange-Lüderitz Shelf Southern Africa Continental Margin.* Unpublished MSc thesis, Department of Geological Sciences, University of Cape Town, South Africa, 75pp.

Maslanyj, M.P., Light, M.P.R., Greenwood, R.J. and Banks, N.L., 1992. Extension tectonics offshore Namibia and evidence for passive rifting in the South Atlantic. *Marine & Petroleum Geology*, **9**, 590 - 601.

McArthur, J.M., Howarth, R.J. and Bailey, T.R., 2001. Strontium Isotope Stratigraphy: LOWESS Version 3: Best fit to the marine Sr-isotope curve for 0-509 Ma and accompanying look-up table for deriving numerical age. *Journal of Geology*, **109**, 155-170.

McHugh, C.M.G. and Olson, H.C., 2002. Pleistocene chronology of continental margin sedimentation: New insights into traditional models, New Jersey. *Marine Geology*, **186**, 389-411.

McHugh, C.M.G., Damuth, J.E. and Mountain, G.S., 2002. Cenozoic mass-transport facies and their correlation with relative sea-level change, New Jersey continental margin. *Marine Geology*, **184 (3-4)**, 295-334.

McLachlan, I.R. and McMillan, I.K., 1979. Microfaunal biostratigraphy, chronostratigraphy and history of Mesozoic and Cenozoic deposits on the coastal margin of South Africa. *Geokongess 77: Geological Society of South Africa Special Publication*, **6**, 161-181.

McLachlan, I.R. and Pieterse, E., 1978. Preliminary palynological results: Site 361, Leg 40, Deep Sea Drilling Project. *In:* Bolli, H.M., Ryan, W.B., *et al. (eds). Initial Reports, Deep Sea Drilling Project*, **40**, pp. 857-882.

University of Cape Town

McLaughlin, P.I., Brett, C.E., McLaughlin, S.L.T and Cornell, S.R., 2004. High-resolution sequence stratigraphy of a mixed carbonate-siliciclastic, cratonic ramp (Upper Ordovician; Kentucky–Ohio, USA): insights into the relative influence of eustasy and tectonics through analysis of facies gradients. *Palaeogeography, Palaeoclimatology, Palaeoecology*, **210 (2-4)**, 267-294.

McMillan, I.K., 1986. Cainozoic planktonic and larger foraminifera distributions around Southern Africa and their implications for past changes of oceanic water temperatures. *South African Journal of Science*, **82**, 66-69.

McMillan, I.K., 1989. *Victoriella conoidea* (Rutten, 1914): A guide to foraminifera for the later Aquitanian (Early Miocene) marine rocks of southern Africa. *South African Journal of Geology*, **92 (2)**, 95-101.

McMillan, I.K., 1990. Foraminiferal biostratigraphy of the Barremian to Miocene rocks of the Kudu 9A-1, 9A-2 and 9A-3 boreholes. *Communications of the Geological Survey. Namibia*, **6**, 23-29.

McMillan, I.K., 1992. Benthonic and planktonic foraminifera from the lower Santonian outcrop at Wanderveld IV, near Bogenfels, southern Namibia. Abstracts: Géologie Africaine: 11th Colloque African de Micropaléontologie (Libreville, Gabon, May 1991), *Elf-Aquitaine Mémoire*, **13**, 412.

McMillan, I.K., 1993. Foraminiferal biostratigraphy, sequence stratigraphy and interpreted chronostratigraphy of marine Quaternary sedimentation on the South African continental shelf. *South African Journal of Science*, **89**, 83-89.

Meadows, M.E., Dingle, R.V., Rogers, J. and Mills, E.G., 1997. Radiocarbon chronology of Namaqualand mudbelt sediments: Problems and Prospects. *South African Journal of Science*, **93**, 321-327.

Melguen, M., 1978. Facies evolution, carbonate dissolution cycles in sediments from the eastern south Atlantic (DSDP Leg 40) since the Early Cretaceous. *In:* Bolli, H.M., Ryan, W.B., *et al. (eds). Initial Reports, Deep Sea Drilling Project*, **40**, pp. 981-1024.

Metzger, J. M., Flemings, P. B., Christie-Blick, N., Mountain, G. S., Austin. J. A. and Hesselbo S. P., 2000. Late Miocene to Pleistocene sequences at the New Jersey outer continental shelf (ODP leg 174A, sites 1071 and 1072). *Sedimentary Geology*, **134**, 149-180.

Miall, A.D., 1992. The EXXON global cycle chart: an event for every occasion. *Geology*, **20**, 787-790.

Miall, A.D., 1995. Whither stratigraphy? *Sedimentary Geology*, **100**, 5-20.

Miall, A.D. and Miall, C.E., 2001. Sequence stratigraphy as a scientific enterprise: the evolution and persistence of conflicting paradigms. *Earth-Science Reviews*, **54 (4)**, 321-348

Middleton, X.V. 2003. *Petrographic and Geochemical Evidence for the Origin of Phosphorites and Phosphate Rocks from the West Coast of Southern Africa*. Unpublished MSc thesis, Department of Geological Sciences, University of Cape Town, 112pp.

Miller, K.G., Browning, J.V., Pekar, S.F. and Sugarman, P.J., 1997. Cenozoic evolution of the New Jersey Coastal Plain: changes in sea-level, tectonics, and sediment supply. *In:* Miller, K.G., and Snyder, S.W. (*eds*). *Proceedings of ODP, Scientific Results*, **150X**, pp. 361-374.

Miller, K.G., Mountain, G.S., Browning, J.V., Kominz, M., Sugarman, P.J., Christie-Blick, N., Katz, M.E. and Wright, J.D., 1998. Cenozoic global sea level, sequences, and the New Jersey transect: Results from coastal plain and continental slope drilling. *Reviews of Geophysics*, **36**, 569-601.

Miller, K.G., Mountain, G.S., the Leg 150 Shipboard Party, Members of the New Jersey Coastal Plain Drilling Project, 1996. Drilling and dating New Jersey Oligocene-Miocene sequences: Ice volume, global sea-level, and Exxon Records. *Science*, **271 (5252)**, 1092-1095.

Miller K.G., Wright J.D. and Fairbanks R.G., 1991. Unlocking the ice house: Oligocene-Miocene oxygen isotopes, eustasy, and margin erosion. *Journal of Geophysical Research*, **96** (B4), 6829-6848.

Monteverde, D.H., Miller, K.G. and Mountain, G.S., 2000. Correlation of offshore seismic profiles with onshore New Jersey Miocene. *Sedimentary Geology*, **134**, 111-127.

Moore, J. M and Moore, A. E., 2004. The roles of primary kimberlitic and secondary Dwyka glacial sources in the development of alluvial and marine diamond deposits in Southern Africa. *Journal of African Earth Sciences*, **38 (2)**, 115-134.

Morse, J.W. and Berner, R.A., 1995. What determines sedimentary C/S ratios? *Geochimica et Cosmochimica Acta*, **59**, 1073-1077.

Mozley, P.S. and Carothers, W.W., 1992. Elemental and isotopic composition of siderite in the Kuparuk Formation Alaska: Effect of microbial and water/sediment interaction on early pore water chemistry. *Journal of Sedimentary Petrology*, **62**, 681–692.

Murray, J. and Renard, A.F., 1891. *Deep-Sea Deposits*. Reports on the Scientific Results of the H.M.S. Challenger 1873-76, H.M.S.O., London, 525pp.

University of Cape Town

Murray, L.G., Joynt, R.H., O'Shea, D.O'C., Forster, R.W. and Kleinjan, L., 1970. The geological environment of some diamond deposits off the coast of South West Africa. *In:* Delany, F.M. (*ed*). The Geology of the East Atlantic Continental Margin. *Reports of the Institute of Geological Sciences* **No. 70/13**, 119-141.

Murray, R.W., Christensen, B.A., Kalbas, J.L. and Kryc, K.L., 2002. Pliocene export production and terrigenous provenance of the Southern Cape Basin, southwest African margin. *Marine Geology*, **180**, 133-150.

Naish, T.R., Woolfe, K.J., Barrett, P.J., Wilson, G.S., Atkins, C., Bohaty, S.M., Bücker, C.J., Claps, M., Davey, F.J., Dunbar, G.B., Dunn, A.G. Fielding, C.R., Florindo, F., Hannah, M.J., Harwood, D.M., Henrys, S.A., Krissek, L.A., Lavelle, M., van der Meer, J., Mcintosh, W.C., Niessen, F., Passchier, S., Powell, R.D., Roberts, A.P., Sagnotti, L., Scherer, R.P., Strong, C.P., Talarico, F., Verosub, K.L. Villa, G., Watkins, D.K., Webb P.N. and Wonik, T., 2001. Orbitally induced oscillations in the East Antarctica ice sheet at the Oligocene/Miocene boundary. *Nature*, **413**, 719-723.

Ndwamise, J.P., 1995. *A Sedimentological Study of Vibracores from the Middle Shelf West of Robben Island.* Unpublished Honours Project, Department of Geological Sciences, University of Cape Town, South Africa, 34pp.

Nelson, G., 1985. Notes on the physical oceanography of the Cape Peninsula upwelling system. *In:* Shannon, L.V. (*ed.*). *South African Colour and Upwelling Experiment.* Sea Fisheries Research Institute, Cape Town, pp. 63-95.

Odin, G.S., 1988. Glaucony from the Gulf of Guinea. *In:* Odin, G.S. (*ed*). *Green Marine Clays.* Elsevier, Amsterdam, pp. 225-247.

Odin, G.S. and Fullagar, P.D., 1988. Geological significance of the glaucony facies. *In:* Odin, G.S. (*ed*). *Green Marine Clays.* Elsevier, Amsterdam, pp. 295-332.

Odin, G.S. and Lamboy, M., 1988. Glaucony from the margin off northwestern Spain. *In:* Odin, G.S. (*ed*). *Green Marine Clays.* Elsevier, Amsterdam, pp. 249-275.

Odin, G.S. and Matter, A., 1981. De glauconiarum origine. *Sedimentology*, **28**, 611-641.

Okey, T.A, 1997. Sediment flushing observations, earthquake slumping, and benthic community changes in the Monterey Canyon head. *Continental Shelf Research*, **17**, 877-897.

Ollier, C.D. and Pain, C.F., 1997. Equating the basal unconformity with the palaeoplan: a model for passive margins. *Geomorphology*, **19**, 1-15.

Padmanabhan, E. and Mermut, A.R., 1996. Submicroscopic structure of Fe-coatings on quartz grains in tropical environments. *Clays and Clay Minerals*, **44 (6)**, 801-810.

Pagani, M., Arthur, M.A. and Freeman, K.H., 1999. Variations in Miocene phytoplankton growth rates in the Southwest Atlantic; evidence for changes in ocean circulation. *Paleoceanography*, **15**, 486-496.

Parker, R.J., 1971. *The Petrography and Major Element Geochemistry of Phosphorite Nodule Deposits on the Agulhas Bank, South Africa.* Unpublished MSc thesis, Department of Geological Sciences, University of Cape Town, 94pp.

Parker, R.J., 1975. The petrology and origin of some glauconitic and glauco-conglomeratic phosphorites from the South Africa continental margin. *Journal of Sedimentary Petrology*, **45 (1)**, 230-242.

Parker, R.J. and Siesser, W.G., 1972. Petrology and origin of some phosphorites from the South African continental margin. *Journal of Sedimentary Petrology*, **42 (2)**, 434-440.

Partridge, T. C., 1998. Of diamonds, dinosaurs and diastrophism: 150 million years of landscape evolution in southern Africa. *South African Journal of Geology*, **101 (3)**, 167-184.

Partridge, T.C. and Maud, R.R., 1987. Geomorphic evolution of southern Africa since the Mesozoic. *South African Journal of Geology*, **90 (2)**, 179-208.

Partridge, T.C. and Maud, R.R., 2000. Macro-scale geomorphic evolution of southern Africa. *In:* Partridge, T.C. and Maud, R.R. (*eds*). *The Cenozoic of Southern Africa.* Oxford University Press, Inc., New York, pp. 3-18.

Peizhenn, Z., Molnar, P and Downs, W.R., 2001. Increased sedimentation rates and grain sizes 2-4 Myr ago due to the influence of climate change on erosion rates. *Nature*, **410**, 891-897.

Pether, 1994a. *The Sedimentology, Palaeontology and Stratigraphy of Coastal Plain deposits at Hondeklip Bay, Namaqualand, South Africa.* Unpublished MSc thesis, Department of Geological Sciences, University of Cape Town, 313pp.

Pether, J., 1994b. Molluscan evidence for enhanced deglacial advection of Agulhas water in the Benguela current, off southwestern Africa. *Palaeogeography, Palaeoclimatology and Palaeoecology*, **111**, 99-117.

Pether, J., Roberts, D.L. and Ward, J.D., 2000. Deposits of the West Coast. *In:* Partridge, T.C. and Maud, R.R. (*eds*). *The Cenozoic of Southern Africa.* Oxford University Press, Inc., New York, pp. 33-54.

Petroleum Agency SA, 2002. *The Petroleum Agency SA: Poster Display for the AAPG 2002 Conference, Houston, Texas.* http://www.petroleumagencysa.com/aapg2002/images/1.jpg.

University of Cape Town

Pickford, M., 1998. Onland Tertiary marine strata in southwestern Africa: Eustasy, local tectonics and epeirogenesis in a passive continental margin setting. *South African Journal of Science*, **94 (1)**, 5-8.

Pickford, M., 2000. Neogene and Quaternary vertebrate biochronology of the Sperrgebiet and Otavi Mountainland, Namibia. *Communications of the Geological Survey of Namibia*, **12**, 359-365.

Pickford, M. and Senut, B., 1999. Geology and palaeobiology of the central and southern Namib Desert southwestern Africa. *Memoir of the Geological Survey of Namibia*, **18**, 1-155.

Posamentier, H.W. and Vail, P.R., 1988. Eustatic controls on clastic deposition II – sequences and systems tract models. *In*: Wilgus, C.K., Hastings, B.S., Kendall, C.G.St.C., Posamentier, H.W., Ross, C.A. and Van Wagoner, J.C. (*eds*). *Sea-level Changes: An Integrated Approach*, SEPM Special Publication, **42**, 125-154.

Posamentier, H.W., Jervey, M.T. and Vail, P.R., 1988. Eustatic controls on clastic deposition I – conceptual framework. *In*: Wilgus, C.K., Hastings, B.S., Kendall, C.G.St.C., Posamentier, H.W., Ross, C.A. and Van Wagoner, J.C. (*eds*). *Sea-level Changes: An Integrated Approach*, SEPM Special Publication, **42**, 109-124.

Postma, D., 1983. Pyrite and siderite oxidation in swamp sediments. *Journal of Soil Science*, **34 (1)**, 163-182.

Powers, M.C., 1953. A new roundness scale for sedimentary particles. *Journal of Sedimentary Petrology*, **23**, 117-119.

Préat, A., Mamet, B., De Ridder, C., Boulvain, F. and Gillan, D., 2000. Iron bacterial and fungal mats, Bajocian stratotype (Mid-Jurassic, northern Normandy, France), Sedimentary Geology, 137 (3-4), 107-126

Puig, P., Ogston, A.S., Mullenbach, B.L., Nittrouer, C.A and Sternberg, R.W., 2003. Shelf-to-canyon sediment-transport processes on the Eel continental margin (southern California). *Marine Geology*, **193**, 129-149.

Pye, K., 1983. Red Beds. *In:* Goudie, A.S. and Pye. K. (*eds*). *Chemical Sediments and Geomorphology: Precipitates and Residua in the Near-Surface Environment.* Academic Press Inc., London, pp. 227-263.

Pye, K. and Mazzullo, J., 1994. Effects of tropical weathering on quartz grain shape: An example from northeastern Australia. *Journal of Sedimentary Research*, **A64 (3)**, 500-507.

Quilty, P.G., 1977. Cenozoic sedimentation cycles in Western Australia. *Geology*, **5**, 336-340.

Raab, M.J., Brown, R.W., Gallagher, K., Carter, A. and Weber, K., 2002. Late Cretaceous reactivation of major crustal shear zones in northern Namibia: constraints from apatite fission track analysis. *Tectonophysics*, **349**, 75-92.

Rack, F.R., 1993. A geologic perspective on the Miocene evolution of the Antarctic Circumpolar Current system. *Tectonophysics*, **222** (3-4), 397-415.

Raiswell, R. and Berner, R.A., 1985. Pyrite formation in euxinic and semi-euxinic conditions. *American Journal of Science*, **285**, 710-724.

Ramsay, P.J. and Cooper, J.A., 2002. Late Quaternary sea-level change in South Africa. *Quaternary Research*, **57**, 82-90.

Rao, V.P., Lamboy, M. and Dupeuble, P.A., 1993. Verdine and other associated (glaucony, phosphate) facies from surficial sediments of the southwestern continental margin of India. *Marine Geology*, **111**, 133-158.

Rau, A.J., 2002. *A Late Quaternary History of Agulhas-Benguela Interactions from Two Sediment Cores on the Western Continental Slope of South Africa.* Unpublished PhD thesis, Department of Geological Sciences, University of Cape Town, South Africa, 190pp.

Rau, A.J., Rogers, J., Lutjeharms, J.R.E, Giraudeau, J., Lee-Thorp, J.A., Chen, M-T. and Waelbroeck, C., 2002. A 450-kyr record of hydrological conditions on the western Agulhas Bank Slope, south of Africa, *Marine Geology*, **180**, 183-201

Roberts, D.L. and Brink, J.S., 2002. Dating and correlation of Neogene coastal deposits in the Western Cape (South Africa): Implications for neotectonism. *South African Journal of Geology*, **105**, 337-352.

Rogers, J., 1977. Sedimentation on the continental margin of the Orange River and the Namib Desert. *Bulletin of the Joint Geological Survey/University of Cape Town Marine Geoscience Group*, **7**, 1-162.

Rogers, J., 1980. First report on the Cenozoic sediments between Cape Town and Elands Bay: *Open-file Report Geological Survey of South Africa*, 1-136pp.

Rogers, J., 1982. Lithostratigraphy of Cenozoic sediments between Cape Town and Eland's Bay. *Palaeoecology of Africa*, **15**, 121-137.

Rogers, J. and Bremner, J.M. 1991. The Benguela Ecosystem. Part VII. Marine-Geological Aspects. *Oceanography and Marine Biology: An Annual Review*, **29**, 1-85.

Rogers, J. and Li, X.C., 2002. Environmental impact of diamond mining on continental shelf sediments off southern Namibia. *Quaternary International*, **92 (1)**, 101-112.

Rogers, J., Pether, J., Molyneux, R., Genis, J., Kilham, J.L.V., Cooper, G. and Corbett, I.B., 1990. Cenozoic geology and mineral deposits along the west coast of southern Africa and the Sperrgebiet. *Guidebook Geocongress '90 Geological Society of South Africa*, PR1: 1-111.

University of Cape Town

Rossetti, D.F., 2001. Late Cenozoic sedimentary evolution in northeastern Pará, Brazil, within the context of sea-level changes. *Journal of South American Earth Sciences*, **14**, 77-89.

Rozendaal, A., Gresse, P.G., Scheepers, R, and Le Roux, J.P., 1999. Neoproterozoic to Early Cambrian Crustal Evolution of the Pan-African Saldania Belt, South Africa. *Precambrian Research*, **97**, 303-323.

Rust D.J. and Summerfield, M.A., 1990. Isopach and borehole data as indicators of rifted margin evolution in southwestern Africa. *Marine and Petroleum Geology*, 7, 277-287.

SACS, 2002. http://www.geoscience.org.za/sacs/newlith.htm

Sarkar, A., Sarangi, S., Ebihara, Bhattacharya, S.K. and Ray, A.K., 2003. Carbonate geochemistry across the Eocene/Oligocene boundary of Kutch, western India: implications to oceanic O_2-poor condition and foraminiferal extinction. *Chemical Geology*, **201**, 281-293.

Sancetta, C., Heusser, L. and Hall, M.A., 1992. Late Pliocene climate in the Southeast Atlantic: Preliminary results from a multi-disciplinary study of DSDP Site 532, *Marine Micropaleontology*, **20**, 59-75.

Sarg, J.F., 1988. Carbonate sequence stratigraphy. *In*: Wilgus, C.K., Hastings, B.S., Kendall, C.G.St.C., Posamentier, H.W., Ross, C.A. and Van Wagoner, J.C. *(eds). Sea-level Changes: An Integrated Approach*, SEPM Special Publication, **42**, 155-181.

Scasso, R.A. and Castro, L.N., 1999. Cenozoic phosphatic deposits in North Patagonia, Argentina: Phosphogenesis, sequence-stratigraphy and paleoceanography. *Journal of South American Earth Sciences*, **12 (5)**, 471-487.

Scheepers, R., 1995. Geology, geochemistry and petrogenesis of Late-Precambrian S-, I- and A-type granitoids in the Saldania belt, Western Cape Province, South Africa. *Journal of African Earth Sciences*, **21 (1)**, 35-58.

Schlager, W., 1993. Accommodation and supply - a dual control on stratigraphic sequences. *Sedimentary Geology*, **86 (1-2)**, 111-136.

Scholtz, A., 1985. The palynology of the upper lacustrine sediments of the Arnot Pipe, Banke, Namaqualand. *Annals of the South African Museum*, **95 (1)**, 1-109.

Schulz, M.S. and White, A.F., 1999. Chemical weathering in a tropical watershed, Luquillo Mountains, Puerto Rico III: Quartz dissolution rates. *Geochemica et Cosmochemica Acta*, **63 (3/4)**, 337-350.

Scrutton, R.A. and Dingle, R.V., 1976. Observations on the processes of the sedimentary basin formation at the margins of southern Africa. *Tectonophysics*, **36**, 143-156.

Senut, B., Pickford, M., Ward, J., De Wit, M. Spaggiari, R. and Morales, J., 1996. Biochronology of the Cainozoic sediments at Bosluis Pan, Northern Cape Province, South Africa. *South African Journal of Science*, **92 (5)**, 249-251.

Shackleton, N. and Kennett, J., 1975. Paleotemperature history of the Cenozoic and the initiation of Antarctic glaciation: Oxygen and carbon isotope analyses in DSDP Sites 277, 279 and 281. *In*: *Initial reports of the Deep Sea Drilling Project*, **29**, 743-755.

Shanmugam, G., 2002. Ten turbidite myths. *Earth-Science Reviews*, **58**, 311-341.

Shanmugam, G., 2003. Deep-marine tidal bottom currents and their reworked sands in modern and ancient submarine canyons. *Marine and Petroleum Geology*, **20 (5)**, 471-491.

Shannon, L.V., 1985. The Benguela Ecosystem Part 1. Evolution of the Benguela, physical features and processes. *Oceanography and Marine Biology: An annual review*, **23**, 105-182.

Shannon, L.V. and Nelson, G., 1996. The Benguela: Large scale features and processes and system variability. *In:* Wefer, G., Berger, W.H., Siedler, G. and Webb, D.J. *(eds). The South Atlantic: Present and Past Circulation.* Springer-Verlag, Berlin Heidelberg, pp. 163-210.

Shields, G. and Stille, P., 2001. Diagenetic constraints on the use of cerium anomalies as palaeoseawater redox proxies: an isotopic and REE study of Cambrian phosphorites. *Chemical Geology*, **175**, 29-48.

Shipbboard Scientific Party, 1998a. Site 1085. *In*: Wefer, G., Berger, W.H. and Richter, C., *et al.*, (*eds*). *Proceedings of the Ocean Drilling Program, Initial Reports*, **175**, pp. 385-428.

Shipbboard Scientific Party, 1998b. Site 1086. *In*: Wefer, G., Berger, W.H. and Richter, C., *et al.*, (*eds*). *Proceedings of the Ocean Drilling Program, Initial Reports*, **175**, pp. 429-457.

Shipbboard Scientific Party, 1998c. Site 1087. *In*: Wefer, G., Berger, W.H. and Richter, C., *et al.*, (*eds*). *Proceedings of the Ocean Drilling Program, Initial Reports*, **175**, pp. 457-484.

Siesser, W.G., 1971. *Petrology of Some South African Coastal and Offshore Carbonate Rocks and Sediments.* Unpublished PhD thesis, Department of Geological Sciences, University of Cape Town, South Africa, 232pp.

Siesser, W.G., 1972. Limestone lithofacies from the South African continental margin. *Sedimentary Geology*, **8**, 83-112.

Siesser, W.G., 1976. Calcareous nannofossils in Pleistocene sediment cores from the South African continental slope. *Transactions Royal Society of South Africa*, **42 (2)**, 107-147.

University of Cape Town

Siesser, W.G., 1978a. Leg 40 results in relation to continental shelf and onshore geology. *In:* Bolli, H.M., Ryan, W.B., *et al.* (*eds*). *Initial Reports, Deep Sea Drilling Project,* **40**, 965-980.

Siesser, W.G., 1978b. Aridification of the Namib Desert: Evidence from oceanic cores. *In:* Van Zinderen Bakker. (*ed*). *Antarctic Glacial History and World Palaeoenvironments,* Balkema, Rotterdam, pp. 105-113.

Siesser, W.G., 1980. Late Miocene origin of the Benguela upwelling system, *Science*, **208**, 283-285.

Siesser, W.G. and Dingle, R.V., 1981. Tertiary sea-level movements around southern Africa. *Journal of Geology*, **89**, 83-96.

Siesser, W.G. and Rogers, J., 1976. Authigenic pyrite and gypsum in South West African continental slope sediments. *Sedimentology*, **23**, 567-577.

Siesser, W.G., Scrutton, R.A., and Simpson. E.S.W., 1974. Atlantic and Indian Ocean margins of southern Africa. *In:* Burk, C.A. and Drake, C.L., (*eds*). *The Geology of Continental Margins.* Springer-Verlag New York, pp. 641-654.

Simpson, E.S.W and Forder, E., 1968. The Cape Submarine Canyon. *Fisheries Bulletin, South Africa,* **5**, 35-38.

Smith, R.A. and Mason, T., 2002. *Sedimentary Environments and Trace Fossils of Tertiary Oasis Deposits in the Central Namib Desert, Namibia.* Abstract. 16th International Sedimentological Congress, Rand Afrikaans University, Johannesburg, South Africa, 338-339.

SOEKOR, 1994. *Orange Basin*, Republic of South Africa Licensing Round Information Brochure.

SOEKOR, 1996. *Major Offshore petroleum exploration opportunities, South Africa.*

South African Committee for Stratigraphy (SACS, 1980). Stratigraphy of South Africa. Part 1 (Comp. L.E. Kent). Lithostratigraphy of the Republic of South Africa, South West Africa/Namibia and the Republics of Bophuthatswana, Transkei and Venda: *Handbook of the Geological Survey of South Africa*, **8**, 1-690.

Spezzaferri, S., McKenzie, J.A. and Isern, A., 2002. Linking the oxygen isotope record of late Neogene eustasy to sequence stratigraphic patterns along the Bahamas margin: results from a paleoceanographic study of ODP Leg 166, Site 1006 sediments. *Marine Geology*, **185 (1-2)**, 95-120.

Spönemann, J. and Hagedorn, J., 2000. Morphotektonik im südwestlichen Afrika zwischen Heidelberg und Lüderitz. *Göttinger Geographische Abhandlungen*, **107**, 1-112.

Stevenson, I., 1992. *A Detailed Seismic Stratigraphic Approach to Interpreting High-Resolution, Shallow-Seismic Data from the Middle Shelf off Southern Namaqualand.* Unpublished Honours Project, Department of Geological Sciences, University of Cape Town, 93pp.

Stevenson, I. and Bamford, M.K., 2002. A submerged Late Cretaceous podocarpaceous forest, west coast, South Africa. *South African Journal of Science*, **98**, 181-185.

Stevenson, I. and McMillan, I.K., *in press*. Cretaceous incised valley fills of the Namaqualand coast. *Journal of the Geological Society of London.*

Stille, P. and Clauer, N., 1994. The process of glauconitization: chemical and isotopic evidence. *Contributions to Mineralogy and Petrology,* **117**, 253-262.

Sugarman, P.J. and Miller, K.G., 1997. Correlation of Miocene sequences and hydrogeologic units, New Jersey Coastal Plain. *Sedimentary Geology*, **108**, 3-18.

Tankard, A.J., 1974. Petrology and origin of the phosphorite and aluminium phosphate rock of the Langebaanweg-Saldanha area, south-western Cape Province. *Annals of the South African Museum,* **65 (8)**, 217-249.

Tankard, A.J., 1975. The marine Neogene Saldanha Formation. *Transactions of the Geological Society of South Africa*, **78**, 257-264.

Tankard, A.J., 1976. Pleistocene history and coastal morphology of the Ysterfontein-Elands Bay area, Cape Province. *Annals of the South African Museum,* **69 (5)**, 73-119.

Tankard, A.J and Rogers, J., 1978. Late Cenozoic palaeoenvironments on the west coast of Southern Africa. *Journal of Biogeography*, **5**, 319-337.

Taylor, S.R. and McLennan, S.M., 1985. *The Continental Crust, Its Composition and Evolution.* Blackwell, London, 312pp.

Taylor, P. D. and Wilson, M.A., 2003. Palaeoecology and evolution of marine hard substrate communities. *Earth-Science Reviews*, **62**, 1-103.

Theron, J.N., Gresse, P.G., Siegfried, H.P. and Rogers, J., 1992. *The Geology of the Cape Town Area. Explanation: Sheet 3318 (1:250 000 scale).* Geological Survey of South Africa, 140pp.

Thomas, R. J., De Beer, C. H. and Bowring, S. A., 1996. A comparative study of the Mesoproterozoic late orogenic porphyritic granitoids of southwest Namaqualand and Natal, South Africa. *Journal of African Earth Sciences,* **23(3)**, 485-508.

University of Cape Town

Tönsing, T., Malan, J. and Young, P., 2002. *A Confined Slump Feature in the Upper Aptian Third Order 13A Sequence, Bredasdorp Basin, Offshore South Africa.* Abstract. 16th International Sedimentological Congress, Rand Afrikaans University, Johannesburg, South Africa, 34-36.

Turner, P., 1980. *Developments in Sedimentology, 29: Continental Red Beds*, Elsevier Scientific Publishing Company, The Netherlands, 562pp.

Tyson, P.D. and Partridge, T.C., 2000. Evolution of Cenozoic climates. *In*: Partridge, T.C. and Maud, R.R. (*eds*). *The Cenozoic of Southern Africa*. Oxford University Press, Inc., New York, pp. 371-387.

Uenzelmann-Neben, G., Spiess, V. and Miller, H., 2002. *Cenozoic Development of the Sedimentation in the Orange Fan Area, Southeast Atlantic.* Final report for DFG research grant Ue 49/4 within priority program "Ocean Drilling Program/Deep Sea Drilling Project", AWI, Bremerhaven, 31pp.

Vail, P.R., Mitchum, R.M., Todd, R.G., Widmier, J.M., Thompson, S., Sangree, J.B., Bubb, J.N. and Hatlelid, W.G., 1977. Seismic stratigraphy and global changes of sea level. *In*: Payton, C.E. (*ed*). Seismic Stratigraphy: applications to Hydrocarbon Exploration. *Memoir of the American Association of Petroleum Geologists*. **26**, pp. 49-212.

Van der Wateren, F.W. and Dunai, T.J., 2001. Late Neogene passive margin denudation history-cosmogenic isotope measurements from the central Namib Desert. *Global and Planetary Change*, **30**, 271-307.

Van Wagoner, J.C., Posamentier, H.W., Mitchum, R.M., Vail, P.R., Sarg, J.F., Loutit, T.S. and Hardenbol, J., 1988. An overview of the fundamentals of sequence stratigraphy and key definitions. *In*: Wilgus, C.K., Hastings, B.S., Kendall, C.G.St.C., Posamentier, H.W., Ross, C.A.

Van Zinderen Bakker, E.M., 1984. Aridity along the Namibian coast. *Palaeoecology Africa*, **16**, 149-160.

Vidal, L., Bickert, T., Wefer, G. and Röhl, U., 2002. Late Miocene stable isotope stratigraphy of SE Atlantic ODP Site 1085: Relation to Messinian events. *Marine Geology*, **180**, 71-85.

Wåhlin, A.K., 2002. Topographic steering of dense currents with application to submarine canyons. *Deep Sea Research Part I: Oceanographic Research Papers*, **49**, 305-320.

Wåhlin, A.K., 2004. Downward channelling of dense water in topographic corrugations. *Deep Sea Research Part I: Oceanographic Research Papers*, **51 (4)**, 577-590.

Ward, J.D. and Corbett, I., 1990. Towards an age for the Namib. *In:* Seely, M. (*ed*). Namib ecology: 25 years of Namib research. *Transvaal Museum Monograph*, **7**, 17-26.

Watkins, R.T., Nathan, Y. and Bremner, J.M., 1995. Rare earth elements in phosphorite and associated sediment from the Namibian and South African continental shelves. *Marine Geology*, **129**, 111-128.

Wefer, G., Berger, W.H. and Richter, C., *et al.*, 1998. Introduction: Background, scientific objectives, and principal results for Leg 175 (Benguela Current and Angola-Benguela upwelling Systems). *Proceedings of the Ocean Drilling Program, Initial Reports*, **175**, 7-23.

Wickens, H. de V. and McLachlan, I.R., 1990. The stratigraphy and sedimentology of the reservoir interval of the Kudu 9A-2 and 9A-3 boreholes. *Communications of the Geological Survey, Namibia,* **6**, 9-22.

Williamson, M.D. and Stevenson, I.R., 1999. *A Seismic Stratigraphic Investigation of a Quaternary-aged Forced Regressive Wedge of Orange River Origin.* Abstract. International Geological Correlation Programme Project No. 396, 4th annual conference 'Continental shelves in the Quaternary", Cape Town, South Africa, 42.

Woodborne, M.A.W., Rogers, J. and Jarman, N., 1989. On the role of kelp in the transportation of cobbles and boulders along the south west coast of South Africa. *Geo-Marine Letters*, **9 (2)**, 109-118.

Zachos, J., Pagani, M., Sloan, L., Thomas, E. and Billups, K., 2001. Trends, rhythms, and aberrations in global climate 65 Ma to Present. *Science*, **292**, 686-693.

University of Cape Town

APPENDIX 1 – CORE LOGS

PAGES

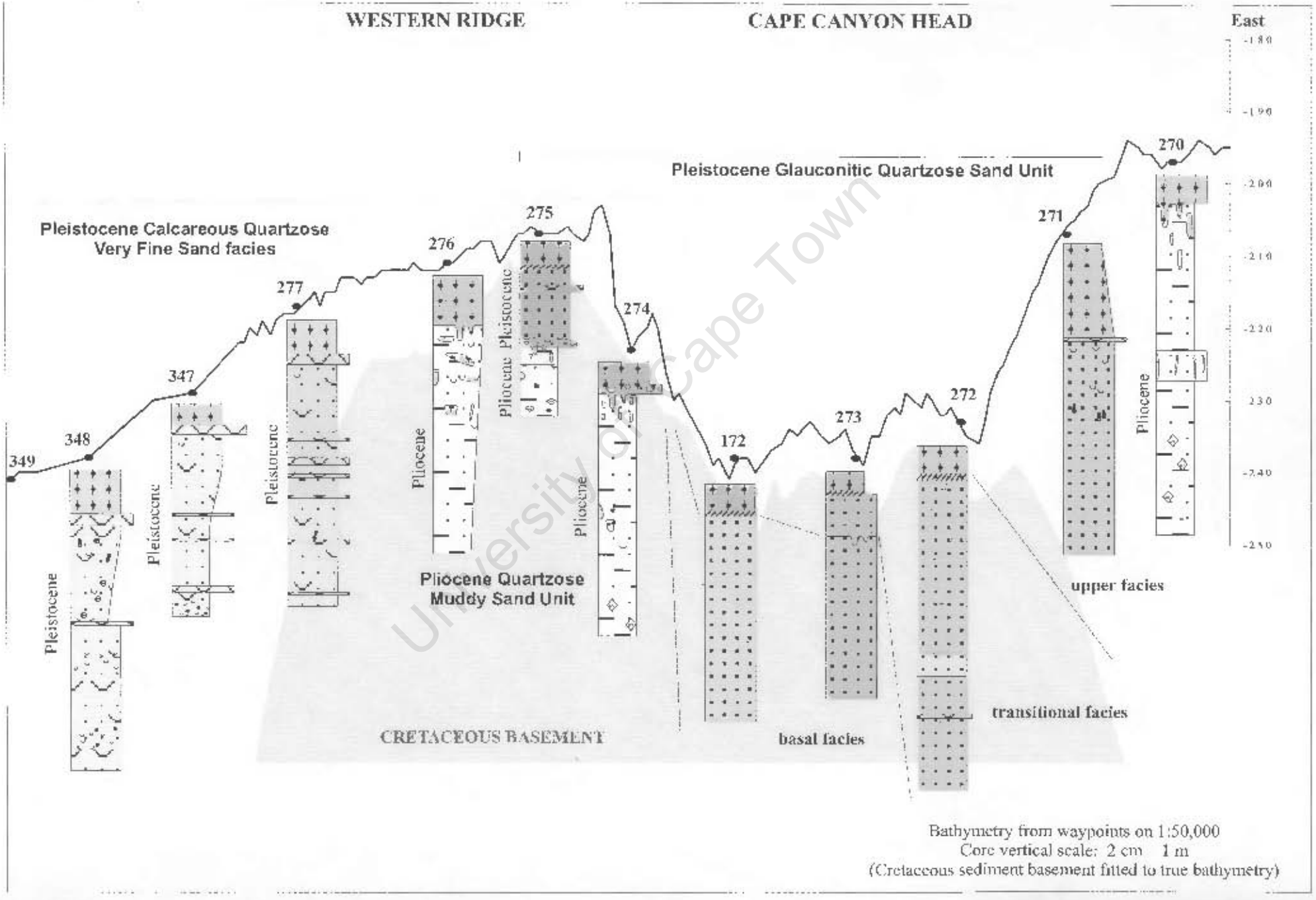
Northern Transect cross-section A1-2
Log for cores 270, 271, 272, 273, 172, 274, 275, 276, 277, 347, 348 ..... A1-3 to A1-13

Central Transect cross-section A1-14
Logs for cores 16, 106, 69, 107, 108, 109, 110, 111, 112, 113, 114,
115,116, 118, 119, 120, 122, 123, 125, 126, 128, 129 ..... A1-15-A1-29

Southern Transect cross-section A1-30
Logs for cores 175, 177, 178A, 179, 190, 186, 187 ..... A1-31-A1-37

Log for Cores 159 ..... A1-38
Log for Cores 324 ..... A1-39

University of Cape Town

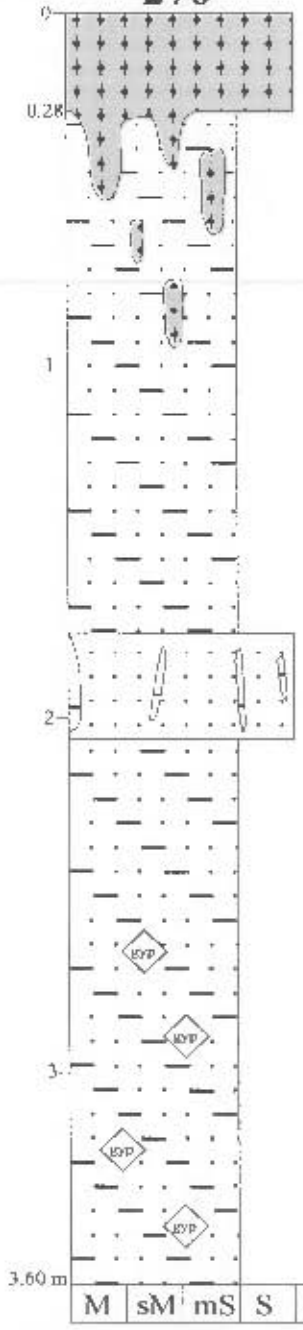


University of Cape Town

270

Holocene

Pliocene



M | sM | mS | S | gS | sG | G

-1: 7-12 cm: Moderately well to well sorted, fine to medium sand
M: 7.2% S: 92.5% G: 0.3% $CaCO_3$: 7.1%
Gravel: <fP PCL & Bv-ShF with well md to ang qz & PCG granules
XRD: qz-cc-mica-kaol-feldspar (plag>>K'spar) + 14Å smectite peak

-2: 23-30 cm: Moderately well to well sorted, fine to medium sand
M: 7.2% S: 92.6% G: 0.2% $CaCO_3$: 6.3%
Gravel: well md to ang Qz & PCG granules & minor ShF

-3: 44-50 cm: Well sorted, muddy very fine sand
M: 45.2% S: 54.78% G: 0% $CaCO_3$: 1.7%
Sand: Dominated by <125 µm angular quartz (including trace red-stained grains) with trace glc, bF and SSp.
XRD: qz-cc-mica-kaol-plag + 14Å smectite peak
Sample collected in upper upper bioturbated interval - contaminated by recent material, including mollusc (?N. bicuspidata) ShF.

-4: 106-113 cm: Very well sorted, muddy very fine sand
M: 46.8% S: 53.2% G: 0% $CaCO_3$: 1.8%
Sand: Dominated by <125 µm angular quartz (including trace red-stained grains) with a minor >125 µm fraction composed of 70% qz, 15% glc & 15% SkF (py-SSp, EchS, bF - poorly preserved *Epistomella pulchella; Frondicularia* sp.)
XRD: qz-cc-mica-kaol-plag + 14Å smectite peak
Predominantly Pliocene sp. (I. McMillan)

28-360 cm: Very well sorted, muddy very fine sand
$CaCO_3$: <2.7%
Light olive grey (5YR 6/2)

184-218 cm: Clean sand with sub-vertical muddy lamellae (bioturbation/rip-up clasts)

-5: 252-261 cm: Very well sorted, muddy very fine sand
M: 36.9% S:63.1% G: 0% $CaCO_3$: 2.0%
Sand: Dominated by <125 µm angular quartz (including trace red-stained grains) with a minor >125 µm fraction composed of qz, glc & SkF (SSp, bF - poorly preserved *Epistomella pulchella;* aggl-bF sp., *Sphaeroidina bulloides*)
XRD: qz-cc-mica-kaol-plag + 14Å smectite peak
Miocene & Pliocene foraminiferal assemblage (I. McMillan)
Dessicated - sampled between two natural horizontal desiccation cracks.

-6: 320-331 cm: Very well sorted, muddy very fine sand
M: 38.2% S: 61.8% G 0% $CaCO_3$: 2.7%
Sand: Dominated by <125 µm angular quartz (including trace red-stained grains) with a minor >125 µm fraction composed of 25% gypsum aggregates, 25% qz, 25% glc, 25% SkF (py-Ssp, EchS, bF - mixed Miocene>Pliocene assemblage) & trace SPG.
XRD: qz-cc-mica-kaol-plag + 14Å smectite peak
Miocene dominant & Pliocene foraminiferal assemblage (I. McMillan)
Last ~40 cm very dry with desiccation cracks. Sampled a single piece (⅔ width of core) between three desiccation cracks.

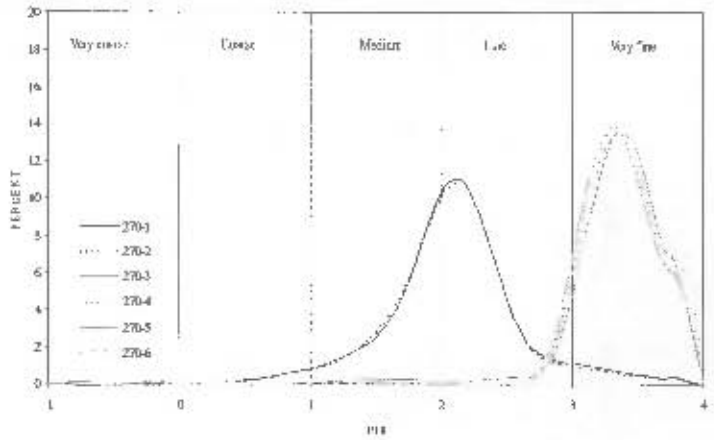
Extra material collected later as bulk reserve sample

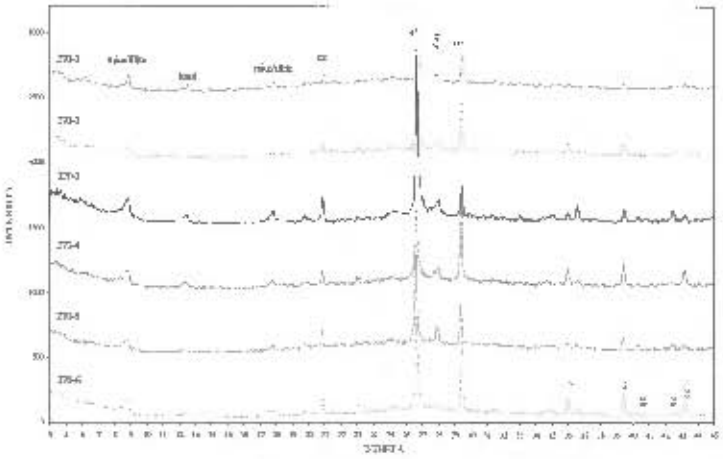
Foraminiferal assemblage

270-4:
Neogloboquadrina pachyderma, Angulogerina sp., *Hanzawaia* sp., *Globocassidulina* sp., *?Nodogenerina* sp., *Cibicidoides* spp., *Oolina* sp., thin elongate *Bolivina* sp., *Bolivina* spp., *Nodosaria* cf. *longiscata*, tiny *Sphaeroidina bulloides*, spiny *Lenticulina* sp., *Lenticulina* spp., *Marginulina/Vaginulina* sp., *Frondicularia* sp., *Epistominella pulchella, Uvigerina* spp., *Nuttallides* sp., *Pullenia subcarinata, Astrononion* sp.

270-5:
Frondicularia sp., *Dentalina* spp., spiny *Uvigerina* sp., *Cibicidoides* sp., *Epistominella pulchella, Lenticulina* spp., fat *Spiroplectinella* sp., *Amphicoryna* sp., *?Nodogenerina* sp. or *? Enantiodentalina* sp., *Pullenia subcarinata, Hanzawaia* sp., *Globulina* sp., *Karreriella* cf. *bradyi* (aggl-bF), *Sphaeroidina bulloides, Gyroidinoides* cf. *soldanii, Cancris* cf. *auriculus.*

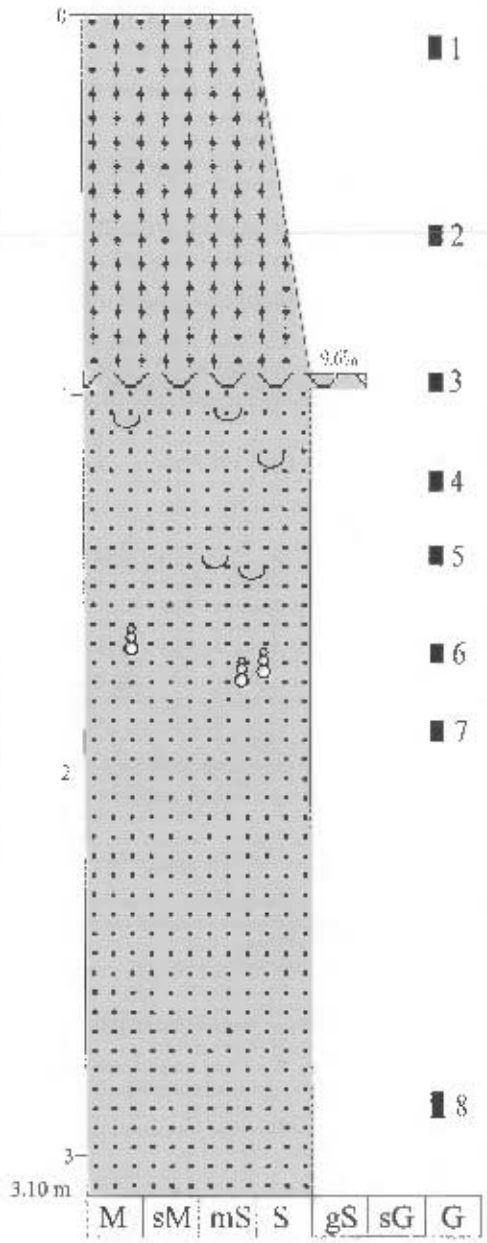
270-6:
Dentalina spp., spiny *Uvigerina* spp., *Cibicidoides* spp., *Epistominella pulchella, Lenticulina* spp., *Sphaeroidina bulloides, Marginulina/Vaginulina* sp., *Amphicoryna* sp.





University of Cape Town

271



-1: 5-11 cm: Moderately well sorted muddy fine sand [58.9% qz : 41.1% glc]
M: 12.4% S: 87.6% G: 0% $CaCO_3$: 5.8%
Sand: 10% Faecal mud (trace pellets); 50% qz; 37% glc, 3% SkF (includes robust Holocene sp., trace SSP and EchS)
XRD: qz-cc-mica-kaol-feldspar (plag>>K'spar)-(pyr)

Samples -1 &-2 include reworked Pleistocene sediments (from foraminiferal assemblage)

-2: 55-60 cm: (Well sorted) Sand
M: 8% S: 92% G: 0% $CaCO_3$: 5.1%
Sand: 60% qz; 37% glc, 3% SkF (includes robust Holocene sp., trace SSP and EchS)
XRD: qz-cc-arag-mica-kaol-feldspar (plag>>K'spar)-(pyr)
61.4% qz : 38.6% glc
Small pyrite peak may be included in arag 2.7 Å peak - with 2nd pyrite small peak between plag & cc at 3.1Å.

-3: 95-100 cm: Gravelly sand, includes shell-rich layer from 95-97 cm.
M: 5.2% S:85.2% G 9.6% $CaCO_3$: 10.6%
Gravel: <cP *T. declivis* (well to poorly preserved) and *A. bulloides* ShF with Bv-ShF, including *L. chuni*, *Hiatella* sp., *Cardiella* sp. and ?*M. pisum*.
Sand: 60% qz, 30% glc, 10% SkF (1% EchS, 3-4% Bv-ShF, diverse bF+pF, Ost & HS)
XRD: qz-cc-mica-kaol-feldspar (plag~K'spar)-(arag-pyr)

-4: 120-125cm: Well to moderately well sorted fine to medium sand [59.7% qz : 40.3% glc]
M: 4.8% S: 94.8% G: 0.4% $CaCO_3$: 8.3%
Gravel: vfP ShF, including *L. chuni*, *Hiatella* sp., *Cardiella* sp., EchS and other Bv-ShF.
Sand: 60% qz, 30% glc, 10% SkF (1% EchS, 2% Bv-ShF, diverse bF+pF, Ost & HS). Single jasper grain and 2 mid lithic fragments. (Qz & glc: see -7)
XRD: qz-cc-mica-kaol-feldspar (plag only)-(arag) No pyrite

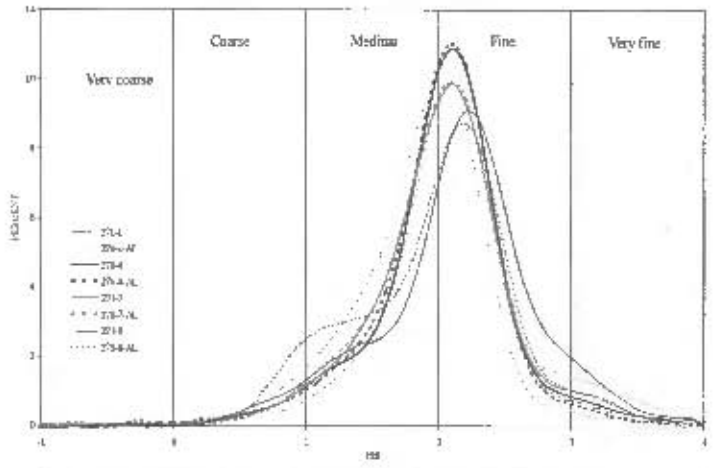
-5: 140-145 cm: Slightly gravelly sand
M: 5.7% S: 91% G: 3.3% $CaCO_3$: 6.6%
Gravel: cP very worn *T. philomela*
Sand: 55% qz, 40% glc, 5% SkF (1% EchS, 2% ShF, diverse bF+pF, Ost & HS)
Qz & Glc: see -7
XRD: qz-cc-mica-kaol-feldspar (plag>>K'spar)-(arag-pyr)

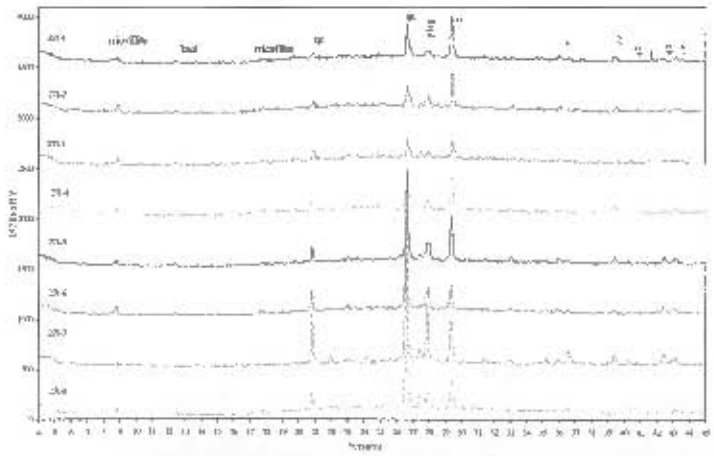
-6: 165-170 cm: Fine to medium Sand
M: 6.3% S: 93.3% G: 0.4% $CaCO_3$: 9.5%
Gravel: vfP G-ShF
Sand: See -7
XRD: qz-cc-mica-kaol-feldspar (plag >>K'spar)-(arag-pyr)

-7: 186-191 cm: Moderately well to well sorted fine to medium slightly gravelly sand
M: 4.8% S: 93.6% G: 1.6% $CaCO_3$: 9.2%
Gravel: cP *Volutocorbis* sp (cf. *abyssicola*) and other ShF.
Sand: 55% qz, 40% glc, 5% SkF (1% EchS, 2% ShF, dec in diverse compared to -6 with pF (*G. bulloides*, *G. inflata*) & Ost)
Qz: f-mS with minor cS component. Qz varies from md to ang & clear, polished to frosted or milky. Glc surface-coating common. Trace red-stained qz present.
Glc: blk polished labels f-mS
XRD: qz-cc-mica-feldspar (plag > K'spar)-(arag)-(mica)-trace kaol

-8: 288-295 cm: Moderately well sorted medium sand (bimodal with a minor medium to coarse fraction) [65.8% qz : 34.2% glc]
M: 5.3% S: 94.7% G: 0% $CaCO_3$: 13.5%
Sand: 60% qz, 30% glc, 10% SkF (1% EchS, 2% ShF, diverse bF+pF (*G. bulloides*, *G. inflata*), Ost & HS)
Qz: f-mS with cS component. Qz varies from md to ang & clear & polished to frosted or milky. Glc surface-coating common.
XRD: qz-cc-mica-kaol-feldspar (plag – K'spar)

271-1: Leaching improves sorting
271-4, -7 & -8: No differences due to leaching



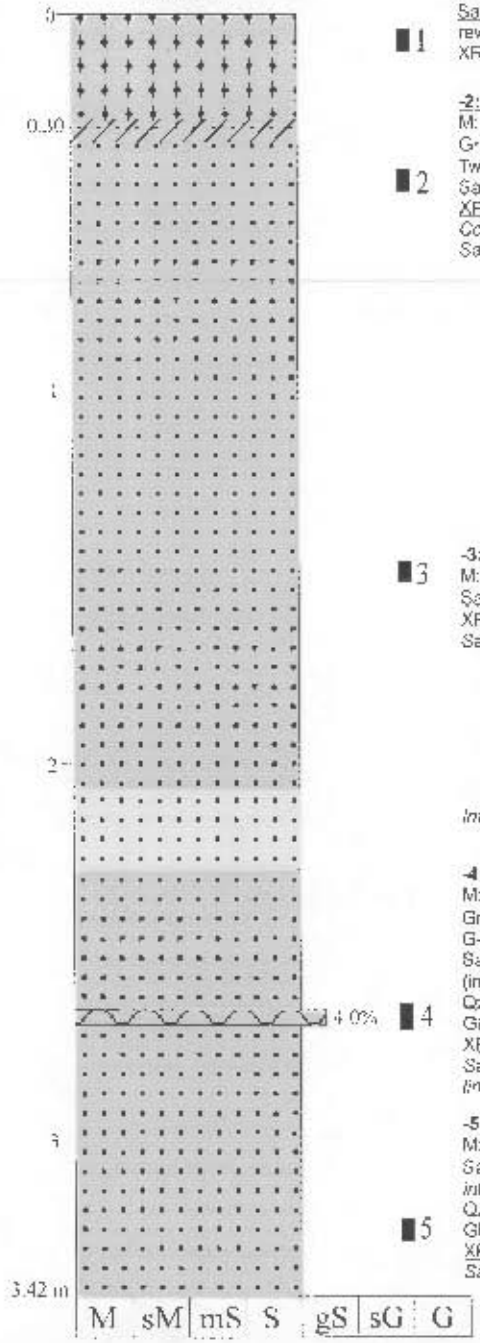


University of Cape Town

272

Holocene

Pleistocene



■1 -1: 6-12 cm: Sanc [46.2% qz, 53.8: glc]
M: 8.7% S: 91.3% G: 0% $CaCO_3$: 6.6%
Sand: 40% qz; 40% glc; 15% faecal mud & 5% SkF. No SSp observed. Qz mud-stained and an increase in reworked Ph component, including polished vcS PCG and SPG present.
XRD: mica-kaol-qz-cc-feldspar (plag~K'spar)

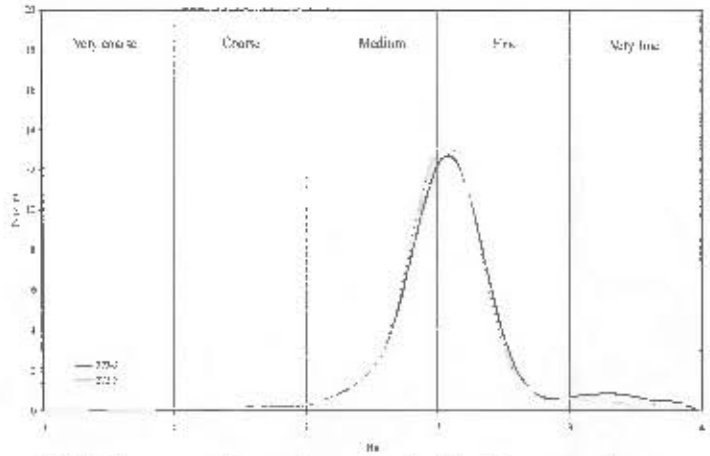
■2 -2: 45-51 cm: Well sorted, fine to medium sand with a small very fine sand population
M: 4.3% S: 95.6% G: 0.1% $CaCO_3$: 6.0%
Gravel: <1P *N. vinctus*, *Polinices* sp., juvenile *Arcella mamoata*, *M. pisum*, scaphopods, otoliths & other ShF
Two qz granules.
Sand: 50% qz, 45% glc, 5% SkF (1-2% SlF; 1% EchS & 1-2% F (increased biodiversity similar to -4)
XRD: mica-kaol-qz-cc-arag-feldspar (plag~K'spar)
Collected from with shell rich upper 1 m, but below obvious presence of Holocene material.
Sample sandy and unconsolidated.

■3 -3: 150-155 cm: Sand
M: 6.0% S: 94.0% G: 0% $CaCO_3$: 5.0%
Sanc: See -5.
XRD: mica-kaol-qz-cc-arag-feldspar (plag>K'spar)
Sample dry and cemented.

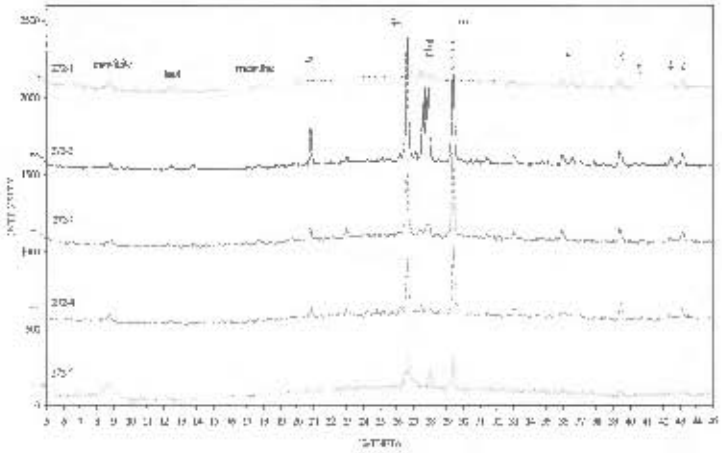
Interval of (wispy) burrowed clean quartz-rich sand

■4 -4: 263-270 cm: Slightly gravelly sand
M: 3.7% S: 92.3% G: 4.0% $CaCO_3$: 6.8%
Gravel: <mP worn *A. bulloides*, *N. vinctus* and brachiopod (cf. *Terebratulina abbysicola*) and other G-ShF.
Sand: 47% qz; 47% glc; 5-6% SkF (2% Bv- & G-SlF, 1% EchS; 2-3% moderate biodiversity (increased biodiversity & bF compared to -5; includes large *Marginulina* sp.).
Qz: slightly less well sorted, f-mS with trace red-stained grains and minor nS.
Glc: fragmented green to black polished grains.
XRD: mica-kaol-qz-cc-arag-feldspar (plag~K'spar)
Sample taken from shell rich layer. Difficult to sample and some shells taken from adjacent to core liner.

■5 -5: 328-334 cm: Well to very well sorted, fine to medium to coarse sand
M: 5.2% S: 94.8% G: 0% $CaCO_3$: 5.0%
Sand: 49% qz, 49% glc; 1-2% F (moderate biodiversity, includes *Bulimina* sp., *G. bulloides*, *G. inflata*, ?*G. laevigata*) and trace EchS
Qz: f-mS with trace red-stained grains
Glc: fragmented green to black polished grains
XRD: mica-qz-cc-felspar (plag only) NOTE: very low intensity peaks except for 10 Å mica peak.
Sample dry and cemented



*NOTE. Decrease in Mica peak upcore and low Kaolinite concentrations



S-IV

University of Cape Town

273

Holocene

Pleistocene

0

0.22

0.45

1

2

2.25 m

M | sM | mS | S | gS | sG | G

■1 -1: 3-7 cm: Recent muddy sand [37.2% qz: 62.8: glc]
M: 12.2% S: 87.7% G: 0.1% $CaCO_3$: 0.4%
Gravel: soft worm tubes with PCG & ShF granules
Sand: 50% glc, 36% qz, 10% Faecal mud & 4% SkF (SSp; robust Holocene pF sp. & reworked Pleistocene pF+bF)
XRD: mica-kaol-qz-cc-feldspar (plag>K'spar)

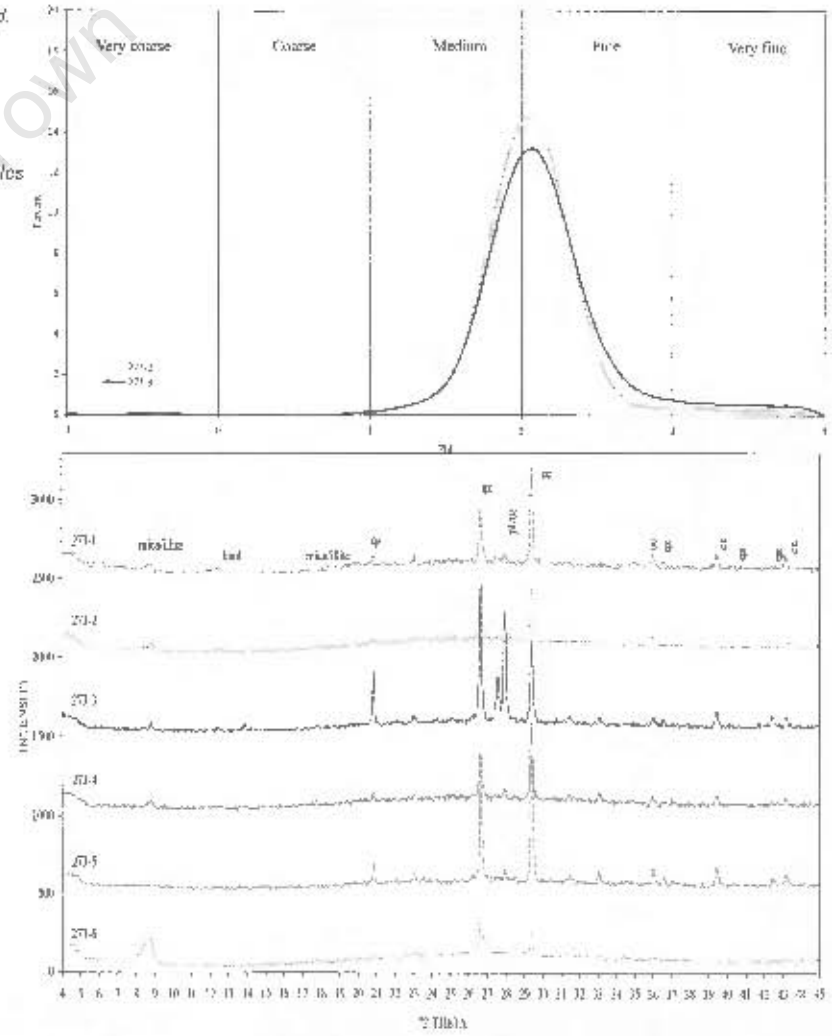
■2 -2: 26-29 cm: Sand [41.5% qz : 58.5% glc]
M: 3.3.0% S: 96.7% G: 0% $CaCO_3$: 5.9%
Sand: 43% qz, 53% glc; 3-4% SkF (Pleistocene pF (*G. bulloides* dominant with *N. pachyderma* present)>bF (slight decrease in biodiversity upcore); Ost & HS) & trace EchS.
XRD: mica-kaol-qz-cc-(arag-pyrite). No feldspar and low intensity counts.
Collected from below obvious presence of recent material. Sample sandy and unconsolidated.

■3 -3: 50-59 cm: Carbonate-rich (well sorted medium) sand [43.6% qz : 56.4% glc]
M: 4.2% S: 95.0% G: 0.2% $CaCO_3$: 9.4%
Gravel: <fP Pcg, EchP, & G-(?*Turritella* sp.) ShF
Sand: 40% qz, 50% glc; 10% SkF (Pleistocene biodiverse pF (*G. bulloides* dominant & *G. universa* present)+bF, Ost & HS;
Glc. dominantly black polished grains with minor to subordinate green grains
XRD: mica kaol-qz-cc-arag-feldspar (plag>K'spar) *[pyrite?] Feldspar absent from other samples*
Collected from cemented interval with bioturbated lower contact.

■4 -4: 70-74 cm: Sand
M: 1.7% S: 98.3% G: 0% $CaCO_3$: 5.1%
Sand: see - 6. Slight increase in abundance (2-3%) & biodiversity with 1% EchS.
XRD: mica-kaol-qz-cc-feldspar (plag only)-(arag-pyrite?)
Collected from below carbonate rich interval.

■5 -5: 123-128 cm. Sand
M. 2.4% S: 97.6% G 0% $CaCO_3$: 5.6%
Sand: see -6.
XRD: mica-kaol-qz-cc feldspar (plag only)-(arag-pyrite)

■6 -6: 203-208 cm: (Well sorted medium) sand [45.4 qz : 54.6% glc]
M: 3.9% S: 96.1% G: 0% $CaCO_3$: 4.5%
Sand: 44% qz; 54% glc; 2% SkF (trace EchS. low biodiversity with bF dominant, including spiny *Uvigerina* sp. & trace *G. inflata*). Trace SPG.
Glc tends to be fractured green grains.
XRD: mica-qz-cc-(plag?)
Collected from base of core – sample dry and cemented



University of Cape Town

Holocene

Pleistocene

0

0.30

1

2

2.35 m

M | sM | mS | S | gS | sG | G

1

-1: 12-16 cm: Sand [30.3% qz : 69.7% glc]
M: 6.5% S: 93.1% G: 0.3% $CaCO_3$: 7.1%
Gravel: fragile gastropod (unidentified) and other ShF
Sand: 55% glc; 37% qz; 0% faecal mud; 8 % SkF (Bv-ShF; EchS & 2% F (dominantly robust Holocene sp.) & trace SSp.
Qz mud-stained.
XRD: mica-kaol-qz-cc-feldspar (plag only)-py-arag?

-2: 56-63 cm Sand
M: 6.0% S: 92.0% G: 0% $CaCO_3$: 6.2%

2

Sand: 59% glc; 40% qz; 1% SkF (slight upcore increase in biodiversity, includes *G. inflata*, *Bulimina* sp., *Globobulimina* sp. etc.). Trace rnd PCG c-vcS; EchS and SSp.
XRD: mica-kaol-qz-cc-feldspar (plag only)-pyrite (No arag)
Collected from well-cemented upper part of unit

3

-3: 115-122 cm: Sand [30.9% qz : 69.1% glc]
M: 4.1% S: 95.9% G: 0.2% $CaCO_3$: 5.5%
Sand: see -4 & -5.
XRD: mica-kaol-qz-cc-feldspar (plag only)-py (No arag)

Sample -4 & -5 include only minor Ph

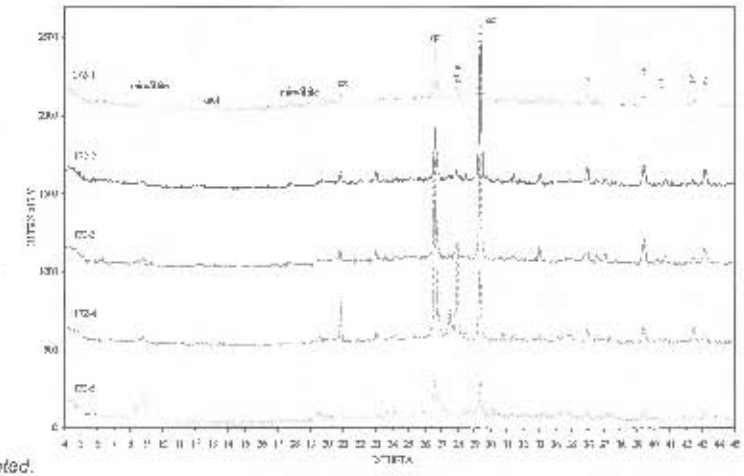
-4: 206-211 cm: Sand
M: 4.2% S: 95.8% G: 0% $CaCO_3$: 5.1%
Sand: 60% glc (see-5); 40% qz (see-5) with trace rnd qz cS: SPG (Sk & T): EchS and pF+bF fragments.
XRD: mica-qz-cc-feldspar (plag+K'spar)-py-arag? No kaol
Collected near base of qz-glc sand.

4

-5: 219-224 cm: (Well sorted, medium) sand [35.6 qz : 64.4% glc]
M: 6.6% S: 93.4% G: 0% $CaCO_3$: 5.1%

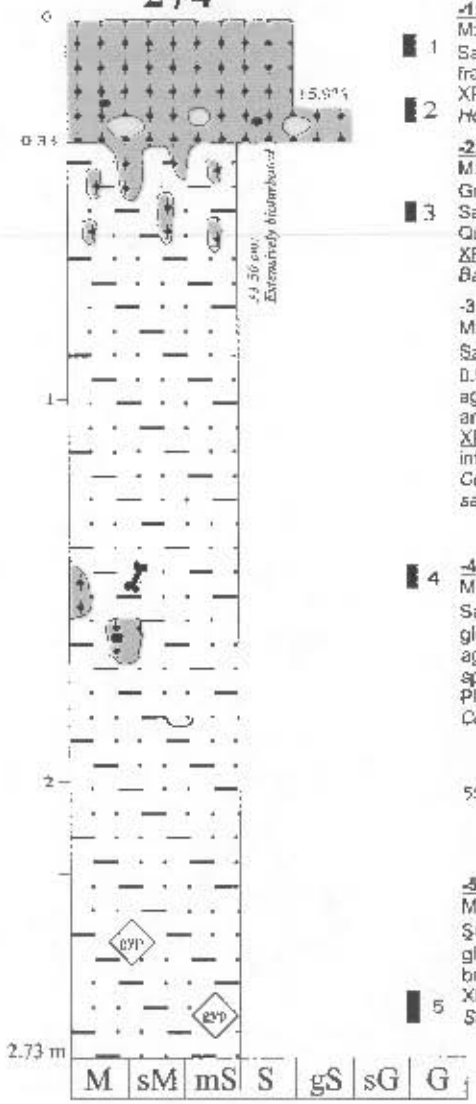
5

Sand: 60% glc; 40% qz with trace EchS and bF (ribbed *Uvigerina* sp.)
Glc: dominantly fragmented green grains with subordinate polished black grains.
Qz: ang to subrnd f-mS with minor rnd qz cS and trace rod-stained grains.
XRD: mica-qz-cc-(plag)
Collected from base of core, which included a higher green mud component. Sample was dry and cemented.



University of Cape Town

274



-1: 6-12 cm: Well sorted, fine to medium sand with a small very fine sand population [33.2% qz : 66.8% glc]
M: 7.0% S: 93.0% G: 0% $CaCO_3$: 7.3%
Sand: 47% qz; 47% glc with 1-2% faecal mud and minor EchS, SSp & robust Holocene sp with pF>bF and trace fragmented Pliocene bF, black glc & SPG.
XRD: qz-cc-mica-kaol-feldspar (plag only)-(pyrite). No kaol.,
Holocene sand with worm tubes (not sampled)

-2: 23-29 cm: Fine to medium gravelly sand
M: 7.3% S: 76.7% G: 15.9% $CaCO_3$: 6.4%
Gravel: cP grey granite (blocky) with qz, granits, PCG (glc mS) granules and SPG (Sk).
Sand: 48% qz; 48% glc; 4% EchS, F (Holocene robust sp with pF>bF) and SSp. Includes a reworked Pliocene Quartzose Muddy Sand component.
XRD: qz-cc-mica-feldspar (plag>K'spar)-pyrite. No kaol and note high intensity counts.
Basal Holocene lag

-3: 50-55 cm: Very well to well sorted, muddy very fine sand [95.9% qz : 4.1% glc]
M: 30.7% S: 69.3% G: 0% $CaCO_3$: 3.4%
Sand: Dominated (98.5%) by <125 µm angular quartz (including trace red-stained grains); 1% py-SSp & 0.5% glc & Ph. The minor >125µm fraction composed of 40% qz; 40% glc; 10% gypsum cemented aggregates & 10% SkF (5% py-SSp; EchS & bF - mixed brown-Miocene>Pliocene) with trace SPG (T) and Ph-Bv-ShF.
XRD qz-cc-mica-kaol-feldspar (plag only). No pyrite or arag - 2.7 Å peak from mica. Note the high intensity counts.
Collected below obvious bioturbation - may be some contamination. Material cemented and difficult to sample.

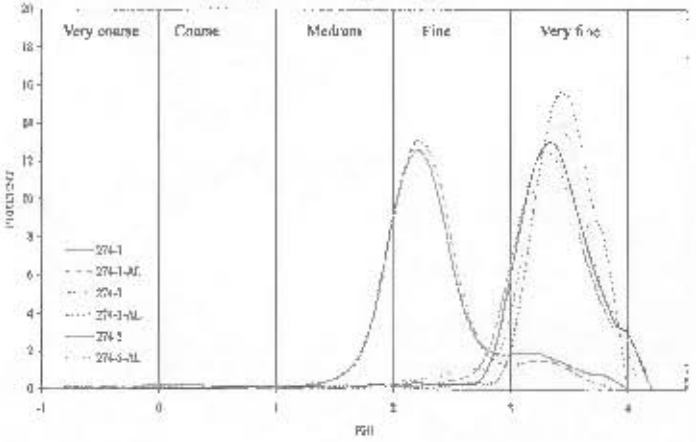
-4: 145-151 cm: Muddy very fine sand
M: 22.1% S: 77.4% G: 0.4% $CaCO_3$: 2.9%
Sand: Dominated (99%) by <125 µm angular quartz (including trace red-stained grains) and <1% SSp, glc & Ph with the minor >125µm fraction composed of 35% qz; 35% glc; 20% gypsum cemented aggregates & 10% SkF (py-SSp; EchS & bF - mixed brown-Miocene+Pliocene (includes *Nodogenerina* sp.) assemblage; trace F with py-infilling).
Pliocene foraminiferal assemblage (I. McMillan)
Collected from typical Quartzose Muddy Sand and includes bone fragment.

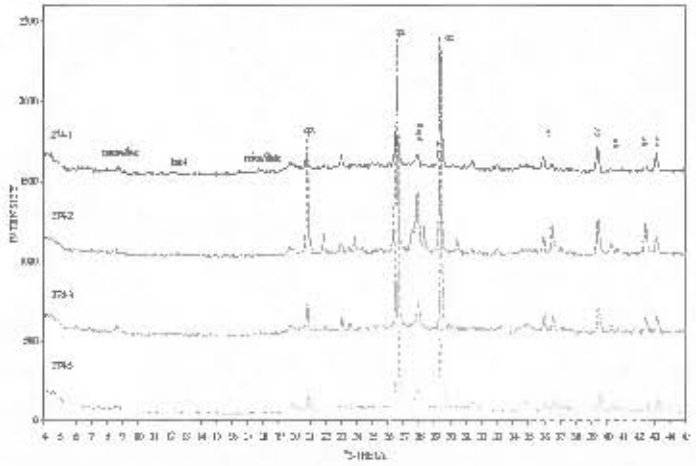
55 to 273 cm Uniform sand with well developed wispy lamellae of less muddy sand

-5: 256-264 cm: Well sorted, muddy very fine sand [94.5% qz : 5.5% glc]
M: 19.6% S: 80.4% G: 0% $CaCO_3$: 2.7%
Sand: Dominated (99%) by <125 µm angular quartz (including trace red-stained grains) and <1% SSp, glc & Ph with the minor >125µm fraction composed of 45% qz, 45% glc and 10% SkF (bF - mixed brown-Miocene>Pliocene assemblags) with gypsum-cemented aggregates & trace SPG (T).
XRD: qz-cc-mica-kaol-feldspar (plag only)-(pyrite)
Sample collected from base of core. Gypsum common.

FORAMINIFERAL ASSEMBLAGE:
274-4
Nodogenina (*Stilostomella*) sp., *Hanzawaia* sp., *Dentalina* spp., *Marginella* sp., *Cibicidoides* sp., *Vaginulina* sp., *Uvigerina* sp. (cf. *bassensis*), *Brizalina* sp., *Lagena semilineata*, *Gyroidinoides ?nipponicus*

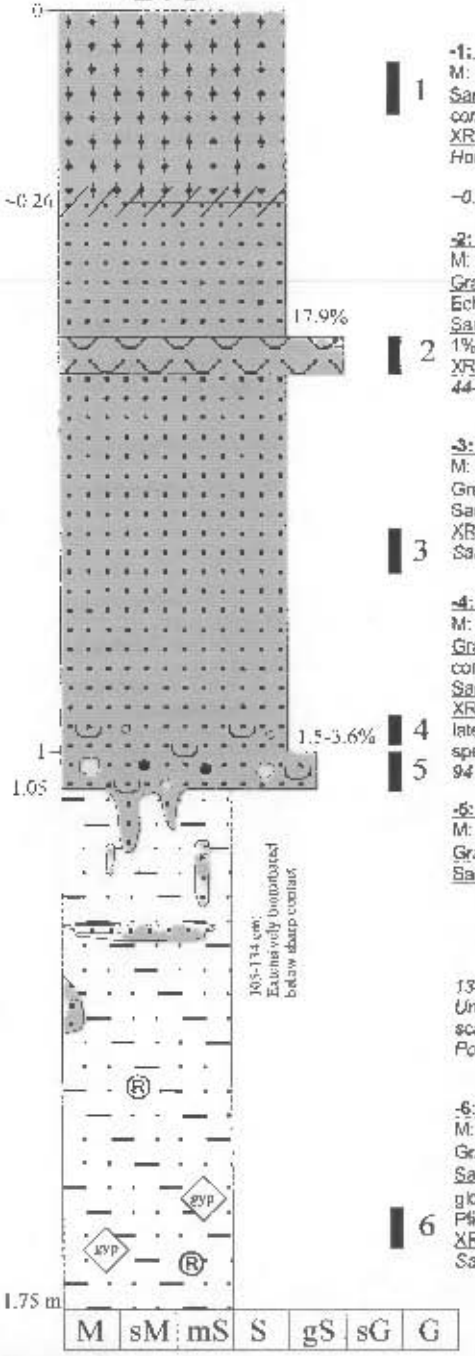
274-1: Acid leaching does not remove the small bimodal very fine population, but improves sorting slightly.
274-3: Leaching improves sorting to very well sorted.
274-5: Leaching improves sorting to very well to well sorted





University of Cape Town

275



-1: 7-14 cm: Well sorted, fine sand with a small very fine sand population [31.5% qz : 68.5% glc]
M: 3.9% S: 96.1% G: 0% $CaCO_3$: 6.6%
Sand: 68% glc; 30% qz; 2% SkF (1% SSp & EchS, 1% F (includes *G. bulloides*, aggl-bF *Discamimina compressa* & robust Holocene pF sp.) No obvious faecal mud.
XRD: qz-cc-mica-feldspar (plag>K'spar). Odd 3.30 Å peak and no kaol.
Holocene material including a high concentration of EchS.

1

~0.26-1.05 m: Quartz Glauconite Sand with shell fragments <2mm

-2: 44-49 cm: Gravelly sand
M: 4.0% S: 78.1% G: 17.9% $CaCO_3$: 5.6%
Gravel: vcP well-preserved *L. chuni*, *T. declivis* (with colour), *Nassarius* sp. (*cf. vinctus*); *Cardiolla* sp., EchP, *Anomia* sp., fish scales, worn Bv and G (*T. declivis*) ShF & PCG (glc mS & vfS qz casts).
Sand: 90% glc>qz; 5% pF>bF (*G. inflata* & *G. menardii* dominant), 2-3% SPG (Sk) & Ph; 2% Bv-ShF, 1% qz cS & 1% EchS. TRACE MUSCOVITE
XRD: qz-cc-mica-feldspar (plag>K'spar)-pyrite. No kaol and note high intensity counts.
44-49 cm: Shell lag composed of T. declivis and Bv-ShF.

2

-3: 70-76 cm: Very well to well sorted fine sand [28.6% qz : 71.4% glc]
M: 3.5% S: 95.9% G: 0.6% $CaCO_3$: 9.1%
Gravel: Well-preserved mP *Amalda bulloides*, fish scales, Bv-ShF, PCG (glc mS & qz vfS cast) granules.
Sand: (see -2) 90% glc>qz; 10% SkF (3% ShF and 7% increased biodiversity pF+bF), EchS & Ost.
XRD: qz-cc-mica-kaol-feldspar (plag only)-(arag-pyrite)
Sampled between shell lag and basal gravel lag

3

-4: 96-100 cm: Slightly gravelly sand
M: 5.0% S: 93.5% G: 1.5% $CaCO_3$: 9.5%
Gravel: <mP well-preserved *L. chuni*, *Cardiolla* sp., Bv-ShF, grey granite granules, worn Bv and coralline algae.
Sand: (see -3) ~87% glc>qz; 13% SkF (3% Bv- & G-ShF and 10% pF+bF), EchS, Ost & HS.
XRD: qz-cc-mica-kaol-feldspar (plag only)-(arag-pyrite)
latest Pleistocene deep water assemblage with transitional (*G. inflata* + *G. dutertrei*) to cool water species (*G. bulloides* + *N. pachyderma*) (I. McMillan)

4

94 to 105 cm: Increase in size and concentration of worn shell fragments

5

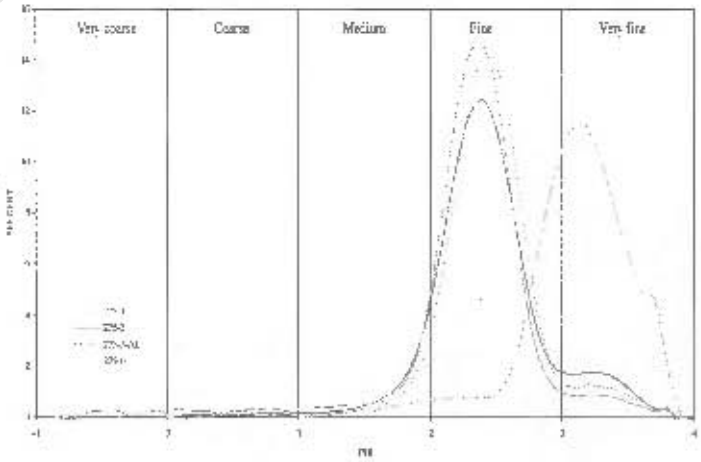
-5: 100-105 cm: Slightly gravelly sand
M: 4.0% S: 92.4% G: 3.6% $CaCO_3$: 8.9%
Gravel: <mP pink granite (blocky); grey granite and ang qz fP and PCG granules.
Sand: (see -4)

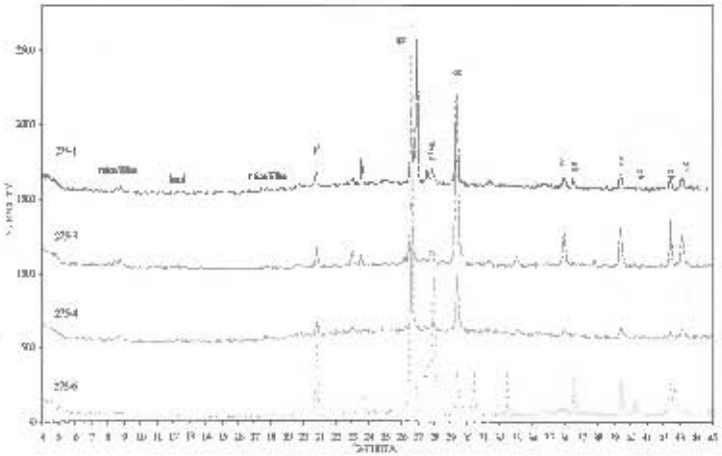
134 to 175 cm:
Uniform muddy sand with well developed wispy lamellae of less muddy sand. Reduced patches scattered throughout.
Possibly transitional to Glauconitic Muddy Sand facies

-6: 161-167 cm: Well to moderately well sorted, muddy very fine sand [90.26% qz : 9.74% glc]
M: 24.1% S: 75.8% G: 0.1% $CaCO_3$: 4.0%
Gravel: vfP PCG (qz vfS) and ?py-cemented qz aggregates
Sand: Dominated (99%) by <125 µm angular quartz (including trace red-stained grains) and <1% SSp, glc, F & SPG with the minor >125 µm fraction composed of glc and bF (mixed brown-Miocene> Pliocene assemblage) with gypsum-cemented aggregates, qz & trace SPG (T). No EchS or SSp.
XRD: qz-cc-(mica)-feldspar (plag & K'spar)
Sampled below bioturbated contact. Gypsum crystallization common.

6

FORAMINIFERAL ASSEMBLAGE:
275-4:
Globorotalia inflata, ?Globoquadrina dutertrei, Neogloboquadrina pachyderma, Globigerina bulloides, Fissurina sp., *Brizalina* sp., *Bulimina* sp. ribbed *Lagena* sp. *(Lagena striata), Globobulimina turgida, Uvigerina* spp., *Lobatula lobatula, Planulina ariminesis*





University of Cape Town

276

Holocene

Pleistocene

Pliocene

0

0.49

1

2

2.77 m

Bioturbated to 130 cm

49-53 cm

134-138 cm

208-204 cm

M | sM | mS | S | gS | sG | G

■ 1

-1: 7-14 cm: Sand [54.4% qz : 45.6% glc]
M: 5.3% S: 94.7% G: 0% $CaCO_3$: 6.7%
Sand: 48% qz vfS; 48% glc (black & ph-glc F-infillings); 4-5% EchS, SSp, robust pF>bF with minor faecal mud & pellets
XRD: qz-cc-feldspar (plag~K'spar)-py No kaol or mica
Holocene material

■ 2

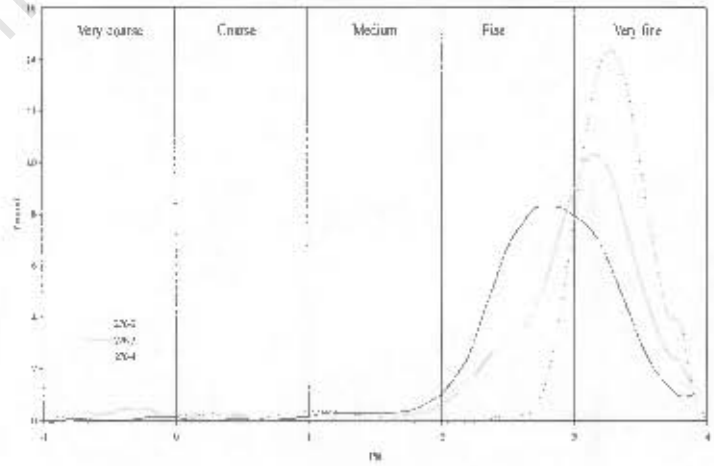
-2: 38-45 cm: Well to moderately well sorted fine to very fine sand [70.3% qz : 29.7% glc]
M: 4.6% S: 95.4% G: 0% $CaCO_3$: 6.5%
Sand: sce -1 (includes trace *G. bulloides*)
XRD: qz-cc-mica-kaol-feldspar (K'spar>plag)-py. Note 3.08 Å peak.
Sampled interval, which included worm ShF

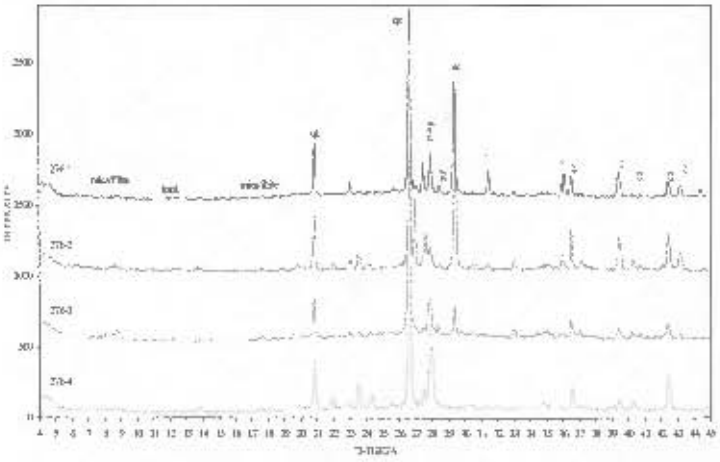
■ 3

-3: 62-66 cm: Moderately well sorted fine to very fine slightly gravelly sand [70.3% qz : 29.7% glc]
M: 6.6% S: 90.2% G: 1.2% $CaCO_3$: 5.6%
Gravel: *N. vinctus*; *T. declivis* & other G-ShF, scaphopods, EchP, *Carditella* sp. & other Bv-ShF, SPG (T), fish scales, granite & qz granules.
Sand: Mixture of vf qz sand & Pleistocene qz-glc fS, which includes *G. inflata*, other pF & bF & minor ShF.
XRD: qz-(cc)-mica-kaol-feldspar (plag only)-py
Sampled within upper bioturbated interval.

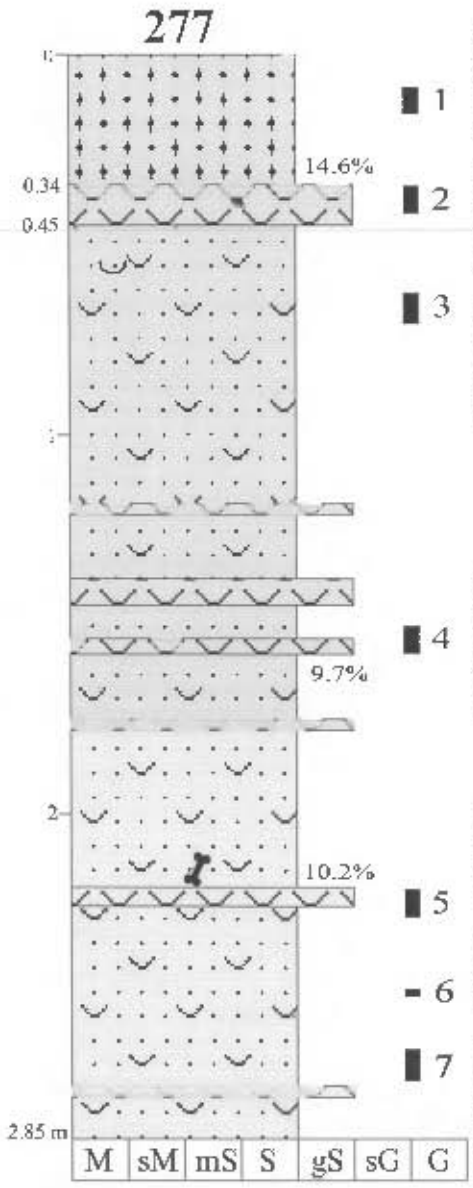
■ 4

-4: 251-258 cm: Moderately well sorted muddy sand (Sorting poor because of coarse gypsum-cemented grains) [97.8% qz : 2.2% glc]
M: 15.2% S: 84.5% G: 0% $CaCO_3$: 3.7%
Sand: <125 µm composed of 99% qz with <1% SSp, SPG & F. >125 µm dominated by gypsum-cemented aggregates, glc, Ph-fragments. SPG (T & Sk) and Miocene/Pliocene bF.
XRD: qz-feldspar (plag >K'spar)-(mica). No kaol-cc-py.
Sampled from base. Core cemented & may be some contamination along core liner.





University of Cape Town



1

-1: 8-15 cm: Sand [72% qz : 28% glc]
M: 5.6% S: 94.3% G: 0.1% $CaCO_3$: 13.3%
Gravel: vfP G-ShF, grey granite, SPG & PCG
Sand: 75% qz>glc; ~25% reworked-SkF (ShF; EchS; pF (including *G. bulloides, O. universa etc*)-bF; Ost) and 1-2% SSp.
XRD: qz-cc-musc-kaol-feldspar (K'spar>plag)-py

2

-2: 34-41 cm: Gravelly sand [67.2% qz : 32.8% glc]
M: 4.0% S: 81.5% G: 14.6% $CaCO_3$: 18.1%
Gravel: vcP well-preserved *L. chuni* and *T. declivis*, with minor well-preserved hooked *Patella* sp., scaphopods, other Bv-ShF, SPG (Sk & T), fish scales and EchP with grey granite, PCL and PCG vfP. Very worn and reworked *A. bulloides* and *L. chuni* ShF also present.
Sand: see -4, but pF dominated by more transitional species *G. inflata* & *N. pachyderma*.

3

-3: 62-70 cm: Moderately well to well sorted fine to very fine sand (leaching improves sorting to well sorted) [77.5 qz : 22.5% glc]
M: 5.1% S: 94.5% G: 0.3% $CaCO_3$: 18.4%.
Gravel: tP worn *L. chuni* and other Bv-ShF with SPG vfP
Sand: see -4, but includes only trace qz cS & no Miocene bF, SPG or PCG.
XRD: qz-cc-musc-kaol-feldspar (plag~K'spar)-py-arag

4

-4: 150-157 cm: Moderately well sorted fine to very fine gravelly sand [75.6% qz : 24.4% glc]
M: 3.5% S: 86.8% G: 9.7% $CaCO_3$: 13.1%
Gravel: cP *L. chuni* (worn and well-preserved, but bored) with minor scaphopods, *M. pisum*, *Cardiella* sp., otoliths and worn Bv-ShF. Trace mP PCL, vfP ss1 and PCG (glc mS & qz vfS cast) & pink granite granules.
Sand: 55% vf qz (includes ~3% cS); 20% glc & 25% SkF (2-3% Bv-ShF; 1% EchS; pF+bF (includes Miocene fragments) & Ost). Trace SPG (T) with single vcS PCG (glc mS).
Sampled interval with well-developed glc-rich bands adjacent to a shell-rich layer.

5

-5: 218-226 cm: Gravelly sand [56.7% qz : 13.3% glc]
M: 5.2% S: 84.6% G: 10.2% $CaCO_3$: 10.5%
Gravel: cP L. chuni (well-preserved) and SPG. Minor *M. pisum*, *Cardiella* sp., otoliths, EchP and worn Bv-ShF. Trace qz, grey granite and PCG (qz cS) granules.
Sand: 65% qz vfS; 10% glc & 25% SkF (3-4% Bv-ShF; diverse pF+bF; Ost; HS & trace EchS)

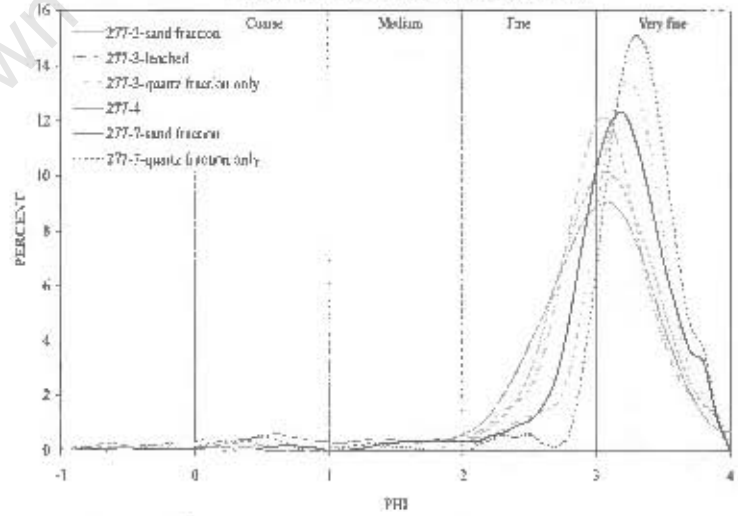
6

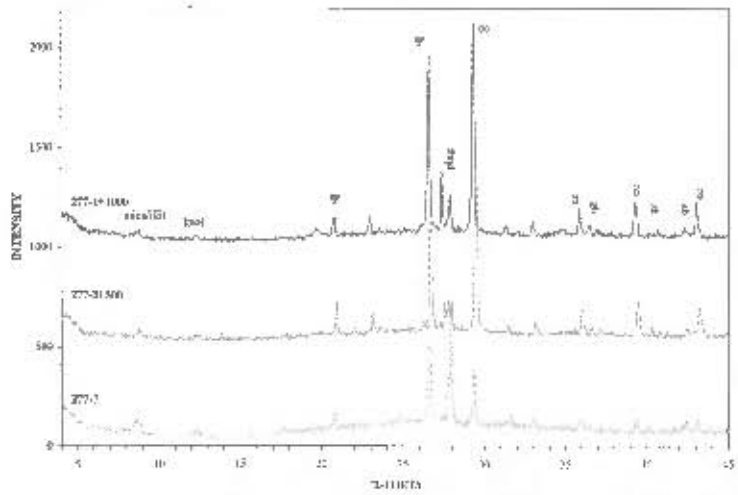
-6: 245 cm: Slightly gravelly sand [90.1% qz : 9.9% glc]
M: 5.6% S: 91.4% G: 3.0% $CaCO_3$: 12.8%
Gravel: cP *L. chuni*, *Anomia* sp., *Polinices* sp., EchP, scaphopod, SPG & trace PCG granules.
Sand: see -7.

7

-7: 261-269 cm: Moderately well sorted fine very fine sand [88.9% qz : 11.1% glc]
M: 3.8% S: 95.7% G: 0.4% $CaCO_3$: 10.1%
Gravel: vfP Bv-Shf, including *L. chuni*, *Anomia* sp., *Carditella* sp. and EchP.
Sand: 65% qz vfS; 10% glc & 25% SkF (2-3% scaphopod & Bv-ShF; 1% EchS; biodiverse pF+bF (includes large bF *Marginulina* sp.; aggl-bF; Miocene sp.; pF: dominant *G. inflata* and *O. universa etc.*); 1% Ost & HS)
XRD: qz-feldspar (plag~K'spar)-cc-musc-kaol-py-arag

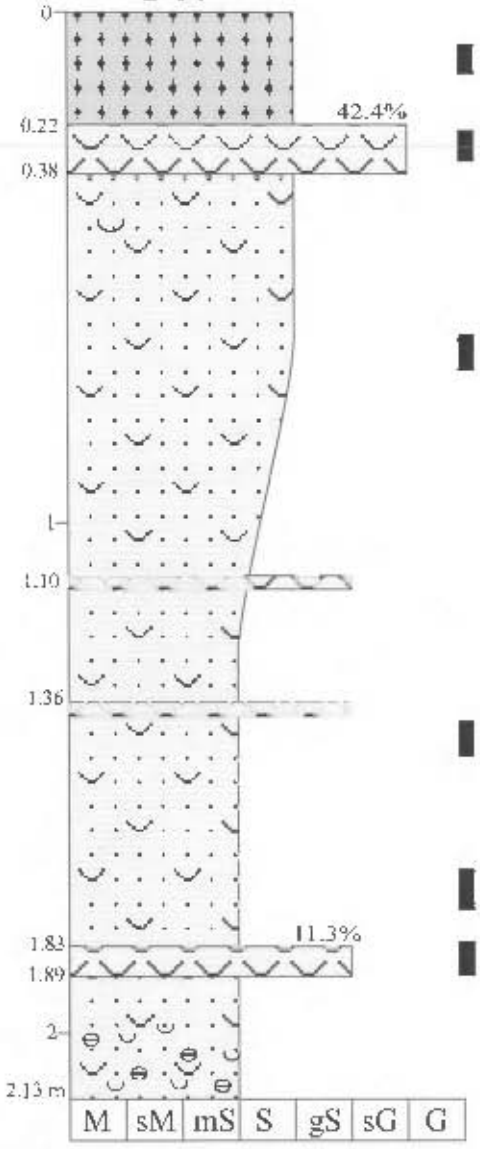
Leaching improves sorting and fines mean grain size, with magnetically separated quartz-only samples most similar to Quartzose Muddy Sand facies (3.11 ϕ (277-3) and 3.24 ϕ (277-7))





University of Cape Town

347



-1: 10-16 cm: Sand [66.9% qz : 31.1% glc]
M: 6.8% S: 93.2% G: 0% $CaCO_3$: 9.1%
Sand: 58% qz, 25% glc, 10% SkF (robust Holocene sp. & reworked Pleistocene sp.); 5% laccal mud and 1-2% SSp.
XRD: qz-cc-mica-feldspar (plag>Kspar)-(py-arag). No kaol.
Holocene material

-2: 29-29 cm: Muddy sandy gravel
M: 6.1% S: 51.5% G: 42.4% $CaCO_3$: 28.5%
Gravel: Imbricated shell lag, includes articulated cP *L. chuni* often with cemented casts and minor scaphopods. *Anomia* sp., *Cardiella* sp., SPG, EchP, otoliths and ShF.
Sand: 45% qz; 15% glc & 40% SkF (5% Bv-ShF; robust Holocene pF and Pleistocene pF, including *G. bulloides* & *O. universa* etc; EchS; SPG & Ost) Trace qz cS & PCG (y/c mS & qz vfs cast).

-3: 63-70 cm: Sand [94.2% qz : 5.8% glc]
M: 6.7% S: 91.7% G: 1.5% $CaCO_3$: 7.4%.
Gravel: Worn Bv and scaphopoc ShF.
Sand: 85% qz; 5% glc and 10% SkF (see -6)
XRD: qz-cc-mica-kaol-feldspar (plag only)-arag-(pyr). No kaol & no cc>qz.
Sampled area below shell lag with lower shell concentrations.

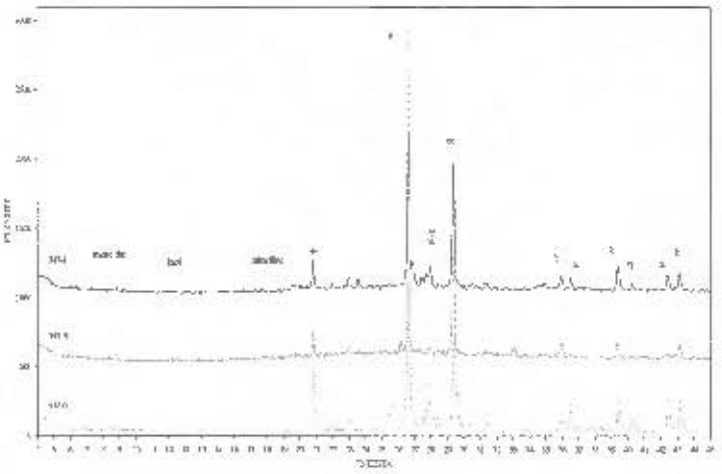
110 cm: Fragile fine shell layer

136-139 cm: Concentration of shell fragments

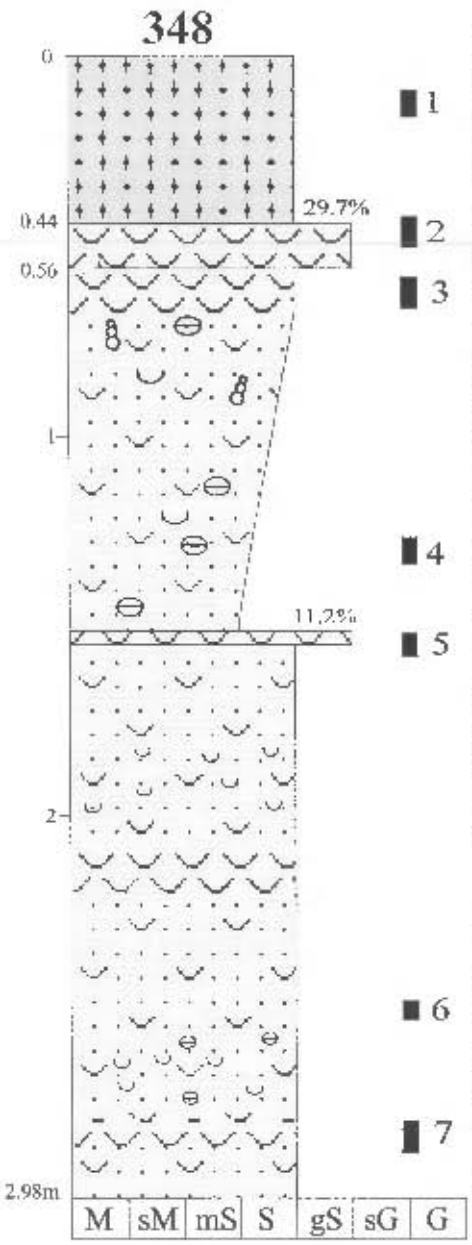
-4: 139-145 cm: Slightly gravelly muddy sand
M: 11.6% S: 87.1% G: 1.4% $CaCO_3$: 8.6%
Gravel: <mP *Hiatella* sp. (bored), vfP G-ShF (including *Polinices* sp. and *Conus* sp.) and vfP Bv-ShF (including *L. chuni*).
Sand: see -6, includes trace OsL
Sampled in interval of scattered shell concentrations

-5: 169-177 cm: Muddy sand
M: 12.0% S: 88.0% G: 0% $CaCO_3$: 7.6%
Sand: see -6, but only 10% SkF with fewer ShF (no bry)
Sampled in interval of lower shell concentrations

-6: 182-189 cm: Gravelly muddy sand [92.8% qz : 7.2% glc]
M: 13.4% S: 75.5% G: 11.3% $CaCO_3$: 9.8%
Gravel: cP worn *L. chuni* and other vfP G and Bv ShF.
Sand: 60% qz, ~5% glc & 15% SkF (2-3% Bv-ShF, trace bry, 1% EchS, biodiverse bF (includes agglu-hF)>sF (*G. bulloides* & *O. universa* etc.)
XRD: qz-cc-feldspar (plag only) pyr-(arag). No clay minerals
Sampled area with typical scattered articulated L. chuni and associated shell fragments
183-189 cm: Shell-rich layers (slightly reduced patches)
Refusal lag composed of articulated L. chuni.



University of Cape Town



-1: 9-16 cm: Fine Sand <250 µm) [76.5%qz : 21.5% glc]
M: 7.5% S: 92.4% G: 0% $CaCO_3$: 10.5%
Sand: 80% qz; 10% glc (vf-fS black polished grains) & 10% SkF. Trace SSp (py-infilling)
XRD: qz-cc-mica-feldspar (plag only)-(py-arag). No kaol.
Holocene material

-2: 42-50 cm: Gravelly sand
M: 5.0% S: 65.2% G: 29.7% $CaCO_3$: 29.5%
Gravel: Articulated well-preserved *L. chuni* with *V. abyssicola*, *N. vintus*, *M. pisum*, *Cerditella* sp., *Hiatella* sp. *Anomia* sp., scaphopods and other SHF. Well-cemented *L. chuni* casts common.
Sand: 50% qz vfs (incl. 3% qz cS); 10% glc & 40% SkF (5% Bv-ShF, pF–bF (incl. aggl-bF *Discammina compressa*), 1% EchS, trace Ost, HS & SSp).
XRD: qz-cc-musc-(kaol)-feldspar (plag only)-arag-(py). cc>qz
Shell lag composed of imbricated L. chuni etc.

-3: 58-66 cm: Well sorted, very fine sand
M: 6.5% S: 91.9% G: 1.6% $CaCO_3$: 16.8%.
Gravel: Dominated by *Anomia* sp. ShF with *A. bulloides*, *L. chuni* and scaphopod vfP ShF.
Sand: 60% qz vfs (incl. 3% qz cS); 10% glc & 30% SkF (Bv-ShF, pF–bF (incl. aggl-bF), EchS & trace Ost. (pF includes *G. bulloides*, *O. universa*, *N. pachyderma*).
XRD: qz-cc-mica-feldspar (plag only) (py-arag) No kaol & cc>qz
Slightly higher glauconite concentrations due to bioturbation

-4: 127-135 cm: Muddy sand [95% qz : 5% glc]
M: 10.5% S: 89.1% G: 0.4% $CaCO_3$: 5.6%
Gravel: mP *Hiatella* sp. with scaphopods and other Bv-ShF.
Sand: <125µm 90% qz vfs, 5% glc & 5% SkF. >125 µm Bv-ShF, pF–bF (incl. aggl-bF), EchS & trace Ost. (pF includes *G. bulloides*, *O. universa*, *N. pachyderma*). Trace qz cS.
Sampled between articulated L chuni.

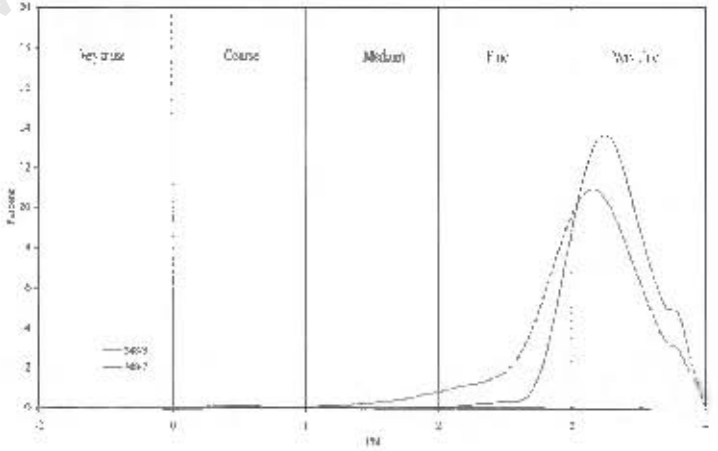
-5: 152-158 cm Gravelly muddy sand
M: 12.4% S: 76.4% G: 11.2% $CaCO_3$: 5.6%
Gravel: Articulated well-preserved *L. chuni* with *Hiatella* sp., scaphopods and other Bv-ShF.
Sand: <125µm 90% qz vfs; 5% glc & 5% SkF. >125 µm Bv-ShF, pF–bF (incl. aggl-bF), EchS & trace Ost. (pF includes *G. bulloides*, *O. universa*, *N. pachyderma*). Trace qz cS.
XRD: qz-cc-mica-kaol-feldspar (plag only)-arag-(py). cc>qz.
Shell layer at 152-157 cm

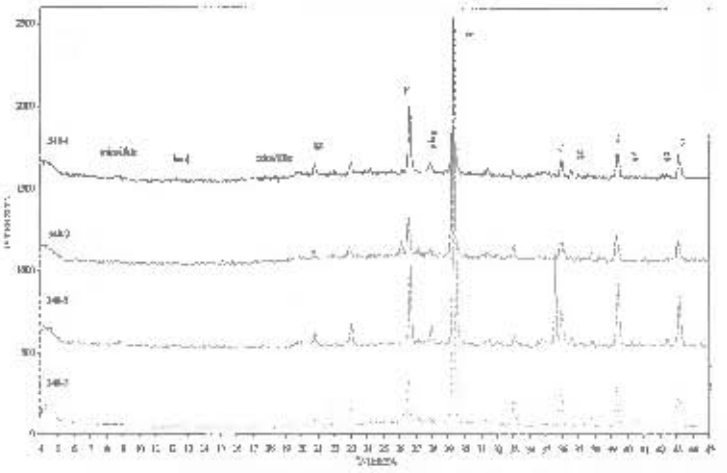
Increased concentration of fine shell fragments above a very shell-rich interval from 209-221 cm. Shell layer composed predominantly of coarse (>2 mm) bivalve fragments, scaphopods and other fragile shell fragments. (Similar interval from 279-221 cm)

-6: 248-253 cm: Sand
M: 8.1% S: 91.9% G: 0% $CaCO_3$: 9.7%
Sand: <125µm 80% qz vfs; 5% glc & 15% SkF. >125 µm Bv-ShF, pF–bF (incl. aggl-bF), EchS, Ost. (pF includes *G. bulloides*, *O. universa*, *G. inflata* present)
Cool deep water late Pleistocene foraminiferal assemblage (I. McMillan)
Sampled typical unit between shells and shell concentrations - much more cemented.

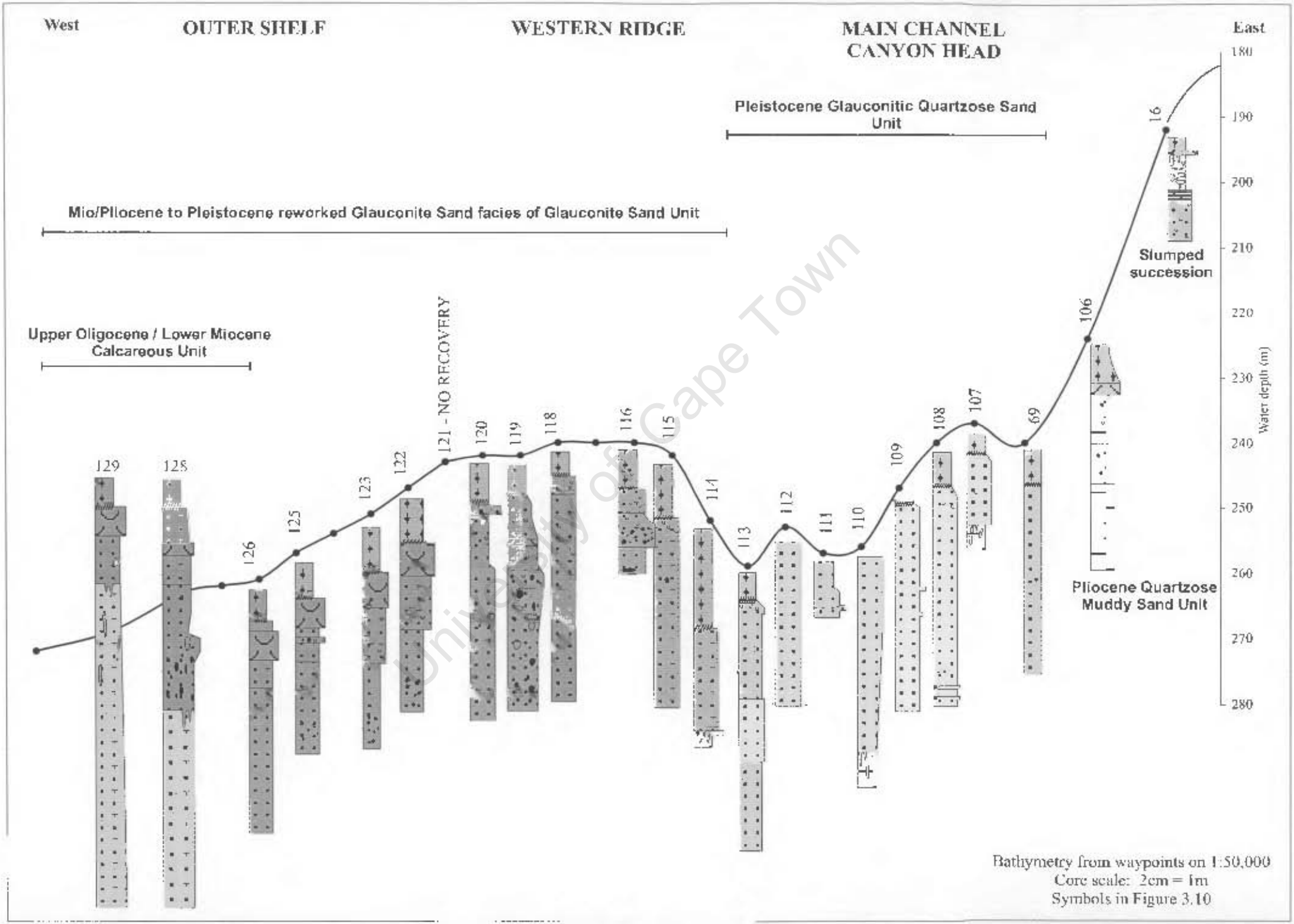
-7: 280-288 cm: Very well sorted very fine sand
M: 5.7% S: 93.1% G: 1.2% $CaCO_3$: 9.7%
Gravel: Dominated by scaphopods (<1 cm) with otoliths and vfP Bv ShF
Sand: <125µm 85% qz vfs; 5% glc & 10% SkF. >125 µm only F (pF–bF), trace Ost.
XRD: qz-cc-mica-kaol-feldspar (plag only)-arag-py. cc>qz.
Cool deep water late Pleistocene foraminiferal assemblage (I. McMillan)
Scattered shell concentration nearest base of core.

Scattered whole articulated L. chuni and shell fragments present throughout unit
FORAMINIFERAL ASSEMBLAGE
348-6:
abundant *Pullenia subcarinata, Globigerinella aequilateralis, Lobatula lobatula, Globorotalia truncatulinoides, Marginulina* sp., *Globigerina bulloides, Orbulina bilobata, O. universa, Globorotalia inflata, Ehrenbergina* sp., *Siphonaperta martinae* (aggl-bF), *Globobulimina turgida* & *?Glandulina* sp. Ostracods include *Ambostracon keeleri.*
348-7:
abundant *Cassidulina laevigata, Brizalina spathulata, Angulogerina* sp., *Gravelinopsis* sp., tiny *Neogloboquadrina pachyderma, Globorotalia scitula, Hoeglundina elegans, Globigerina bulloides, Orbulina universa, Globorotalia inflata*

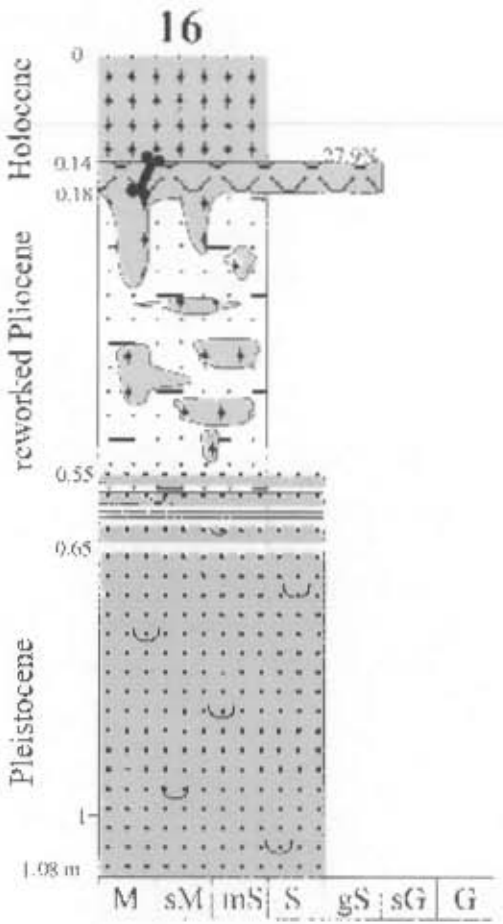




University of Cape Town



University of Cape Town



■1 -1: 14-16 cm Gravelly muddy sand
M 16.5% S: 55.6% G: 27.9% $CaCO_3$ 11.6%
Sand: 55% qz, 35% glc, 10% biogenics (diverse bf>pf, HS, no Ost, trace Bv-ShF, EchS.)
Gravel: cP vf qz equant sst with bV shF, SPG and fish scales
Basal lag includes bone and scattered shell fragments

18-65 cm: Very disturbed interval possibly due to slumping. Upper portion extensively bioturbated with some evidence of coarser qz-glc sand laminae. Well developed layers of qz glc sand towards base of unit with shell fragments concentrated in these layers.

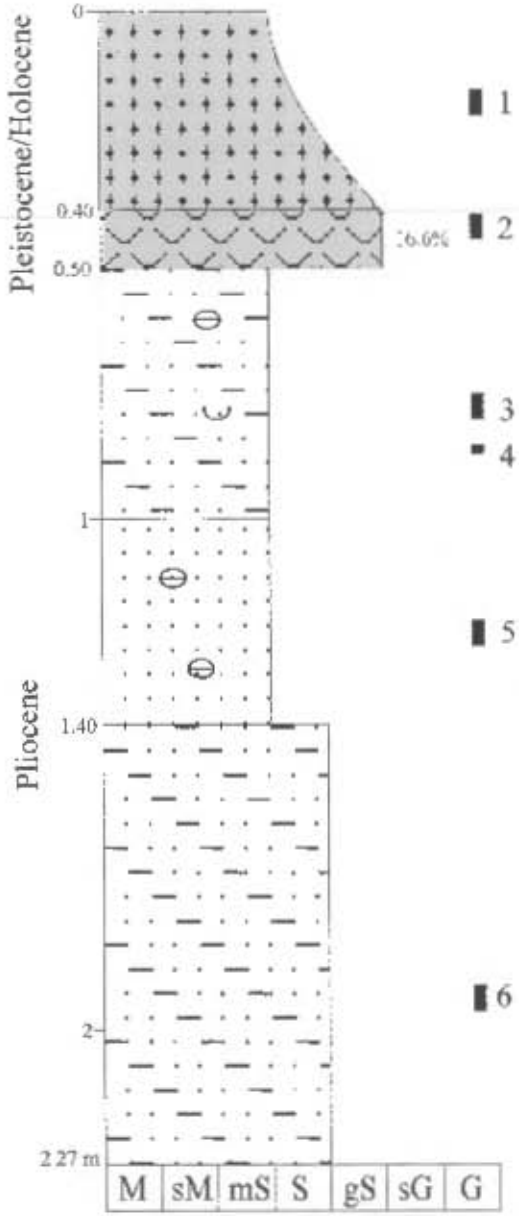
■2 -2: 51-54 cm Muddy sand
M: 27.6% S: 72.4% G: 0% $CaCO_3$: 18.0%
Sand: typical Quartzose Muddy Sand (69% <125 µm qz; 1% glc & SSp), but includes ~20% glc, Pleistocene b+pF, SSp, Ost, EchS, Ph-SPG (tune)

Sampled qz-rich area, but some contamination.

■3 -3. 80-85 cm: Qz glc Sand with worn ShF
M: 9.4% S: 90.1% G: 0.5% $CaCO_3$: 22.6%
Sand (f-mS at ~250 µm): 50% qz, 30% glc, 20% SkF (b>pF, Ost, HS EchS, Bv-ShF, including *G. inflata*) with trace granite cS and qz cS

University of Cape Town

106



■ 1

1: 15-20 cm: Muddy sand
M: 27.9% S: 71.9% G: 0.2% $CaCO_3$: 7.3%
Sand: 58% qz, 46% glc, 5% ShF (mixed fragmented Pleistocene sp. and robust Holocene pF; trace EchS & Ssp), 2% faecal mud.
Gravel: Qz and PCG granules
(Holocene unit above shell lag increase in glc up-unit)

■ 2

-2: 40-45 cm: Gravelly muddy sand
M: 16.8% S: 56.7% G: 26.6% $CaCO_3$: 17.0%
Sand: 60% qz, 25% vf-f blk glc, 10% p+bF, 5% ShF (Bv, hooked *Patella* sp., EchS). **Qz**: vf ang with trace cS - no Holocene mud-staining). **p+bF**: typical diverse Pleistocene assemblage with HS, OST.
Gravel: *T. sanginae, T. declivis, Neopycnodonte cochlear, P. abbreviatus, Hiatella* sp., *Dosinia* sp. *Anomia* sp., *A bulloides* and *N. vinctus*, EchP and trace SPG and

-3: 85-90 cm: Well sorted (.46 phi) slightly gravelly muddy very fine (3.01 phi) quartz sand
M: 13.5% S: 86.0% G: 0.5% $CaCO_3$: 4.5%

■ 3

Sand: see -6
Gravel: qz granules
Collected below any obvious shell fragments

■ 4

-4: 90 cm: articulated *Pitar abbreviatus*

100-140 cm: Slightly mud-rich interval, more typical Quartzose Muddy Sand

■ 5

-5: 120-125 cm: Quartzose muddy sand [(A/L) 80.5% qz : 19.5% glc]
M: 22.4% S: 77.26% G: 0.33% $CaCO_3$: 5.2%
Sand: ~5% f-m glc otherwise <125 µm (99% qz; 1% glc & Ssp). Includes *O. universa, Nodogenerina* sp.
Gravel: ?micrite-cemented *in situ* qz sand.

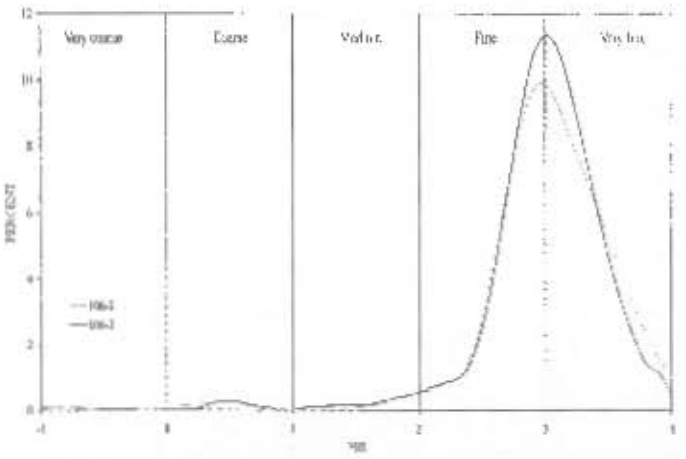
(More typical Quartzose Muddy Sand)

50-227 cm: Atypical Quartzose Muddy Sand - with relative abundance of glc and ShF - slumped interval

■ 6

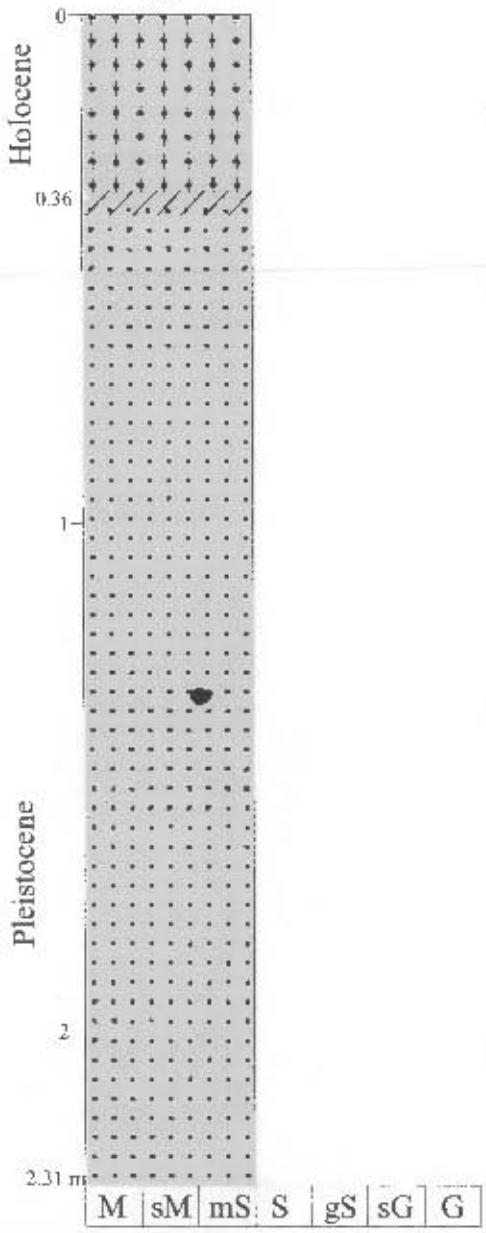
-6: 192-197 cm: Well sorted, glauconite-rich fine to very fine (2.99 phi) quartz sand [(A/L) 82.1% qz : 17.9% glc]
M: 9.9% S: 90.1% G: 0% $CaCO_3$: 4.8%
Sand: ~50% <125 µm (99% qz; 1% glc & Ssp) ~50% >125 µm: f-m qz-glc sand with minor ShF, Ost, EchS, p+bF (reworked Pleistocene sand). F includes Miocene fragmented sp.

(A/L: acid leached)



University of Cape Town

69



■ 1 **-1:** 17-22 cm: Muddy sand [(A/L) 55.7% qz : 44.3% glc]
M: 21.5% S: 78.4% G: 0.1% $CaCO_3$: 4.8%
Sand: 54% qz, 44% glc, 2% SkF (EchS, moderate p+bF biodiversity with robust Holocene pF, but no Ssp)
Gravel: single qz granule

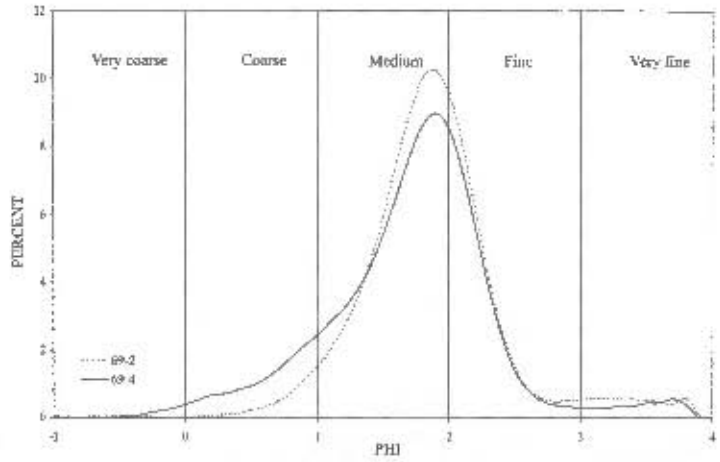
■ 2 -2: 50-55 cm: Muddy sand [(A/L) 58.7% qz : 41.3% glc]
M: 10.9% S: 89.1% G: 0% $CaCO_3$: 5.5%
55% qz, 40% glc, 5% SkF (p+bF including *G. bulloides, C. laevigata* and moderate biodiversity, EchS, 1% ShF and trace Ost). **Glc:** blk, polished with ~ 1% PP and Ph-ShF

36-231 cm: Uniform mottled medium quartz-glauconite sand, with a change in appearance of glc upcore from typical Pliocene green glc (-4 & -3) to Pleistocene blk, polished pellets (-2 & -1).

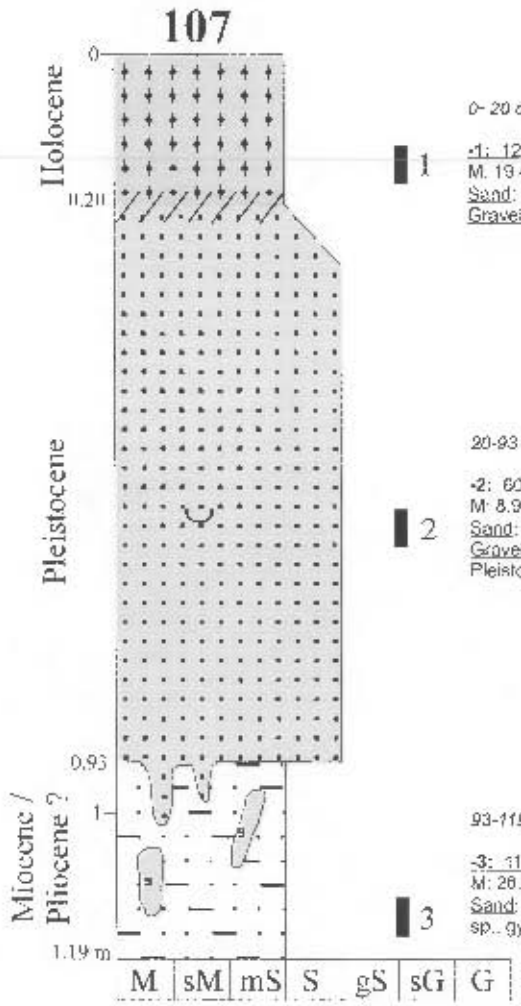
■ 3 **-3:** 134-136 cm: (Muddy) sand
M: 11.8% S: 88.2% G: 0% $CaCO_3$ 4.6%
Sand: see -4

■ 4 **-4:** 200-205 cm: Muddy glc qz sand [(A/L) 66.9% qz : 33.1% glc]
M: 12.5% S: 87.5% G: 0% $CaCO_3$: 4.7%
Sand: 64 % qz, 34% glc, 2% SkF (low diversity, includes aggl. bF), trace Ph-ShF, SPG, EchS. **Qz:** mod sorting with a cS component. **Glc:** green, fractured polished surface (compare to Mio/Pliocene)

Possible equivalent to mid Miocene sediment of Core 319 - requires further bio- & Sr-stratigraphic work



University of Cape Town



0- 20 cm: Holocene faecal pellet muddy sand

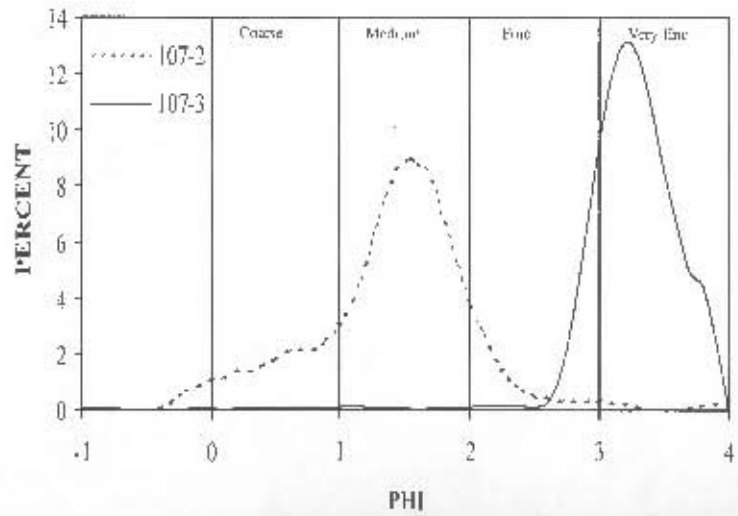
-1: 12-17 cm: Muddy sand [(A/L) 69.5% qz : 30.5% glc]
M: 19.4% S: 80.5% G: 0.2% $CaCO_3$: 4.7%
Sand: similar to -2 with both Pleistocene and Holocene pF, but mud-stained qz, trace SSp and trace EchS.
Gravel: 1X qz and 3X PCG granules

20-93 cm: Uniform mottled quartz-glauconite sand with sparse bivalve shell fragments scattered throughout unit.

-2: 60-65 cm: Moderately well sorted medium sand with a coarse sand component [(A/L) 72.9% qz : 27.1% glc]
M: 8.9% S: 89.3% G: 1.8% $CaCO_3$: 5.4%
Sand: 70% qz, 25% blk glc, 2% SkF (EchS, moderate biodiversity p>bF (*G. bulloides* present), 1-2% PCG
Gravel: <1P pink granite with PCG and qz granules, ste lths and Bv-Shl (including *Anomia* sp.). PCG of various types including qz vfS and glc mS. (No typical latest Pleistocene Ost, Agnl, bF or HS present) **Qz:** bimodal with dominate mS with minor mod- to w-md cS.

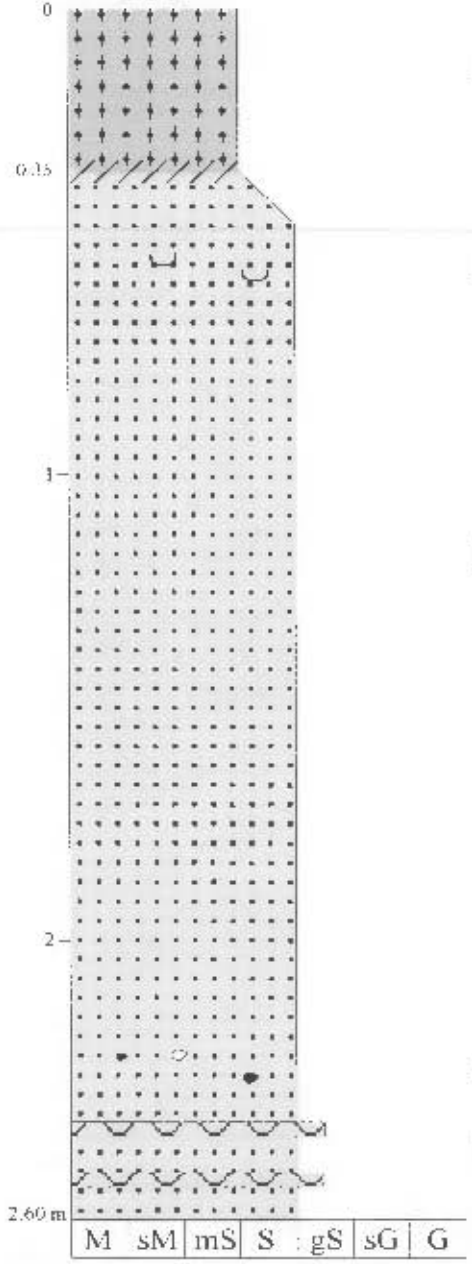
93-119 cm: Extensively biturbated below sharp contact

-3: 111-116 cm: Muddy quartzose sand
M: 28.1% S: 71.9% G: 0% $CaCO_3$: 3.7%
Sand: <125 mm: 99% ang qz & 1% glc, bF and SSp. >125 mm: *Nodogerina* sp.; ?*Nodosaria* sp., gypsum-cemented aggregates, EchS and contamination from above.



University of Cape Town

108



■ 1 **-1:** 10-15 cm: Muddy sand
M: 15.7% S: 84.3% G: 0% $CaCO_3$: 4.2%
Sand: see -2, but includes 2-3% faecal mud and qz mud-stained with a Holocene foram. assemblage incl. *Marginulina* sp. and trace EchS.
0 ~35 cm: Holocene faecal pellet muddy sand

■ 2 -2: 50-55 cm Sand [(A/L) 79.1% qz : 20.9% glc]
M: 5.4% S: 93.1% G: 1.5% $CaCO_3$: 5.3%
Sand: See -3 to -5, but includes 3-5% Pleistocene b+pF, Ost, HS assemblage with 1%g+Bv ShF.
Gravel: <mP *P. abbreviatus*, *L. chuni*, *Cardiella* sp., scaphopods, otoliths and EchP, vfP worn *T. declivis* and other ShF, 5X glc-stained qz and 1X PCG granules.
Sample includes small concentration of well preserved bivalves.

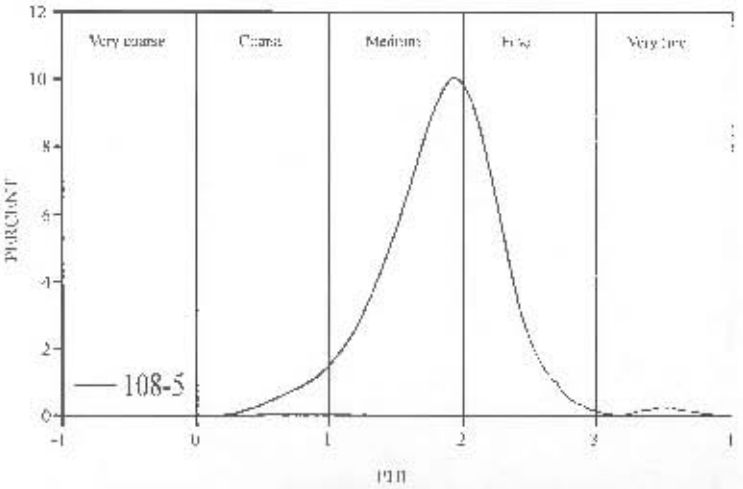
■ 3 **-3:** 115-120 cm: Sand
M: 4.1% S: 95.9% G: 0% $CaCO_3$: 3.1%
Sand: See -5. Includes trace Ph, pF-SkF, PCG fragments, SPG and 1X pink feldspar grain. **Qz:** relative abundance of pink grains, milky to clear w-md grains present. **Glc:** blk, polished w th minor to subordinate green pellets

~35-250 cm: Uniform mottled medium glauconite quartz sand with an coarser quartz-rich patches. Decrease in cementation up-core.

■ 4 -4: 225-230 cm. Sand [(A/L) 77.2% qz : 22.8% glc]
M: 4.2% S: 95.2% G: 0.6% $CaCO_3$: 3.5%
Sand: See -5, but inc. in mS blk, polished glc
Gravel: rounded PCG (cast?) and glc-stained qz granules, otolith and Ph-SPG

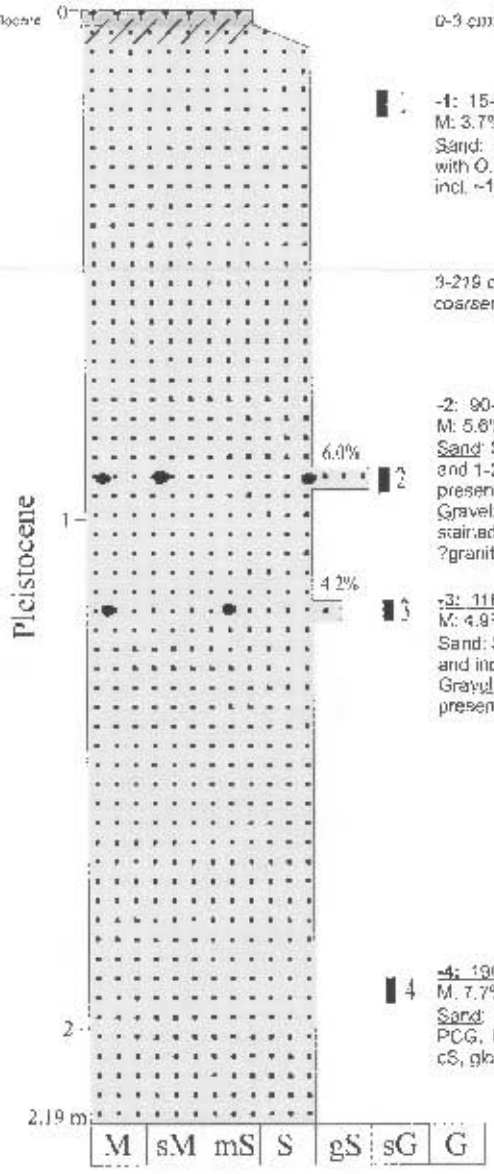
■ 5 -5: 200-205 cm: Moderately well sorted medium sand with a minor cS qz component
[(A/L) 80.7% qz : 19.3% glc]
M: 6.9% S: 92.9% G: 0.2% $CaCO_3$: 2.6%
Sand: 79% qz, 19% glc, 1-2% SkF (ShF, EchS, low diversity b+pF). **Qz:** ang to w-md. milky to frosted. **Glc:** 1-mS blk & green fractured grains.
Gravel: v. wum: Bv-ShF and ?co-cemented *in situ* sand

Two thin layers at 240 & 250 cm with concentrations of worn shell fragments



University of Cape Town

109



0-3 cm: Thin faecal pellet muddy sand

-1: 15-20 cm: Sand [78.0% qz : 22.0% glc]
M: 3.7% S: 96.2% G: 0.1% $CaCO_3$: 4.7%
Sand: 75% qz, 20% glc, 5% SkF (moderate biodiversity pF>bF with *O. universa*, *G. inflata* > *G. bulloides* (no aggl bF and Ost.) incl. ~1% EchS and 1% ShF)

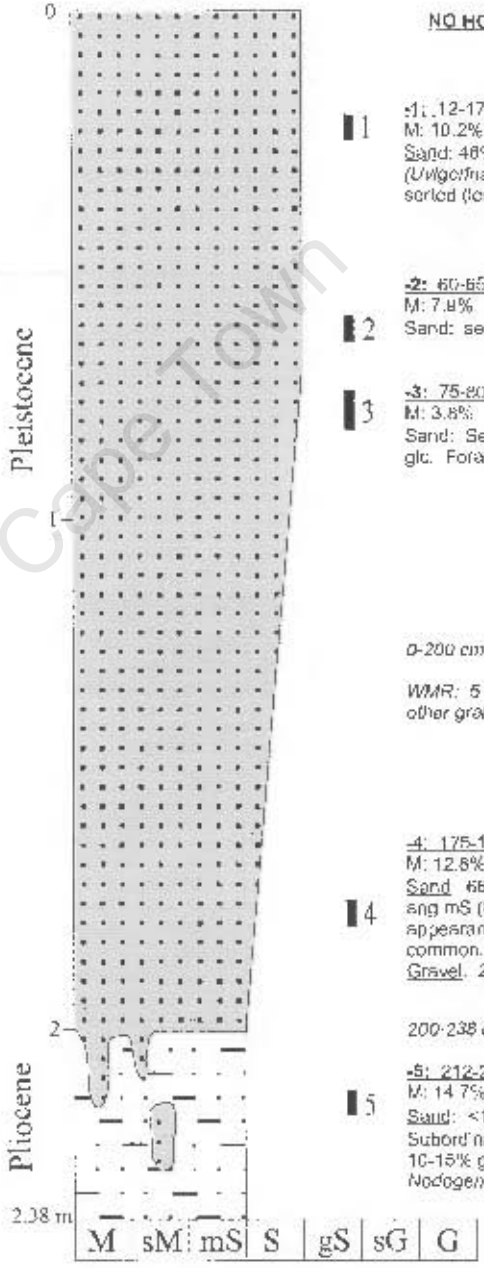
3-219 cm: Uniform mottled medium glauconite quartz sand with coarser quartz-rich patches.

-2: 90-95 cm. Gravelly sand [79.8% qz : 20.2% glc]
M: 5.6% S: 88.4% G: 6.0% $CaCO_3$: 3.9%
Sand: See -2 (also b.modal), but with <1% SkF, but no forams and 1-2% PCG and Ph-ShF present. Single jasper sand grain present
Gravel: <mP PCG (mixed with qz cS; glc mS; qz vfz) and glc-stained qz granules (PCG>>qz). <mP grey granite, biolite ?granite and agate lithic fragments present).

-3: 116-121 cm: (Gravelly) sand
M: 4.9% S: 90.9% G: 4.2% $CaCO_3$: 4.0%
Sand: See - 4, but with a bimodal qz (& trace PCG) cS component and includes 1% SkF (ShF & trace bioF)
Gravel: <IP 1X pink granite, PCG>qz and 1X PCL. Single agate present.

-4: 190-195 cm: Sand [81.3% qz : 18.7% glc]
M: 7.7% S: 92.3% G: 0% $CaCO_3$: 2.6%
Sand: 80% qz, 20% glc (fractured green pellets dominant), trace PCG, **NO BIOGENIC GRAINS**. **Qz:** well sorted mS with minor cS, glc-staining common and trace red-stained grains present.

110



NO HOLOCENE

-1: 12-17 cm: Muddy sand
M: 10.2% S: 89.8% G: 0% $CaCO_3$: 4.8%
Sand: 46% qz, 48% glc (green >> black pellets), 1% Pleistocene F (*Uvigerina* spp. and *Bulimina* spp., trace *G. inflata*, EchS). **Qz:** better sorted (less cS)

-2: 60-65 cm: Sand
M: 7.8% S: 92.1% G: 0% $CaCO_3$: 5.6%
Sand: see -3

-3: 75-80 cm: Sand [55.4% qz : 44.6% glc]
M: 3.8% S: 96.2% G: 0% $CaCO_3$: 5.3%
Sand: See -4, but better sorted with less qz cS. Slight inc. in blk glc. Forams dominated by *G. inflata* and spiny *Bulimina* sp.

0-200 cm: Uniform medium glc qz sand

WMR: 5 cm well-rounded quartzite pebble with trace jasper, and other granules at 134 cm.

-4: 175-180 cm. Muddy sand [66% qz : 34% glc]
M: 12.8% S: 86.4% G: 0.8% $CaCO_3$: 4.5%
Sand: 66% bimodal qz, 32% glc, 2% SkF. **Qz:** mod sorted with sng mS (trace red-stained grains) and cS component. Diverse appearance ang to w-rnd, frosted, clear, milky and glc-staining common.
Gravel: 2X qz, 2X PCG (gl ms) and gypsum aggregates

200-238 cm: Quartz muddy sand

-5: 212-217 cm: Muddy sand
M: 14.7% S: 85.3% G: 0% $CaCO_3$: 3.5%
Sand: <125 um 99% qz with trace SSP and 1% glc (no F). Subordinate >125 µm fraction (more than usual) incl. 40% qz fS, 10-15% green glc, 25% p+bF (incl. aggl. bF, *O. universa*, *Nodogenerina* sp, EchS, Ph-bone and SSp

University of Cape Town

111

Holocene

Pleistocene

0-54 cm: Uniform mottled medium quartz-glauconite gravelly sand.

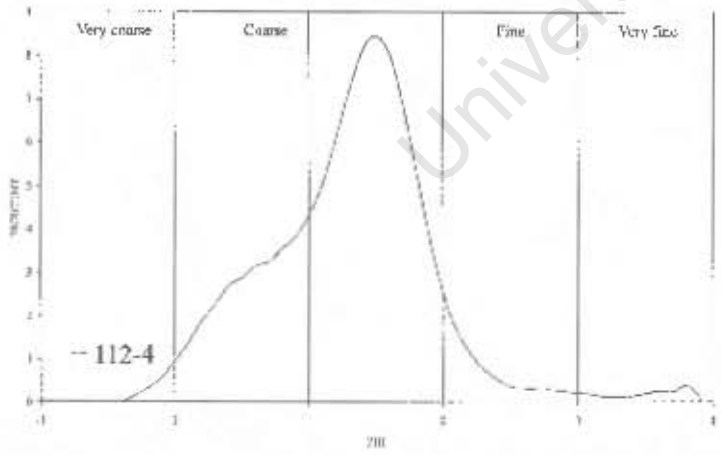
6.4%

2

-2: 42-47 cm: Gravelly sand [58.0% qz : 42.0% glc]
M: 6.6% S: 86.0% G: 6.4% $CaCO_3$: 5.6%
Sand: 57% qz, 41% glc (fractured green pellets), 1% PCG, 1% LchS and trace F. **Qz**: mod to well sorted sand with minor qz cS.
Gravel: <mP PCG (mixed brn to blk - qz nS, glc mS) with vfP PCG > qp
Sample includes isolated pebbles at 45 cm

0.54 m

M | sM | mS | S | gS | sG | G



112

Pleistocene

1

1.72 m

NO HOLOCENE

1

-1: 15-20 cm: Sand
M: 8.7% S: 91.3% G: 0% $CaCO_3$: 4.6%
Sand: well sorted with ~49% qz, 49% (green) glc, 2% SkF (incl 1% LchS with ribbed *Uvigerina* spp., *Globobulimina* sp., *Bulimina* sp., *L. lobatula* and *G. inflata* and ?Miocene *Dentalina* sp.) No Ost, HS

2

-2: 42-47 cm: Sand [60.6% qz : 39.4% glc]
M: 4.5% S: 95.5% G: 0% $CaCO_3$: 4.4%
Sand: See -3 & -4, but includes 2% SkF (EchS, pF>bF with *G. bulloides* > *G. inflata*, moderate biodiversity, includes no Ost, HS).

0-172 cm: Uniform mottled medium glauconitic quartz sand. No scattered shell fragments.

3

-3: 132-138 cm: Sand
M: 6.7% S: 93.3% G: 0% $CaCO_3$: 4.2%
Sand: Seu -4, but includes single jasper grain

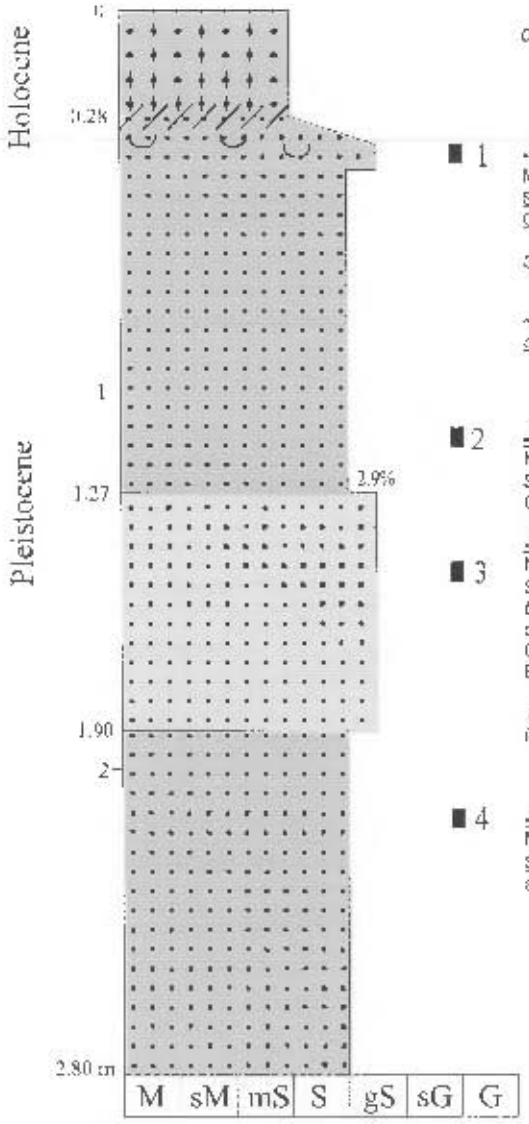
4

-4: 148-153 cm: Sand [69.5% qz : 30.5% glc]
M: 6.8% S: 93.2% G: 0% $CaCO_3$: 4.1%
Sand: 70% qz, 30 % green glc with trace gypsum-cemented aggregates, SPG, and PCG. **NO BIOGENIC GRAINS.**
Qz: Bimodal mS with cS component

M | sM | mS | S | gS | sG | G

University of Cape Town

113



0~28 cm. Holocene faecal pellet muddy sand

■ 1

-1: 35-40 cm: Slightly gravelly sand [55.7% qz 44.3% glc]
M: 8.4% S: 87.6% G: 4.1% $CaCO_3$: 7.1%
Sand: 55% qz, 40% glc, 5% SkF (1% ShF, EchS, high biodiversity with *G. inflata*). No Ost, HS. **Qz:** slightly bimodal with cS component
Gravel: fP PCG (very mixed)>qz granules (glc-stained). SPG (Sk & T)

31-41 cm: Sparsely scattered shells

~28-280 cm. Uniform mottled medium glauconitic quartzose sand. Glauconite-rich laminae tend to be finer grained

■ 2

-2: 110-115 cm: Sand [59.4% qz : 40.6% glc]
M: 5.9% S: 93.8% G: 0.3% $CaCO_3$: 5.0%
Sand: very similar to -4, but 2-3% SkF (pF>bF, lower species biodiversity and *G. inflata* dominant with *G. dutertrei* present)
Gravel: 4X PCG granules

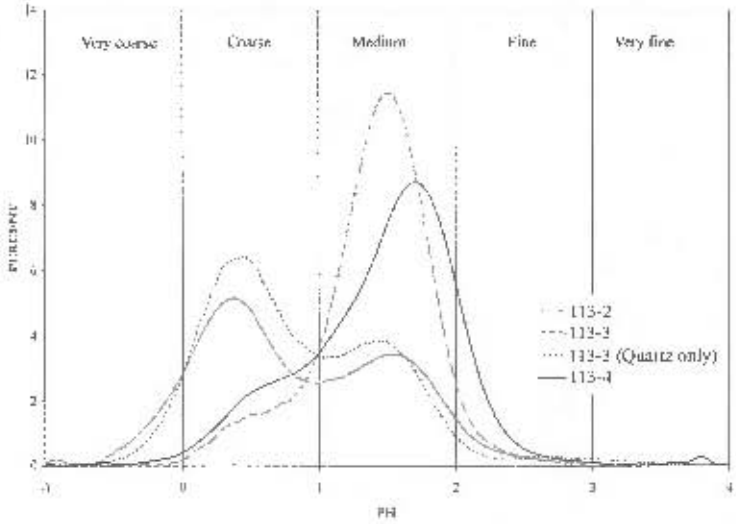
■ 3

-3: 145-150 cm. (Gravelly) sand [74.0% qz : 26.0% glc]
M: 4.4% S: 92.7% G: 2.9% $CaCO_3$: 5.9%
Sand: 70% qz, 25% glc, 5% SkF (ShF, 1% EchS, mod to high biodiversity p=bF with *G. bulloides, O. universa* and *G. inflata*. Ost). **Qz:** strongly bimodal (see magnetically separated qz fraction)
Gravel: <fP PCG>qz (relative abundance of orange-stained qz as well as glc-stained) with Bv-ShF and scaphopods.

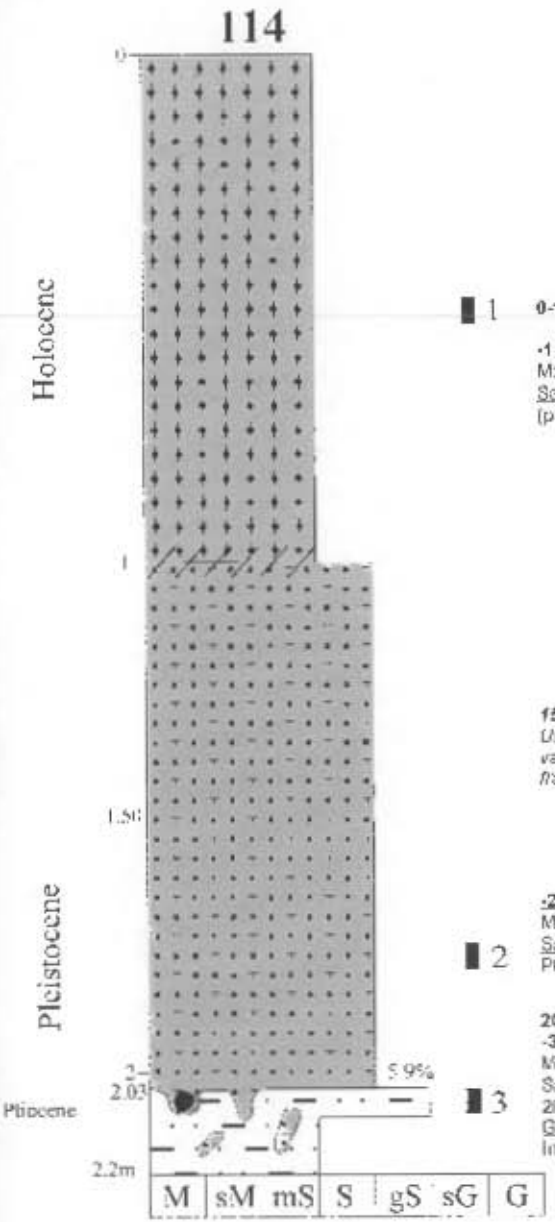
127-190 cm: Coarser grained sand to gravelly sand with higher quartz concentrations. No internal structures (laminations, bioturbation etc.) observed.

■ 4

-4: 210-215 cm: Sand [56.0% qz : 44.0% glc]
M: 2.8% S: 97.2% G: 0% $CaCO_3$: 6.3%
Sand: mod to well sorted 55% qz, 42% green to blk glc with 3% Ph (PCG, orange/amber Ph and Ph-ShF), trace pF (often broken)



University of Cape Town



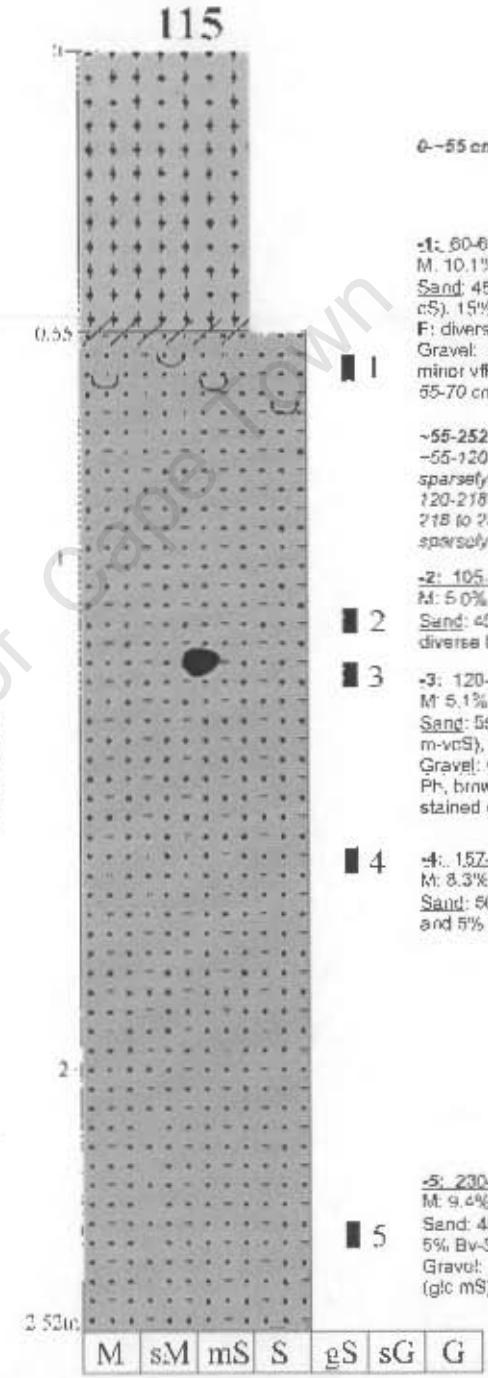
0-150 cm: RECENT FAECAL PELLET MUDDY SAND

-1: 48-53 cm, Muddy sand [28.2% qz : 71.8% glc]
M: 15.9% S: 84.1% G: 0% $CaCO_3$: 10.3%
Sand: 50% blk glc, 5% Au, 15% qz, 10% F and 10% SkF (pF mostly) with trace EchS and SSp

150-203 cm: GLAUCONTIC SAND
Uniform mottled medium quartz-glauconite sand. No variation in grain size. Sparsely scattered shell fragments throughout.

-2: 190-195 cm: Sand [28.4% qz : 71.6% glc]
M: 5.0% S: 95.0% G: 0% $CaCO_3$: 10.9%
Sand: 65% blk glc, 10% Au, 20% qz Au: incl SPG-T, PCG, PP and Ph-Forams

203-220 cm: QUARTZOSE MUDDY SAND
-3: 205-210 cm: Gravelly muddy sand
M: 25.5% S: 68.0% G: 5.9% $CaCO_3$: 6.0%
Sand: 90% qz vfS, 10% glc and trace F. >125 mm: 80% glc, 20% qz, trace EchS, trace b+pF with Ph-F)
Gravel: 1 vdP and vfP irregular dark-brown PCG (glc+qz fvS). Interval extensively bioturbated.



0-55 cm: RECENT FAECAL PELLET MUDDY SAND

-1: 50-65 cm, Slightly gravelly muddy sand [26.4% qz : 73.6% glc]
M: 10.1% S: 88.6% G: 1.3% $CaCO_3$: 17.5%
Sand: 45% blk & grn glc, 10% Au (5% PCG (glc mS)), 20% qz (5% qz m-cS). 15% F and 5% SkF (Bv mostly) with trace EchS, Ost, HS and Ssp.
F: diverse pF~hF
Gravel: <mP ShF (*T. declivis*, at least 5 Bv species, EchP, Bry, G) with minor vfP and dark-brown PCG (glc mS) and md green-stained qz.
55-70 cm: scattered shell fragments

~55-252 cm: GLAUCONITIC SAND
~55-120 cm: Uniform mottled medium (quartz) glauconite sand with sparsely scattered shell fragments.
120-218 cm: Finer sand with occasional fine quartz-rich lamellae present.
218 to 252 cm: Uniform mottled medium (quartz) glauconite sand with sparsely scattered shell fragments.

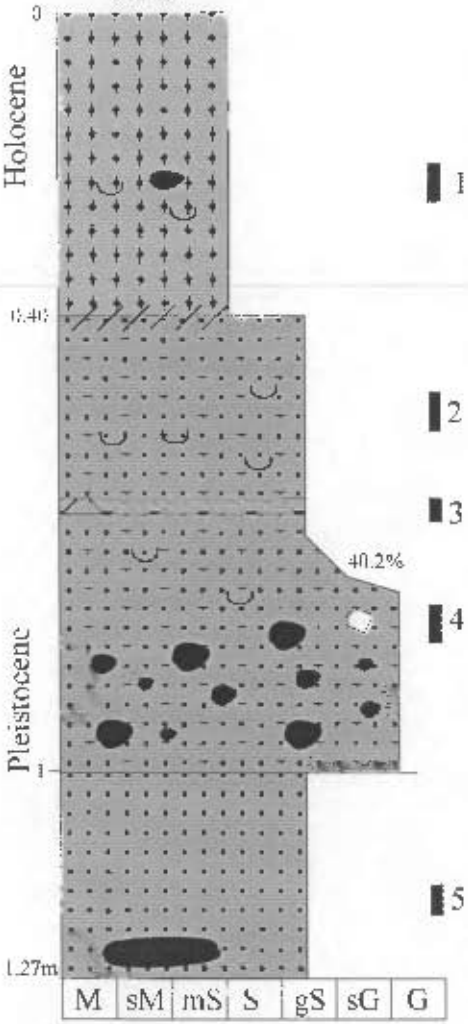
-2: 105-110 cm: Sand
M: 5.0% S: 95.0% G: 0% $CaCO_3$: 16.3%
Sand: 45% blk to grn glc, 15% Au, 25% qz (5-8% m-vcS), 10% Pleistocene diverse b=pF and 5% SkF with 1% EchS and trace Ost and HS.

-3: 120-125 cm, Muddy slightly gravelly sand [17.8% qz : 82.2% glc]
M: 5.1% S: 94.4% G: 0.5% $CaCO_3$: 16.0%
Sand: 55% blk to grn glc, 15% Au (incl 1% vcS PCG (glc mS)), 15% qz (5% m-vcS), 2-3% pF and 5% SkF with 1% EchS and trace Ost and HS.
Gravel: vfP md to sub-md Ph, including dark-brown PCG (glc mS), black Ph, brown PCG (qz (& glc) vfS), brown Ph, amber Ph-ShF, md green-stained qz and md pink granite vfP.

-4: 157-162 cm: Sand
M: 8.3% S: 91.7% G: 0% $CaCO_3$: 11.9%
Sand: 50% blk (to grn) glc, 15% Au, 20% qz (10% m-vcS), 2-3% p>bF and 5% SkF with EchS.

-5: 230-235 cm: Sand [14.7% qz : 85.3% glc]
M: 9.4% S: 90.4% G: 0.3% $CaCO_3$: 17.6%
Sand: 45% blk (to grn) glc, 10% Au, 15% qz (2% m-vcS), 25% p>bF and 5% Bv-ShF with EchS, HS.
Gravel: vfP to fP worn Bv- and EchP-ShF with a single dark-brown PCG (glc mS) and a Ph/micrite-cemented *in situ* glc aggregate.

University of Canterbury



0–40 cm: RECENT FAECAL PELLET MUDDY SAND

-1: 20-25 cm: Slightly gravelly muddy sand
M: 16.4% S: 82.1% G: 1.5% $CaCO_3$: 16.1%
Sand: 50% blk glc, 10% Au, 20% qz (1% m-vcS), 15% robust pF and 10% Bv-ShF with EchS & SSp and 5% FP.
Gravel: Single irregular cP dark-brown PCG (glc mS)
Scattered shell fragments present

-2: 50-55 cm: Slightly gravelly sand [13.0% qz : 87.0% glc]
M: 5.0% S: 93.1% G: 1.9% $CaCO_3$: 22.6%
Sand: 40% blk glc, 15% Au, 10% qz (3% m-vcS), 25% Pleistocene diverse p=bF and 5% Bv-ShF with 1% EchS, Ost & HS.
Gravel: vcP *T. declivis* and *T. sanguinea*. <mP Bv-ShF, EchP, with minor vfP dark-brown PCG (glc mS), micrite-cemented crs md qz and md brown PCG (qz (&glc) vfS), amber Ph-ShF, Ph-cemented *in situ* sand, md green-stained frosted qz and Ph-vertebrae.

84-86 cm: 2 cm thick shell layer

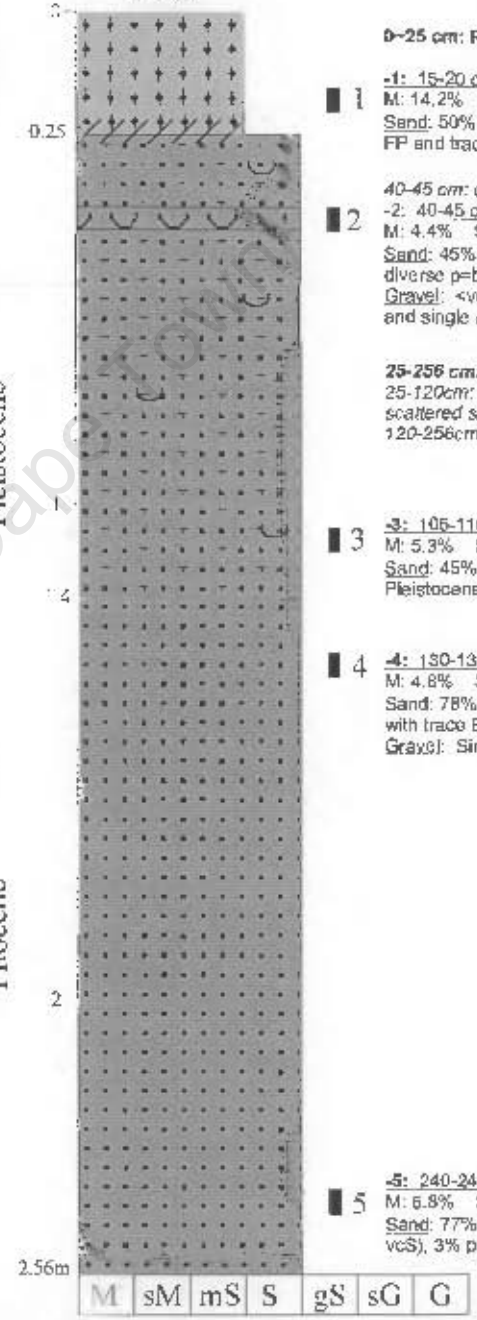
-3: 84-87 cm: Slightly gravelly sand
M: 5.2% S: 91.2% G: 3.6% $CaCO_3$: 19.6%
Sand: 40% blk glc, 15% Au, 10% qz (3% m-vcS), 20% Pleistocene diverse p=bF and 10% Bv-ShF with 1% EchS, Ost & HS.
Gravel: <mP worn diverse ShF (Bv>G) and worn tubes, with minor vfP md dark-brown and brown Ph-cemented glc+qz vfS and md green-stained frosted qz. Single mP brown Ph-cast (qz (& glc) vfS).

-4: 78-83 cm: Muddy sandy gravel [14.2% qz : 85.8% glc]
M: 6.3% S: 53.5% G: 40.2% $CaCO_3$: 13.9%
Sand: 38% blk glc, 10% Au, 15% qz (2% m-vcS), 30% Pleistocene diverse p=bF and 5% Bv-ShF with 1% EchS, Ost & HS.
Gravel: vcP irregular black to dark-brown PCG (glc mS), brown PCG (md qz (& glc) cS) and brown Ph-Bv casts (qz-glc vfS) with amber Ph-Sh dominate. mP micrite-cemented md qz cS and fP md brown Ph, single mP blocky pink granite, <mP brown Ph-casts and <mP worn Bv fragments. vfP include dark-brown PCG (glc mS), brown PCG (qz (& glc) vfS) and md green-stained qz.

-5: 115-120 cm: Slightly gravelly muddy sand [15.9% qz : 84.1% glc]
M: 10.8% S: 86.6% G: 2.6% $CaCO_3$: 13.8%
Sand: 35% blk glc, 10% Au, 20% qz (1% m-vcS), 30% Pleistocene diverse p=bF and 5% Bv-ShF with EchS, Ost & HS.
Gravel: <mP ShF (Solitary coral, Bv (incl. *L. chuni*), hooked limpet, scaphopod, Bry and G) with minor otoliths and vfp brown PCG (qz (&glc) vfS).
Increase in mud content below gravel lag and the last 27 cm of the core was poorly preserved (very dry and cemented).

120-127 cm: Cemented small cobble bagged by WMR (see Figure 7.8)

~40-127 cm: GLAUCONITIC SAND
~40-78 cm: Shell-rich
78-100 cm: Phosphorite gravel layer
100-127 cm: Dried and poorly preserved muddy sand



0–25 cm: RECENT FAECAL PELLET MUDDY SAND

-1: 15-20 cm: Muddy sand
M: 14.2% S: 85.8% G: 0% $CaCO_3$: 18.0%
Sand: 50% blk glc, 10% Au, 20% qz (3% m-vcS), 15% pF with 5% FP and trace EchS & SSp.

40-45 cm: concentration of shell fragments

-2: 40-45 cm: Slightly gravelly sand [4.0% qz : 96.0% glc]
M: 4.4% S: 92.3% G: 3.3% $CaCO_3$: 22.3%
Sand: 45% blk glc, 20% Au, 10% qz (<1% m-vcS), 20% Pleistocene diverse p=bF and 5% Bv-ShF with 1% EchS.
Gravel: <vcP EchP, cP & fP *L. chuni* and minor other ShF (Bv & G) and single *Dentalium* sp.

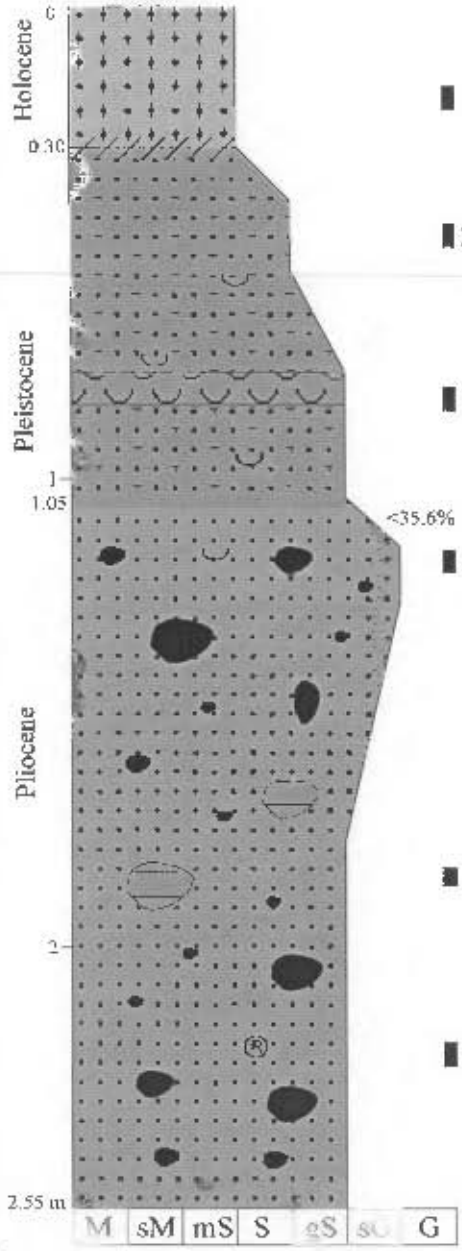
25-256 cm: GLAUCONITIC SAND
25-120cm: Uniform speckled glauconite sand with sparsely scattered shell fragments
120-256cm: Uniform glauconite sand

-3: 105-110 cm: Sand
M: 5.3% S: 94.7% G: 0% $CaCO_3$: 19.8%
Sand: 45% blk (to gm) glc, 20% Au, 10% qz (<1% m-vcS), 20% Pleistocene diverse p=bF and 5% Bv-ShF with 1% EchS, Ost & HS.

-4: 130-135 cm: Sand
M: 4.8% S: 95.1% G: 0.1% $CaCO_3$: 14.0%
Sand: 78% (blk) to gm glc, 10% Au, 10% qz (<1% m-vcS), 1-2% pF with trace EchS.
Gravel: Single fP sub-md dark-brown PCG (glc mS).

-5: 240-245 cm: Sand
M: 6.8% S: 93.2% G: 0% $CaCO_3$: 13.8%
Sand: 77% (blk) to gm glc, 10% Au, 10% qz (<1% m-vcS), 3% pF with trace EchS and cS ShF.

University of Cape Town



0-~30 cm: RECENT FAECAL PELLET MUDDY SAND

1 -1: 15-20 cm: Muddy sand
M: 20.1% S: 79.8% G: 0.1% $CaCO_3$: 19.3%
Sand: 50% blk glc, 10% Au, 20% qz (<1% m-vcS), 15% pF with 5% FP and cemented aggregates and trace EchS & SSp.
Gravel: Single vfP sub-md green-stained frosted qz

2 -2: 45-50 cm: Sand [6.7% qz : 93.3% glc]
M: 7.2% S: 92.1% G: 0.7% $CaCO_3$: 24.8%
Sand: 40% blk to (gm) glc, 20% Au, 10% qz, 20% p>bF, 10% ShF with 1% EchS.
Gravel: <mP ShF (diverse Bv sp., G, EchP, Bry) and 2 green-stained frosted qz grains.

3 *78-85 cm: Shell layer with articulated fragile bivalves (includes WMR: N. virctus, A. bulloides, L. churii, P. abbreviatus)*
-3: 80-85 cm: Gravelly muddy sand
M: 12.3% S: 71.7% G: 16.0% $CaCO_3$: 24.2%
Sand: 40% blk to (gm) glc, 20% Au (PP, SPG), 15% qz (1% mS), 15% p=bF, 10% ShF (Bv, scaphopods) with 1% EchS.
Gravel: <cP v. worn ShF (Bv > Dentalium sp.), otolith and minor vfP SPG. Minor vfP dark-brn PCG (glc mS), brn PCG (glc cS) and glc-stained frosted qz grains.

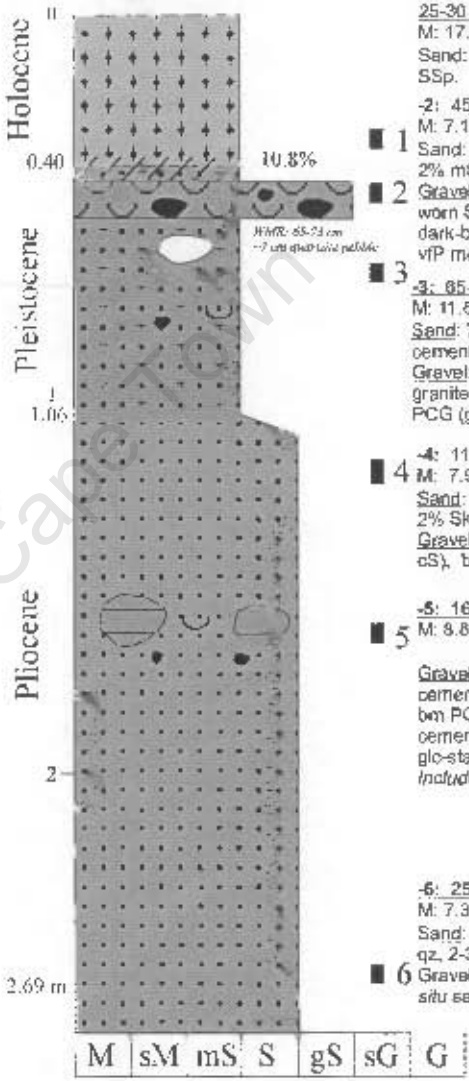
4 -4: 115-120 cm: Muddy sandy gravel
M: 8.1% S: 56.4% G: 35.6% $CaCO_3$: 18.0%
Sand: 75% gm glc, 10% Au, 10% qz (<1% mS), 4% p>bF, trace Bv-ShF & Ost.
Gravel: sC Ph-cemented *in situ* sand, cP brn PCG with clasts (incl. brn PCG (qz (& glc) cS), vfP Ph-cemented *in situ* sand and dark-brn PCG (glc mS).

30-255 cm: GLAUCONITIC SAND
30-105 cm: Uniform speckled glauconite sand with sparsely scattered shell fragments
~105-~255 cm: Uniform glauconite sand with mud-rich patches between 160-165 cm.

5 -5: 168-172 cm: Gravelly muddy sand [11.0% qz : 89.0% glc]
M: 13.8% S: 77.6% G: 8.7% $CaCO_3$: 19.2%
Sand: 75% gm glc, 10% Au and 15% qz (<1% mS)
Gravel: <mP Ph cemented *in situ* sand with vfP dark-brn PCG (glc mS) and brn PCG (qz (& glc) cS). (Cement completely Ph)

105-255 cm: Includes *in situ* cemented aggregates

6 220-225 cm: Gravelly muddy sand [5.2% qz : 94.8% glc]
M: 14.8% S: 56.8% G: 28.4% $CaCO_3$: 26.9%
Sand: 60% gm glc, 25% Au and 15% qz. Lots of cemented aggregates - mostly gypsum and pyrite/siderite
Gravel: sC & <mP Phmicrite-cemented *in situ* sand with trace Ph-Pc ShF and md brown PCG (qz (& glc) vfS). (Partial and variable replacement of micrite-cement)



0-~40cm: RECENT FAECAL PELLET MUDDY SAND
25-30 cm: Muddy sand
M: 17.2% / S: 82.4% / G: 0.4% $CaCO_3$: 18.9%
Sand: 50% blk glc, 10% Au, 20% qz, 25% SkF, 5% FP with EchS & SSp.

1 -2: 45-50 cm: Gravelly sand from within 45-55 cm shell-rich interval
M: 7.1% S: 82.1% G: 10.6% $CaCO_3$: 22.9%
Sand: 40% blk glc, 15% Au (PCG (glc mS), Ph-F, SPG), 20% qz (1-2% mS), 15% p=bF, 10% Bv-ShF with 1% EchS.

2 Gravel: vcP *T. declivis* ShF's (with original colour), other cP very worn ShF incl. *L. churii*, Bv, G, *D. plumbissulatum*, otoliths, <mP dark-brown PCG (glc mS) & vfP brown Ph-casts (qz (& glc cS) and vfP md green-stained frosted qz. (Gravel mixed ShF-Ph pebbles)

3 -3: 65-70 cm: Slightly gravelly muddy sand [3.3% qz : 96.7% glc]
M: 11.6% S: 85.3% G: 2.9% $CaCO_3$: 12.9%
Sand: 70% gm glc, 10% Au, 15% qz (<1% mS), 2% SkF with 2% Fe-cemented aggregates of *in situ* sand.
Gravel: <mP md brown PCG (qz (& glc) vfS), mP weathered blocky granite, <mP worn ShF (*L. churii* & Bv), vfP Ph-ShF, dark-brown PCG (glc mS) and md green-stained frosted qz.

4 -4: 117-123 cm: Sand
M: 7.9% S: 91.7% G: 0.4% $CaCO_3$: 13.0%
Sand: 80% blk (to gm) glc, 15% Au (PCG, SPG, Ph-pF), 5% qz, 2% SkF.
Gravel: vfP dark-brown PCG (glc mS), blk Ph, brn PCG (md qz cS), brn PCG (qz vfS) and glc-stained frosted qz.

5 -5: 160-165 cm: Gravelly muddy sand [6.2% qz : 93.8% glc]
M: 8.8% S: 76.8% G: 14.4% $CaCO_3$: 15.2%

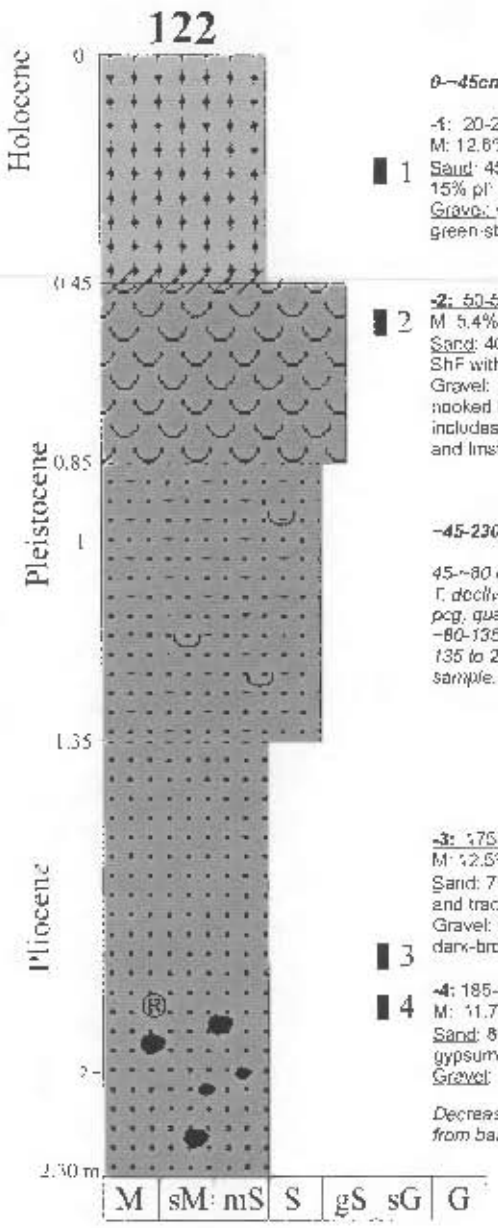
Gravel: vcP & vfP angular brn PCG (biogenic-qz fS) with micrite-cemented clasts of a similar biogenic-qz vfS, <mP irregular dark-brn PCG (glc mS), brn Ph-mollusc casts (qz (& glc) vfS), <fP Ph-cemented *in situ* sand, micrite-cemented md qz cS, Ph-ShF, md glc-stained frosted qz and trace vfP ShF.
Includes brown mud-rich intervals with shell and pebble material.

-5: 250-255 cm: Sand [2.2% qz : 97.8% glc]
M: 7.3% S: 92.2% G: 0.5% $CaCO_3$: 13.0%
Sand: 80% blk (to gm) glc, 10% Au (PCG, SPG, Ph-pF), 5-7% qz, 2-3% SkF (to=pF, aggl. bF) with SPG and G-cast.

6 Gravel: Three vfP dark-brn PCG (glc mS) and a Ph-cemented *in situ* sand.

120
~40-269 cm: GLAUCONITIC SAND
~40-106 cm: Uniform olive-grey speckled glauconite sand with oxidised iron rich concentration at 65 cm.
~106-~269 cm: Uniform glauconite sand with mud-rich patches between 160-165 cm.

© University of Canterbury



0–45cm: RECENT FAECAL PELLET MUDDY SAND

-1: 20-25 cm: Muddy sand
M: 12.6% S: 87.3% G: 0.1% $CaCO_3$: 19.7%
Sand: 45% blk glc, 15% Au (PCG, PP, Ph-pF), 20% qz (<1% m-vcS), 15% pF (incl. ~5 % fragments) with 5% FP and trace EchS & SSp.
Gravel: vfP md dark-brown PCG (glc mS), brown Ph and sub-rnd green-stained frosted qz granules.

-2: 50-55 cm: Slightly gravelly sand
M: 5.4% S: 89.7% G: 4.9% $CaCO_3$: 23.5%
Sand: 40% blk glc, 15% Au, 20% qz (<1% m-vcS), 15% diverse b-pF & 10% ShF with EchS.
Gravel: vcP *A. bulloides* ShF, <mP diverse G & Bv ShF incl. *Hiatella* sp., hooked limpets, scaphopods, EchS, EchP and otoliths. Minor Ph present includes vfP Ph-ShF and <mP irregular dark-brown PCG (Au+qz+F f-mS) and limst with md brown PCG clast.

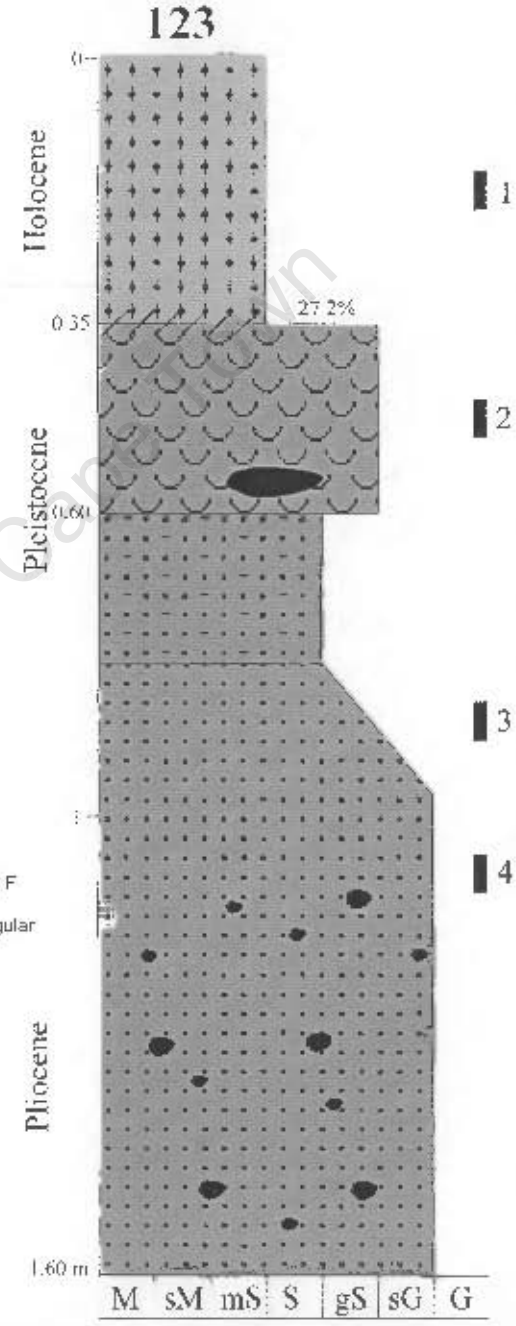
45–230 cm: GLAUCONITIC SAND

45-~80 cm: Shell-rich interval with discrete shelly layers (WMR: includes T. declivis, L. chuni), scaphopods) Pebbles include quartz conglomerate, pcg, quartzite etc.
~80-135 cm: Speckled glauconite sand with scattered shell fragments
135 to 230 cm : Green mud-rich interval. Cemented and difficult to sample.

-3: 175-180 cm: Slightly gravelly muddy sand [2.7% qz : 97.3% glc]
M: 12.5% S: 84.8% G: 2.7% $CaCO_3$: 22.8%
Sand: 75% grn glc, 130% Au (PCG and SPG) and 10% qz (<1% mS) woth 2% F and trace Pc-ShF.
Gravel: < mP md brown Ph-mollusc casts (qz (& glc) vfS) and vfP angular irregular dark-brown PCG (glc mS).

-4: 185-190 cm: Muddy sand
M: 11.7% S: 87.5% G: 0.8% $CaCO_3$: 16.8%
Sand: 80% grn glc, 15% In situ cemented aggregates, 5% qz with trace pF & gypsum aggregates.
Gravel: <mP angular irregular dark-brown PCG (glc mS).

Decreasing concentration of phosphatised shell and PCG (glc-rich) pebbles from base of core to ~190 cm



0–35cm: RECENT FAECAL PELLET MUDDY SAND

-1: 15-20 cm: Muddy sand
M: 15.6% S: 84.4% G: 0% $CaCO_3$: 19.6%.
Sand: 50% blk glc, 10% Au (PCG, PP, Ph-pF), 20% qz (<1% m-vcS), 15% pF (incl. ~5 % fragments) with 5% FP and trace EchS & SSp.

45-50 cm: Gravelly sand
M: 5.0% / S: 67.8% / G: 27.2% $CaCO_3$: 23.2%
Sand: 40% blk glc; 15% Au; 15% qz vfS; 15% F (p-b); 15% ShF (EchP, Bv, G) with minor EchS, Ost and qz mS.
Gravel: sC angular irregular dark-brn PCG (glc mS), <mP diverse Bv and IP dark-brown PCG (md qz (& glc) cS).

~35-160 cm: GLAUCONITIC SAND
35-~60 cm: Shell-rich interval with concentration of shell fragments (WMR: includes L. Chuni)
60-80 cm: Speckled glauconite sand with scattered shell fragments80- 160 cm: A green mud-rich unit which includes scattered Ph pebbles

-3: 80-85 cm: Slightly gravelly medium sand
[2.7% qz : 97.3% glc]
M: 7.5% S: 90.2% G: 2.3% $CaCO_3$: 18.5%
Sand: 70% grn glc; 10% Au; 13% qz vfS; 5% F and 2% Bv-ShF with minor qz mS.
Gravel: < mP ShF, including worn Bv and other Bv, Br, *Dentalium* sp., EchS and otoliths and vfP dark-brown PCG (glc mS), brown Ph-casts (qz (& glc) vfS) and sub-rnd green-stained frosted qz. (Gravel mixed ShF-Ph pebbles)

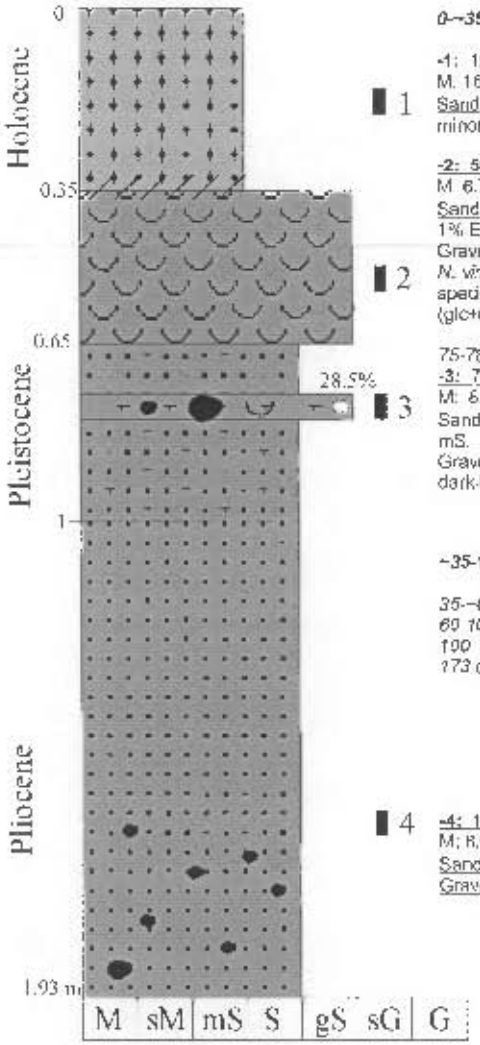
WMR: 80-85 cm: Pebble lag with quartzite (4 cm) and schist (5 cm) pebbles

-4: 105-110 cm: Muddy sandy gravel
[3.1% qz : 96.9% glc]
M: 6.4% S: 47.5% G: 46.2% $CaCO_3$: 15.6%
Sand (mS): 75% grn glc; 5% Au; 13% qz vfS; 2% F and 5% *in situ* Ph-cemented aggregates with minor qz mS.
Gravel: sC Ph (& oc) cemented *in situ* sand

SAND DESCRIPTION NOTES :
F: includes all foraminiferal fragments
Au: Mix of Ph-pF test with glc infilling, yellowish-brown Ph fragments, Ph-ShF, PCG (glc mS), PP, SPG (teeth & bone) and trace Ph mollusc casts (qz vfs).

University of Canterbury

125



0–35cm: RECENT FAECAL PELLET MUDDY SAND

-1: 15-20 cm: Muddy sand
M: 16.7% S: 83.3% G: 0% $CaCO_3$: 18.1%
Sand: 50% blk glc, 15% Au, 20% qz vfS, 15% F (p>b) and 5% FP with minor SSp, EchS and qz mS.

-2: 50-55 cm: Gravelly sand [3.4% qz : 96.6% glc]
M: 6.7% S: 86.2% G: 7.1% $CaCO_3$: 22.2%
Sand: 40% blk glc, 15% Au, 20% qz vfS, 15% F(p>b), 10% ShF (Bv, G), 1% EchS with minor Ost and qz mS.
Gravel: <vcP of *T. declivis* and Bv-ShF incl. *L. chuni*, *Pecten* with <mP of *N. vinctus*, *A. bulloides*, *M. pisum*, EchP and EchS, Bry and other fP G species. *L. chuni* and *A. bulloides* very worn. Two vfP dark-brown PCG (glc+qz mS).

75-78 cm: gravelly layer
-3: 75-80 cm: Gravelly muddy sand [2.5% qz : 97.5% glc]
M: 6.1% S: 63.4% G: 28.5% $CaCO_3$: 18.3%
Sand: 75% grn glc, 10% Au, 10% qz vfS, 5% F with minor EchS and qz mS.
Gravel: cP of *in situ* ph/micrite-cemented glc sand with vfP of angular dark-brown PCG (glc+qz mS), rnd green-stained frosted qz and Bv ShF.

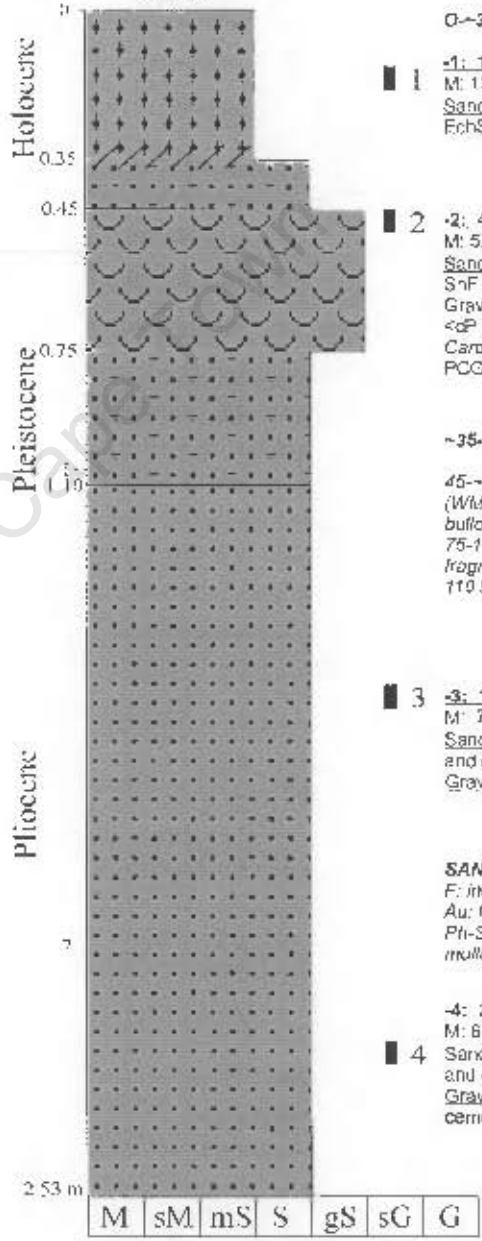
~35-160 cm: GLAUCONITIC SAND

35–65 cm: Shell-rich interval with concentration of shell fragments 60-100 cm. Speckled glauconite sand with scattered shell fragments 100-193 cm. A green mud rich unit with scattered Ph pebbles below 173 cm.

-4: 125-130 cm: Sand [3.2% qz : 96.8% glc]
M: 8.0% S: 91.9% G: 0.1% $CaCO_3$: 16.10%
Sand: 70% grn glc, 10% Au, 15% qz vfS, 4% F and 1% qz mS
Gravel: angular vfP qz and Bv-ShF

SAND DESCRIPTION NOTES :
F: includes all foraminiferal fragments
Au: Mix of Ph-pF tes with glc infill, yellowish-brown Ph fragments, Ph-SkF, PCG (glc mS), PP, SPG (teeth & bone) and trace Ph mollusc casts (qz vfs).

126



0–35 cm: RECENT FAECAL PELLET RICH MUDDY SAND

-1: 15-20 cm: Muddy sand [4.9% qz : 95.1% glc]
M: 13.5% S: 86.5% G: 0% $CaCO_3$: 19.9%
Sand: 50% blk glc, 15% Au, 20% qz vfS, 15% F (p>b) with minor EchS, SSp and qz mS.

-2: 45-50 cm: Gravelly medium sand [4.2% qz : 95.8% glc]
M: 5.1% S: 88.9% G: 56.0% $CaCO_3$: 24.6%
Sand: 40% blk glc, 10% Au, 20% qz vfS, 15% F (p–b, aggl.); 14% ShF (Bv, Solitary coral), 1% EchS with minor Ost and qz mS.
Gravel: cP *Volutocorbis abyssicola* and Ph-bone fragments with <cP *T. declivis*. Bry. otoliths, hooked limpet sp., vfP *L. chuni*, *Cardiella* sp. and other small Bv and G. Three vfP ang dark-brown PCG.

~35-253 cm: GLAUCONITIC SAND

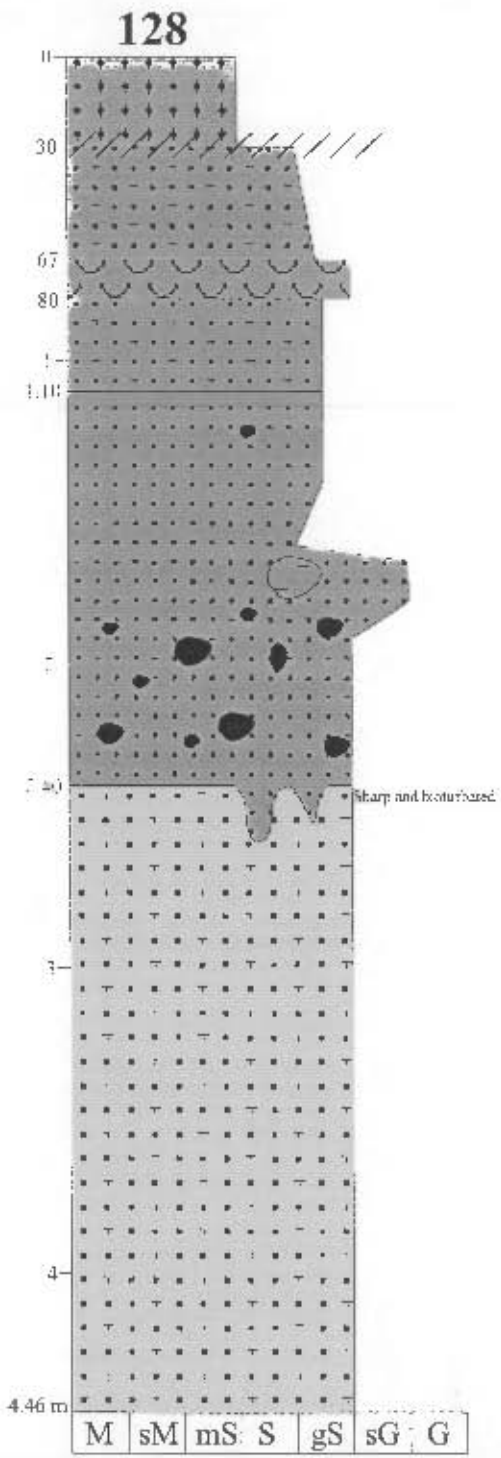
45–~75 cm: Shell-rich interval with discrete shelly layers (WMR: Includes L. Chuni (often articulated) and A. bulloides.
75-110 cm: Speckled glauconite sand with scattered shell fragments with increasing concentration upcore.
110 to 239 cm : Uniform glauconite sand

-3: 140-145 cm: Medium sand
M: 7.3% S: 92.6% G: 0.1% $CaCO_3$: 18.1%
Sand: 60% grn glc, 15% Au, 15% qz vfS 10% F with minor EchS and qz mS.
Gravel: vfP of micrite-cemented glc aggregates and a ShF.

SAND DESCRIPTION NOTES :
F: includes all foraminiferal fragments
Au: Mix of Ph-pF tes with glc infill, yellowish-brown Ph fragments, Ph-SkF, PCG (glc mS), PP, SPG (teeth & bone) and trace Ph mollusc casts (qz vfs).

-4: 220-225 cm: Medium Sand [3.4% qz : 96.6% glc]
M: 6.4% S: 93.4% G: 0.2% $CaCO_3$: 18.5%
Sand: 70% grn glc; 10% Au; 15% qz vfS: 5% F with minor EchS and qz mS.
Gravel: vfP of ang dark-brown PCG (glc+qz mS) and Ph/micrite cemented glc aggregate.

University of Canterbury



■ 1

-1: 20-25 cm: Moderately well to well sorted medium muddy sand **[128-1]** [9.8% non-mag : 75.5% mag : 14.7% semi-mag (A/L: 4.8% qz : 95.2% glc)] M: 11.9% S: 86.1% G: 0% $CaCO_3$: 21.7%.
Sand: 40.5% blk glc, 11.3% Au (yellowish-brown md Ph fS-cS & pF); 25.8% qz vfs, 0.3% qz mS; 4.9% F (pF>bF, aggl.); 16.9% SkF (F) and 0.3% EchS with minor SSP and SPG.

■ 2

-2: 40-45 cm: Moderately well to well sorted medium sand. [14.2% non-mag : 81.0% mag : 4.8% semi-mag] M: 2.9% / S: 96.7% / G: 0.3%
Sand: 31.6% blk glc; 17.7% Au (yellowish-brown md Ph fS-cS & pF); 23.4% qz vfs; 0.4% qz mS; 11.0% F (pF>bF, aggl.); 15.6% SkF (F~ShF) and 0.4% EchS with minor SPG.
Gravel: includes fP of worm Bv and G ShF and an ang vfP light-brown Ph-cemented *in situ* sand.

■ 3

-3: 60-65 cm: Moderately sorted slightly gravelly medium sand [17.7% non-mag : 79.7% mag : 2.6% semi-mag] M: 3.9% S: 94.2% G: 1.9%
Sand: 37.9% blk glc; 15.6% Au (yellowish-brown md Ph fS-cS & pF); 15.1% qz vfs; 0.3% qz mS; 10.6% F (pF>bF, aggl.); 11.3% SkF (F>Bry, Bv-ShF), 0.6% EchS and 0.3% OsL with minor EchS and SPG.
Gravel: <mP Bry, <fP *M. plaum*, solitary corsi, vfP *Cavitella* sp. and other Bv, SPG and a subrnd qz grain.

■ 4

-4: 80-85 cm: Moderately to moderately well sorted slightly gravelly medium sand **[128-2]** [13.1% non-mag : 85.5% mag : 1.5% semi-mag (A/L: 4.1% qz : 95.9% glc)] M: 6.9% S: 90.5% G: 2.6% $CaCO_3$: 25.5%

■ 5

Sand: 33.3% blk glc; 9.1% Au (yellowish-brown md Ph fS-cS & pF); 20.3% qz vfs; 0.4% qz mS; 12.3% F (pF>bF) and 24.8% SkF (F>Bv-ShF) with minor EchS and SPG.
Gravel: <mP Bv-ShF, solitary corsi, vf-fP *A. chami*, Bv-Bru-G-Bry-Ech ShF, *Centalium* sp. and an ang qz grain.

-5: 90-95 cm: Moderately well to well sorted slightly gravelly med um sand [8.6% non-mag : 90.2% mag : 1.2% semi-mag] M: 5.5% S: 92.1% G: 2.4%
Sand: 47.5% blk glc; 16.5% Au (yellowish-brown md Ph fS-cS & pF); 17.0% qz vfs; 0.3% qz mS; 7.4% F (pF>bF) and 9.3% SkF (F~Bv-ShF) with minor EchS.
Gravel: <mP Bv-ShF (incl. ??) and a vfP G. vfP Ph (black Ph, dark-brown PCG (glc mS), brown PCG cast (qz (& glc) vfS). Ph/micrite-cemented *in situ* sand, ShF with minor sub-md qz, otoliths and SPG. Bv Sh-F tend to be thick shelled and worn.

■ 6

-6: 120-125 cm: Moderately well to well sorted slightly gravelly medium sand [4.4% non-mag : 94.7% mag : 0.9% semi-mag] M: 7.6% S: 90.9% G: 1.5%
Sand: 66.1% gm glc; 4.7% Au (yellowish-brown md PhfS-cS, minor pF); 23.0% qz vfs; 7.2% F (b~p) with minor qz mS, PP and a single pyrite aggregate.
Gravel: vfP-fP of brown PCG (Au+qz+F f-mS) and brown PCG crs earthy glc.

■ 7

-7: 150-155 cm: Moderately well to well sorted medium sand **[128-3]** [4.6% non-mag : 94.5% mag : 0.9% semi-mag] M: 9.7% S: 90.3% G: 0% $CaCO_3$: 22.5%
Sand: 66.0% gm glc; 10.5% Au (yellowish-brown md PhfS-cS & pF); 21.1% qz vfs; 3.3% F (b>p) with minor qz mS, SPG (tooth/bone) and a single Ph-cemented *in situ* sand.

■ 8

-8: 170-175 cm: Moderately well to well sorted muddy sandy gravel (medium sand) [7.9% non-mag : 78.5% mag : 13.6% semi-mag] M: 8.4% S: 48.2% G: 43.4%
Sand: 48.1% Au (pF); 34.5% gm glc; 9.5% qz vfs; 0.4% qz mS; 2.3% F (p>b, aggl.) and 5.3% Ph/gypsum (& Pyrite) cemented aggregates with minor SPG (tooth/bone) an PP.
Gravel: Single ang vcP of Ph/micrite-cemented *in situ* glc mS with minor qz and F. vfP-fP A/A and irregular dark-brn PCG (Au f-mS).

■ 9

-9: 208-216 cm: Moderately well to well sorted gravelly muddy medium to fine sand (mean of 1.99 phi) [1.3% non-mag : 35.8% mag : 42.9% semi-mag] M: 9.1% S: 63.7% G: 27.2%
Sand: 62.7% Au (pF); 21.0% gm-blk glc; 5.4% qz vfs; 10.8% SkF (F p>b, aggl.) with minor Bv-ShF, qz mS and SPG (tooth/bone).
Gravel: Single vcP irregular clast-rich dark-brn PCG (Au+qz+F f-mS). Clast incl. light-brown PCG (SkF). vfP of mixed Ph-types (light-brn casts, brn Ph, dark-brn PCG.

■ 10

Minor fP Pc-ShF and Bv-ShF.
-10: 225-230 cm: Moderately well sorted gravelly muddy fine sand **[128-4]** [27.6% non-mag : 42.5% mag : 29.8% semi-mag (A/L 5.4% qz : 94.6% glc)]
M: 10.5.9% S: 69.9% G: 19.6% $CaCO_3$: 46.8%
Sand: 66.6% Au (pF); 7.9% gm-blk glc; 3.1% qz vfs; 1.4% F (p>b, aggl.), 1% Bv & EchP-ShF with minor qz mS, blk rnd Ph vcS, PCG (glc mS) vcS and SPG (Sk & T).
Gravel: <cP irregular Ph, dominated by dark-brown PCG (Au+qz+F f-mS) *In situ* cemented sand mP, fP-vfP also include casts, dark-brown Ph cast in brown Ph-cemented biogenic sand. Pc-ShF and a subrnd qz vfP

■ 11

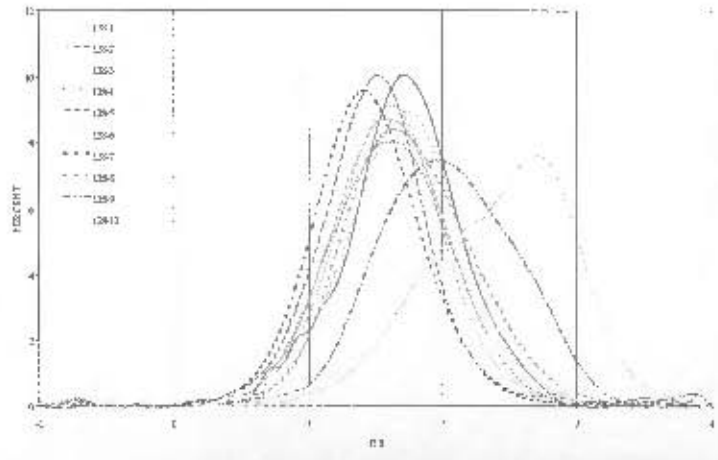
-11: 265-270 cm: Gravelly muddy sand **[126-5]**
M: 14.0% S: 74.8% G: 11.0% $CaCO_3$: 75.4%
Sand (~250mm): 42.6% Au (ph>glc), 33.2% F (p=b), 21.6% ShF, 2.6% qz, ~1% ostracods
Qz: vf-fS ang, trace md cS **Glc:** earthy green/brown mixed mineral. **Ph:** Includes both F-tests replaced with amber Ph and amber Ph fragments.
ShF: F-tests, Ech, Bv, bF: Incl. aggl. & other med-srs bF
Gravel: mP Bry, Pc, ShF, Sharks-Tooth and PCG (brown Ph glc>qz)

■ 12

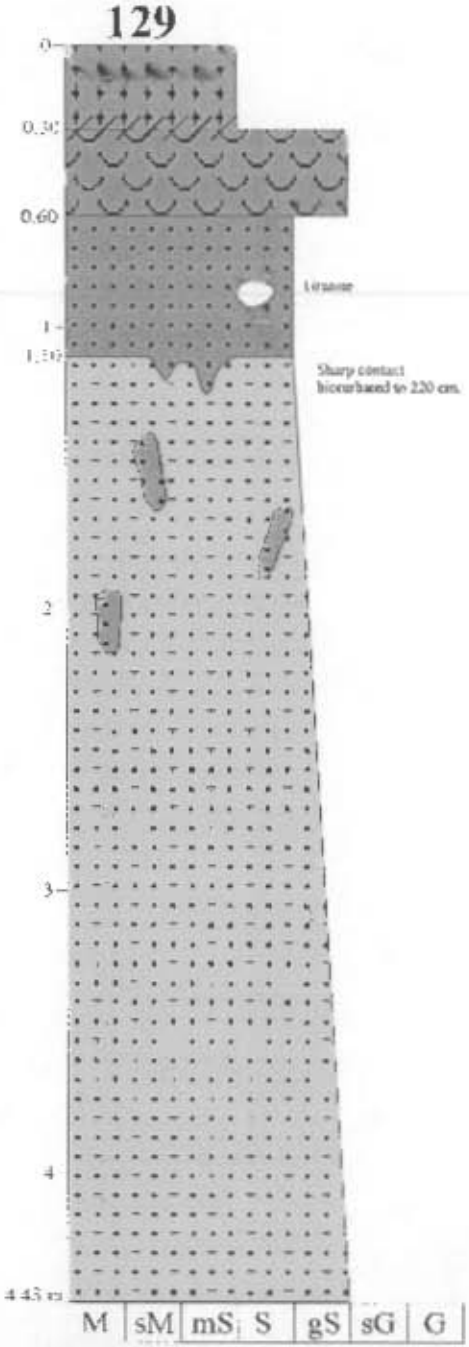
-12: 315-320 cm: Slightly gravelly muddy sand **[128-6]**
M: 16.9% S: 79.7% G: 3.4% $CaCO_3$: 73.8%
Sand (~250mm): 42% Au (ph=glc), 35% F (p=b), 20% ShF, 2-3% qz
Gravel: mP Bry, Pc, ShF and EchS. fP art-Br, CFA-cemented *in situ* sand, Bry and PCG (amber qz cS, minor glc mS)

■ 13

-13: 407-412 cm: Gravelly muddy sand **[128-7]**
M: 15.8% S: 77.7% G: 6.5% $CaCO_3$: 70.5%
Sand (~250mm): 43.5% Au (ph=glc), 34.0% F (p=b), 17.7% ShF, 4.8% qz. **Qz:** vf-fS ang, trace md cS. **Glc:** earthy green/brown mixed-mineral. **Ph:** Includes both F tests replaced with amber Ph and amber Ph fragments
Gravel: mP Bry, Pc, ShF (partially Ph), PCG (amber cement) fP art-Br, Ph



Property of Cape Town



0–~30 cm: RECENT FAECAL PELLET RICH MUDDY SAND
-1: 15-20 cm: Muddy sand [129-1] M: 16.3% S: 83.6% G: 0.1% $CaCO_3$: 21.5%
Sand: 50% blk glc, 10% Au, 20% qz vfS, 15% F (p>b) and 5% FP with minor SSp, EchS and qz mS.
■ 1 Gravel: vfP worn ShF

-2: 20-25 cm: Gravelly muddy sand [129-2] M: 11.3% S: 82.4% G: 6.3% $CaCO_3$: 25.1%
■ 2 Sand: 40% blk glc, 12% Au, 13% qz vfS, 15% Pleistocene diverse p=bF and 15% ShF with EchS and qz mS.
Gravel: cP *L. chuni*, G-ShF (*Volutocorbis abyssicola?*) and worm tubes. <mP worm ShF (Bv>G), otolith, *Caralloia* sp. and 2 vfP dark-brown Ph-cemented glc with qz cS in one vfP.

~30-110 cm: GLAUCONITIC SAND
~30-60 cm: Shell rich interval with well defined shell lags at 40-45 and 55-58 cm.

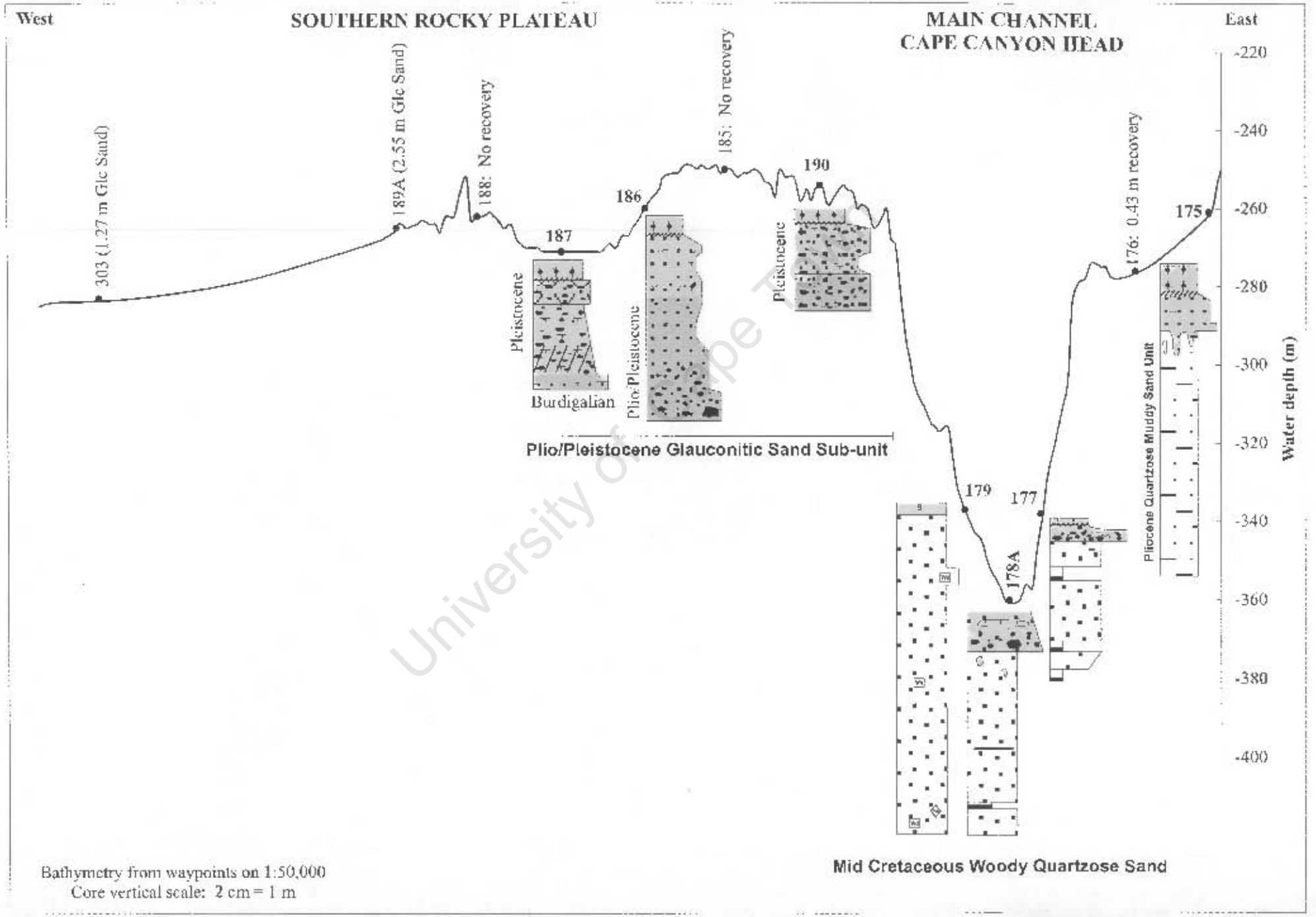
■ 3 -3: 86-91 cm: Sand
M: 5.0% S: 95.0% G: 0.3%
■ 4 ~2 cm angular cP of a fine grained Cape Granite, displaying low grade metamorphism in thin-section.
Sand: 70% blk glc, 15% Au, 10% qz vfS, 5% Pleistocene diverse p=bF and trace Bv-ShF with EchS and qz mS.

-4: 102-107 cm: Slightly gravelly sand
M: 4.8 S: 92.6% G: 2.6%
■ 5 Sand: 65% blk glc, 20% Au, 10% qz vfS, 5% Pleistocene diverse p=bF & Ph>pF with EchS and qz mS.
Gravel: mP Bry, Pc, ShF (partially Ph), <mP irregular dark-brown PCG (Au+qz+F f-mS), brown Ph-cast (qz & ShF *fS*) and Ph/micrite-cemented *in situ* sand.

-5: 135-140 cm: Slightly gravelly muddy sand [129-3] [57.6% non-mag : 37.4% mag : 5.0% semi-mag]
M: 20.1% / S: 76.9% / G: 3.0% $CaCO_3$: 72.6%
Sand (~250mm): 43.8% Au (ph=glc), 38.4% F (p=b), >3.9% ShF, 3.9% qz **Qz:** vf-fS ang, trace md cS. **Glc:** earthy green/brown mixed mineral. **Ph:** includes both F tests replaced with amber Ph and amber Ph fragments
Gravel: vcP Pc-ShF, <mP ShF (incl. Pc & Bry), light-brown Ph-cemented biogenic-glc-qz sand with partial ph of biogenic grains.

■ 6 -6: 393-398 cm: Gravelly muddy sand [129-4]
M: 22.5% / S: 65.4% / G: 12.1% $CaCO_3$: 73.3%
Sand (~250mm): Au (ph=glc), F (p=b), ShF, qz
Gravel: <cP Pc, ShF (partially Ph), light brown Ph-cemented *in situ* sand.

University of Cape Town

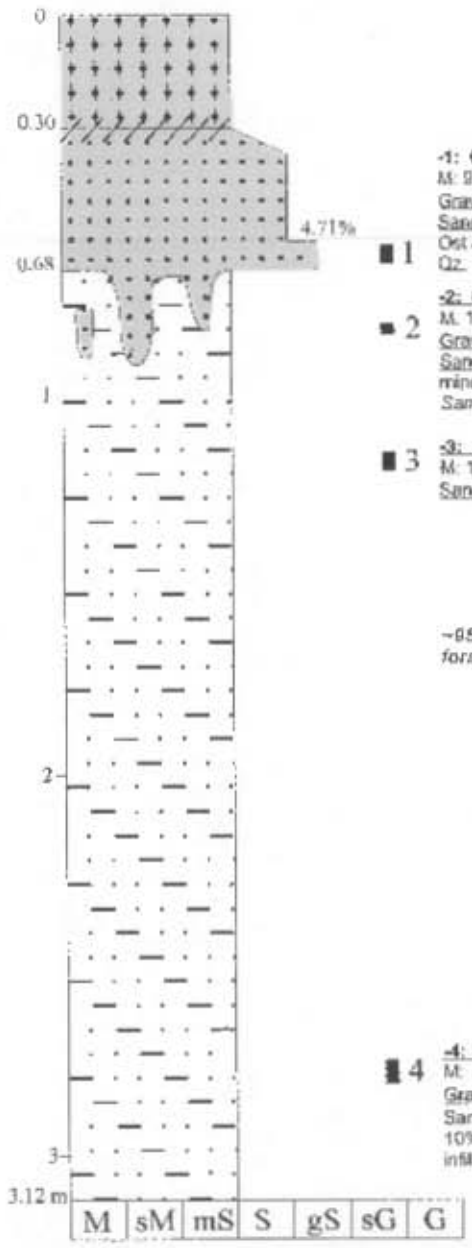


University of Cape Town

175

latest Pleistocene Holocene

Pliocene



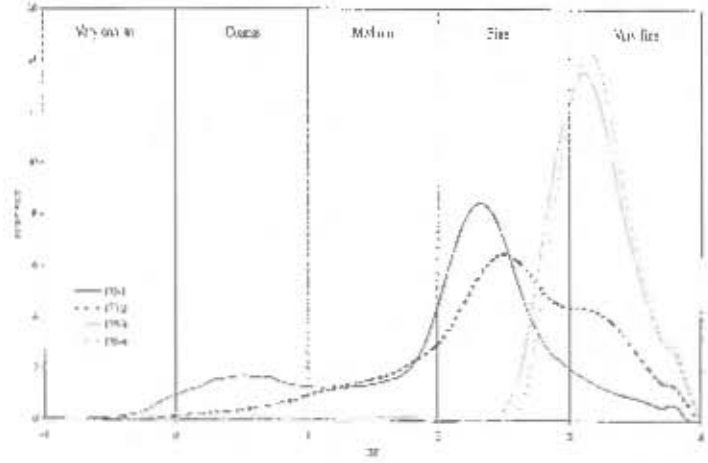
-1: 61-66 cm: Moderately sorted slightly gravelly fine sand.
M: 9.2% S: 86.1% G: 4.7% $CaCO_3$: 20.7%
Gravel: <mP *M. pisum, A. bulloides* ShF; with fP ssl, SPG, fragile *Anomia* sp.; Bv-ShF; PCG (glc mS) & qz.
Sand: Bimodal - 80% qz; 20% glc (Black polished) & 20%SkF (latest Pleistocene Bv-ShF; EchS: pF>bF; trace Ost & HS); minor Ph (ShF Bv-casts, Sk, T & Amb) and PCG; trace grey feldspar grains.
Qz: ang vfS - subrnd/rnd cS. Varies from polished (milky to clear) to frosted; glc-surface coating common on cS.

-2: 61-64 cm: Moderately sorted slightly gravelly muddy fine sand.
M: 11.6% S: 87.3% G: 1.1% $CaCO_3$: 11.7%
Gravel: Ribbed Bv-ShF with SPG; qz; PCG (glc mS) & gypsum aggregates
Sand: Trimodal distribution - dominant fS (black glc - qz - F (pF+bF) and vfS qz component with a minor cS component. cS dominated by Bv-ShF; EchS, Ph (Sk & Amb), F & trace PCG.
Sampled shell concentration in burrow.

-3: 115-120 cm: Well sorted muddy very fine quartz sand
M: 11.1% S: 88.9% G: 0% $CaCO_3$: 3.1%
Sand: see -4.

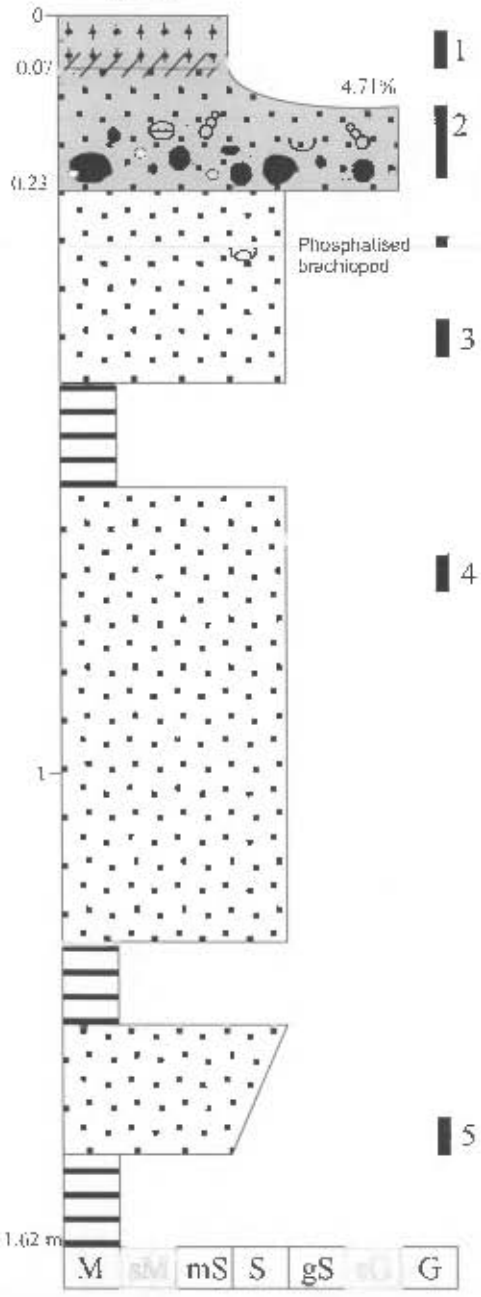
~95-312 cm: A uniform, very well sorted, muddy very fine angular quartz sand with minor foraminifera (bF >> pF) and trace sponge spicules. F often worn & infilled with glc)

-4: 275-281 cm: Well sorted muddy very fine quartz sand
M: 14.2% S: 85.7% G: 0.1% $CaCO_3$: 3.2%
Gravel: Ph-vertebrae and unknown brachiopod (J. Pether, *pers. comm.*, 2003)
Sand: <125 µm: 99% qz; 1% glc & SSp. Minor >125 µm: ~30% qz; 30% glc & Ph-ShF/bone, 30% F, 10% EchS & SSp. F includes Miocene/Pliocene assemblage - Miocene fragmented & minor glc-infilling. Minor gypsum-cemented aggregates and SPG



University of Cape Town

177



latest Pleistocene-Holocene

mid Cretaceous

-1: 2-7 cm: Moderately well sorted slightly gravelly muddy medium sand.
M: 19.6% S: 76.9% G: 1.5% $CaCO_3$: 6.2%
Gravel: PCG=qz granules
Sand: 58% qz; 38% glc; 2% F (robust Holocene pF>bI: sp.); 2 % faecal mud & trace EchS & SSp. Qz (& glc) mud-stained)

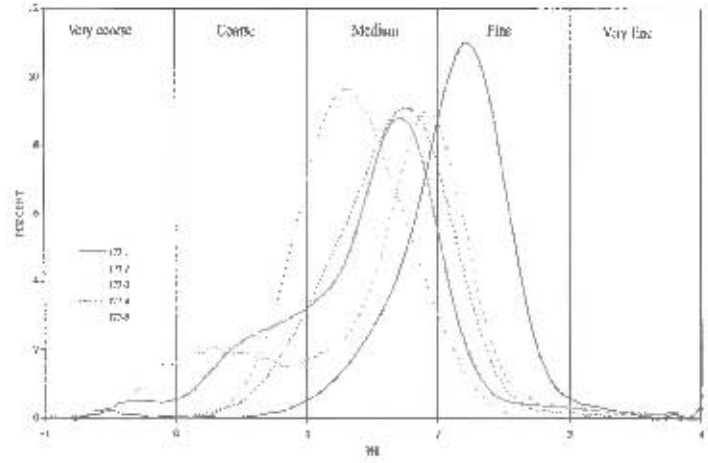
-2: 12-23 cm: Moderately sorted sandy gravel.
M: 3.2% S: 33.6% G: 63.2% $CaCO_3$: 12.6%
Gravel: <cP PCG (glc mS with m-nor qz mS-fP) dominated with minor Ph-casts; minor mP-vfp (dominant) rnd qz & trace ShF (increasing towards top of lag) . ShF include *T. declivis, articulated Dosinia lupinius and Nuculana bicuspidata* fragment
Sand: Bimodal 70% qz; 20% glc; 5% Ph & 5% SkF (latest Pleistocene Bv-ShS, EchS, biodiverse pF (abundant *G. inflata*)=bF (incl. *C. laevigata* & aggl-bF)) Dominant fS (qz ~ blk glc & minor SkF, Amb Ph, PCG) and minor cS (abundant qz (ang - rnd) & PCG with minor ShF & EchS)

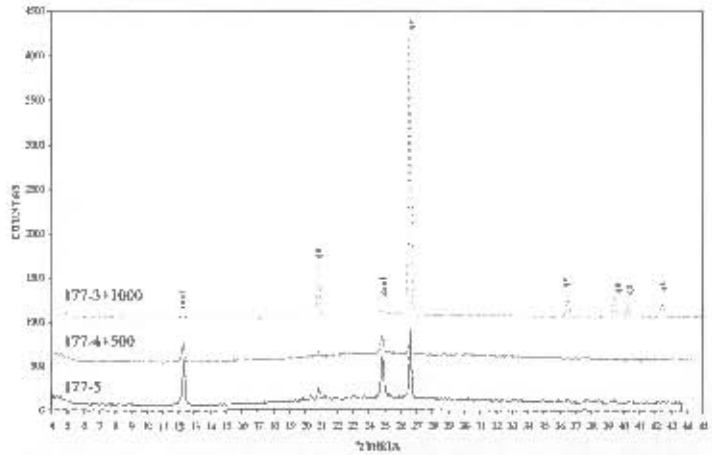
-3: 40-45 cm: Well sorted medium sand
M: 1.2% S: 98.8% G: 0% $CaCO_3$: 0.2% ($CaCO_3$ free in acid test)
Sand: see -5, with minor brown-mud staining of qz.
XRD: qz-(kaol)

-4: 71-78 cm: Well sorted medium sand
M: 2.0% S: 98.0% G: 0% $CaCO_3$: 0.4% ($CaCO_3$ free in acid test)
Sand: see -5
XRD: qz-kaol

25 to 152 cm: A well sorted upward coarsening (fine to medium) quartz sand with interbedded dark brown mud-rich intervals.

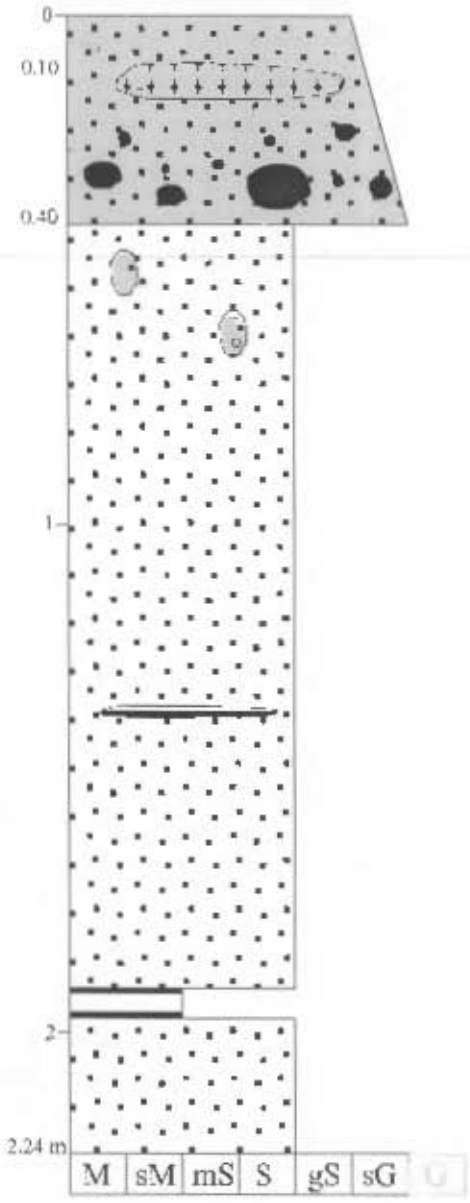
-5: 146-150 cm: Well sorted muddy fine sand
M: 10.4% S: 89.6% G: 0% $CaCO_3$: 0.4%
Sand: Subang to subrnd qz, with occasional well -rnd qz; minor ochre-staining observed. Qz typically slightly pink and frosted. Subordinate brown-mud staining of qz.
XRD: qz-kaol
(Trace very worn vf-fS carbonate (ShF?) present - slight effervescence in acid test)





University of Cape Town

178A



-1: 10-16 cm: Moderately well sorted gravelly medium sand
M: 8.2% S: 79.8% G: 12.0%
Gravel: <fP mc PCG > qz (often glc-stained). PCG dominated by CFA-cemented glc mS (with md lithic fragment & mc qz clasts), but includes all types with single layered example.
Sand: 70% qz; 20% blk glc; 8% PCG & trace F (robust Holocene pF sp.)
10-16 cm: Holocene muddy sand probably included during coring

-2: 29-37 cm: Moderately sorted muddy sandy gravel.
M: 5.9% S: 27.2% G: 67.0%
Gravel: <cP irregular PCG dominated by glc mS with qz mP & Bv clasts) & Ph-casts (G & calc-algae).
Sand: Bimodal distribution with dominant mS (66% qz; 20% blk glc; 10% Ph, 2% gypsum & trace F. Minor cS dominated by PCG (glc mS) > qz (ang-mc). SPG (T) & trace grey feldspar.

-3: 61-69 cm: Well to moderately well sorted slightly gravelly muddy medium quartz sand.
M: 9.7% S: 85.6% G: 4.6% $CaCO_3$: 1.3% ($CaCO_3$ free in acid test)
Gravel: <mP gypsum-cemented qz aggregates & qz vfP.
Sand: 100% qz with trace muscovite & gypsum crystallization on qz present.
Qz typically subang-subrnd & slightly frosted with minor ochre-stained qz present. Trace cS-vcS subrnd qz, often glc-stained, are present due to bioturbation.
Minor bioturbation to ~67 cm. Includes coarser sand blebs with phosphorite pebbles

-4: 79-86 cm: Moderately well sorted medium sand
M: 6.2% S: 93.8% G: 0% $CaCO_3$: 0.1% ($CaCO_3$ free in acid test)
Sand: 100% qz - typically subang-subrnd & slightly frosted with minor ochre-stained qz present. Gypsum crystallization on qz present.

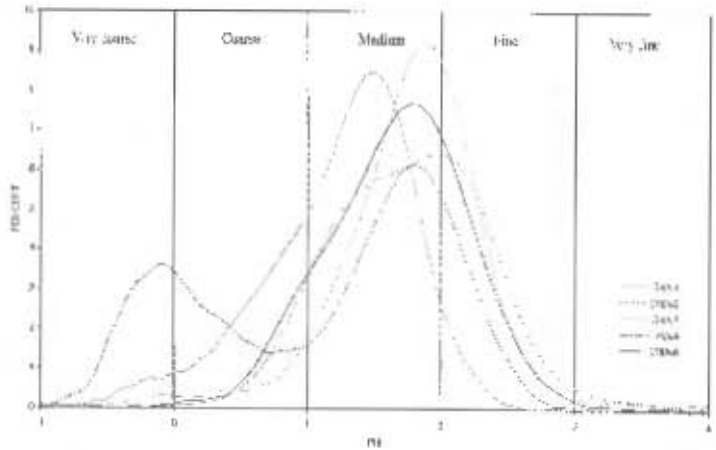
137 cm: <1 cm thick mud-rich stringer

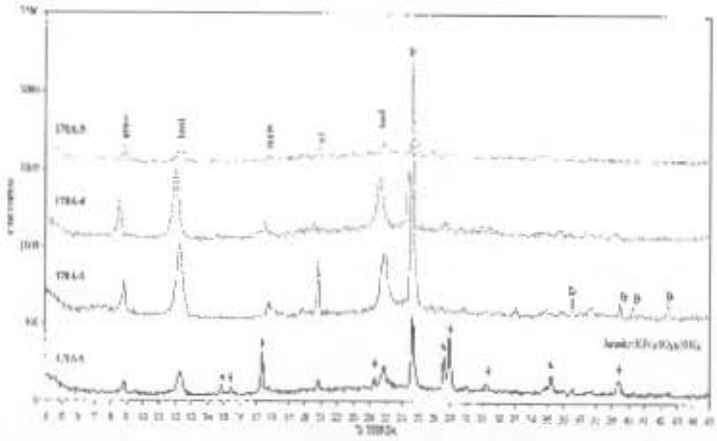
25 to 162 cm: A well sorted medium quartz sand with interbedded dark brown mud-rich intervals. Composed of sub-angular to sub-rounded quartz, with occasional well rounded quartz grains and minor ochre-staining observed. The quartz typically slightly pink and frosted. Minor wood fragments, pyrite and mica and trace megaspores and amber present in sample 178A-5.

-5: 181-195 cm: Sandy mud.
M: 59.7% S: 40.3% G: 0% $CaCO_3$: 1.0% ($CaCO_3$ free in acid test)
Sand: Subang to subrnd qz with minor wood fragments (partially pyritised), pyrite framboids & muscovite. Trace megaspores and yellow amber present. Qz slightly pink and frosted with minor ochre-stained qz present.
***Palynological analyses by S. de Villiers: mid-Cretaceous age**

-6: 09-209 cm: Moderately well sorted medium sand.
M: 4.8% S: 95.2% G: 0% $CaCO_3$: 0.8% ($CaCO_3$ free in acid test)
Sand: 100% qz - typically subang-subrnd. Qz slightly pink & frosted with minor ochre-stained qz present.

Ochre-coloured Jarosite ($KFe_3(SO_4)_2(OH)_6$) crystallization/alteration common on cut surface and along core liner.



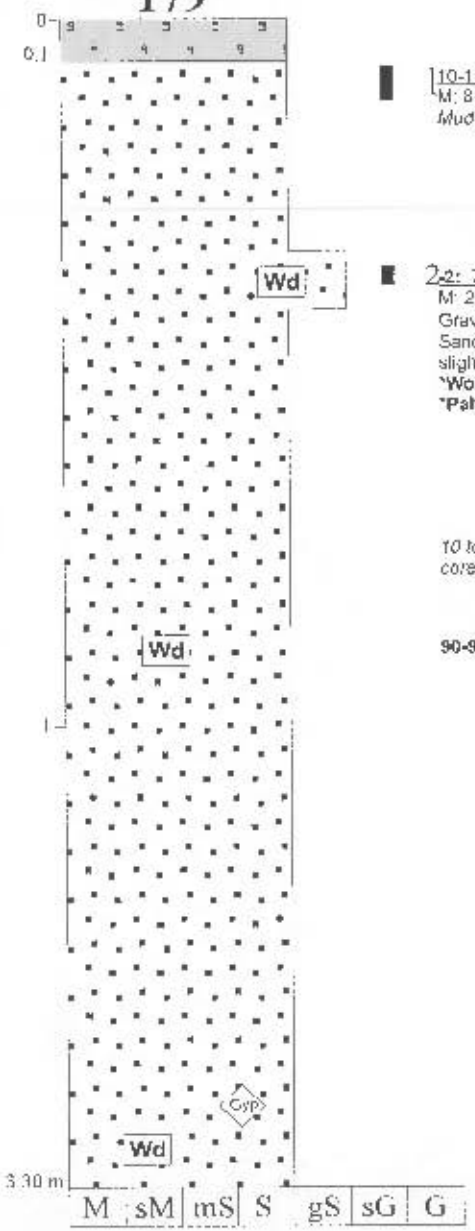


University of Cape Town

Pleistocene-Holocene

mid Cretaceous

179

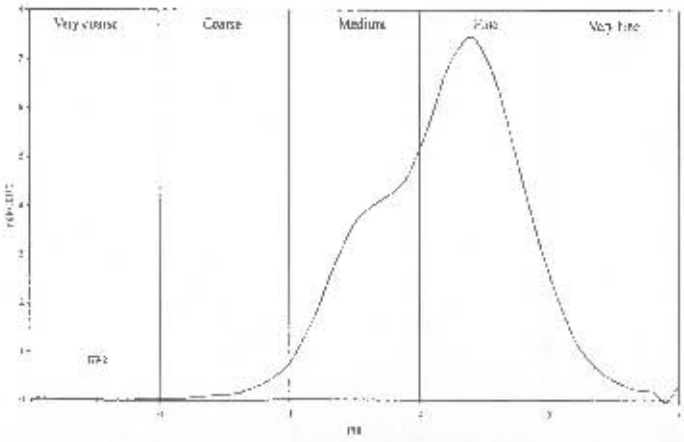


10-16 cm: Moderately well sorted gravelly medium sand
M: 8.2% / S: 79.8% / G: 12.0%
Muddy Holocene sand included during coring

2-2: 70-80 cm: Moderately well sorted gravelly muddy fine sand.
M: 20.0% S: 72.8% G 7.3% $CaCO_3$: 1.8% ($CaCO_3$ free in acid test)
Gravel: Pyritised wood fragments
Sand: Bimodal - dominated by subang to subrnd qz, with occasional well-rnd qz; minor ochre-staining observed. Qz typically slightly pink and frosted. Subordinate brown-mud staining of qz. Minor mS dominated by py-wood.
***Wood sample sent to M. Bamford: Gymnosperm (*Araucarian*); Permian to Cretaceous**
***Palynological analyses by S. de Villiers: mid-Cretaceous age**

10 to 162 cm: Upward fining unit with an upcore increase in mud content. Whole core stained by jarosite along cut surface & core liner

90-95 cm: Wood sample sent to M. Bamford by WMR: Angiosperm; Uppermost Cretaceous to Miocene



University of Cape Town

190

Holocene

Pliocene/Pleistocene

0.13

45-47 cm ■ bF/EchS: 0.7-1.4 Ma

0.66

86-91 cm ■■■■ bF/EchS/ShF: 0.5-1.4 Ma

1.02 m

Sr-isotopic ages

M	sM	mS	S	gS	sG	G

1

2

3

4

-1: 21-28 cm: Moderately sorted muddy sandy gravel. Grain size analysis shows a bimodal distribution with dominant medium and coarse to very coarse fractions.
M: 4.1% S: 21.8% G: 74.3%
Sand: 40% black lobate glc; 15% Au (Ph-pF, PP); 20% F (p>b); 10% SkF (Bv-ShF>F); 15% qz (vfS & 2% m-cS md clear to green-stained grains. Trace EchS, Sp and SPG (Sk & T). cS dominated by qz (ang to md, frosted and green-stained) with ~40% PCG (glc mS, casts of qz vfS, glc- & micrite-cemented lmst with 5% ShF (worn Bv).
Gravel: Dominated by <vcP irregular dark-brown PCG (glc (& qz) mS with clasts, incl. Ph-ShF). <mP brown PCG Bv & G casts (qz (& minor - subordinate glc) vfS) - Ph-Sh may be partially preserved. Occasional cS md qz present in cemented casts. Casts tend to be md & reworked. Minor <mP *T. declivis* and other Bry & Bv-ShF, <vfP green-stained frosted submd qz.

-2: 51-56 cm; 29-37 cm: Moderately well sorted gravelly medium sand. Bimodal grains size distribution, although considerably less cS.
M: 5.4% S: 75.6% G: 19.0%
Sand: 40% black lobate glc; 15% Au (Ph-pF, PP); 20% F (p>b); 10% SkF (Bv-ShF>F); 15% qz (vfS & 2% m-cS md clear to green-stained grains. Trace EchS, Sp and SPG (Sk & T). cS dominated by Qz (ang - md, frosted & green-stained) with ~40% PCG (glc mS), PCG casts (qz vfS), glc- & micrite-cemented lmst with 5% ShF (worn Bv, Bry).
Gravel: Dominated by <vcP irregular dark-brown PCG (glc (& qz) vfS with clasts, incl. Ph-ShF). <mP brown PCG G & Bv casts (qz (minor - subordinate glc) vfS where Ph-Sh may be partially preserved. Casts tend to be md & reworked. <mP co-cemented crs md qz & glc. Minor vfP Ph-ShF, otoliths and green-stained frosted sub-md qz.

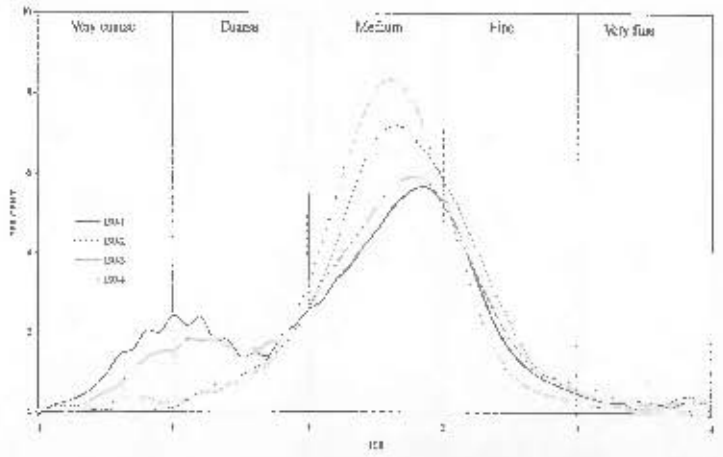
-3: 71-77 cm: Moderately sorted muddy sandy gravel (gravel). Grain size analysis shows a bimodal distribution with mS & cS fractions.
M: 3.9% / S: 16.2% / G: 79.9%
Sand: 50% black lobate to fractured green glc; 15% Au (Ph-pF, PP); 10% F (p>b); 5% SkF (Bv-ShF>F); 20% qz (vfS & 2% m-cS md clear to green-stained grains. Trace EchS, Sp, Ost and SPG (Sk & T). cS dominated by brown PCG (glc mS), PCG casts (qz vfS qz), glc- & micrite-cemented lmst (Qz Glc Calc Sand).
Gravel: Dominated by <sC irregular submd brown PCG (glc (& qz) mS with clasts, incl. Ph-ShF - polished surfaces and rounded grains darker). <mP brown PCG G & Bv casts (qz (minor - subordinate glc) vfS casts, where Ph-Sh may be partially preserved. Casts tend to be md & reworked. Single mP well md green-stained frosted qz. Minor vfP Ph-ShF, green-stained frosted sub-md qz and ShF.

-4: ~80-102 cm: Moderately well sorted sandy gravel.
M: 4.7% S: 43.8% G: 51.5%
Sand (mS): 60% fractured green glc; 10% Au (Ph-pF, PP); 10% F (p>b); 10% SkF (Bv-ShF>F); 10% qz (vfS & 2% m-cS md clear to green-stained grains. Trace EchS and SPG (bone & teeth). Minor cS dominated by PCG (brown PCG (glc mS), PCG casts (qz vfS), glc- & micrite-cemented lmst (Qz Glc Calc Sand).
Gravel: Dominated by <sC irregular sub-md brown PCG (glc (& qz) vfS) with clasts, incl. Ph-ShF. <mP brown PCG G & Bv casts (qz (minor - subordinate glc) vfS) - Ph-Sh may be partially preserved. Casts tend to be md & reworked. Minor vfP Ph-ShF and green-stained frosted submd qz.
(Most of gravel fraction show some rounding as evidence of reworking)

~80 - 102 cm: Sand includes increased abundance of green glauconite
Only partial core section sampled/preserved, sampled available material

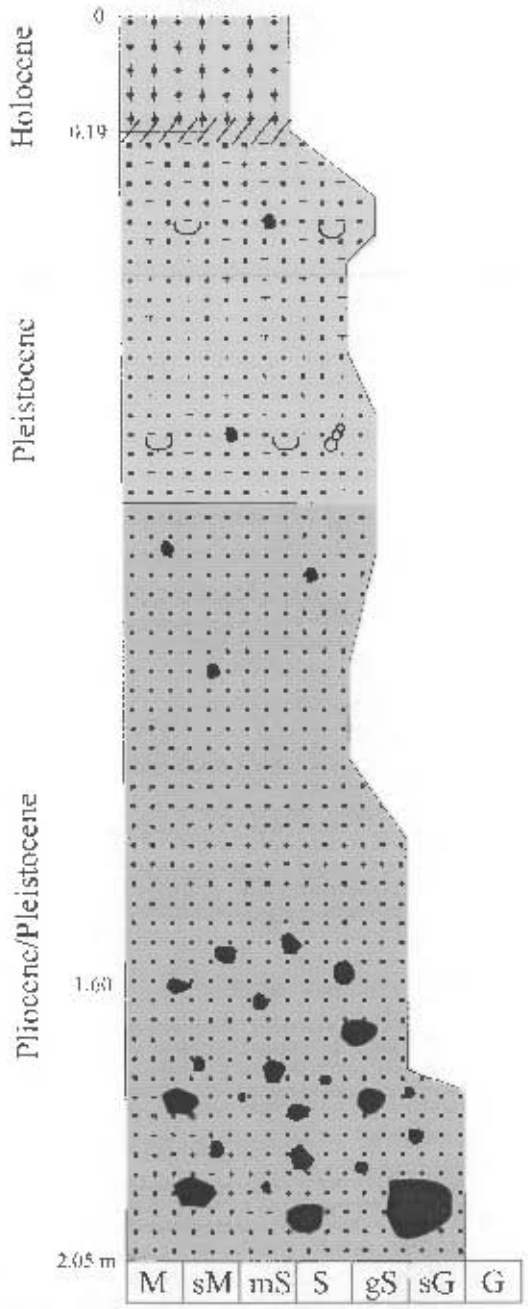
The working half of the core was jigged and the >2 mm fraction preserved.
Gravel: Dominated by vfP to cP of irregular clast-rich brown PCG (glc mS with rare crs md qz); subordinate <mP brown PCG casts (qz (&glc) vfS) & Ph Pc-ShF present Clasts and <mP incl. brown PCG casts (qz (& glc) vfs), lmst (Lower Miocene Calcareous Sand - B-Au-Qz and B-Au), Ph-lmst and cc-cemented (Fe-rich) crs md qz+ShF+glc (occasionally partially Ph). light-brown PCG (phospho-glc fS). Minor, SPG (<mP teeth), often green-stained frosted sub-md qz vfP and vfP Bry, G, otoliths, scaphopods & worm Bv-ShF (<mP). Include 2 mP granite (white and pink) and a PCG-clast of a mP greenish Malmesbury mudstone disc.
Encrusting bry & bF present.

FORAMINIFERAL ASSEMBLAGE:
190-4: mixed assemblage includes rare Pliocene, abundant Pleistocene & Holocene species. The latest Pleistocene assemblage includes some littoral species, deposited not far from the shoreline. Depositional environment a complex mixture of deep water to littoral.



University of Cape Town

186



1 **-1:** 9-14 cm: Muddy medium sand
M: 20.0% S: 79.1% G: 0%
Sand: 45% black polished rnd to lobate glc; 15% Au (orange to black Ph, Ph-pF and PCG); 10% F (p>b); 10% SkF (F); 20% qz (vfS & 2% m-cS rnd clear to green-stained grains. Trace Sp, EchS and SPG (bone & teeth).

2 **-2:** 30-35 cm: Slightly gravelly muddy medium sand
M: 11.4% S: 87.3% G: 1.3%
Sand: 40% black polished rnd to lobate glc; 20% Au (orange to black Ph, Ph-pF and PCG); 15% F (p>b, incl aggl. sp); 15% SkF (Bv, G, Bry & ShF >F); 10% qz (vfS & 2% m-cS rnd clear to green-stained grains. 1% EchS and trace Ost. SPG (teeth).
Gravel: cP Bv & EchP with <fP Bv, G, Bry and EchP ShF's. 2 Ph (rnd brown PCG (glc mS) and amber/brown PCG (qz and glc vfS) and single rnd frosted qz vfP

3 **-3:** 48-53 cm: Medium sand
M: 6.1% S: 93.9% G: 0%
Sand: 40% black polished rnd to lobate glc; 20% Au (orange to black Ph, Ph-pF and PCG); 15% F (p>b); 15% SkF (F>Solitary coral & ShF); 10% qz (vfS & 2% m-cS rnd clear to green-stained grains. Trace EchS. *(Note less ShF, aggl. bF, Ost & EchS than above otherwise similar)*

4 **-4:** 67-72 cm: Slightly gravelly muddy medium sand
M: 10.0% S: 89.9% G: 0.1%
Sand: 40% black polished rnd to lobate glc; 20% Au (orange to black Ph, Ph-pF and PCG). 15% F (p>b); 15% SkF (F>Solitary coral & ShF); 10% qz (vfS & 2% m-cS rnd clear to green-stained grains & 1% EchS.
Gravel: vfP ShF (Bv & EchP), cc-cemented biogenic-glc sand and a vfP brown PCG (qz+glc vfS)

5 **-5:** 86-94 cm: Slightly gravelly medium sand
M: 9.5% S: 90.2% G: 0.3%
Sand: 60% black lobate to green fractured glc; 10% Au (orange to black Ph, Ph-pF and PCG); 10% SkF (F, incl. stained *Operculina* sp.); 5% F (p incl. *G. inflata*>b); 15% qz (vfS & 2% m-cS rnd clear to green-stained grains & trace EchS, Pelletal Ph & SPG (tooth)
Gravel: vfP mixed Ph granules, including brown PCG (glc mS), amber/brown PCG (qz+glc vfS), cc- and light-brown Ph cemented biogenic-glc vfS and a single ShF.

6 **-6:** 115-120 cm: Medium sand
M: 5.0% S: 95.0% G: 0%
Sand: 65% black lobate to green fractured glc; 15% Au (orange to black Ph, Ph-pF and dominant PCG); 5% SkF (F, Incl. stained *Operculina* sp.); 5% F (p incl. *G. inflata* >b); 10% qz (vfS & 2% m-cS rnd clear to green-stained grains & trace EchS & Pelletal Ph.

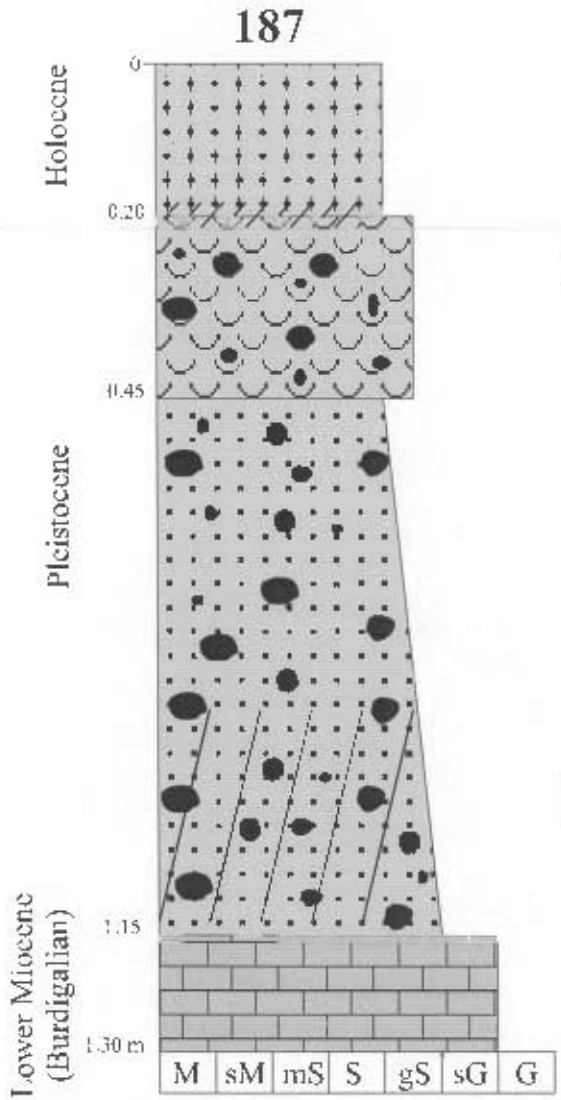
7 **-7:** 148-153 cm: Gravelly medium sand
M: 7.4% S: 87.6% G: 5.0%
Sand: 40% black polished rnd to lobate glc; 20% Au (orange to black Ph, Ph-pF and PCG); 15% F (p>b); 10% SkF (F); 15% qz (vfS & 2% m-cS rnd clear to green-stained grains. Trace EchS and SPG (bone & teeth). *(pF rich and different glc - blacker & better polished)*
Gravel: cP angular brown PCG (glc mS), with <fP mixed Ph pebbles, including A/A, amber/brown PCG (qz+glc vfS), cc- and light-brown cemented biogenic-glc vfS, Ph-ShF and a single rnd frosted green-stained qz.

8 **-8:** 168-172 cm: Gravelly muddy medium sand
M: 14.6% S: 75.2% G: 10.2%
Sand: 60% black lobate to green fractured glc; 25% Au (orange to black Ph, Ph-pF and PCG); 5% F & SkF-F; 10% qz (vfS & 2% m-cS rnd clear to green-stained grains. Trace Pelletal Ph, and micrite and ph-cemented grains. No obvious G. inflata

9 Gravel: cP blocky cemented lmst (partially Ph - light brown) overlain by crs rnd qz, ShF and glc in Fe-rich cement, a mP intraclast-rich angular brown PCG (glc mS with clast Ph-glc-lmst) and <fP mixed Ph pebbles, dominated by brown PCG (glc mS - darkun in colour with increasing roundness), amber/brown Bv cast PCG (qz+glc vfS) and cc-cemented (Fe-rich) crs rnd qz+ShF+glc. Trace ShF and rnd frosted green-stained qz.

-9: 168-172 cm: Muddy sandy gravel
M: 25.2% S: 30.7% G: 44.1%
Sand: 56.8% green fractured glc; 30% Au (60% Ph-cemented *in situ* sand with orange to black Ph and Ph-pF); 10.8% qz (vfS & .05% m-cS rnd clear to green-stained grains and 1.0% F & SkF-F. vcS fraction Incl Ph-cemented *in situ* sand, PCG mollusc cast (vfS qz) and other PCG's. No obvious *G. inflata*
Gravel: vcP and <mP angular clast-rich brown Ph-cemented glc mS with rare crs rnd qz. Irregular surfaces of vcP polished black and increased roundedness results on darker colour.. Clasts incl. Ph-lmst, Bv casts and cc-cemented crs rnd qz, ShF and glc.
<mP also includes casts of amber/brown qz+glc vfS, cc-cemented biogenic-glc vfS, cc-cemented (Fe-rich) crs rnd qz+ShF+glc, Ph-ShF and vfP rnd frosted green-stained qz.

University of Cape Town



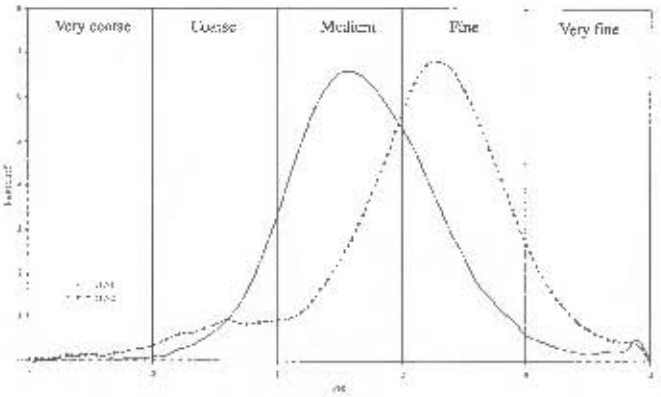
-1: 26-31 cm: Moderately well sorted medium sand.
M: 3.3% S: 92.0% G: 4.7%
Sand: 40% black lobate to green fractured glc, 15% Au (Ph-pF, PP); 20% F (p>b); 10% SkF (Pc-ShF>F); 15% qz (vfS & 2% m-cS rnd clear to green-stained grains. Trace Sp, 1% EchS, HS and SPG (bone & teeth).
Gravel: <fP of Ph and ShF in equal proportions. Ph dominated by sub-rnd brown PCG (ph-glc & trace crs rnd qz - rounding darkens appearance of PCG). Trace Ph-ShF and fP of cc- to light-brown PCG (biogenic ph-glc). ShF incl cP *Dentalium* sp., with <fP Bra, G (>3 sp.), Bv (>3 sp.), Bry and EchP.

20-45 cm: speckled, shell-rich interval
45-85 cm: black, Ph pebble- rich interval

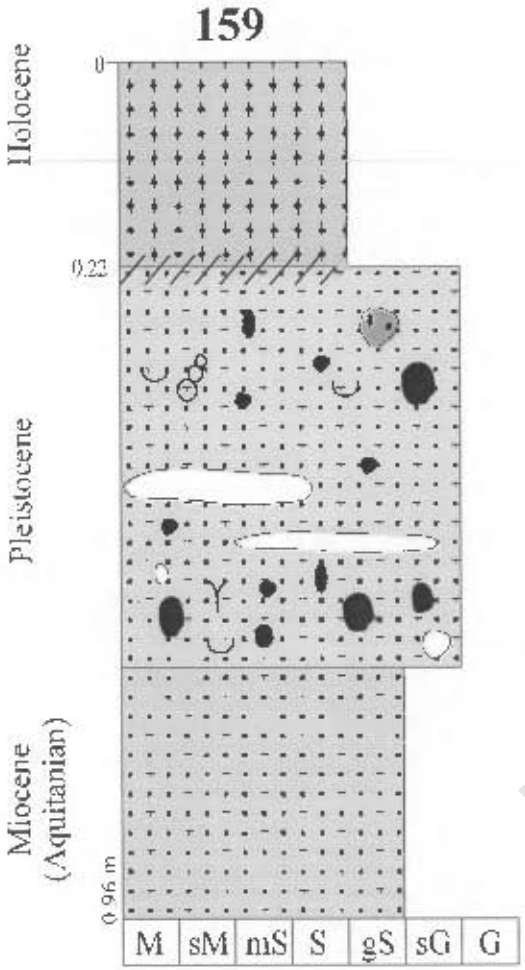
~85 - 115 cm: gradational contact with increase in ShF down-core. Very cemented interval.

-2: 51-56 cm: Moderately sorted gravelly muddy fine sand
M: 11.0% S: 76.0% G: 13.0%
Sand: 70% Au (Ph-pF, Ph-SkF, PP, SPG (bone & teeth)); 10% black rnd glc; 10% F (p (incl *G. inflata*-b incl. aggl. sp.); 5% SkF (Bv-ShF>F), 5% qz (vfS & 2% m-cS rnd clear to green-stained grains). Rare robust scaphopods present.
Gravel: <mP of Ph and ShF in equal proportions. Ph dominated by irregular brown PCG (ph-glc with trace crs rnd qz). Rare Ph-Bv casts of similar material preserved. Trace Ph-ShF, fP of cc- to light-brown PCG (biogenic_ph-glc), SPG (vfP tooth), irregular dark brown PCG (glc mS and glc+qz vfS) and vfP sub-rnd brown to green stained qz. ShF dominated by Bv (predominantly Pc-ShF), Bry, Bra and EchS. Bry with glc in zooecia.

-3: 120-125 cm: Muddy sandy gravel
M: 14.9% S: 42.3% G: 42.8%
Sand (~250 mm): 56.1% Au (ph>glc), 33.5% F (p=b-trace aggl-bF & vcS *Dentalina* sp.), 8.7% ShF (Bv>>Bry, Bra), 1.6% qz
Qz: vf-fS ang. trace rnd cS. **Glc**: earthy green/brown ph-glc. Ph: both F-tests replaced with amber Ph and amber Ph Sh-F.
Gravel: <cP Bv (Pc) and cc-cemented *in situ* sand. Trace fP amber PCG Bv cast (qz and glc vfS) and Bry & Bra ShF.



University of Cape Town



0.90 m: Sr- isotopic age of 24.1-24.3 Ma

Foraminiferal assemblage 159-5:
Victorella conoides, *Gaudryina* sp., *Quinqueloculina* cf. *vulgaris* *, *Spiroplectinella* sp., flat *Spiroplectinella* sp., *Cibicidoides* spp., *Globigerina* spp., flat Nonion sp., small rounded margin *Nonion* sp., *Lenticulina* sp., *Quinqueloculina* spp.*, *Pyrgo* sp., *Globulina* sp., *Eponides* "*miocenica*", *Triloculina* cf. *tricarinata**, *Siphonaperta* sp., *Sigmoilina* sp.*, Ostracod
*. Aquitanian innermost shelf deposit with some hypersaline indicators

1

-1: 7-12 cm: Slightly gravelly muddy fine qz-glc-pF-FP sand
M: 11.1% S: 86.3% G: 2.6%
Sand: ~60% qz, 30% blk glc, 5% pF, 5% FP (and muddy agg.), trace EchS & brown Ph.
Gravel: fP SPG-T, vfP brown PCG G-cast, brown PCG (glc>qz), subrnd to w-rnd qz, amber ph and md sandstone

0-~23 cm: Recent faecal pellet muddy sand
~23-68 cm: Qz-glc-pF sandy gravel

2

-2: 33-37 cm: Sandy gravel
M: 4.0% S: 52.6% G: 42.5%
Sand: see 159-4
Gravel: cP-vcP *T. declivis* and Bv (*Peclen*), vcP blk/brn PCG (vfP to vfS qz, glc), cP ph-PCG (of co-cemented underlying carbonate sand with vfP qz, hm Ph, glc, Bry), vfP to fP brown PCG casts (Bry, G & B), brown PCG (glc>qz), subrnd to w-rnd qz, amber ph, ShF (Bv) and fP SPG-T.

3

-3: 51-56 cm: Muddy sandy gravel
M: 8.0% S: 52.4% G: 39.6%
(No reserve sample)
Sand: see 159-4
Gravel: vfP to mP Bry (zoecia filled with glc), vfP to fP subrnd to w-rnd qz, brown PCG (glc>qz), brown PCG (Bv, G & scaphopod) casts (glc>qz), black Ph and trace amber Ph.

37-68 cm: reworked/gradational contact
68-96 cm: Amber coloured authigenic skeletal carbonate sand

4

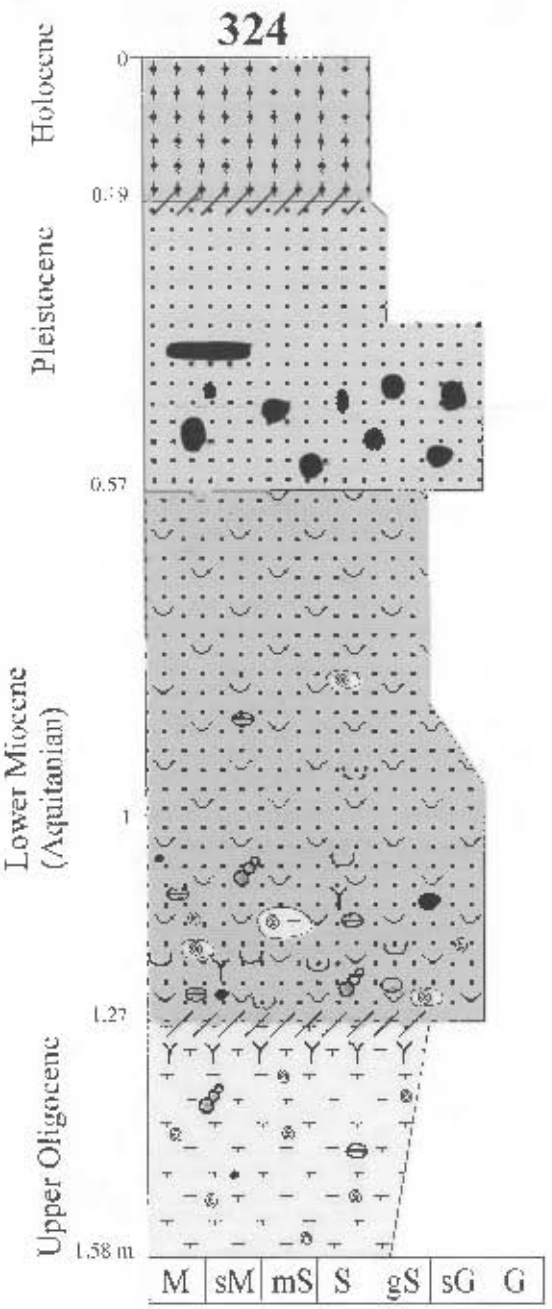
-4: 64-68 cm: Muddy sandy gravel
M: 8.9% S: 22.7% G: 70.4%
Sand: 52.1% qz, 29.2% glc, 9.7% ShF, 8.1% pF & 0.8% bF. Minor brown PCG (glc), brown PCG casts and EchS.
Qz: ang. fS to mS, dominant, minor sub-rnd to rnd cS to vcS with glc surface coating. **Glc**: black to earthy green. **Sh-frag:** Bry dominant (with glc in znoecium) pF: incl. *G. inflata*.
Gravel: vfp to vcP co-cemented clasts (incl. vcP Bv) of underlying Qz Glc Calc Sand facies (larger clasts above sample 9 X 8 cm and 7 X 5 cm), cP bry-encrusted brown PCG Bv-cast (crs qz & glc), vfP to fP sub-rnd to w-rnd qz, brown PCG (glc), brown PCG casts (glc>qz), black Ph, trace amber Ph and Bry (zoecia filled with glc).

5

-5: 85-90 cm: Gravelly muddy sand
M: 17.0% S: 66.4% G: 16.6%
Sand: 36.7% ShF, 33.9% (ph-)glc, 23.4% qz, 2.6% bF, 2.4% pF and 0.8% Bry. Trace amber ph.
Qz: mS, ang-rnd. **Glc**: earthy green/brown mixed-mineral. **bF**: incl. *V. conoidea*. Most calcareous and quartz grains have very tiny red (Fe) crystal precipitate on surfaces.
Gravel: vfP to mP co-cemented in-situ sand, vfP to fP Bry (zoecia filled with glc) and other ShF. Trace vfP amber PCG (qz>glc).

Co-nemented clasts of underlying Quartzose Authigenic (glc) Biogenic Sand (larger clasts 9 X 8 cm and 7 X 5 cm)

University of Cape Town



1

-1: 6-11 cm: Sand
M: 7.8% S: 92.2% G: 0%
Sand: Green/brown glc(-ph) & amber-stained Sh-frag dominant, sub-ordinate qz (any vfS to md cS), minor bF (incl. agglutinated, pF (incl G. *inflata*), EchS, & amber ph. (reworked early Miocene sediment?)

2

-2: 19-32 cm: Slightly gravelly muddy sand
M: 14.6% S: 82.6% G: 2.8%
Sand: Blk glc & pF dominant, subordinate qz (any vfS to md cS), minor bF, EchS, Sp, ShF, Ph (brown PCG (glc mS) & amber).
Gravel: vfP to fP md. amber PCG (qz>glc), vfP any. brown PCG (glc>qz) & a single cc-cemented vfP (blk glc > qz, F)

3

-3: 45-52 cm: Muddy sandy gravel with the sand fraction composed predominantly of glauconite, quartz, pF and shell fragments (Bv, Bry & larger bF)
M: 5.8% S: 31.3% G: 62.9%
Sand: 35% glc, 30.0% qz, 21.9% pF (incl pF-frag) & 13.1% ShF (with trace EchS & -P; bF (incl larger and agglutinated bF) & Bry)
Qz: clear, ang to submd vfS. Minor (~5%), w-md frosted qz cS (surface cracks filled with glc) **Glc:** (2/3 blk vfS to cS: 1/3 reworked vfS earthy green/brown mixed-mineral). **Ph:** minor w-md brown PCG (glc>qz) **pF:** includes Pleistocene *G. inflata*.
Gravel: vfP to mP ang brown PCG (glc>qz) dominant. Sub-ordinant cc-cemented vcP (blk glc > qz, F and SPG). Minor worn vfP to fP ShF (incl. *L. Chuni*) and vfP Bv.

4

-4: 59-65 cm: Gravelly muddy quartzose, shelly, glauconitic sand (shell fragments coarser grained and amber-stained)
M: 23.0% S: 64.3% G: 12.7%
Sand: 51.6% glc(-ph), 33.5% ShF, 12.6% qz, , 1.2% pF, 0.8% bF and 0.4% PCG (qz>glc) - See 324-5.
Gravel: vfP to mP ShF (Bv-Pecten dominant, minor bry), fP of Bv & G amber PCG casts, sub-rnd amber PCG (qz>glc), Ph=-ShF, a single larger bF and pink-stained re-crystallised ShF, which have *in situ* sand cc-cemented on surfaces.

37-68 cm: reworked/gradational contact
68-96 cm. Amber coloured authigenic skeletal carbonate sand

5

-5: 77-82 cm: Gravelly muddy quartzose, shelly, glauconitic sand (shell fragments coarser grained and amber-stained)
M: 26.1% S: 66.9% G: 7.0%
Sand: 48.7% glc(-ph), 29.6% ShF, 15.9% qz, , 2.2% bF, 1.8% pF, 0.9% cc-cemented qz aggregates and 0.9% Ph-ShF.
Qz: clear, ang to submd vfS. Minor (~5%), w-md frosted qz cS (surface cracks filled with Fe-rich coating) **Glc:** earthy green/brown mixed-mineral dominant. **Ph:** minor w-md amber PCG (qz>glc), amber Sh-frag, SPG & trace PP. **Sh-frag:** vary from vfS (resembles qz) to vcS, incl Bv & Bry (zooecium typically filled with glc). **bF:** includes trace larger bF and *Dentalina* sp.
Gravel: vfP to mP ShF (Bv, Pec>Bry) and cemented aggregates of the Quartzose Foraminiferal Muddy Sand, incl larger bF. fP of amber PCG Bv casts & an ang green/brown glc & minor qz black-brown PCG's. ShF have *in-situ* sand cc-cemented on surfaces.

324-5 shows increase in vf glc(ph) at expense of qz relative to 324-6

6

-6: 105-110 cm Muddy sandy phosphoritic gravel, with the sand fraction composed predominantly of quartz, glauconite/phosphorite and shell fragments (Bv and Bry) (Shelly material typically amber (ph) stained)
M: 11.7% S: 39.0% G: 49.3%
Sand: 32.9% qz, 32.9% (ph-)glc, 26.0% ShF, 3.7% pF, 2.3% bry, 1.8% bF and 0.5% PP
Qz: vf, clear, ang to submd. Subordinate (<10%) crs, w-rnd frosted qz (surface cracks filled with Fe-rich coating) **Glc:** earthy green/brown mixed-mineral dominant. **Ph:** minor w-rnd amber PCG (qz>glc), amber ShF, SPG & trace PP. **ShF:** vary from vfS (resembles qz) to crs, incl Bv & Bry (zooecia typically filled with glc). **bF:** includes trace larger bF and *Dentalina* sp.
Gravel: vfP to mP light brown PCG (G/Bv casts) and md frags of amber PCG (qz>glc) pebbles, fP Sh-frag (Bv-Pecten > Bry), cemented aggregates of the Quartzose Foraminiferal Muddy Sand, incl. larger bF, minor fine pebbles of cemented crs md qz and drk-brown PCG and amber Ph-ShF. Minor ang green/brown glc (& qz) black-brown PCG granules. Encrusting Bry common.

7

-7: 132-137 cm: Gravelly muddy glauconitic quartzose sand with ~16% coarse sequin benthic foraminifera and other shell fragments. (Calcareous material typically red-stained)
M: 17.6% S: 61.2% G: 21.1%
Sand: 59.3% qz, 22.2% glc(-ph), 16.3% (larger) bF & other ShF, 1.8% pF and <1% EchS & Ph.
Qz: clear, ang to submd vfS. Minor w-rnc frosted qz cS (surface cracks filled with Fe-rich coating) **Glc:** earthy green/brown mixed-mineral dominant. **Ph:** minor w-rnd PCG (qz>glc) & amber grains, trace PP. **bF:** dominated by larger bF, but increased biodiversity with *Dentalina* sp. present. **ShF:** varies from vfS (resembles qz) to vcS, incl Bv & Bry (zooecia typically filled with glc).

8

Gravel: vfP to mP of amber w-rndPCG (qz>glc), G/Bv casts with encrusting bry and ShF (Bv & Bry) & larger bF (<4 mm).

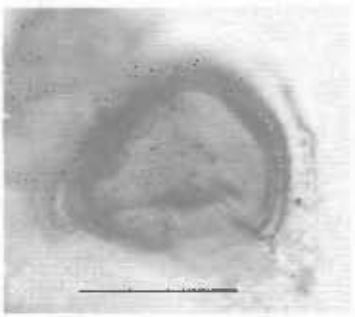
-8: 152-156 cm. Slightly gravelly muddy quartz sand with ~15% coarse sequin benthic foraminifera (All calcareous material red-stained)
M: 31.0% S: 66.1% G: 3.0%
Sand: 70.5% qz, 14.7% (larger) bF (& bF-frag), 6.9% glc, 4.2% pF, 1.1% ph and <1% EchS.
Qz: clear, ang to submd vfS. Trace w-rnd frosted qz cS. **Glc:** earthy green/brown mixed-mineral dominant. **Ph:** w-md PCG (qz) & amber grains.
Gravel: larger bF (<4mm) and vfP to fP of amber Ph: (w-md PCG & G/Bv casts) & single Bv-frag.

WMR Sr-ages (foram): 25.8-27.2 Ma

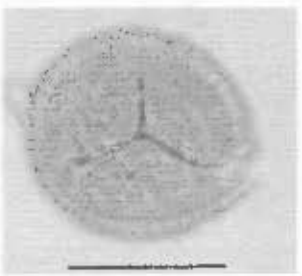
University of Canterbury

APPENDIX 2 – PALYNOLOGICAL ASSEMBLAGE

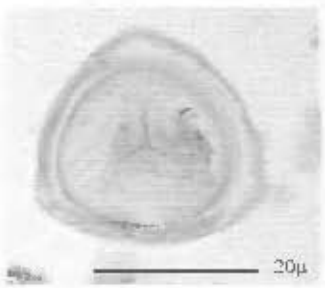
Spores Plate 1



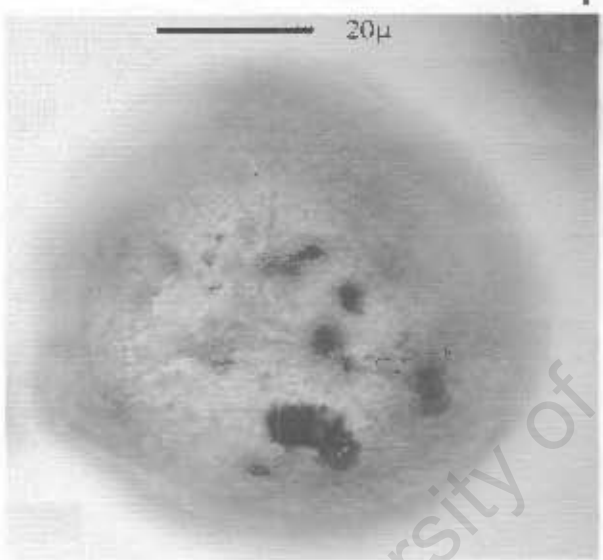
1



2



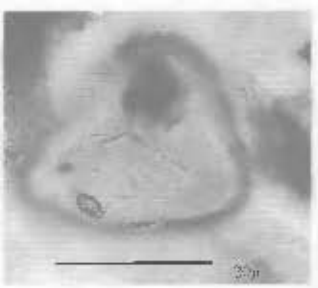
3



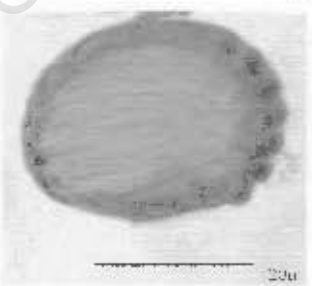
4



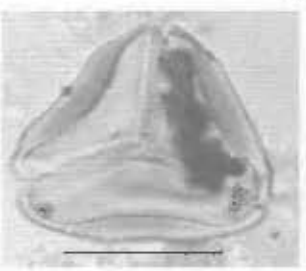
5



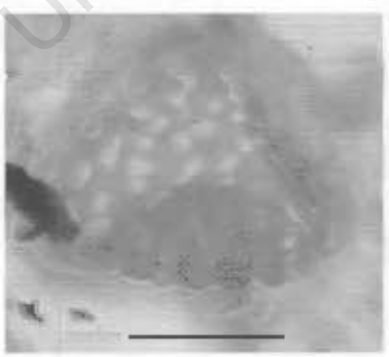
6



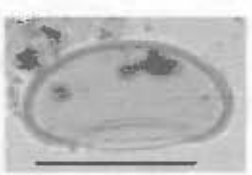
7



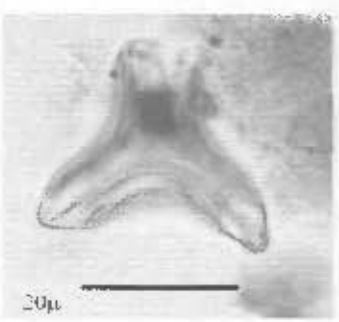
8



9



10



11

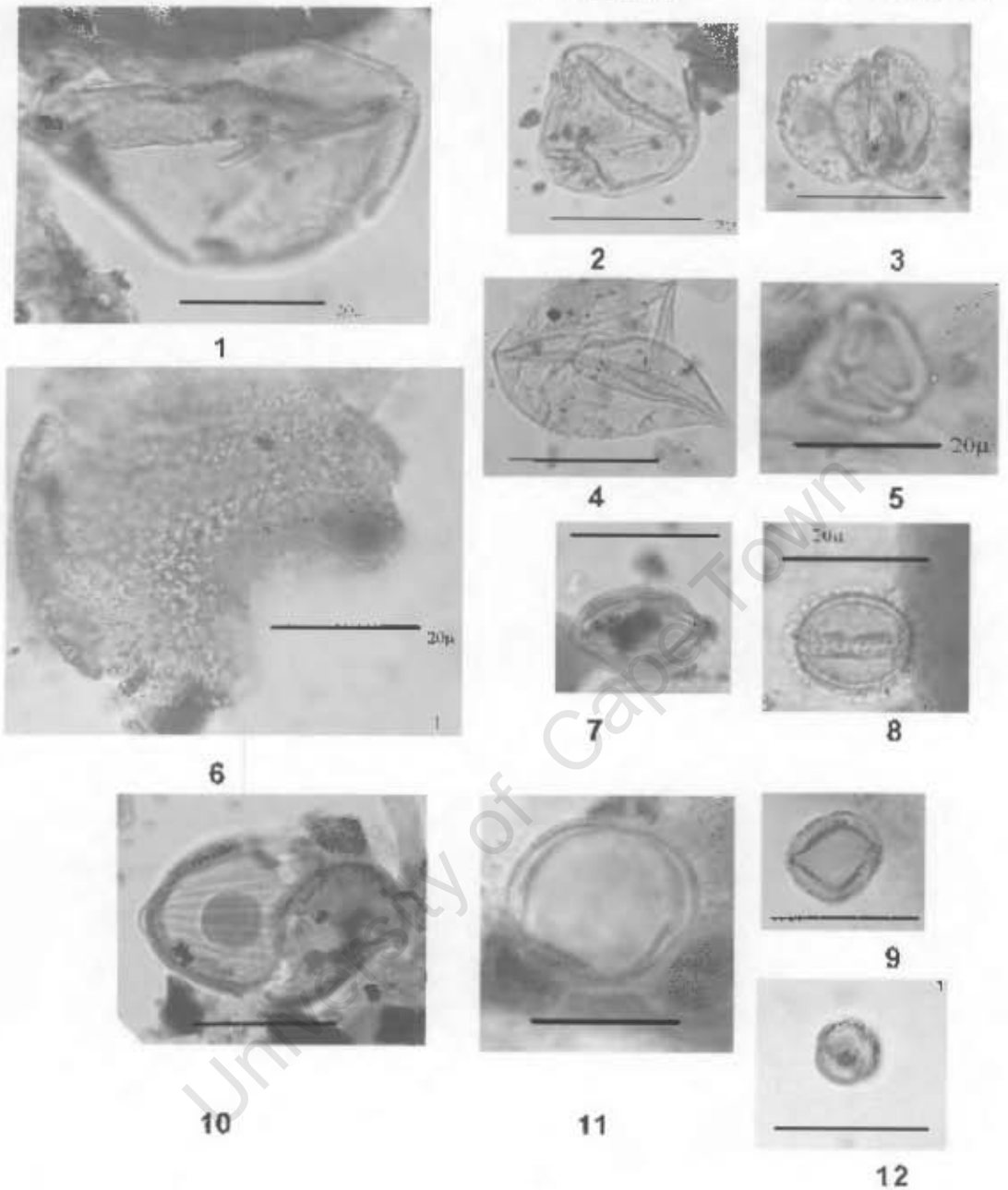
University of Cape Town

Spores

All scale bars 20µ

1: *Aequitriradites* sp.
2: *Camarozonosporites* sp.
3: *Cingulatisporites* sp.
4: *Densoisporites* sp.
5: *Polypodiaceoisporites* sp.
6: *Cyathidites minor*
7: *Cicatricososporites* sp.
8: *Gleicheniidites circinidites*
9: *Ischyosporites* sp.
10: *Laevigatosporites* sp.
11: *Gleicheniidites* sp.

Pollen Plate 2



All scale bars 20μ

University of Cape Town

Pollen

1. *Araucariacites* sp.
2. *Inaperturopollenites* sp.
3. *Podocarpidites* sp.
4. *Taxodiaceaepollenites* sp.
5. Tricolpate pollen D
6. *Incrotonipollis* sp.
7. *Rhoipites* sp.
8. *Clavatipollenites* sp.
9. *Nyssapollenites* sp.
10. *Ephedripites* sp.
11. *Tricolporites* sp.
12. *Triangopollen* sp.

Cape Canyon Palynomorph age ranges

AGE	Mya	TAXON	*Cyathidites minor*	*Laevigatosporites* sp.	*Aequitriradites* sp.	*Dictyotosporites* sp.	*Ephedripites* sp.	*Araucariacites* sp.	*Clavatipollenites* sp.	*Polypodiaceoisporites* sp.	*Podocarpidites* sp.	*Inaperturopollenites* sp.	*Camarozonosporites* sp.	*Ischyosporites* sp.	*Gleicheniidites circinidites*	*Gleicheniidites* sp.	*Cicatricosisporites* sp.	*Taxodiaceaepollenites* sp.	*Nyssapollenites* sp.	*Rhoipites* sp.	*Tricolporites* sp.	Tricolpate pollen D	*Ilexpollenites* sp.	*Triangulopollen* sp.	
Pleistocene	2		●	●							●	●						●	●	●	●				
Pliocene	5		●	●						●	●	●				●	●	●	●	●	●			●	
Miocene	23		●	●				●	●	●	●	●				●	●	●	●	●	●			●	
Oligocene	38		●	●				●	●	●	●	●				●	●	●	●	●	●			●	
Eocene	55		●	●			●	●	●	●	●	●		●	●	●	●	●	●	●	●	●	●	●	
Palaeocene	65		●	●			●	●	●	●	●	●	●	●	●	●	●	●	●	●	●	●	●	●	
Maastrichtian	69		●	●	●	●	●	●	●	●	●	●	●	●	●	●	●	●	●	●	●	●			
Campanian	76		●	●	●	●	●	●	●	●	●	●	●	●	●	●	●	●	●	●	●	●			
Santonian	82		●	●	●	●	●	●	●	●	●	●	●	●	●	●	●	●	●	●	●				
Coniacian	88		●	●	●	●	●	●	●	●	●	●	●	●	●	●	●								
Turonian	94		●	●	●	●	●	●	●	●	●	●	●	●	●	●	●								
Cenomanian	100		●	●	●	●	●	●	●	●	●	●	●	●											
Lower Cretaceous	141		●	●	●	●	●	●	●	●	●	●													
earlier sediments			●	●																					

● Indicates that similar palynomorph found in sediments attributed with this age

Not to be published

APPENDIX 3 – REE DATA

The sample locations are included in Appendix 1.
The letter "c" and "r" imply position of analysis at either core or rim respectively, with a 2 added if more than one analysis undertaken at core or rim.

	Holocene								Pleistocene								
	128-1-1	128-1-2	128-1-3	128-1-4c	128-1-4r	128-1-5c	128-1-5r	128-1-5r2	128-3-1	128-3-2	128-3-3	128-3-4	128-3-5c	128-3-5r	128-3-6c	128-3-6c2	128-3-7c
Ca	53331.58	13826.66	344749.56	33320.89	167687.90	230945.40	577079.33	316771.12	84912.56	15568.47	6116.91	144249.70	823.96	23658.46	3505.35	0.00	293771.28
Sc	5.261	6.426	9.930	3.794	2.925	0.001	3.179	4.728	5.286	4.931	6.325	8.161	4.312	5.404	4.161	5.156	4.436
Ti	183.387	135.366	852.982	184.496	489.901	576.211	1458.755	880.657	234.987	92.279	89.108	389.851	87.780	152.081	119.179	133.632	791.513
V	233.714	239.206	213.164	168.176	153.929	70.524	202.105	208.546	345.607	267.858	269.780	148.632	180.094	207.729	224.347	239.900	305.166
Ni	10.069	11.417	9.856	8.339	9.074	3.561	9.040	10.914	11.072	10.516	10.422	13.458	8.144	6.825	26.059	23.268	10.085
Ga	20.438	26.693	25.135	19.871	18.832	8.611	23.436	23.415	33.053	26.257	29.939	25.794	17.602	18.323	22.259	23.975	26.294
Rb	271.513	266.215	282.575	118.906	125.653	66.745	191.368	179.488	274.673	262.793	259.227	272.099	136.404	142.653	149.398	142.157	166.353
Sr	233.159	63.996	1278.900	163.222	720.273	918.876	2281.469	1447.720	364.880	71.586	30.531	652.751	30.844	137.475	43.758	17.036	1272.428
Y	103.872	47.428	207.959	98.626	309.586	132.352	512.776	752.768	186.872	44.928	24.925	279.828	17.658	119.309	30.391	9.858	466.265
Zr	23.734	29.550	26.760	54.658	46.127	12.649	40.694	42.753	19.419	24.359	27.462	18.545	42.093	47.766	36.234	44.852	32.211
Nb	2.787	2.534	2.327	3.636	2.549	1.020	3.023	2.900	2.363	2.327	2.832	1.720	3.445	4.032	3.526	3.679	3.094
Ba	4.332	2.413	13.012	46.355	57.003	7.761	17.790	13.567	4.158	1.075	0.823	4.911	1.057	2.914	2.099	1.935	8.034
La	48.545	20.284	129.625	46.317	162.306	62.553	306.197	456.890	90.994	19.422	10.419	160.252	9.782	58.643	13.521	3.021	269.271
Cu	50.281	23.655	151.426	49.119	191.605	65.476	208.425	361.824	136.050	23.590	14.229	186.058	16.056	72.903	16.268	4.545	252.148
Pr	8.535	4.096	18.696	9.785	27.427	8.516	33.214	63.494	18.279	3.940	2.370	24.660	2.771	13.296	3.569	0.911	36.340
Nd	40.023	19.920	84.192	39.839	112.766	38.480	145.337	282.422	83.900	18.281	11.021	111.615	9.004	58.903	12.784	4.577	165.947
Sm	7.801	3.899	15.862	7.371	20.905	5.621	23.972	52.532	16.872	3.916	2.474	20.556	1.586	11.782	2.946	1.038	29.060
Eu	1.930	0.956	3.570	2.286	5.479	1.447	5.874	12.480	3.851	0.874	0.680	5.010	0.442	2.856	0.682	0.292	6.809
Tb	1.456	0.706	2.745	1.484	3.778	1.275	4.509	8.778	2.856	0.676	0.440	3.683	0.337	1.984	0.482	0.133	5.454
Gd	10.318	4.765	19.389	8.733	26.598	8.561	35.055	64.403	23.019	4.758	3.042	26.688	1.955	14.748	3.410	0.940	38.136
Dy	9.092	4.452	17.265	8.026	23.154	7.617	30.759	57.696	17.517	4.329	2.606	23.408	1.936	11.580	2.938	1.128	34.342
Ho	2.188	0.989	4.091	2.160	6.266	2.126	8.542	13.474	4.126	1.016	0.574	5.578	0.411	2.654	0.696	0.243	8.612
Er	5.980	2.923	11.752	5.641	16.285	6.107	24.609	39.199	11.218	2.794	1.615	15.431	1.240	6.723	1.986	0.721	24.730
Tm	0.758	0.372	1.507	0.872	2.262	0.768	3.432	5.197	1.457	0.378	0.207	2.021	0.109	0.937	0.417	0.094	3.359
Yb	5.134	2.592	10.322	4.484	14.981	5.627	22.684	32.826	9.585	2.430	1.426	13.343	0.918	6.173	1.495	0.605	21.341
Lu	0.759	0.403	1.606	0.959	2.451	0.999	4.210	5.156	1.467	0.352	0.200	2.099	0.160	1.013	0.317	0.163	3.562
Hf	0.605	0.771	0.977	1.257	1.287	0.191	0.816	0.930	0.463	0.507	0.632	0.662	1.032	1.096	0.924	1.144	0.885
Ta	0.016	0.037	0.078	0.125	0.102	0.009	0.096	0.060	0.019	0.019	0.019	0.033	0.019	0.070	0.012	0.072	0.084
Pb	3.237	1.615	10.027	2.367	4.167	2.805	7.176	6.287	3.917	1.611	1.194	7.506	0.812	1.491	1.843	2.520	2.692
Th	0.389	0.796	0.679	0.585	0.753	0.146	0.496	0.932	0.266	0.147	0.242	0.553	0.188	0.620	0.307	0.228	0.204
U	59.617	13.340	310.141	21.801	67.087	58.506	215.958	218.101	40.283	15.291	9.635	114.935	5.006	18.337	13.602	5.544	142.733
Co	1.253	1.726	3.912	2.526	1.935	0.456	3.703	3.637	1.107	0.971	0.942	0.909	1.220	1.183	2.721	1.551	0.563

University of Plymouth

	Oligocene/Miocene												Eocene							Coniacian		
	324-5-1	324-5-2	324-5-3	324-8-1	324-8-2	324-8-3	324-8-4	159-5-1A	159-5-1B	159-5-2	159-5-3	159-5-4	1407-1	1407-1B	1407-2	1407-3	1418-1	1418-2	1418-3	4396-1	4396-2	4396-3
Ce	15286.38	4905.86	80706.98	11563.65	12512.11	273292.26	1714.99	373000.35	294795.43	96330.43	5690.10	435049.24	215.50	732.15	17330.22	2688.74	735.34	752.55	900.22	3689.48	16550.42	2019.43
Sc	14.597	11.584	13.944	14.361	13.207	14.018	19.590	29.637	26.328	11.276	8.830	16.537	5.255	8.093	12.802	17.362	4.850	3.764	5.256	21.185	25.162	21.940
Ti	432.545	796.418	371.290	331.873	362.778	726.751	533.053	1411.981	1251.907	468.533	505.792	1254.506	87.474	158.097	211.017	309.607	107.256	57.264	116.946	298.201	610.266	192.830
V	305.465	957.297	170.568	325.635	385.422	105.041	567.479	295.803	292.702	164.712	322.068	158.308	146.357	186.113	343.258	212.065	117.746	86.276	96.777	499.534	519.680	521.363
Ni	63.069	189.050	45.417	66.108	69.169	23.130	93.719	138.672	134.265	58.714	142.550	51.764	20.402	23.262	9.566	12.750	6.320	7.571	10.807	11.472	14.494	10.446
Ga	10.155	12.923	11.397	10.439	10.812	11.998	12.229	9.980	9.180	8.376	9.056	8.709	8.673	10.279	20.078	13.227	9.631	8.174	8.952	36.931	39.702	43.048
Rb	206.821	228.566	230.873	223.453	218.131	222.541	185.471	208.441	198.469	233.720	202.878	231.879	266.298	246.503	272.741	265.235	258.644	246.624	238.823	267.164	268.902	277.677
Sr	68.741	34.225	411.152	50.773	56.978	1109.640	14.402	1162.465	921.447	310.143	21.222	1382.419	1.893	2.845	71.723	18.772	6.742	5.821	7.666	12.043	81.625	9.263
Y	53.213	18.487	184.153	46.949	37.497	359.401	2.957	1102.512	871.504	265.268	12.274	545.408	0.037	0.067	61.755	14.292	0.060	0.030	0.105	0.151	47.543	0.210
Zr	34.582	51.146	27.155	41.244	38.039	15.831	50.672	56.096	52.547	28.058	45.009	34.021	20.209	30.531	41.754	44.297	22.457	17.469	23.629	60.681	67.970	75.710
Nb	3.851	11.340	1.652	2.436	2.851	1.041	3.171	5.250	5.020	2.140	5.276	1.857	1.576	2.409	9.007	3.226	1.706	1.480	1.574	6.390	6.961	16.679
Ba	1.529	2.053	3.656	1.900	1.695	9.657	2.133	11.468	10.126	2.957	1.636	10.699	0.898	1.170	1.890	2.467	1.514	0.812	3.078	14.496	29.333	15.860
La	40.234	12.523	172.799	34.184	29.587	387.776	1.952	942.321	742.623	217.652	9.572	507.961	0.038	0.050	48.079	11.365	0.021	0.020	0.363	0.184	42.798	0.139
Ce	66.782	18.836	251.473	52.900	53.900	778.115	3.376	1748.602	1411.691	423.465	16.245	921.615	0.108	0.143	179.385	45.070	0.045	0.000	0.353	0.618	153.461	0.478
Pr	9.377	3.009	31.180	6.161	6.038	72.559	0.485	211.762	172.648	52.103	2.383	101.993	0.009	0.015	15.186	3.660	0.010	0.011	0.034	0.053	15.555	0.041
Nd	43.305	13.824	137.920	28.020	31.049	314.731	2.254	942.721	772.068	238.748	10.987	442.691	0.020	0.060	67.674	15.923	0.004	0.101	0.112	0.188	70.798	0.201
Sm	9.701	3.160	27.134	6.409	6.883	62.097	0.545	198.759	168.049	51.796	2.456	86.975	0.004	0.006	16.551	4.127	0.000	0.000	0.017	0.045	16.936	0.049
Eu	2.098	0.710	6.044	1.957	1.586	16.321	0.138	43.657	36.708	11.314	0.598	19.265	0.003	0.008	3.884	0.954	0.007	0.017	0.005	0.017	3.724	0.009
Tb	1.366	0.464	3.818	1.190	0.980	8.666	0.071	27.832	23.383	7.091	0.341	12.258	0.000	0.002	2.306	0.531	0.001	0.002	0.006	0.005	1.982	0.007
Gd	9.469	3.269	29.324	8.338	7.023	63.199	0.498	198.483	166.129	50.723	2.534	90.009	0.000	0.007	15.204	3.551	0.010	0.010	0.056	0.056	13.706	0.047
Dy	7.303	2.524	21.440	6.411	5.233	47.070	0.469	150.108	125.693	38.022	1.860	68.251	0.015	0.017	12.154	2.954	0.011	0.017	0.040	0.066	10.719	0.050
Ho	1.348	0.476	4.170	1.277	1.001	9.267	0.102	28.621	23.266	7.178	0.374	13.549	0.000	0.005	2.182	0.540	0.000	0.000	0.006	0.005	1.912	0.004
Er	3.194	1.294	9.807	2.715	2.317	21.555	0.219	66.328	53.796	16.635	0.736	31.205	0.010	0.006	5.308	1.231	0.008	0.001	0.020	0.019	4.249	0.036
Tm	0.352	0.164	1.080	0.314	0.262	2.593	0.019	7.597	6.227	1.880	0.102	3.684	0.000	0.000	0.668	0.202	0.000	0.000	0.000	0.001	0.520	0.003
Yb	1.984	0.929	5.827	1.692	1.432	14.488	0.193	41.733	33.940	10.494	0.546	20.621	0.010	0.022	4.130	1.008	0.020	0.017	0.018	0.019	2.827	0.037
Lu	0.254	0.125	0.744	0.206	0.180	1.924	0.025	5.040	4.160	1.324	0.075	2.690	0.009	0.006	0.528	0.132	0.006	0.014	0.010	0.006	0.403	0.005
Hf	1.157	1.633	0.600	1.403	1.181	0.272	1.782	1.760	1.805	0.955	1.685	0.872	0.412	0.677	0.674	1.040	0.595	0.463	0.608	1.514	1.781	1.571
Ta	0.068	0.095	0.025	0.042	0.035	-0.003	0.076	0.131	0.135	0.068	0.133	0.054	0.008	0.031	0.059	0.076	0.020	0.404	0.030	0.056	0.152	0.071
Pb	4.304	20.014	4.503	2.812	4.202	7.486	3.709	16.151	12.640	4.537	3.956	13.957	1.281	1.749	0.739	2.424	0.811	0.654	1.806	0.587	2.508	0.750
Th	1.304	2.134	2.012	2.453	0.957	0.056	0.590	10.209	8.359	3.186	1.133	5.360	0.041	0.059	1.507	2.632	0.096	0.145	0.216	0.109	19.351	0.133
U	2.236	2.447	0.979	2.010	1.446	22.136	0.930	27.060	20.980	6.275	1.814	34.590	1.038	1.246	3.520	2.542	0.104	0.107	0.130	0.154	0.877	0.121
Co	11.469	30.107	8.423	12.202	13.294	5.816	17.207	20.307	15.171	10.271	21.789	8.958	9.859	12.670	2.101	4.994	2.670	2.245	2.648	2.990	4.066	2.187

University of Rhode Island

	Pliocene																	
	128-7-1	128-7-2	128-7-3	119-6-1	119-6-2	119-6-1	281-3-1	30-7-1	30-7-2	30-7-3B	147-120-1	147-120-2	147-120-3	190-4-4B	128-10-1	128-10-2	128-10-3	128-10-4
Ca	280397.25	936.09	280053.64	20786.85	5936.81	31879.94	392657.11	1240.24	1486.46	821?2.29	339.86	177575.66	10355.33	-340.43	1u9917.59	97805.66	-6.25	613962.91
Sc	7.205	5.254	6.446	7.303	6.720	6.250	15.013	6.033	8.335	9.715	0.105	7.139	0.583	1.425	8.548	10.995	11.290	8.429
Ti	551.075	0.000	630.406	180.490	202.315	161.656	943.657	126.877	0.00u	297.832	156.529	484.307	160.047	56.033	472.233	435.347	352.251	1466.616
V	198.071	126.865	220.039	125.942	118.252	151.575	185.740	115.636	111.800	185.621	248.526	226.072	257.265	135.590	219.859	238.762	216.681	254.101
Ni	12.489	7.601	10.863	12.360	10.432	13.975	15.845	8.930	0.663	11.844	12.942	17.492	14.733	12.120	12.374	14.622	13.226	17.830
Ga	28.250	26.856	26.085	23.124	23.140	19.196	19.184	13.107	14.184	13.423	40.586	45.295	45.299	14.920	27.430	26.648	25.146	35.800
Rb	288.667	269.279	296.068	220.627	277.922	260.374	304.697	311.576	308.184	306.033	326.753	382.799	361.414	371.922	388.818	440.706	429.864	430.093
Sr	813.344	7.592	1036.671	113.883	29.819	136.878	1470.041	6.533	7.922	338.207	4.683	758.588	54.236	5.829	609.803	463.783	10.304	2461.152
Y	104.406	0.625	175.772	50.436	6.214	41.565	329.571	0.075	0.294	167.605	0.092	265.543	36.369	0.042	168.059	121.088	1.786	275.943
Zr	19.718	16.146	20.857	30.872	20.056	27.092	31.469	21.323	23.915	25.153	27.865	20.196	24.810	14.396	27.223	37.709	45.317	23.073
Nb	2.430	1.767	2.239	3.783	2.580	2.734	3.197	2.125	2.356	2.531	2.770	2.503	3.089	1.438	3.163	3.156	4.470	2.003
Ba	6.941	4.379	8.995	2.516	2.417	2.123	12.766	1.309	1.460	3.706	1.792	8.365	1.929	0.648	6.937	5.546	2.779	19.847
La	67.909	0.754	101.954	20.583	3.857	22.505	256.884	0.021	0.196	126.604	0.045	128.184	15.384	0.001	67.773	53.073	0.930	169.199
Ce	74.650	1.111	130.068	34.614	5.644	34.101	361.672	0.050	0.437	238.131	0.096	154.751	16.840	0.029	116.314	96.225	1.856	190.277
Pr	8.604	0.145	15.209	4.572	0.867	4.440	39.022	0.003	0.052	26.414	0.010	20.928	2.415	0.008	16.330	12.010	0.251	22.706
Nd	37.951	0.642	66.916	20.902	4.224	19.761	165.566	0.035	0.243	117.741	0.037	97.113	10.415	0.025	75.712	54.231	1.258	100.710
Sm	6.572	0.135	12.476	4.201	0.958	4.111	30.950	0.005	0.070	24.851	0.251	18.492	3.681	0.000	15.595	11.174	0.267	18.100
Eu	1.520	0.057	2.835	0.985	0.205	0.917	6.680	-0.004	0.002	5.328	0.000	4.495	0.843	-0.005	3.524	2.727	0.054	4.255
Tb	1.162	0.019	2.081	0.739	0.156	0.676	5.241	0.001	0.008	5.884	0.003	3.208	0.596	0.005	2.691	1.946	0.045	3.090
Gd	6.096	0.093	15.566	5.122	1.007	4.577	36.394	0.001	0.031	26.863	0.003	22.986	4.116	-0.004	18.759	13.203	0.303	23.380
Dy	7.598	0.128	13.485	4.710	0.994	4.160	32.641	0.005	0.050	23.143	0.018	20.190	3.057	0.002	16.050	12.059	0.251	19.981
Ho	1.838	0.028	3.237	1.057	0.234	1.006	7.412	0.002	0.014	4.904	0.001	4.836	0.805	0.004	3.961	2.648	0.042	4.015
Er	5.223	0.064	9.505	2.858	0.569	2.845	19.901	0.010	0.020	12.600	0.004	13.647	2.181	0.002	10.742	7.268	0.138	13.681
Tm	0.708	0.002	1.234	0.379	0.073	0.368	2.007	0.000	0.004	1.611	0.001	1.853	0.291	-0.002	1.462	0.980	0.020	1.877
Yb	4.744	0.051	8.277	2.584	0.474	2.500	17.600	-0.014	-0.002	10.140	0.011	12.398	1.924	-0.012	9.326	6.430	0.008	12.003
Lu	0.704	0.006	1.391	0.373	0.003	0.386	2.054	-0.004	-0.002	1.432	0.016	2.020	0.302	-0.004	1.383	0.982	0.010	1.927
Hf	0.614	0.710	0.684	0.871	1.330	0.053	1.089	0.016	1.019	0.989	0.934	0.689	0.753	0.311	1.287	1.778	2.348	1.086
Ta	0.034	0.047	0.028	0.057	0.102	0.035	0.041	0.056	0.060	0.064	0.058	0.070	0.066	0.011	0.121	0.105	0.176	0.064
Pb	4.178	1.309	5.531	1.907	2.091	3.274	12.706	1.055	1.855	5.582	1.542	6.742	1.794	2.221	7.392	11.183	3.232	14.170
Th	0.177	0.151	0.383	0.418	0.516	0.570	0.409	0.058	0.177	5.092	0.026	0.194	0.375	0.033	1.474	0.912	0.870	0.320
U	412.403	5.801	314.031	11.897	3.310	22.857	174.823	0.869	0.866	43.647	2.647	111.456	13.254	1.883	65.081	94.599	6.787	105.039
Ca	1.224	0.578	1.079	1.452	1.395	1.376	2.308	1.136	1.391	2.179	1.022	1.375	1.002	1.661	1.216	2.444	2.249	1.366

ODP Publications